Targeted Release from Lyso-thermosensitive Liposomal Doxorubicin (ThermoDox®) Using Focused Ultrasound in Patients with Liver Tumours



Paul C. Lyon
Keble College
University of Oxford

A thesis submitted to the Nuffield Department of Surgical Sciences for the degree of Doctor of Philosophy
Michaelmas Term, 2016

Supervised by: Professor C.C. Coussios, Professor F.V. Gleeson & Professor R. Carlisle

© Copyright by Paul Christopher Lyon 2016

Abstract

Targeted Release from Lyso-thermosensitive Liposomal Doxorubicin (ThermoDox®) Using Focused Ultrasound in Patients with Liver Tumours

Paul C. Lyon, Keble College

Submitted for the degree of Doctor of Philosophy, Michaelmas Term, 2016

The TARDOX study is a Phase I first-in-man proof-of-concept study which aims to demonstrate the safety and feasibility of targeted delivery of a thermo-sensitive liposome in combination with mild hyperthermia induced using an extracorporeal Focused Ultrasound (FUS) device. ThermoDox® is a specially formulated long-circulating and thermosensitive liposome, activated by conditions of mild hyperthermia, to release its cytotoxic doxorubicin content. FUS offers non-invasive and non-ionising approach to tumour therapy, classically by the mechanism of thermal ablation (High Intensity Focused Ultrasound, HIFU) rather than hyperthermia.

Nine patients have received intervention; a single treatment cycle of ThermoDox® combined with FUS to a single target primary or secondary liver tumour using an ultrasound-guided extracorporeal FUS device (Model JC200 Focused Ultrasound Tumor Therapeutic System, Haifu Medical). Five cases proceeded with real-time thermometry and four without. In those with thermometry, optimal hyperthermia (T>39.5°C for over 300 cumulative and 60 continuous seconds, and CEM_{43} < 60 minutes) was achieved in 4/5.

Core tumour biopsies were used for drug quantification studies using high performance liquid chromatography. In an interim analysis, of the evaluable tissue samples analysed to date, an average of 8.41 μg/g ± 4.37 SD of intratumoral doxorubicin was demonstrated in those receiving optimal hyperthermia under real-time thermometry (n=2) and 6.75 μg/g ± 0.13 SD in those whose intervention proceed without thermometry (n=2). Overall, an average of 7.58 μg/g ± 2.70 SD of doxorubicin was seen in the included post-delivery samples analysed to date (n=4). This compares to an average of 2.48 μg/g ± 1.26 SD in evaluable samples taken immediately prior to FUS-mediated delivery (n=4).

Microscopic analysis of post-delivery biopsies demonstrated intercalation of doxorubicin in the nuclei of tumour cells in 6/6 patients with adequate tissue samples, evidencing that release of bioavailable drug from the administered liposomes has been achieved. Radiological follow-up at two weeks with ^{18}F-FDG PET-CT demonstrated unequivocal localised response in 3/4 evaluable patients receiving optimal hyperthermia and 2/4 without real-time thermometry (subjective response in 1 of the remaining 2), despite only receiving a single standard dose treatment cycle of doxorubicin. Serious adverse events were limited to transient neutropenia in 4/9 patients, in line with the adverse event profile for doxorubicin, and prolonged hospital stay due to confusion in 1/9.

We have demonstrated that combined treatment with ThermoDox® and extracorporeal targeted FUS hyperthermia is feasible, safe and can enhance intratumoral drug delivery, providing localised response in human liver tumours refractory to standard chemotherapy. This study, which builds on decades of research efforts in targeted liposome delivery using FUS, is one of the earliest studies to translate ultrasound-mediated tumour targeting into the clinic. The use of chemotherapy in combination with FUS devices, as a non-invasive targeting method, has the potential to transform future clinical treatments for solid organ cancers.

Dissemination

Publications

Several study-related pre-clinical and clinical publications in draft at time of DPhil submission.

Oral Presentations

Selected invited talks & conference attendances:

1. **P.C. Lyon** *et al.*, "TARDOX: Phase I Study of Targeted Delivery of Lyso-Thermosensitive Liposomal Doxorubicin (LTLD) by Focused Ultrasound Hyperthermia to the Liver", invited talk at National Institute of Health, Washington DC, November 2016

2. **P.C. Lyon** *et al.*, "Thermal-mediated Drug Delivery in the Clinics âĂŞ the TARDOX Trial", invited talk at MEIbioeng 2016 (Biomedical Engineering, Medical Engineering and Bioengineering Conference), Keble College, University of Oxford, Sept 2016

3. P.C. Lyon, C. Mannaris, M. Gray, D. Chung, A. Shah, R. Carlisle, F. Wu, M. Middleton, F. Gleeson, **C. Coussios**, "TARDOX: Phase I Study of Targeted Delivery of Lyso-Thermosensitive Liposomal Doxorubicin (LTLD) By Focused Ultrasound to the Liver", Plenary Talk at International Congress of Hyperthermic Oncology, New Orleans, May 2016

4. **P.C. Lyon**, "Clinical HIFU in Oxford: Thermal & Chemo-Ablation of Tumours", invited talk at IDEAL Conference 2016, Oxford, April 2016

5. **P.C. Lyon**, C. Mannaris, M. Gray, L. Folkes, M. Stratford, R. Carlisle, F. Wu, M. Middleton, F. Gleeson, C. Coussios, "Early Clinical Experience of Targeted Delivery of Lyso-Thermosensitive Liposomal Doxorubicin (LTLD) by Focused Ultra-

sound to the Liver", International Symposium of Therapeutic Ultrasound, Israel, April 2016

Poster Presentations

Selected conferences with poster presentations:

1. **P.C. Lyon**, C. Mannaris, M. Gray, L. Griffiths, R. Goldin, L. Folkes, M. Stratford, K. Myers, L. Campo, M. Shipman, N. Fisher, D. Tramonti, R. Carlisle, F. Wu, M. Middleton, F. Gleeson, C. Coussios, "Targeted Drug Delivery in Liver Tumours by Focused-Ultrasound Hyperthermia: Early Results of a Phase I Clinical Trial", BioEngenuity: Improving Human Health Keynotes, University of Oxford, Nov 2016 (*in absentia*)

2. **P.C. Lyon**, L. Griffiths, L. Odondi, C. Mannaris, M. Gray, L. Folkes, M. Stratford, R. Carlisle, F. Wu, M. Middleton, F. Gleeson, C. Coussios, "TARDOX: Early Results of a Phase I Study of Targeted Delivery of Lyso-Thermosensitive Liposomal Doxorubicin (ThermoDox®) By Focused-Ultrasound ", National Cancer Research Institute, Liverpool, Nov 2016 (*in absentia*)

3. L. Odondi, **P.C. Lyon**, L. Boyle, C. Mannaris, M. Gray, L. Folkes, M. Stratford, R. Carlisle, F. Wu, M. Middleton, F. Gleeson, C. Coussios, "TARDOX: Safety and Feasibility of Targeted Delivery of Lyso-Thermosensitive Liposomal Doxorubicin (ThermoDox®) By Focused-Ultrasound Hyperthermia for Liver Tumours", National Cancer Research Institute, Liverpool, Nov 2016 (*in absentia*)

4. **P.C. Lyon**, J. Martin, R. Carlisle, C. Coussios, P. Jakeman, M. Woodcock, "Use of Flow Cytometry to Quantify Cytotoxic Effects Caused by HIFU-Induced Hyperthermia", International Symposium of Therapeutic Ultrasound, Utrecht, 2015

Abbreviations

ANOVA	Analysis of Variance
Casp3	Caspase-3
CCA	Cholangiocarcinoma
CD31	Also known as: Platelet Endothelial Cell Adhesion Molecule-1
CEST	Chemical Exchange Saturation Transfer
CEM_{43}	Cumulative Equivalent in Minutes at 43°C
CE-MRI	Contrast-Enhanced MRI
CK	Cytokeratin
CT	Computed Tomography
CTCAE	Common Terminology/Toxicity Criteria for Adverse Events
DAPI	4',6-Diamidino-2-Phenylindole
DAQ	Data Acquisition
DC	Duty Cycle
DDS	Drug Delivery System
EPR	Enhanced Permeability and Retention
^{18}F-FDG	Fludeoxyglucose 18-F
FUS	Focused Ultrasound
FFT	Fast Fourier Transform
FSC	Forward Scatter
FWHM	Full Width Half Maximum
GA	General Anaesthetic
GCP	Good Clinical Practice
GLP	Good Laboratory Practice
HAE	Hepatic Artery Embolisation
HCC	Hepatocellular Carcinoma
H&E	Hematoxylin and Eosin
HIFU	High Intensity Focused Ultrasound
HFJV	High Frequency Jet Ventilation
HPLC	High Performance Liquid Chromatography
I_{SPTP}	Spatial Peak-Temporal Peak Intensity
IBME	Institute of Biomedical Engineering (University of Oxford)
IHC	Immunohistochemistry
L/D	LIVE/DEAD®
LLOQ	Lower Limit of Quantification
LTSL	Lyso-thermosensitive Liposome

LTLD	Lyso-thermosensitive Liposomal Doxorubicin
USgFUS	Ultrasound Guided Focused Ultrasound
mCRC	Metastatic Colorectal Carcinoma
MPHP	Mixed Pool Human Plasma
MPS	Mononuclear Phagocyte System
MRgFUS	MR Guided Focused Ultrasound
MHRA	Medicines and Healthcare Products Regulatory Agency
MRI	Magnetic Resonance Imaging
MWA	Microwave Ablation
NSTL	Non-Temperature Sensitive Liposome
PAM	Passive Acoustic Mapping
PBS	Phopshate Buffered Saline
PCD	Passive Cavitation Detection
PEG	Polyethylene Glycol
PERCIST	PET Response Criteria in Solid Tumours
PET	Positron Emission Tomography
pLINFU	Pulsed Low Intensity Non-focused Ultrasound
PRF	Pulse Repetition Frequency
RECIST	Response Evaluation Criteria in Solid Tumours
REILD	Radio-embolisation-induced Liver Disease
RFA	Radio-frequency Ablation
SAE	Serious Adverse Event
SIRT	Selective Internal Radiation Therapy
SSC	Side Scatter
TACE	Trans-arterial Chemo-embolisation
TD	ThermoDox®
TSL	Thermo-sensitive Liposome
TTSL	Traditional Temperature Sensitive Liposome

Statement of Originality

I hereby declare that this submission is my own work and to the best of my knowledge it contains no materials previously published or written by another person, or substantial proportions of material which have been accepted for the award of any other degree or diploma at the University of Oxford or any other educational institution, except where due acknowledgement is made in the thesis. Any contribution made to the research by others, with whom I have worked at the University of Oxford or elsewhere, is explicitly acknowledged in the thesis. I also declare that the intellectual content of this thesis is the product of my own work, except to the extent that assistance from others in the project's design and conception or in style, presentation and linguistic expression is acknowledged.



Paul C. Lyon

Michaelmas Term, 2016

Word Count

Words in main text: 49438 (excluding abstract, acknowledgements, dissemination, headings, tables, figure captions & appendices and bibliography)

Words outside main text: 12615 (headings, tables, figure captions & bibliography, excluding appendices)

Words in appendices: 4580

Number of tables & figures: 160 (including appendices)

Acknowledgements

It has been an absolute privilege to lead this early phase clinical trial from concept through to clinical data collection. This has only been possible due to an extensive and sustained world-wide research effort in focused ultrasound technology and the development of drug delivery systems. In advance of me taking post in Oxford, a huge amount of collaborative work between research institutes and industrial partners has led to gaining many of the necessary regulatory approvals to make this clinical research study possible, and I will forever be indebted to all involved along the way.

Perhaps most importantly, my personal gratitude goes to each of the patients who has agreed to participate in this early phase study, including those who did not make it to treatment. I stand in awe at the selfless individuals who have put themselves forward for the study. Their willingness to go through the hardship of a clinical study for the benefit of cancer research, whilst in the knowledge that their own lifetime is limited, is truly inspiring.

Undoubtedly this exciting translational project would not have got off the ground without the steadfast support of my supervising Professors and the world-class research facilities at Oxford. I would like to express upmost gratitude to the following people. Professor Constantin Coussios has been a driving force in this translational work, since long before I had heard about the emerging field of focused ultrasound, and he has continued to support me every step of the way, from my first day in Oxford, personal ultrasound tutoring in early pre-clinical experiments, through to our ethics committee meeting, the early treatments and the clinical data interpretation and dissemination. Even beyond the clinical study, he has been a great support in my future career endeavours as an academic clinician. His expert knowledge of focused ultrasound and targeted drug delivery, combined with his enthusiasm for clinical translation, has inspired and motivated a great number of early researchers to make bold steps forward, not least myself. Professor Fergus Gleeson has given me tremendous clinical and scientific support throughout and has

always made time for me despite a fully-booked diary. He has been instrumental in all aspects of the clinical translation and his technical expertise in radiology is a pleasure to observe. Furthermore, he has enthused me to pursue an Academic Clinical Fellowship in Clinical Radiology at Oxford, which I am delighted to have recently taken post. Professor Robert Carlisle has been a fantastic scientific critique, adviser and mentor, and has continued to review the countless scientific documents I have put in front of him at a moments notice to a very high standard. I truly hope that my future career in Oxford means I continue to develop collaborations with all three of my supervising Professors and other clinical Professors in the field.

This study would not have been possible without Professor David Cranston's foresight into the potential of clinical HIFU several years ago, and the efforts of himself and his colleagues (Professor Feng Wu, Dr. James Kennedy, Dr. Rob Ritchie, Mr. Tom Leslie, Dr. Gail Ter Haar) to put the Oxford HIFU experience forward to gain CE-marking of the Chinese devices for use in Europe. In collaboration with Chongqing HAIFU™ Company, Professor Feng Wu has been involved in developing HIFU technology for two decades and has made an outstanding contribution to the field of clinical HIFU. As a HIFU clinical fellow in Oxford, it has been a great privilege to work alongside such a world-leading expert. He has taught me a great deal about the clinical considerations of HIFU and has always made time for my endless questions, both in study design and during clinical treatments.

I am extremely grateful to Professor Mark Middleton for his willingness to take on this rather unique research proposal as Chief Investigator, his continued expert guidance on the design and running of the clinical protocol, his great contribution to patient recruitment, and his remarkable ability to give individual focus and time to the study, despite this being one of many run under his remit. My gratitude extends to the research oncology team who have believed in the study, guided me, and given outstanding clinical care to the patients throughout, including Finn Tysoe, the lead study research nurse, Dr. Simon Lord, Dr. Sarah Blagden, Dr. Victoria Woodcock, Dr. Nick Coupe, Dr. Karin Hershleb, Dr. Astrid Lappid, Dr. Ricardo Fernandes, Dr. Laura Spiers, Sam Suter and

Leny Hellings.

Due to the multidisciplinary and complex nature of this study, I cannot hope to provide an exhaustive record of the acknowledgements that are due, and take this opportunity to extend my thanks to anybody that I have omitted to mention directly. The Oncology Clinical Trials Organisation and Oxford Clinical Trials Research Unit have been instrumental in guiding the study through the numerous rigorous regulatory hurdles and quality assurance processes, and this would not have been possible without the help and support of a great number of other individuals. Special mention must go to Lucy Griffiths (formerly Boyle), who has expertly lead the OCTO administrative burden from day one and has done so with great professionalism and knowledge.

I would like to personally thank Dr. Daniel Chung, Dr. Mark Anderson, Dr. Mark Little and Dr. Aarti Shah of the Radiology Department, in going the extra mile to assist in the screening and the treatments, and for providing invaluable advice on the analysis of clinical radiology data. High-frequency jet ventilation is a technique requiring advanced anaesthetic skills which have been put into practice with great expertise by Dr. Shaun Scott and Dr. Amy Swinson, who have provided smooth anaesthesia for all of the cases.

Dr. Michael Stratford and Dr. Lisa Folkes took on the difficult challenge of quantifying doxorubicin in tiny tumour samples, using their many years of combined expertise in extraction and quantification, with astonishing efficiency and rigour, for which they deserve a great deal of credit. I would also like to express my gratitude to all of the excellent members of the Good Clinical Practice laboratory, namely Dr. Kevin Myers, Nita Fisher, Daniella Tramonti and Leticia Campo and the Sample Handling Laboratory. Prof. Robert Goldin also deserves special mention for his expert eye in the analysis of histopathological specimens.

Over the years, many post-doctoral researchers at Oxford have paved the way for early clinical projects such as this, and, in particular I would like to thank Dr. Jamie Collin and Dr. Eleonora Mylonopoulou for their relevant contributions. Most recently Dr. Michael Gray and Dr. Christophoros Mannaris have imparted a great amount of

intellect to further both pre-clinical and clinical aspects of the study, and this extends far beyond their chosen area of expertise (ultrasound).

Funding for the study was generously provided by the Oxford Biomedical Research Centre, as part of the National Institute for Health Research. I would also like to thank the Nuffield Department of Surgical Sciences, and in particular Professor Freddie Hamdy, for supporting this DPhil under the device-targeted therapies sub-theme. Celsion Corporation deserve special recognition, not least for being the first company to produce a thermosensitive liposome to clinical-grade, but for their enthusiasm and support for the study, and finally, funding the study drug.

This thesis marks the culmination of book theory, research and clinical experience gained over several degrees and clinical placements in numerous cities across England, including Oxford, over the last two decades. I dedicate this thesis to my mother and my late father, as they have supported me in my research pursuits throughout and have never laid judgement on my previously rather nomadic lifestyle, and I will remain eternally grateful to them.

Finally I will forever be appreciative of my devoted wife, Caroline, who has given me a tremendous level of personal support and wisdom, and has been incredibly understanding for those times where research commitments have impacted our time together. Marrying Caroline in Oxford in the summer of 2015 will always remain one of my happiest memories, and having five Oxford Professors in attendance was an exceptional privilege.

After such great pre-clinical advances in ultrasound-targeted drug delivery across the globe, I truly hope that this study marks one of the very first steps towards the translation 'from knife, to needle, to nothing', in ultrasound targeted treatment of solid organ cancers.

Contents

1 Introduction **1**

1.1 Motivation 1

1.2 Current Treatment Options for Liver Tumours 2

1.2.1 Surgery & Systemic Chemotherapy 2

1.2.2 Minimally Invasive Treatments 4

1.2.3 Non-Invasive Treatments 10

1.3 High Intensity Focused Ultrasound for Tumour Ablation 12

1.3.1 Introduction to Therapeutic Ultrasound 12

1.3.2 Evolution of Extracorporeal Clinical HIFU of the Liver 15

1.3.3 Histological Changes in Ablative HIFU 24

1.3.4 Clinical Summary 29

1.4 Triggered Liposome Release by Focused Ultrasound for Localised Drug Delivery 30

1.4.1 Challenges in Drug Delivery 30

1.4.2 Doxorubicin & Mechanism of Action 32

1.4.3 Liposomal Drug Delivery Systems 34

1.4.4 Heat-Triggered Liposomal Drug Delivery Systems 37

1.4.5 Lyso-Thermosensitive Liposomal Doxorubicin 40

1.4.6 Hyperthermia for Targeted Delivery of Thermosensitive Liposomes 42

1.4.7 Focused Ultrasound Devices for Localised Hyperthermia 45

1.4.8 Previous Pre-Clinical Studies 49

1.5 Clinical Application of Focused Ultrasound for Localised Drug Delivery by Hyperthermia 58
1.5.1 Rationale for Clinical Trial 58
1.5.2 Previous Clinical Studies 60
1.5.3 TARDOX Clinical Study 62
1.5.4 Other Clinical Studies 65
1.5.5 Summary 66

2 Pre-Clinical Studies **68**

2.1 Characterisation of Clinical Thermometry Devices 69
2.1.1 AngioDynamics Thermistor 69
2.1.2 Medtronic Thermocouple 74
2.1.3 Validation of Clinically-approved Thermometry Devices 77
2.2 Volumetric Hyperthermia Using Clinical FUS Device 82
2.2.1 Calibration of the JC200 Therapeutic Device 84
2.2.2 Materials for Volumetric Heating Optimisation 94
2.2.3 Method for Volumetric Heating Optimisation 98
2.2.4 Results 101
2.2.5 Summary 105
2.3 Analytical Methods for Doxorubicin Delivery 107
2.3.1 Doxorubicin Quantification in Tumour and Plasma by HPLC . . . 109
2.3.2 Doxorubicin Quantification in Plasma by Direct Fluorometry . . . 118
2.3.3 Doxorubicin Delivery Studies by Fluorescence Microscopy . . . 126
2.4 Analytical Methods for Cell Viability 133
2.4.1 Cell Viability Studies by Flow Cytometry 134
2.4.2 Cell Viability Studies by Microscopy 147
2.4.3 Summary 151

3 Clinical Study **154**

3.1 TARDOX Overview 154

3.1.1 Study Design 154

3.1.2 Practical Considerations 155

3.1.3 Study Endpoints 159

3.2 Safety & Feasibility 161

3.2.1 Thermal Dose Threshold 166

3.2.2 Inertial Cavitation Thresholds 168

3.2.3 Focused Ultrasound Pressure Estimations 169

3.2.4 Real-time Clinical Thermometry Data 172

3.2.5 Power Predictions 183

3.2.6 Cell Viability by Microscopy 188

3.3 Pharmocokinetics & Bio-Distrubution of Doxorubicin 215

3.3.1 Doxorubicin Quantification in Plasma by HPLC 215

3.3.2 Doxorubicin Quantification in Plasma by Dequenching Assay . . 219

3.3.3 Doxorubicin Quantification by HPLC in Tumour Biopsy 223

3.3.4 Doxorubicin Bio-availability by Fluorescence Microscopy 229

3.4 Radiological Outcomes 238

4 Discussion, Conclusion & Future Work **259**

4.1 Safety & Feasibility 259

4.2 Summary of Clinical Results 261

4.2.1 Case Summary 261

4.2.2 Evidencing Non-Ablative Regimes 266

4.2.3 Interim Analysis of Primary Endpoint 267

4.3 Key Study Challenges 268

4.3.1 Clinical & Logistical Challenges 268

4.3.2 Technical Challenges 270

4.3.3 Scientific Challenges 275
4.4 Study Limitations 276
4.5 Ethical Considerations 277
4.6 Future Work 278
4.6.1 Other Clinical Studies 278
4.6.2 Technological Advances 279
4.6.3 Simulating Parameters for Volumetric Hyperthermia 282
4.7 Conclusions 283
4.8 Summary 283

5 Appendices **285**
5.1 Laboratory Methods 285
5.1.1 Live/Dead Staining of a Cell Suspension for Flow Cytometry . . . 285
5.1.2 Tissue Cell Recovery Protocol 286
5.1.3 Markers & Fluorophores Used in Fluorescence Microscopy . . . 288
5.1.4 Stains Used in Immunohistochemistry for Microscopy 290
5.1.5 Summary of Microscopy Protocols 290
5.2 Regulatory Approvals 292
5.2.1 Research Ethics Committee Approval 292
5.2.2 Medicines and Healthcare products Regulatory Agency Approvals 302
5.3 Previous Medical Histories 306

CHAPTER 1

Introduction

1.1 Motivation

In 2012 there were 14.1 million new cancer cases, 8.2 million cancer deaths and 32.6 million people living within five years of a cancer diagnosis worldwide. Lung, breast, colorectal, prostate and gastric cancer are the five most frequently occurring cancers [1]. Lung, breast and colorectal cancer alone account for 40% of total cases diagnosed and they represent the leading causes of cancer-related death, resulting in almost 2.5 million deaths each year worldwide [2]. The main cause of death is the development of metastases, with the liver being one of the most common sites of spread. Studies have shown that in selected cases the treatment of distant metastases, either surgically and/or with systemic therapy, improves survival [3, 4].

For patients with primary colorectal tumours, liver metastases are diagnosed in 10-25% at the time of bowel resection and, eventually, up to 70% of this group develop liver metastases [5, 6]. Life expectancy for patients with colorectal metastases without treatment is dismal and ranges from 5 to 9 months with a median survival after diagnosis of 6 months [7–9]. Surgical resection of liver metastases offers the best opportunity for survival, but only the minority of cases are operable and offers five-year survival rates of 58% at best [10].

Breast cancer affects 1 in 9 women and most commonly disseminates to the lung, bone, liver and lymph nodes [11]. 15% of patients with breast cancer have liver metastasis at the time of diagnosis, and as many as 50% of patients with disseminated (stage IV) disease will develop liver metastases [12–16]. Those with regional disease have 84% relative five-year survival and once distant metastasis has occurred, this survival rate rapidly declines to just 24% [17].

Approximately a third of patients with non-small cell lung cancer have liver metastases at the time of diagnosis [18], which reduces the five-year survival rate from 36% to just 1% [19, 20].

Primary liver cancers are the third highest cause of cancer-related death globally [21], and in England, account for around 1% of all cancer cases with a 20% survival rate at one year [22]. Hepatocellular carcinoma (HCC), also known as malignant hepatoma, is the most commonly occurring primary liver cancer, accounting for 45% of cases in England [23], and has risk factors including hepatitis B and C and cirrhosis. Cholangiocarcinoma (CCA), cancer of the biliary tract, accounts for 40% of primary liver cancers in England and is the most common cause of death from primary liver cancer in the UK, where it has an annual mortality rate of 1500 [24].

1.2 Current Treatment Options for Liver Tumours

1.2.1 Surgery & Systemic Chemotherapy

Primary liver resection remains the gold standard in the treatment of colorectal liver metastasis, as it is the only treatment shown to have long-term curative potential [25], offering 40% survival at 5 years [26]. However, only a minority (10-20%) of patients are surgical candidates due to either the cancer being too locally advanced, extra-hepatic, or being unfit for surgery due to co-morbidities [27]. A large trial involving neoadjuvant chemotherapy has shown it is possible to convert some previously inoperable patients

to the resectable group with survival benefit becoming comparable to that of primary resection [26]. However, of the larger group with primarily unresectable tumours, the majority (84%) remained inoperable. Furthermore, most of those patients who are fortunate enough to undergo resection of isolated liver metastases subsequently progress, with common sites of recurrence in the liver (in 43 % of resections) or lung (in 31 %) [28, 29]. For those with liver metastases from breast cancer, only a highly selected group are eligible for liver resection as an adjuvant treatment to systemic therapy, such as hormonal and chemotherapy, as such patients typically will have associated metastases at other sites [30]. Similarly for those with liver metastases from lung cancer, liver resection has been a subject of controversy and is generally the exception. However with improved safety in liver surgery and reducing operative mortality, it may be offered as an acceptable adjuvant treatment option in tertiary referring centres for selected cases of oligo-metastatic, and ideally single site liver disease in those who are fit for surgery [31].

Systemic chemotherapy is the accepted standard-of-care for patients with inoperable liver metastasis. Despite advances in systemic chemotherapy, it remains a palliative treatment, as long-term survival is a rare event. For example, in patients with colorectal liver metastasis, systemic chemotherapy with 5-fluorouracil (5-FU) has a response rate of only 20% with a median response duration of 6 months [32]. In the same patient group, combined chemotherapy regimens, such as 5-FU and leucovorin, have improved the median overall survival to approximately 12 months [33, 34] but with a trade-off of increased systemic toxicity. In endocrine-resistant metastatic breast cancer, first-line systematic therapy typically consists of antracyclines, such as doxorubicin, and taxanes, such as paclitaxel [35]. The aim of therapy is prolonged symptom-free survival, but only a relatively modest survival benefit is achievable [36]. In patients with disseminated lung cancer, regimens including platinum-based chemotherapy agents, such as cisplatin, can control symptoms and improve quality of life in those with a good performance status, but again, ultimately, systemic therapy can only modestly prolong survival.[37].

Available treatment options for primary liver cancers are dependent on staging and

background liver condition. In HCC, again resection is the gold standard for localised disease, but is not an option in cirrhosis, often the underlying cause for HCC. Consequently there is the additional option for total hepatectomy and liver transplant in cirrhotic HCC, should a suitable donor be found. Early diagnosis and treatment of HCC can achieve survival rates of 60-70%. However, due to a lack of alternative treatment options, prognosis in advanced disease or progressive disease following local therapy is dismal [38–40]. Sorafenib has been shown to increase median survival in those with advanced HCC by almost three months over placebo in a Phase III trial of over 600 patients [41], a magnitude of effect which caused contentious debate when NICE considered the healthcare economics of the drug [42, 43]. In the case of CCA, again surgery offers the only chance of cure, but the majority of cases are inoperable due to presence of extra-hepatic metastasis at diagnosis. A study looking at survival rates in CCA diagnosed in European adults between 1990-1999 demonstrated age-standardised five-year relative survival rate of around 12% [44]. A recent UK study has demonstrated a six-month progression free survival of 57% using combination chemotherapy [45].

1.2.2 Minimally Invasive Treatments

Minimally invasive ablative techniques in the treatment of patients with discrete liver tumours which are radiologically detectable are in demand, driven by an ageing population, the high proportion of cases unsuitable for surgery and limitations of systemic therapies. Ablative minimally-invasive therapies include radio-frequency (RFA) and microwave ablation (MWA), percutaneous ethanol injection, laser and cryoablation [46]. Such techniques have the advantage of shorter length of hospital stay and lower complication rates, when compared to surgery, but have the disadvantage of less well proven survival benefits, although much clinical research activity is on going in this regard. The majority of the current literature for ablative therapies relates to treatment of hepatocellular carcinoma (HCC) rather than metastatic liver disease, and to date there are no published trials comparing outcomes between ablative technologies [47]. However abla-

tive technologies are showing encouraging outcomes for the treatment of metastatic liver disease as an adjunct to chemotherapy and/or surgery and consequently are playing an increasingly important role.

Radio-frequency Ablation

RFA is the most frequently used local treatment modality for primary and secondary liver tumours. The technique involves placement of an ablation catheter into the target tissue, under Ultrasound or CT guidance, and aims to deliver enough thermal energy to kill cells throughout the entire tumour volume, as well as ablating an additional cuff of normal liver parenchyma (margin). Figure 1.1 demonstrates a schematic of the ablation zone for one clinically-available RFA device. Needle placement can be done percutaneously or intra-operatively by either laparoscopic or open approach. A drawback of RFA is that for larger tumours, upwards of 2.5 cm diameter, local control becomes less predictable as the ablation margin becomes more difficult to attain, and multiple ablations may be required to treat the tumour volume.

A large study has shown that for colorectal liver metastases of diameter 2.5 cm or less, complete local control could be obtained in 78%, but for tumours over 4.0 cm control drops to only 32% [48]. The study demonstrated that RFA can provide palliation, by extending life expectancy to a median survival of 36 months, representing a significant improvement over chemotherapy alone, which has a medial survival of 19.5-24 months [49, 50]. Another study followed progression in 88 patients with isolated colorectal liver metastases under 4.0 cm, who were candidates for resection, but who underwent percutaneous RFA. The study demonstrated complete radiological tumour necrosis in 60%, and 26% remained disease free at a median follow-up of 26 months [51, 52].

Repeat RFA is an option in recurrence; however, risk of local progression after repeat ablation is almost twice that of primary RFA [53]. A recent study evaluated survival outcomes in over 300 patients with colorectal liver metastases treated with RFA and the five-year survival of this patient cohort was shown to be 24-33% post ablation [54].

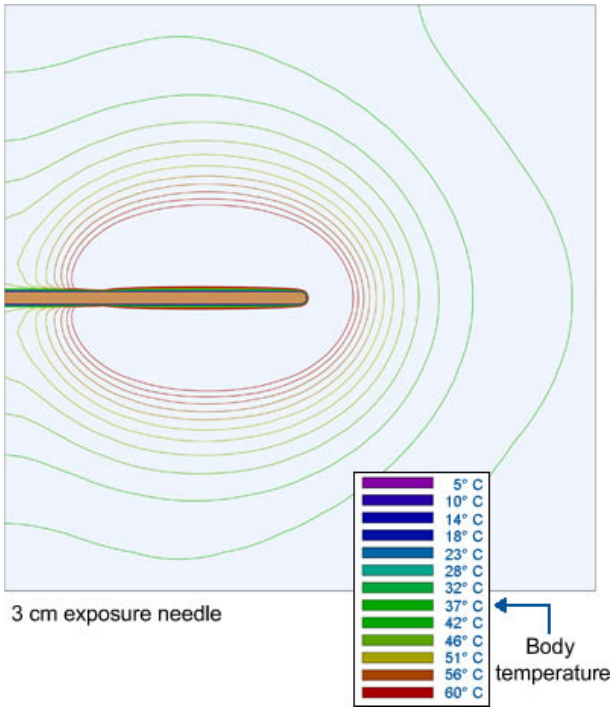


Figure 1.1: Schematic of ablation zones using Covidian Cool-tip water-cooled RFA probe. Not to scale. Figure reproduced from Cool-tip RF Ablation System literature with permission from Medtronic Ltd. (formally Covidien).

In the treatment of liver tumours, although generally safer than surgical resection, minimally invasive ablative techniques generally suffer from similar complications, the most common of which include bleeding, hepatic abscess, injury to bile duct, injury to adjacent bowel, hepatic failure and late track seeding [55–59]. A large RFA study looked at complication rates in over 2000 patient in multiple centres, reporting a mortality rate of 0.3% and a major complication rate of 2.2%. Bleeding (0.5%) and abscess formation (0.3%) were the most common acute complications and track seeding was the most common delayed complication (0.5%) [60].

In the treatment of colorectal liver metastases, although the use of RFA as an adjunct to chemotherapy has demonstrated a significant progression-free survival benefit when compared to chemotherapy alone, the overall survival benefits remains uncertain [61]. In addition such treatments must be radiologically amenable to accurate targeting of the tumour or tumours and thus only a limited number of metastatic tumours in the liver can

be successfully treated by RFA.

Microwave Ablation

More recently MWA technology has developed and several studies have demonstrated it to be a safe and effective ablation modality, using either CT or ultrasound guidance [62–65]. Unlike RFA which has a self-limiting ablation zone, MWA has the advantage of being able to rapidly heat beyond the margin of charred tissue, and consequently is now gaining commercial ground.

Outcome data for MWA in the treatment of hepatic metastasis is rather limited. A randomised study of 30 patients with metastatic colorectal cancer assigned to either surgical resection or laparoscopic MWA did not show a significant difference in mean survival times, with a three-year survival rate of 14%, comparable to that of other ablative technologies in this patient group [47]. Another similar randomised study is currently recruiting at a single centre, which aims to demonstrate comparable local disease control at 2-years [66].

Cyoablation

Cryoablation has been shown to be a relatively safe and effective treatment for advanced liver malignancies in selected patients [67–69], and median survival of 13-32 months has been reported in those with colorectal metastases [70]. Cryoablation may have a role as an adjunct to resection of liver metastases that are amenable to surgery in patients with multiple liver metastases.

Trans-arterial Embolisation

Trans-arterial techniques offer an alternative minimally invasive but non-ablative treatment modality. Hepatic artery embolisation (HAE) has an established role in the treatment of hepatomas and neuroendocrine tumours resulting in 50-60% and 80-90% re-

sponse rates respectively, with a modest survival benefit [71]. The technique relies on the selective blood supply to the liver metastasis via the hepatic artery, thus selectively starving the cancer cells of a blood supply, whilst normal liver parenchyma remains largely supplied by the portal vein [72]. The response tends to be transient due to the development of collateral circulation and no survival benefit has been shown in the treatment of colorectal metastases with embolisation alone [73, 74].

Trans-arterial Chemo- and Radio-embolisation

Attempts to utilise this unique anatomical feature have also been applied to targeted chemotherapy alone; however, several Phase III trials have failed to demonstrate a survival benefit in hepatic arterial chemotherapy over systemic chemotherapy [71].

Drug-eluting bead trans-arterial chemo-embolisation (DEB-TACE) and selective internal radiation therapy (SIRT) [75] offer two alternative techniques, under investigation in patients who have liver metastasis either refractory or not amenable to other treatments. Using chemotherapeutic (DEB-TACE) or radioactive (SIRT) microspheres which are delivered trans-arterially, the arterial microvasculature of the target liver tumour(s) are embolised where further local therapeutic effects can be obtained. In the case of chemo-embolisation, the dual ischaemic and cytotoxic insult has theoretical benefits beyond either of the individual components of treatment [71]. However although response rates are relatively high, all patients eventually develop disease progression [71]. However, the interventional radiology procedures are technically challenging even in skilled hands, multiple embolisation procedures are often required for maximum benefit. Furthermore, radio-embolisation-induced liver disease (REILD) is a relatively uncommon but significant risk, defined as jaundice and ascites 1 to 2 months after a radio-embolisation procedure, in the absence of tumour progression or bile duct occlusion [76]. One prospective study evaluated 45 patients without chronic liver disease who underwent radio-embolisation for the liver in a single institution and 9 (20%) went on to develop REILD in the first 90 days [77]. All these patients had received chemotherapy pre- or

post- procedure and population analysis strongly suggested that this sinusoidal obstruction syndrome results from a combined effect of radiation and chemotherapy.

A previous study included 30 patients who received between one and three chemo-embolisation procedures using combination of cytotoxic agents. Radiological response was seen in 63% of the cases but all responses were transient. Median survival was extended to 29 months after initial diagnosis of liver metastasis and just 8.6 months after initiation of chemo-embolisation [71]. A more recent randomised study between the DEB-TACE and SIRT in the treatment of HCC found no difference in time to progression, progression free survival (216 days for DEB-TACE vs. 180 for SIRT), or overall survival [78]. Hepatic artery radio-embolisation studies are ongoing, notably the global FOLFOX Phase III study which is following outcomes in patients randomised between systemic chemotherapy with or without embolisation as a first line treatment in patients with unresectable liver-only or liver-predominant metastatic colorectal cancer [79].

Irreversible Electroporation

Since an initial study in 2003 showing tumour reduction in a *in vivo* murine model [80], the use of high-intensity pulsed electric fields have been used clinically to ablate tumours by percutaneous insertion of electrodes, accurately positioned adjacent to the target tissue. Most recently the technology has had success in the treatment of pancreatic [81], kidney [82] and liver [83] tumours. One irreversible electroporation system, NanoKnife®, is manufactured by AngioDynamics (Latham, New York) and has Food and Drug Administration (FDA) approval for surgical ablation of soft tissue, but can also be used in organs 'off-label' [83]. One recent study looked at the use of the technique for ablation of liver, kidney and lung tumours with patients under general anaesthesia and the most significant clinical side effects were self-limiting ventricular tachycardias and pneumothoraces [84]. Whilst clinical results are still in their infancy, the non-thermal technology appears effective, reproducible and relatively safe, unaffected by the heat-sink effect of vessels, and further trials are underway.

Whilst surgery remains the definitive treatment, targeted treatment of liver tumours with ablative and trans-arterial techniques allows localised, minimally-invasive therapy with lowered toxicity profiles, and has a growing role in the treatment of patients with progressive liver disease. Unfortunately the majority of patients with metastatic liver disease from breast, lung and colorectal cancer or primary liver cancers are unsuitable for these therapies; thus palliative chemotherapy has defaulted as the mainstay of treatment. Nevertheless, the availability of ablative modalities has perhaps re-stimulated interest in developing an additive or synergistic combination therapy for such patients combined chemotherapy and heat.

1.2.3 Non-Invasive Treatments

Radiotherapy

The field of radiation therapy has been active since the early twentieth century, and it has a very well established role in the treatment and palliation of disseminated cancer. Ionising radiation is directed at tumour deposits and damages the DNA of cancer cells such that they are driven to apoptosis. Stereotactic radiotherapy to the liver has emerged as a feasible and effective option in highly selected patients over the last decade [85–87]. However, a significant disadvantage of radiotherapy is the cumulative radiation exposure and the potential for radiation to damage other structures or the highly radiosensitive liver parenchyma in the path of the radiation beam, which may result in radiation-induced liver disease [88, 89]. In addition the current liver radiotherapy systems use 3D-CT guidance with a requirement for respiratory motion control [87], further adding to the radiation burden.

Focused Ultrasound for Ablation

Diagnostic medical ultrasound is a well-known imaging modality which has been used in routine day-to-day clinical practice over several decades because it is safe, cheap and non-invasive. Therapeutic ultrasound is an emerging and versatile technology which offers the same advantages and holds great promise in the treatment of solid organ tumours. This may be achieved by focusing the incident ultrasound waves to a tight focus, which can result in therapeutic effects, such as direct tumour ablation when used at high powers.

Depending on the properties of the tissue medium [90], at sufficiently high rarefactional pressure amplitudes, the ultrasound wave can lead to the formation of gas- and vapour-filled cavities, a process known as acoustically induced cavity nucleation [91]. These nucleated bubbles will then oscillate linearly or nonlinearly in response to the ultrasound excitation, a process known as acoustic cavitation. Inertial cavitation is a process of rapid and unstable expansion during rarefaction, followed by a violent collapse during compression, which can occur over the course of a single acoustic cycle [92]. At the time of collapse, inertial cavities radiate part of the incident energy as broadband acoustic emissions into the surrounding tissue, which may result in dramatically enhanced heating at the focus [91]. Cavitation phenomena have been associated with a wide range of desirable therapeutic effects *in vivo*, including at high intensities, histotripsy and cavitation-enhanced thermal ablation. Section 1.3 describes the use of High Intensity Focused Ultrasound (HIFU) for tumour ablation.

Focused Ultrasound for Drug Delivery

Although the HIFU acronym has historically received widespread use regardless of its intensity [93], more accurately, focused ultrasound (FUS) is a generic term encompassing the full range of therapeutic ultrasound regimes including low-intensity regimes, for example for tissue hyperthermia.

In the treatment of cancer, it has long been known that there is synergy in combining

systemic chemotherapy or radiotherapy with hyperthermia of 40-43°C [94, 95]. This is a phenomena which has been demonstrated in several clinical studies using whole body, regional or localised hyperthermia induced by a range heating modalities, and is the subject of several review articles [96–99].

When used at lower power and/or low pulsed regimens, FUS can be used to induce highly localised hyperthermia to facilitate targeted therapy, when used in combination with systemically administered thermo-liable chemotherapeutics. This may be achieved cheaply, safely, reliably and effectively and in the absence of ionising radiation and off-target effects. Section 1.4.7 describes how this may be achieved in clinical practice.

In addition, at these lower intensities, FUS-mediated cavitation may provide enhanced vascular permeability, improved drug extravasation and deeper penetration through challenging tissue targets such as tumours [100–104] or the blood-brain barrier [105].

1.3 High Intensity Focused Ultrasound for Tumour Ablation

1.3.1 Introduction to Therapeutic Ultrasound

HIFU offers a completely non-invasive approach to solid tumour ablation. It does this by inducing a rapid rise in temperature to exceed 50°C, in a highly-targeted area, for 1-3 seconds resulting in cell protein coagulation and consequent irreversible cell death (coagulative necrosis) with sparing of the surrounding tissues [106].

HIFU has been the subject of medical research for over 60 years. Since Burov first proposed the use of HIFU for oncological treatments in 1956 [107], it has been used for targeted ablation of tumours in many organs including the liver, kidney, breast, prostate, uterus, bladder, pancreas, testes, brain and the eye [108]. Tumour dissemination following HIFU ablation was a concern raised in 1978, by Fry *et al.*, an early HIFU pioneer, who demonstrated increased metastatic potential of implanted medulloblastoma tumours

in the flanks of hamsters, following intense ultrasound [109]. Several studies in small animals have since explored this hypothesis for a variety of tumour types and have failed to confirm it; it is now widely accepted that HIFU ablation of malignant tumours does not result in their dissemination [110–114]. Indeed other pre-clinical [115–117] and clinical studies [118, 119] have demonstrated that ablative therapies, including HIFU, may induce an immune-mediated host response following curative treatment, which protects against further metastatic spread, and possibly even result in abscopal effects, a benefit shared with other ablative therapies [120, 121] and radiotherapy [122–126].

HIFU has an advantage over chemo- and radiotherapy in that it offers a very favourable side effect profile, with no upper limit of tissue tolerance following repeated exposures of (non-ionising) ultrasound [127]. It has the added benefit, over conventional systemic chemotherapy, of being highly-targeted; due to the tight focusing of ultrasound energy, the non-targeted tissues of the body, even tissues in very close proximity to the target, remain completely unharmed. Furthermore, HIFU allows volumetric coverage according to a treatment plan, rather than concentric thermal damage radiating from a central core, as seen with minimally-invasive ablative technologies previously discussed (Section 1.2.2), or treatment of just the well-perfused margins, as is often the case with systemic chemotherapy.

Safety and feasibility of the extracorporeal approach for HIFU ablation has been demonstrated in China for a wide variety of solid cancers [128] and, in the West, specifically for those of the liver and kidney [129]. Clinically, perhaps one of the largest disadvantage of HIFU over its competing ablative modalities stems from ultrasound's inability to pass through an air-filled space to reach the target lesion, such as in the case of a lung tumour. Treatment time has also been a limiting factor for HIFU, although technology continues to improve in this respect and in experienced hands, the gap between tumour ablation times for RFA/MWA and HIFU is shortening.

In the clinical setting, there are three key mechanisms implicated in the generation of

coagulative necrosis by HIFU:

1. **Heat**: Thermal effect from conversion of mechanical energy into heat, resulting in rapidly induced high peak temperatures for which the cooling effect from nearby blood flow becomes negligible.

2. **Inertial Cavitation**: Acoustic cavitation effects from the rapid expansion and collapse of small gaseous nuclei naturally present in tissue fluid, the endothelial wall and sub-cellular organelles [130].

3. **Vascular Destruction**: Damage to vasculature supplying the target tumour indirectly leading to consequent tumour hypoxia.

In collaboration with the University of Oxford, the Oxford University Hospitals NHS Trust has extensive clinical HIFU experience. The first extracorporeal HIFU device in Europe was used for a study performed at the Churchill Hospital between 2002 and 2004 [129]. The study used an ultrasound-guided focused ultrasound (USgFUS) device to treat 30 patients with tumour deposits in the kidney or liver, and demonstrated both safety and efficacy. These were the first clinical trials of HIFU ablation of tumours in the Western world [131]. These studies led to European Conformity (CE) marking of the Model JC and JC-200 Focused Ultrasound Tumor Therapeutic Systems (Chongqing HAIFU™ Company, Chongqing, China) for non-invasive treatment of the liver, breast, pancreas, uterus, bone and soft tissues in 2005 and 2009, for respective devices.

The TARDOX study is a Phase I proof of concept clinical study which forms the basis of this thesis. For the first time in man, the study aims to demonstrate feasibility of extracorporeal FUS to non-invasively attain and sustain intratumoral hyperthermia in target liver tumours in combination with a thermo-liable chemotherapy delivery agent [132]. In particular, in addition to demonstrating safety, the study aims to demonstrate enhanced tumour-targeted delivery of systemically administered thermo-sensitive liposomal doxorubicin under non-ablative FUS regimes. The study is introduced further in Section 1.5 and the following chapters present pre-clinical and clinical results.

1.3.2 Evolution of Extracorporeal Clinical HIFU of the Liver

Several pre-clinical studies using small and large animal models for ablation in the liver and kidney, of normal parenchyma and tumours, have been performed *ex vivo* and *in vivo* and are presented. For the studies described, one can assume HIFU was applied in continuous wave mode unless otherwise specified as a pulsed exposure.

In 1977 Frizzell *et al.* established thresholds for focal ultrasonic lesions in rabbit liver, kidney and testicle using a 2 MHz device, but organs were exteriorised through surgical incisions, and thus whilst the experiments were performed using *in vivo* perfused liver, this was not an extracorporeal approach [133]. The device used had a focal length of 5 cm, and was tested at the first and third harmonic of its fundamental frequency using exposures of up to a minute. A 2 MHz frequency was shown to provide near optimal depth of penetration for localised heating in solid organs. At 6 MHz, much lower intensity thresholds were found for lesion formation. In this study, tissue damage was presumed to be by predominantly thermal mechanisms, based on another study, which determined an in situ focal intensity threshold of 200 W/cm^2, above which non-thermal effects contribute to tissue destruction [134]. Over the years, several other groups have looked at *in vivo* animal tumour models for HIFU ablation in exteriorised livers, with promising results in terms of accuracy of lesion placement and safety [110, 135, 136], but extracorporeal HIFU was the crucial step needed to translate into clinical practice.

In the early 1990s, attempts at *in vivo* extracorporeal HIFU ablation in the porcine liver and kidney by Vallancien *et al.* [137] used a system of multiple 1 MHz piezo-ceramic elements arranged in a concave dish, to target a common focal volume. Derived from piezo-electric lithotripters, these, when combined, generated very high focal intensities of over 10 kW/cm^2 and hence produced lesions using a predominantly cavitation-based, rather than purely thermal, mechanism. Although these large animal studies and ultimately early human trials [138] demonstrated the device's ability to form extracorporeal lesions in organs at depth, proceeding with the multiple and sizeable generators

required ultimately proved to be impractical and too unreliable for clinical use.

In 1992, Yang *et al.* performed extracorporeal liver ablation in rabbits using a ultrasound guided prototype system through a subcostal approach. The 4 MHz device consisted of a single ceramic transducer which combined both imaging and therapeutic elements, with a 3.5 cm focal length. Using a cubic matrix of 10x10x10 insonation points of 4 s exposures each, with 1 mm separation. The in situ intensity (I_{SPTP}) was 1.5 kW/cm^2. Histological analysis revealed a sharp demarcation of 1 cm^3 coagulation necrosis in 9 of 10 animals, and it was suggested this non-invasive approach may replace laparotomy for liver tumours [139]. In addition this early USgFUS study, along with others, noted the immediate appearance of hyperechoic changes in the target volume when examined under the guiding diagnostic ultrasound, a phenomenon since exploited by clinical USgFUS devices for real-time treatment monitoring. Several similar studies using rabbit tumour models followed with similarly promising results [140, 141].

In the late 1990s, Visioli *et al.* performed an early Phase I dose escalation study for FUS treatment of localised tumours using an extracorporeal transducer (0.56 MHz fundamental, driven at 1.69 MHz) housed on a gantry for movement in three dimensions, without use of anaesthesia [142]. The study included attempted HIFU ablation of six metastatic liver tumours from a variety of primary tumours, with target volumes of 1.3-2.9 cm^3. Using 1 second exposures with in situ focal intensities (I_{SP}) of 745-1490 W/cm^2 for 4-9.5 cm focal depths (assuming 1.0 dB attenuation of acoustic energy per cm of soft tissue, with the addition of 0.5 dB for skin). Whilst curative intent was not the goal, the study demonstrated that the treatment was well tolerated for the five patients with liver tumours, and the remaining 12 patients who received, kidney, prostate or bone tumour ablations.

At around the same time, between 1997-2001, using the ultrasound-guided Model-JC HIFU System (Chongqing HAIFU™ Company, described in Section 1.3.2) over one thousand patients were treated in China with ablative HIFU for a range of solid malignancies

at a range of depths. An extremely low major complication rate was observed [128]. Of this large cohort, 474 patients with malignant liver tumours were treated with a mean diameter of 8.18±3.37 cm. In the liver cohort, the median survival rate was 13.4 months. For this USgFUS device, grey-scale changes (hyperechoic changes) are typically used to determine the therapeutic threshold of ablation, as a surrogate marker for coagulative necrosis [143, 144]. This phenomenon of an area of temporarily increased echogenicity, known as the transient hyperechoic zone, can last for 30-90 minutes and is believed to represent microbubbles of water vapour, and cellular debris [145]. Following comparison between several radiological imaging modalities, contrast-enhanced MRI (CE-MRI) was deemed to be the best method for rapid assessment of therapeutic response of the target tumour, with successful ablation being demonstrated by a lack of perfusion in the HIFU treated region. This early and well-powered study demonstrated that complete tumour ablation is feasible and that cure may even be possible using HIFU for tumour ablation.

Between 2002-2004, Illing *et al.* performed a study which demonstrated safety and feasibility of extracorporeal HIFU for solid tumour deposits [129]. Thirty patients were treated with a single HIFU session using the same Model-JC HIFU System in Oxford; 22 patients had liver tumours (mostly colorectal metastases) and the remaining had renal tumours. Of the liver patients, seven went on to have liver resection. All treatments were performed under a GA with a double lumen endotracheal tube for single lung ventilation to minimise respiratory movement of the target. Transient discomfort and skin toxicity at the treatment site were the commonest adverse-events. Of all thirty patients treated, according to common toxicity criteria (CTC Version 2, 1998), seven patients had grade 1 skin toxicity, self-resolving pin-head blisters, and only one patient had a grade 2 event, a larger partial thickness blister which also resolved spontaneously. 13% suffered from a low-grade fever, self-resolving by 24 hours, consistent with the previously reported 'post-ablation syndrome' [145]. All patients were well enough to be discharged the day following treatment. Of those evaluable patients receiving HIFU to the liver, 20/20 had radiological evidence of ablation on CE-MRI at day 12, and 6/6 had histological evidence

following resection. Of the eight kidney patients, four went on to have subsequent surgical resection, and only one of these (25%) showed features of ablation both macroscopically and by histology (Figure 1.4). Radiological response of ablation was demonstrated in four (67%). Accuracy was evaluated using CE-MRI and lesions were placed directly on target in 88% of cases overall, and within 5 mm for the remaining cases, all lying within the normal surgical resection margins.

In 2006, an MRI-guided FUS (MRgFUS) device (ExAblate 2000 system, InSightec, Israel) was used to safety ablate benign liver tumours in four dogs under GA using induced apnoeas over 20-30 s to control respiratory motion [146]. Using the real-time temperature mapping capabilities the group achieved accurate lesion placement. The same group went on to treat the normal liver in five pigs, again with impressive results [147].

Towards the end of the century, Daum *et al.* used MRgFUS device with a continuous-wave 256-element phased ultrasonic array offering electronic beam steering (1.1 MHz, 12 cm diameter) to generate larger-volume lesions in a more clinically-relevant porcine liver and kidney model [148]. A subcostal abdominal approach was used in five *in vivo* liver cases and two *ex vivo/in situ* liver cases, the latter group chosen to test under respiratory motion-free conditions. By rapidly cycling a series of multiple focus fields over a 20 second continuous exposure period, using their previously published method [149] these researchers were able to generate a cross-sectional focal region of 0.5x0.5 or 1.0x1.0 cm^2. Using the smaller focal volume, lesions of greater than 2 cm^3were reliably achieved, although the size of lesion on autopsy was somewhat variable for lesions formed at the same power, thought to be due to a combination of varied rib anatomies and propagation paths. Post-sonication T2-weighted MR images were able to detect liver-lesion volumes for lesions formed with high temperatures, although respiratory motion artefact weakened this correlation. Using this strategy, the study demonstrated the feasibility of achieving clinically-relevant ablation volumes using MR thermography to detect unwanted heating of the ribs. The study also highlighted the possibility of using a

phased-array to treat between the ribs, increasing the available acoustic window for liver treatments, a method that was already under investigation by other groups at the time [150–152].

Overall, clinical studies in ablation of liver tumours have demonstrated feasibility, accuracy and safety of HIFU ablation in the liver with a promising degree of efficacy. Whilst this section has focused on HIFU ablation in the liver, successful clinical outcomes in extracorporeal HIFU have equally been demonstrated in several other solid tissues including the uterus, kidney, breast, bone and pancreas, across several clinical institutions.

Of this group, the kidney is rather a special case and has perhaps posed the greatest challenge to treat. This is in part due to the defocusing effect of the surrounding perinephric fat [153]. In addition, in highly-perfused organs such as the kidney, there is a consequent high level of conductive cooling [154]. To compensate for these characteristics, higher pressures are likely to be required before successful ablation is achieved. With increased power there is increased the risk of pre-focal heating [153] and consequent skin toxicity [129]. Published clinical studies in extracorporeal HIFU treatment of kidney tumours have not involved MRgFUS and been limited to USgFUS studies to date [128, 129, 142, 155, 156]. The most recent study demonstrated successful ablation in approximately two-thirds of attempted treatments [155], and, whilst promising, a higher success rate is sought before the modality can become adopted as a preferred treatment to surgical excision.

Despite promising results from early phase prospective studies in the West, there is a paucity of much-needed later phase randomised studies, which compare outcomes in cancer patients treated with HIFU with the many competing minimally-invasive treatment modalities available, and this is, in part, attributable to ethical considerations. In favour of continued HIFU research is the large and ever-increasing body of evidence demonstrating the excellent safety profile of HIFU for oncological treatment, its clin-

ical efficacy and its ability to retreat tumours without cumulative radiation damage to surrounding tissues. This has made it an attractive area for continued pre-clinical and clinical studies worldwide, and progress continues to be made year-on-year.

Clinical Considerations in Extracorporeal HIFU

In the clinical setting, HIFU ablation of solid organ tumours may be performed for different indications. In early-stage cancers, a curative outcome is desired, and as such the HIFU-targeted region will typically encompass the tumour and a normal tissue margin of 1.5-2 cm. With advanced-stage cancers, the goal of HIFU treatment typically shifts to palliation with the aims being to retard growth, reduce tumour size and symptoms, and ultimately, to improve the quality of life [128].

Given the wide-range of clinical applications for HIFU, there are currently a variety of optimised clinical HIFU devices on the market for extracorporeal [128, 129, 157–159], interstitial [160] or intracavitary use [161], the first being the only truly non-invasive approach. Interstitial applications include an intravascular approach for cardiac ablation [162], whilst intracavitary applications include the trans-rectal approach for the prostate [163]. Promising clinical outcomes for extracorporeal liver and kidney ablations have been demonstrated using a variety of device designs: hand-held or non-portable, US- or MR-guided, single element or phased array, concave or cylindrical transducers with parabolic reflectors. Transducers built for delivering ablation at short distances, for use in interstitial or intracavitary devices, tend to operate at the higher frequencies of 3-4 MHz [164], producing smaller, well-defined lesions. Whilst such devices have been used to perform *ex-vivo* [165] or laparoscopic [166] liver and kidney ablations in animal studies, they are not suitable for extracorporeal ablations in human subjects due to their smaller transducer diameters and higher frequencies, with consequent inadequate depth of penetration. For successful extracorporeal liver or kidney HIFU ablation, in order to create ablative lesions with clear demarcation, clinical devices must employ higher powers, and transducers with less curvature in order to achieve the required increased depth of pene-

tration of 5-15 cm [167]. Devices must be capable of generating in situ focal intensities in the region of 1.5 kW/cm^2 [142]. As the attenuation coefficient of most tissues is directly related to the ultrasound frequency [168], clinical extracorporeal devices [164] require lower operating frequencies (0.8-1.6 MHz) to facilitate this increased depth of penetration [169].

A major obstacle in extracorporeal HIFU ablation of the liver and kidney is that the incident focused ultrasound must cross the protective rib cage in order to reach the target organ. Ribs obstructing the ultrasound path undergo very high levels of absorption and reflection of the transmitted energy, and thus begin to heat up, with consequent unwanted thermal effects of the overlying tissues and skin, a major off-target effect of ablative treatments across the ribs [169]. As the rib position becomes closer to the focal point, the off-target temperature rises are greater and the focal intensity decreases due to rib shadowing [170], both being undesirable results, as consequently higher powers are required to achieve ablation thus pushing the rib temperature up further.

Extracorporeal clinical devices employ either single or multiple-element transducers with a large diameter, upwards of 10 cm, due to physical limitations, at the cost of device portability. With increasing transducer diameter the larger surface area reduces the energy density crossing the skin, fat, muscle and ribs, thus minimising off-target effects for the same focal intensity, when compared with a smaller transducer. In addition, a larger transducer will naturally reduce the potential impact of rib shielding due to a larger area of incident wave transmission. This is because larger diameter transducers transmit energy through several intercostal spaces simultaneously whilst, small diameter transducer will typically transmit through a single intercostal space and thus, for some target positions, may undergo a significantly greater shielding effect from a single rib lying within the transmitted ultrasound field.

In addition to reducing the energy density transmitted across the costal wall, minimising rib heating, larger diameter transducers have greater curvature consequent with

increased depth of penetration, making them ideal for extracorporeal use. Since their introduction by McGough *et al.* [150] and Botros *et al.* [171, 172] in the late 1990s, phased array HIFU devices have been under active development [149, 170, 173–182] due to their ability to steer the focus through the intercostal spaces, thus minimising unwanted effects such as rib heating and reflections. Phased array devices have typically been designed for non-portable extracorporeal applications using large diameter multiple element transducers, however portable phased array devices are now emerging [183]. HIFU devices with this 'beam-steering' technology are now in clinical use. These include the Sonalleve MRgHIFU device (Philips Healthcare) [158], although this is not yet a clinically established technique for transcostal liver and kidney ablations.

Clinically approved extracorporeal HIFU therapeutic devices employ FUS, typically coupled through water or gel, to provide thermal and non-thermal tissue effects at a precise anatomical location, under MR (MRgFUS) or ultrasound guidance (USgFUS). When used at high intensity for typical ablative application, clinical HIFU devices produce a characteristic “cigar-shaped” thermal lesion at the target, lying along the direction of ultrasound propagation. For example, a typical 0.94 MHz HIFU field used clinically for ablation, as produced by the Model JC-200, typically generates very small lesions of 10-20 mm along the beam axis and 1-2 mm transversely. Thus in order to produce clinically-relevant conformal and confluent volumes of ablation, such devices require placement of lesions side-by-side [184].

The Model-JC and JC200 Tumour Therapy Systems (Chongqing HAIFU™ Company) are extracorporeal clinical devices approved by China's State Food and Drug Administration (SFDA) and are CE marked for use in Europe. The devices are indicated for use in solid tumours including primary and metastatic liver cancer, kidney cancer, pancreatic cancer, breast cancer, primary and metastatic malignant bone tumours, soft tissue sarcomas, and benign tumours such as uterine fibroids and breast fibroadenomas. The devices have since been used to treat a large number of patients worldwide, including in China, Japan, Korea, United Kingdom, Italy, Spain, Russia, Romaina, Ukraine and Saudi Arabia

[185]. An interchangeable therapeutic transducer lies in the centre of the treatment table immersed in a reservoir of degassed water, and can be moved with millimetric precision in orthogonal axes via a computer console. The Model-JC has operating frequencies of 0.8-1.6 MHz and generates free field focal intensities of 5-15 kW/cm^2 at focal lengths of 9-15 cm [186]. The Model JC200 has operating frequencies of 0.8-2.4 MHz with a maximum free field focal intensity of 25 kW/cm^2 for similar focal depths. Both devices have a co-axially aligned 3.5 MHz diagnostic ultrasound probe, which lies in a central aperture of the therapy transducer. These diagnostic probes can be used to provide on-line targeting and feedback based on the presence or absence of hyper-echoic signal following attempted ablation. By controlled translational movements of the transducer along orthogonal axes, driven from the operating interface, the device offers a conventional dot-by-dot approach to forming rows, slices and volumes (Figure 1.2), and a linear mode, which provides lines of continuous sonication for more rapid 'dose painting' of the target volume.

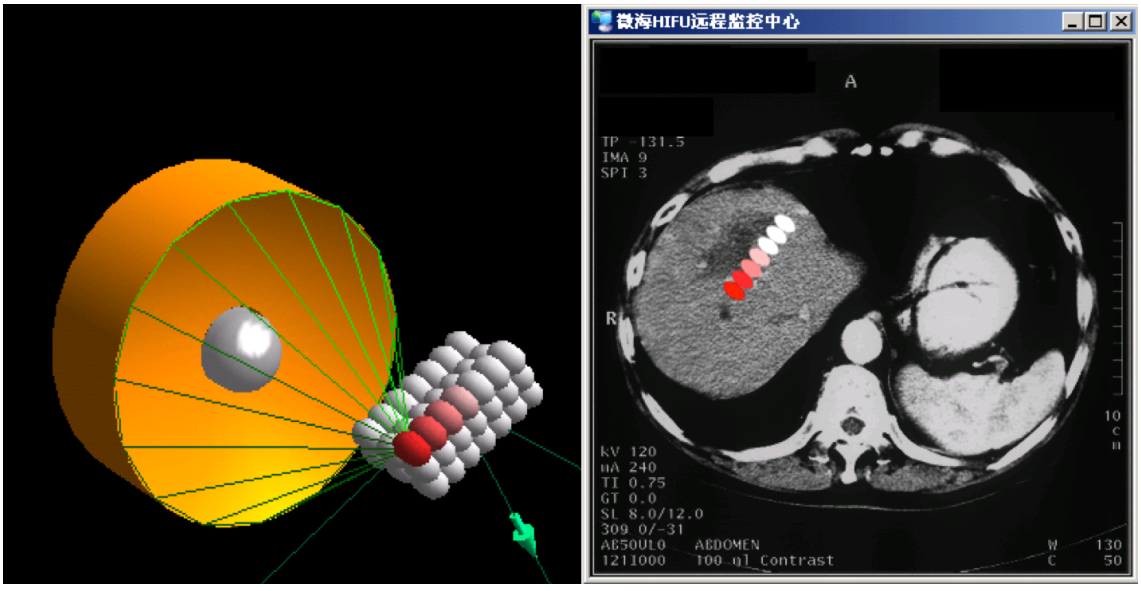


Figure 1.2: LEFT: Schematic of Chongqing USgFUS system and how, by translating the transducer in 3D space using a motorised rig, multiple exposures can be stacked together for the formation of rows, slices and a volume of ablation. RIGHT: Overlay of the current treatment slice on an axial contrast CT image, and in particular the targeting of a large liver tumour, shown by reduced contrast enhancement. Images produced by Chongqing HAIFU™ Company and obtained courtesy of Prof. David Cranston, Oxford, UK

Depending on the target organ, ablative HIFU can be performed with the patient fully conscious, under light sedation or under regional or general anaesthetic (GA) [187]. Whilst light sedation allows the patient to provide verbal feedback based on their sensations, such as pain from nerve stimulation, it offers no respiratory control.

Respiratory-related movements have long been an important consideration for targeted therapy of the upper abdominal organs [188]. Movements of the liver have been quantified as 24.4±16.4 mm in the cranio-caudal direction, and of the kidneys, ~16-17 mm [189]. For HIFU ablation of intra-abdominal tumours, GA is usually required in order for the patient to remain immobile throughout the treatment [187], although one clinical study proceeded without [142]. Furthermore accurate placement of one lesion next to another in order to form rows and volumes requires a stable target organ, and the already relatively long treatment times make breath holding impractical. Under GA, increased control over ventilation using respiratory gating [187], lung separation techniques, such as bronchial blocking and double-lumen intubation for single lung ventilation [155, 190, 191], have proved to be of great value for stabilisation of upper abdominal target organs in HIFU ablations. High-frequency jet ventilation (HFJV), which has a role in RFA of the liver [192] and heart [193–195] and has shown benefit in microwave lung ablation [196], also offers a less-invasive alternative for HIFU anaesthesia and consequently is used in the TARDOX study (Oxford experience, unpublished). Another group has developed a sophisticated motion tracking platform integrated within an MRgFUS device, for ablation of abdominal targets such as the liver [197].

1.3.3 Histological Changes in Ablative HIFU

The mechanisms for the effects on neoplastic tissues induced by HIFU are likely to comprise both direct and indirect destructive effects [198–200]. Evidence from pre-clinical studies has shown that HIFU can induce thermal damage in small vessels, depriving cancer cells of vital nutrients and oxygen [201–204]. This mechanism is likely to contribute

to the instantaneous and irreversible cell death insults from the direct and instantaneous thermal and cavitation effects of HIFU [202]. Between 1997-99, Wu *et al.* examined vessel destruction in 164 patients receiving extracorporeal HIFU for solid malignancies histologically, the majority being liver tumours [205]. Comprehensive radiological follow-up was performed, including contrast-enhanced MRI, colour Doppler US imaging, digital subtraction angiography (DSA) and dynamic radionuclide scanning. All modalities revealed a reduction, or absence, of blood supply in the treated region, indicating successful ablation. Thirty patients went on to have conventional surgery 1-2 weeks post-HIFU and histopathology revealed homogenous coagulation necrosis of tumour tissue and severe destruction of small blood vessels including arteries and veins in the treated region. It is known that the neoplastic microvasculature is more sensitive to hyperthermia-induced injury than that of normal tissue due to key histological differences, thus potentiating secondary tumour cell death [206–208]. This study concluded that HIFU induces neoplastic tumour vessel damage and this mechanism likely to contribute to coagulative necrosis by secondary tumour death.

Since the early pre-clinical histological studies of HIFU lesions in tissue [200, 202, 209–211] several clinical studies involving surgical resection post-HIFU have been undertaken that have employed histological analysis to confirm the presence, and extent, of ablation in tissue sections [129, 201, 212–214]. Haematoxylin and eosin (H&E) stain (Figure 1.4) can be used to demonstrate coagulative necrosis and irreversible cell death, by identifying the histological features of nuclear pyknosis, erythrocyte disruption, loss of cell membrane detail, granular protein deposits on vessel walls, endothelial damage and homogenisation of vascular smooth muscle [213, 214]. In particular, lesions in tissue harvested shortly after HIFU have classically been described as demonstrating an 'island and moat' appearance, where some regions of the central 'island' of tissue may look normal due to instantaneous heat fixation [215]. The central area is surrounded by a penumbra or 'moat' of clear cellular debris, and at its outer edge there is a very sharp demarcation from unaffected tissue, with a transition zone as narrow as six cells wide

[200, 202, 213].

Over days, the irreversibly damaged cells at the centre of the lesions will disaggregate and demonstrate the absence of distinct nuclei or cytoplasm [216]. In the boundary between treated and untreated cells, granulation tissue appears around 7 days and there is infiltration by fibroblasts, which are involved in scarring and repair processes [213, 217]. Typically, small blood vessels of the target region less than 0.5-2 mm in diameter, depending on flow rate, are significantly damaged and occluded, with irreversible destruction of endothelial cells [202, 218], resulting in a delayed secondary response due to reduced blood supply to the tumour [205, 213, 219]. NADH-diaphorase is a standard histochemical vitality stain, which has been utilised for electron microscopy of snap-frozen sections of HIFU-ablated tumour tissue, having the advantage over H&E in its ability to differentiate non-viable heat-fixed cells [215, 220–222]. Several other vitality stains have also been used for histological analysis post-ablation including cytokeratins and triphenyl tetrazolium chloride (TTC). Cytokeratin immunohistochemistry, for example CK8/18, are epithelial specific, and have utility in histological subtyping of carcinomas. In addition cytokeratins can offer information on cell vitality and have an advantage over NADH-diaphorase in that the stain works in paraffin sections and may demonstrate improved morphology [223]. The absence of cytokeratin staining has been used in the identification of ablated regions in various tumour types following treatment with a variety of devices, including HIFU [223–226].

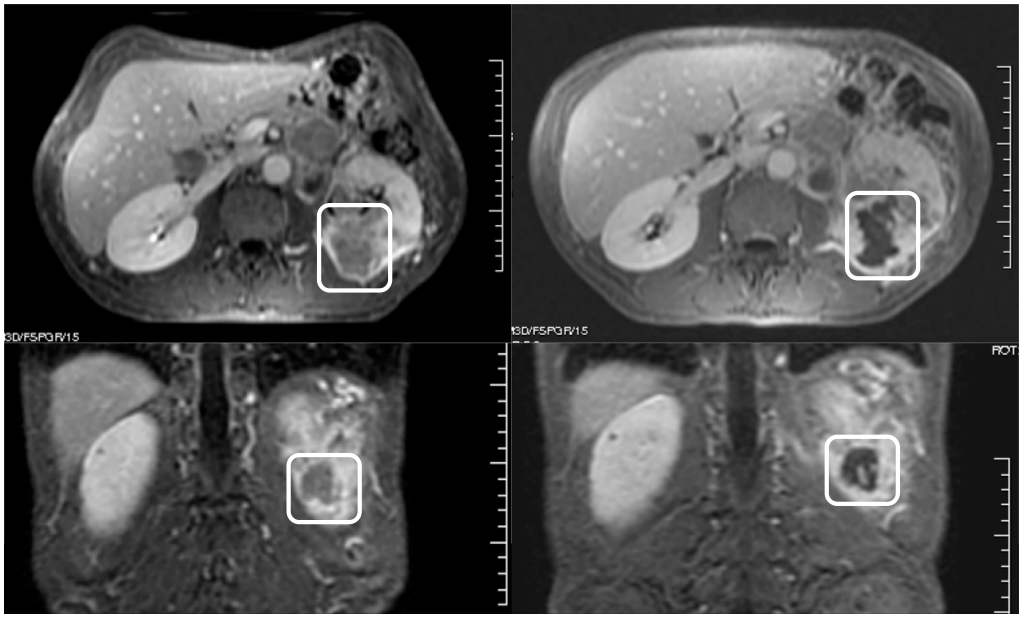


Figure 1.3: Axial (above) and coronal (below) Contrast-enhanced MRI images taken prior (left) and 12 days post HIFU ablation (right), demonstrating a sharply demarcated region of reduced perfusion in the treated left kidney lesion (white oval). Images obtained from data generated on ethically approved clinical trial, courtesy of James Kennedy, Oxford, UK [227]

Whilst histology will remain the gold standard for assessing the presence and margins of HIFU ablation, outside early phase studies, obtaining clinical tissue is rarely possible. Contrast-enhanced cross-sectional imaging, in the form of MR or CT, provides a reliable and non-invasive alternative [128]. In the early weeks following HIFU treatment, CE-MRI demonstrates a lack of central enhancement in the ablation zone, consistent with coagulative necrosis and destruction of tumour vasculature so that contrast cannot penetrate the region. The associated surrounding thin peripheral rim of enhancement is known as benign peri-ablational enhancement [145] and corresponds to an early inflammatory reaction [205]. CE-MRI has now become the imaging modality of choice in the assessment of response following HIFU ablation for most tumour types, including renal tumours (Figures 1.3 & 1.4). To ensure the full extent of tumour ablation, timely radiological evaluation by CE-MRI, or other suitable imaging modality, is critical in oncology patients. However as microscopic foci of tumour cells cannot be visualised radiologically [145], early radiological evaluation is only a surrogate marker of treatment success,

and consequently there is a need for further clinical studies with long-term follow-up and survival data.

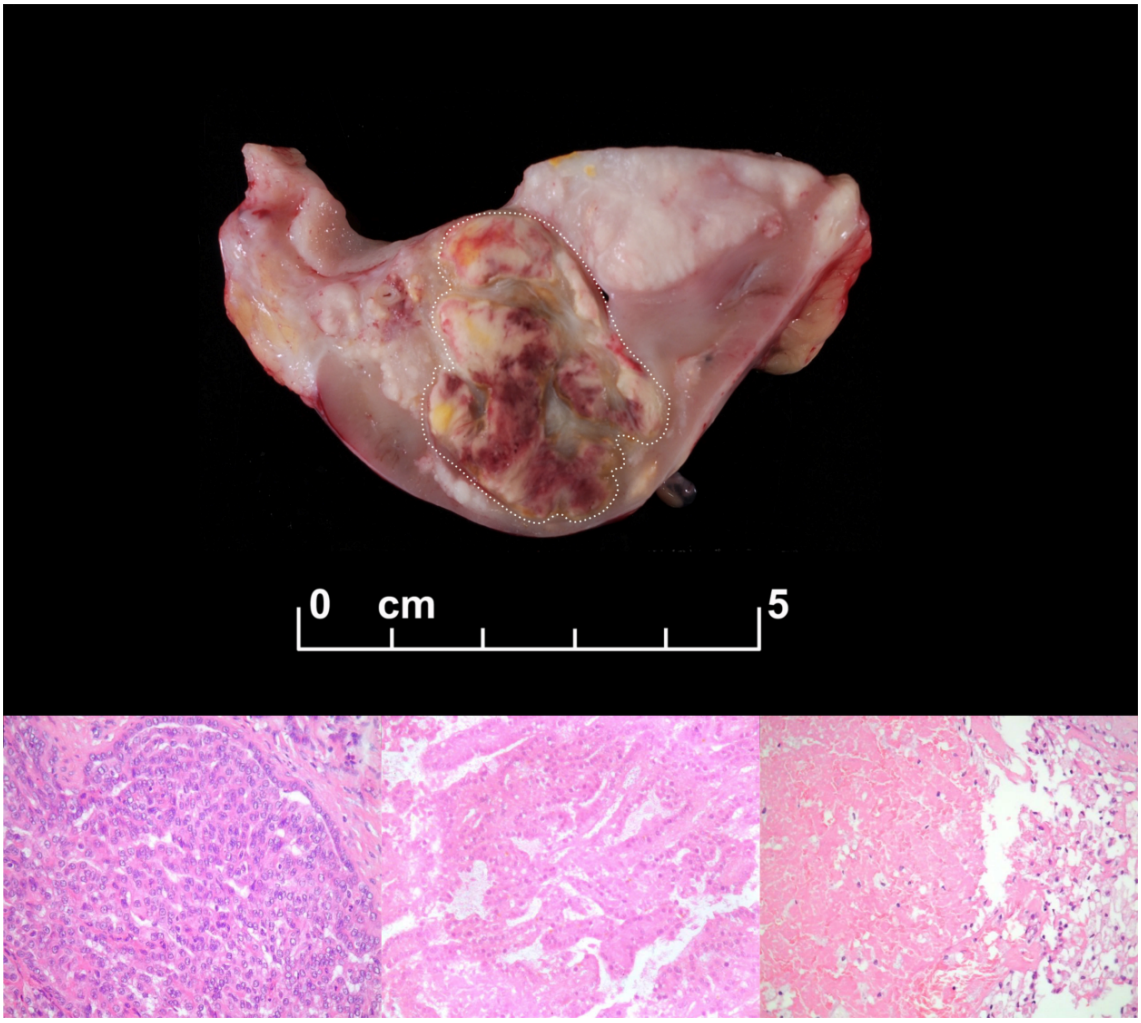


Figure 1.4: TOP: Macroscopic view of the same large renal tumour treated with HIFU and subsequently surgically excised. The white dotted region represents the macroscopic borders of the tumour and ablated region. Several haemorrhagic regions are visible within. BOTTOM: Haematoxylin and eosin (H&E) stained sections of the same tumour, resected days later, showing viable solid variant papillary carcinoma in untreated tumour (left), heat-fixed ablation zone retaining architecture and nuclear outline in treated tumour (middle) and marginal area of ablation zone of treated tumour showing liquefactive necrosis with inflammatory response with macrophage infiltration on the right of the image (right). Images obtained from data generated on an ethically approved clinical trial, courtesy of James Kennedy, Oxford, UK [227]

1.3.4 Clinical Summary

The truly non-invasive and non-ionising nature of HIFU coupled with its versatility, repeatability and favourable safety profile makes it a very attractive treatment modality for solid tumours. The absence of any increased risk of metastasis and evidence of enhancement of the immune response [118, 119] further strengthens its case. However, as with other competing therapies, HIFU ablation of solid organ tumours has its limitations, including the relatively lengthy treatment times compared with RFA/MWA, and the obstruction of the propagation path to some target regions by the presence of bone or air filled structures. This said, for the liver, the lack of associated morbidities such as haemorrhage, infection, fistula formation, transfusion requirement and intensive care stay provides a clear advantage over surgical resection [228].

There has been an inertia in uptake of clinical HIFU in the UK, and there are only a handful of specialist centres such as Oxford who currently offer clinical HIFU to NHS patients. This may be due to the initial expense of acquiring a therapeutic device, potentially lengthy treatment times and the initially steep training requirements for the HIFU operator. This said, both academic and clinical interest continues to grow across the globe and the paradigm shift "from knife to needle to nothing" [229] in the non-invasive treatment of solid organ malignancies through HIFU is taking ever closer steps to clinical acceptance. However, the use of low intensity focused ultrasound systems, when used in combination with chemotherapy agents with triggered-release properties, may address some of HIFUs current shortcomings; an even safer treatment modality with shorter treatment times and the possibility for portable extracorporeal devices make this a hugely attractive research area.

The safety, feasibility, efficacy and limitations of extracorporeal HIFU for treatment of malignant tumours in both curative and palliative settings have been discussed. Ablative HIFU will not be discussed further, and the remainder of this thesis will be concerned with the use of HIFU devices for generation of mild hyperthermia for purposes of targeted

drug delivery.

1.4 Triggered Liposome Release by Focused Ultrasound for Localised Drug Delivery

1.4.1 Challenges in Drug Delivery

Conventional chemotherapy is essentially the only treatment option for patients with multi-focal liver disease. Despite advances in chemotherapy and its delivery, objective response in this patient group remains poor and represents a great societal and economic cost across the globe. In the United States alone, the cost of all cancer care was $124.5 billion in 2010 [230], of which chemotherapy is a significant contributor with an estimated average price-tag of $161,000 for a typical chemotherapy regime for metastastic colorectal cancer in 2004 [231]. In the United Kingdom, according to a 2011 BUPA report, the current annual cost of second- and third-line chemotherapy to the NHS is ~£400m, a cost which could be greatly reduced if first-line treatments could be made more effective. The shortcomings of chemotherapy can be attributed both to the limitation of maximum dose, governed by systemic toxicity of intravenously injected agents, and to the challenge of achieving widespread intratumoral drug penetration to all tumour cells [232].

For a cancer treatment to be curative, it must have access to all tumour cells, as the survival of even minimal cell burden could form the focus of tumour recurrence. In 1955, using histological sections of bronchial carcinoma, Thomlinson & Gray first demonstrated that the amount of necrotic tissue was related to the size of the tumour itself [233]. As central necrosis was observed in all tumours of radius greater than 200 μm, but never in tumours under 160 μm, it was concluded that this was due to an oxygen diffusion limit from the nearest blood vessel, with cells beyond that limit being anoxic and unable to proliferate. Furthermore it was hypothesised that a rim of chronically hypoxic,

but viable cancer cells, surrounds each necrotic core. Indeed hypoxic tumour cells in poorly perfused tumour regions have been shown to promote drug resistance, tumour progression and metastasis through several mechanisms [234] and thus are a dangerous target cell population which limit the effectiveness of systemic chemotherapy.

For any blood-borne therapeutic agent, there must be extravasation and penetration beyond the perivascular space to reach all cancer cells within a tumour [235]. Systemic chemotherapy relies on indiscriminate passive diffusion from vessels, and thus there is a trade-off between providing adequate dosage for tumour penetration and limiting the dose to avoid off-site, or adverse, effects. Several factors combine to make the tumour a challenging environment into which to deliver drugs. Tumour vasculature has a significantly different architecture from that found in normal tissue, having a highly heterogeneous complex and dense branching pattern with enlarged vessels and absent lymphatic drainage [236, 237]. Furthermore, tumour microvasculature has intercellular spaces of up to 500 nm, six times larger than fenestrated endothelia in the liver, and hundreds of fold larger than normal tissue beds, leading to a leaky microenvironment [238–242]. This, in turn, causes unregulated extravasation of fluid and solutes into the tumour interstitial space and increased interstitial fluid pressure (IFP) [243]. Because the IFP is roughly equivalent to the pressure within the microvasculature (~20 mmHg), convection from the vascularised regions to the rest of the tumour is very limited and molecular movement through the tumour becomes entirely diffusion-driven [244].

The maximum distance between a cell and the nearest blood vessel in healthy tissues rarely exceeds 100 μm, a remarkable feature of the human body. As tumour cells may proliferate more rapidly than the endothelial cells of blood capillaries, this has the effect of forcing vessels apart, increasing this distance to up to 180-200 μm in some tumour types [232, 233, 245]. This renders the passive, diffusion-driven delivery mechanism to these high pressure and hypoxic regions even more challenging and leads to perhaps the biggest barrier to successful delivery: poor drug penetration to tumour cells furthest from blood vessels. One *in vivo* study has shown that the concentration of systemically

administered doxorubicin decreases exponentially with increasing distance from tumour vessels, and falls to half its perivascular concentration at a distance of 40-50 μm [246].

As a result of these features, systemically administered drugs will tend to concentrate around the periphery of solid tumours where perfusion is rich. Following intravenous delivery all agents achieve a degree of uptake into the periÂŋvascular space adjacent to blood vessels. However in the more avascular central regions, delivery becomes diffusion-limited, rather than by convection, due to low pressure gradients [237]. Indeed, the larger the agent, the more inefficient passive diffusion becomes [247].

To date, purely pharmacological approaches have therefore failed to address what is essentially a three-fold challenge: (i) to deliver therapeutically significant concentrations of active agents to the tumour vasculature while minimising off-target effects; (ii) to release the therapeutic agent "on-demand" at the target site; and, (iii) to improve the distribution and spread of the therapeutic agent against the intratumoral pressure gradient in order to achieve a therapeutically relevant concentration throughout the tumour.

1.4.2 Doxorubicin & Mechanism of Action

Doxorubicin (adriamycin) is an anthracycline antibiotic with potent broad-spectrum anti-tumour activity [248, 249]. It has been used as an anti-cancer agent for over three decades, and it continues to be one of the most widely used chemotherapy agents in clinical practice, typically as a combination therapy. Doxorubicin is one of the most effective drugs in the treatment of solid tumours, and in particular, breast, lung and ovarian cancers. In addition it also offers significant activity against bladder, gastric, liver, thyroid, bone and paediatric kidney tumours as well as soft tissue sarcoma and some haematological malignancies [250]. Its potent anti-neoplastic effect against these wide ranging cancers, combined with its inherent ability to fluoresce even at low concentrations, make it an excellent theranostic agent for both pre-clinical and clinical studies alike.

In the clinical setting, doxorubicin is typically administered intravenously, and cir-

culates systemically in order to exert its anti-tumour effects. Free doxorubicin is able to enter cells (influx) through a process of passive diffusion, following an initial rapid uptake phase of over just seconds, thought to be due to drug adsorption to phospholipids in the cell membrane. Once intracellular, doxorubicin has a high affinity for several cellular components including double-stranded DNA (nuclear binding accounting for the vast majority), double-stranded RNA, dinucleotides, lysosomes and phospholipid components [251].

Doxorubicin is selectively transported to the nuclei of neoplastic and proliferating cells. It has been proposed that once intra-cellular, doxorubicin preferentially targets the cytoplasmic proteasomes of these highly-proliferating (tumour) cells [252]. From there, the proteasome complex is transported to the nucleus by an ATP-dependent nuclear pore-mediated mechanism, where doxorubicin dissociates to bind to the double-stranded DNA, for which it has an even higher affinity. The mechanism of doxorubicin's activity has long been the subject of debate, but current understanding is that several cytotoxic pathways are at play, ultimately leading to apoptosis:

1. Proteases: inhibition of protease activity suppressing cell growth and metabolism [253].

2. DNA-mediated effects: nuclear accumulation and its intercalation [254] hinders the progress of topoisomerase II, required for DNA transcription and synthesis of macromolecules [255], and results in double-strand breaks [256].

3. Regulation of gene expression: through enhanced or suppressed binding of transcription factors, such as SP-1 [257, 258].

4. Free radicals: the production of free radical-generating metabolites (semiquinone and aglycone), leading to oxidative cellular damage. This mechanism is also thought to contribute to cardiomyopathy, a dose-dependent and significant adverse effect [259].

1.4.3 Liposomal Drug Delivery Systems

The use of macromolecular Drug Delivery Systems (DDS), such as those composed of liposomes [260], polymers [261] or nanoparticles [262], can enhance the pharmacological effect of chemotherapeutics by improving pharmacokinetics and pharmocodynamics [263]. The requirements of a targeted DDS are to (1) retain its content from manufacture to point of delivery, (2) evade the bodies natural defence mechanisms, (3) target the specific tumour site and only then (4) release its cytotoxic agent [264]. In the early sixties, Bangham *et al.* first identified the potential of a swollen phospholipid system, initially coined 'bangosome', which became known as the liposome [265]. Further pioneering research in the 1960-70s by Gregoriadis and others [265–270], led to the realisation that liposomes could potentially be used as drug delivery vehicles due to their versatile biocompatible membranes and aqueous core, allowing incorporation of hydrophilic drugs. Furthermore their inert nature, limited toxicity and biodegradability at to the attraction of their use as DDS [271].

As liposomes are unable to influx freely into cells, in order to exert their cytotoxic effects, liposomes must either release their contents extra-cellularly, for passive diffusion, or by interact with cells using one of the following mechanisms: [272]:

1. Adsorption: depending on the surface properties of the liposomes, if the attractive forces exceed the repulsive forces the liposome will be adsorbed directly into the cell membrane.

2. Endocytosis: the cell membrane engulfs the liposome and it enters the cytoplasm using an energy-driven process.

3. Fusion: the liposome merges with the cell membrane such that liposomal content is delivered directly into the cell.

4. Lipid exchange: components of the lipid bilayer (lipids, cholesterol, membrane bound molecules) are exchanged with components of cell membranes.

In early studies, liposomes were noted to suffer from rapid opsonisation and uptake by the mononuclear phagocyte system (MPS), resulting in rapid clearance from the circulation. The development of 'stealth liposomes' by incorporating polyethylene glycol (PEG) into the lipid membrane (PEGylation), has greatly extended circulation times, from hours to days, due to evasion of uptake by the MPS [273–275]. A further optimisation has included the use of cholesterol in the membrane to reduce leakage of encapsulated content [276, 277].

One approach to improve targeting efficiency is the use of conjugated ligands which interact with over-expressed cancer cell surface receptors such as folate [278]. Conjugated ligands such as peptides, proteins, carbohydrates, and various other small molecules can promote receptor-mediated endocytosis of the liposome. Antibody conjugation has led to a new generation of 'immunoliposomes', which offer a unique opportunity for specific cellular targeting. However only modest improvements in targeting efficiency have been reported, due to rapid clearance of the formulations by the MPS [279].

Liposomal formulations are under investigation for clinical use in intravascular delivery of anti-cancer, anti-fungal, gene therapy agents and vaccines, by vascular, inhalational and topical delivery mechanisms, but only a small minority of formulations have been approved for clinical use [280]. Liposomal DDS are currently approved for use in oncological clinical practice and there are many on-going clinical trials in this area (Tables 1.1 & 1.2). The first human study to demonstrate the use of PEGylated liposomes for prolonged circulation was performed in 1994 [281], shortly after which the encouraging results of the first clinical study of PEGylated liposomal doxorubicin (Doxil™) for Kaposi's sarcoma were published [282]. In 1995, Doxil™ became the first FDA-approved liposomal pharmaceutical, or indeed nano-drug, and is indicated for the treatment of metastatic breast and ovarian cancer [283–286]. Of note, FDA approval was based on equivalent therapeutic efficacy but reduced adverse effects. Other well-known chemotherapeutic liposomal formulations approved for use in Europe include Myocet® (containing doxorubicin), also indicated for breast cancer [287] and DaunoXome® (con-

taining daunorubicin) for Kaposi's sarcoma [288].

Liposomal formulations of typical mean size 100 nm, such as Doxil™ are of particular interest. By virtue of their size (50-450 nm [289]), these lipid-based nano-medicines will tend to preferentially accumulate across the leaky tumour vasculature due to a passive targeting phenomenon known as the enhanced permeability and retention (EPR) effect [290]. As a result of this process, liposomes are seen to accumulate in solid tumour and remain there for several days rather than minutes [291]. In particular, intravenously administered liposomes preferentially accumulate in the perivascular space of tumours, as they are unable to penetrate further [292, 293]. A review of the last 10 years of data on nanoparticle delivery has identified that a median 0.7% of administered nanoparticle dose is found to be delivered to solid tumour [294].

One study has shown Doxil™ distribution falling off rapidly further than 10 μm from the nearest vessel [295], in contrast to bioavailable drugs, such as free doxorubicin, which may penetrate up to an order of magnitude further [246]. Consequently, such non-temperature sensitive liposomes (NTSLs) are designed to degrade slowly following passive accumulation to reduce systemic toxicity, thus delivering sustained concentrations of bioavailable drug [296]. Doxil™ is a stealthed NTSL, designed to accumulate by the EPR effect and slowly release its chemotherapeutic content over days-to-weeks with peak bioavailability at 48 hours [297]. Despite FDA approval, the mechanism for intratumoral release of doxorubicin still remains to be elicited [298].

Key advantages of such liposomal preparations are longer circulation times and the ability to attenuate drug-related systemic toxicity, thus increasing the therapeutic index [299, 300]. However, despite great advances in the manufacture of clinically approved liposomes (Tables 1.1 & 1.2), only modest improvements in clinical outcomes have been demonstrated in the treatment of cancer patients [301].

Despite the EPR effect, a major limitation of systemically-administered liposomal agents is their low therapeutic index: the dose required to produce a successful anti-

tumour effect remains toxic to normal tissues, and, at lower doses, antitumor activity is hindered by a failure to penetrate beyond the perivascular space [302]. Furthermore, as NTSL are primarily designed to be stable in circulation, they fail to release more than a third of their cargo upon reaching the perivascular space in the tumour [303]. Whilst the passive accumulation and slow release of PEGylated NTSLs may be efficacious in some circumstances such as schedule-dependent drugs [304, 305], the activity of other drugs and in particular anti-cancer agents, such as doxorubicin, is dependent on peak concentrations [296, 306]. In the absence of a triggered release mechanism, such passive release may create a situation whereby tumour cells are exposed to persistently low levels of mutagenic drugs rather than peak chemoablative levels. This may create conditions ideal for the development of resistance rather than treatment. It is notable that only a single liposomal anti-cancer agent (Doxil™) has received approval in the last decade.

1.4.4 Heat-Triggered Liposomal Drug Delivery Systems

Since their introduction by Yatvin and Weinstein in the late 1970s [307, 308], thermosensitive liposomes (TSLs), or traditional TSLs (TTSLs), have offered great promise as targeted delivery systems to improve on the passive release profiles of NTSLs. A large body of work driven by Needham and Dewhirst [280, 309] has since led to the development of novel low-temperature sensitive liposomes, also known as lysolipid thermally sensitive liposomes (LTSLs). Incorporation of a phospholipid, lysolecithin, facilitates opening of pores in the lipid bilayer at a transition threshold temperature which is above body temperature but below that which is intrinsically damaging to the cell [310]. Indeed, chemotherapy agents can now be packaged inside biocompatible LTSLs which are specifically formulated to be stable at 37°C but release their cargo at temperatures as low as 39°C. In addition, release is more rapid and a higher percentage of drug release can be achieved compared to TTSLs.

When administered systemically, such LTSLs are also formulated to evade the MPS

Products approved	Drug	Indications	Year approved
AmBisome (Gilead)	Amphotericin B	Fungal infections, Leishmaniasis	1990 (Europe), 1997 (USA), 2000
Doxil/Caelyx (Johnson & Johnson)	Doxorubicin	Kaposi's sarcoma Ovarian cancer Breast cancer Multiple myeloma + Velcade	1995 1999 2003 (Europe, Canada) 2007
DaunoXome (Galen)	Daunorubicin	Kaposi's sarcoma	1996 (Europe), 1996 (USA)
Myocet (Cephalon)	Doxorubicin	Breast cancer +cyclophosphamide	2000 (Europe)
Amphotec (Intermune)	Amphotericin B	Invasive aspergillosis	1996
Abelcet (Enzon)	Amphotericin B	Aspergillosis	1995
Visudyne (QLT)	Verteporphin	Wet macular degeneration	2000 (USA), 2003 (Japan)
DepoDur (Pacira)	Morphine sulfate	Pain following surgery	2004
DepoCyt (Pacira)	Cytosine Arabinoside	Lymphomatous meningitis Neoplastic meningitis	1999
Diprivan (AstraZeneca) Estrasorb (King)	Propofol Oestrogen	Anaesthesia Menopausal therapy	1986 2003
Lipo-Dox (Taiwan Liposome) Marciibo (Talon)	Doxorubicin Vincristine	Kaposi's sarcoma, breast and ovarian cancer Acute lymphoblastic leukaemia	2001 (Taiwan) 2012 (USA)

Table 1.1: Liposomal and lipid-based products approved for clinical use and marketed. Reproduced with minor modification from Advanced Drug Delivery Reviews, 65(1), Allen & Cullis, Liposomal drug delivery systems: From concept to clinical applications, p41, 2013, with permission from Elsevier, references available in original manuscript [283].

Products in clinical trials	**Drug**	**Indications**	**Clinical Study Phase**
SPI-077 (Alza)	Cisplatin	Solid tumours	Phase II*
CPX-351 (Celator)	Cytarabine: daunorubicin	Acute myeloid leukemia	Phase II
CPX-1 (Celator)	kinotecan HCl:floxuridine	Colorectal cancer	Phase II
MM-398 (Merrimack)	CPT-11	Gastric and pancreatic cancer Glioma and colon cancer	Phase II Phase II
MM-302 (Merrimack)	ErbB2/ErbB3-targeted doxorubicin	ErbB2-positive breast cancer	Phase I
MBP-436 (Mebiopharm)	Transferrin-targeted oxaliplatin	Gastric cancer and gastro-oesophageal junction	Phase II
Brakiva (Talon)	Topotecan	Relapsed solid tumours	Phase I
Alocrest (Talon)	Vinorelbine	Newly diagnosed or relapsed solid tumours	Phase I
Lipoplatin (Regulon)	Cisplatin	Non-small cell lung cancer	Phase III
L-annamycin (Callisto)	Annamycin	Adult relapsed ALL Pediatric relapsed ALL and acute myelogenous leukemia Doxorubicin-resistant breast cancer	Phase I Phase I Phase II*
ThermoDox® (Celsion)	Thermosensitive doxorubicin	Primary hepatocellular carcinoma Refractory chest wall breast cancer Colorectal liver metastases	Phase III Phase II Phase II
Endo-Tag-1 (Medigene)	Cationic liposomal paclitaxel	Pancreatic cancer Triple negative breast cancer	Phase II Phase II
ALN-TTR ALN-PCS	siRNA targeting transthyretin (TER)	TIR amyloidosis	Phase I
ALN-VSP (Alnylam)	siRNA targeting PCSK9 RNAi targeting liver cancer	Hypercholesterolaemia Liver cancer and liver metastases	Phase I Phase I
TKM-PLK1 TKM-ApoB (Tekmira)	RNAi targeting polo-like kinase (POLO) RNAi targeting apoB	Liver tumours High levels of LDL cholesterol	Phase I Phase I
Stimuvax (Oncothyreon/Merck)	Anti-MUCI cancer vaccine	Non-small cell lung cancer	Phase III
Exparel (Pacira)	Bupivacaine	Nerve block Epidural	Phase II Phase I

Table 1.2: Liposomal and lipid-based products approved for investigational use in clinical trials. *Development terminated. Reproduced with minor modification from Advanced Drug Delivery Reviews, 65(1), Allen & Cullis, Liposomal drug delivery systems: From concept to clinical applications, p41, 2013, with permission from Elsevier, references available in original manuscript [283].

and remain in the blood stream for several hours. At peak circulating levels, if regional hyperthermia is applied to a target tumour site, there is the potential for instantaneous and localised release of chemo-ablative levels of bioavailable drug, whilst avoiding rapid systemic drug release. In using such a delivery systems, the intratumoral concentration of delivered drug depends on several factors; i) the plasma concentration of the LTSL, ii) the drug content of the liposome, iii) the pharmacokinetic release profile of the liposome, and iv) the total exposure time to hyperthermia [311]. LTSLs are now available for clinical use as investigational medicinal products. Such LTSLs rapidly release chemotherapeutic contents upon reaching levels of mild hyperthermia of around 40-42°C.

1.4.5 Lyso-Thermosensitive Liposomal Doxorubicin

At the turn of the millennium, Needham *et al.* developed a LTSL formulation containing doxorubicin, which, whilst stable at 37°C, was optimised for rapid release of drug in conditions of only mild hyperthermia (39-40°C) [312]. Based on this formulation, Celsion Corp., Columbia, MD, have developed lyso-thermosensitive liposomal doxorubicin (LTLD, LTSL-doxorubicin) for clinical use, under the commercial name of ThermoDox® [280]. LTLD releases bioavailable doxorubicin when exposed to mild hyperthermia as the trigger. Release (80-100% of encapsulated drug) is rapid when heated to 41.3 °C for 20-40 seconds, whilst at 39°C only minimal release (15%) is seen [313]. More recently Lindner *et al.* have developed a liposome with similar thermal release properties using a different formulation [314, 315].

Many pre-clinical studies incorporating the use of LTLD for targeted delivery have already been completed, and a number of clinical studies are in the pipeline, in progress or nearing-completion. Early pre-clinical and clinical studies involving LTLD utilise fluorescence-based quantification assays to better understand its pharmacokinetics in the plasma, and assess intratumoral delivery. Whilst doxorubicin remains encapsulated in its liposomal form, its fluorescence emission is significantly quenched. Thus in these

studies, quantification assays will generally incorporate de-quenching steps, such as the use of heating, homogenisation, solvents or detergents, to achieve maximal release and determine total doxorubicin levels. This de-quenching effect is illustrated *in vitro* by heating in Figure 1.5 and is discussed in more detail in Section 2.3.2.

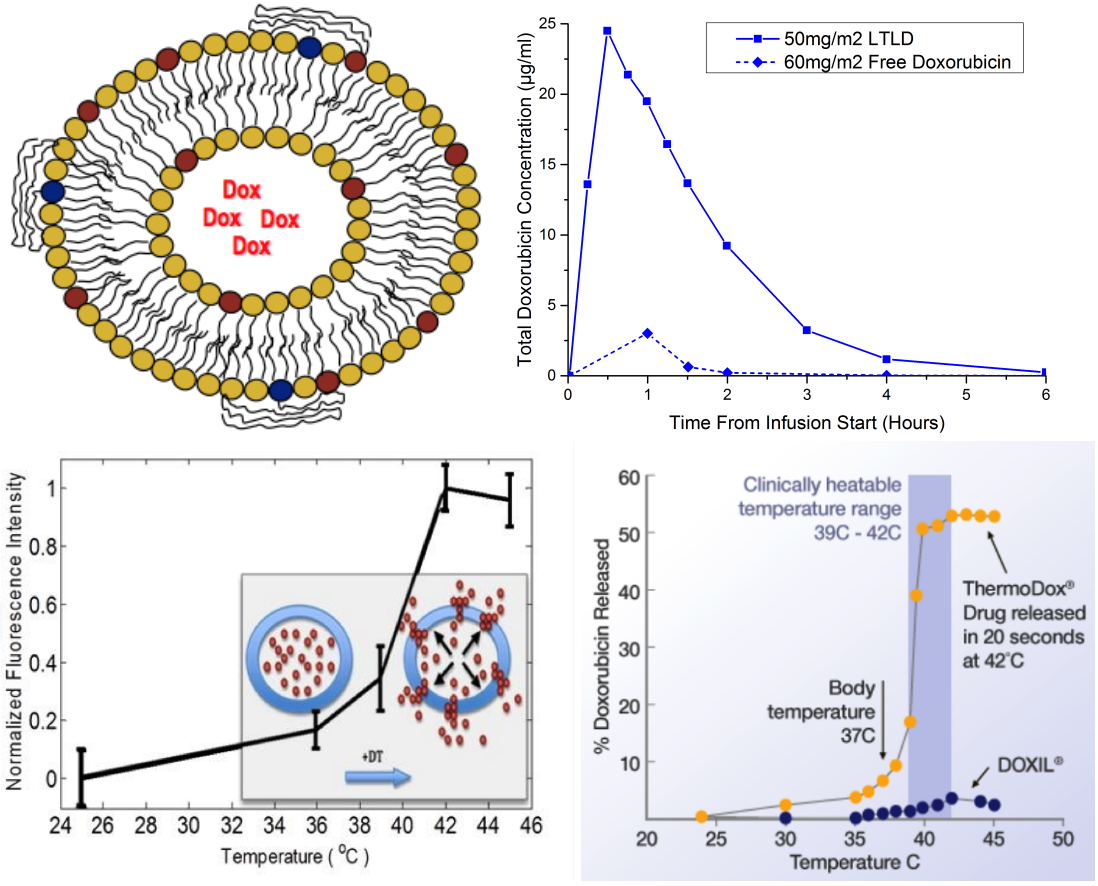


Figure 1.5: Composition and pharmacokinetics of LTLD. TOP LEFT: ThermoDox® composition, obtained courtesy of Celsion Corporation. Doxorubicin is contained within a phospholipid membrane (Yellow=DPPC, Red=MSPC, Blue-DSPE-PEG). TOP RIGHT: Plasma total circulating doxorubicin in humans after intravenous injection of LTLD over 30 minutes (Poon *et. al* [316]) or conventional doxorubicin over 60 minutes (Swenson *et. al* [317]). BOTTOM LEFT: Plot of fluorescence intensity for LTLD for 6-minute exposures to varying degrees of hyperthermia in a water bath, figure provided courtesy of Eleonora Mylonopoulou, Institute of Biomedical Engineering, Oxford [318]. BOTTOM RIGHT: ThermoDox® release profile, obtained courtesy of Celsion Corporation.

LTLD is available for intravenous administration at the maximum tolerated dose of 50 mg/m^2 of the patient's body surface area over a 30-minute period. The pharmacokinetic profiles of encapsulated and free doxorubicin in patients with liver tumours treated with

RFA combined with LTLD have been evaluated in a previous study [316]. LTLD circulation is extended for several hours over free doxorubicin due to its PEGylated liposomal carrier. The LTLD pharmacokinetic data has been combined with data from another study, which performed pharmacokinetic analysis for conventionally administered doxorubicin [317]. The marked increase in the pharmacokinetic profile for LTLD over that of a slightly higher dose of doxorubicin is illustrated in Figure 1.5(b). Of note, the peak therapeutic levels in the first two hours post-infusion provide an optimal and clinically convenient window during which regional heating modalities can be administered.

1.4.6 Hyperthermia for Targeted Delivery of Thermosensitive Liposomes

When considering hyperthermia-mediated chemotherapeutic delivery to solid tumours using LTSLs, regional hyperthermia of around 41-43°C theoretically enhances efficacy by the following key mechanisms in synergy:

1. Enhanced tumour blood flow: hyperthermia increases the potential flow for drug delivery using any systemically administered chemotherapeutic [319, 320]. However, at higher temperatures the converse becomes true and tumour perfusion may ultimately decrease below that of unheated tumour. This effect of decreased perfusion at temperatures of 43°C and above has been demonstrated in several *in vivo* studies [319, 321]. Another group has developed a mathematical pharmacokinetic model of targeted drug delivery of LTSLs by FUS [322]. The study suggests that tumour perfusion decreases linearly with time during application of hyperthermia at 43 °C, and rapidly induced high temperatures (50°C for just 20 seconds) will result in near instantaneous termination of blood flow, both detrimental for initial drug delivery. These studies emphasise the need for controlled levels of hyperthermia above the release threshold whilst minimising time above 43°C.

2. Increased permeability of tumour vasculature: hyperthermia is hypothesised to increase pore size in the microvasculature and thus improve diffusivity. In the presence of circulating liposomes, there is enhanced liposomal accumulation in the tumour interstitium and therefore delivery of a higher total dose than by EPR alone [292, 301, 323]. Up to a limit governed by the clearance of the LTSL from the circulation, the longer the duration of hyperthermia the more potential for liposomal accumulation.

3. Instantaneous release of LTSLs: such release is thought to occur both intra-vascularly and, to some extent, in the tumour interstitium, when the level of hyperthermia exceeds the release threshold. Such instantaneous release is thought to expose tumour cells to a rapid and lethal insult from a steep concentration gradient of chemotherapeutic, penetrating further than would be possible with free drug or slower release from NTSL. Key to current understanding is that the release time of LTSLs in a hyperthermic tumour matches the transit time through the microvasculature, where the majority of release is thought to happen [301]. Indeed application of hyperthermia following the intravenous infusion when plasma levels are highest is optimal. This is in stark contrast to NSTLs which take 24-48 hours to accumulate and subsequently release [296].

4. Direct cytotoxic effect: mild hyperthermia alone provides a direct cytotoxic effect even in the absence of chemotherapeutic, through mechanisms or protein denaturation or immune stimulation [324].

5. Enhanced chemotherapeutic effect: the use of hyperthermia as a delivery mechanism is particularly attractive, as, when used simultaneously with specific chemotherapeutics, it is understood there is supra-additive enhancement of chemotherapeutic effect, without increased systemic toxicity [325–329]. Specifically in the case of doxorubicin, this enhanced cell kill effect [330] has been seen *in vivo* [331] and is thought to be due to increased cellular uptake and due to mechanisms relating to

inhibition of nucleic acid synthesis and DNA-repair [332].

6. Anti-angiogenic effect: in addition to cytotoxic effects on the target cancer cells, it has been demonstrated that this rapid and localised delivery of high dose of chemotherapeutic agent via heated LTSLs has an anti-angiogenic effect with consequent tumour-regression, thought to be due to a direct cytotoxic effect on tumour vasculature endothelial cells [333, 334].

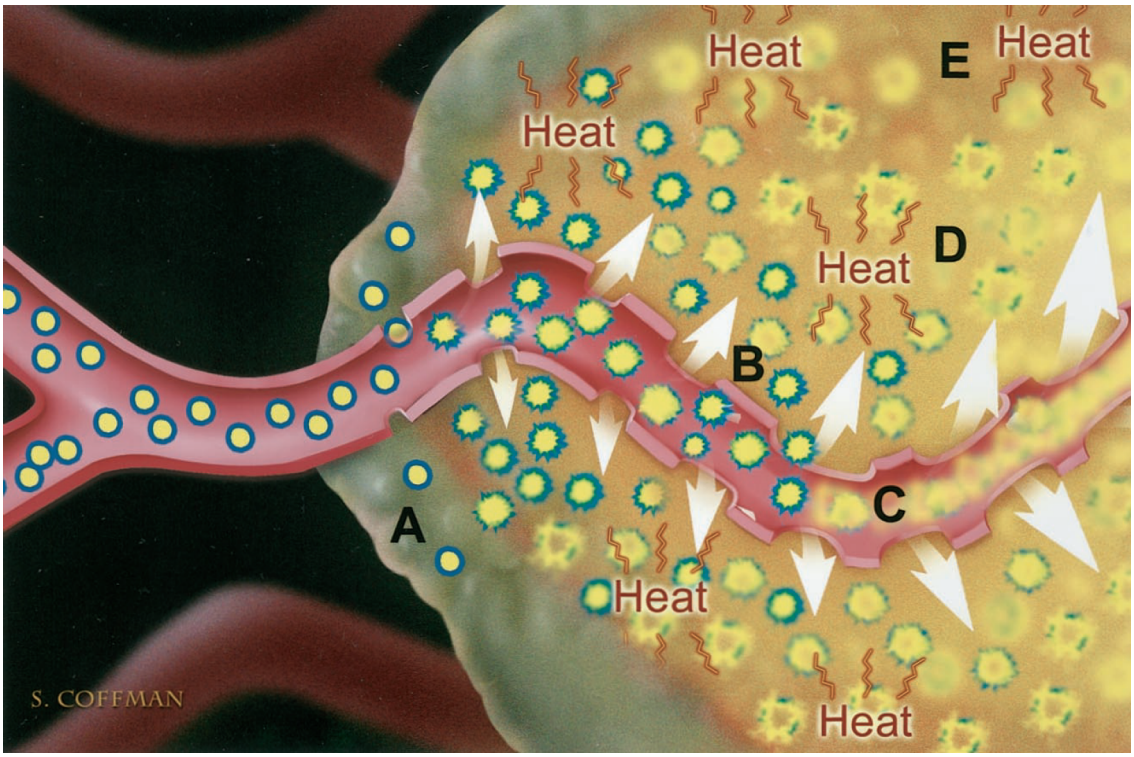


Figure 1.6: Schematic which illustrates the potential mechanisms involved in combination hyperthermia and liposomal therapy for solid tumors. (A) liposomes (blue circles with yellow content) preferentially extravasate from pores in tumor vessel walls. (B) Hyperthermia increases tumour pore size and thus increases tumor liposome extravasation (mechanism 2). (C) Hyperthermia triggers drug release (yellow) from liposomes in the tumour vessel (mechanism 3). (D) Hyperthermia can trigger liposomal drug release in the tumour interstitium (mechanism 3). (E) Hyperthermia can be directly cytotoxic to tumour cells (mechanism 4). Reprinted from Cancer Research, 2000; 60(24): 6955, Kong *et al.*, Efficacy of Liposomes and Hyperthermia in a Human Tumor Xenograft Model: Importance of Triggered Drug Release, with permission from AACR [301].

Several of these mechanisms are illustrated in Figure 1.6. There are several *non-invasive* methods which have been used to induce localised hyperthermia both pre-clinically and clinically, which include:

1. Immersion of body part in a warm water bath to allow conductive hyperthermia. A low-tech, low cost option which lacks tumour targeting capacity.

2. Loco-regional hyperthermia by microwave devices, such as the Celsius TCS Hyperthermia System (Celsius42+ GmbH, Cologne, Germany), with limited tumour targeting capacity in that surrounding tissues are also exposed to hyperthermic conditions.

3. Locally applied microwave or ultrasound heat pads for superficial heating (such as those used in the on-going DIGNITY trial for recurrent breast wall cancer [335], which also uses ThermoDox®), but offers no real depth of penetration.

4. USgFUS and MRgFUS devices, which offer greater targeting abilities at greater depths, with potential for tighter temperature control (discussed further in the following section) but involving the requirement of scarce and potentially expensive equipment and highly-trained users.

1.4.7 Focused Ultrasound Devices for Localised Hyperthermia

Different mechanisms for delivering thermal energy to the target site to release LTSLs are under investigation clinically; these include minimally invasive techniques such as RFA to improve ablation margins, or the non-invasive modality of HIFU to provide regional hyperthermia alone. Although the HIFU acronym has historically received widespread use regardless of its intensity [93], it is perhaps more precise to use FUS to describe devices used to achieve targeted hyperthermia, as this more generic term applies to devices used to generate both hyperthermia and ablation.

Given FUS has the potential to transmit energy and associated temperature rises into the body at precise locations non-invasively, safely, precisely, painlessly and repeatedly, it is an attractive modality for targeting solid organ tumours for drug delivery by regional hyperthermia. The goal is to optimise clinical devices and heating strategies to attain a

rapid, relatively uniform and sustained bulk temperature rise isolated to the target volume alone.

Subject to the appropriate regulatory and ethics approval, both USgFUS and MRgFUS therapeutic HIFU devices can be utilised clinically at intensities below the ablative threshold in order to induce regional hyperthermia for the purpose of targeted drug delivery, without tissue destruction through thermal or cavitation effects [336]. This said, depending on the FUS parameters, mechanical effects, namely cavitation and radiation force, may still play some part in release of the drug at the target site in addition to the predominately thermal mechanism [337].

In order to achieve a sub-ablative drug delivery regime, strategies must be employed to significantly reduce the energy delivered to a given focal spot within the target volume, so as to avoid cytotoxic levels of heat deposition within the target volume. This may be achieved by reducing acoustic power for a given transducer geometry, pulsing the ultrasound to reduce the duty cycle, or minimising dwell time in a particular tissue volume by moving the ultrasound beam. In practice, a combination of these approaches may be required. Such strategies would ideally sustain hyperthermia, typically in the region of 40-43°C, over clinically relevant tumour volumes for between tens of minutes and a few hours, whilst achieving rapid initial heating, tight temperature control and uniform heating throughout the target volume. As significantly lower time-averaged ultrasound intensities are being delivered, the risks of off-target effects such as skin burns and damage to other vital structures is lower than for ablative HIFU.

The operating software for most USgFUS and MRgFUS extracorporeal clinical devices can drive precise movements of the transducer in an automated fashion, according to a pre-determined treatment plan. Phased arrays offer further opportunity for rapid translations of the focus without moving the transducer. In the case of a USgFUS system, because the diagnostic ultrasound only acquires two-dimensional images, the probe must be moved perpendicular to the imaging plane obtained to visualise the whole tar-

get tumour area prior to the FUS exposure. During treatment, the tissue volume to be warmed can be mapped into parallel cross-sectional areas, or slices, built up from rows of adjacent exposures (Figure 1.7), as previously discussed for ablative HIFU (Figure 1.2). However, rather than treating slices from deep-to-superficial, as typically performed in ablation, slice skipping can be used in order to trap heat. Further optimisations of this USgFUS approach to volumetric hyperthermia, such as changing from traditional dot mode to moving beam mode, are possible and are discussed in Chapter 2.

Ultrasound-guided Focused Ultrasound for Hyperthermia

When USgFUS devices, such as the Model JC200, are used to ablate tissue, a co-axially aligned diagnostic ultrasound B-mode probe of 3.5-5 MHz is used to monitor the appearance of echogenic changes in real time, which are consistent with tissue boiling [91, 338]. However this method has limited use in the context of hyperthermia for drug delivery and cannot provide the much sought after feature of temperature mapping (thermography) [339]. Despite many advances in the field of real-time ultrasound thermography [340–346], although anticipated, such technology is not yet clinically available for USgFUS devices [93].

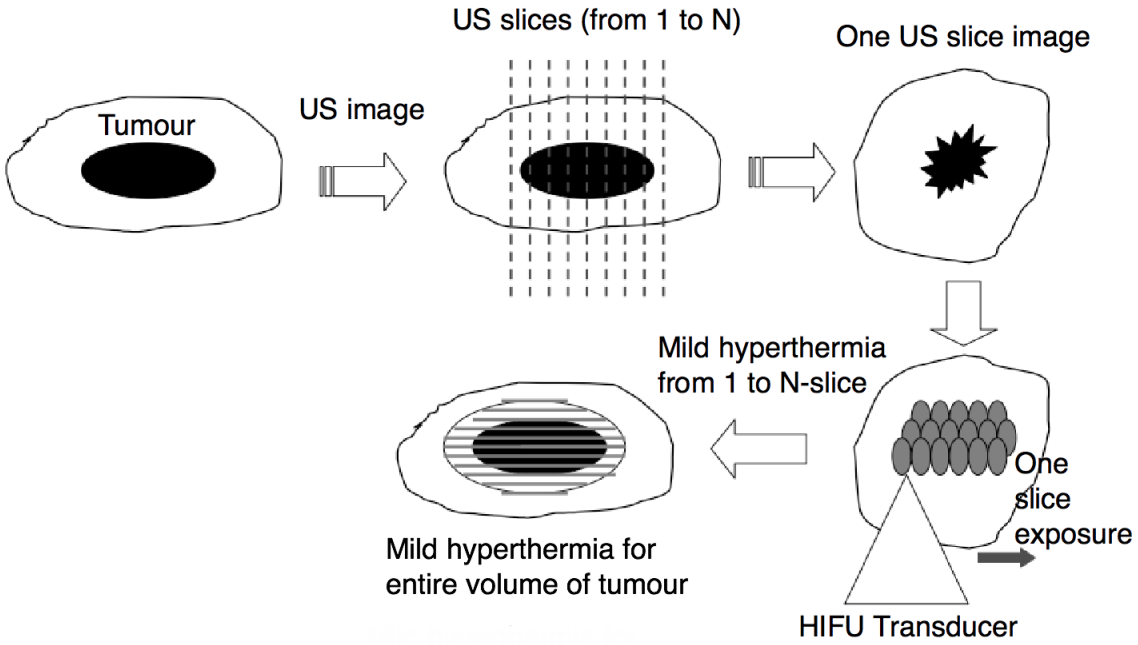


Figure 1.7: Schematic representation of the row-by-row, slice-by-slice approach used to induce mild hyperthermia into the target tumour volume by an USgFUS device running in traditional dot mode. Figure produced from within the research group, with modification.

MR-guided Focused Ultrasound for Hyperthermia

For MRgFUS systems, typically spiral or circular raster paths are applied to generate hyperthermia using closed-loop control algorithms [93]. The Philips Sonalleve system, a 1.2 MHz 256-element phased array MRgFUS device (Sonalleve 1.5T, Philips Medical Systems, Vantaa, Finland [158]) is one such commercially available device costing approximately US$1 million, and has a spatial peak, temporal average in situ focal intensity (I_{SPTA}) of 120 W/cm^2 at 7.5 W$_{ac}$ and 55 W/cm^2 at 35 W$_{ac}$, at a focal depth of 15 mm in tissue (attenuation coefficient of 0.5 dB/cm/MHz). It has been used to achieve volumetric sonication by a proprietary automated beam steering control algorithm that translates the focal point between specific locations following circular trajectories, in an attempt to maximise heat diffusion for more uniform heat deposition. This method was developed

following research efforts by Moonen *et al.* [347–350] and Köhler *et al.* [351].

A recent preclinical study demonstrated generation of 40°C intratumoral hyperthermia [352] using the device. Using concentric sonication subtrajectories with a binary feedback control algorithm over slices of 7 mm thickness, and powers of 20-35 W_{ac}, this device was used to tightly control volumetric intratumoral hyperthermia in ten tumour-bearing rabbits *in vivo* between 40.4-41.3°C (SD 1.0-1.5°C) at 10-18 mm focal depths from skin. The study did not evaluate for tissue damage using rigorous methods, but no macroscopically evident thermal damage was seen and thermal dose was well below the cumulative equivalent minutes at 43°C threshold (CEM_{43}). CEM_{43} is based on model by Sapareto and Dewey [353] and is a common standard used to define the transition from mild to ablative levels of hyperthermia [351, 354] (Section 3.2.1).

Heating patterns may be affected by variability in the vascularity and perfusion of tumours between patients or even in the same patient [355]. Obtaining real-time spatiotemporal feedback from clinical FUS devices is of particular importance in ablative therapies and drug delivery alike. For MRgFUS devices, such as the Sonalleve MR-HIFU (Philips Medical Systems, Vantaa, Finland) [158], non-invasive volumetric heating feedback is available in real-time or cumulatively, providing a much sought after platform for non-invasive heating and monitoring. The Sonalleve is able to provide temperature measurements to an accuracy of 1°C in stationary tissue and 2-3°C in moving tissues such as liver, however only temperature increases from baseline are interpretable, not absolute values [356]. Cumulative temperature measurements are derived from Sapareto and Dewey's thermal dose model [353].

1.4.8 Previous Pre-Clinical Studies

Pre-clinical studies have played a crucial role in advancing the first LTSL and LTLD formulations into the clinical arena. The challenge of attaining peak levels of intratumoral free drug compatible with deep penetrance is key to successful treatment outcomes, and

ease of tissue recovery in pre-clinical models has facilitated the assessment of doxorubicin delivery using a range of NTSLs, TSLs and various heating modalities for regional hyperthermia, including FUS. Doxorubicin's inherent fluorescence has proved extremely valuable in establishing both plasma and tumour pharmacokinetics using fluorescence-based assays, whilst fluorescence microscopy has been utilised in assessing tumour penetration.

As previously discussed, the peak distance of tumour cells from the closest blood vessel may be as much as 200 μm in tumour tissue and consequently at adequate concentration, penetration depths greater than this would be therapeutic in the treatment of solid organ tumours. In respect of the therapeutic threshold of doxorubicin, there is variability, depending on histological tumour type. A previous in vitro study has demonstrated intracellular doxorubicin concentrations of 60 ng/mg are required, in order to exceed a 99% cell kill in non-small cell lung cancer [357]. A total intratumoral doxorubicin concentration in excess of 20 μg per gram of wet tumour mass would generally be considered to be therapeutic, although based on the fractional cell kill hypothesis [358], multiple cycles are required for complete cell kill. Clinically, the use of FUS targeting to increase intratumoral concentration and penetration of delivered drug is aimed at improving therapeutic efficacy for the same systemic dose, and ultimately may render previously unresponsive tumours treatable, in addition to potentially reducing the number of treatment cycles.

With regards to the third proposed mechanism regarding instantaneous release discussed previously, Gasselhuber *et al.* have developed a computational pharmacokinetic model to simulate tissue heating by FUS and consequent TSL-based doxorubicin delivery [322, 359]. The model demonstrates increasing doxorubicin delivery with up to 2 hours of hyperthermia with maximal intracellular doxorubicin concentrations of ~15-23 μg/g in the target region. The simulated results were validated in an *in vivo* rabbit tumour model. The same group also performed pharmacokinetic simulations to compare delivery of doxorubicin in various forms: free, stealth liposomes and LTSL with intra- and extravascular triggered release, the former being released immediately after administration,

and the latter being allowed to accumulate for 24 hours before release [359]. Simulated delivery to doxorubicin-sensitive cells in a mouse model revealed peak intracellular tumoural drug concentrations of 3.4, 0.4, 100.6 and 15.9 μg/g and peak bioavailable tumoural drug concentrations of 1.6, 0.2, 77.3 and 7.5 μg/g respectively, correlating well with an *in vivo* study discussed below [301]. LTSL simulations assumed locally triggered release by a modality capable of providing 30 minutes of uniform hyperthermia. Simulations demonstrated that liposomal extravasation made a negligible contribution for LTSL when intra-vascular triggered release was applied. Mylonopoulou *et al.* developed and characterised a cell-embedding tissue-mimicking material with similar thermal and acoustic properties to liver for application to FUS-mediated drug delivery, validated using LTLD with an embedded hepatoma cell line (HuH-7) [360].

Due to significant effort from many research groups, there is an established body of evidence from *in vivo* studies demonstrating that the combination of LTLD and FUS-mediated regional hyperthermia selectively increases intratumoral concentration and penetration of doxorubicin over non-heated control tumours. Furthermore, several studies have demonstrated safe and efficacious targeted delivery using FUS with improved survival outcomes. These studies will be discussed in general chronological order.

As early as the mid-1970s, small animal models have been used to demonstrate enhanced outcomes attributable to liposomal DDS in the absence of hyperthermia [361, 362]. In 1978 Yatvin *et al.* developed the first traditional temperature sensitive liposomes (TTSL) and introduced the great clinical potential of hyperthermia-triggered release [307] and further in vitro studies with improved formulations followed [363, 364]. In the 1990s, several pioneering small animal studies using TTSLs containing a range of chemotherapeutics including doxorubicin and cisplatin, delivered by regional hyperthermia in the range of 42-45°C for durations of up to an hour, evidenced both increased delivery and improved outcomes [365–371]. Whilst this research was groundbreaking, clinical translation of TTSLs was limited by the difficulty in achieving uniform regional hyperthermia of beyond 42°C in the clinical setting. Furthermore as these TTSL demon-

strated relatively slow drug release, in order to achieve maximal release, exposure to these levels and durations of hyperthermia rapidly approach the thermal dose limit for complete cell death according to the thermal isoeffect dose (TID) model of Spareto and Dewey [353, 372–374] and thus more physiologically relevant release profiles have been sought.

To address these limitations, the LTSL formulation developed by Needham *et al.* was validated in 2000 in a pre-clinical human tumour xenograft model [301, 309]. Free doxorubicin was compared with three long-circulating liposomal formulations given with and without regional hyperthermia at 42°C; i) NTSL, ii) TTSL releasing at 42-45°C over a 30 minute exposure, and, iii) LTSL releasing at 39-40°C in just seconds. In the presence of hyperthermia, the LTSL group showed the largest concentration of delivered drug (25.6 μg/g tumour, $p<0.04$), was the only group to demonstrate significant DNA-bound doxorubicin ($p<0.02$), and also demonstrated both the most pervasive doxorubicin fluorescence on microscopy and the largest antitumour effect. The authors highlighted the importance of standardising factors influencing overall efficacy of the delivery mechanism, and distinguished hyperthermia-induced liposomal delivery from hyperthermia-triggered liposomal drug release. Whilst in liposomal form, doxorubicin is non-bioavailable and cannot easily penetrate beyond the perivascular space, or bind to DNA, to achieve its cytotoxic effect. Key to this study, when comparing the LTSL group with TTSL and NTSL groups, the DNA-bound doxorubicin and the pervasive fluorescence both indicate higher levels of drug bioavailability and thus release.

In 2005, Laginha *et al.* looked at doxorubicin pharmacokinetics in mice with orthotopically implanted mammary carcinoma injected with free doxorubicin or NTSLs with different release rates, including Doxil™ as a slow release comparitor formulation [303]. Neither LTSLs nor hyperthermia were used in this study. For the group given Doxil™, the time taken to reach the maximum intratumoral drug concentrations was 24-48 hours post-injection, compared to 30 minutes with free doxorubicin. This reflects the additional time taken for the larger liposomes to extravasate through the pores of the

tumour vasculature to reach the interstitium by the EPR effect. The longer circulating time for Doxil™was also demonstrated, in stark contrast to free doxorubicin, with an area under the time-versus-concentration 87-fold higher at 7 days. Bioavailability was assessed using a nuclear extraction technique which showed 95% of free doxorubicin was nuclear-bound, and thus bioavailable, by 24 hours, whereas only 49% of Doxil™ was nuclear-bound at 7 days.

In 2006, Hauck *et al.* performed a Phase I dose escalation study of LTSLs combined with local hyperthermia in dogs with spontaneous tumours (carcinomas or sarcomas), and included pharmacokinetic analysis [375]. Three treatments using a thirty-minute infusion of LTSL-doxorubicin were given at three weekly intervals. Hyperthermia was induced during, and for one hour after, infusion using a microwave device. Intratumoural thermometry probes were used to record temperature. The drug was tolerated well by most dogs with dose-limiting toxicities of grade 4 neutropenia and acute death secondary to liver failure. Plasma total doxorubicin concentrations were shown to be maximal at the end of the infusion. intratumoral doxorubicin concentration was significantly associated with intravenous drug dose administered ($p<0.05$), but remained variable. The variability was attributed to the different vascular densities of tumours, and to potential error from a single biopsy from a heterogenous tumour environment being used for drug quantification.

The first *in vivo* study to use of pulsed HIFU as a source of hyperthermia for triggered release of a LTSL was that of Dromi *et al.* in 2007 [100]. Mice with subcutaneous tumours were injected with free doxorubicin, NTSLs, or LTSLs. Each group was split into a subgroup that was sacrificed immediately, or 24 hours after injection, for tumour recovery, and further divided into those receiving HIFU, or not, immediately prior to sacrifice. Pulsed HIFU (Focus Surgery, 120 pulses with pulse repetition frequency of 1 Hz, 2 mm raster spacing, each exposure giving a spatial average temporal average in situ focal intensity (I_{SATA}) of 1.3 kW/cm^2) at a 10% duty cycle was given for 2 minutes at each raster point, spanning the tumour. Although temperature rises were not monitored in this study,

the same exposure variables had been previously shown to induce temperature elevations of 4-5°C in a similar mouse model [376]. The study demonstrated that the group of mice receiving LTSLs with HIFU at 0 hours was the only group to benefit from a significant increase in the mean intratumoral doxorubicin concentration, which was over three-fold greater than the mean concentration of the other groups. In addition, this treatment group demonstrated significantly enhanced antitumour effects compared with all other groups, suggested to be due to more rapid delivery of higher drug levels. Of the two groups receiving LTSL with or without HIFU at 24 hours, there was no significant difference in the mean intratumoral drug concentrations. This finding suggests that LTSLs were no longer circulating at sufficient concentrations to be released by HIFU and supports the hypothesis that the majority of LTSL release happens during peak circulating levels in the tumour microvasculature whilst the tumour is simultaneously under regional hyperthermia.

In 2010, Staruch *et al.* made a breakthrough in the use of MR thermometry, in a study of *in vivo* delivery of LTSLs in the thigh muscles of 10 rabbits [377]. A pre-clinical, custom-built and MR-compatible FUS rig was placed in the bore of a clinical 1.5T MRI device (Signa, GE Healthcare, Waukesha, WI, USA). Co-registration of the ultrasound focus with the MRI coordinate system was performed using MR thermometry in a gel-phantom. A closed-loop feedback system was used to heat in a circular trajectory. One thigh of each rabbit was used as an unheated control. Of the contralateral thighs, six rabbits received controlled hyperthermia whilst four received ablation. Of those rabbits receiving controlled hyperthermia, the drug concentrations in the heated tissues had a mean 15.8-fold increase over the controls, compared with a mean 9.7-fold increase seen in the ablated thigh tissue. This discrepancy may reflect decreased tumour perfusion resulting from ablation [218] and emphasises the importance of temperature monitoring and control in order to stay under the ablative threshold.

In the same year, Yarmolenko *et al.* studied a range of human xenografts as well as a murine tumour line in a mouse model using the commercialised formulation of LTLD [378]. Of the mice treated with LTLD, tumours exposed to 1 hour of regional hyper-

thermia in a water bath (obtaining tumour temperatures of 43°C) demonstrated a significant average total doxorubicin concentration increase in all five tumour types (FaDu, HCT116, PC-3, 4T07 and SKOV-3) and a significant increase in median growth time in three (FaDu, HCT116, PC-3), over LTLD alone. The study correlates variations in efficacy to *in vitro* cell doubling time and highlights the importance of the consideration of tumour types in studies assessing the efficacy of targeted delivery by tumour growth time or survival.

Theranostic LTSLs with co-encapsulated paramagnetic MRI contrast agents have already been developed, offering a surrogate marker of release using MRgFUS systems. Such a delivery paradigm offers the potential for more efficient optimisation of hyperthermia regimes in addition to avoiding the need for tissue sampling. Following *in vivo* studies using manganese-loaded LTSLs as a contrast agent for 'dose painting' [379, 380], de Smet *et al.* demonstrated delivery of LTSLs containing a gadolinium-based and clinically-approved T1-weighted MRI contrast agent in a rat model in 2011 [311]. Using a 3T clinical MRgFUS device, the study demonstrated good correlation between T1-weighted MRI mapping interleaved between FUS exposures and both doxorubicin and gadolinium concentrations present in the excised tumours. At around the same time, two further studies in this field were published, both testing novel formulations of LTSLs containing gadolinium-based contrast agents co-encapsulated with doxorubicin *in vivo* [381, 382].

In 2011, Ranjan *et al.* came another step closer to clinical translation of targeted delivery of LTSLs [383]. Using a clinical MRgFUS system (Phillips Sonalleve, 1.5T) with MR thermometry, the study delivered clinical-grade LTSLs to rabbits with VX2 tumours. One group received free doxorubicin, and the remaining two groups received LTSL with and without 30 minutes of MRgFUS within 1 hour of drug infusion for non-invasive regional hyperthermia. Rabbits were euthanised and tissues harvested to study the bio-distribution of drug. Tumours treated with LTSL and MRgHIFU demonstrated a mean intratumoral doxorubicin concentration of 30±9 μg/g tissue, a significant 7.6-

fold increase over free doxorubicin and a significant 3.4-fold increase over LTSL alone ($p<0.05$). Furthermore, the last treatment group demonstrated significantly more specific delivery to the target region, with a 43.5-fold increase in intratumoral concentration over adjoining muscle tissue, compared to a 12.5-fold increase for the LTSL group alone.

Following the early MR-based study previously discussed, in 2012 Staruch *et al.* used a pre-clinical MRgFUS system for focused ultrasound hyperthermia (FUH) to deliver LTLD to VX2 tumours in rabbits [384]. Real-time MR thermometry was used to inform precise temperature control. Twelve rabbits with tumours transplanted to both thighs had a single tumour treated with FUS for regional hyperthermia, using a feedback control loop based on MR thermometry. Plasma pharmacokinetic analysis revealed that 47% of total injected dose was still circulating at 30-minutes following the infusion start in the LTLD group, compared with minimal circulating drug in the group injected with free doxorubicin (Figure 1.8).

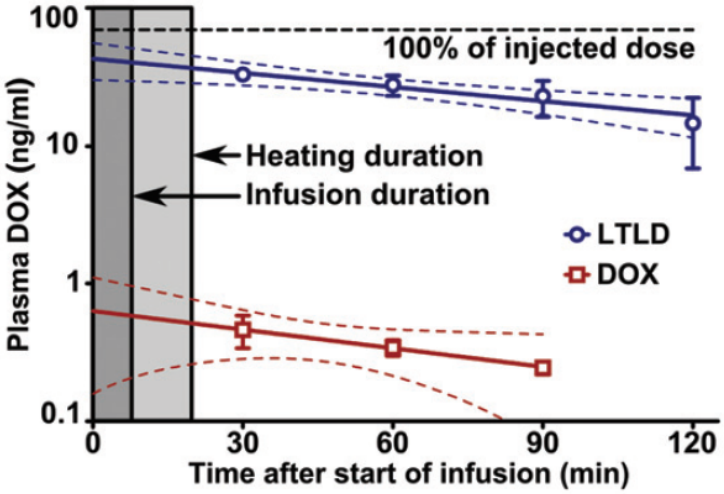


Figure 1.8: Plasma concentration of LTLD vs. free doxorubicin groups in an *in vivo* study of MRgFUS-targeted delivery of LTLD to rabbit VX2 tumours. Reprinted from International Journal of Hyperthermia, 2012; 28(8): 783, Staruch *et al.*, Enhanced drug delivery in rabbit VX2 tumours using thermosensitive liposomes and MRI-controlled focused ultrasound hyperthermia, with permission from Taylor and Francis (http://www.tandfonline.com) [384].

Doxorubicin delivery was assessed from fluorescence of tumour homogenates whilst microregional distribution was studied using fluorescence microscopy. The study re-

vealed an impressive mean intra-tumoral doxorubicin concentration of 76.3 μg/g in the group treated with LTSD and regional hyperthermia, which was over 26-fold higher than that in unheated tumours ($p<0.017$). Furthermore, no significantly enhanced delivery was seen in heated tumours treated with free doxorubicin over those receiving doxorubicin alone. Fluorescence microscopy of snap-frozen sections from a heated tumour demonstrated co-localisation of a nuclear stain with doxorubicin fluorescence that penetrated beyond the perivascular space, indicating diffusion of bioavailable doxorubicin and thus validated release. In contrast, the unheated tumour sections demonstrated that penetration was confined to perivascular regions only. Tumour microscopy spatial distribution studies demonstrated a doxorubicin penetration depth of over 150 μm from the closest vessel in the LTSD/FUS group compared to around 50 μm in the group receiving LTSD alone.

Three years later the same group published a follow-up study focusing on therapeutic efficacy, using the same tumour model [385]. In this study a clinical MRgFUS system (Sonalleve [158], previously described) was used for application of 20 minutes of regional hyperthermia at 42°C using concentric circular trajectories for cylindrical volume coverage in a closed feedback control algorithm. Efficacy was evaluated using tumour progression, based on follow-up contrast-enhanced T1-weighted MRI scans and calculated tumour volumes. Of the twelve rabbits treated, at time of treatment the average tumour volume was 0.9±0.35 cm^3 and the maximum dimension was 1.68±0.75 cm. The six animals receiving LTLD alone had rapid tumour progression exceeding the allowed tumour size end-point of maximal dimension greater than 6 cm at 24 days, whilst those receiving combined regional hyperthermia all saw at least a transient decrease in tumour volume, of which four survived to the study end point of 60 days. Of the remaining two, one reached the tumour size end-point whilst the final rabbit was sacrificed early due to hyperthermia-related toxicity.

Since 2010, groups have also been looking at novel LTLD formations in an attempt to improve on the thermo-responsiveness of the most clinically advanced formulation of

LTSD (ThermoDox®), used in several of the above studies. Tagami *et al.* presented a formulation with 90-100% release in 2.5 minutes at 40-42°C *in vitro*, which demonstrated enhanced tumour regression in vivo when used in combination with regional hyperthermia via a water bath [386]. Park *et al.* described another formulation (STL) which showed over 95% release within 10 seconds at 42°C in vitro, and statistically significant tumour regression in the STL over LTSD when delivered with FUS in a murine tumour model [387].

Finally, another group has observed benefit in use of a pulsed low intensity non-focused ultrasound regime (pLINFU) designed for tumour sonoporation and extravasation of intact liposomes from the vasculature, prior to release by a non-thermal low intensity ultrasound -mediated regime [388], a mechanism also explored by other studies [389, 390]. These studies are beyond the scope of this chapter and are not discussed further.

1.5 Clinical Application of Focused Ultrasound for Localised Drug Delivery by Hyperthermia

1.5.1 Rationale for Clinical Trial

There is an unmet clinical need in the treatment of patients with unresectable primary and secondary liver tumours, where prognosis remains poor despite advances in chemotherapy and minimally-invasive therapies.

Over several decades there has been a significant research effort in the development of LTSLs which are now beginning to emerge for clinical use, with ThermoDox® being the first to make it to clinical-grade production for investigational use. In addition there has been a vast amount of work performed in *in-vivo* tumour models using LTSLs with FUS for targeted drug delivery have clearly demonstrated efficacy of enhanced drug

delivery. Table 1.3 summarises some of the findings from key pre-clinical studies using ThermoDox®, one study demonstrating a extremely impressive 26-fold increase over ThermoDox® alone in the intratumoral concentration of drug along with enhanced drug penetration [384].

Study	**Tumour Model**	**FUS Regime**	**Dox+HT** (μg/g)	**TD alone** (μg/g)	**TD+HT** (μg/g)	**Fold Inc.**
Dromi, 2007 [100]	Balb/c mice, JC	20 min., 42°C	0.9	1.2	3.5	2.9
Ranjan, 2012 [383]	Rabbits, VX2	30 min., 41°C	-	8.8	30.0	3.4
Staruch, 2012 [384]	Rabbits, VX2	20 min., 42-43°C	~7.0	3.4	76.3	26.7

Table 1.3: Summary of intra-tumoural concentrations obtained key pre-clincial studies using free doxorubicin and ThermoDox®with and without hyperthermia (HT) induced by focused ultrasound (FUS).

The HEAT [391] and OPTIMA [392] studies previously discussed have used ThermoDox® in the treatment of primary liver tumours with RFA in late-phase clinical studies looking overall survival as the primary endpoint. However, the great potential for non-invasive focused-ultrasound targeted drug delivery has yet to be exploited in a clinical study, and in particular at this very early stage there is a need for a proof-of-concept study which obtains histological tumour samples by biopsy or resection in order to quantify intratumoral drug delivery as the primary endpoint.

Oxford has world-class expertise in the use of the JC200 (Chongqing HAIFU™ Company, previously discussed) therapeutic device in the liver and kidney, leading to CE marking for tumour therapy, which, prior to TARDOX, has involved ablative therapies only. With available ultrasound and drug delivery expertise at the Institute of Biomedical Engineering, Oxford in combination with the support of the Nuffield Department of Surgical Sciences, the Department of Radiology, the Department of Oncology, the Oncology

trials management (Oncology Clinical Trials Office) at Oxford and Celsion Corporation, USA there has been no better time or place to translate this concept to a world-first study to demonstrate the capabilities of FUS-mediated targeted drug delivery to the liver.

The hope is that once the feasibility, safety and efficacy of the LTLS/FUS paradigm has been evidenced clinically, by early phase studies such as the TARDOX study, many potential applications of this targeted delivery approach with emerge, in addition to the treatment of liver cancers. Several other organs are targetable non-invasively with fixed or hand-held extracorporeal devices such as the pancreas, kidney, uterus, bladder, breast, thyroid and brain. Many more organs are accessible with interstitial or intracavitary devices, such as the prostate. There is also great potential to explore targeted delivery of other chemotherapy agents by a variety of drug delivery systems including thermosensitive liposomes. There is great promise that we may see such device and drug targeting in routine oncology practice in years to come, with reduced morbidity, improved prognoses and at a great saving to the future cost of oncology healthcare.

1.5.2 Previous Clinical Studies

In the 1980s, Lopez-Berestein *et al.* and then Gabizon *et al.* published the earliest clinical trials involving the use of liposomes in cancer patients [393, 394], ultimately leading to the clinical use of NTSLs for a range of different indications today [283]. Since the approval of LTLD (commercialised as ThermoDox®) for investigational use, several studies involving microwave, radio-frequency and FUS-mediated targeted delivery of doxorubicin have been completed, are currently underway or are in the development stage.

To date, the most clinically advanced studies using targeted LTSL delivery have been concerned with improving outcomes in RFA of liver tumours. Such studies seek to supplement localised tumour ablation by releasing doxorubicin in the hyperthermic tumour margins thus potentially extending the volume of cell kill, and, theoretically re-

ducing recurrence. In 2009, following Phase I dose escalation studies for RFA/LTLD [391, 395], Poon & Borys published the findings demonstrating a safety and a significant dose-response effect in the treatment of hepatocellular carcinoma (HCC) [316]. In 2008, Celsion opened a randomised, double-blind, global multicenter Phase III trial (Hepatocellular Carcinoma Study of RFA and ThermoDox®, or HEAT [396]) comparing RFA + 50 mg/m^2 of ThermoDox® versus RFA alone in over 700 patients with newly diagnosed and unresectable HCC. Recruitment has completed for this study and follow-up of survival outcomes is ongoing. The primary endpoint of overall survival was not met in the HEAT trial and one may postulate several potential reasons for this:

1. Tumours over a particular size may not be amenable to complete destruction as cancer cells may be sited beyond the ablation zone and the surrounding zone of hyperthermia where ThermoDox® is expected to have cytotoxic effects.

2. In the near instantaneous ablation of the tumour, the microvasculature of the tumour is rapidly destroyed and thus the transport route for ThermoDox® becomes reduced such that only peripheral tumour vessels can deliver drug to the tumour bulk.

3. Inter-operator and inter-institutional variability in RFA treatment technique and exposure times, with short exposure times potentially failing to release enough of the circulating dose of ThermoDox® for chemo-ablation.

4. The use of progression-free survival as a primary endpoint and a secondary endpoint of overall survival are surrogate markers for efficacy of the delivery modality and do not evidence the underlying delivery mechanism for ThermoDox® delivery

Post-hoc analysis was indicative that LTLD treatment markedly improves progression-free survival and overall survival in the subset of patients having optimal RFA [397]. Consequently, the subsequent pivotal Phase III OPTIMA study, which initiated in June 2014, focuses on the subset of HCC patients who are amenable to optimal RFA, with

intermediate solitary lesions of 3-7 cm, and having standardised treatment times of over 45 minutes [392]. Again the primary endpoint pertains to the overall survival with progression free survival as a secondary endpoint, and recruitment is currently ongoing.

Data from the HEAT study has demonstrated that LTLD has a well-established and safe toxicity profile, consistent with that of doxorubicin. The most frequent adverse events in patients treated with LTLD at a 50 mg/m^2 dose are myelosuppression (60%), haematological adverse event (related or unrelated) (45%) and alopecia (40%) [398]. Other toxicities reported in greater than 5% of patients include pyrexia, fatigue, nausea and decreased appetite. To date, no significant hypersensitivity or anaphylactoid reactions have been reported in clinical studies using LTSD. Cumulative doxorubicin cardiotoxicity is a serious risk, which limits lifetime exposure [399]. Although formulations of PEGylated liposomal doxorubicin reduce this risk, it remains significant, and consequently such pharmaceuticals typically have a maximum lifetime dose of ~600 mg/m^2 [400]. Whilst not directly translatable to the FUS/LTLD delivery mechanism, the drug safety data captured from this large Phase III study has facilitated ethical approval for other early phase trials involving other heating modalities capable of inducing regional hyperthermia in the absence of ablation, such as FUS.

In 2014, Zagar *et al.* published the results of two Phase I trials using LTLD in patients with chest wall recurrences of breast cancer, by definition an advanced and difficult to treat cohort of patients [401]. The study designs were similar, other than the permitted dose was higher (up to 50 mg/m^2 of LTLD) in the second study following dose escalation in the first. Hyperthermia was applied using superficial microwave or ultrasound hyperthermia devices with temperature monitoring by thermistor. The primary endpoint was identification of the maximum tolerated dose (MTD). Objective response was evaluated radiologically according to largest tumour diameter (RECIST criteria [402]). The study revealed a MTD of 50 mg/m^2 and an impressive overall local objective response in almost half of the 29 evaluable patients, five demonstrating complete response.

1.5.3 TARDOX Clinical Study

The TARDOX Phase I proof of concept study opened in Oxford, UK, in 2014 and at the time of writing has recruited and treated its first nine patients, with the first treatment in March 2015 [132]. The diagnoses and previous medical histories for the patients treated can be found in Section 5.3. The regulatory approval letters are found in Section 5.2.

This study seeks to evidence enhanced delivery of LTLD to liver tumours at depth by use of extracorporeal USgFUS, delivered intercostally, to generate localised and sustained targeted hyperthermia, whilst avoiding FUS-induced ablation by remaining well below the thermal dose limit previously discussed (CEM_{43}). In the early stages of the study (Part I), real time thermometry data is acquired following insertion of a clinically approved thermometry device through a co-axial needle placed in the target tumour under ultrasound-guidance (Figure 1.9). In later stages of the study (Part II) there will be no real-time thermometry and settings will be chosen based on previous clinical data (Section (3.2.5) and potentially computational models (Section 4.6.3). This method has inherent limitations, which are discussed in Section 4.4. More detail on the study design is available in Section 3.1.1.

In order to determine if FUS-enhanced delivery is clinically achievable, one or more core biopsies are taken through the same co-axial needle and used to estimate total intratumoral doxorubicin concentration, using a validated quantification technique based on a previously published method [403]. In addition, biopsy samples are analysed using fluorescence microscopy to explore the bio-distribution of doxorubicin, and, in particular, intercalation with DNA at the cell nuclei (hypothesised to a predominant site of the potent anti-proliferative and cytotoxic effects of doxorubicin [404]), evidencing doxorubicin bioavailability and thus FUS-mediated liposomal release.

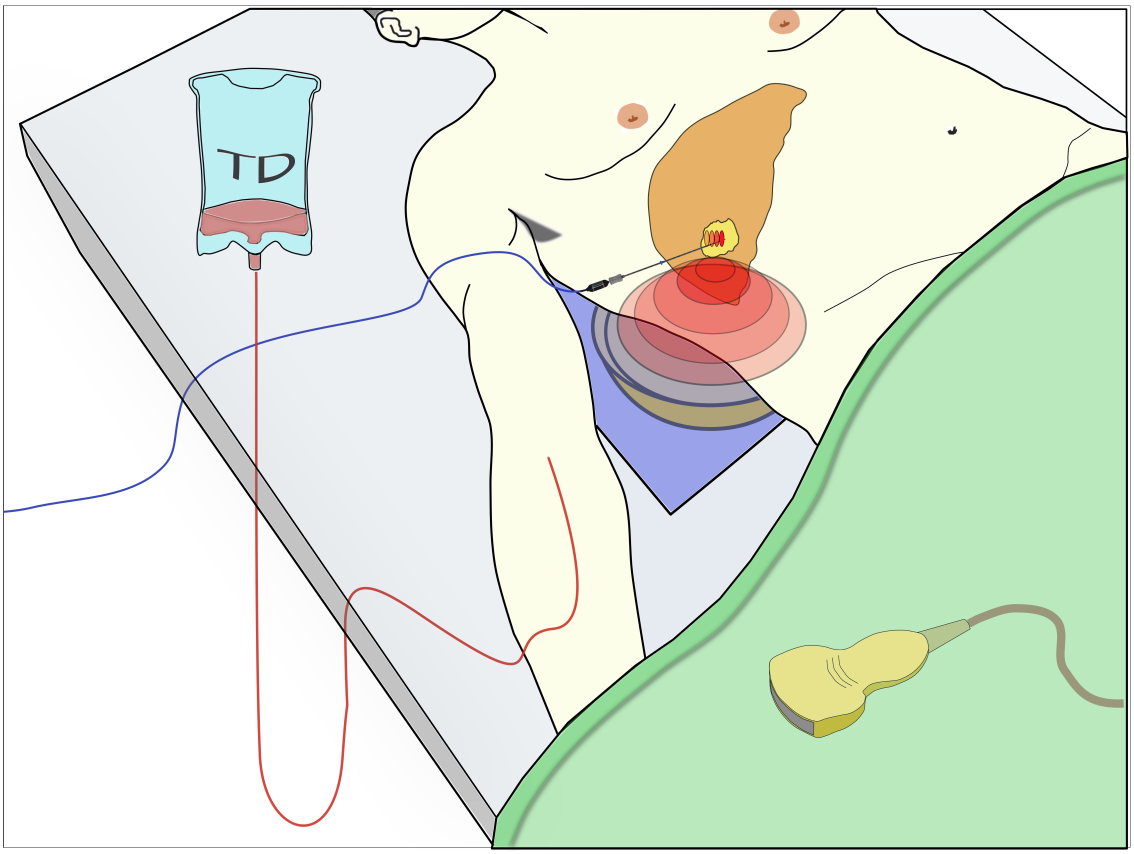


Figure 1.9: Schematic which illustrates the TARDOX study intervention, involving targeted drug delivery of ThermoDox® to a liver tumor using the focused ultrasound system. Patient typically lies supine with posterior chest wall immersed into the water bath. The transducer is aligned with the target liver tumour using the built-in ultrasound guidance system (B-mode). Central thermistor alone is shown, inserted through a co-axial needle placed under portable ultrasound guidance into the core of the same target tumour, above the water level. ThermoDox® is administered intravenously prior to inducing FUS hyperthermia in the target tumour.

Key Research Hypotheses

The TARDOX study proposes the following hypotheses and the study design incorporates objectives and endpoints specifically for testing them:

1. It is feasible and safe to non-invasively deliver sustained volumetric targeted hyperthermia to a selected liver tumour using a clinically-approved extracorporeal FUS device, in combination with a thermosensitive liposome delivered intravenously (ThermoDox®).

2. For the target tumour, following exposure to optimal levels of FUS for mild hyperthermia alone, there will be absence of cell death consistent with non-ablative levels of hyperthermia.

3. For the target tumour, whilst there are therapeutic levels of circulating ThermoDox®, exposure to optimal levels of FUS for mild hyperthermia will result in both increased *total* intratumoral concentration of doxorubicin and increased *bioavailability* (i.e. FUS-triggered liposomal release).

4. For the target tumour, when compared with any available control tumour in the liver (receiving ThermoDox®alone), there will be any isolated radiological response in the target tumour following combined treatment (ThermoDox® and FUS).

Further details on the TARDOX study design and the clinical results up to the time of writing are presented in Chapter 3.

1.5.4 Other Clinical Studies

Several other early phase FUS/LTLD clinical studies are currently in the pipeline, including the indications of primary breast and recurrent chest wall breast cancer and pancreatic cancer. In addition pre-clinical studies exploring delivery of FUS/LTLD across the blood brain barrier to treat Glioblastoma Multiforme (GBM) using a phased-array trans-cranial FUS delivery system have been underway since 2014 (Brigham and Women's Hospital and Harvard Medical School). Most recently the blood brain barrier has been opened non-invasively in man for the first time using FUS with an intravenously administered ultrasound contrast agent (microbubbles) for the delivery of liposomal doxorubicin [405], paving the way for future clinical studies utilising trans-cranial targeting by FUS/LTSLs.

1.5.5 Summary

Despite a wealth of encouraging pre-clinical results for FUS-targeted delivery of LTSLs, clinical studies have only recently begun to gain momentum. The relatively limited clinical investment seen to date is a is likely to be consequence of the requirement for expensive equipment, training investment and a general clinician and interventional focus on the competing minimally-invasive techniques for thermal tumour ablation. Progress has been further hindered due to the relatively immature and emerging technologies available for real-time monitoring and correlation with drug delivery, be it by ultrasound monitoring strategies or MR thermometry, or co-encapsulation of surrogate markers of release for detection on MRI.

In order to achieve mainstream acceptance for such a novel targeted delivery technology, operator feedback from the device is of paramount importance in order to provide confidence in drug delivery and, more specifically, release from liposomes. Consequently perhaps the most rapidly transforming technological advance of all would be the adoption of a clinically accepted method of non-invasive monitoring of LTSL delivery.

MR thermometry [356, 406] has become established as the gold standard in monitoring temperature rises in tissue consequent with release, but comes at considerable expense, and has traditionally been hindered by lack of temporal and spatial resolution over a wide field of view as well as its inability to detect cavitation directly. However, using a technique known as proton resonance frequency (PRF) shift [406, 407], one study has recently demonstrated rapid multi-plane MR thermometry *in vivo* at focal depths of up to 6 cm [350]. The technique achieved 2.5 mm resolution over a large field of view, over 5 coronal, and, 1 sagittal slice of 7mm thickness, with an acquisition time of less than 3 seconds, performed simultaneously with volumetric FUS exposure. Whilst spatially homogeneous temperature diffusion and regular temperature rises in the target region were used to evidence absence of cavitation, ultrasound-based methods remain superior. Research to further improve temporal resolution using the PRF shift method is

on-going [408].

Ultrasound-based monitoring methods, including passive acoustic mapping (PAM) [102, 409–413] and ultrasound thermometry [340–346], hold great promise due to their significantly reduced cost and improved resolution. However, there is a need for more formalised industry standards and integration of such technologies in clinical FUS devices before adoption. Other MR-based monitoring methods, such as co-loading of paramagnetic agents [381, 382], or alternatively MR-spectroscopy techniques such as chemical exchange saturation transfer (CEST) [414] may hold the future for localisation of drug release in real-time.

The use of FUS for drug delivery has been a highly anticipated area of clinical research for many years, and with the continued advances in monitoring techniques interest continues to grow. Clinical FUS devices continue to advance further in their utility for drug delivery as well as ablative therapy, and this continues to represent an area of much active research and reviews [93, 415].

The FUS/LTSL paradigm has great potential to improve clinical outcomes in oncological treatments of solid organs and has potential to be highly impactful, thus justifying the huge amount of research effort and resources that have been, and continue to be, applied to this field. Success of such clinical studies could potentially revolutionise the future of chemotherapy delivery for ultrasound-accessible solid organ tumours; over the next decade, customised targeted chemotherapy regimens using LTSLs triggered non-invasively by regional hyperthermia may become a reality in routine clinical practice, especially if the FUS parameters required can be achieved using more readily available and inexpensive machines.

The background and rationale for the TARDOX clinical study has been presented and the remainder of this thesis will describe pre-clinical and clinical results obtained in order to realise this key first-in-man study.

CHAPTER 2

Pre-Clinical Studies

Several key issues needed to be addressed in preparation for treating patients in the TARDOX study. A clinically approved invasive thermometry device, that could yield measurements of acceptable accuracy (on the order of 1°C), first had to be identified and fully characterised against reference thermometry devices, both in the absence, and in the presence, of ultrasound excitation. Secondly, the clinically available HIFU device (Chongqing HAIFU, JC200) had to be fully characterised and calibrated, in order to enable treatment planning and a direct correlation between predicted and measured temperature rises during clinical intervention. Thirdly, protocols for generating mild hyperthermia using a highly focused ultrasound beam over a relevant volume (some 27-64 cm^3) for extended periods of time (in excess of 20 minutes) had to be developed and optimised, as this represented a departure from conventional volumetric spot-by-spot ablation over timescales of seconds. Lastly, quantitative Good Laboratory Practice (GLP) methods had to be developed in order to detect and quantify drug concentrations in limited tumour biopsy and plasma samples, and to assess cell viability and liposomal release following ultrasound exposure. Studies aimed at addressing these key preclinical challenges are described below.

2.1 Characterisation of Clinical Thermometry Devices

This section introduces two different clinically-approved thermometry devices, one a thermistor, the other a thermocouple, which have ultimately been used to attain real-time thermometry data in the Part I of the TARDOX study. Both devices are compatible with the 18G co-axial needle used by the Temno® biopsy system, used to obtain tissue biopsies in the clinical study. In completing this characterisation work, acknowledgement goes to post-doctoral researcher, Dr. Christophoros Mannaris, Institute of Biomedical Engineering, University of Oxford (IBME) for his assistance in experimental design and data acquisition for thermometry devices exposed to an ultrasound field.

2.1.1 AngioDynamics Thermistor

Thermistors are in essence semiconductors whose resistance demonstrates temperature dependence, thus allowing temperature measurements to be made. Thermistors can be classified as having either a negative (NTC) or positive temperature coefficient (PTC). NTC thermistors are the most common, and typically used in clinical applications; as temperature increases the resistance decreases.

The AngioDynamics NTC thermistors [416] (Microsulis Acculis MTA Accu5i Temperature Probes, Ref: 900-314) are sterile, single-use, disposable 18G 20 cm thermometry devices, constructed from stainless steel. They are certified for clinical use to monitor temperatures up to 70°C. They are supplied in a pair, one with a four-pin male ODU connector, the other with a 6-pin version. In either case only two wires are required as these are essentially 2-wire 10 kOhm thermistors. As the manufacturers' hardware can only provide a digital readout without real-time data acquisition capabilities, a decision was made to use a custom acquisition system allowing recorded thermometry to a resolution of a tenth of a second. Custom ODU® female connectors were made up to allow data transmission from the active male pins of the device connector, which when used

clinically, allowed packs to remain sterile until the moment of use. The connectors were wired to a HP Agilent Module board (16-channel module 34902A) which in turn was inserted into a HP Agilent 34970A data acquisition (DAQ) unit. The unit was connected to a Microsoft Windows PC running a custom LabView client (Figure 2.1), via a serial connector (RS-232). The LabView client automatically configures the HP DAQ based on user input. The client has been designed to enable thermometry to be written to file at regular intervals during an acquisition in case of a power failure or computer crash, rather than holding potentially large amounts of thermometry data in memory.

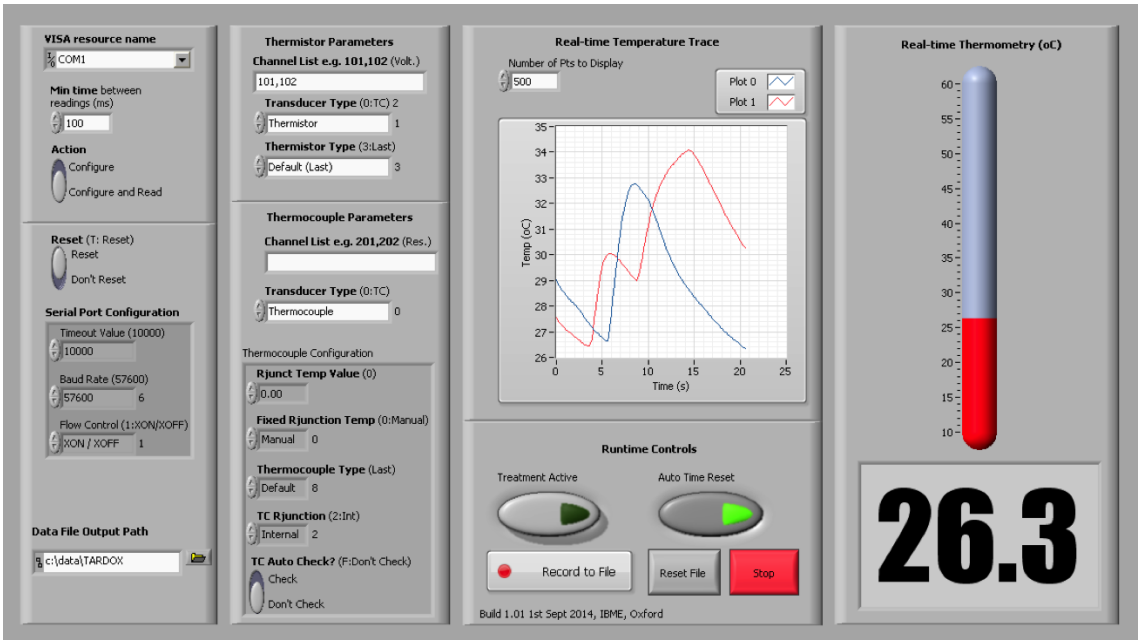


Figure 2.1: Screen capture of custom LabView client used to obtain real-time thermometry data via AngioDynamics thermistors. In this case two thermistors are acquiring data in parallel on separate channels wired into the same module and the thermometry trace is updated in real-time. Acknowledgement: Dr. Jamie Collin for developing an early LabView client which has subsequently been enhanced with various features.

The thermistors were characterised using a 1 MHz transducer in a degassed and filtered water tank at room temperature, using a standard setup with a matching network, amplifier and oscilloscope. The sharp-tipped thermistor was inserted into a rigid gel phantom supplied by Chongqing HAIFU™Company, typically used to confirm alignment of clinical USgFUS devices. The phantom was chosen due to its attenuating and thermal

properties, resulting in a local heating effect when exposed to a low-energy FUS beam, detectable by the thermistor. Whilst in the co-axial orientation, a Ultrasonic Measurement System with a 3D positioning system and client (UMS, Precision Acoustics) was used to move the thermistor relative to the fixed transducer. The setup used is shown in Figure 2.2.

The thermistor was thermally characterised in each cartesian axis. For a given axis the thermistor was first thermally aligned in all axes to achieve the maximal temperature rise ('sweet-spot'). Then, from this starting position, the thermistor was only moved in the selected axis such that the tip of the needle was at the focus of the transducer. This was achieved using pulse-echo signals interpreted on the oscilloscope.

In the same axis, a manual scan was performed at 2 or 0.2 mm resolution using fixed exposures of the same pressure and duty cycle, and the temperature rises and cool-down periods were continually recorded for each exposure. Subsequently a power ramp was performed at the sweet-spot of the thermistor. The results are shown in Figure 2.3 and in summary, demonstrate that the most sensitive part of the thermistor is 10-14 mm from the tip and that the device appears capable of recording temperatures of up to 140°C.

In interpreting these experimental results it must be kept in mind that the very presence of the thermometry device in the ultrasound field leads to an elevated and artifactual temperature reading due to viscous heating around the device as well as heat conduction through the needle shaft and the possible occurrence of cavitation on the needle tip [417, 418]. However the purpose of these experiments was to characterise the point of maximum sensitivity on the thermistor, not to characterise such artefacts or formally validate the clinically-approved thermistor, both of which are outside the scope of this work.

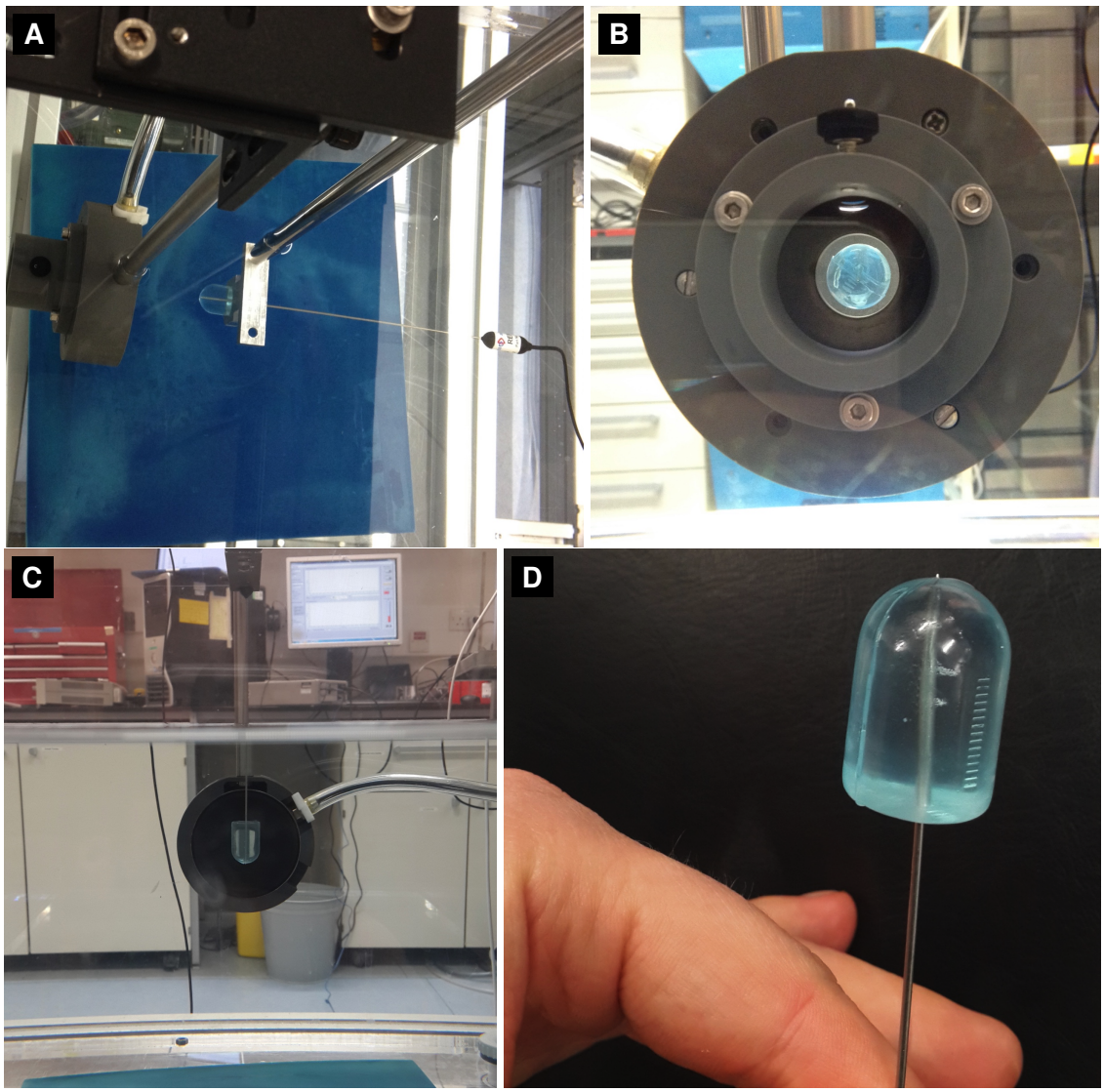


Figure 2.2: Experimental setup for characterising AngioDynamics thermistor inserted into a transparent and rigid gel phantom with attenuating properties (Chongqing HAIFU™Company). **A:** Top view of thermistor orientated co-axially via a 3D positioning system with the rigid 1 MHz transducer in a tank of degassed water. **B:** View of co-axially orientated thermistor through the central aperture of the transducer. **C:** Side view of thermistor orientated vertically, perpendicular to the transducer. **D:** Close up of thermistor inserted into gel phantom, such that probe tip flush with curved face.

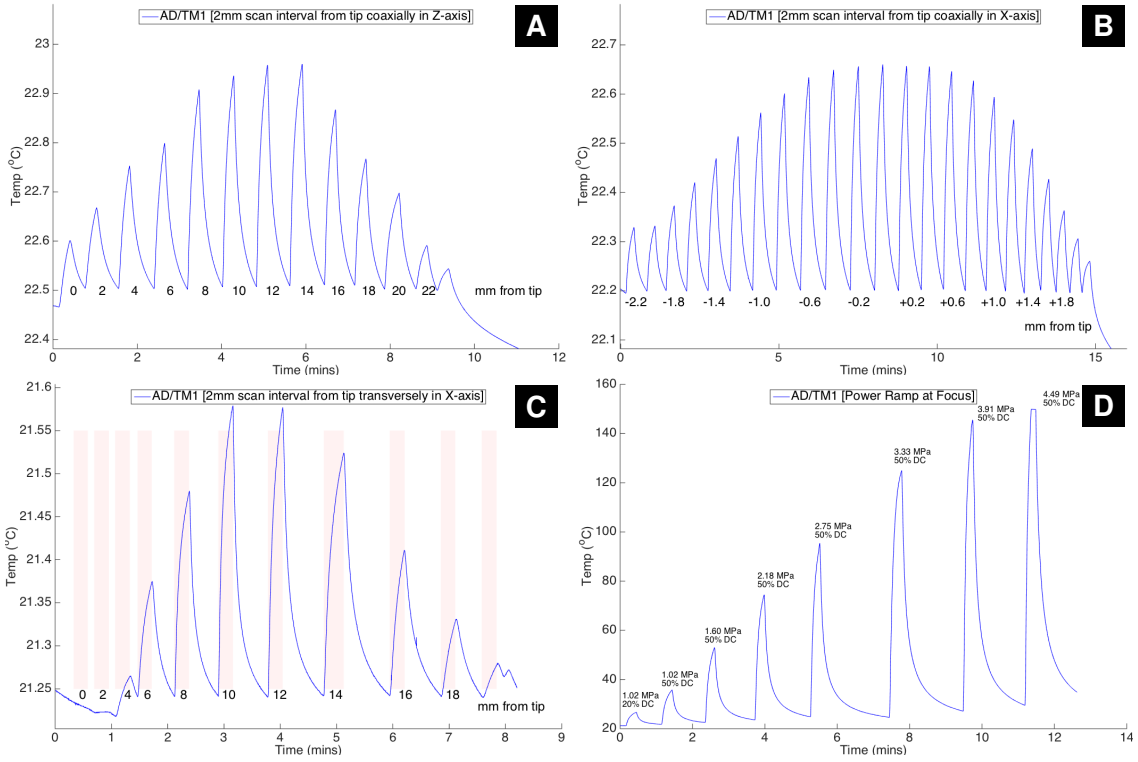


Figure 2.3: Temperature traces acquired from FUS exposures applied to the AngioDynamics thermistor. The first three traces were acquired using the 1 MHz transducer at a pressure of 0.44 MPa and a 5% DC. **A:** With the thermistor in co-axial orientation, 2 mm steps performed from the tip to proximal shaft. **B:** With the thermistor in the same orientation, 0.2 mm steps performed transversly. **C:** With the thermistor in vertical orientation, 2 mm steps performed from the tip to proximal shaft, demonstrating the maximum sensitivity at 10-14 mm from the tip. Pink regions indicate the times periods during which FUS exposures were active. **D:** Power ramp performed at the site of maximum sensitivity in vertical orientation, with individual parameters shown for each exposure peak. The final exposure resulted in temperatures which the device was no longer able to record, and thus the trace has been truncated at the highest recordable value.

During the clinical study, AngioDynamics probes were successfully used with this HP DAQ system in the treatment of the first four patients. However, the supplier ceased to manufacture these thermistors, which were manufactured with intended use for thermometry during RFA treatments. A variety of other clinical temperature devices were subsequently tested for suitability for use on the clinical study, and the Medtronic thermocouple was chosen given its acceptable signal-to-noise ratio and value for money.

2.1.2 Medtronic Thermocouple

Thermocouples consist of two different electrical conductors which form a junction which generates temperature-dependent voltages, by the thermoelectric effect. Depending on the properties and type of the thermocouple, conversion tables can be used to convert voltage to temperature. However, unlike thermistors, thermocouples also require a reference temperature measured by an independent sensor, in order to compensate for temperature fluctuations at the 'cold-junction' and this is known as (dynamic) cold-junction compensation.

The Medtronic (formally Covidien™) thermocouple (Cool-tip™ RF Ablation Remote Temperature Probe E-Series, 20cm, Ref: RTP20) was also characterised. Again, custom ODU® female connectors were preparing for compatibility with the four-pin male ODU connectors, facilitating direct connection of these thermocouples without the need for modification. The HP DAQ may be configured for thermocouples and device was used for the following characterisation experiment by initially calibrating at room temperature, but without dynamic cold junction compensation.

The thermocouples were characterised using a similar setup to the thermistors, with the same 1 MHz transducer in a degassed and filtered water tank at room temperature. The thermocouples are blunt-tipped and so could not penetrate the rigid phantom used previously. Instead one was immersed in a custom-phantom holder containing glycerol solution (Sigma 86-89%, Ref: 49781-500mL), another attenuating medium, with front and back acoustic windows. The rigid circular phantom body (Figure 2.4) meant it was not possible to characterise this probe in the co-axial orientation, as previously performed for the AngioDynamics probe with the rigid phantom. Similarly, whilst in the vertical orientation, the same 3D positioning system was used to move the thermocouple relative to the fixed transducer.

Both the previously characterised AngioDynamics thermistor and the new Medtronic thermocouples were thermally characterised in a single axis using the same principles

as before. For the thermocouple a manual scan was performed at 1 mm resolution and then rescanned at a finer 0.25 mm resolution around the sensitive region. A brief power test was also performed at the sweet-spot of the thermocouple. The results are shown in Figure 2.5. In summary, in the vertical orientation, the setup reproduces the finding of the sweet-spot at 10-14 mm from the tip for the thermistor, but only 3-4 mm from the tip for the thermocouple. The clinical relevance of this is that the biopsy is taken 7-24 mm from the tip of the thermometry device (Figure 2.21), and thus samples an area of tissue slightly more peripheral to where the thermometry readings are taken. Consequently this may lead to under-estimation of the level of heat induced doxorubicin release in the tissue, depending on the size of the planned volume; a 'sampling' limitation of the clinical study.

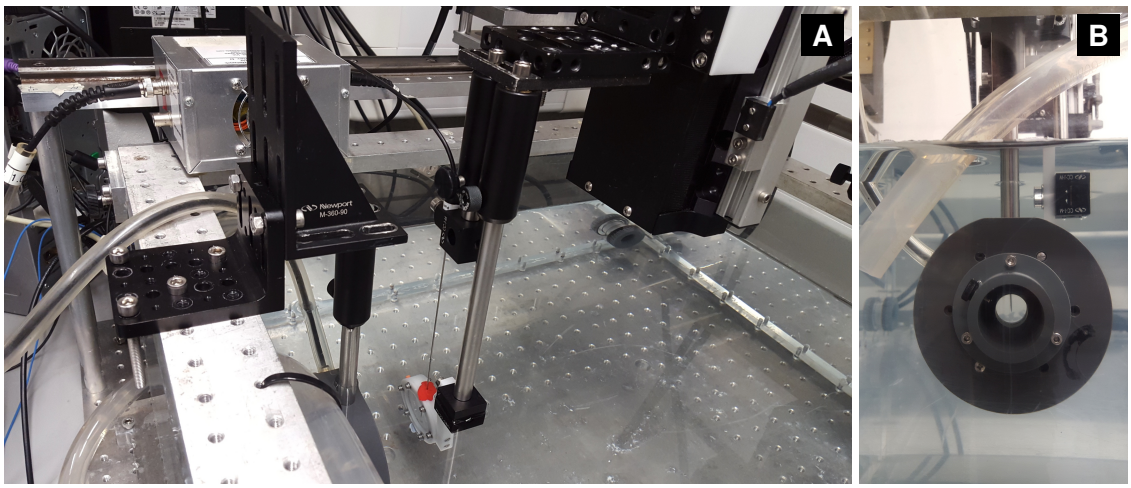


Figure 2.4: Experimental setup for characterising Metronics thermocouple (or AngioDynamics thermistor) inserted into a custom-made water-tight phantom holder containing glycerol solution (acknowledgement: Shunning Bian for phantom design). **A:** Top view of thermistor orientated vertically into the glycerol via a 3D positioning system with the rigid 1 MHz transducer in a tank of degassed water. **B:** View of vertically orientated thermistor through the central aperture of the transducer.

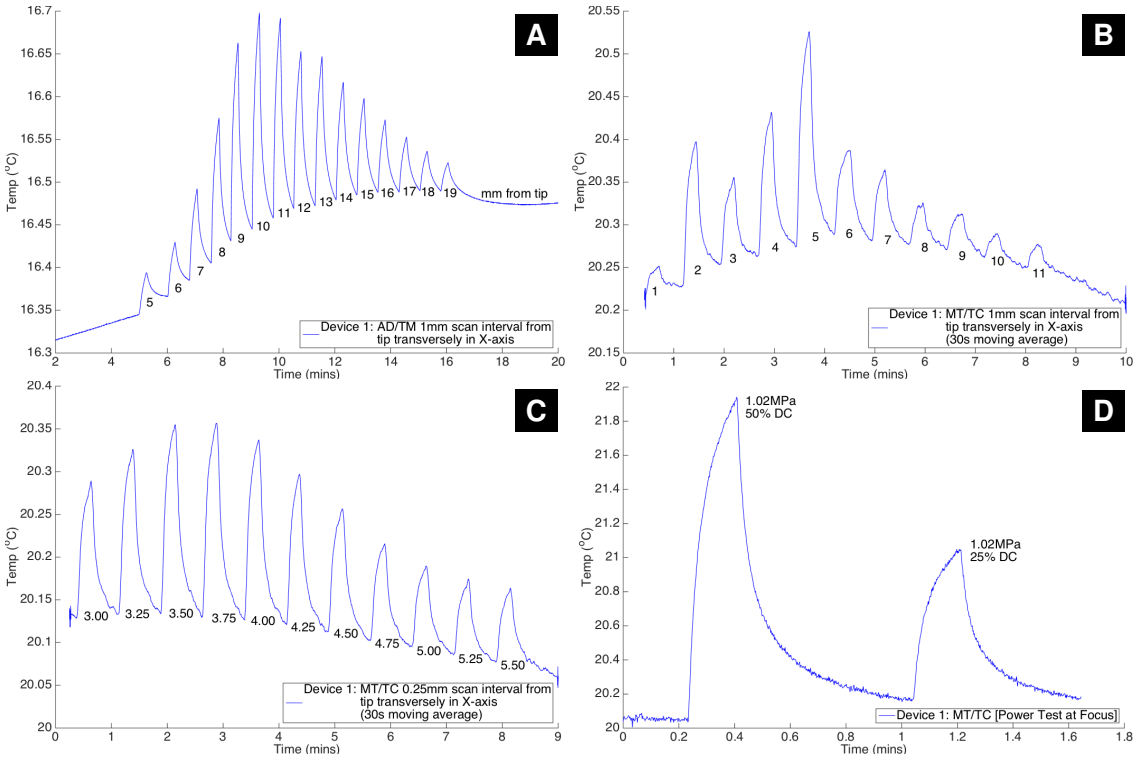


Figure 2.5: Temperature traces acquired from FUS exposures applied to the AngioDynamics thermistor and MedTronic thermocouple. All traces were acquired using the 1 MHz transducer at a pressure of 1.02 MPa and a 5% DC, except the last trace which explored higher DC. Note that due to subtle warming of the glycerol solution it become impractical to wait in order to keep a constant baseline. **A:** With the AngioDynamics thermistor in vertical orientation, 1 mm steps performed transversely 5 mm from the tip to proximal shaft. **B:** With the Medtronic thermocouple in the same orientation, 1 mm steps performed transversely from the tip. **C:** With the thermistor in the same orientation, 0.25 mm steps performed around the sweet-spot, demonstrating the maximum sensitivity at 3-4 mm from the tip. **D:** Power ramp performed using the thermocouple in the same orientation at the site of maximum sensitivity, with individual parameters shown for each exposure peak.

Over the HP DAQ, the National Instruments Hi-Speed USB Carrier (NI USB-9162) appears to offer reduced signal variability and ease of configuring cold junction compensation, and as such has since been selected for data acquisition when using this thermocouple clinically. Only one of the clinical cases used the uncompensated HQ DAQ system for this thermocouple type (Section 3.2.4). The LabView client has been enhanced to include the functionality to read from this additional hardware, in parallel with the HP DAQ if necessary.

The HP DAQ module has accuracy specifications of ±0.08°C for thermistors and

±1°C for T-type thermocouples [1], in addition to a ±0.05°C conversion accuracy for the DAQ unit itself and the error of the thermometry device itself [2]. Similarly the NI DAQ device has a ±1.2°C error for a T-type thermocouple, which again is additive to the error of the thermometry device itself [3]. Clinical thermistors and thermocouple devices typically come with an expected error tolerance of ~±1°C, thus resulting in a root sum squared error tolerance of up to ~±1.56°C. However, the validation work in the following section demonstrates that, in practice, the correlation between devices is much tighter at physiologically-relevant temperatures.

2.1.3 Validation of Clinically-approved Thermometry Devices

In order to receive CE approval, clinical thermometry devices must already be validated for clinical use and it is not the aim of this thesis to rigorously re-validate these products. However, given the data acquisition is performed using systems other than the intended manufacturer devices, for the reasons previously mentioned, it is prudent to ensure that the temperature readings are close to what might be expected in a pre-clinical setting. Consequently validation work was performed to confirm that the AngioDynamics thermistors and Medtronic thermocouples correlated well with other thermometry devices. This also helps to validate the pre-clinical hyperthermia work performing using AngioDynamics thermistors, for clinical translation to use the Medtronic thermocouples.

In order to validate readings from clinical thermometry devices, they were immersed in a conical flask containing iced water and brought up to the hyperthermic temperature range by placing the flask on a hot plate set to over 100°C. A magnetic stirring bar was used to minimise natural variations in water temperature. The clinical thermometry devices were connected to DAQ system as previously described (Sections 2.1.1 & 2.1.2) and data was acquired in parallel using a modified LabView client (Figure 2.6). In addition to the clinical devices, two Omega T-type thermocouples were used (Omega mini

[1] HP 34970A User's Guide, Page 16
[2] HP 34970A User's Guide, Page 345
[3] NI 9211 Data Sheet, 6/11/2014, Page 6

hypodermic probe, Ref: HYP0-33-1-T-G-60-SMPW-M and Omega thermocouple probe, Ref: HYP2-21-1-1-/2-T-G-48-SMPW-M). These were connected to a PC on two independent channels using the Pico® Technology USB TC-08 Data Logger (PicoLogger). In addition room temperature was recorded using a cold-junction temperature from the same device, on a third channel, although on this device dynamic cold-junction compensation was deliberately not performed. The experimental set up can be seen in Figure 2.7.

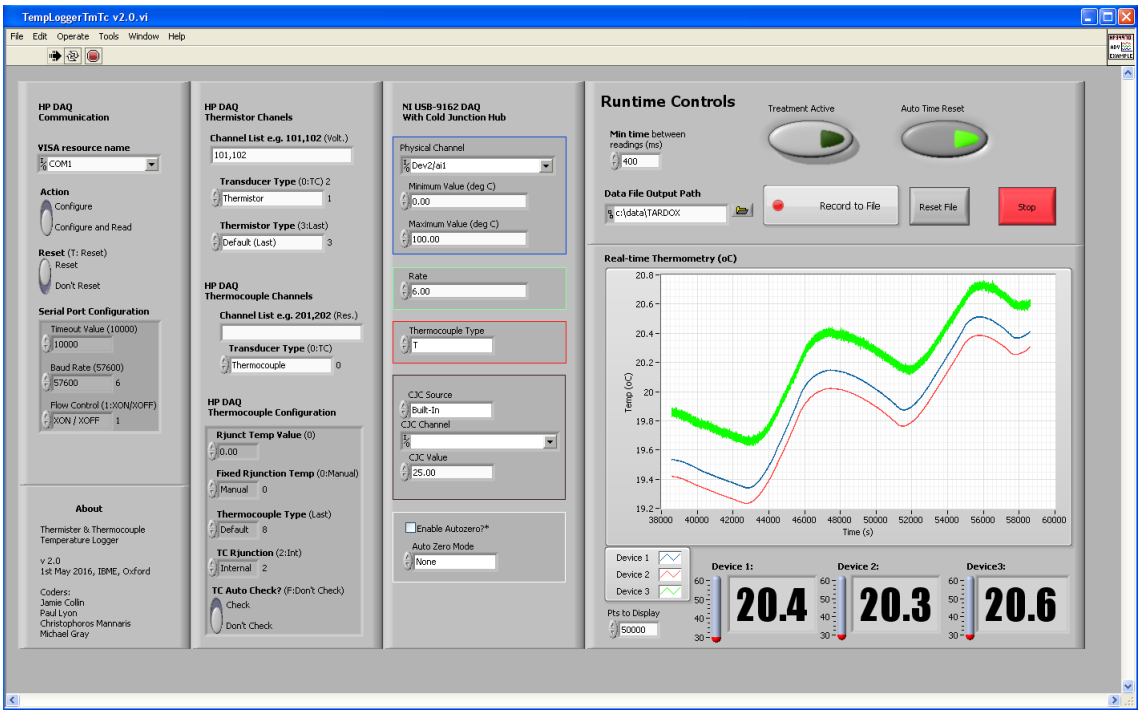


Figure 2.6: Screen capture of a modified LabView client used to obtain real-time thermometry data via AngioDynamics thermistors and/or Medtronic thermocouples. In this case two AngioDynamics thermistors (red and blue traces) and one Medtronic thermcouple (green trace) are acquiring data in parallel, whilst immersed into water and allowed to equilibriate with room temperature overnight. Eight-hour period of complete trace shown. Temperature differences are likely due to regional differences in the water temperature whilst, temperature changes are likely due to air-conditioning. Note the thermocouple has slightly more variance than the thermistors, which can easily be smoothed using a moving average function.

The results are shown in Figure 2.8 and in summary they demonstrate that the devices perform reproducibly, regardless of using the ODU connectors or a hard-wired connection. All of the T-type thermocouples, including the Medtronic probes, provide near identical thermometry curves within a few tenths of a degree. The AngioDynam-

ics thermistors produced thermometry curves of similar morphology within ±2°C at the extremities of temperature (0 and 50°C). Although it cannot be determined which clinical thermometry device records the most correct temperature, the thermocouple readings were noted to be closer to the manual thermometer used. There are of course limitations in this experimental setup to consider, such as regional variations in water temperature despite the magnetic stirrer. Perhaps more crucially, it has previously been demonstrated that the most sensitive regions of the clinical devices are at different positions along the shafts (AngioDynamics thermistor 10-14 mm, Medtronic thermocouple 3-4 mm) (Section 2.1). The final thermometry trace shown in Figure 2.9 was generated overnight using the same experimental setup in the absence of a hot plate to warm the flask, such that temperature changes were due to natural equilibration with room temperature. The variability in the cold junction temperature likely represents air temperature changes due to activation and deactivation of the air-conditioning unit. As expected, the clinical thermocouple was unaffected by these perturbations due to cold-junction compensation, whilst the pre-clinical thermocouples, which are not compensated, were clearly affected.

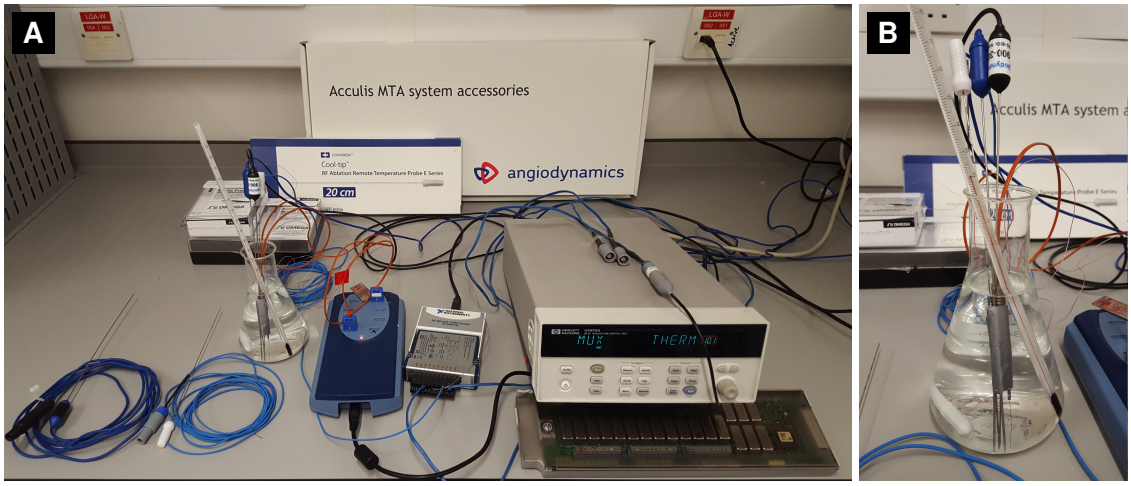


Figure 2.7: A: Thermometry equipment used to compare readings from AngioDynamics thermistors (shown bottom, left most, with 6- or 4-pin ODU male connector) and Medtronic thermocouples (white top, shown bottom, next left most, with 4-pin ODU male connector) against Omega T-type thermouples (HYP0-33 mini-hypodermic probe shown top left, on top of its box, and HYP2-21 thermocouple probe, shown immersed in water). The data acquistion systems from left to right are: PicoLogger (blue) for Omega thermocouples, National Instruments (silver/white) for Medtronic thermistors, HP (grey/cream) for AngioDynamics thermocouples, with spare female ODU connectors taped to top, and a spare unwired module in front which loads into the rear of the unit. **B:** Close up of 250 mL conical flask containing water at varied temperatures, a stiring bar (white, at base), a household thermometer, and a bound bundle of thermometry devices: two AngioDynamics thermistors (long, black/white top from newer batch and blue/black top from older batch, the former being connected via ODU connector, the latter being directly hard-wired to the module), one Medtronic thermocouple (long, white top, connected to NI DAQ system) and two Omega type-T thermocouples (short, mini-hypodermic probe with fine pink lead and short, thermocouple probe with orange lead, both connected to PicoLogger by their standard Omega connectors).

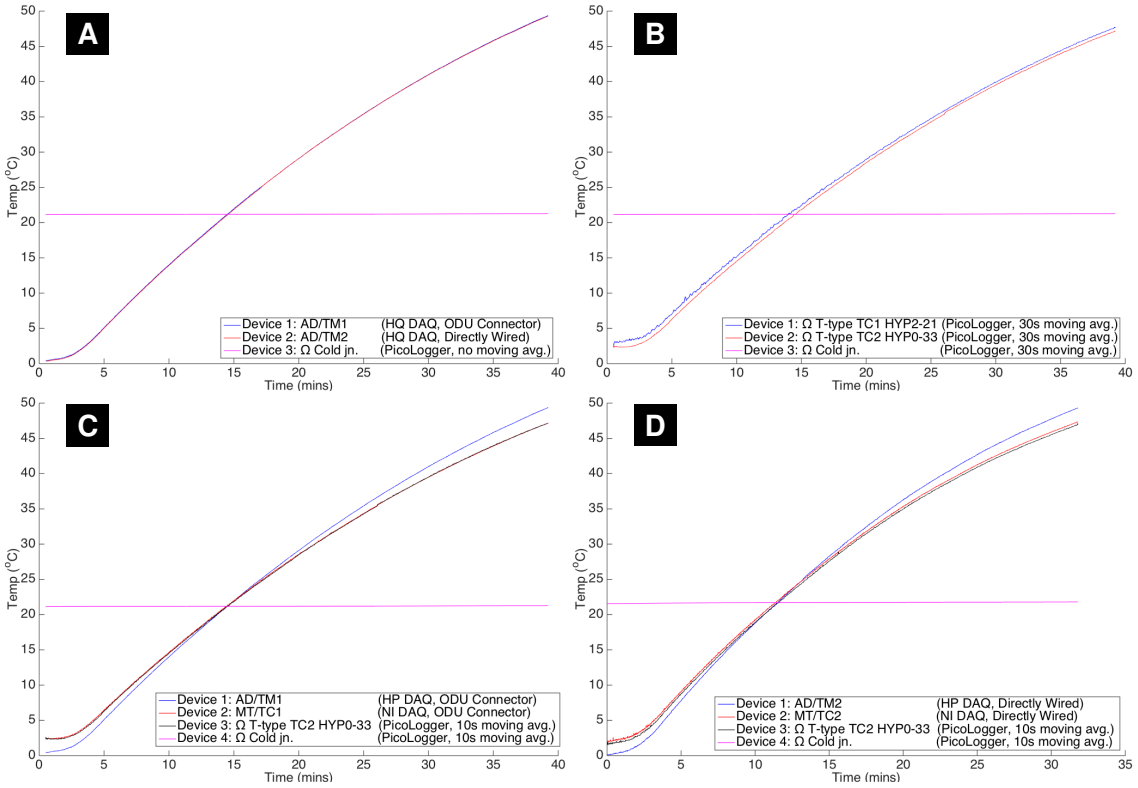


Figure 2.8: Comparison of temperature readings obtained from iced water warmed on a hot plate through to ~50°C. In all cases the cold-junction temperature was taken from the PicoLogger device, and represents room temperature (pink trace). Plots A-C were acquired in parallel for the same ice warming experiment, whilst the remaining plot was acquired subsequently. **A:** Traces for two AngioDynamics thermistors, one hard-wired, one connected via ODU connector. Traces almost indistinguishable, showing high correlation. **B:** Traces for two Omega T-type probes, showing a good degree of correlation. **C:** Traces for ODU-connected AngioDynamics thermistor, ODU-connected Medtronic thermocouple and one of the Omega thermocouples, demonstrating a high degree of correlation across the clinical and pre-clinical thermocouples and a reasonable degree of correlation between the thermistor and the thermocouples. In particular, at room temperature all devices correlate very well, however note that the thermistor reads higher and lower than the thermocouples at hot and cold temperature extremes respectively, with a maximum variation of approximately ±2°C at 0 and 50°C. **D:** A repeat of same experiment performed with fresh iced water, with the exception of reading from AngioDynamics thermistor and Medtronic thermocouples both directly wired to their respective DAQ units without connector, demonstrating reproducibility and independence on connection mode. It was not possible to run two Medtronic probes in parallel in this experimental setup due to limitations with the existing LabView client.

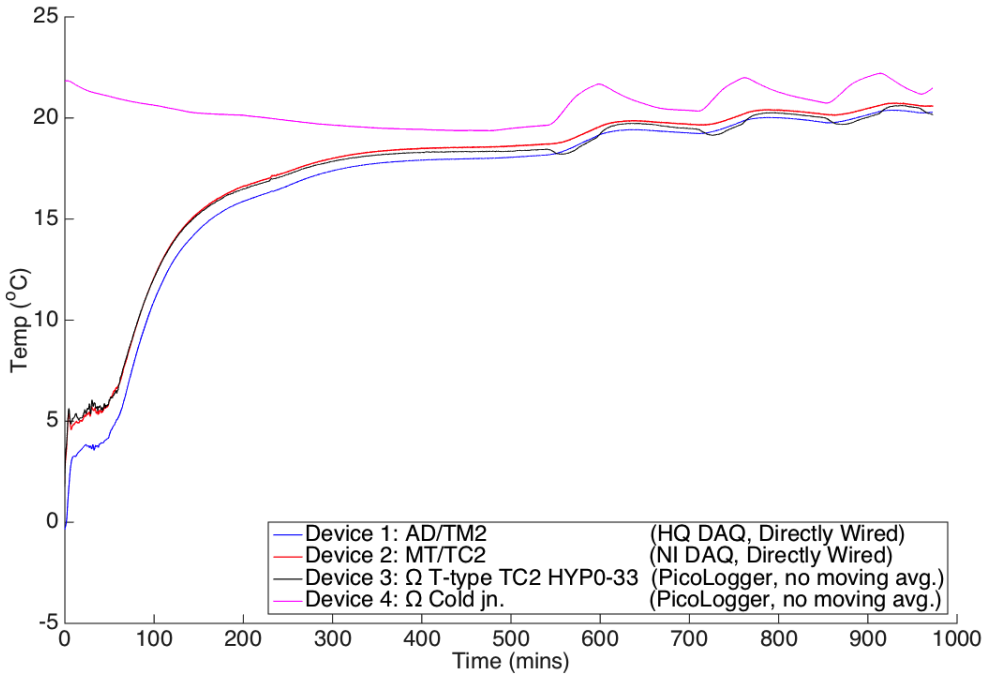


Figure 2.9: Comparison of temperature readings obtained from the same experimental set up in fresh iced water allowed to equillibriate with room temperature over night in the absence of a hot plate. The cold-junction temperature was taken from the PicoLogger device, and represents room temperature (pink trace). Note the fluctuations in room temperature which are likely due to air conditioning triggers. The PicoLogger thermocouple trace (black) dips where the cold-junction temperature peaks, clearly demonstrating the lack of dynamic cold-junction compensation and an inverse relationship. However the Medtronic thermocouple follows the same trend as the room temperature fluctuations, due to dynamic cold-junction compensation, and correlates well with the thermistor as previously seen.

2.2 Volumetric Hyperthermia Using Clinical FUS Device

The use of FUS to induce mild hyperthermia has already been introduced in Section 1.4.7. One of the key challenges of the clinical study is to achieve and sustain a temperature in excess of 39.5°C, which is required for release over the entire tumour volume using minimum input FUS energy, for a duration compatible with the pharmacokinetics of the drug. ThermoDox® is administered systemically and maintains high circulating levels for around 1-2 hours, with circulating plasma levels of over 50% and 25% of peak at 1 and 2 hours post-infusion respectively (Figure 1.5), giving a convenient clinical window during which FUS can be applied to a target tumour. Celsion advise limiting the length

of hyperthermia to 3 hours after initiation of the infusion [398].

Clinically, the driving power of the clinical FUS device is determined by attenuation and obstruction in the tumour propagation path, which is likely to contain, from outside in: skin, subcutaneous fat, muscle, ribs (Figure 2.10), connective tissues, liver capsule, normal liver parenchyma including vessels and ultimately liver tumour. Whilst it is difficult to include all these features in an *ex vivo* pre-clinical model, such a model is an excellent first step before clinical translation. For perhaps the first time, strategies to obtain optimal hyperthermia in a pre-clinical model have been explored using a clinical ultrasound-guided device. This initially involved early work heating agar gel 'phantoms' incorporating either microbeads [419] or silica [420] as attenuating agents to produce a tissue-mimicking model, and more recently *ex vivo* liver tissue has been tested using the clinical device. For the sake of brevity this section will focus on the *ex vivo* work only, which more closely translates to the clinical cases.

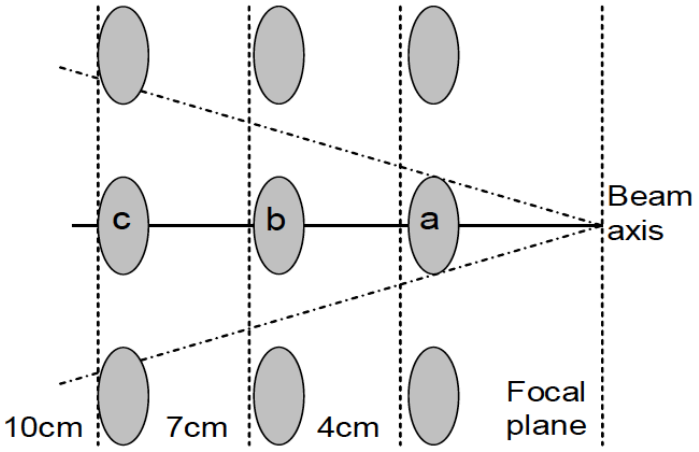


Figure 2.10: Figure reproduced from DPhil thesis courtesy of Dr. James Kennedy, University of Oxford. Using a membrane hydrophone, porcine ribs were placed in an HIFU field at (a) 4 cm, (b) 7 cm, and, (c) 10 cm from the focus of a 1.7 MHz Teleson transducer with 84 mm diameter element and 15 cm focal length. A membrane hydrophone with a 0.5 mm sensitive element was used to plot the beam pattern of pressure intensity, normalised to that in the absence of ribs. At the focus, pressure amplitudes were reduced to 38%, 64% and 60% for rib positions (a), (b) and (c) respectively.

Given the JC200 therapeutic device (Chongqing HAIFU™Company), previously described in Section 1.3.2), is used for the clinical study, the same device was used to

optimise hyperthermia strategies in *ex vivo* liver tissue prior to patient treatments. In particular the JC200 J081C-170 HIFU Treatment Head (serial number 20099-44) was used for all pre-clinical experiments and indeed clinical treatments (Figure 2.11). This particular transducer has a driving frequency of 0.95 MHz, a focal length of 145 mm and a diameter of 200 mm, resulting in a focus with a transverse âĂŞ3-dB beam-width of 1.2 mm and an axial âĂŞ3-dB length of 9.5 mm [153].

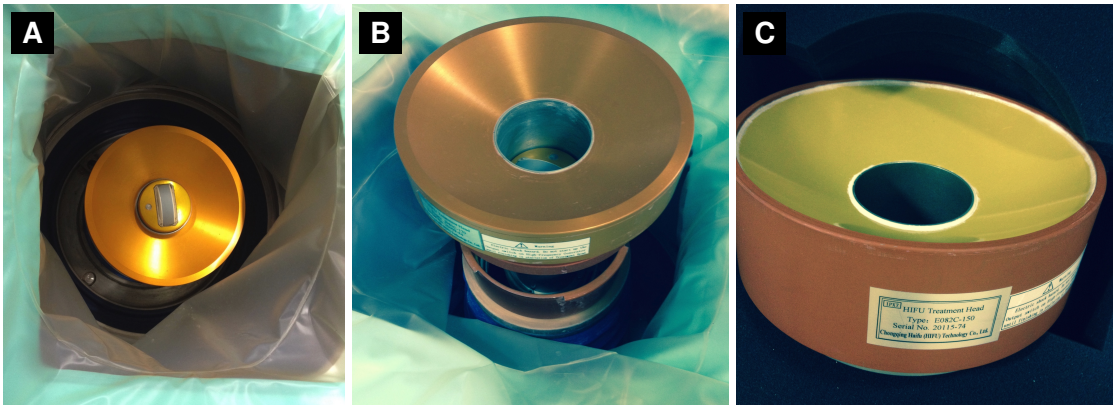


Figure 2.11: JC200 Tumour Therapy Systems (Chongqing HAIFU™Company) and removal of the exchangable treatment head (tranducer). **A:** treatment head in position in the unfilled water bath, demonstrating the co-axially aligned B-mode device used for ultrasound guidance. **B:** After unscrewing the treatment head it can be separated from the central motorised positioning system. **C:** Treatment head used for all pre-clinical and clinical studies in this thesis in isolation. The corresponding beam pattern produced by this transducer is shown in Figure 2.17.

2.2.1 Calibration of the JC200 Therapeutic Device

As with any HIFU transducer in pre-clinical or clinical use, due to risks of transducer delamination, crystal fracture and electrical problems leading to transmitted pressure changes, for safety and quality assurance, calibration of transducers is necessary at regular intervals. The JC200 device is calibrated on a yearly basis by a Chongqing HAIFU engineer, using a radiation force balance following its annual service. With assistance from post-doctoral researchers, Dr. Christophoros Mannaris and Dr. Michael Gray (IBME), attempts have been made to further characterise the FUS output field from the JC200. This has been a challenge for a number of reasons:

1. From an electronics perspective, the JC200 is a 'black-box', in that it is not possible to monitor electrical power output to the transducer itself, only to set it via the user inferface

2. Even at its lowest user-defined power setting of 32 W, 1% DC, the JC200 will cavitate and destroy most standard acoustics laboratory hydrophones when acoustically aligned to the focus

3. In attempting to monitor JC200 output by hydrophone, in addition to the added electronic noise of B-mode pulse/echo signals, the JC200 produces additional noise in the form of unpredictable 'transients' and great care and expertise is required to distinguish the noise from true hydrophone readings on the monitoring oscilloscope

Before attempting to calibrate the JC200, a 75 μm Precision Acoustics hydrophone was used safely off-axis (with the focal point some mm away from the hydrophone when in a co-axial configuration) in order to gain an appreciation of the output at varying DC and Pulse Repetition Frequency (PRF), at a fixed power of 32 W. These results are best appreciated by reference to Figure 2.12.

Using the same experimental setup in acoustic alignment with the 75 μm hydrophone at the lowest possible power settings resulted in a non-linear trace (Figure 2.13), with the presence of harmonics following Fast Fourier Transform (FFT). It was felt that any higher pressures at the focus would damage this hydrophone and so no further characterisation was performed with it.

Given these difficulties, an attempt to further characterise the JC200 was made using an implantable needle-shielded hydrophone (ONDA HNA-0400, effective diameter 400 μm) manufactured by ONDA Corporation, and the setup is shown in Figure 2.14. This particular hydrophone, with its larger diameter, is designed for robustness in the mapping HIFU acoustic fields (1-20 MHz), as a trade-off for sensitivity. The manufacturer stress

tests these hydrophones for one hour at 1.5 MHz, 50% DC in degassed water providing a exposure intensity of 715W/cm^2 temporal-average, and 1430 W/cm^2 pulse average, corresponding to 15 MPa peak positive and 3.7 MPa peak negative pressures [421]. However despite being able to withstand high field pressures, it has minimal protection against damage caused by inertial cavitation.

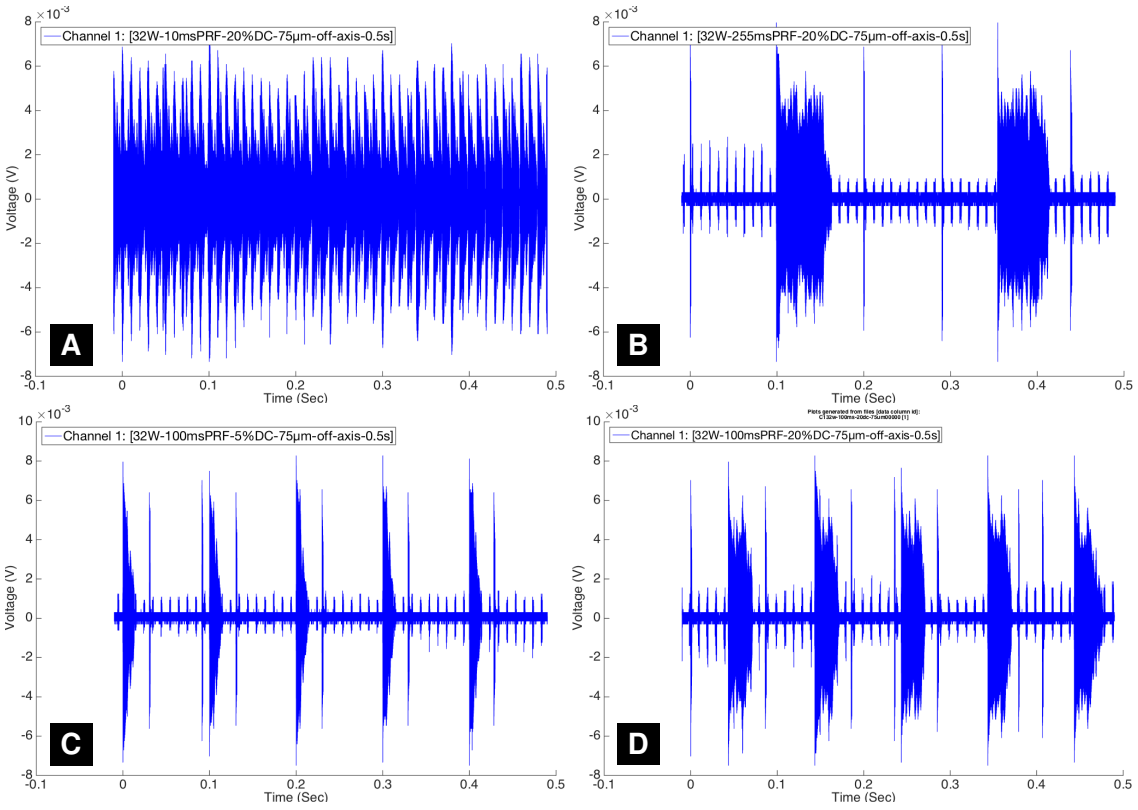


Figure 2.12: Waveforms of duration 0.5 s captured from the JC200 using LeCroy WaveSurfer on a near-aligned (within 2 mm) but not perfectly aligned 75 µm Precision Acoustics hydrophone. Note all traces have short-bursts of background noise: the frequent low amplitude (<2V) spikes throughout of unknown origin and less frequent large amplitude spikes every 1/100th of a second due to B-mode acquistion. TOP: Comparison of PRF at a fixed DC of 20%, PRF of 10 ms **(A)** vs. 255 ms **(B)**. Note that regardless of the PRF the overall exposure time and thus energy delivered is equivalent, but the frequency at which the pulses fire is modified. BOTTOM: Comparision of DC at a fixed PRF of 100 ms, DC of 5% **(C)** vs. 20% **(D)**. Note that as the DC is four times greater at 20% DC, the overall FUS exposure time and thus energy delivered is also four times greater and is equivalent to the energy delivered with the exposure parameters for the first plot which was also at 20% DC with a shorter PRF.

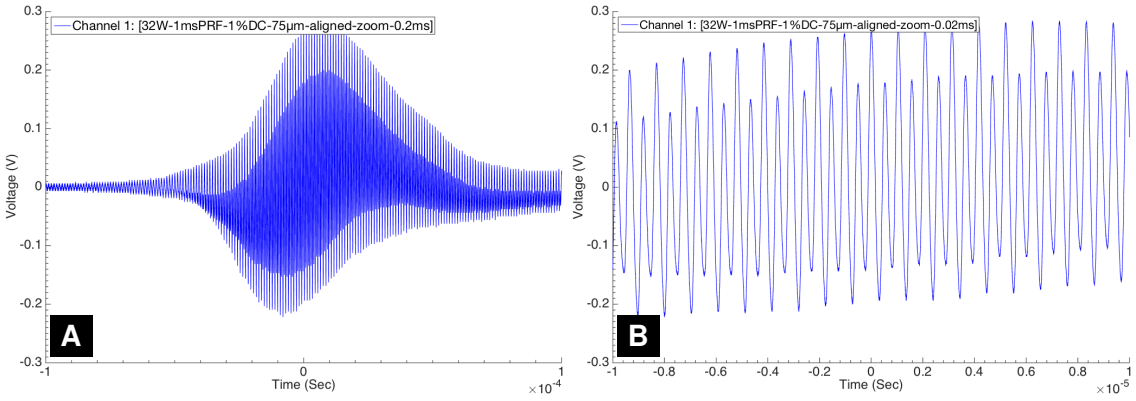


Figure 2.13: Waveforms captured from the JC200 using LeCroy WaveSurfer by a perfectly aligned 75 µm Precision Acoustics hydrophone, using 32 W, 1 ms PRF, 1% DC. **A:** A trace captured of 0.2 ms duration. There is a low-frequency baseline oscillatory component, which is thought to be a transient due to the flexible/deformable nature of the hydrophone, and not related to the source. Such low frequency oscillation was not seen with the more rugged (ONDA) hydrophone. **B:** The first 0.02 ms of the same trace, demonstrating linear and non-linear components over the 20 cycles captured for this ~1 MHz transducer ($1x10^{6} * 0.02x10^{-3}$).

From the ONDA certificate of calibration, at 1 MHz the sensitivity, s, is -242 decibel (dB) relative to 1V/µPa (legacy units). Thus, this hydrophone sensitivity per unit pressure, or transfer factor, c, with the pre-amplifier and D/C coupler in use, can be derived as follows [422]:

$$c = 10^{\frac{s}{20}}\text{V/µPa}$$

$$c = 10^{12}.10^{-12.1} = 10^{-0.1}\text{V/MPa}$$

$$c = 794\text{mV/MPa}$$

This sensitivity was validated against a well-characterised Precision Acoustics (PA) 0.5 mm hydrophone using a 1 MHz single element transducer in our laboratory, and resultant pressures were in close agreement up to 3 MPa peak-to-peak, after which the PA hydrophone began to saturate. The same acoustic equipment was used with the ONDA in the absence of the pre-amplifier. The average ratio of the peak-to-peak output voltages with and without the pre-amplifier, before the point of saturation, was determined to be

20.4, giving a sensitivity of 39 mV/MPa without the pre-amplifier (Figure 2.16).

The JC200 was calibrated using the ONDA hydrophone without the pre-amplifier, as a safeguard to minimise hydrophone non-linearity. At 0.97 MHz, 32 W, 1% DC and 5 ms Pulse Repetition Frequency (PRF) the transducer was acoustically aligned to the ONDA hydrophone. Sampling was performed on a LeCroy WaveSurfer at a high temporal resolution of 2 giga-samples/second. In perfect alignment to the focus, even at these minimal power settings, again it was noted that the oscilloscope trace was non-linear, as with the PA hydrophone, with visible harmonics on the FFT (Figure 2.15). A beam pattern was then created in the axial field by using the 3D positioning system to scan varied positions of the hydrophone in 0.1 mm steps, whilst keeping the JC200 fixed (Figure 2.17). The full width half maximum (FWHM) was determined to be approximately 1.7 mm, which fits well with the transverse diameter of the focal area reported in the literature of 1-2 mm [184, 423].

Whilst this gives us an estimate of the output pressure (MPa) of the JC200 at the lowest possible power settings, it does not reveal how pressure scales with power. In order to determine focal in situ intensities for larger powers, if performed at the focus, any power ramp would risk of destroying the hydrophone. Instead, as an approximating method, the hydrophone was subsequently aligned to the first side lobe of the beam pattern, where a near-linear trace was obtained on the oscilloscope. Pressures were compared to those at the focus at the same power settings, and a linear correction ratio calculated and subsequently used to estimate focal pressures based on the power ramp at the first side lobe. As cavitation is a stochastic process, care was taken to only use well-formed traces, and attention was paid to regularly check for visible bubbles on the hydrophone tip, which were removed using syringed water. Figure 2.18(A) shows the estimated linear power:pressure relationship based on uncorrected readings from the first side lobe. The ratio of the peak-to-peak pressure between the focus and the first side lobe, found in the beam pattern exercise was 2.506, thus this was the correction factor used to generate Figure 2.18(B). The extrapolated readings were fitted to a pure quadratic equation ($Power\ \alpha\ Pressure^2$)

and the equation shown on the figure can be used to predict peak-to-peak pressures for any output power generated by the JC200, up to its maximum output power of 400 W.

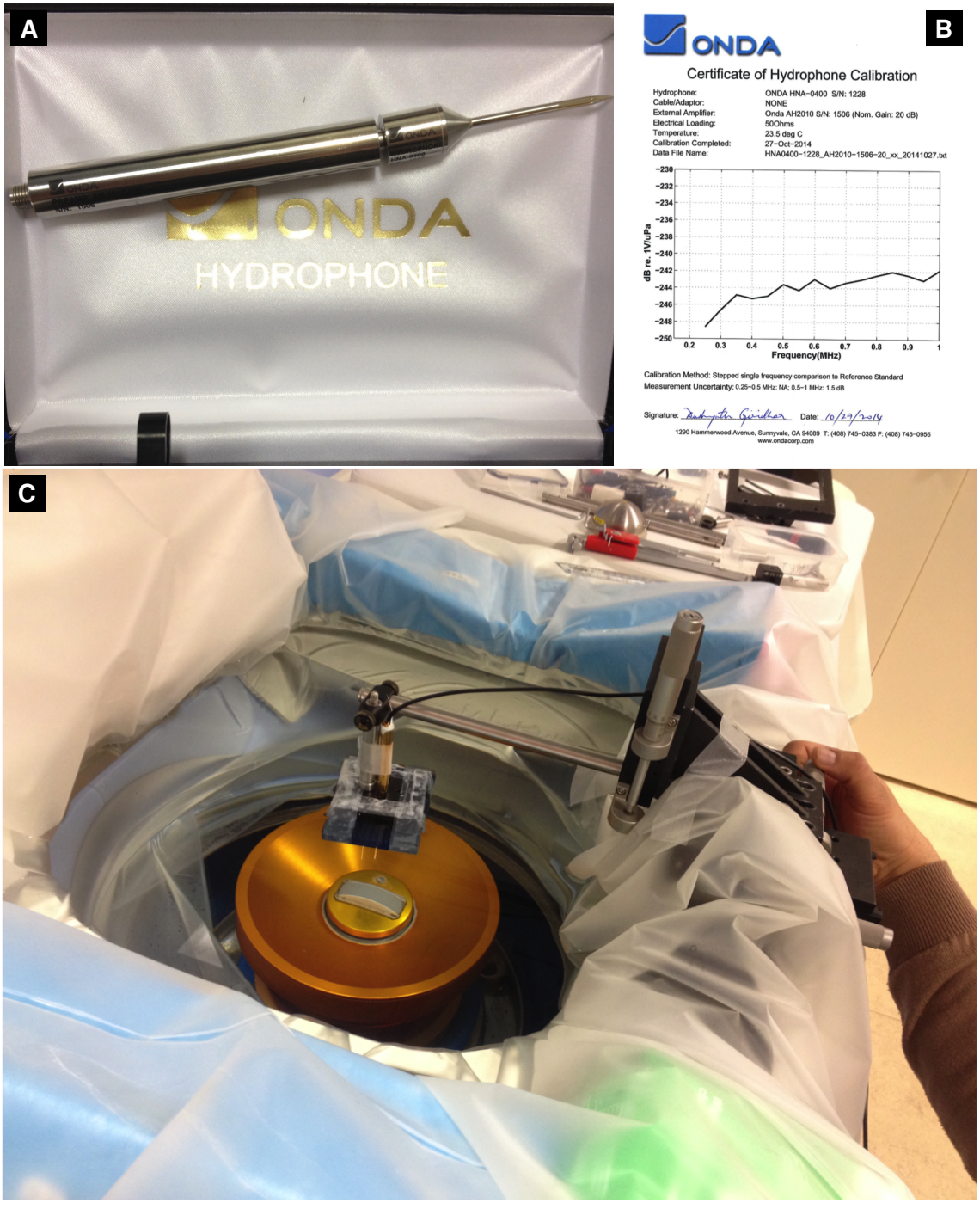


Figure 2.14: A: ONDA Hydrophone (ONDA Corporation), demonstrating the pre-amplifier and the sensitive needle tip. **B:** Certificate of calibration for the hydrophone. **C:** The ONDA hydrophone mounted on a 3D positioning ganty over the JC200 transducer. Note the hydrophone is centred through acoustic blocking material designed to avoid reflections.

Recent radiation force balance data, generated by the Chongqing HAIFU™ engineer during annual service, was used to validate this quadratic fit. Powers of 50 W and 100 W applied to the equation yield Peak-to-Peak pressures of 18.94 and 24.52 MPa respectively, which compare favourably with the pressure output predicted from radiation force balance measurements, namely 16.2 and 23.0 MPa (acknowledgement: Dr. Michael Gray). Errors on the order of this magnitude are expected due to non-linearity at the focus even at minimal power settings for the JC200, uncertainties in the absolute sensitivities of both the hydrophone and radiation-force balance, the assumptions used in the RF balance conversion and some degree of scaled error from the extrapolation method used. Note that in addition, a small degree of new pitting on the hydrophone tip was noted following this calibration exercise. However, before and after calibration on the JC200, the ONDA hydrophone was calibrated against a smaller 1 MHz transducer, and there was no change in sensitivity.

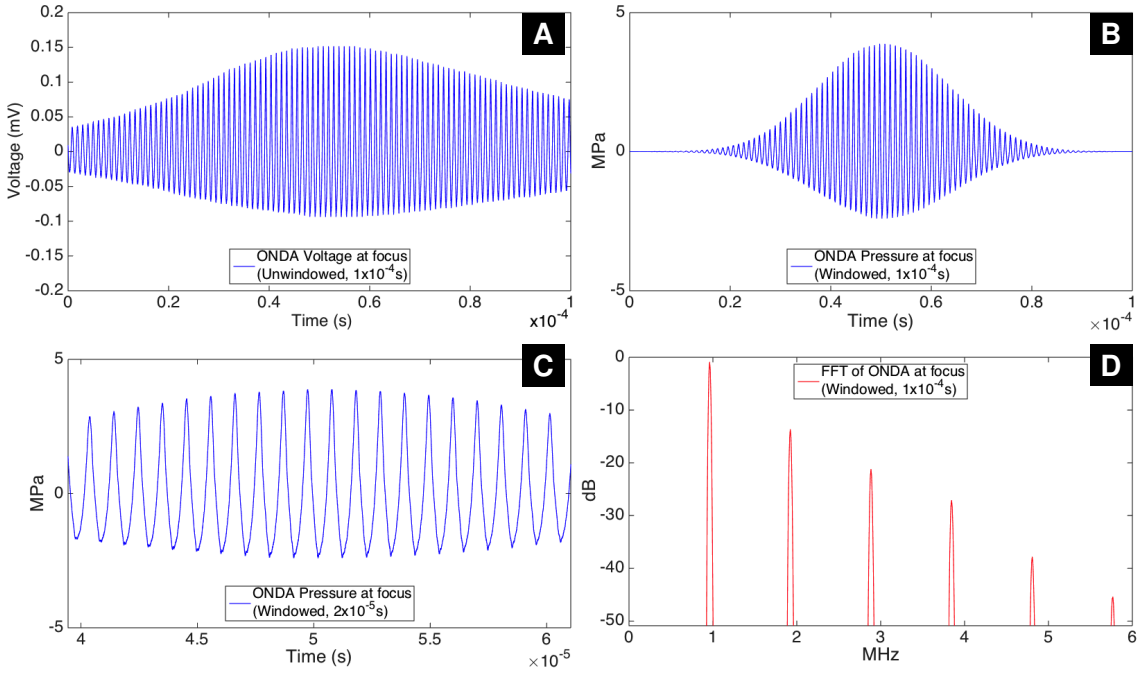


Figure 2.15: ONDA hydrophone waveform at the focus of the JC200 (driven at 0.97 MHz, 32 W, 1% DC, 5 ms PRF) and its Fast Fourier Transform (FFT). **A:** The output captured on the oscilloscope over 0.0001 ms. **B:** The same trace coverted into pressure calculated using the ONDA sensitivity at 1 MHz, which has had a Blackman-Harris window applied ('windowed') for a cleaner FFT. **C:** A closer look at the same pressure waveform from 0.4-0.6 x10^{-5} s, demonstrating features of non-linearity. **D:** The final FFT demonstrating discrete components at each of the harmonics.

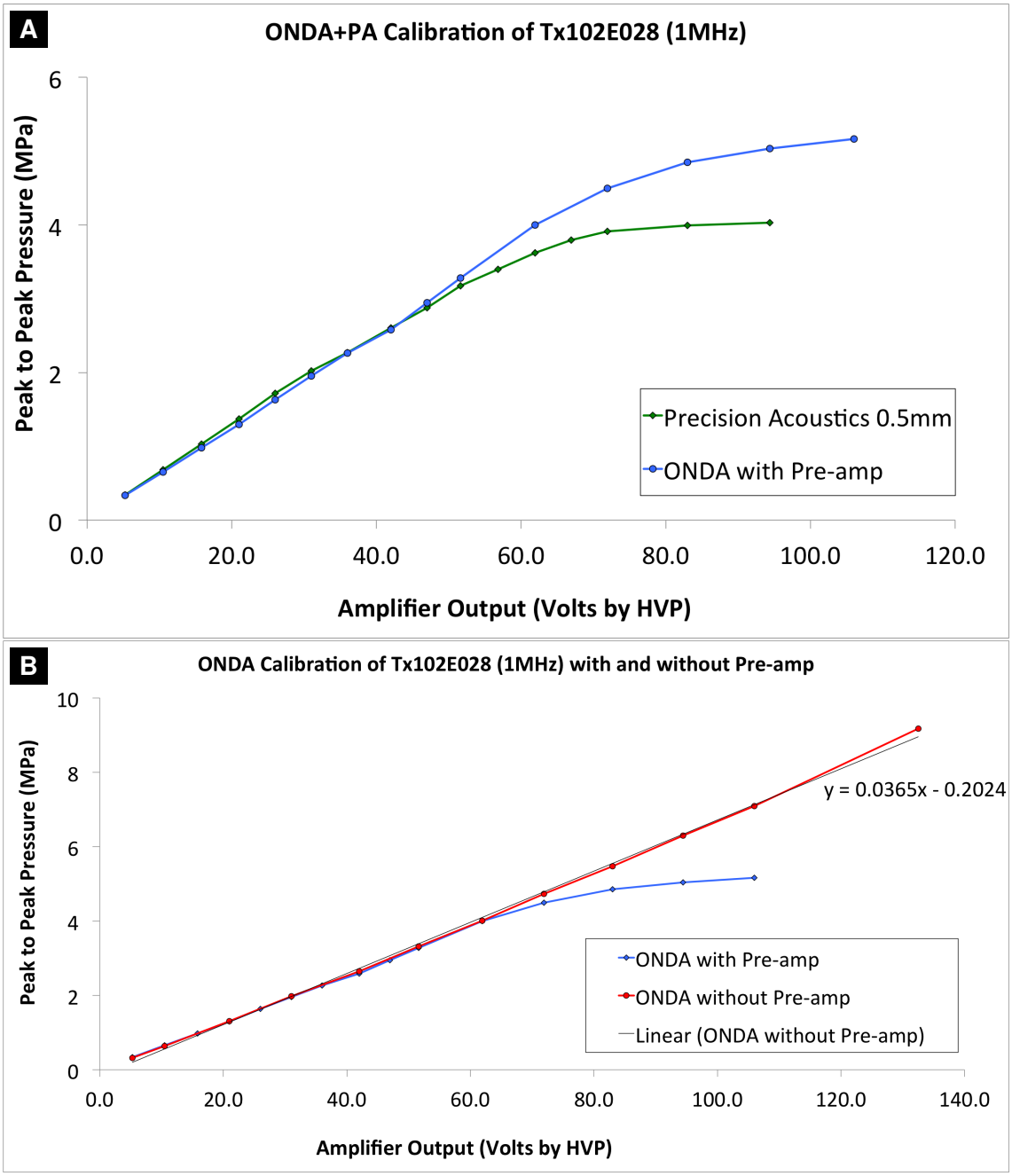


Figure 2.16: ONDA calibration of a 1 MHz transducer in degased water in IBME, performed using same function generator. **A:** Comparison of the ONDA hydrophone with pre-amplifier against a Precision Acoustics 0.5 mm hydrophone with a sensitity of 248 mV/MPa, demonstrating a close correlation up to 3 MPa peak-to-peak. **B:** Comparison of the same ONDA calibration with the pre-amplifier against a plot in the abscence of the pre-amplifier, adjusted by a factor of 20.4 to bring the two into correlation. Linear fit shown for the plot without the pre-amplifier. Note that in the presence of the pre-amplifer, the hydrophone begins to saturate at 4 MPa peak-to-peak whilst without the pre-amplifier it can be used to accurately read pressures of over 10 MPa peak-to-peak without saturation.

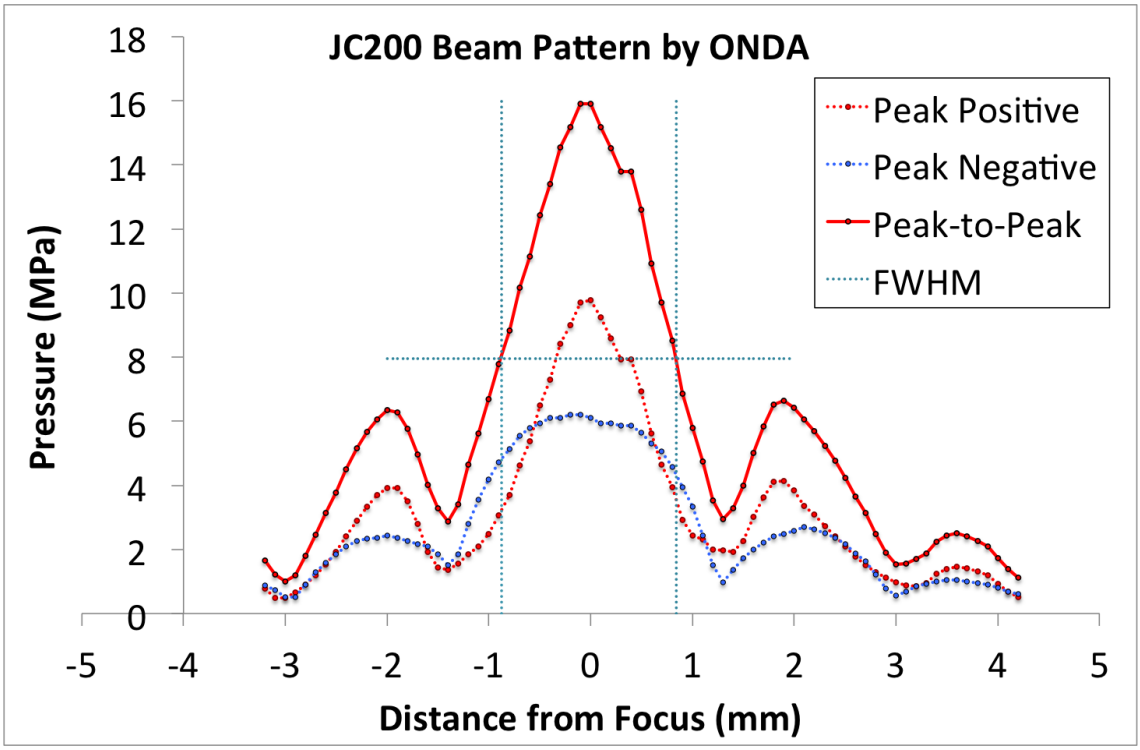


Figure 2.17: Beam pattern generated in the axial field by the JC200 at 32W, 1% DC and 5 ms PRF, by manual movements on the ONDA hydrophone using the 3D gantry with 0.1 mm resolution in the X-axis only. The full width at half maximum (FWHM) is 1.72 mm, indicated by light blue dotted lines. The maximum pressures at the focus and first side lobe are 15.90 and 6.35 MPa peak-to-peak respectively. Pressures at the focus may represent an underestimate due to the presence of non-linearity. The first side lobe appears of greater amplitude, relative to the peak positive, than one may expect for a focused beam pattern and this is thought to be in part due to the geometry of the single element transducer with its central cut-out for the B-mode probe (Figure 2.11).

In summary, hydrophone calibrations served to confirm the spatial extent of the HIFU focus, and the magnitude of the pressure amplitude deployed by the device at its lowest output power setting of 32 W (output voltage not reported by JC200). This became the most commonly used power setting in subsequent pre-clinical experiments. For clinical cases, by using a side-lobe power ramp extrapolated to the focus, the powers required to generate the typical free-field pressure amplitude range of 19-28 MPa at 1 MHz (Table 3.6) could be estimated hereafter.

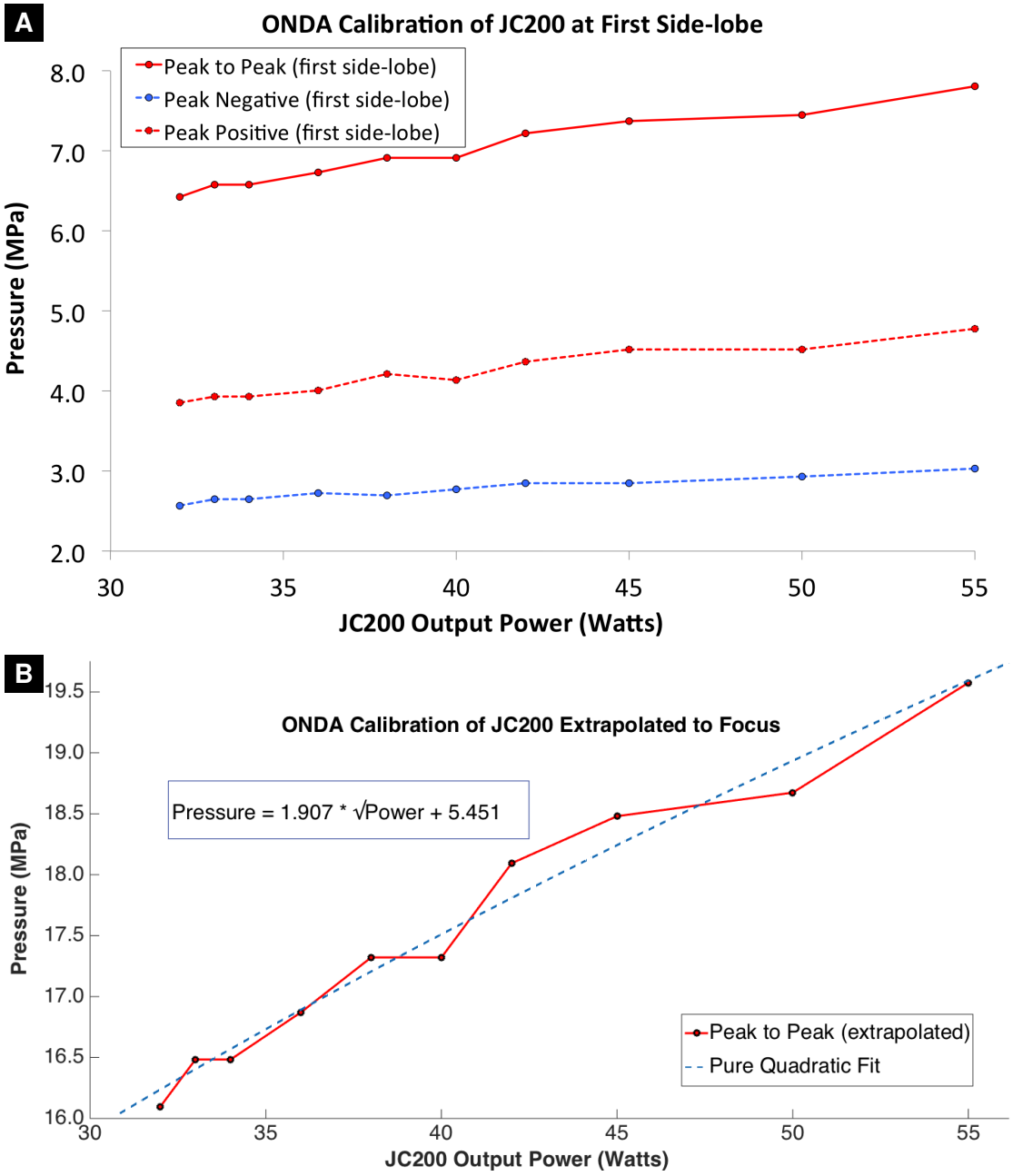


Figure 2.18: Approximated JC200 calibration based on extrapolation of a calibration performed at the first side lobe, using 1% DC and 5 ms PRF. **A:** peak-negative, peak-positive and peak-to-peak pressures generated whilst aligned to first side lobe (uncorrected for true focus). **B:** extrapolated peak-to-peak focal pressures, predicting those at the true focus, based on the previously calculated conversion factor of 2.506. Pure quadratic fit and its equation for the free-field focal peak-to-peak pressures shown. Fit Parameters: R-square=0.9748, Root Mean Square Error (RMSE) = 0.1902, Sum of Squares due to Error (SSE) = 0.2893.

2.2.2 Materials for Volumetric Heating Optimisation

Once calibration of clinical HIFU device was completed, the next step was to optimise the HIFU exposure parameters in order to achieve volumetric heating over timescales of tens of minutes, using the lowest possible acoustic energy input to the patient. In order to complete these experiments, the JC200 was filled with degassed water at room temperature (19.5°C). This temperature was chosen as, whilst not physiological, it allowed equilibrium of liver tissue temperature with room temperature even after partial immersion in the water bath. Full immersion was not possible due to limited depth of water bath (Figure 2.19). Hotter or colder temperatures would have resulted in temperature inhomogeneity within the liver tissue even before heating.

Fresh bovine liver was obtained from Mutchmeats Ltd., a local abattoir and wholesale butcher. Livers were arranged for delivery as soon as possible following slaughter, such that they arrived within 2 hours of slaughter and were typically still warm. To prepare them, livers were immediately examined and homogenous tissue volumes were selected which avoided large vessels. The volumes were sectioned to the required dimensions and degassed in phosphate buffered saline (PBS) solution for a minimum of one hour to remove trapped gas in the tissue, which would otherwise interfere with the FUS field.

A custom holder was manufactured from Delrin® of internal dimensions 10x10x10 cm, with a 10x10 cm, 50 μm thick Mylar acoustic window beneath, and loaded with degassed liver. A 3D gantry was attached to the bed of the therapeutic device enabling the holder to be suspended in the water bath above the JC200 transducer and interfacing air bubbles were removed.

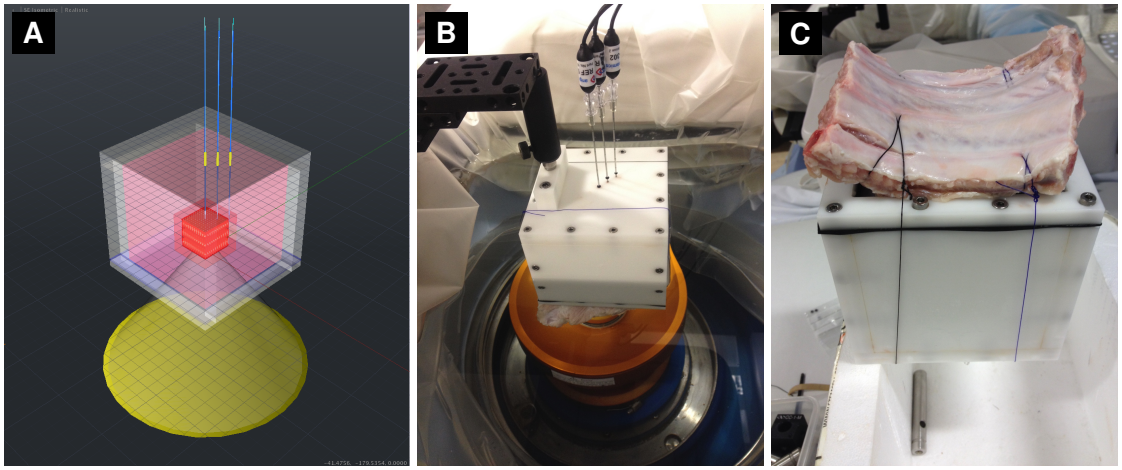


Figure 2.19: The co-axial configuration of thermistor insertion. **A:** 3D model of Delrin® holder (white), containing liver (pink) positioned over the JC200 transducer (yellow). The centre heating cube in the liver (red) is 3x3x3 cm and is covered with dot mode exposures. The larger covering heating cube (transparent red) is 4x4x4 cm. Both of these heating cubes are spanned with co-axially loaded thermistors (blue) with respect to the JC200 beam axis. **B:** Experimental setup on JC200 device, demonstrating rig and partial immersion into water bath. Note all thermistors are inserted through 18G co-axial needles to the same axial depth, using rubber 'O' rings to minimise movements. **C:** Underside of holder demonstrating the attachment of degassed ribs to overlay the acoustic window using surgical sutures, used in a subset of the experiments only.

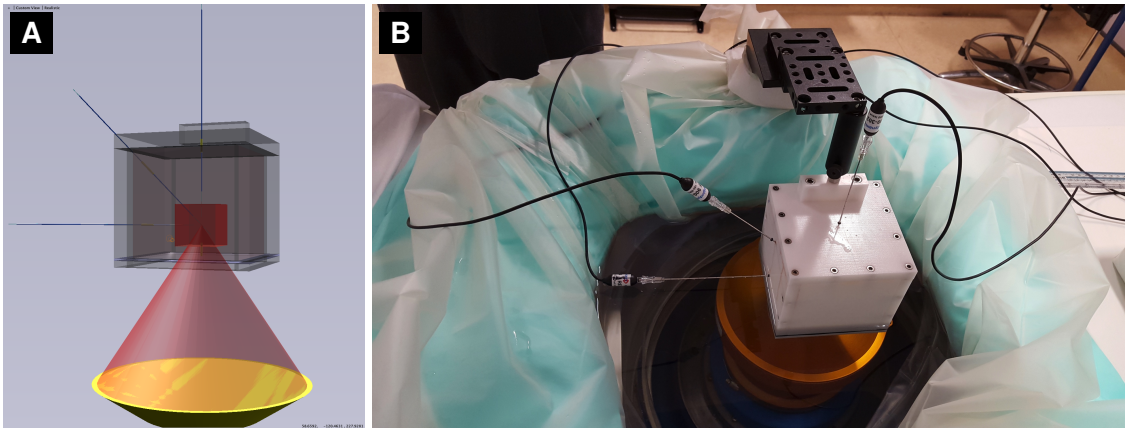


Figure 2.20: The 45° configuration of thermistor insertion. **A:** 3D model of holder (white), containing liver (pink) positioned over the JC200 transducer (yellow). The centre heating cube in the liver (red) is 4x4x4 cm and is covered with dot mode exposures and is spanned by thermistors (blue) orientated at 0, 45 & 90° relative to the horizonal. **B:** Experimental setup on JC200 device without ribs before the water level was brought up. Air trapped when bringing the water level up was removed using a syringe.

Clinically approved thermistors (TM) (AngioDynamics, described in Section 2.1.1) were used to thermally characterise target virtual FUS 'heating cubes' within the liver, in-

serted through 18G co-axial needles (Temno®, CTT1820) in a co-axial or angled configuration (Figure 2.19). The angled configuration was included to more accurately reflect the clinical situation, in that the thermistor is rarely loaded in a perfect co-axial orientation and is more typically at around 45° (Figure 2.20). In another experimental setup, a fibre optic hydrophone (FOH) (Precision Acoustics) was used to further validate the range of temperature rises seen on the thermistors (Figure 2.21). A section of degassed porcine rib cage was used to mimic blocking effects of the human rib cage in some experiments (Figure 2.19).

Several clinically approved thermometry devices are now commercially available, typically used for RFA or MWA monitoring [416]. This clinical study requires an 18-gauge (18G) probe of 20 cm length for compatibility with the Co-axial Temno® (ACT) Biopsy Device, given the same co-axial needle is utilised for both biopsy and thermometry acquisition, thus only requiring a single percutaneous entry point.

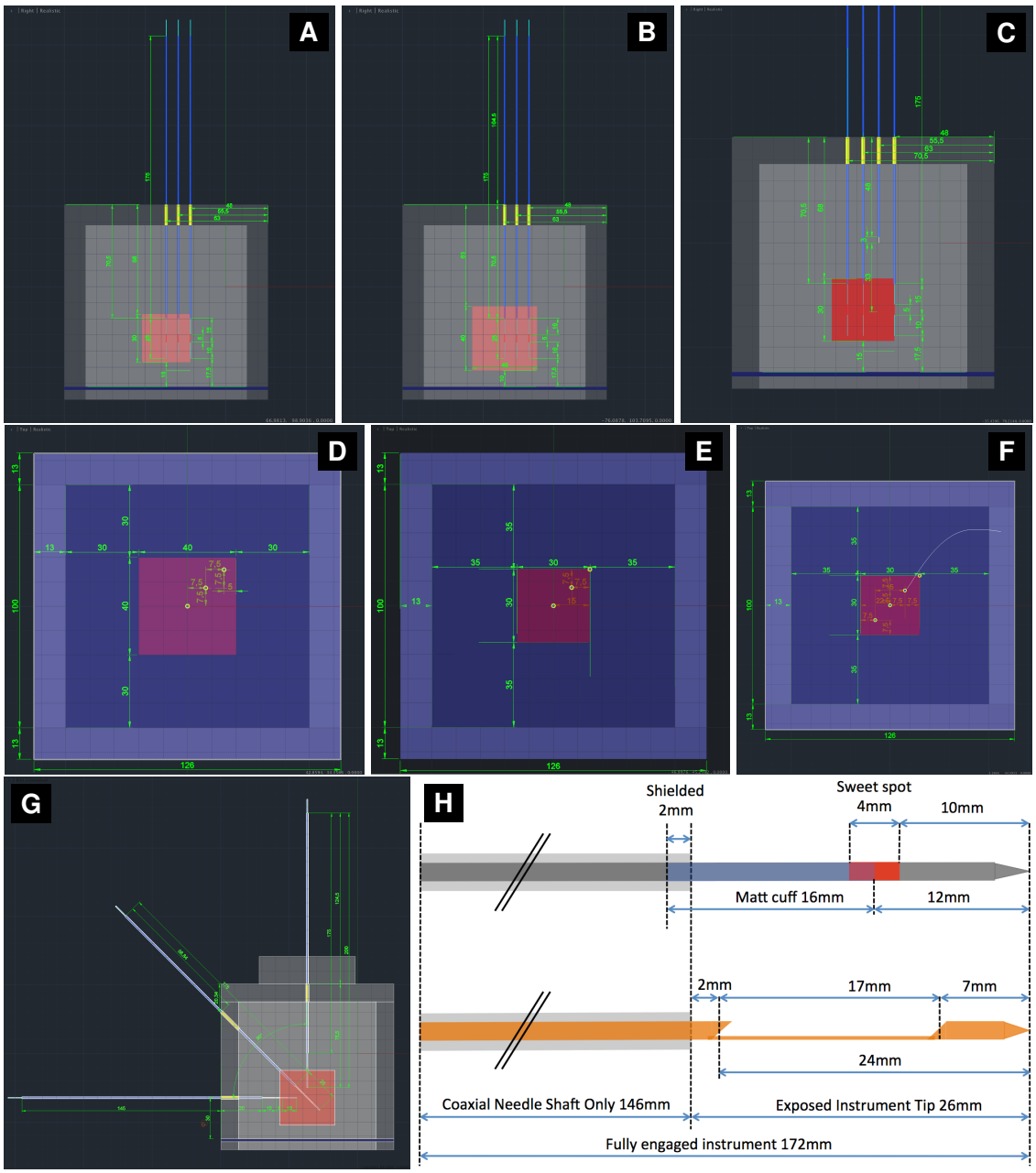


Figure 2.21: Thermistor positioning planning for the thermometry experiments. **A-B:** Side plan view for 3x3x3 cm **(A)** and 4x4x4 cm **(B)** heating cubes in co-axial configuration and a 4x4x4 cm cube **(C)** with addition of a fibre optic hydrophone. **(D-F)**: Top plan view for the same. **G:** Side plan view for a 4x4x4cm cube in 0,45,90° configuration. **H:** Schematic demonstrating the thermal 'sweet spot' of the AngioDynamics thermistor (thermally characterised in Section 2.1.1) relative to the core biopsy needle. Note the thermal sweet spot lies within the core biopsy region if the co-axial needle remains stationary and both instruments are fully engaged.

2.2.3 Method for Volumetric Heating Optimisation

Even at a fixed power setting, several other exposure settings on the clinical HIFU device need to be determined, including transducer movement speed (1-6 cm/s), duty cycle, and motion path to span the intended treatment volume. The experiment was set up in order to identify an ultrasound exposure protocol that deposited the minimum total acoustic energy input to the patient in order to raise the temperature of an oncologically relevant volume (initially 3x3x3 cm^3) by about 5 degrees within a matter of minutes, and sustain such hyperthermia for 20 minutes or more. The reason why these timescales are important is because this time interval represents the period of time when the majority of ThermoDox® liposomes are still in circulation post-administration (Figure 1.5). The possibility of heating a larger volume (4x4x4 cm^3) using these optimised protocols was also explored.

Experiments were carried out at 32 W (the lowest power the JC200 is capable of generating) using a 0.96 MHz transducer which is typically used in most clinical cases. Target volumes, consisting of contoured cubes of volume 27 cm^3 or 64 cm^3, were exposed to FUS using automated plans generated on the JC200 user console, based around the geometric centre. In both cases, clipping of the acoustic field by the holder was negligible (Figure 2.22).

The B-mode guidance feature of the JC200 was used to visually align to the co-axially loaded reference thermistor, which was positioned such that the thermal sweet spot was at the geometric centre of the heating cube, hereon referred to as the geometric centre. Single shots at low power and low DC were then used to thermally align with greater accuracy (the JC200 is accurate to 1 mm in all coordinates). As this was not an exercise in calibration, the mounted 3D positioning gantry, such as that used in hydrophone calibration, was not required. The reference thermistor was used to obtain the bulk tissue temperature, and all other thermistors and the FOH were used to measure off centre and peripheral temperatures.

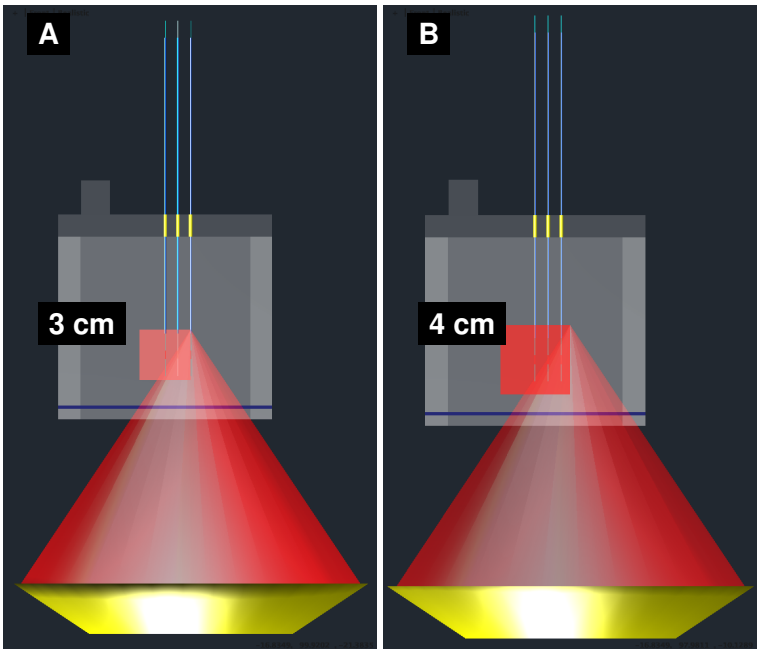


Figure 2.22: Modelling of the JC200 transducer incident FUS beam against the phantom using AutoCAD. A cone with a base diameter of 20 cm and a height of 15 cm was used to model the FUS output from the JC200 transducer, closely matching that of the transducer previously described. **A:** No clipping of the incident FUS observed when focus positioned in the extremity of the 27 cm^3 heating cube. **B:** Negliable clipping of the incident FUS observed when focus positioned in the extremity of the 64 cm^3 heating cube.

Based on a user-defined planned volume, the JC200 is capable of generating plans for both dot mode (single shots between transducer movements) and linear mode (continuous sonication during transducer movement), (Figure 2.24). In linear mode, there is no dwell time at any point in space during sonication. This is contrary to dot mode which has a minimum exposure (dwell) time of 1 second. For example, at a 50% DC and a 100 ms PRF, the pulse length is 50 ms on, 50 ms off. In linear mode, if the transducer moves at 6 mm/s (the maximum speed, and the speed used throughout pre-clinical and clinical work presented), it means that each time the JC200 fires, the transducer will have moved 0.3 mm from the location of the last exposure. Both methods were explored at varied treatment parameters in order to optimise speed and maintenance of induction of hyperthermia.

Exp. No.	TM Config.	Planned Vol. (cc)[a]	Mode	Dot Int. (on:off:int.) / Lin. Speed	Cycles(Duty Cycle)	Ribs	Fig.
1(a)	Co-ax	27	Dot	1s:1s:2mm	1(100%)	N	2.25(A)
1(b)	Co-ax	27	Dot	1s:1s:4mm	1(100%)	N	2.25(B)
1(c)	Co-ax	27	Lin	6mm/s	2(25,25%)	N	2.25(C)
1(d)	Co-ax+FOH	27	Lin	6mm/s	4(25,10,8,6%)	N	2.25(D)
2(a)	Co-ax	27	Lin	6mm/s	2(25,25%)	Y	2.26(A)
2(b)	Co-ax	27	Lin	6mm/s	3(50,10,8%)	Y	2.26(B)
2(c)	0,45,90°	64	Lin	6mm/s	0.38(50%),0.62(20%)	N	2.26(C)
2(d)	Co-ax	64	Lin	6mm/s	0.5(50%),0.5(20%)	Y	2.26(D)

Table 2.1: Summary of *ex vivo* hyperthermia experiments performed on the JC200. A pulse interval of 100 ms / 10 Hz was used in all cases. A slice thickness of 2 mm and a row distance (minimum depth interval) of 12mm was used in all cases.

[a]The intended volume for coverage by FUS, on which the modeling and thermistor positioning was based. The resultant prescribed volume reported by the JC200 refers to the volume which is bounded by user-defined coordinates, which is used to generate FUS treatment plans, and is independent of the treatment plan parameters. In practice, prescribed volume is often considerably larger than the initially planned treatment volume, and this is thought to be due to the algorithm the JC200 uses to define boundaries from user-defined coordinates, which generates curves rather than straight lines (Figure 2.24). For example, in these particular experiments, the 27 cm^3 planned volumes resulted in a prescribed volume of ~39 cm^3 whilst the 64 cm^3 planned volumes had a prescribed volume of ~92 cm^3.

For each experiment, summarised in Table 2.1, holders loaded with liver were partially immersed into the water bath which was then filled to the highest level possible (Figure 2.19). Holders and contents were allowed to equilibrate to water temperature before any treatment plan was commenced.

The 27 cm^3 heating cube spanned a 3 cm depth (1.5-4.5 cm) from the acoustic window, whilst the 64 cm^3 cube spanned a 4 cm depth (1-5 cm). Treatments were slice-by-slice with slice thickness (distance between planes) of 2 mm, resulting in 16 slices of 3 rows each for 27 cm^3 and 21 slices of 4 rows for 64 cm^3. Slice separation of four was used in all experiments as a method to trap heat, meaning that after any given slice, the next three were skipped, before resuming the heating plan, which cycled back to the early slices rather like a modulo function.

In order to form rows in single shot (dot) mode, a 2-mm spacing was first used in

Experiment 1, followed by a 4-mm spacing in Experiment 2. In order to form rows in linear mode, the default behaviour of the JC200 is to move the transducer from the start position on any given row to the end of that row, and back to the start position, whilst exposing to FUS at a speed 6 mm/s, before stopping FUS to move onto the next row.

2.2.4 Results

The purpose of Experiment 1 was to explore the utility of linear mode over dot mode, and not necessarily to control the temperature within the tight limits, especially given the absence of ribs. Dot mode with 2 mm trans-axial separation and a row separation of 12 mm (resulting in 3 rows), took over an hour to span the entire 27 cm^3 planned volume target (39 cm^3 prescribed, see footnote in Table 2.1 for information on prescribed volume) (Experiment 1(a), Figure 2.25(A)), limiting the potential ability to treat larger tumours clinically due to the half-life of circulating drug. Coverage time was reduced to just 35 mins using a wider dot separation of 4 mm, but the same row separation, requiring 13.8 kJ (432 s of HIFU time x 32 W in continuous wave) for a ΔT of 5-10°C in the absence of ribs (Experiment 1(B), Figure 2.25(b)).

By contrast, linear mode at 25% DC covered the same target volume in under 15 minutes and slighted exceeded this ΔT requiring only 4.1 kJ, demonstrating a dramatic improvement in time and energy efficiency for volumetric hyperthermia (Experiment 1(c), Figure 2.25(C)). Using this optimised linear mode, refined control of ΔT over a prolonged period of over 45 minutes could be achieved by lowering the DC from 50% for the initial induction phase of 15 minutes to lower values for maintenance. In this case, the FOH recorded a comparable ΔT profile, validating the TM readings by an independent method (Experiment 1(d), Figure 2.25(D)).

Experiment 2 was designed to more closely reflect how the heating protocol might work in clinical practice with more considered temperature control, and explored the effect of the presence of ribs. The addition of ribs reduced the resultant ΔT by over half

(Figure 2.26(A)), and with DC control the optimal range of hyperthermia (ΔT=4-8°C) was achieved centrally in under 8 minutes and peripherally in under 30 minutes (Experiment 2(b), Figure 2.26(B)). A larger planned volume of 64 cm^3 (92 cm^3 prescribed) was covered in 32 minutes and the angle of the TM was found to be inconsequential, further validating its use in clinical cases (Experiment 2(c), Figure 2.26(C)). Even in the presence of ribs, again it was possible to achieve optimal hyperthermia across the extent of this larger volume in under 30 minutes (Experiment 2(d), Figure 2.26(D)).

Following these controlled hyperthermia experiments, none of the Experiment 2 exposure parameters shown in Table 2.23 resulted in either greyscale changes on the JC200 B-mode images or visible ablative damage when examined macroscopically. Examination was performed by dissecting *ex vivo* liver tissue into quarters initially, as per Figure 2.23, followed by further sectioning at axial depths of small intervals (<1 cm).

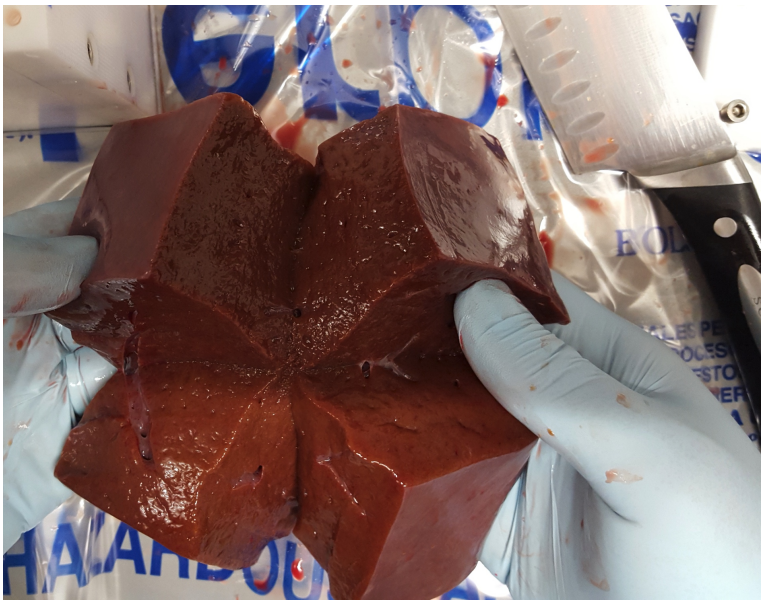


Figure 2.23: Macroscopic view of *ex vivo* liver sample from Experiment 2. Layer closest to acoustic window examined, which was treated with FUS for hyperthermia and subsequently sectioned into quarters demonstrating the absence of ablative change.

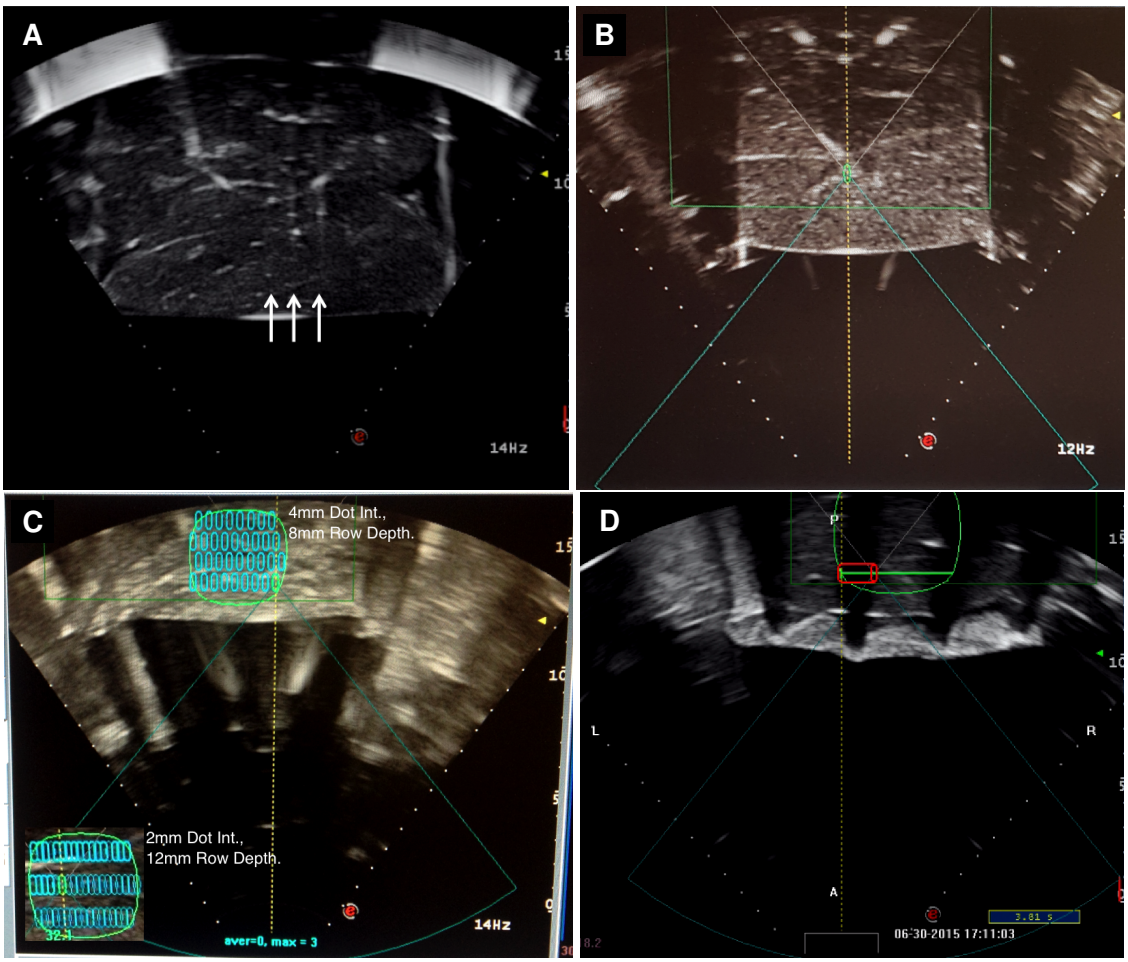


Figure 2.24: B-mode images captured on the JC200 device during *ex vivo* liver hyperthermia experiments. **A:** Experiment 2(a+b) - three co-axial needles and their thermistors entering liver co-axially, JC200 probe at 45° rotation in order to capture all probes in a single B-mode. Thermistor tips cannot be clearly distinguished, only co-axial needle shafts. **B:** Experiment 2(c) - co-axial needle is shown entering liver from the top left at 45°, with the HIFU focus approximately near the tip of the thermistor. Note the echo poor shadow distally to the co-axial needle through which the diagnostic ultrasound cannot penetrate. Also note the echogenic horizontal line to the left of the tip, which is due to a small amount of air-trapping between two layered liver sections used to fill the holder. **C:** A example of a single slice of a 27 cm^3 treatment plan covered by dot mode with 4 mm dot separation and 8 mm row separation. South-West corner inset - 2 mm dot separation and 12 mm row separation for comparison, taken from Experiment 1(b). The transducer has completed the slice and is currently on the last unit of the slice. **D:** Experiment 2(d) - rib shadowing is seen for each of the four ribs in the rib cage section, which are aligned in the axis of the foreground and background (pointing out from the page). Note the linear mode sweep is in progress (red oval), with the transducer translating to the right at 6mm/s, and the focus is just about to enter the next intercostal space. Using this system, the FUS beam does not turn on and off selectively over ribs and their spaces and energy is delivered indiscriminately, according to the treatment plan.

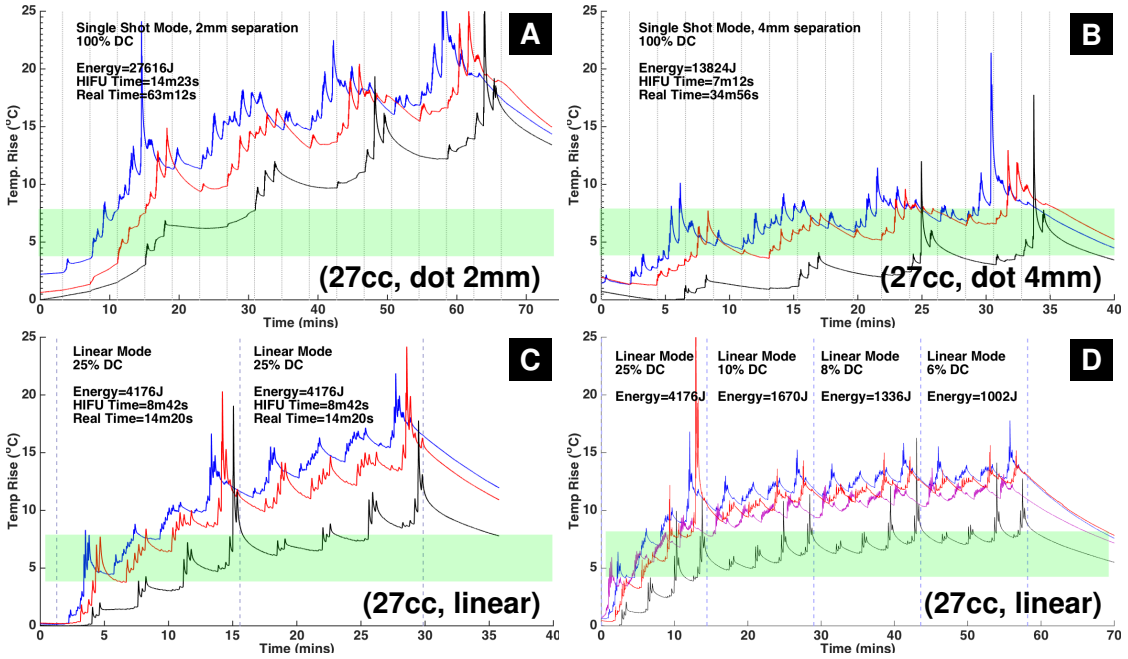


Figure 2.25: Thermometry traces obtained from several *ex vivo* liver preparations in the absence of ribs, shown as a temperature increase (ΔT) from room temperature. All plots obtained in co-axial TM configuration (Figure 2.19). Green shaded areas represent target range of hyperthermia. The blue trace represents centrally located TM, the black and red traces represent peripheral TMs. Grey dotted lines in **(A)** and **(B)** represent different treatment slices and horizontal blue dashed lines in **(C)** and **(D)** represent start and end of FUS cycles. Input energy obtained from JC200 reports and corrected for DC. HIFU time refers to time when the transducer is delivering energy as if continuous wave, and disregards DC. **A+B:** Comparison of single shot mode (one cycle, 1s on, 1s off, 100% DC) using 2 mm **(A)** or 4 mm **(B)** dot separation. **C+D:** Multiple treatments in linear mode, demonstrating the utility of DC modifications to induce and sustain central and peripheral hyperthermia. In particular plot **(D)** demonstrates maintenance of a prolonged period of hyperthermia (up to 1 hour) and validates TM temperature increases by FOH (purple=FOH and red=TM equidistant from blue central trace by TM).

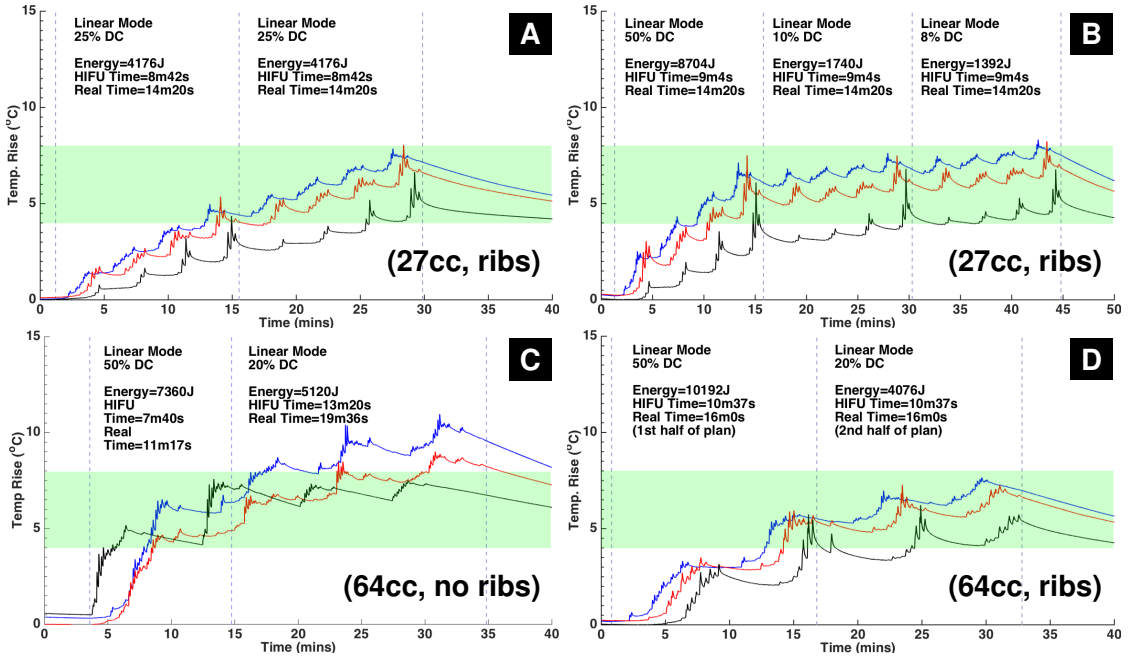


Figure 2.26: Thermometry traces obtained from several *ex vivo* liver preparations in the presence of ribs, with the exception of **(C)**, shown as a temperature increase (ΔT) from room temperature. Plots obtained in co-axial TM configuration (Figure 2.19) with the exception of **(C)** which was performed in the 0,45,90° configuration (Figure 2.21). Green shaded areas represent target range of hyperthermia. The blue trace represents centrally located and co-axially loaded TM, the black and red traces represent peripheral TMs. Horizontal blue dashed lines represent start and end of FUS cycles (**A,B**) or modification of DC (**C,D**). Input energy obtained from JC200 reports and corrected for DC. HIFU time refers to time when the transducer is delivering energy as if continuous wave, and disregards DC. **A+B**: Comparison of single shot mode (one cycle, 1s on, 1s off, 100% DC) using 2 mm **(A)** or 4 mm **(B)** dot separation. **C+D:** Multiple treatments in linear mode, demonstrating the utility of DC modifications to induce and sustain central and peripheral hyperthermia. In particular plot **(D)** demonstrates maintenance of a prolonged period of hyperthermia (up to 1hr) and validates TM temperature increases by FOH (purple=FOH and red=TM equidistant from blue central trace by TM).

2.2.5 Summary

In the confines of current practical limitations, the JC200 transducer use for the pre-clinical and clinical studies has been calibrated with a reasonable degree of confidence and its beam-form has been characterised.

An optimised exposure regime for sustained large-volume hyperthermia using the capabilities of an existing clinical USgFUS system, the JC200, has been identified. In the pre-clinical model, the use of linear mode at a fixed, low input FUS power of 32 W

has been shown to generate target hyperthermia in clinically-relevant volumes of up to 64 cm^2 in the presence of ribs, for over 30 minutes and potentially for durations on the order of several hours. By fixing the power and modifying the DC during or between cycles of the FUS treatments, it is possible to rapidly induce and maintain the required levels of hyperthermia that are required for sustained ThermoDox® release in the clinical context.

However, limitations of this *ex vivo* model are as follows:

1. Non-physiological baseline temperature
2. Absence of perfusion (both macro and micro vasculature)
3. Insulating effect of Delrin® custom holder, further reducing conductive losses
4. Absence of skin, fat and connective tissue layers
5. Absence of tumour
6. Absence of significant depth of penetration to the target

In Part I of the clinical study, real-time thermometry feedback provides the opportunity to dynamically modify parameters such as power and DC during a clinical treatment for hyperthermia. Based on these pre-clinical results, despite their inherent limitations, due to having real-time thermometry it was deemed that we could translate the heating strategies demonstrated here to patients treated in Part I of the study. The addition of the tissues (skin, fat, connective tissues) to the propagation path and the greater tumour depths seen clinically are likely to increase power requirements to levels in excess of 32 W in order to induce the required level of hyperthermia, and may of course also alter the degree of non-linearity of the ultrasound wave as it travels through different tissues such as fat. Furthermore as in the clinical case the presence of perfusion means that there are greater conductive losses away from the target tissue than pre-clinically. Consequently, it follows that once adequate hyperthermia is induced, in the clinical case it is likely that

the drop in DC required to maintain hyperthermia is less than seen in these non-perfused pre-clinical models.

Based on these pre-clinical results, when choosing initial parameters for the clinical cases these important differences were considered. The clinical thermometry data from Part I of the study is presented in Chapter 3, Section 3.2.4. With an increasing amount of clinical thermometry data for various tumour anatomies, acoustic modelling has bridged the gap to Part II of the study, where no real-time thermometry is obtained and required treatment parameters are calculated using the experience gained in Part I and mathematical modelling. This is discussed in detail in the following section. At the time of writing five patients have been treated in Part I and two patients in Part II.

2.3 Analytical Methods for Doxorubicin Delivery

A key feature of the TARDOX clinical study is that the primary endpoint relates to enhanced drug delivery to the tumour, not clinical efficacy (radiological response). In order to be able to deliver on this objective, methods needed to be developed that could reliably detect and quantify doxorubicin in blood and in small tissue samples obtained through biopsies. This section describes the development and validation of such techniques.

As previously discussed in Section 1.4.2, doxorubicin potentiates its potent anti-neoplastic effects by several mechanisms including intercalation into cellular DNA [249]. When doxorubicin is intercalated into DNA, its fluorescence becomes significantly reduced ('quenched'). This has been demonstrated in our laboratory using a simple experimental setup in which calf thymus DNA was added, at increasing concentrations, to dilutions of doxorubicin in phosphate buffered saline, and direct fluorometric analysis was then performed using a 96-well plate (Figure 2.27). The plots demonstrate that adding DNA leads to a high degree of quenching up to a transition point at which no further quenching is possible, presumably because all of the doxorubicin has already intercalated. A recent study has examined the fluorescence properties of doxorubicin more

closely using double-stranded salmon DNA [424].

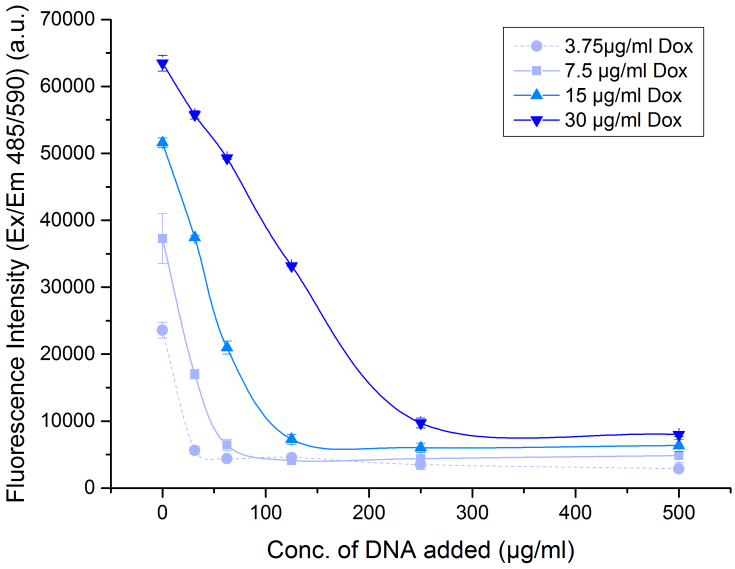


Figure 2.27: Effect of DNA intercalation on doxorubicin fluorescence. Doxorubicin (Sigma, Ref. D1515-10MG), diluted in phosphate buffered saline (PBS) to concentrations of 60, 30, 15 and 7.5 µg/mL, was mixed 50:50 with calf thymus DNA (Life Technologies, Ref. 15633-019), at concentrations of 500, 250, 125, 62.5, 31.25 µg/mL in PBS, and left at room temperature for 1 hour in the dark. 200 µL aliquots of each combination were added in quadruplet to a 96-well plate and fluorometry was performed on the Omega FLUOstar fluorometer at excitation/emission of 485/590 nm and a gain of 1300. Fluorescence was averaged and plotted for each doxorubicin concentration (n=4, error bars represent standard deviation).

Consequently in order to detect its presence in tissue *in vivo*, a method with very high sensitivity would be required to distinguish concentrations in its nuclear-bound form. Confocal microscopy, and in particular fluorescence lifetime imaging microscopy (FLIM) is one option for intracellular and nuclear doxorubicin quantification [425]. Alternatively, if the doxorubicin can first be unbound from nucleic acids and proteins, before fluorometric analysis, it is no longer quenched and thus sensitivity can be dramatically improved. The use of enzymatic digestion of nucleic acids using DNAse and RNAse enzymes was explored in our laboratory, however due to a very high binding affinity and low levels of release, success was limited and more robust methods were sought.

The following sections introduce the method development for doxorubicin quantifi-

cation in tissue and/or plasma, using three different techniques which all rely on doxorubicin's inherent fluorescence at low concentrations, namely (i) high performance liquid chromatography, (ii) direct fluorometry and (iii) confocal fluorescence microscopy.

2.3.1 Doxorubicin Quantification in Tumour and Plasma by HPLC

A sensitive, robust and validated method is required to determine intratumoral concentration of low-levels of doxorubicin in small tissue samples (biopsy) in order to evaluate the primary endpoint of the study, which pertains to enhanced doxorubicin delivery (Section 3.1.3).

Lead by the Bio-analysis Core (acknowledgements: Dr. Michael Stratford, Dr. Lisa Folkes, Dr. Kevin Myers) with scientific input from the clinical team, a Good Laboratory Practice (GLP) assay has been developed for determination of doxorubicin concentration in plasma and tissue samples. The assay has been validated and has been implemented clinically. The assay is detailed formally as a standard operating procedure (SOP) held under version control by the Good Clinical Practice (GCP) Laboratories (at time of writing: LAB/SOP/069 version 4). In this section, the procedure is presented more intuitively, with a worked example for clarity.

The assay builds on previously published techniques of liquid-liquid solvent extraction from tissue and high performance liquid chromatography (HPLC) with fluorescence detection for doxorubicin quantification in tumour lysate. These techniques have been implemented in pre-clinical models with relatively large tissue masses, due to the ability to harvest tumours in their entirety, but we present a validated technique sensitive enough to determine doxorubicin concentration in clinical samples with masses of as little as 1 mg. This is an essential feature of the assay as tissue sample is extremely limited; a liver biopsy core taken with an 18G needle is typically around 5 mg in mass [426]. For a given tissue biopsy obtained from the clinical study, as well as determining doxorubicin concentration, it is intended to perform cell viability and microscopy studies. Consequently,

in the clinical study, each sample is divided in approximate halves using a fresh scalpel blade in a sterile receiver and one half is placed in a pre-weighed cryovial (Figure 2.28), re-weighed and frozen at -80°C for subsequent processing in order to determine the concentration of total doxorubicin by HPLC, to address the primary endpoint (Section 3.1.3). Plasma samples are spun off from venous blood samples, collected in EDTA Vacutainers, and frozen at -80°C.

On the day of analysis, tissue and plasma samples are removed from the freezer and crucially, to prevent losses or introduction of impurities, stay in the vial in which they were stored until solvent extraction of the drug has been performed. The first step is to add a small volume of working solution and pure water to the vial. In particular this working solution contains daunorubicin, another anthracycline with a distinct fluorescence signature to that of doxorubicin, which is used as an internal standard for the assay. Next, a clean stainless steel ball-bearing is added to the vial, and the vial placed in a holder for homogenisation using the Mikro Dismembrator U device (Sartorius), which rapidly oscillates in order for the ball-bearing to lyse all cells (Figure 2.29). This step is carried out in a cold room to minimise doxorubicin degradation and production of its metabolites due to heat.

Following tissue homogenisation, solvent extraction is required in order to isolate doxorubicin from tissue proteins. A solvent extraction technique similar to that of Al-Abd *et al.* [427] was selected, which uses acetone and concentrated zinc sulphate solution and offers a high dose recovery. These are added to the vial, mixed thoroughly, and centrifuged at 4°C, in order to produce a supernatant containing both the anthracyclines.

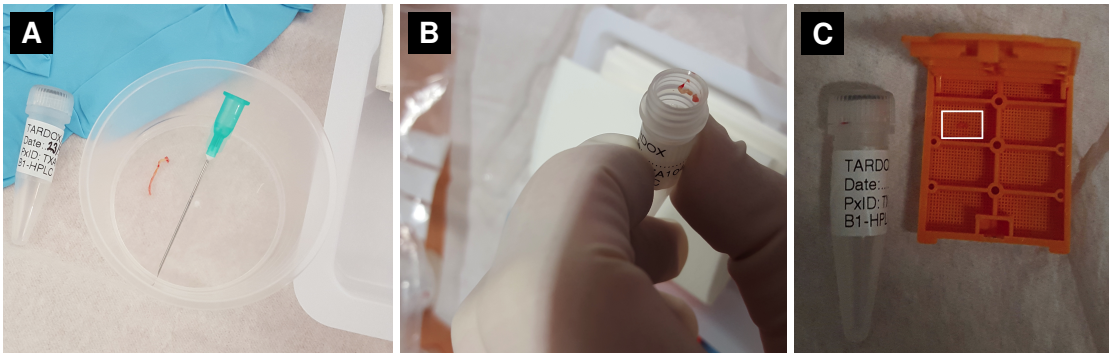


Figure 2.28: **A:** 18G biopsy core taken from a patient treated on the clinical study. **B:** Image of approximately half of this tissue mass inserted into a pre-weight cryovial from another biopsy sample. The cryovial is inserted into a ZipLock™ bag to keep it dry, and then placed on ice for transport to the Bioanalysis Core for weighing and immediate freezing at -80°C. **C:** The remaining half of the biopsy core is placed into a micro cassette (white rectangle) and fixed in formalin and paraffin embedded.

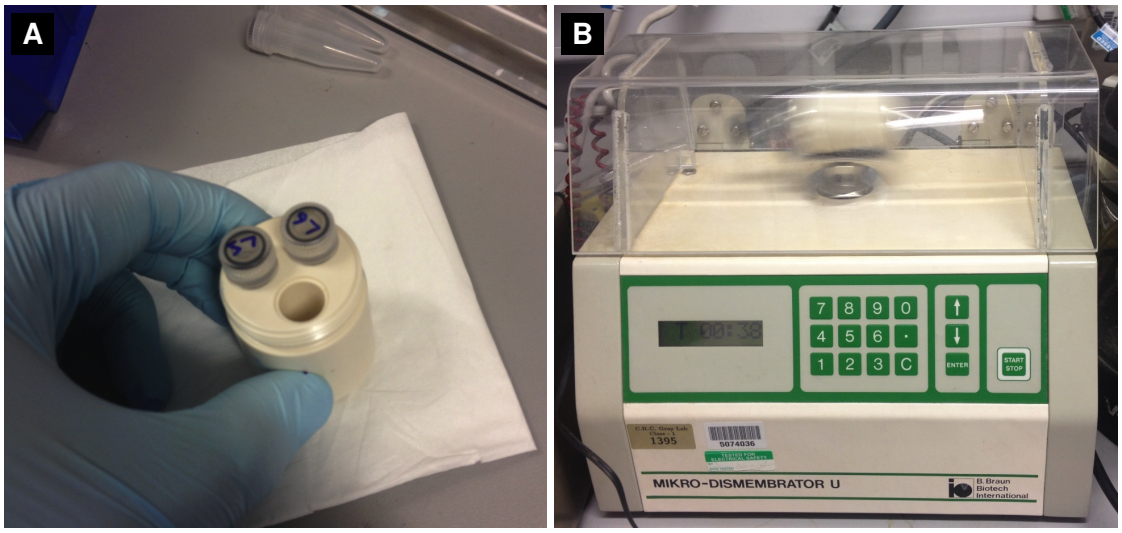


Figure 2.29: **A:** Ball-bearing and 100 µL of internal standard (IS) added to cryovial containing a tissue sample (not visible and sample loaded into a custom holder prior to replacing screw top (not shown). **B:** Mikro Dismembrator in action, demonstrating how vigorous oscillations can be used to lyse tumour tissue into a homogenate.

The majority of the supernatant is transferred to a clean brown open-top glass tube ready for evaporation to dryness, using a centrifugal vacuum evaporator. The residues from the dried extracts are redissolved in 100 µL of a predominantly aqueous solution (90% 10 mM formic acid, 10% acetonitrile), transferred to injection vials and 30 µL of each is injected onto the HPLC column via an auto-sampler using the Alliance Waters

2695 control unit (Figure 2.30). Separation of chemicals in the analyte is performed on a reverse-phase Gemini C6-Phenyl column (3 μm, 3x150 mm, Phenomenex), in which a 6-carbon chain is used as a linker to attach phenyl to the silica surface. The carbon chains make the silica hydrophobic, allowing compatibility with aqueous-based polar solvents.

The solvent is pumped through the column at high pressure, and is predominately aqueous phase. 10 mM formic acid is used as the aqueous phase and mixed with a smaller amount of organic phase, pure acetonitrile. An elution gradient is used such that the solvent begins at just 12% organic phase, which over time increases to 40% and then drops back to 12%. When the gradient is such that the affinity of the anthracyclines for the solvent is greater than that for the column, then they will move through the system more quickly. The gradient thus helps to reduce the run time whilst ensuring there is an adequate difference in elution time between doxorubicin and daunorubicin, due to subtle differences in their affinity to the column, such that their fluorescent peaks can be distinguished because of differences in their chemical structures. As the analyte elutes off the column the anthracyclines are detected using the Alliance Waters 474 fluorescence unit configured for excitation/emission at 480/560 nm. Fluorescence chromatograms are generated for automated analysis by the Empower Chromatography Data Software.

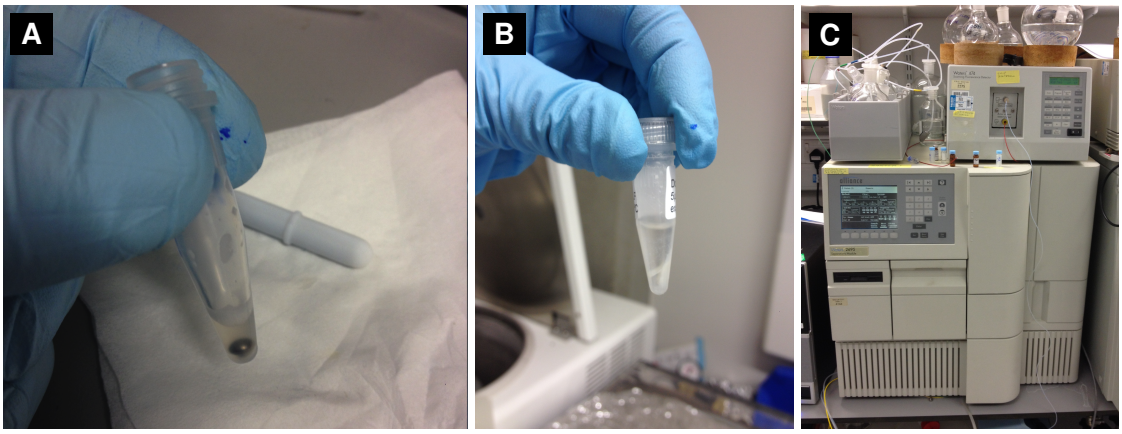


Figure 2.30: A: Cryovial containing steel ballbearing prior to its removal with a magnet. **B:** Cryovial demonstrating separation layers post solvent extraction (for a plasma sample), with protein precipitate separating the two layers. The majority of the supernatant is isolated using a pipette, and contains the analytes and IS. **C**: Alliance Waters 2695 Control Unit (base device) and Alliance Waters 474 Fluorescence Unit (on top).

In order to validate clinical results, pre-prepared quality control samples containing known concentrations of doxorubicin were run before and after the patient samples, and in addition blank samples were run. Using this method, HPLC results can be used to calculate doxorubicin tissue concentrations, and indeed plasma samples (which do not even require the homogenisation step).

A plasma calibration curve is generated by spiking commercially available plasma (50 μL) with doxorubicin at pre-determined concentrations. Recall that each sample for injection also contains the internal standard, added as a 100 μL aliquot at a concentration of 1 μg/mL, prior to solvent extraction, and consequently the ratio for the area under the peaks for both can be calculated and plotted with linear regression. A typical peak-area ratio table used to generate the calibration curve is illustrated in Table 2.2. Values from tables such as this can be used to calculate concentrations of doxorubicin for any clinical plasma or biopsy analyte, and for this example, this is illustrated in Figure 2.31).

Dox. Conc. μg/mL	**Peak area ratio: Dox./Int. std.**	**Calc. Dox. Conc. μg/mL**	**% Deviation from Nominal Conc.**
0.10	0.08	0.10	0.0
0.20	0.17	0.20	1.0
0.50	0.42	0.49	-2.0
1.00	0.83	0.96	-4.7
2.00	1.76	2.03	1.5
5.00	4.56	5.23	4.6

Table 2.2: Calculated values and percentage deviation from nominal concentrations for an illustrative plasma calibration curve. Peak area ratios obtained from spiked plasma samples using the HPLC device at the Bioanlaysis Core. Doxorubicin concentrations calculated using Empower software.

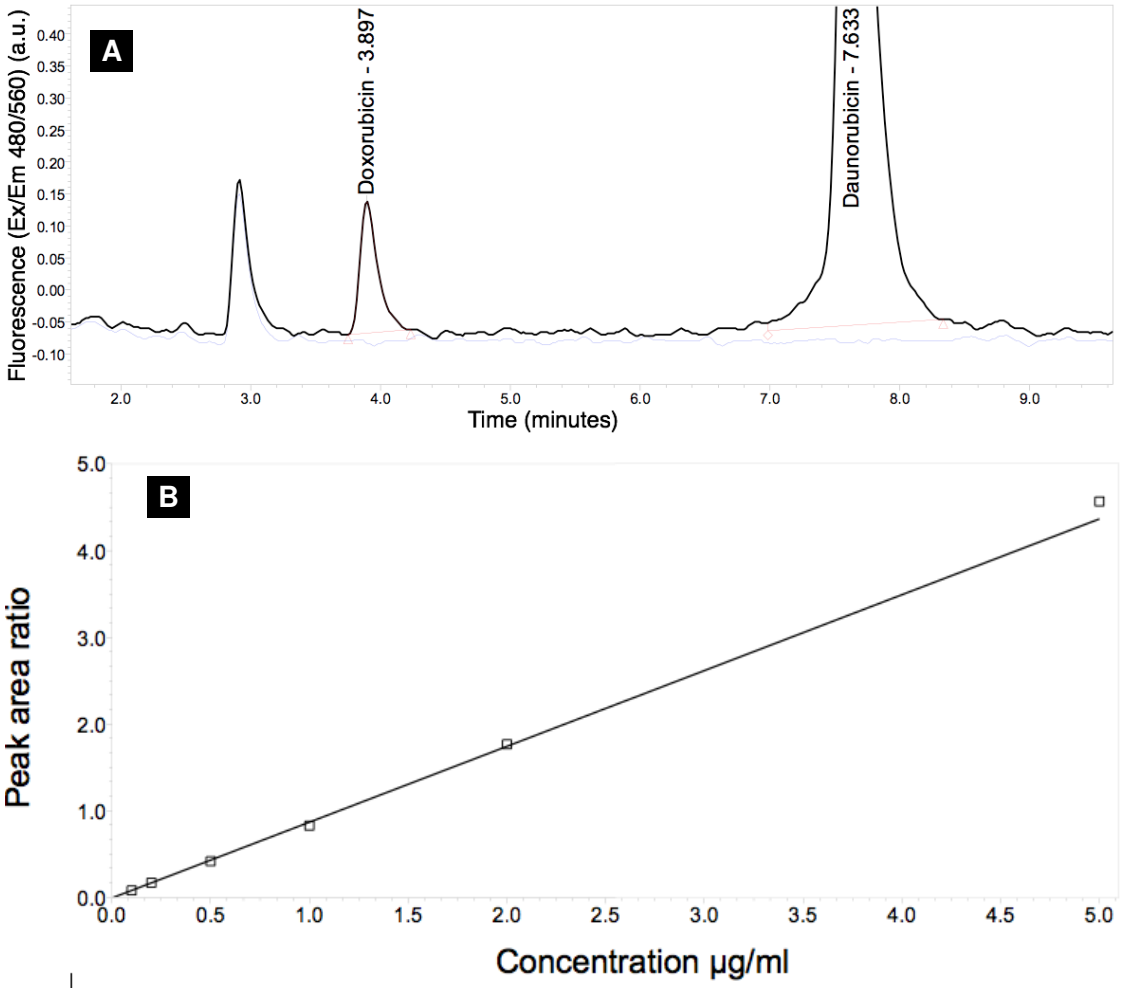


Figure 2.31: A: Illustrative HPLC Chromatogram obtained for the 0.1 µg/mL standard for the plasma calibration curve, with the daunorubicin internal standard and a blank plasma control extract (faint blue line). Note that for the particular elution gradient used here was used for the first two patients in Part I of the study. Over a 10 minute run time, doxorubicin elutes at 3.9 minutes and daunorubicin at 7.6 minutes, and the 'control peak' at 3 minutes, also appearing in the control plasma, is thought to be due to fluorescence from plasma proteins or possibly chemical sample impurity and can be ignored. **B:** Plasma calibration curve demonstrating the linear relationship between concentration of doxorubicin and fluorescence intensity following extraction of spiked control plasma. Acknowledgement: Dr. Michael Stratford.

The Empower software automatically looks up the Dox/IS ratio on the calibration curve, such as the one shown, generated during the same batch of HPLC runs. The software can then be used to calculate the concentration of doxorubicin in the analyte and derive the concentration of doxorubicin in the original plasma or tissue sample. A worked example best illustrates this calculation in practice for a plasma sample:

1. For a plasma analyte obtained from the extracted plasma component, if the area under the doxorubicin peak was 9.0 and that of the daunorubicin peak was 2.0, the peak area ratio would be 4.5.

2. By reading our peak area ratio off the calibration curve, we can see that we have extracted 5 μg/mL of doxorubicin from our injection of 30 μL of reconstituted analyte, which equates to 0.15 μg in total.

3. Thus in our full 50 μL volume of analyte we have recovered $0.15x(100/30) = 0.5$ μg in total.

4. If 0.5 μg of doxorubicin was extracted from an original plasma sample aliquot of 50 μL before solvent extraction, we can infer that the plasma must have contained 10.0 μg/mL of *total* doxorubicin at the time of sampling, assuming the dose was evenly distributed in the venous circulation. Note that this assay is unable to distinguish liposomal doxorubicin from released doxorubicin in the plasma sample, and this is addressed by a second plasma assay (Section 2.3.2).

Again, a worked example best illustrates the calculation in practice for a tumour sample:

1. For a tumour analyte obtained from a 2 mg tissue mass, if the area under the doxorubicin peak was 0.84 and that of the daunorubicin peak was 2.0, the peak area ratio would be 0.42.

2. By reading our peak area ratio off the calibration curve, we can see that we have extracted 0.5 μg/mL of doxorubicin from our injection of 30 μL of reconstituted analyte, which equates to 0.015 μg in total

3. Thus in our full 50 μL volume of analyte extracted from 2 mg of tissue we have recovered 0.05 μg in total

4. If 0.05 μg of doxorubicin was extracted from an original tissue mass of 2 mg before solvent extraction, we can infer that the tumour must have contained 25.0 μg/g of doxorubicin at the biopsy site, assuming that the density of liver is 1.0 g/cm^3.

These examples are for illustrative purposes and are not based on real clinical data. However, the examples reflect that the concentrations of doxorubicin expected to be found in the tumour extracts will be much lower than that of plasma samples. Consequently, in practice the patient plasma is diluted 10-fold in control plasma before extraction, so that they therefore can be analysed with the same calibration curve as the biopsies, and readjusted for dilution following these calculations.

Clinical results are subject to the following run acceptance criteria, also defined in the analytical plan:

- The determined concentration of calibration standards must be less than 15% deviation from nominal concentration
- Linear regression fit must have a correlation coefficient of >0.99
- The quality control (QC) samples (0.06, 0.5 and 4 μg/mL of doxorubicin in plasma), run in duplicate both pre- and post- patient samples must be within 15% of their nominal value
- Plasma blanks should have minimal or no interference at the doxorubicin and daunorubicin elution times (blank controls)
- In addition retention time is checked in case of drift, which is expected to be minimal

Plasma samples, once spun off from EDTA tubes of whole blood, are extracted using the same technique as biopsy samples, but without homogenisation step, typically during the same HPLC run as the biopsies. Clinical HPLC results can be found in Section 3.3.

For application to the clinical samples, extensive validation work has been performed including the following (acknowledgement: Dr. Lisa Folkes):

1. QCs include intra- and inter-assay plasma source variations, using plasma from three different single sources

2. Specificity using blank plasmas to demonstrate the absence of interfering peaks at doxorubicin and daunorubicin elution times (Figure 2.32)

3. Lower limit of quantification (LLOQ) has been validated to 0.05 µg/mL and the lower limit of detection (LLOD) remains undetermined

4. Inter- and intra-day precision and accuracy

5. Dose recovery, which is discussed below

6. Stock stability, validating samples frozen at -80°C, for up to two freeze/thaw cycles and at room temperature for 1 hour

This list serves as an overview of the validation work performed and in depth discussion of the finer details is outside of the scope of this chapter. Further information in the form of a validation report (GI/VAL/015) is available from the Bioanalysis Core.

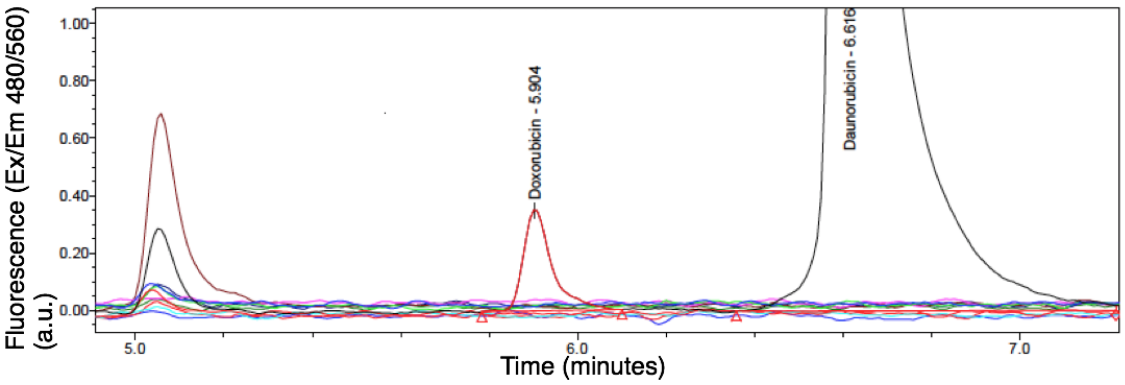


Figure 2.32: Chromatograms of blank plasmas from 10 individuals, only one sample was spiked with 0.1 µg/mL doxorubicin and to another sample, the internal standard was added prior to solvent extraction. Note this assay uses a different elution gradient, used from the third patient onwards, and demonstrates a later elution times of 5.9 minutes for doxorubicin and 6.6 minutes for daunorubicin.

Dose recovery is an important consideration; it should be high enough to avoid compromising sensitivity, and it should also be independent of concentration so that it does not bias results. Validation work has shown that the dose recovery is typically around 75%. This is in part due to incomplete solvent extraction and because it is impractical to take the full volume of supernatant after solvent extraction. As all standards are made up in plasma, a biological matrix, this means that any losses seen in the clinical samples will also be reflected in the standards. Making up the standards in plasma was a primary consideration of the assay design. In the case of clinical tissue samples, as it is not practical to make up realistic standards using a tissue matrix, again plasma is used as a surrogate biological matrix and it is assumed recovery will be the same. Due to normalisation of results by the internal standard, any losses during processing will be accounted for and therefore will not influence the final determined concentrations.

2.3.2 Doxorubicin Quantification in Plasma by Direct Fluorometry

It is understood that in the case of systemically-circulating ThermoDox®and the absence of a release-trigger, the vast majority of doxorubicin will remain encapsulated both in the intra- and perivascular spaces for some hours, due to its high stability at body temperature. The majority of intravenously administered liposomes are rapidly taken up by the MPS, predominately in the liver [428]. PEGylation significantly extends the circulation time of ThermoDox® (Figure 1.5) and evasion of the MPS is thought to be one of the major underlying mechanisms for this [429].

Celsion Corporation, the manufacturer of ThermoDox®, and several other research institutions have performed a number of *in vivo* studies which have examined the plasma pharmacokinetics of ThermoDox® in rats, rabbits, dogs and pigs (ThermoDox® Investigator's Brochure, unpublished, confidential & proprietary). Whilst many of these studies have compared the concentration of total circulating doxorubicin in groups receiving ThermoDox® or free doxorubicin, pre-clinical data on the proportion of circulating dox-

orubicin which remains encapsulated post-injection is yet to be published. One clinical study by Poon & Borys attempted to elicit this for patients with primary liver tumours who received ThermoDox® and RFA [316]. However, unfortunately the methodology used to identify the relative proportions free vs. encapsulated doxorubicin has since been identified as being flawed and the publication is pending a revision. Only the total doxorubicin can be interpreted (Figure 2.33).

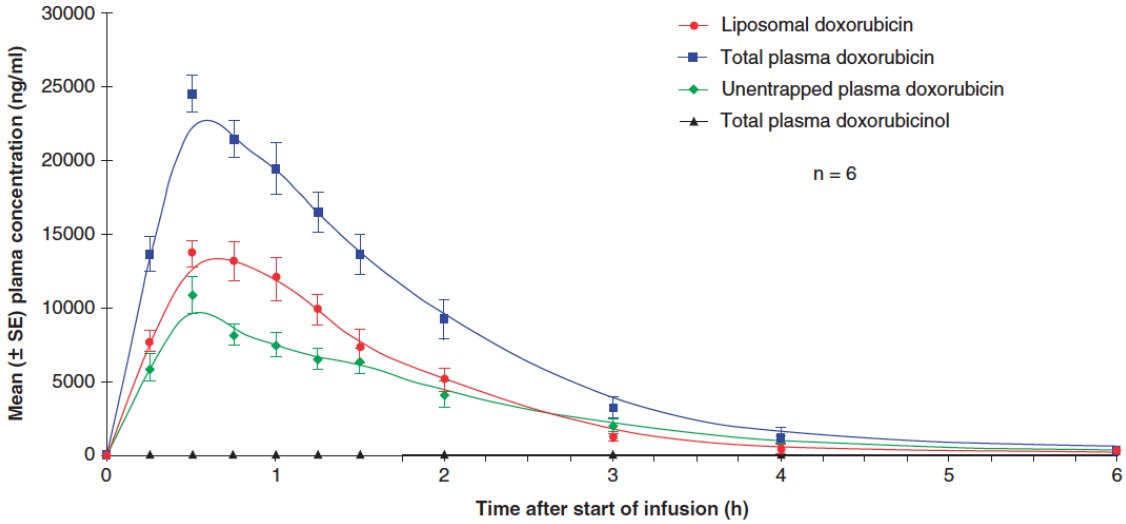


Figure 2.33: Average total, encapsulated and free plasma doxorubicin concentrations for six hours following a 50 mg/m^2 infusion of ThermoDox® in six liver cancer patients treated with ThermoDox®+RFA. Maximal levels of doxorubicin are demonstrated immediately following the 30 minute infusion. Reprinted from Expert Opinon on Pharmacotherapy, 2009; 10(2): 337, Poon & Borys, Lyso-thermosensitive liposomal doxorubicin: a novel approach to enhance efficacy of thermal ablation of liver cancer, with permission from Taylor and Francis (http://www.tandfonline.com) [316]. Due to a potential misinterpretation in the quantification method for encapsulated and free doxorubicin used in this study, only the total plasma doxorubicin can be interpreted with confidence.

The concept of long circulating unreleased ThermoDox® is supported by previous *in vivo* studies at our institution. Using CD-1 nude mice bearing HCT-116 tumours, targeted tumour drug delivery was performed using HIFU with ThermoDox®. Pharmacokinetic analysis was able to demonstrate that ThermoDox® remains encapsulated in the circulation, and that HIFU moves doxorubicin out of the circulation into the tumour (Figure 2.34). Of note, the pharmacokinetic assay used to determine plasma concentrations of

doxorubicin was able to distinguish released from unreleased ThermoDox®. These results are of great relevance, as not only do they demonstrate efficacy of the delivery method *in vivo*, they emphasise the potential of capturing plasma pharmacokinetics in better understanding the mechanism of intratumoral delivery.

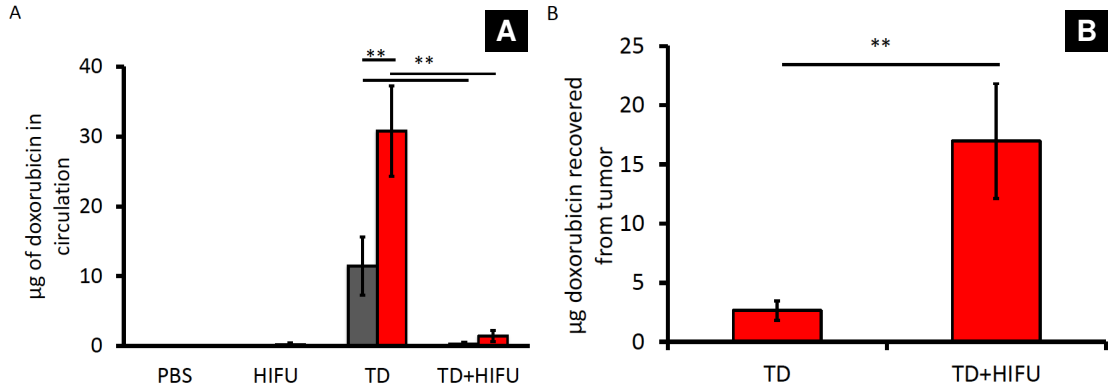


Figure 2.34: Plasma and tumour pharmacokinetics for a small animal *in vivo* study combining ThermoDox® and HIFU, performed in Oxford. Fluorescence values were obtained using an Omega FLUOstar well-plate reader at 485/590 nm excitation and emission. Mice were injected with 80 µg of ThermoDox® and HIFU exposure of the tumour performed at 1.06 MHz using three repeats of a 9x9 rasta scan of continous wave, 6 second bursts for approximately 20 minutes in total. **A:** Plasma samples were taken and analysed for fluorescence without heating (grey bars) and then heated to achieve full release and re-measured (red bars). Results of the plasma pharmacokinetic studies indicate that ThermoDox® was effectively removed from the circulation in the group receiving HIFU exposure. Furthermore in the group receiving ThermoDox® alone, there was an approximate 3-fold increase in fluorescence intensity following heating of plasma samples, demonstrating that circulating doxorubicin remained in liposomal form. **B:** The total tumour doxorubicin load was calculated by excising and homogenising tumours and comparing fluorescence to identically treated tumours spiked with known ThermoDox® concentrations, demonstrating that the circulating ThermoDox® removed from the circulation in the HIFU-exposed group is shifted into the tumour, resulting in approximately 8-fold increase in intra-tumoural concentration of doxorubicin over the group receiving ThermoDox® alone. N = 3, standard deviation shown, ** = $p<0.005$. Results representative of 2 experiments. Acknowledgement: Prof. Robert Carlisle. (Unpublished)

For any liposomal formulation the natural fluorescence of doxorubicin becomes quenched, when encapsulated to high efficiency [430]. This means there is an opportunity to measure the relative fluorescence of a plasma sample both before and after a dequenching step, in order to demonstrate if the majority of the doxorubicin remains in its encapsulated form, or if it has been released in its free, or *bioavailable*, form. Several dequenching assays have been used in pre-clinical studies typically involving chemical (solvents or de-

tergents) or mechanical (homogenisation) disruption of the liposome. For ThermoDox®, hyperthermia provides another convenient release method, and indeed has been used with fluorometric assays to characterise its release properties pre-clinically, both in our institution and by the manufacturer (Figure 1.5). There are alternative methods to dequenching assays, including micro filtration. Indeed such a technique is used to analyse the encapsulation efficiency in the manufacture of ThermoDox®. However this technique comes at the disadvantage of expense and a requirement for filter maintenance, where as the selected method is cheap and has a low maintenance overhead.

The HPLC assay previously presented (Section 2.3.1) can be used to quantify the total circulating doxorubicin concentration in any clinical plasma sample. Typically no further assay would be required as it would be unnecessary duplication and discrepancy between the assays may leave results open to interpretation. However given the lack of clinical data in this regard, that we have excess plasma and can determine the quenching-ratio with relative ease, an additional dequenching assay has been included in the study, which serves to provide a richer understanding of the delivery pharmacokinetics in the clinical context. The dequenching assay used for plasma samples obtained on the clinical study is presented in the remainder of this section. The assay must be run on the day of sample collection, as freezing the samples would result in liposomal fracture. The same principles cannot be applied for measuring release properties of the tumour sample, as the homogenisation and solvent extraction steps required to obtain the analyte for fluorometry, are themselves both dequenching methods.

In the plasma quantification assay discussed, using doxorubicin's natural fluorescence, the concentrations are read from a standard curve prepared in a similar biological matrix (mixed-pool human plasma, MPHP). Whilst the concentrations referenced from the curve for heated samples are a true representation of the total doxorubicin levels, comparable to the HPLC values, one must interpret the results for unheated samples with care; the fluorescence values are quenched and thus do not represent absolute concentrations. The unheated concentrations must be taken in the context of the heated counter-

parts; the 'quenching-ratio' can be derived by dividing the fluorescence of the heated by the unheated plasma sample. From this ratio, one can get an impression of the proportion of the total doxorubicin that was in liposomal form at the time of sampling. For example, if the heated and unheated samples read similar concentrations from the standard curve, it would imply the sample largely consisted of free doxorubicin. Conversely clinical-grade ThermoDox® is highly encapsulated and has a quenching-ratio of ~3-fold (Figure 2.35) or more (Section 3.3.2) and thus plasma samples demonstrating similar ratios can be interpreted to have similarly high levels of encapsulation. Using this method, it follows that clinical plasma samples that demonstrate a quenching-ratio of between 1 (fully-released) and the upper limit for a given batch (fully-encapsulated) are partially-released or mixed samples.

The assay is detailed formally as a work instruction held under version control by the Good Clinical Practice Laboratories (WIN/041). In the remainder of this section, the procedure is presented intuitively, with a worked example for clarity.

Aliquots of the top calibration standard, containing 32 μg/mL of doxorubicin, were prepared in advance in MPHP, and frozen. At the time of the assay, one of these standards is defrosted and a 2:1 serial dilution in MPHP is used to prepare doxorubicin standards through 16, 8, 4, 2, 1 and 0.5 μg/mL. In addition pre-prepared QC samples at high, medium and low concentrations of doxorubicin in MPHP are defrosted.

Patient plasma is taken off ice and equal aliquots from each sample are transferred into paired eppendorfs and diluted 1 in 2 in MPHP. One of the eppendorfs is heated in a water bath for 15 minutes at 42°C, validated for full release, whilst the other is kept at room temperature. In duplicate, each of the standards, QCs and clinical plasma samples (heated and unheated, diluted 1 in 2) are plated on a 96-well plate along with MPHP blanks, in 200 μL aliquots. The plate is read directly on a fluorometer (Omega POLARstar OPTIMA plate reader) using an excitation/emission of 485/590 nm. No internal standard is used in this assay, as with the HPLC assay, as the fluorometer cannot

distinguish emitted light between closely related wavelengths and can only detect total emissions. A blank-corrected four-parameter linear regression fit is calculated to generate a standard curve using specialist software (Figure 2.37), and quenched and total doxorubicin concentrations can be referenced from the standard curve using averaged unheated and heated readings respectively.

To illustrate how the dequenching assay works in practice, a clinical-grade ThermoDox® vial for pre-clinical use, containing doxorubicin at a concentration of 2 mg/mL, was defrosted from the -80°C freezer and diluted in MPHP to make a standard curve, with a top nominal doxorubicin concentration of 32 µg/mL. Fluorescence was measured in heated and unheated standards using the same methods and equipment as per the standard operating procedure. An approximate 3-fold increase in the fluorescence intensity after heating to maximal release was observed (Figure 2.35).

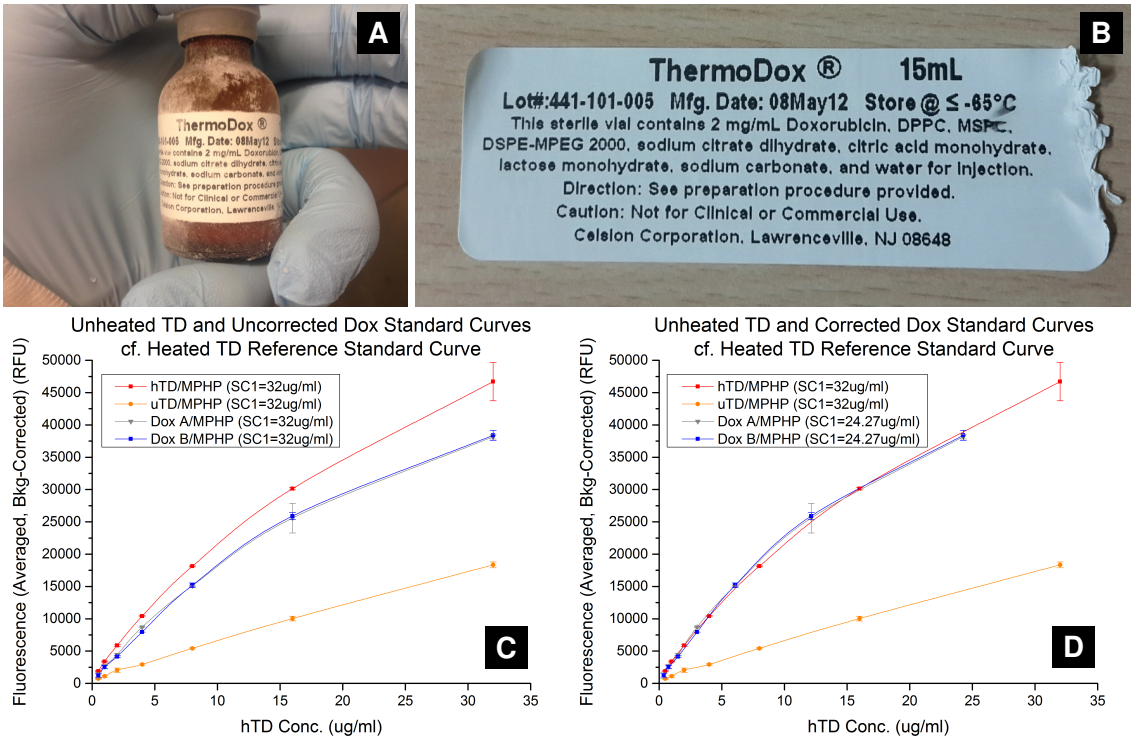


Figure 2.35: A-B: Clinical-grade ThermoDox® vial **(A)** and its label **(B)** supplied by Celsion Corporation for pre-clinical use (Lot: 441-101-005). **C:** ThermoDox® release profile assessed against two uncorrected independently prepared doxorubicin calibration curves (Dox A and Dox B) in the GCP lab. **D:** As for (C) with corrected concentrations. RFU=Relative Fluorescence Units. uTD=unheated ThermoDox® hTD=heated ThermoDox®.

These fluorescence curves were plotted against two standard curves for the same nominal concentrations prepared by independent operators, using an initial batch of pre-prepared doxorubicin standards, frozen at -20°C. The first plot demonstrates the heated ThermoDox® curve reads higher than the two doxorubicin standard curves, which demonstrate an approximately one third reduction in fluorescence intensity. This suggests that the top doxorubicin standards were too dilute or the ThermoDox® preparation was too concentrated relative to the intended (nominal) concentration.

Using the method previously described (Section 2.3.1), HPLC was used as an independent means to verify the doxorubicin concentration of the contents of the same ThermoDox® vial and the initial batch of standards and QCs. It was identified that the ThermoDox® concentration was within 1% accuracy, whilst the nominal concentration of the doxorubicin and QCs was approximately a third lower than anticipated. It is believed this discrepancy was the consequence of issues around solubility and degradation. In particular, (i) difficulties concerning dissolving doxorubicin powder into small volumes of plasma directly when making up the initial standards and QCs, leading to use of mild heating and degradation, (ii) losses due to adsorption and degradation in polypropylene containers [431], and, (iii) degradation of items over time during their storage in a -20°C, rather than -80°C, freezer. Further HPLC analysis was performed six-months later, which revealed the appearance of new decomposition products, which were not present in an earlier HPLC analysis of aliquots of the same items (Figure 2.36). Subsequent work has demonstrated that doxorubicin is unstable in mixed pool human plasma when stored at -20°C, with a very high level of degradation of doxorubicin (circa 90%) in all standards and QCs at 1 year, whilst at -80°C, degradation has been shown to be negligible over the same period of time. Thus the dequenching assay has been modified and revalidated based on doxorubicin stocks stored in plasma at -80°C (Section 3.3.2).

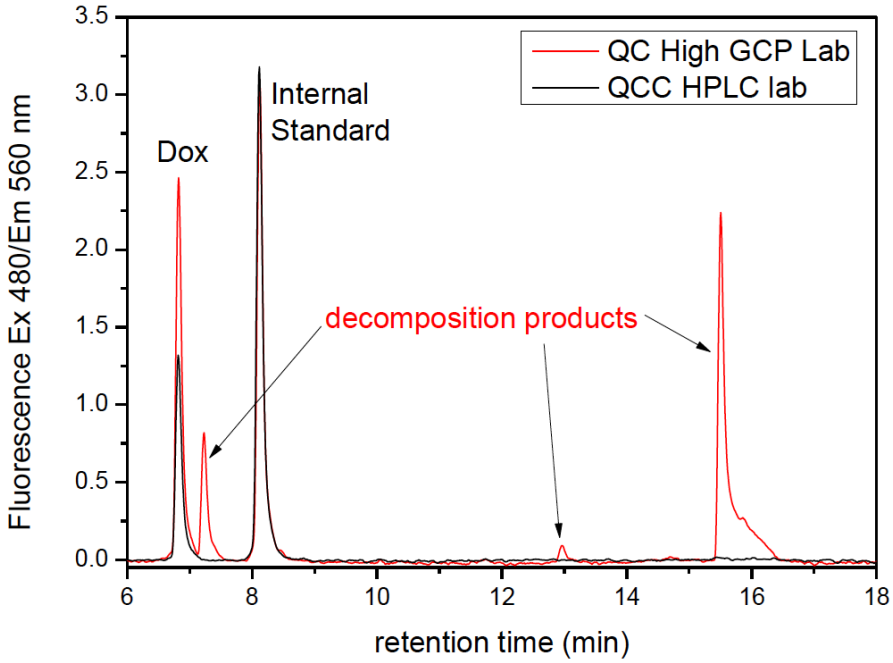


Figure 2.36: HPLC analysis of an inital batch of QC samples prepared for the plasma dequenching assay, subsequently stored at -20°C for 6 months before analysis, demonstrating doxorubicin degradation products. Performed using same HPLC method as previously discussed in Section 2.3.1

Due to the degraded standards and QCs, only the absolute fluorescence readings for the plasma samples obtained from the first four patients can be used with certainty and the corresponding concentrations can only be estimated using an averaged standard curve subsequently generated from validated standards (Figure 3.35). Since the problem was identified, standards and QCs were remade using an ultra-sonicator to dissolve doxorubicin powder into a small volume of PBS, before MPHP, avoiding the need for heat. New items have been stored at -80°C in line with HPLC validation work demonstrating long-term stability at this temperature. Before freezing, the standard curve and QC stock solutions were analysed by HPLC and concentrations were found to be within 1% of the stocks previously prepared in the Bio-analysis Core. The standard curve generated for these stocks is shown in Figure 2.37. The plasma from the fifth patient forward has used these new standards and QCs and thus the standard curves can be relied upon to derive doxorubicin concentrations, subject to continued stability testing with HPLC. The

clinical results for the dequenching assay can be found in Section 3.3.2.

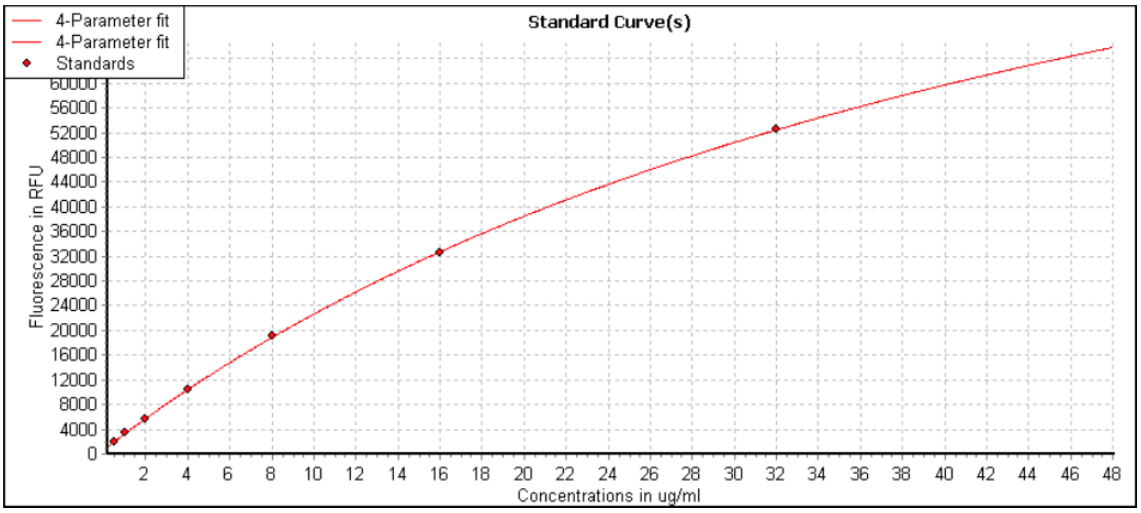


Figure 2.37: Doxorubicin standard curve prepared in MPHP to mimic the clinical biological matrix, derived from a serial dilution of top standard of 32 µg/mL in MPHP during validation of the assay. Curve generated using the Omega MARS Data Analysis Software to calculate a four-parameter linear regression fit from blank-corrected and averaged fluorescence values obtained over duplicate wells on a 96-well plate.

2.3.3 Doxorubicin Delivery Studies by Fluorescence Microscopy

The mechanism for nuclear uptake of free doxorubicin has previously been discussed in Section 1.4.2. As the cell nucleus is the main 'sink' for doxorubicin, it follows that in the minutes following injection, the more ThermoDox® that is released in the tumour vasculature or interstitium (Figure 1.6), the higher the nuclear concentration will be (up to a point of saturation). However, at around 2 hours post-exposure and at the point of apoptosis, one *in vitro* study using the HeLa cell line has demonstrated that the fluorescence of nuclear doxorubicin may rapidly decrease [425]. In our clinical study, the timing of the final biopsy immediately after the FUS exposure (Figure 3.2), which is typically of duration of 45-90 minutes, represents a convenient post-delivery window to obtain tissue for immediate fixation, ideally before significant apoptosis ensues and nuclear doxorubicin fades.

One of the key study aims concerns how to evidence the release of doxorubicin from ThermoDox® achieved using FUS (Section 1.5.3). Whilst doxorubicin remains encapsulated as ThermoDox® it is non-bioavailable and can only be enter the cell by one of the mechanisms previously discussed (Section 1.4.3). In the first few hours following infusion, and at the time of tissue biopsy, there is little time for these slower processes to occur to any great extent following extravasation by the EPR effect [290, 291]. Thus, in the absence of a release trigger, such as FUS-mediated hyperthermia, negligible doxorubicin is expected to become nuclear-bound in the first few hours following infusion.

Using an *in vivo* murine tumour model, one study by Laginha *et al.* has distinguished bioavailabile and non-bioavailable doxorubicin in tumour tissue following delivery of free doxorubicin and liposomal doxorubicin formulations [303]. The study emphasises that, in the case of liposomes, only released drug has biological activity. Consequently a method to estimate the bioavailable fraction is presented, by comparing extracted levels of drug between isolated nuclei and whole tissue [303]. The study postulates that nuclear doxorubicin provides a reasonable first approximation to bioavailable doxorubicin in cells. The study also demonstrated that, by passive delivery alone, the maximum intratumoral drug concentrations were reached at 30 minutes for free doxorubicin and 24-48 hours for Doxil™, the latter having a dose area under the curve the first 7 days ($AUC_{0\text{-}7}$) of 87- and 45-fold higher for total and nuclear doxorubicin respectively.

Thus in the tissue biopsies obtained from the clinical study, the demonstration of nuclear doxorubicin in the tissue sample obtained post-infusion and post-FUS would provide strong support of the hypothesis of FUS-mediated release. The absence of nuclear doxorubicin in samples obtained post-infusion but pre-FUS would further strengthen this hypothesis. The exploratory endpoint which examines this hypothesis of FUS-mediated release is detailed in Section 3.1.3.

Flow cytometry and microscopy were both considered as potential methods to evidence nuclear doxorubicin in tissue obtained on the clinical study. One previous study has

utilised flow cytometry to quantify intracellular doxorubicin directly in cell lines [432]. Another study, also using flow cytometry, has employed an indirect method to quantify nuclear accumulation of doxorubicin in cell lines, based on competition for nuclear binding sites with a Hoechst stain [433]. This method could potentially be combined with the cell recovery method which is introduced in Section 2.4.1. Where flow cytometry gains in its ability to rapidly quantify without subjective bias, this comes at the cost of qualitative information regarding tumour morphology and doxorubicin distribution, which only microscopy analysis of tumour sections can offer. In addition, due to small biopsy masses, cell yield may be as small as a few hundred cells, which permits only a single flow-cytometry run, thus limiting versatility of the assay.

In our laboratories, using fluorescence microscopy, an *ex vivo* mouse liver model was used to demonstrate the rapid nuclear uptake and diffusion capabilities of free doxorubicin into liver tissue. The liver was harvested immediately after sacrifice. Within 90 minutes of harvest, small sections (~50 mg) were cut with a scalpel and immersed into Dulbecco's Modified Eagle's Medium (DMEM), spiked with doxorubicin (Apollo Scientific) at concentrations of 10 and 100 μg/mL. The concentrations used are on the order of, and over 30-fold of, cytotoxic doses typically used in *in vitro* cell line suspension studies [434] (5 μmol = 2.72 μg/mL). The tissue was left at room temperature in the dark for 1 or 3 hours before retrieval, DMEM wash and fixation in 4% formaldehyde overnight, followed by subsequent paraffin embedding. The Leica TP1050 Tissue Processor was used to dehydrate the samples and the ThermoScientific Histostar Paraffin-embedder was used to embed them. Paraffin sections were cut at 4 μm using the Leica RM2235 Microtome. Without using a permeabilisation step, the slides remained waxed and were mounted using a hard-setting DAPI mounting media and a coverslip of thickness compatible with the confocal microscope. DAPI is a fluorescent nuclear stain which stains both permeabilised cells, and to a lesser degree, live cells.

Microscopy analysis, performed within 1 week, revealed that doxorubicin freely penetrated into the nuclei in the surrounding periphery of the tissue section at easily de-

tectable levels at 1 hour, even at the lower dosing concentration. However, using this particular standard fluorescence microscope (Nikon Eclipse Ti), doxorubicin could not be distinguished from background fluorescence at tissue penetration depths of greater than ~300 μm. Incubation time increased nuclear intensity in the periphery but did not appreciably increase depth of penetration, where as the higher concentration dramatically improved the depth of penetration even at 1 hour. Given this experiment is *ex vivo*, clearly its findings are of limited value, but nevertheless serve to demonstrate both the role of fluorescence microscopy in identifying nuclear doxorubicin and the unhindered penetration of free doxorubicin through healthy liver tissue when in high concentration, even in the absence of an active circulation.

The dose of intratumoral doxorubicin required to exhibit therapeutic effects *in vivo* is dependent on several factors including the tumour type, bioavailability, peak levels as well as exposure levels over time (AUC). This said, in pre-clinical studies, values of around 18-20 μg/g of total doxorubicin are typically seen to be the minimum therapeutic dose in solid tumours [435], of which only a proportion will be nuclear-bound. Another *in vitro* study suggests *intracellular* doxorubicin concentrations of approximately 60 ng/mg are required for greater than 99% cell kill [436]. In order to detect such low concentrations of doxorubicin within a relatively highly auto-fluorescent liver tumour biopsy sample using a fluorescence microscope, it follows that optimisation of specificity and sensitivity are important. A spectral-unmixing approach [437] has been optimised using the Zeiss 710 confocal microscope, to isolate the doxorubicin fluorescence signature in DAPI-stained samples obtained from the clinical study, offering improved sensitivity and specificity over the Nikon microscope and the broad TRITC filter. In particular the unmixing profile has been designed to be compatible with a number of selected immunofluorescent (IF) fluorochromes, used to stain the clinical samples for other features (Appendix 5.1.3, Table 5.2).

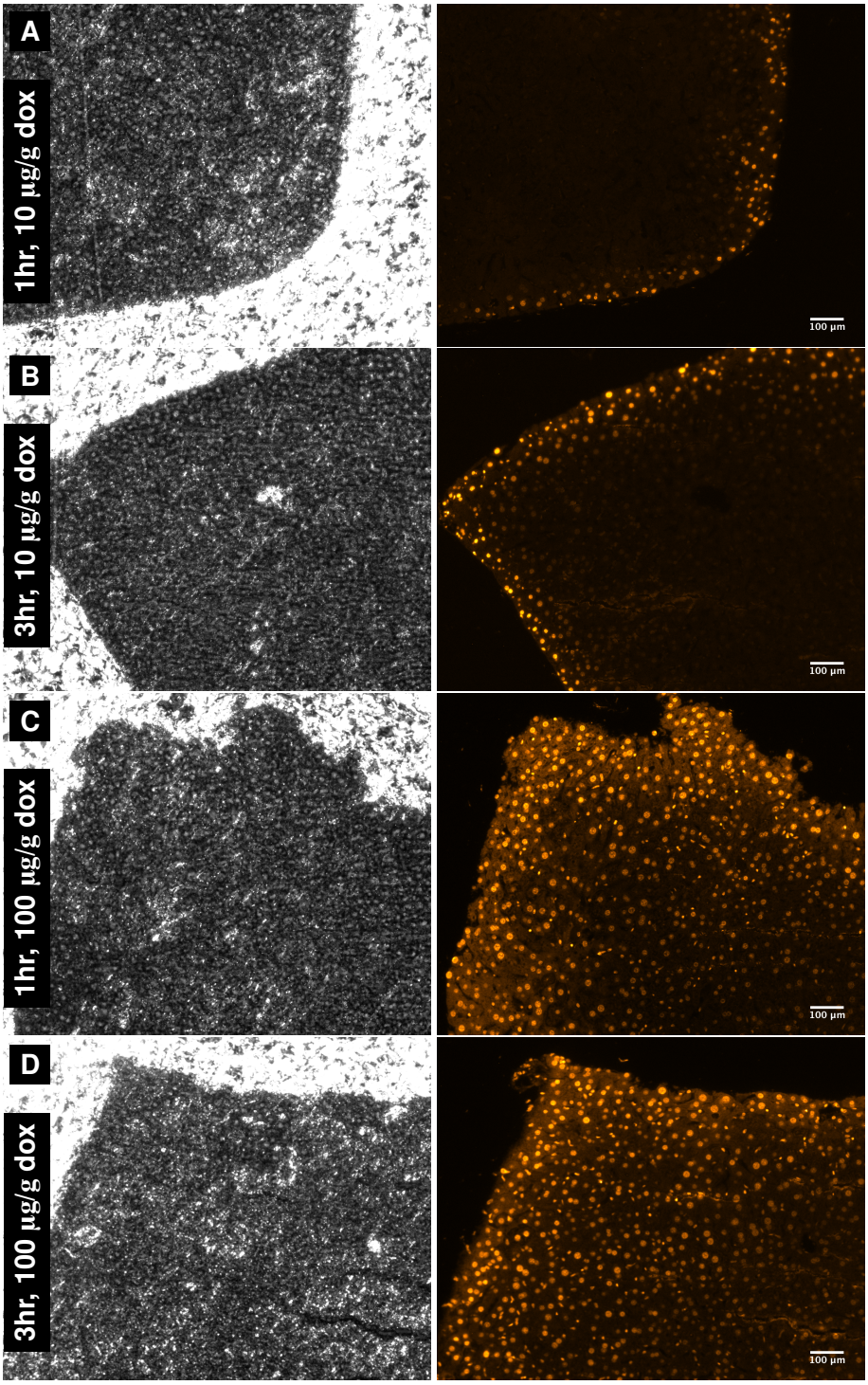


Figure 2.38: Nuclear uptake of doxorubicin in *ex vivo* mouse liver relative to exposure time and concentration. Microscopy performed in 4 µm-thick paraffin-embedded sections of freshly-harvested mouse liver immersed in 10 µg/g of doxorubicin/PBS for (A) 1 hour and (B) 3 hours before fixation, and 100 µg/g for (C) 1 hour and (D) 3 hours before fixation. Images acquired on Nikon Eclipse Ti microscope using x10 objective and a monochrome detector (DS-QiMC). LEFT: bright-field paraffin section, demonstrating the tissue border (dark) against the paraffin (bright). RIGHT: Corresponding section demonstrating nuclear doxorubicin (orange), captured with the TRITC filter for doxorubicin, using a 1 second exposure and a gain of x1.4.

By using doxorubicin-exposed mouse liver samples, previously described, in unprocessed (waxed) section, the Zen software was used to generate an unmixing spectra for doxorubicin and DAPI, capable of identifying low levels of nuclear doxorubicin in clinical liver tumour samples. Figure 2.39 demonstrates the unmixing process on the Zen workstation, with doxorubicin spectra. To validate that the spectrally unmixed signal corresponds to nuclear-bound doxorubicin, its fluorescence signature compared favourably to that captured in a previous study which examined the spectra for doxorubicin bound to double-stranded salmon DNA at a similar excitation wavelength [424].

Using this spectral profile, Figure 2.40 shows a composite unmixed image generated from a DAPI-mounted mouse liver sample, previously exposed to 100 μg/mL doxorubicin, and again the doxorubicin is clearly visualised in the peripheral nuclei. At a depth of ~200 μm there is a clear transition through cells demonstrating co-localisation for both doxorubicin and DAPI (purple), to nuclei staining only for DAPI (blue) at deeper depths. It is likely this is due to competitive nuclear staining between doxorubicin and DAPI, such that in the peripheral cells this high concentration of nuclear doxorubicin interferes with the formation of the usual fluorescent DAPI-complexes formed with DNA [438], and this phenomenon has been observed in at least one other study involving yeast cells [439].

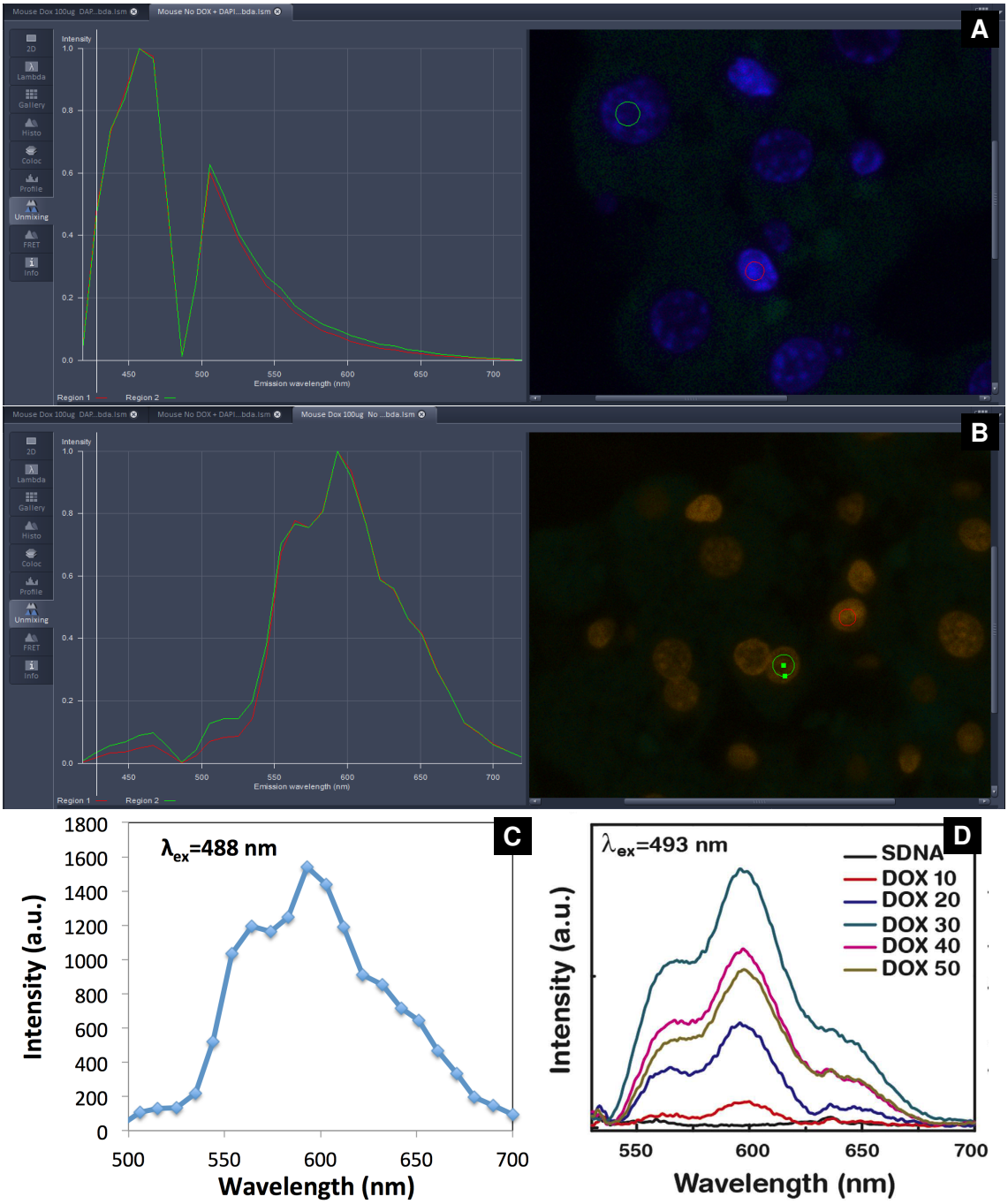


Figure 2.39: Screenshots of the Zeiss Zen software used for spectral unmixing, demonstrating spectral profiles for DAPI and doxorubicin. **A:** Spectral profile and image for nucleus in DAPI-stained control mouse liver in the absence of doxorubicin. Note the notch at 485 nm is due to presence of a dichroic mirror. **B:** Spectral profile and image for nucleus in doxorubicin-exposed mouse liver in the absence of DAPI. Acknowledgement: Mark Shipman, Ludwig Institute, University of Oxford for spectral setup. **C:** Spectral profile for doxorubicin-only sample at an 488 nm excition, replotted from (B). **D:** Plot showing spectra published for doxorubicin-exposed salmon nuclei at a similar excitation wavelength (493 nm). Reprinted from Scientific Reports, 2015; 5(12722): 4, Gnapareddy *et al.*, Characteristics of Doxorubicin Hydrochloride Drug-Doped Salmon DNA Thin Films, with permission from Nature Publishing Group [424].

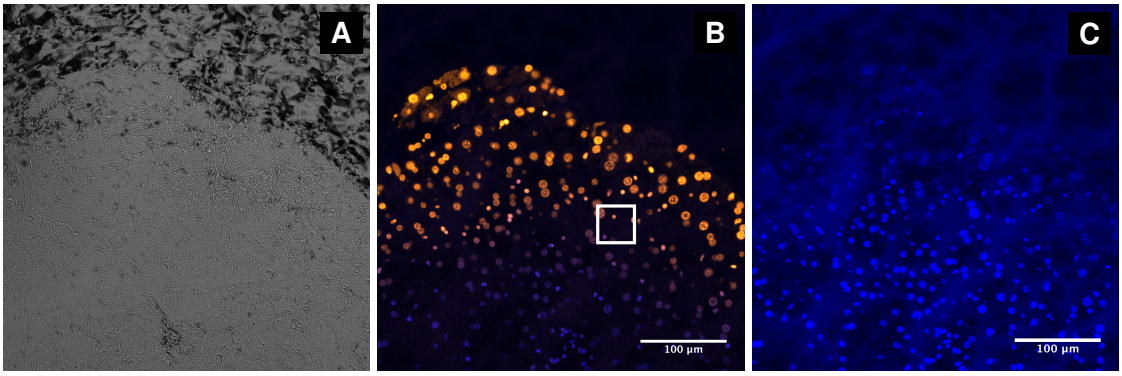


Figure 2.40: A DAPI-mounted FFPE section of mouse liver exposed to 100 µg/mL of doxorubicin, prepared as previously described. Captured on a Zeiss 710 confocal microscope at x20. **A:** bright-field. **B:** composite image spectrally-unmixed for DAPI (blue) and doxorubicin (orange), demonstrating a transistion zone (purple). The transistion zone (one region indicated by white rectangle) represents the colour produced by DAPI and doxorubicin co-localised within the same nuclei. **C:** DAPI-only layer from the same image, which has been intensified to demonstrate there is weak DAPI staining even in the most peripheral nuclei.

In addition to identifying nuclear doxorubicin, further information can be obtained from the clinical samples using confocal fluorescence microscopy. In particular immunofluorescent (IF) staining, using the fluorophores shown in Appendix 5.1.3, can be used in combination in order to identify doxorubicin distribution relative to nuclei and vessels. Furthermore the pan-CK stain can be used as a cell vitality marker and is discussed further in Section 2.4.2. Again a spectral unmixing technique is used to correct spectral bleed-through between different colour channels for these fluorophores. In practice, images are generated from the same tissue section, which is imaged for doxorubicin before, and then re-imaged following IF staining, for subsequent overlay. This is because during the de-waxing process required for IF, a heating step is required, which destroys the doxorubicin fluorescence. Clinical samples which have generated using this technique are shown in Section 3.3.4.

2.4 Analytical Methods for Cell Viability

Another key hypothesis (Section 1.5.3) underpinning the TARDOX study is that ultrasound-mediated hyperthermia alone, in the absence of a drug, should not induce any direct cell

death due to ablation. In other words, any cell death and subsequent radiological response in the target tumour is due to chemo-ablative effects rather than instantaneous thermal and mechanical ablation by FUS. To address this FUS safety consideration, there is a need for a robust and quantitative method to assess extent of cell death by coagulative necrosis by FUS alone (Section 1.3), independently of the cytotoxic action of the drug.

This endpoint is evaluable, as the study provides a tissue biopsy immediately following the post-drug FUS exposure in both Part I and Part II, before chemo-ablative effects can manifest. It is designed to provide supporting evidence to the Part I thermometry data, which can be used demonstrate a safe thermal dose (Section 3.2.1), and in isolation in Part II. In order to determine the most appropriate method to use for clinical biopsy samples, cell viability in small tissue samples has been explored pre-clinically using both flow cytometry and microscopy.

2.4.1 Cell Viability Studies by Flow Cytometry

Flow cytometry is a well-established technique that has been used to quantify cell death, apoptosis and other characteristic effects in various cell lines exposed to different hyperthermia regimens in many *in vitro* studies [440–455].

In our laboratory, an optimised cell recovery method has been combined with a cell viability assay, which uses flow cytometry, for potential application to analyse clinical tissue samples. In particular the assay was designed to be practical for tissue masses of as little as 4-5 mg, as obtained with an 18G core biopsy device, and to be compatible in the presence of intracellular doxorubicin. Doxorubicin has a broad emission spectrum [456] (Figure 2.39), which potentially may interfere with a number of commonly used fluorophores used in assessing cell viability, such as propidium iodide (PI) (Figure 2.41).

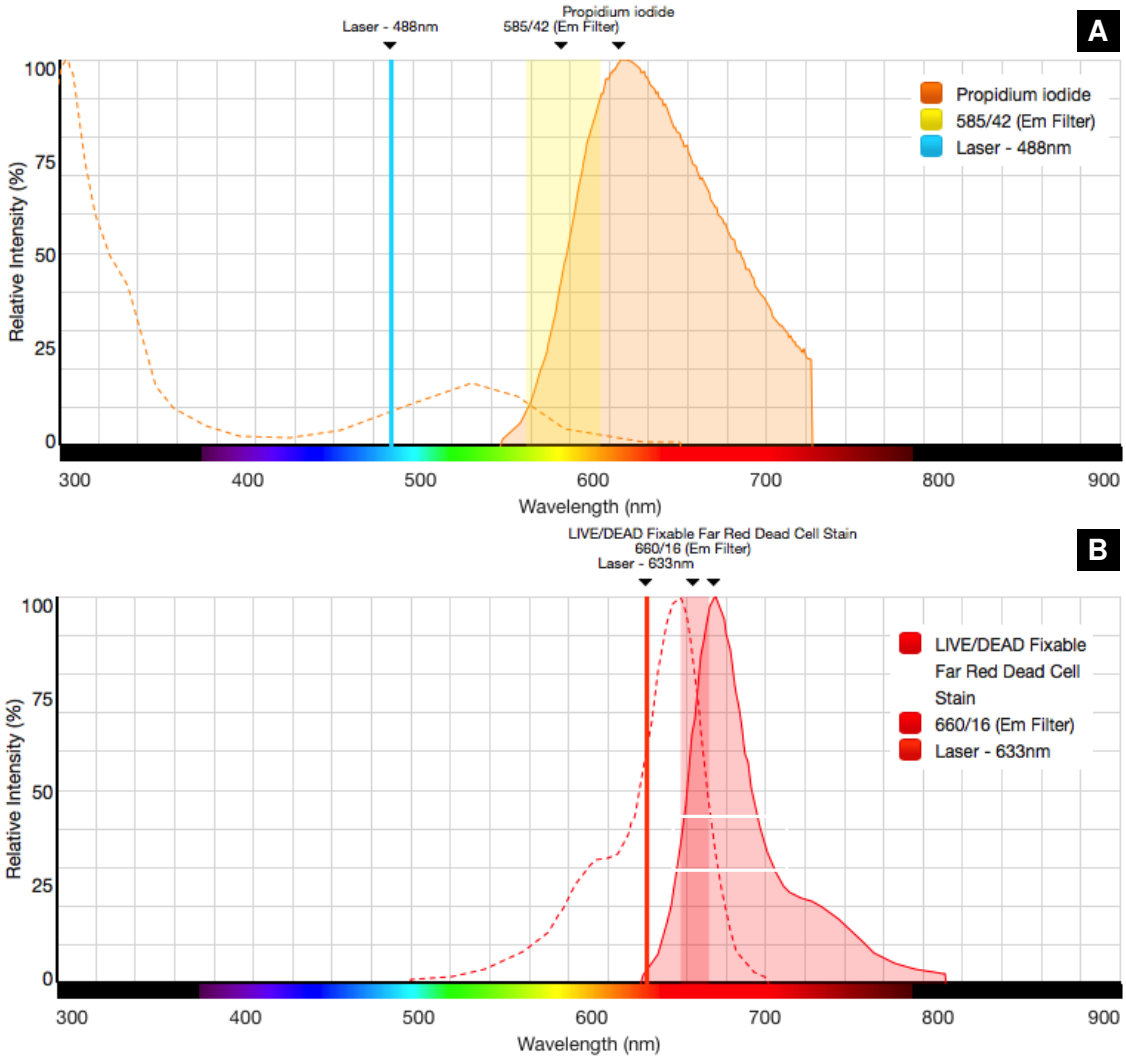


Figure 2.41: Excitation (dotted lines) and emssion spectra (solid lines) for cell viability fluoreophores, generated by LifeTechnologies™ Fluorescence SpectraViewer. **A:** Propidium iodide (PI) stain is excited using the blue (argon) laser (488 nm) and its broad emission specta may be detected using the orange detector 585±42 nm or higher wavelength detectors. **B:** LifeSciences™ Far Red LIVE/DEAD® (L/D) stain is excited using the red laser (633 nm) and its narrow emission spectra is best detected using the far red detector 660±16 nm. Note that doxorubicin typically has a excitation of ~480 nm with a peak emission of ~590nm, overlapping the emission spectra for PI, but clear of that for the L/D stain, although exact values are somewhat solvent-dependent [425, 456].

The PI stain is a cell-impermeant dye that is excluded from viable cells with excitation and emission maxima of 535 and 617 nm with weak fluorescence on the surface of cells. Once inside a cell whose membrane has been compromised, it intercalates with DNA, enhancing its florescence 20- to 30- fold. LifeTechnologies™ manufacture an alternative

LIVE/DEAD (L/D) stain with a range of fluorophore options. It is a cell-impermeant, amine-reactive dye which similarly exhibits weak fluorescence in healthly cells, as only cell surface amines are available for reaction. However the stain has a 50-fold increase in fluorescence when entering a compromised cell membrane, this time due to binding to intra-cellular protein amines. In particular both stains are used to distinguish live and dead cells, and on their own they are not able to identify apoptotic cells.

The far red LIVE/DEAD (L/D) vitality stain was chosen, as it has emission spectra well away from that of doxorubicin's. The function of the L/D stain in the presence of intracellular doxorubicin has been demonstrated by a simple experiment in which HT29 cells were grown in DMEM with 10% FCS (HII Foetal Calf Serum, LifeTechologies™, Ref: 10500-064) and 1% Penicillin-Streptomycin (LifeTechnologies™, Ref: 15140-122) in culture flasks. When confluent, cells were trypsinised into a suspension, centrifuged, and re-suspended in the same cell media. Cell suspensions were incubated with doxorubicin or not, and then stained for L/D or PI, with an unstained control, before flow cytometry. The results are shown in Figure 2.42, and demonstrate that the PI viability plot for the doxorubicin-exposed sample gives a false impression of complete cell death due to the overlapping emission spectra. The L/D viability plot, however, shows no cell necrosis due to doxorubicin, which is as one would expect, given the exposure time is so short (read within an hour of exposure).

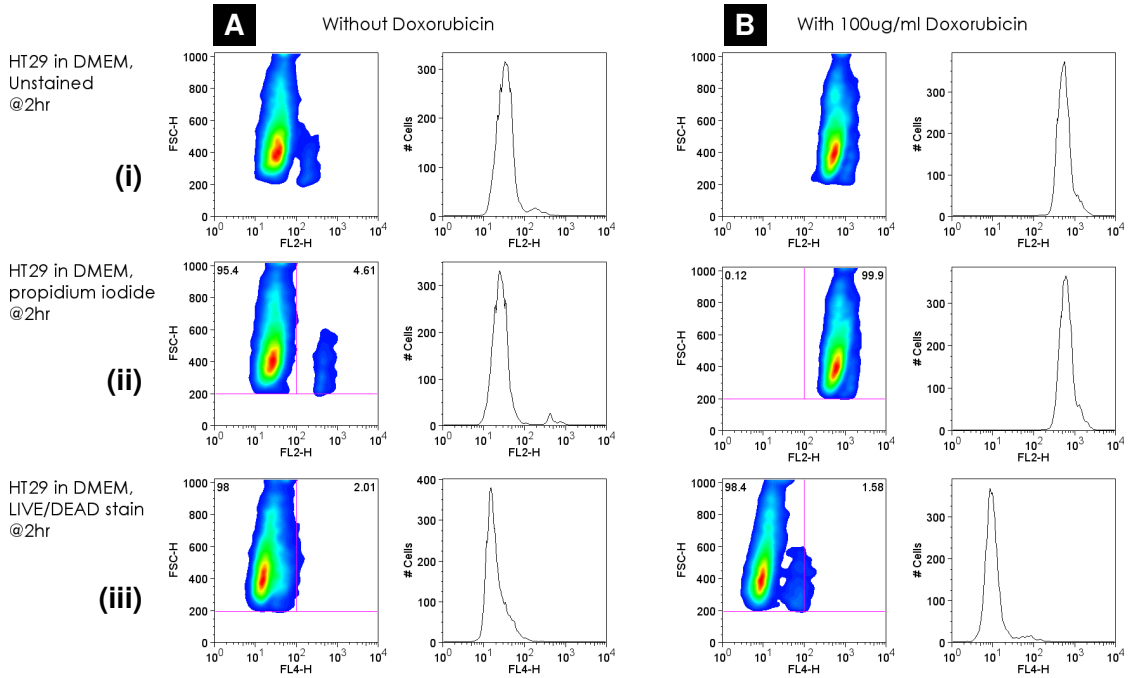


Figure 2.42: Evaluation of cell viabliity stains in viable cancer cells by flow cytometry using the BD FACSCalibur™ Cell Analyzer. Each plot shown with corresponding histogram. HT29 cells (colorectal cancer cell line, American Type Culture Collection, ATCC® HTB-3™) were cultured and suspended in DMEM (High glucose Dulbecco's Modified Eagle Medium, LifeTechnologies Ref: 11965-092). Cells were either doxorubicin-free (**A**), or exposed to high-dose doxorubicin for 2 hours (**B**). Cells from each group were either unstained ((i), Ex/Em 488±42 nm), stained with PI ((ii), Ex/Em 488±42 nm), or the far red L/D stain (LifeTechnologies™ Far Red LIVE/DEAD® stain) ((iii), Ex/Em 660±16 nm)). In the stained samples, gating was used to distinguish viable (<100 FL units) from non-viable cells (>100 FL units) for both detection channels. Due to interference of doxorubicin fluorescence, the PI stain gives a false impression of cell death, with strongly positive staining to the right of the horizontal threshold (**B(ii)**), whilst the L/D stain is unaffected and demonstrates weak staining only predominately to the left of the horizontal threshold (**B(iii)**). Plots generated using FlowJo Data Analysis Software. Acknowledgement: Mick Woodcock, Bioanalysis Core, University of Oxford for assistance and demonstrating use of the flow cytometer.

Subsequently, flow cytometry was used to determine levels of cell death in cell suspensions obtained from the following pre-clinical models, discussed over the following three sections:

1. HT29 cell line exposed to hyperthermia and/or doxorubicin insult,
2. *Ex-vivo* bovine liver tissue exposed to hyperthermia, and,
3. *Ex-vivo* bovine liver tissue exposed to ablative (or sub-ablative) levels of HIFU

Cell viability Using Cell Line Exposed to Doxorubicin and/or Hyperthermia

Preliminary studies involved exposure of cell suspensions of the same HT29 cell line to doxorubicin as well as hyperthermic insult. Following a gentle vortex, the cell suspension was split four ways with two tubes receiving doxorubicin solution (Doxorubicin, 100 mg, Apollo Scientific, Ref: BID0120, Batch No: AS444828), made up in phosphate buffered saline (DPBS, no calcium, no magnesium, LifeTechnologies, Ref: 14190-250) up to a final concentration of 100 μg/mL, the remaining two tubes received no drug. Tubes with and without drug were then heated to 47°C in a water bath, or simply placed in a CO_2 incubator at 37°C. Following 30 minutes of 47°C hyperthermia (as confirmed by reference to a temperature-monitored control tube) or normothermia, the contents of each tube was aliquoted between four different 5 mL sterile FACS tubes (BD Falcon round-bottom polystyrene tubes, Catalog No. 352058), each being used to represent a different time point. Samples were protected from light and kept in a CO_2 incubator at 37°C with loose tops, when not being assayed. Using the method detailed in Section 5.1.1 without fixation, cell viability was assessed using flow cytometry at 2, 6, 48 and 72 hours, relative to initial doxorubicin exposure. Due to adherence of cells to the FACS tubes, trypsinisation was required before they could be assayed.

Doxorubicin did not interfere with the L/D stain emission spectra, which could clearly be distinguished by the far-red detector. The maximal trend to cell death (positive L/D stain) was observed in the HT29 samples receiving both doxorubicin and heat insult, where under 10% of cells remained viable at 72 hours (Figure 2.44). With reference to the flow cytometry plots (Figure 2.43) a subpopulation of cells demonstrate a trend for increased cell granularity (side-scatter, SSC) following insult, in keeping with early apoptosis [457]. The appearance of the separate particles with low light scatter properties (SSC and forward scatter, FSC) in these cell cultures is most likely due to the formation of apoptotic bodies [458, 459], and are largely absent from the control.

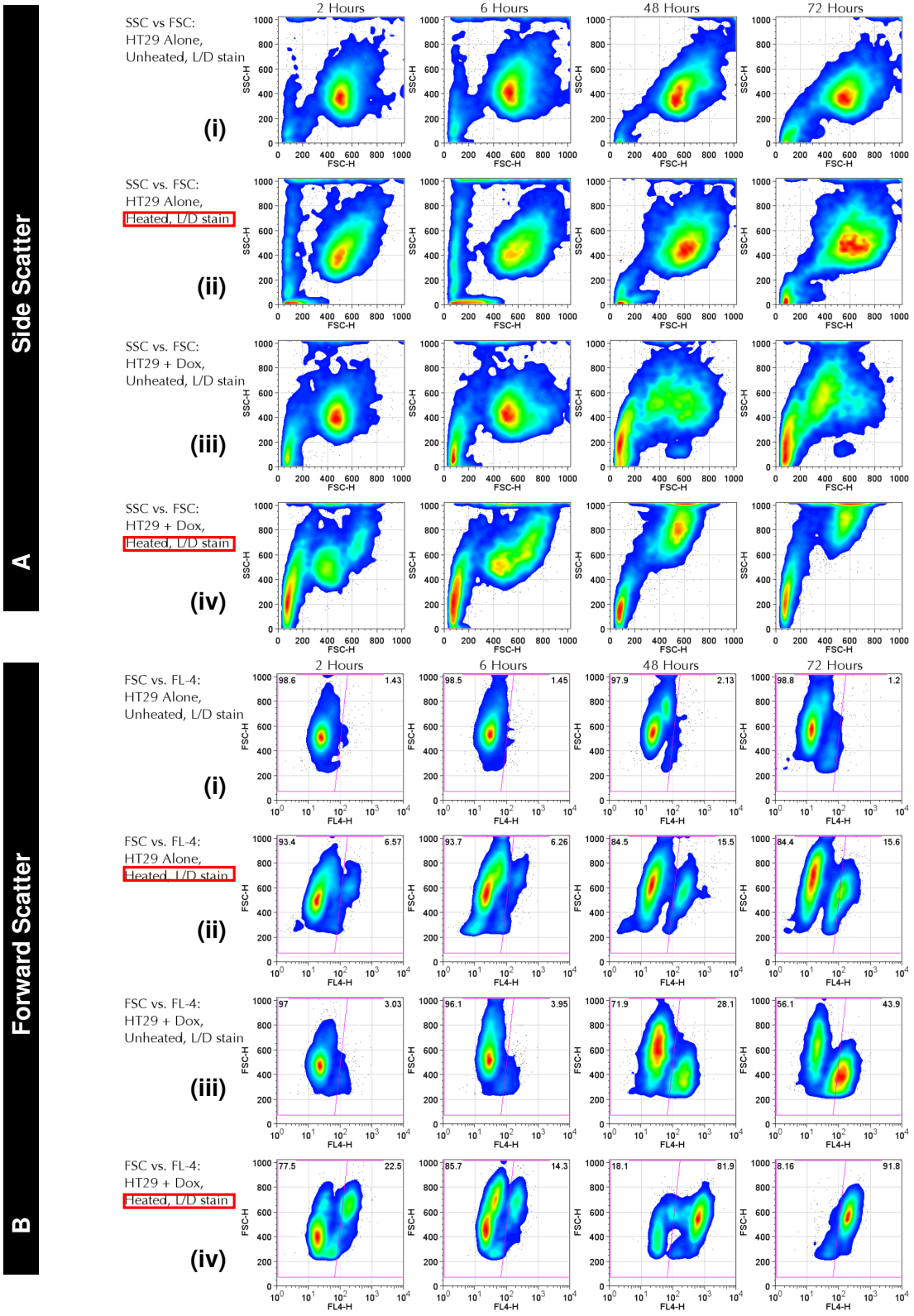


Figure 2.43: Flow cytometric studies of HT29 cell suspensions with (iii+iv) and without (i+ii) 100 µg/g doxorubicin and with (ii+iv) and without (i+iii) 30 mins. of a hyperthermic insult at 47°C, assayed over 72 hours. **A:** Side Scatter (SSC) vs. Forward scatter (FSC) for the four groups. **B:** Viability analysis of same four groups using L/D stain. FSC vs. FL-4, channel used to detect far-red emission at 660±8 nm. Note at 72 hours, the trend towards cell death is highest in samples treated with doxorubicin and in particular when combined with heat insult.

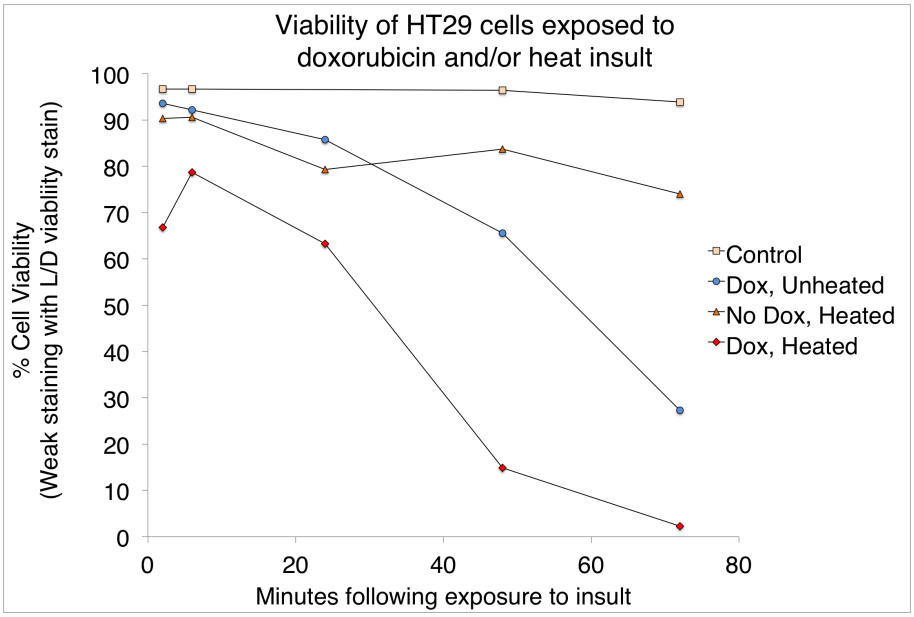


Figure 2.44: Cell viability analysis for HT29 cells exposed to insults of either high dose doxorubicin (100 µg/mg), heat, both or neither. Cells assayed at 2, 6, 24 48 and 72 hours. There is more rapid cell death in the group receiving both insults compared with the groups receiving a single insult. Data obtained from analysis of the flow cytometry plots shown in Figure 2.43 using the threshold show, with a discard of any events with FSC<200.

Cell Viability in *Ex-vivo* Liver Exposed to Hyperthermia

Fresh cow liver was obtained within 2 hours of slaughter, and a peripheral tissue section of 5x5x10 cm was resected. From this section 18 smaller single-piece sections were cut with masses ranging from 71-130 mg. Each section was placed in a ZipLoc® polyethylene bag and 4 mL of RMPI medium (Sigma, Ref: R8758-500ML) added. Air was manually expelled before sealing and custom-made clamps were applied across the seal. Two bags, one control and one for longest heating, also received a thermocouple into the media and liver tissue, using modified clamps. All bags were watertight and all but three were loaded onto a custom-made holder (Figure 2.45), which was immersed in a 44°C water bath. The remaining three bags were placed into a 37°C water bath in a similar manner. Bags were removed from the hyperthermic water bath in triplicates at 60, 120 and 240 minutes, and placed into the 37°C bath along with the controls. Samples were recovered using an enzymatic process as per the cell recovery protocol outlined in Section 5.1.2, with the exception of incubating the resulting suspensions overnight in a CO_2 in-

cubator without fixation, to allow time for the effects of hyperthermic insult to manifest. At both 16 and 40 hours post-recovery, the samples were removed from the incubator, stained with L/D stain and formalin-fixed for same-day flow cytometric analysis.

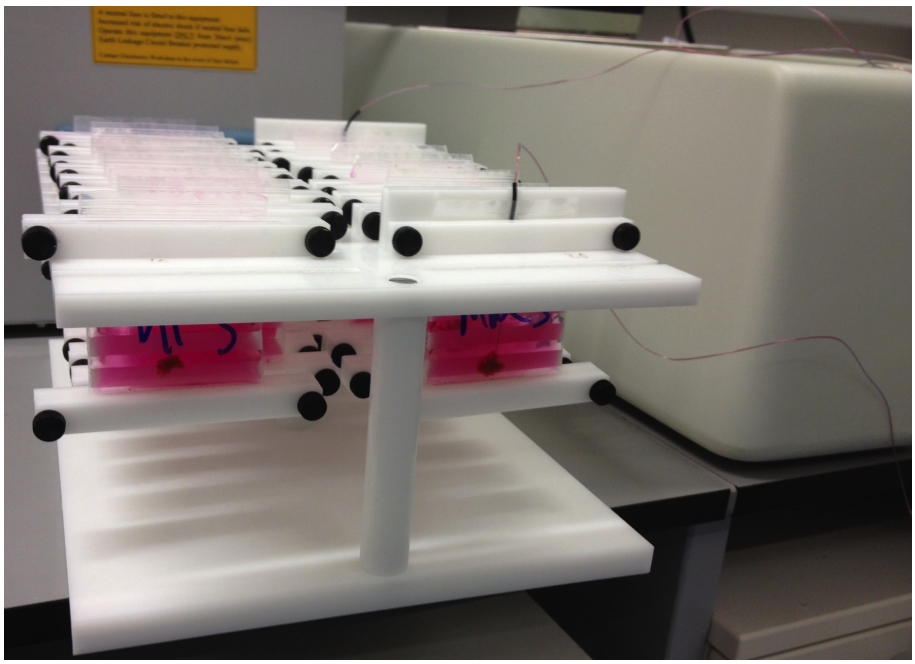


Figure 2.45: Custom rig used to immerse *ex vivo* bovine liver in a water bath for various time periods. Note two ZipLoc® bags were monitored for temperature using thermocouples (Type T Thermocouple, Omega, Ref: HYP-0-33-1-T-G-60-SMPW-M) connected to a PC via a PicoLogger device (already introduced in Section 2.1.3). Acknowledgment: Rig designed by Joe Martin and produced by Jim Fisk of the IBME.

Results: Throughout the treatment period, thermometry traces revealed mean temperatures of 37.4°C and 44.0°C in the hyperthermic and normothermic water baths respectively. 16 hours after exposure to hyperthermia for an hour or more, a statistically significant increase ($p<0.01$) in cell death (L/D staining) was evident compared to the control groups and the two groups treated for durations of less than an hour (Figures 2.46 & 2.47). In addition, these preliminary studies demonstrated that this cell recovery protocol recovered an average of over 3,000 cells per mg of healthy *ex-vivo* liver samples for processed masses, ranging from 2-22 mg.

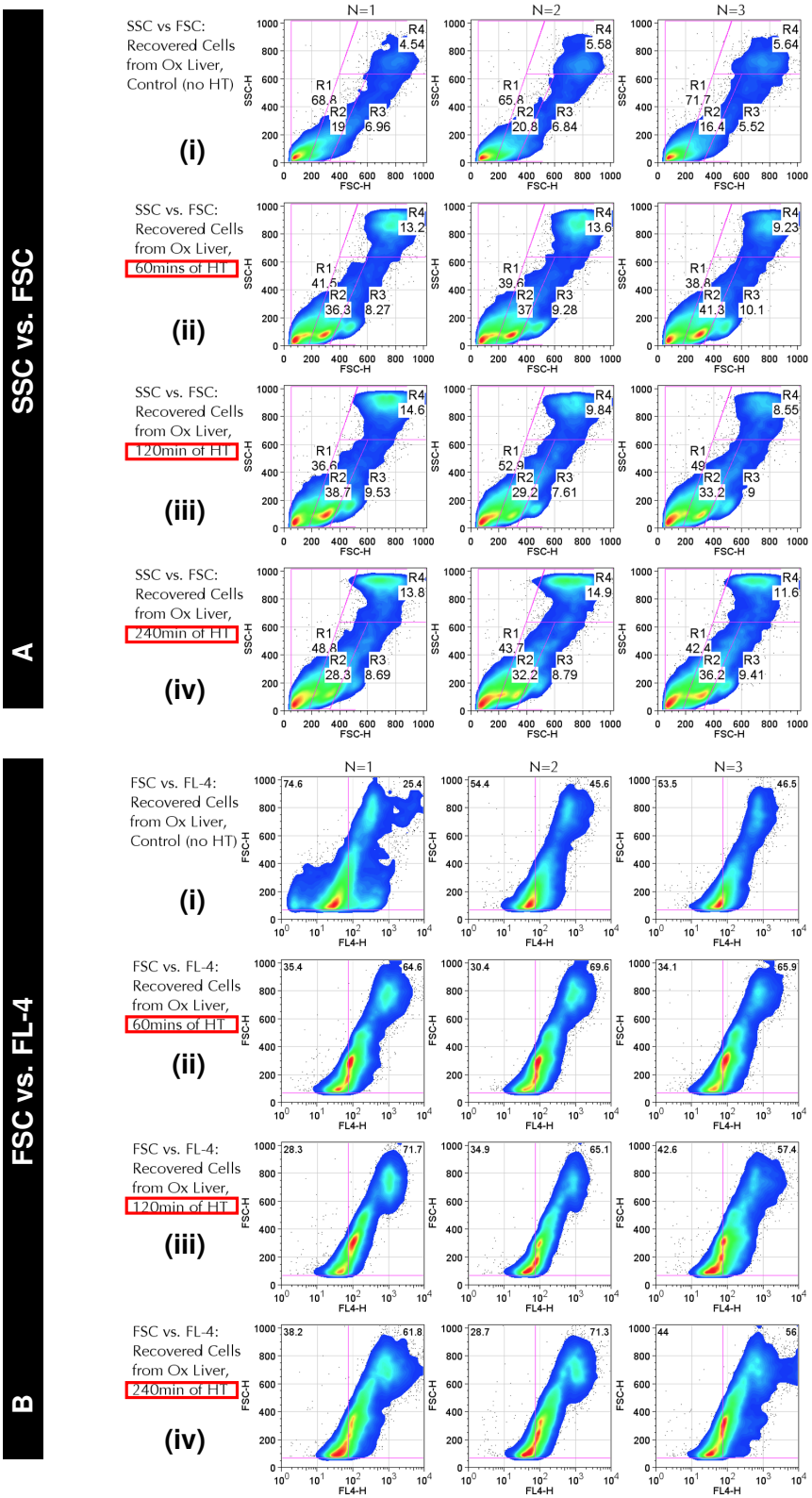


Figure 2.46: Flow cytometric studies of cells recovered from control liver and liver exposed to varying durations of hyperthermia assayed at 16 hours (n=3). Distributions for 0 (i), 60 (ii), 120 (iii) and 240 (iv) minutes of hyperthermia shown. **A:** SSC vs. FSC plots demonstrate subtle trend for increased subpopulations R2 and R4 for heat-treated group compared with control group. **B:** FSC vs. FL-4 plots (FSC<80 discarded) demonstrate trend for increased L/D staining in heat-treated group relative to control group. Plots generated using FlowJo Data Analysis Software.

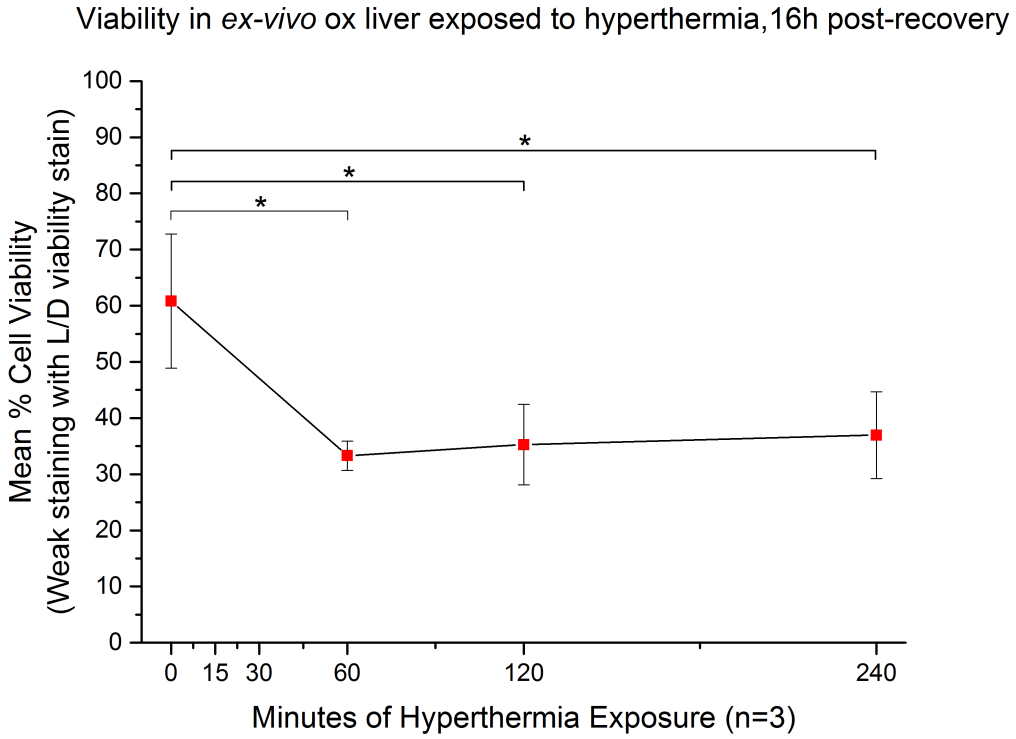


Figure 2.47: Cell viability analysis for *ex vivo* bovine liver hyperthermia experiments. Mean cell viability plot of cells recovered from control liver and liver exposed to varying durations of hyperthermia assayed at 16 hours (n=3). One-way ANOVA with Fisher's LSD revealed $p<0.01$ for all of the groups treated with 60, 120 or 240 minutes of hyperthermia at 16 hours when compared to the control group. Analyses performed using OriginPro v9.1, Origin Lab.

Cell viability in *Ex-vivo* Liver Exposed to HIFU Ablation

Using a custom watertight tissue holder with internal dimensions 5x5x10 cm, liver obtained from a freshly slaughtered cow was cut to size to fill the holder and degassed in PBS. The *ex vivo* liver was exposed to HIFU through a 5x5 cm acoustic window (Mylar sheet) at an axial tissue depth of 2 cm in a degassed water tank at 22°C. Using a 1.067 MHz transducer at the fundamental and a custom 3-axis positioning system, three lesions were created for each of three selected pressures (Low = 6.34 MPa, Medium = 7.27 MPa and High = 8.19 MPa peak-to-peak acoustic pressure). To increase the cross-sectional and thus sampling area for each lesion in a clinically-relevant manner, rather than increasing duration of sonication, each of the individual nine lesions were formed using

10 second continuous wave exposures arranged in a 2x2 grid with 1mm raster spacing in both X- and Y-axes (Figure 2.48). The nine larger lesions had a 1 cm separation in the X- and Y-axes.

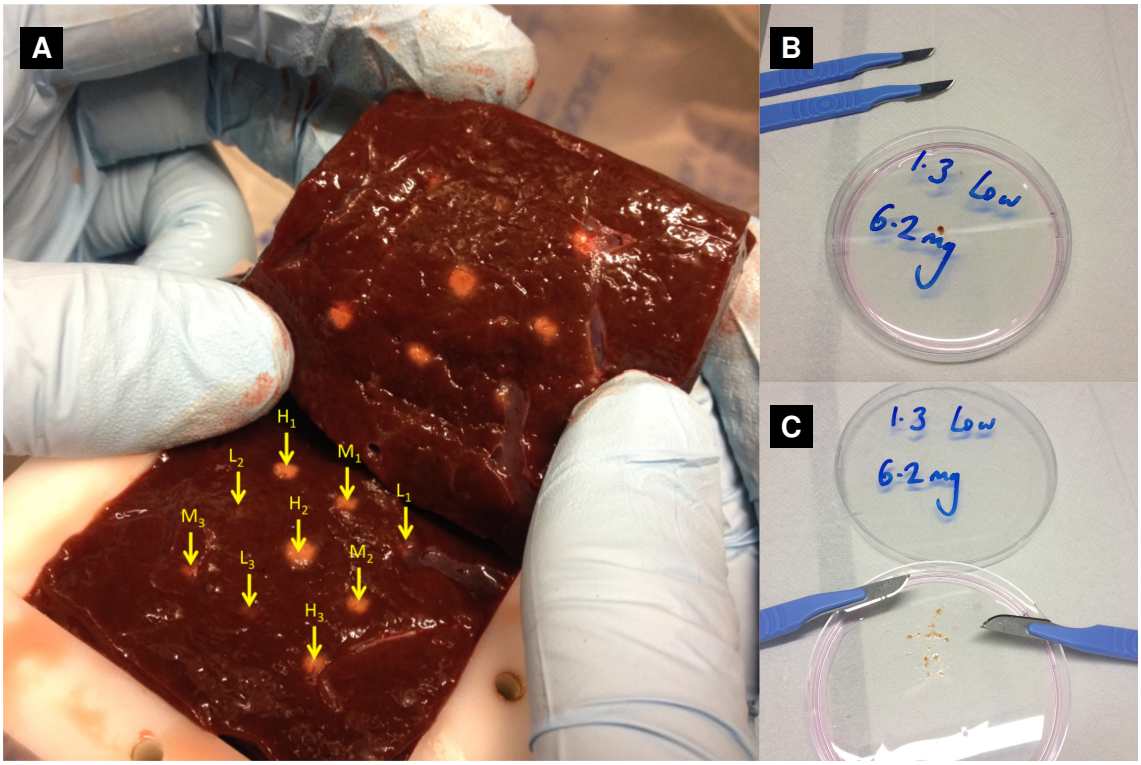


Figure 2.48: Experimental images of ablated *ex-vivo* bovine liver. **A:** n=3 HIFU lesions for each of H=High, M=Medium and L=Low acoustic pressures obtained in freshly harvested degased *ex vivo* bovine liver. Liver tissue remains in watertight tissue holder with the acoustic window removed and has been sliced transversely at the axial focus (2 cm depth). Lesions for each pressure regime are diagonally orientated to help orientate to the (less obvious) low power lesions. Right: A biopsy sample of 6.2 mg mass obtained from the L1 lesion before (B) and after (C) physical disaggregation using crossed scalpels in petri dish, prior to enzymatic digestion.

The core of each lesion was biopsied in addition to three controls taken from non-ultrasound exposed regions. The cell recovery protocol was performed with fixation within 4 hours for all lesions. Fixation was performed within this short post-recovery period to avoid manifestation of cell death due to removal of the liver tissue from its host environment. The following day, resulting cell suspensions were assessed for yield and viability using the described flow cytometery protocol (Section 5.1.1).

Results: Flow cytometric analysis revealed that, compared to control liver, there was a statistically significant increase ($p<0.01$) in both granularity as measured by side-

scatter (SSC) [460] and cell death as measured by highly positive L/D staining in the groups exposed to medium and high pressure compared with the control and low pressure groups (overall means of 9.7% vs. 47.6% and 20.7% vs. 73.6% respectively) (Figure 2.50 and 2.49). Whilst there is a clear shift towards cell death in the high pressure group, a proportion of cells (~20%) remain to the left of the horizontal threshold (weakly staining for L/D), either suggesting thermotolerance in this cancer cell line or the possibility of tissue sampling outside the ablated region. Whilst it is possible to validate these results using further cell viability analyses, such as NADP-H-dependent assays (e.g. MTT), the L/D stain is already a validated cell viability technique and such alternative assays may be associated with a high degree of standard error.

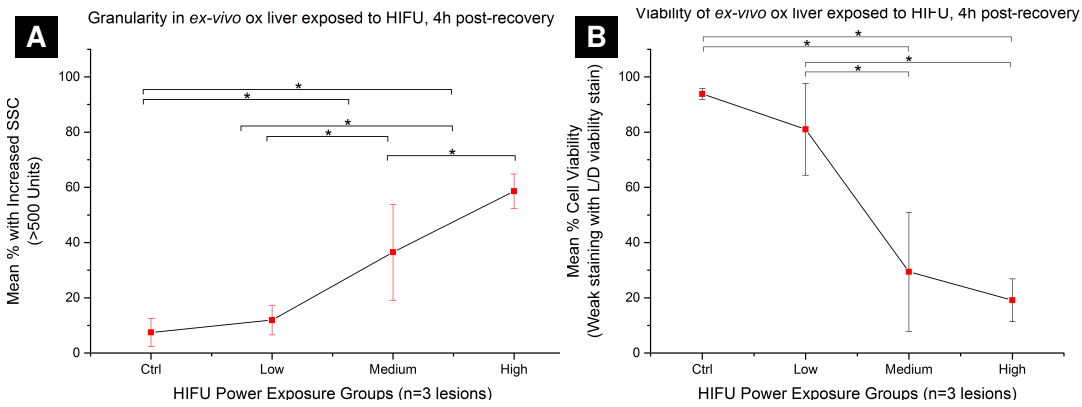


Figure 2.49: Cell granularity (SCC) and viability analysis for *ex vivo* bovine liver HIFU experiments. **A:** Mean granularity analysis of cells recovered from control liver and HIFU-ablated lesions fixed at 4 hours and assayed the following day (n=3). One-way ANOVA with Fisher's LSD revealed $p<0.01$ for increased granularity (SSC) in both the medium and high power groups compared the control. **B:** Mean cell viability plot of the same samples (n=3). One-way ANOVA with Fisher's LSD revealed $p<0.01$ for weak (dead) vs. strong staining (viable) in both the medium and high power groups compared to both the control and low power groups in any combination. **B:** Analyses performed using OriginPro v9.1, Origin Lab.

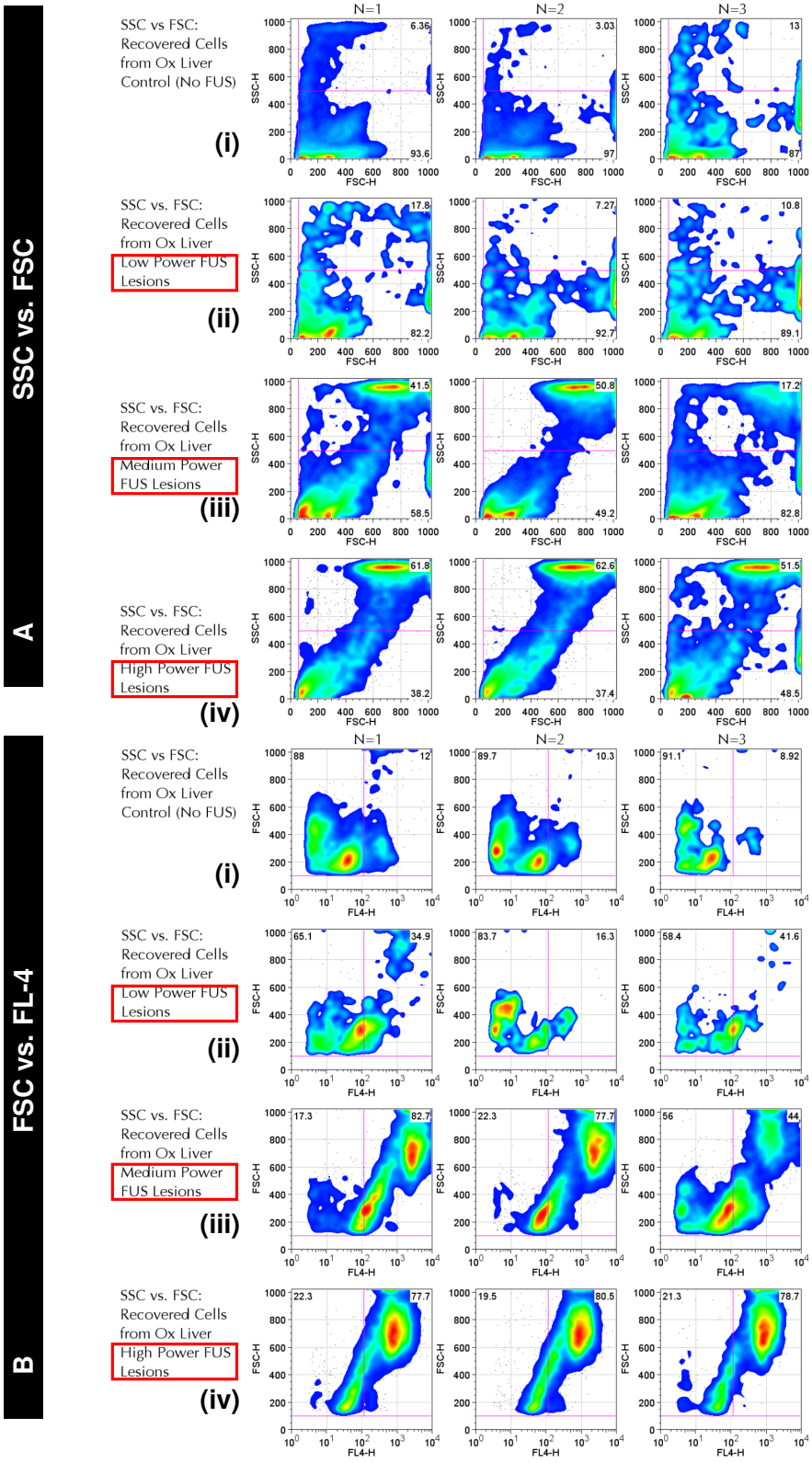


Figure 2.50: Flow cytometric studies of cells recovered from control liver and HIFU-ablated lesions fixed at 4 hours and assayed the following day (n=3). **A**: SSC vs. FSC plots demonstrate a trend for increased SSC suggesting higher cellular granularity with increasing HIFU powers. **B**: FSC vs. FL-4 plots (FSC<100 discarded) demonstrate a strong trend for increased L/D staining intensity with increasing HIFU powers. Plots generated using FlowJo Data Analysis Software.

2.4.2 Cell Viability Studies by Microscopy

Histological changes that may be observed in tissue samples post-HIFU have already been discussed in depth in Section 1.3.3. Due to the previously discussed limitations of routine H&E in assessing ablative damage by FUS, other stains were considered for use in the clinical study, in order to evidence the *absence* of ablative changes. Using existing microscopy sections to obtain this additional clinical data could be used as a further level of evidence to demonstrate any enhancement in drug delivery is attained by drug release at safe levels of hyperthermia.

Cytokeratin (CK) stains are epithelium specific and can be used as a test of cell viability [461]. For example, the CK8 subtype is lost early in apoptosis and has proven utility in distinguishing ablative regions of epithelial tissues. One clinical study by Kreb *et al.*, obtained resected breast tumour tissue immediately following RFA ablation, for formalin-fixation and paraffin section. The study demonstrated the CK8 stain became negative in ablated regions in the time taken to resect, and indeed was superior to NADH in distinguishing ablation zones [223].

Exploratory pre-clinical microscopy studies were performed in our laboratory using a wide-spectrum cytokeratin stain (pan-CK) for vitality assessments, which is compatible with a variety of animal tissues, including ox. The fluorophores used pre-clinically are detailed in Appendix 5.1.3, Table 5.1). Freshly harvested *ex vivo* bovine liver was used to create HIFU lesions, subsequently resected and fixed within 6 hours of slaughter. An acoustic set up similar to that already described in Section 2.4.1 was used, except this time there were two acoustic windows to avoid internal reflections, and an acoustic absorber was placed in the path following the exit window.

Lesions were created using a 1.06 MHz transducer in continuous wave, at a depth of 15 mm in the liver, at low and high acoustic pressures of 6.3 and 8.2 MPa peak-to-peak. To generate each lesion, the Precision Acoustics software client was pre-programmed to automatically move the transducer clockwise over a 2x2 grid with 1 mm spacing, such

that there was a cumulative exposure time of 40 seconds for each individual grid unit. Lesions and control liver were resected from the liver sample and immediately fixed in formalin, and later paraffin-embedded for pan-CK IHC. Results are shown in Figure 2.51, and demonstrate that normal hepatocytes are weakly positive for pan-CK, consistent with the liver being an epithelial derivative (of the foregut). Bile ducts demonstrate a very strong stain, as would be expected for true epithelial structures [462] and has previously been reported [463]. In the HIFU-treated samples, a clear loss of pan-CK in the hepatocytes was demonstrated, which co-registered with the macroscopically visible lesions. Staining of the bile-ducts appears relatively weaker in HIFU-exposed samples, but is relatively unaffected. This exploratory work demonstrates that CK vitality stains, including this pan-CK stain, have the potential to clearly differentiate ablated regions in clinically-obtained tissue samples obtained within minutes-hours of the FUS exposure. H&E staining was also performed, but showed only subtle changes including nuclear pyknosis and increased intra-cellular spacing in the tissue exposed to high-powered HIFU.

Pan-CK IHC staining was performed on a number of human liver tumour samples obtained from a tissue bank in order to observe the level of heterogeneity in the presence of epithelial structures in tumours, staining positive for CK. Selected images are shown from three individual subjects, along with H&E staining of the same samples in Figure 2.51. CK8 immunofluorescence was performed on the same samples in order to optimise the antibodies for clinical samples, and selected images are shown in Figure 2.53. The clinical immunofluorescence staining protocol is summarised in Appendix 5.1.3, Section 5.1.5 along with the fluorophores in Table 5.2).

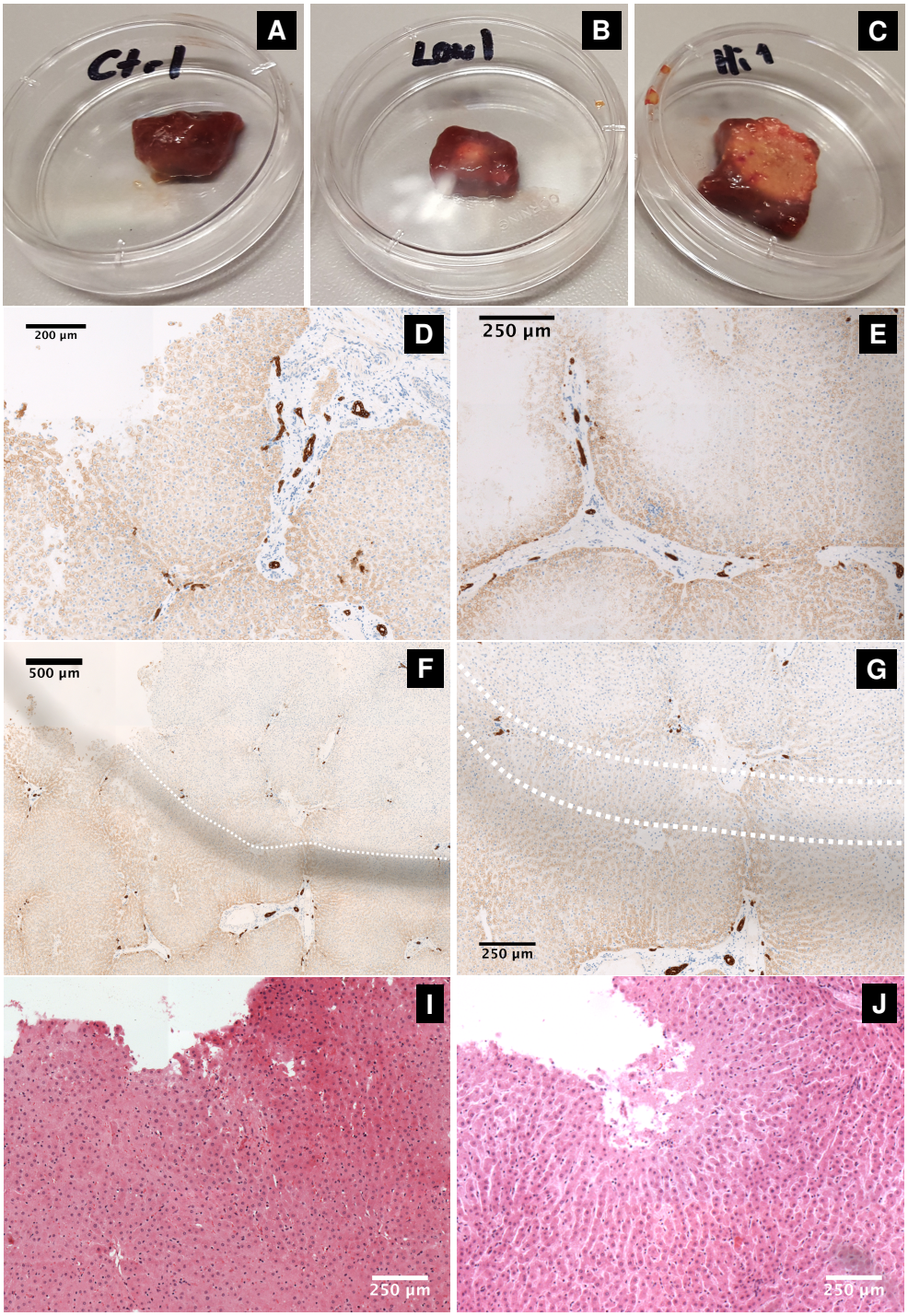


Figure 2.51: Pan-CK Immunohistochemistry in HIFU-ablated *ex-vivo* bovine liver. Resected control liver **(A)**, and lesions created at low **(B)** and high power **(C)**, 6.3 and 8.2 MPa peak-to-peak acoustic pressure respectively. Microscopy for pan-CK immunohistochemistry in control liver at x20 **(D)**, low power HIFU lesion at x20 **(E)**, and high power HIFU lesion at x10 **(F)** and x20 **(G)**. There is a distinct and sharply demarcated region where pan-CK stain is absent in both HIFU-exposed samples, the region being much larger in the high powered HIFU sample, demarcated by white dotted line. The dotted lines in **(G)** demarcate the transistion zone which is under 20 cells wide. There is an artefact in **(F)** and **(G)** due to marking of the slide around the region of absent pan-CK stain with a marker pen. H&E staining of control (I) and high power HIFU **(J)** lesions at x20. Acknowledgement: Leticia Campo for optimisation and application of staining protocols.

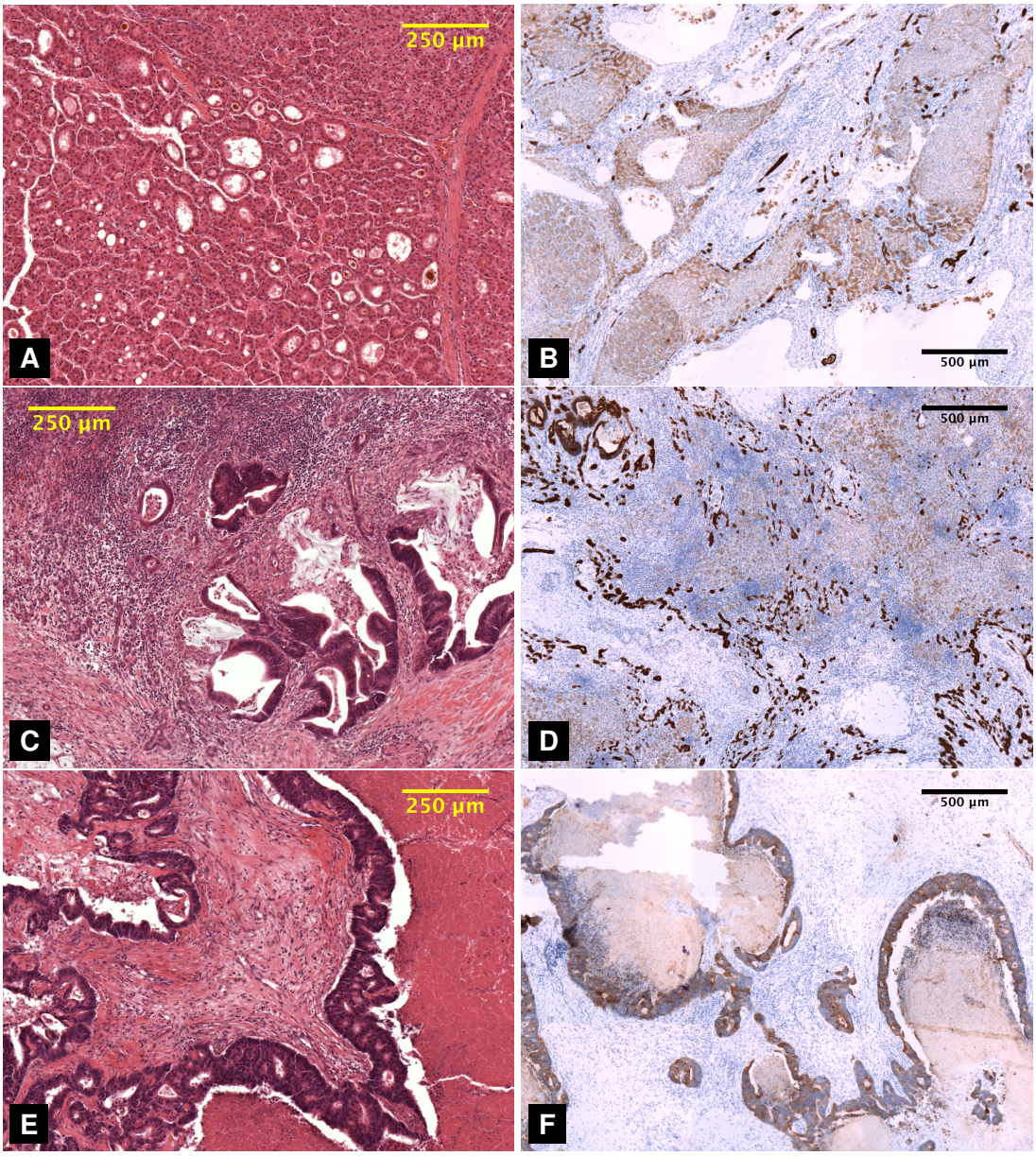


Figure 2.52: Pan-CK Immunohistochemistry in human liver tumour samples, obtained from Oxford Centre for Histopathology Research (OCHRe). **(A)** moderately differentiated HCC, **(C,D)** metastatic colorectal carcinoma, and **(E)** metastatic adenocarcinoma at x20 stained with H&E. **(B, D, F):** the respective samples stained with pan-CK at x10 demonstrating a wide variation in staining. Acknowledgement: Leticia Campo for optimisation and application of staining protocols and OCHRe for providing the tissue.

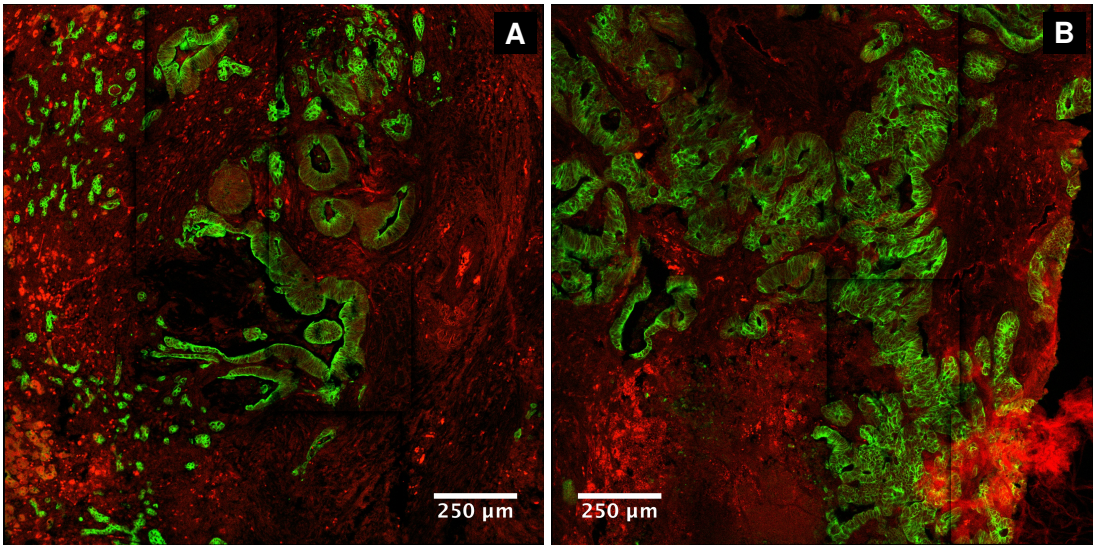


Figure 2.53: CK8 (Green, cell viability marker) and CD31 (Red, vascular marker) Immunofluorescence in human liver tumour samples, obtained from Oxford Centre for Histopathology Research (OCHRe). **(A)** metastatic colorectal carcinoma, and **(B)** metastatic adenocarcinoma at x20 demonstrating heterogeneity of glandular structures. Acknowledgement: Leticia Campo for optimisation and application of staining protocols, Mark Shipman for assistance in image acquistion and OCHRe for providing the tissue.

2.4.3 Summary

Using pre-clinical models, analytical methods to quantify total and bioavailable doxorubicin in tissue and plasma have been presented. In addition it has been demonstrated that, with optimised cell recovery techniques, flow cytometry can offer a rapid, sensitive and highly quantitative method to assess cell viability in tissue obtained from 18-14G liver biopsy cores of masses in the range of 5-20 mg [426]. The cell recovery method described (Section 5.1.2) could also be adapted to obtain cell suspensions for use with other analytical methods including, for example, single cell genome sequencing for use in oncogenetic studies [464].

In 18G tissue biopsy samples obtained in this clinical study, of approximate mass of 5 mg for a good biopsy, quantification of total doxorubicin and, in particular, its bioavailability, is a particularly difficult problem. Previous studies have utilised flow cytometry to quantify intracellular doxorubicin [432, 433] in different cell lines. However in the

clinical study, biopsy tissue must be shared between the doxorubicin quantification assay (evaluating the the primary endpoint) and the cell viability studies, reducing available tissue mass further. For masses of under 5 mg the technique begins to loose statistical relevance as the cell yield becomes small in tumour tissues. There are also practical considerations to take into account; a reasonably complex cell recovery protocol must be performed on the same day of intervention, and ideally immediately post-biopsy, in order to fix cells before natural *ex vivo* cell death ensues.

Thus in the quantification of doxorubicin levels in tissue, the fluorescence HPLC assay provides the most ideal solution. Where the HPLC method gains in sensitivity, and its ability to distinguish doxorubicin from its metabolites, it has the disadvantage that the solvent used for chromatography releases any encapsulated doxorubicin. For tissue samples, an additional nuclear isolation step has been discussed as an alternative to *estimate* bioavailable doxorubicin, but with such limited tissue masses this becomes impractical for this clinical study. Thus in tumour samples, the HPLC method presented can only be used to determine total intratumoral doxorubicin. For analysis of release and distribution of drug other methods are required.

Similarly, when considering clinical plasma samples, exact quantification of the bioavailable quantity of doxorubicin is not achievable using fluorescence HPLC, without first performing separation of free from encapsulated doxorubicin. Thus, the HPLC method presented can, again, only be used to determine total circulating doxorubicin. Separation by ultra-filtration has been used in the quality control of ThermoDox® production to ensure efficient encapsulation (Global Investigational Medicinal Product Dossier, Feb 2014, Celsion Corporation). However the additional ultra-filtration equipment comes at some expense, and is prone to blocking. The dequenching method discussed is an alternative simple technique that can be used to estimate the split between encapsulated and free doxorubicin in the circulation. As there is an abundance of available plasma, both the HPLC method and the dequenching method are used to analyse clinical samples from the study and clinical results are available in Section 3.3.

Fluorescence microscopy has been selected as the method of choice for demonstrating doxorubicin distribution, bioavailability and cell viability in tissue. This is because it has the advantages of practicality and facilitates multiple slices and stains from a single sample rather than a single shot assay. In addition it can provide morphological information including distribution of doxorubicin relative to vessels and other histological features. Clinical microscopy results are available in Sections 3.3.4 and 3.2.6.

CHAPTER 3

Clinical Study

3.1 TARDOX Overview

This feasibility study hypothesises that enhanced intratumoral delivery of doxorubicin can be achieved using the FUS/LTLD paradigm, for the same total systemic dose of doxorubicin. The following sections summarise key design aspects of the TARDOX study. The latest revision of the TARDOX study protocol is available from the Oxford University Hospitals NHS Foundation Trust Intranet for clinicians, or directly from the EPCTU. An overview of the study protocol's outcome measures and eligibility criteria are available on the ClinicalTrials.gov website (Identifier: NCT02181075).

3.1.1 Study Design

The TARDOX study is a single site Phase I study run at the Churchill Hospital in Oxford, under the clinical remit of Prof. Mark Middleton as the Chief Investigator. Prof. Constantin Coussios and Prof. Fergus Gleeson are the principal investigators for the study, whilst Prof. Feng Wu is the clinical HIFU consultant. The study is run through the Oncology Clinical Trials Office (OCTO), which is integrated with the Cancer Centre in the Churchill hospital. The study is an open-label design, with all participants receiving a single treatment cycle of ThermoDox® and FUS under a general anaesthetic. The study

has two parts: Part I, which involves implantation of an invasive thermometry device prior to FUS treatment and the taking of sequential tissue biopsies; and Part II, with no real-time thermometry and only a final post-FUS tissue biopsy.

3.1.2 Practical Considerations

Patients with either liver metastases or primary liver tumours are potentially eligible for screening. Other inclusion and exclusion criteria are covered in the clinical protocol. As part of the consent process, it is explained to participants that only a single liver tumour can be chosen for treatment in this Phase I study. Furthermore, as is often the nature with early-phase studies such as this, participation involves a high degree of altruism; it is explained that the study does not have curative intent, merely an aim to demonstrate the safety and feasibility of targeted drug delivery. This is reflected in the study endpoints, discussed in the following section. This said, participants with limited tumour burden in the liver may potentially benefit from receiving the study intervention, if indeed targeted drug delivery is proven successful and the tumour is responsive to enhanced levels of delivered doxorubicin, which may be incentivising in some participants.

Screening involves an ultrasound examination of the liver and only those participants with liver tumours that are potentially targetable by FUS are invited to continue on the study. The study runs in two parts. The purpose of Part I is to obtain real time bulk thermometry data during FUS exposure, using an indwelling thermometry device positioned in the core of the tumour (Figure 1.9). This clinical data is essential in optimising the clinical treatment parameters required to induce mild hyperthermia in a volume of perfused liver tumour for targeted drug delivery in the clinical setting. Extensive optimisation of FUS treatment plans using a pre-clinical *ex vivo* liver model has previously been discussed (Section 1.4.7).

Due to the requirement for an indwelling thermometry device in Part I, for a tumour to be treatable, it must be possible to visualise a target region within it transcostally,

from both the JC200 diagnostic ultrasound below the level of the water, and via a hand-held ultrasound device above the level of the water. This is so that FUS treatment and thermometry can be performed synchronously without need for patient repositioning. In addition, the co-axial needle used to insert the thermometry device provides a convenient port through which the three tumour biopsies can be taken during the procedure. Whilst this configuration provides crucial thermometry data, this requirement has the disadvantage of limiting patient selection to those with liver tumours in anatomical positions favourable for such triangulation. In practice, technical feasibility in Part I has been limited to target tumours in liver segments VI/VII (Figure 3.1), and even in these locations, Part I interventions have typically been technically challenging for the radiologist and FUS operator alike, due to mutual compromise in patient positioning. This restriction added to the challenge of recruitment, and contributed to the overall under-recruitment of the study.

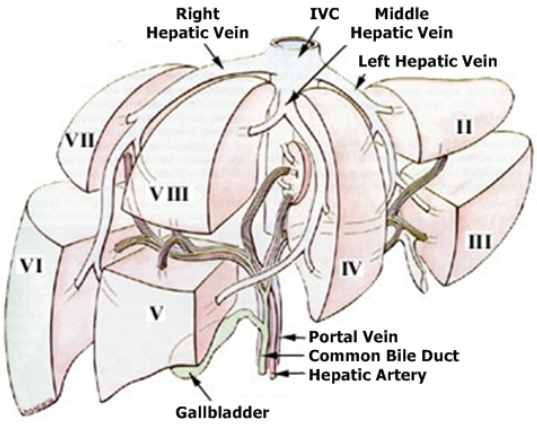


Figure 3.1: Couinaud classification: anatomy of the liver segments. Source: http://www.stefajir.cz/files/Liver_Segments.JPG

Part II more closely reflects how the TARDOX study may be adopted to more routine clinical practice. Collective Part I thermometry data is used in order to predict optimal FUS exposure parameters in the absence of thermometry. In Part II, temperature feedback is not available for the FUS operator; thus, whilst the absence of greyscale changes on the B-mode images provides confidence that parameters are below the ablative threshold, it

is not possible to be certain that optimal temperatures for drug release are being obtained during the procedure. However, the advantage to Part II is that it becomes completely non-invasive, other than a biopsy performed *after* the FUS procedure to validate drug delivery. Furthermore, no such ultrasound triangulation is required, therefore tumours in any liver segment can potentially be treated, as the patient may be positioned optimally for FUS exposure. At the point of biopsy, following FUS exposure and whilst still under the general anaesthetic, the patient can be repositioned to facilitate biopsy before the patient is recovered, thus Part II is technically much more straight-forward than Part I.

Due to more flexibility in target tumour position, the cohort of participants who are suitable for Part II is potentially greater than Part I. This said, in very large tumours with no distinguishing land-marks one must take caution in Part II. It may be possible to treat a partial tumour volume optimally, yet sample an unheated part of the same tumour under ultrasound-guidance, as there is no pre-existing co-axial needle to guide the radiologist as in Part I. This would clearly be of detriment to the study outcomes and thus such tumours may be deemed Part I candidates, if feasible, or alternatively not be offered the intervention. This highlights the great advantage of opening both parts of the study in parallel rather than progressing from Part I to Part II.

The protocol has been designed to include the option of adding ultrasound-based strategies for monitoring drug-delivery, which may include passive acoustic mapping [102, 409–413] and ultrasound thermometry [340–346]. Whilst such strategies would be highly desirable, particularly in Part II, at the current time they have not been applied, in part due to existing complexity of the Part I intervention and due to the relative immaturity of such methods for clinical application.

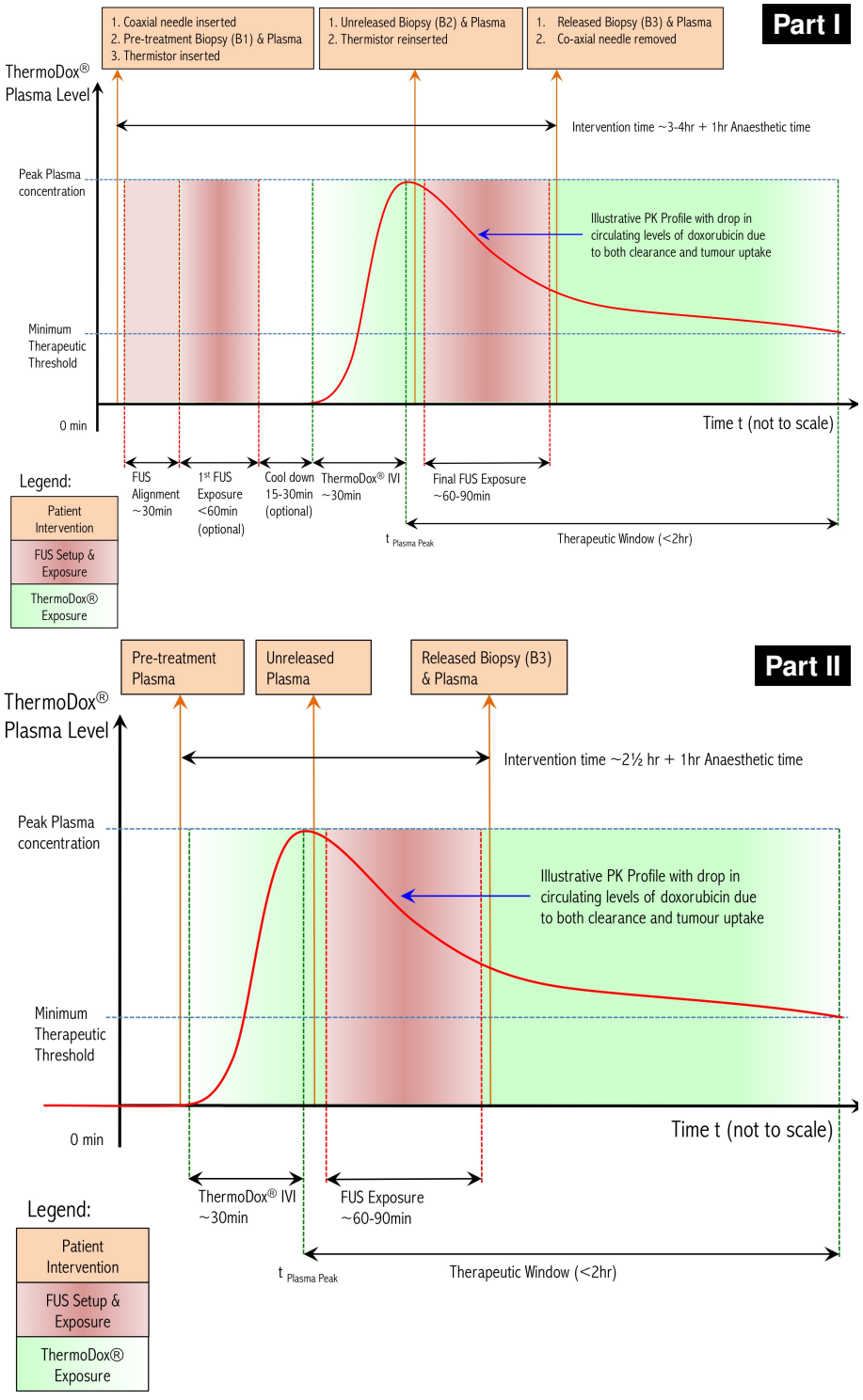


Figure 3.2: TARDOX study protocol timelines. IVI = Intravenous Infusion. Drug clearance curves not based on clinical PK data and are not to scale. Green shaded areas represent periods where drug is circulating in the absence of FUS. Pink shaded regions represent periods where FUS is being applied. In both cases the final FUS exposure overlaps the period where circulating drug is highest. Orange boxes represent interventions required for sampling (blood and biopsy) and thermometry. **Part I:** timeline demonstrating how the FUS parameters are first optimised prior to the drug infusion, under conditions of real-time thermometry, before being re-applied after drug infusion. **Part II:** timeline demonstrating a much simpler protocol involving a single FUS phase following the drug infusion.

In Part I, three intratumoral biopsies are performed specifically to evaluate the primary endpoint, and EDTA blood samples are obtained at synchronous time-points. In Part II, the first two biopsy samples are not required (Figure 3.2), but blood samples are obtained as for Part I. The final biopsy in Part II is repeated, such that there is redundancy. This is primarily to protect the evaluability of the primary endpoint - as the HPLC assay is a single shot assay which may be subject to human error or experimental failure on occasion. The biopsy and plasma samples collected during the intervention have the following naming conventions:

1. Pre-Treatment (B1) (biopsy in Part I only): The samples taken before any drug is infused.

2. Unreleased (B2) (biopsy in Part I only): The samples taken shortly following infusion of ThermoDox®, i.e. at the maximum circulating levels

3. Released (B3): The samples taken following the post-drug FUS has been given

3.1.3 Study Endpoints

The full study protocol details the study objectives and endpoints. In brief, the study's primary endpoint pertains to quantifying delivered intratumoral doxorubicin by HPLC analysis of biopsy samples, as described in Section 2.3.1. Specifically, the primary endpoint is defined as:

> *"A demonstrable two-fold increase in, or value exceeding 10* μg/g *of, the concentration of intratumoral doxorubicin at the treated tumour site following FUS-induced mild hyperthermia, in at least 50% of evaluable participants."*

This primary endpoint incorporates HPLC data from both Part I and II patients. In Part I, the increase in intratumoral concentration is determined by comparing the total

dose of doxorubicin between the second ('Unreleased') and the final ('Released') biopsy; In Part II, where there is only a final Released biopsy, the total doxorubicin concentration contained within it is compared to an average of the concentration in all evaluable Unreleased biopsies from Part I. The ideal control is tissue from a further control tumour exposed to systemic drug in the absence of FUS, taken at a near-synchronous time point. However due to ethical considerations, the number of biopsies that can be taken has an upper limit, and a single entry point further reduces potential harm to the patient.

Secondary endpoints address safety of both the drug and ultrasound-mediated hyperthermia, classified according to the common toxicity criteria adverse events (NCI CTCAE version 4). For hyperthermia in particular, secondary endpoints ensure that, in Part I, the hyperthermia remains within the desired range (and not exceeding 47°C) and, furthermore, in both parts of the study, there is no microscopic evidence of FUS-mediated ablation. The MRI scan performed the day following intervention (Section 3.4) also provides a further level of evidence in this regard, but does not pertain to an endpoint.

The first tertiary endpoint seeks to distinguish between encapsulated and bioavailable doxorubicin in tissue, which the HPLC assay cannot differentiate, by one of the following methods:

1. Presence of nuclear doxorubicin on fluorescence microscopy. Such fluorescence is a consequence of doxorubicin intercalation in DNA, an event which cannot occur without liposomal release

2. MR-spectroscopy methods of identifying accumulation of intratumoral ThermoDox® doxorubicin or their metabolites non-invasively, such as Chemical Exchange Saturation Transfer (CEST)[1].

[1]Currently there is no published MR-spectroscopy method or pulse-sequence which can determine the presence of ThermoDox® doxorubicin or their metabolites in the liver *in vivo*. Whilst such methods are under investigation pre-clinically at the Radiology Research Institute, Oxford, to date existing CEST pulse sequences do not have the required level of sensitivity. Consequently, to date, no clinical data has been collected to evaluate this endpoint and it will not be discussed further.

3. A decrease of in total doxorubicin plasma levels over time-matched clearance levels, following FUS-induced release[2,3].

The second tertiary endpoint relates to radiology evidence of response in the target and control tumours by cross-sectional (CT, MRI) and functional imaging (PET-CT) to assess efficacy, using standard radiological criteria, namely CHOI [465], RECIST [466] and PERCIST [467].

3.2 Safety & Feasibility

The cases performed to date have demonstrated feasibility of targeted drug delivery to the liver using FUS. Currently nine patients have been treated on the study; five in Part I and the remaining four in Part II. Table 3.1 details the demographics and tumour types for those patients treated on the study. The clinical samples obtained for the last two patients treated in Part II remain under analysis.

Patient ID	Part	Treatment Date	Sex	Age	Height (cm)	Weight (kg)	BMI	ASA Grade	Diagnosis
TXA101	I	24/03/15	M	50	172	67.0	22.6	II	Primary HCC
TXA102	I	06/05/15	F	60	158	60.3	22.4	II	Breast met.
TXA103	I	23/09/15	M	66	178	80.7	25.5	II	mCRC
TXA104	I	04/11/15	F	64	150	45.7	20.2	III	mCRC
TXA105	I	09/03/16	M	49	181	82.0	25.5	II	mCRC
TXB101	II	22/06/16	M	53	185	125.3	36.6	III	Lung met.
TXB102	II	20/07/16	F	63	158	61.7	24.7	II	mCRC
TXB103	II	09/11/16	F	53	162	72.0	27.4	III	mCRC
TXB104	II	11/01/17	M	65	171	79.0	27.0	III	mCRC

Table 3.1: Attributes of those patients treated on the study (met.=metastasis, HCC=hepatocellular carcinoma, mCRC=metastatic colorectal cancer). Several more patients were screened for the study, but did not make it to treatment.

[2]Plasma pharmacokinetics have previously discussed in Section 2.3.2

[3]Currently only clinical PK data for ThermoDox® when used in combination with RFA is published (Figure 2.33), as it may not be ethical to give ThermoDox® without evaluating its release by some intervention. Thus, as time-matched clearance levels in the absence of any other intervention are not available, this endpoint is currently non-evaluable. If the PK data becomes available in the future, such as a randomised-controlled trial involving ThermoDox® vs. ThermoDox®+intervention, this endpoint may be re-explored.

Table 3.2 details the tumour attributes for each patient treated, whilst Table 5.4 gives more information on the prior treatment history. Figure 4.1 shows the pre-treatment B-mode for the target tumour for patient TXB101, within the JC200 operators console. Of note, in this particular case, as the tumour was relatively small, the prescribed treatment volume of 40.7 cm^3, detailed on the console, was extended beyond the visible tumour margin where possible. Patient treatment times for Part I and II are shown in Table 3.3.

To date the clinical trials using ThermoDox® have demonstrated the safety profile is similar to that of doxorubicin (Table 3.5). Adverse events (AEs) for patients treated on this study are detailed in Table 3.4. Serious adverse events (SAEs) are limited to grade IV neutropenia in 4/9 patients and prolonged hospital stay due to confusion in 1/9. Neutropenia is an expected adverse event, and, in all cases, was transient and without the need for medical treatment with granulocyte-colony stimulating factor (G-CSF). This adverse event is in line with findings from other clinical studies to use the drug, including the HEAT study [398], and overall myelosuppression (leukopenia, neutropenia, lymphopenia, anaemia, and thrombocytopenia) is the most significant AE, and is seen in up to 60% of patients.

Patient ID	Tumour Location (Segment(s))	Tumour Dimensions (mm)	Estimated Volume (cc)[a]	Superficial Depth (mm)	Furthest Depth (mm)	Patient Position
TXA101	V+VI	35x25x30	13.7	35	58	Supine
TXA102	V+VI	62x58x47	88.4	48	124	Supine
TXA103	VI	70x70x58	148.8	80	133	Supine
TXA104	VI	62x47x48	72.2	38	87	Supine
TXA105	VI	66x40x48	66.4	36	79	Supine
TXB101	VI	29x33x37	18.5	52	90	Right lat. decubitus
TXB102	VI	58x98x70	206.8	26	56[b]	Supine + 30° tilt
TXB103	IV	64x76x88	224.1	56	86	Right lat. decubitus
TXB104	VI	55x38x52	56.9	27	67	Right lat. decubitus

Table 3.2: Attributes of target tumours treated on the study. Tumour dimensions taken from the baseline MRI acquired day prior to treatment, and in particular axial LAVA (contrast-enhanced), fat saturated sequences and coronal sequences.

[a]Estimated values calculated using ellipsoid volume, $V = \frac{4}{3}\pi.a.b.c$, where a,b and c are the orthogonal radii

[b]This figure relates to the furthest FUS-exposed depth as, intentionally, only the most superficial (posterior) region of the tumour was covered with FUS (49.9 cm^3), leaving the deeper tumour untreated by FUS. The deepest border of the tumour was 77 mm.

Patient ID	Part	Anaesthetic Time Before Drug Infusion	Anaesthetic Time After Drug Infusion	Total Anaesthetic Time Including Drug Infusion	Mean Anaesthetic Time
TXA101	I	332	65	429	368.6
TXA102	I	251	96	377	
TXA103	I	239	92	355	
TXA104	I	193	82	310	
TXA105	I	232	110	372	
TXB101	II	63	114	205	213.8
TXB102	II	150	119	245	
TXB103	II	76	94	200	
TXB104	II	75	100	205	

Table 3.3: Treatment times for the patients treated on the TARDOX study, including a break down of time spend before and after administration of the study drug.

Patient ID	Grade I	Grade II	Grade III	Grade IV
TXA101	Buttock pain Fatigue Sickness	Alopecia		
TXA102	Red face Back ache Right arm pain Rib pain (right) Anorexia	Urinary tract infection Alopecia		Neutropenia
TXA103	Pain/swelling of right arm Buttock pain			Neutropenia
TXA104	Abdominal pain Fatigue Vomiting Rib pain (right) Thrush Skin discolouration (groin)			Neutropenia
TXA105	Anorexia Nausea Rib pain (right)	Buttock pain Fatigue Respiratory tract infection Alopecia		
TXB101	Rib pain (right)	Alopecia	Neutropenia	
TXB102	Nausea Right upper quadrant pain Alopecia			Neutropenia
TXB103	Alopecia Ankle swelling	Fatigue Anaemia		
TXB104	Confusion[a] Alopecia	Fatigue Nausea & Vomiting Anorexia	Neutropenia	

Table 3.4: Adverse events in the patients treated on the TARDOX study, classified according to the common toxicity criteria adverse events (NCI CTCAE version 4). Note that TXB103 was lost to follow-up after two weeks due to fatigue, and as such the patient withdrew for the study.

[a] Although this was Grade I confusion, the resulting prolonged hospital admission meant it satisfied the criteria for a SAE.

Adverse Event	Percentage
Leukopenia Grade 3 (1000-1999/mm^3)	3.4
Leukopenia Grade 4 (<1000/mm^3)	0.3
Shock, sepsis	1.5
Systemic infection	2.4
Nausea only	15.5
Vomiting ≤ 12 hours	34.4
Vomiting > 12 hours	36.8
Intractable	4.7
Alopecia Partial	22.9
Alopecia Complete	69.5
Weight loss 5-10%	6.2
Weight loss >10%	2.4
Weight gain 5-10%	10.6
Weight gain > 10%	3.8

Table 3.5: Relevant adverse events in 1492 patients with early breast cancer involving axillary lymph nodes who recieved 2 months of adriamycin (doxorubicin) and cyclophosphamide (AC) combination therapy. Data obtained from the National Surgical Breast and Bowel Project (ASABP) implemented protocol B-15 to compare 2 months of AC regime with 6 monhts of conventional cyclophosphamide, metotrexate and fluorouracil (CMF) in patients with breast cancer non-responsive to tamoxifen [468].

3.2.1 Thermal Dose Threshold

Based on a modified Arrhenius-based system, early work by Sapareto and Dewey [372] led to introduction of the concept of a thermal isoeffect dose (TID) model defined by Cumulative Equivalent Minutes at a reference temperature of 43°C (CEM_{43}) [353, 373, 469]. This thermal dose model was designed around the premise that in *in vitro* cell lines, it takes 240 minutes for >96% cell death at 43°C, and this time halves for each subsequent degree rise i.e. t=900s at 47°C, t=3.52s at 55°C, t=0.11s at 60°C.

By integrating a thermal dose profile over time and normalising to an equivalent dose at the reference temperature, the model has been used to predict cell death. The CEM_{43} model was first applied to HIFU ablations *in vivo* by Damianou *et. al* [470] and was later used clinically to quantify hyperthermia-enhanced radiation response in superficial

tumours [471]. The model has become the industry standard for ablative systems [472] and most recently for MRgFUS ablation of fibroids with accurate histopathological correlation [473].

The equation for CEM_{43} as follows, where R can be approximated to 0.5 for most biological tissues above 43°C, and 0.25 below this temperature [474]:

$$CEM_{43} = \int R^{43-T(t)} dt \tag{3.1}$$

Typically, for many soft tissues, the critical thermal dose limit is well reported in the literature as CEM_{43} of 240 minutes. However, in practice CEM_{43} will naturally vary with tissue type and whilst it is known that dose limits in the range of 320-340 minutes in normal liver parenchyma are ablative [475, 476], the onset of functional liver damage is likely to occur at lower values [477]. In the absence of concrete published data, for the purposes of the TARDOX study it seems reasonable to expect CEM_{43} values of less than quarter of 240 minutes to satisfy safety criteria (the absence of thermal ablation of normal liver tissue or liver tumour). For this purpose, a MatLab script has been developed to convert temperature history into CEM at a reference temperature of 43°C, and this has been applied to clinical data (Section 3.2.4). However, Sapareto and Dewey's CEM_{43} model was validated in a subset of human cell lines *in vitro* up to 50°C, and for gradual temperature rises only. It has not been validated *in vivo* for tissues exposed to instantaneous temperature rises above 50°C, i.e. those which occur during ablative HIFU. Indeed, Dewhirst *et. al* identified the lack of application to human tissues [478]. Thus, although it remains a useful metric, a degree of caution should be applied when relying on this model alone to predict presence or absence of coagulative necrosis clinically, when applying FUS in tumours of different histological origins, each with anatomical differences and varying degrees of perfusion. It is for this reason that this clinical study also evaluates available biopsy tissue microscopically, in an attempt to confirm the absence of direct ablative insult due to FUS (3.2.6).

3.2.2 Inertial Cavitation Thresholds

At high rarefactional pressures, the focus of the FUS propagation may place target tissue under enough tension as to create small cavities, which rapidly fill with gas and vapour. This process is known as acoustically induced cavity nucleation [91] and the pressure threshold for these gas pockets, or microbubbles, to form depends on the fluid or tissue medium [90]. Once these nucleation sites are established, further FUS exposures will result in the pulsation of these bubbles, which is a process known as acoustic cavitation. Inertial cavitation is a process of rapid and unstable expansion and violent collapse of such a bubble, which can occur even after a single acoustic cycle [92]. At the time of collapse, inertial cavities radiate energy into surrounding tissue in the form of broadband energy, which may result in dramatically enhanced heating at the FUS focus [91]. At lower pressures, mechanical effects of cavitation and radiation force may contribute to the release of the liposomal contents at the target site [337].

Cavitation phenomena have been associated with a wide range of desirable therapeutic effects *in vivo*, including enhanced vascular permeability, cell membrane permeabilisation, enhanced dose delivery, drug release and penetrance [100–104, 479]. However, pressures required to generate cavitation in tissue are high. The *in vivo* transient (inertial) cavitation threshold in in the thigh muscle of dogs at 1 MHz has previously been found to be at a peak pressure amplitude of almost 6 MPa [336]. Another more recent study has shown the threshold in *in vivo* murine pancreatic tumours to be above 5 MPa peak negative (rarefactional) pressure [104]. Further study is required to determine the inertial cavitation threshold in human liver tumours, and, at best, these figures only serve as an estimate.

Of great relevance here, in clinical USgFUS systems, the appearance of hyperechoic greyscale changes on B-mode images due to tissue boiling are typically used to determine when tissue has been successfully ablated in HIFU treatments [339, 480]. The formation of hyperechoic regions on ultrasound images has been shown to be caused by thermally-

driven formation of large bubbles, a process which likely would occur at higher pressures than would be required for the onset of inertial cavitation only following over-treatment of the target tissue [481]. Thus in the TARDOX study, where no such B-mode changes would be expected, it is conceivable that cavitation effects below the threshold for tissue destruction may be occurring undetected, and this may potentially be providing enhanced drug delivery at the target site, in addition to the hyperthermia-mediated effects, including release of doxorubicin from ThermoDox®.

As the initial onset of cavitation cannot be determined by B-mode imaging, previous pre-clinical studies have typically determined threshold values by listening with a hydrophone which is capable of identifying the presence of broadband emissions, a technique known as passive cavitation detection (PCD). The TARDOX protocol intentionally includes the flexibility to include a PCD device during clinical treatments, although, to date, treatments have not incorporated such a monitoring device. The reason for this is that only a passive cavitation array confocally aligned with the FUS transducer could confirm that any observed cavitation occurred not in the ultrasound propagation path but in the target tumour. However, the limited access for additional instrumentation within the water bath on the clinical FUS device made the insertion of a passive detection array difficult. Finally, in preliminary experiments, it was found that the high level of broadband noise emissions produced by the HIFU device itself made it very challenging to distinguish broadband acoustic emissions occurring at depth within tissue. For these reasons, a PCD device could not ultimately be used in the present study.

3.2.3 Focused Ultrasound Pressure Estimations

In attaining bulk temperatures, FUS must penetrate through skin, subcutaneous fat, muscle tissues between an intercostal space and then connective tissue layers, and often some normal liver parenchyma before reaching the target liver tumour. Each tissue type has its own acoustic properties and, in particular, attenuation coefficient. This means that the incident focal pressure produced by the JC200 transducer in water (free-field) becomes

derated by the time it is transmitted to the target tumour volume in the clinical case. Full treatment parameters for each case are shown in Table 3.9. By taking the JC200 output powers alone, it is possible to estimate the free-field (Figure 2.18) and consequently derated pressures at the axial centre of each treated target tumour. For a FUS field, in the absence of non-linear contributions to heating, the relationship between the pressure attenuation in dB, a_{dB}, and attenuation in linear units for pressure calculations in MPa, a_{lin}, is as follows:

$$a_{dB} = 20.log_{10}(e^{-\alpha.z}) \tag{3.2}$$

$$a_{lin} = 10^{(\frac{a_{dB}}{20})} = e^{-\alpha.z} \tag{3.3}$$

Where α is material-dependent and defined in units of nepers/cm (Np/cm), and z is the depth in cm. At 1 MHz driving frequency, using values averaged from the literature [482–487], α is 0.054 Np/cm in metastatic liver tumours and 0.069 Np/cm in healthy liver parenchyma. If the latter value of 0.069 Np/cm is taken as an average value for $alpha$ over all the tissues encountered in the FUS propagation path, from Equation 3.2, a_{dB} is 0.60 dB/cm, which substitutes into Equation 3.3 as follows:

$$a_{lin} = 10^{(\frac{-0.6.z}{20})} = 10^{-0.03.z} \tag{3.4}$$

Where a_{lin} is the total linear attenuation factor over distance of z. Using Equation 3.4, the estimated derated pressures have been calculated relative to the axial centre point of each targeted tumour volume. Estimated derated pressures are shown in Table 3.6. It should be noted that these calculations have been made assuming all energy remains in the fundamental and there are no non-linear effects. As such, these estimations remain an upper bound of the possible pressure transmitted.

Patient ID	Depth to Centre of Target Volume from Skin (mm)[a]	JC200 Output Power (W)	Free-field Pressure (MPa P-P)[b]	Derated Pressure (MPa P-P)[c]	Duty Cycle (CW/%)
TXA101	47	50	18.9	13.7	CW
TXA102	86	70	21.4	11.8	CW
TXA103	107	100	24.5	11.8	CW
TXA104	63	140	28.0	18.2	50
TXA105	58	130	27.2	18.3	85
TXB101	71	128	27.0	16.5	55
TXB102	41	114	25.8	19.4	42
TXB103	55	140	28.0	17.3	44
TXB104	48	110	25.5	19.9	40

Table 3.6: Summary of JC200 treatment parameters used showning derated pressures at the center point of the FUS-target volumes and duty cycles (DCs). Where multiple powers were used in a treatment, the highest powers and DCs have been taken. CW=Continuous Wave (100% DC).

[a]Mean of proximal and distal lengths in the direction of FUS propagation, as defined in Table 3.2. Where partial tumour volumes were treated, this has been reflected in the depth calculation.

[b]Peak-to-peak powers, based on free-field JC200 calibration in degassed water as, described in Section 2.2.1, before derrating.

[c]Based on the tumour center point, along the axial direction of propagating FUS.

If taking an approximated inertial cavitation threshold of 12 MPa peak-to-peak (Section 3.2.2), derated powers for the FUS treatments performed in this study have just met or exceed this threshold in all cases, whilst remaining below thresholds of ablation and lethal thermal dose. It follows that cavitation may be acting synergistically with hyperthermia-triggered release to provide enhanced liposome transport in addition to extravasation and penetration of released doxorubicin into the tumour by cavitational micro-streaming (Section 1.2.3).

A brief pre-clinical study was performed to determine if mechanical lysis of ThermoDox® was achievable using the clinical device, in the absence of significant FUS-mediated heating. OptiCell™ chambers were filled with 20 μg/mL of ThermoDox® diluted in phosphate buffered saline (PBS), immersed in degassed water and exposed to similar derated pressures to those used clinically at a 50% duty cycle. Liposomal release was not demonstrated (data not included for brevity). However, due to practical considerations, the experiment was performed in degassed water at room temperature, not physiologic

temperatures, and thus is not conclusive. Further work using a pre-clinical experimental setup has shown that at 37°C, closer to the transitional temperature, transient opening of ThermoDox® diluted in PBS is achievable using repeated shockwave exposures in the absence of significant heating, presumably due to a mechanical and/or cavitation effects (data not shown, acknowledgements: Dr. Shamit Shrivastava, Dr. Michael Gray).

3.2.4 Real-time Clinical Thermometry Data

Post-drug thermometry traces were analysed using a custom MatLab script, and the summary of results is available in Table 3.10. In particular, the cumulative time over the drug release threshold was calculated with CEM_{43}. In order the be defined as 'optimal hyperthermia', over the first 1.5 hours post drug infusion, a thermometry trace has to meet the following criteria as a minimum:

1. Cumulative time >39.5°C is in excess of 300 seconds
2. Continuous time >39.5°C is in excess of 60 seconds
3. CEM_{43} less than 25% of that for expected cell death in liver, i.e. under 60 minutes (Section 3.2.1)

These are defined in the statistical analysis plan (SAP) for TARDOX, which is a version-controlled document maintained by OCTO and under the remit of the Oxford Clinical Trials Research Unit (OCTRU) and the Centre for Statistics in Medicine (CSM). The criteria above used to define optimal release are perhaps rather generous, and, in reality, a longer duration of hyperthermia is desirable as the time above the release temperature threshold is likely to be directly related to total drug release, within the bounds of the drug pharmocokinetics. Furthermore temperatures in the range of 41-43°C will ensure maximal release whilst remaining well within safety limits, and may extend the zone of chemo-ablation due to giving a higher temperature gradient to that tissue on the periphery of the exposed volume. It is also important to consider that these temperatures should

ideally be attained as soon as possible after infusion, whilst the circulating ThermoDox® levels are highest. For each patient treated in both Part I and II, the parameters used for treatment planning on the JC200 are shown in Tables 3.7 & 3.8. For Part I patients, the real-time thermometry is shown in Figures 3.3-3.7 and summarised in Table 3.8 and Figure 3.10.

Patient ID	FUS Treatment	Slice Thickness (mm)	Slice Sep. / No. Slices	Mode	Dot Int. (on:off:int.)/Lin. Speed	Row Dist. (mm) (Min. Depth Int.)	Prescribed Units	Prescribed Vol. (cc)
TXB101	Post Drug (i)	2	4/13	Linear	6 mm/s	10		
TXB101	Post Drug (ii)	2	4/13	Linear	6 mm/s	10	72	40.7
TXB101	Post Drug (iii)	2	4/13	Linear	6 mm/s	10		
TXB102	Post Drug (i)	2	4/13	Linear	6 mm/s	10		
TXB102	Post Drug (ii)	2	4/13	Linear	6 mm/s	10	81	49.9
TXB102	Post Drug (iii)	2	4/13	Linear	6 mm/s	10		
TXB103	Post Drug (i)	2	4/13	Linear	6 mm/s	10		
TXB103	Post Drug (ii)	2	4/13	Linear	6 mm/s	10		
TXB103	Post Drug (iii)	2	4/13	Linear	6 mm/s	10	52	30.7
TXB103	Post Drug (iv)	2	4/13	Linear	6 mm/s	10		
TXB103	Post Drug (v)	2	4/13	Linear	6 mm/s	10		
TXB104	Post Drug (i)	2	4/21	Linear	6 mm/s	10		
TXB104	Post Drug (ii)	2	4/21	Linear	6 mm/s	10	83	53.9
TXB104	Post Drug (iii)	2	4/21	Linear	6 mm/s	10		

Table 3.8: Parameters for the treatment plan for each Part II target tumour, as configured on the JC200. A pulse interval of 100 ms / 10 Hz was used in all cases. For more information on prescribed volume see footnote in 3.7.

Patient ID	FUS Treatment	Slice Thickness (mm)	Slice Sep. / No. Slices	Mode	Dot Int. (on:off:int.)/Lin. Speed	Row Dist. (mm) (Min. Depth Int.)	Prescribed Units	Prescribed Vol. (cc)[a]
TXA101	Post Drug (i)	2	4/11	Dot	1s:1s:2mm	8	354	10.5
TXA101	Post Drug (ii)	2	4/11	Dot	1s:1s:2mm	8		
TXA102	Post Drug (i)	2	4/11	Dot	2s:1s:2mm	8	-	Est. 25[b]
TXA102	Post Drug (ii)	2	4/11	Linear	6 mm/s	8		
TXA103	Post Drug (i)	2	4/21	Linear	6 mm/s	12	<158	73.2
TXA103	Post Drug (ii)	2	4/21	Linear	6 mm/s	8 [c]	158	
TXA104	Post Drug (i)	2	4/21	Linear [d]	6 mm/s	12	99	73.4
TXA104	Post Drug (ii)	2	4/21	Linear	6 mm/s	12		
TXA104	Post Drug (iii)	2	4/21	Linear	6 mm/s	12		
TXA104	Post Drug (iv)	2	4/21	Linear	6 mm/s	12		
TXA105	Post Drug (i)	2	4/24[e]	Linear	6 mm/s	12	<129	<90.9
TXA105	Post Drug (ii)	2	4/14	Linear	6 mm/s	12	74	63.8

Table 3.7: Parameters for the treatment plan for each Part I target tumour, as configured on the JC200. A pulse interval of 100 ms / 10 Hz was used in all cases. Prescribed units refers to the total number of dots or linear sweeps which the operator software automatically generates to fill the user-defined treatment volume and within the constraints of the other spacing parameters.

[a]The prescribed volume reported by the JC200 refers to the volume which is bounded by user-defined coordinates, which is used to generate FUS treatment plans. The prescribed volume is thus independent of the coverage mode and unit spacing used in the treatment plan and it includes spaces between treatment units. It can be thought of as the size of tumour volume covered by FUS in a single cycle. The volume covered by a (moving beam) linear unit (single linear sweep makes a row) is typically much greater than that of a dot unit (multiple dots make a row). This explains why the case performed in dot mode, TXA101, has many more prescribed units than the linear mode cases, which are of larger overall prescribed volume.

[b]The prescribed volume was not recorded at the time of treatment and was subsequently not available from the JC200 generated report.

[c]After the first cycle given using a row distance (minimum depth interval) of 12mm, the second complete cycle and third partial cycle used a reduced row distance of 8mm.

[d]This FUS exposure was performed in top-to-bottom slice ordering, rather than the usual slice-to-slice ordering used in all other cases

[e]The initial prescribed volume was divided across 24 slices, which was split over a rib. During treatment, the actual volume covered with FUS was less, as peripheral slices were skipped in the interests of maintaining sufficient temperatures in the region of the thermocouple. When reducing to a smaller volume across 14 slices, temperatures became easier to maintain due to much less transducer translation time across the rib space, thus significantly reduced off time.

Patient ID	FUS Treatment	Start Time	End Time	Real-time	JC200 Power (W)	Duty Cycle	Units Delivered	Energy Delivered (KJ)	FUS 'on' Time (s)
TXA101	Post Drug (i)	15:54	16:19	25m	50	CW	354	21.1	422
TXA101	Post Drug (ii)	16:22	16:27	5m	50	CW	68		
TXA102	Post Drug (i)	14:10	15:05	55m	70	CW	unknown[a]	72.3	1040
TXA102	Post Drug (ii)	15:05	15:25	20m	70	CW			
TXA103	Post Drug (i+ii)	14:00	15:13	72m 56s	100	CW	254	273.3	2733
TXA104	Post Drug (i)	12:39	13:05	26m 0s	140	50	99	71.5	1021
TXA104	Post Drug (ii)	13:06	13:11	5m 9s	140	30	18	7.8	186
TXA104	Post Drug (iii)	13:11	13:32	21m 13s	140	40	81	46.8	835
TXA104	Post Drug (iv)	13:34	13:45	11m 16s	140	50	42	30.3	433
TXA105	Post Drug (i)	13:41	14:14	33m 15s	110	70	213	218.6	2839
TXA105	Post Drug (ii)	14:16	15:01	44m 50s	130	85			
TXB101	Post Drug (i)	11:13	11:33	20m[b]	118	55	72	43.7	673
TXB101	Post Drug (ii)	11:34	11:52	18m	128	55	72	47.4	673
TXB101	Post Drug (iii)	11:54	12:12	18m	128	55	72	47.4	673
TXB102	Post Drug (i)	11:45	12:05	20m	114	42	81	39.1	816
TXB102	Post Drug (ii)	12:08	12:27	20m	114	42	81	39.1	816
TXB102	Post Drug (iii)	12:30	12:50	20m	114	42	81	39.1	816
TXB103	Post Drug (i)	11:36	11:48	12m	140	44	52	30.8	500
TXB103	Post Drug (ii)	11:48	12:00	12m	140	44	52	30.8	500
TXB103	Post Drug (iii)	12:02	12:14	12m	140	44	52	30.8	500
TXB103	Post Drug (iv)	12:15	12:27	12m	140	44	52	30.8	500
TXB103	Post Drug (v)	12:28	12:40	12m	140	44	52	30.8	500
TXB104	Post Drug (i)	11:31	11:53	22m	110	40	83	38.4	873
TXB104	Post Drug (ii)	11:53	12:15	22m	110	40	83	38.4	873
TXB104	Post Drug (iii)	12:15	12:37	22m	110	40	83	38.4	873

Table 3.9: The individual treatments delivered, corresponding to the treatment plans shown in Tables 3.7 & 3.8. All treatment plans used treatment head J081C-170 (S/N 20099-44) at 0.96 MHz, with a 154 mm focal length. Energy delivered was captured from the JC200 treatment reports and has subsequently been corrected for DC, but no such correction for loses due to attenuation and rib blocking have been made. Conversely, FUS 'on' time is represented as if given in CW. The duration of real-time monitored for each FUS treatment does not necessarily represent a single FUS cycle, and may represent multiple cycles.

[a] The same treatment plan was used for planning and treatment thus it is not possible to distinguish how many units were attributed to each. Similarly the energy and FUS on time for this patient delivered during treatment was estimated as a proportion using real-time.

[b] This cycle is slightly longer due to two pauses to check settings.

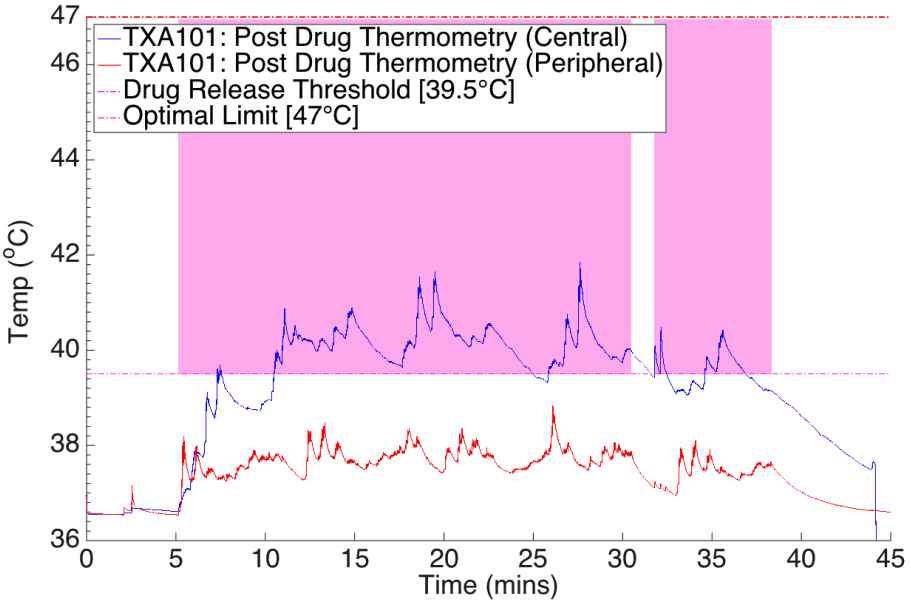


Figure 3.3: Real-time thermometry data captured post-drug infusion and during FUS exposure (pink shaded regions) for TXA101. Acquired using AngioDynamics thermistors both central placed (blue trace) and in the periphery of the tumour (red trace), demonstrating that hyperthermia was localised to the core of the target tumour. $1\frac{1}{5}$ FUS exposure cycles completed at 50 W continous wave in dot mode (1 second on, 1 second off) over a prescribed volume of 10.5 cm^3.

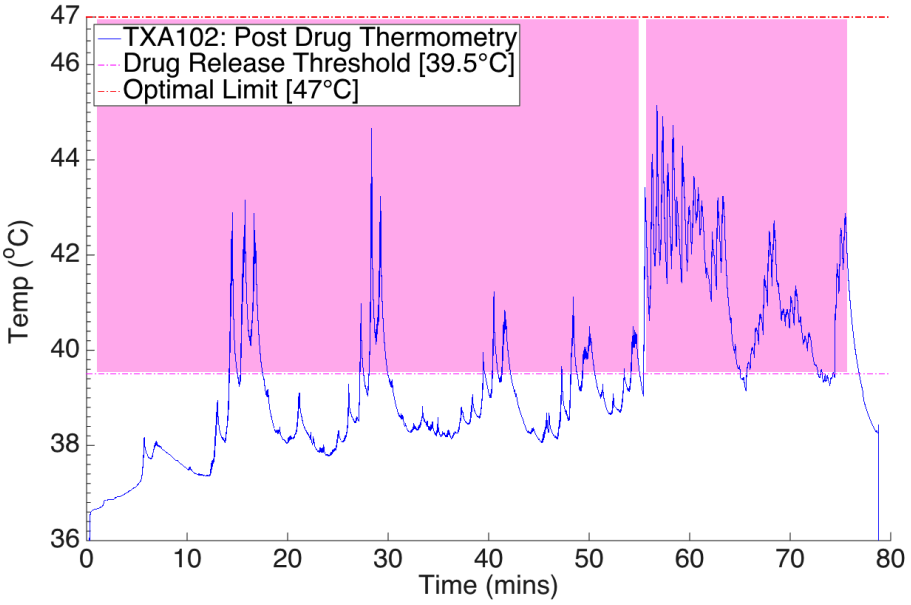


Figure 3.4: Real-time thermometry data captured post-drug infusion and during FUS exposure (pink shaded regions) for TXA102. Acquired using AngioDynamics thermistor. 1 FUS exposure cycle completed at 70 W continous wave in dot mode (2 seconds on, 1 second off) over an estimated prescribed volume of 25 cm^3 followed by 20 minutes of free-hand painting around the region of the thermistor tip in linear mode (6 mm/s) at the same power settings and DC.

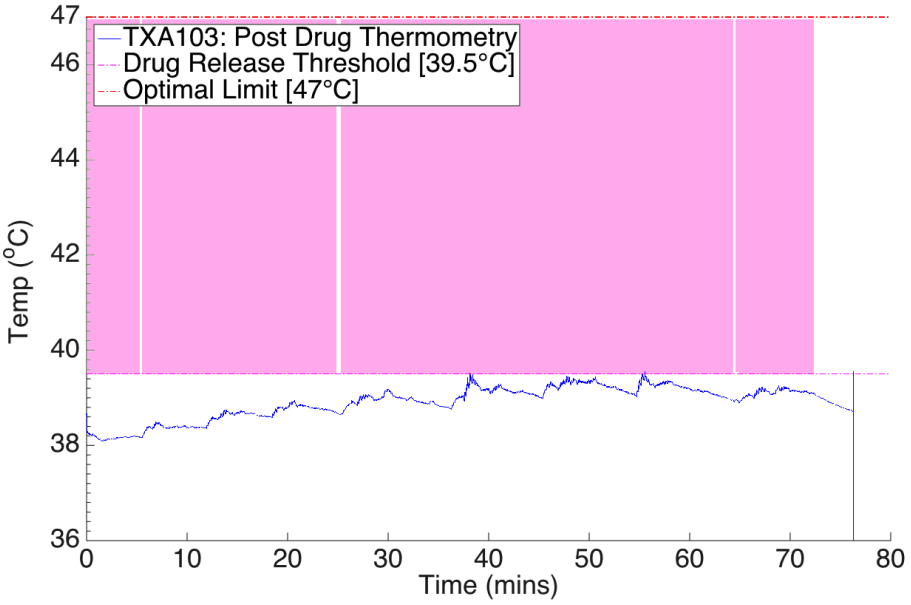


Figure 3.5: Real-time thermometry data captured post-drug infusion and during FUS exposure (pink shaded regions) for TXA103. Acquired using AngioDynamics thermistor. Two complete FUS exposure cycles and a third partial cycle completed at 100 W continous wave in linear mode (6 mm/s) over a prescribed volume of 73.2 cm^3. The first cycle had a row distance of 12 mm, whilst the second and third partial cycle had a smaller row distance of 8 mm.

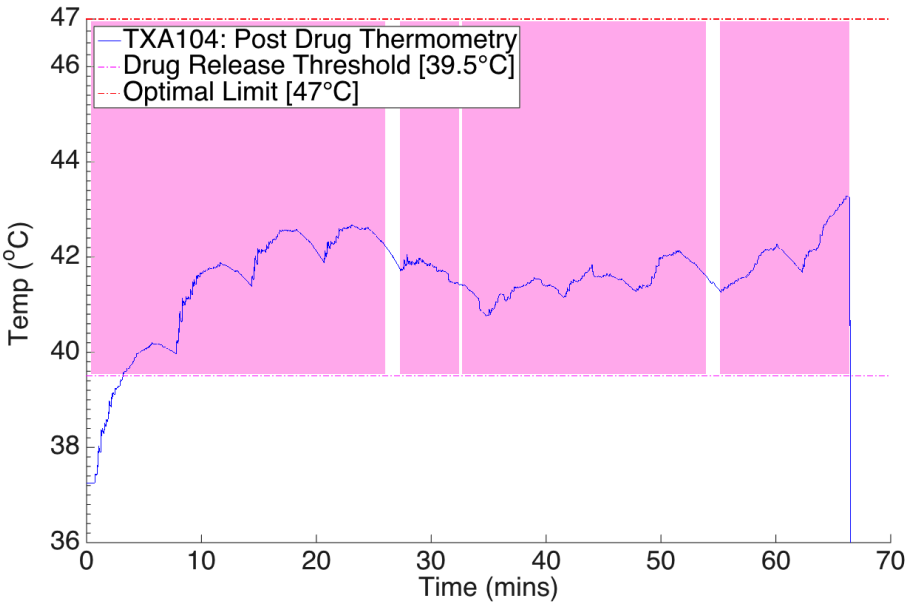


Figure 3.6: Real-time thermometry data captured post-drug infusion and during FUS exposure (pink shaded regions) for TXA104. Acquired using AngioDynamics thermistor. $2\frac{2}{5}$ FUS exposure cycles completed at 140 W in linear mode (6 mm/s) over a prescribed volume of 73.4 cm^3. The first cycle was at 50% DC, the second at 30/40% DC and the final $\frac{2}{5}$ of a cycle at 50% DC.

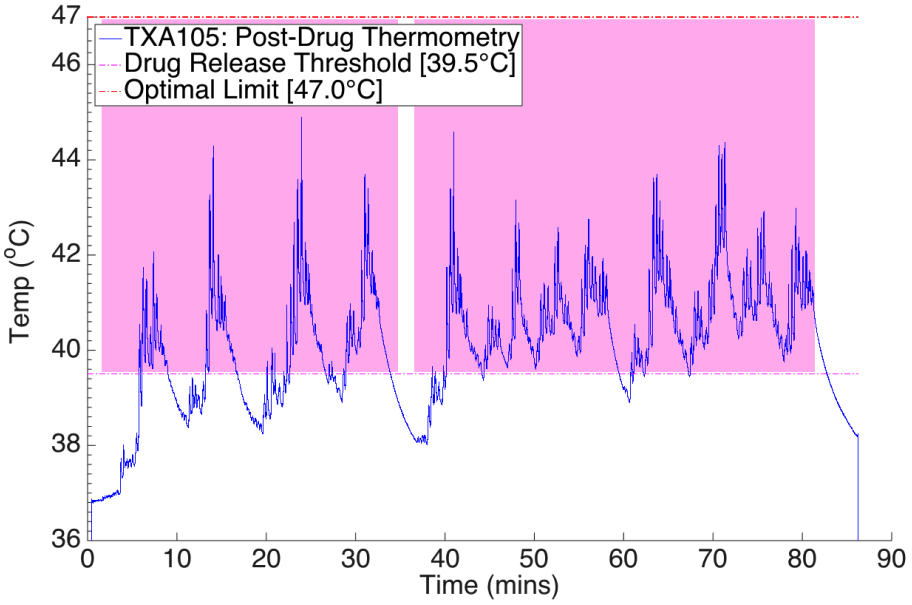


Figure 3.7: Real-time thermometry data captured post-drug infusion and during FUS exposure (pink shaded regions) for TXA105. Acquired using calibrated Medtronic thermocouple without dynamic cold-junction compensation. Trace post-calibrated to the oesopheageal temperature probe at the end of treatment. An initial partial FUS exposure cycle was completed at 118 W, 55% DC in linear mode (6 mm/s) over a initial prescribed volume of 90.9 cm^3, but with skipping. A second complete FUS exposure cycle was completed at 128 W, 55% DC in linear mode (6 mm/s) over a smaller prescribed volume of 63.8cm^3.

Patient ID	FUS Treatment No.	Trace Start Time	Trace Duration	Duration of FUS Treatment	Max. Temp.	Min. Temp.	Mean Temp.	Time 39.5-47°C (culm.)	Time 39.5-47°C (cont.)	CEM_{43}
TXA101	(i+ii)	15:48	53:18	31:57	41.85	36.61	39.75	23:19	14:28	0:35
TXA102	(i)	14:10	55:37	53:51	44.67	36.67	38.63	9:54	9:36	7:45
TXA102	(ii)	15:05	25:00	20:00	45.15	39.14	41.33	19:12		
TXA103	(i)	14:00	1:43	1:29	38.84	37.70	38.12	0:00	0:02	0:17
TXA103	(ii)	14:02	1:28:48	1:11:27	39.56	38.09	38.90	0:06		
TXA104	(i)	12:39	1:11:28	1:03:15	43.29	37.25	41.53	63:20	63:20	14:12
TXA105	(i)	13:41	1:26:16	33:15	44.91	36.83	39.54	16:23	15:20	5:31
TXA105	(ii)	14:16		44:50	44.60	38.00	40.52	40:49		

Table 3.10: Summary of the post-drug thermometry analysis for the Part I patients. Analysis was only applied to the durations during which FUS was being applied (pink shaded regions in the plots).

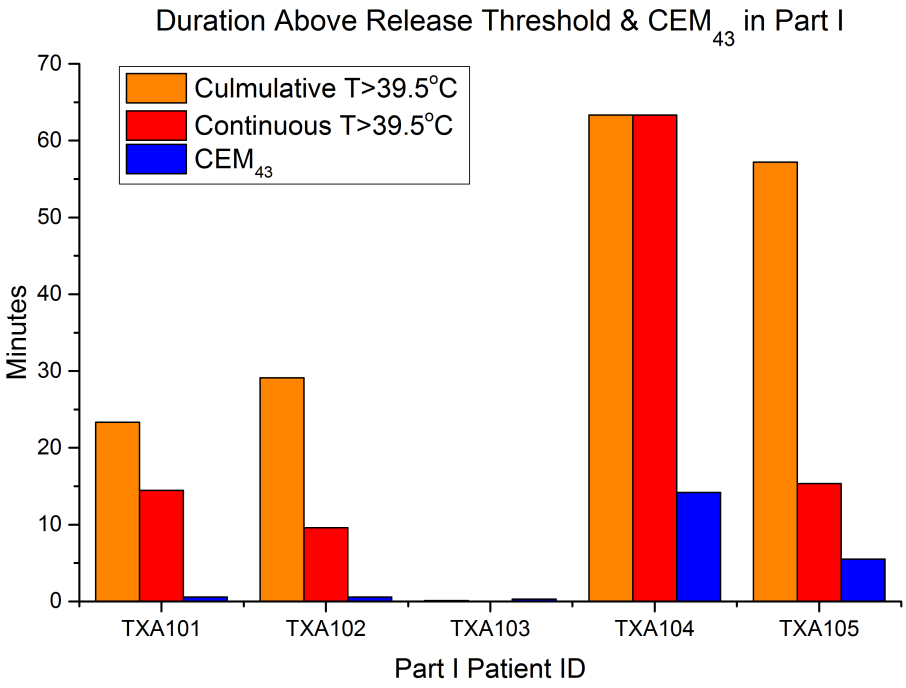


Figure 3.8: Graphical representation of the post-drug thermometry analysis for the Part I patients including cumulative and continous time above the drug release threshold of 39.5°C, and CEM_{43}. Analysis of thermometry data performed using custom CEM_{43} algorithm developed in MatLab (Section 3.2.1.

Interpretation of Clinical Thermometry Results

With the exception of TXA103, all patients received cumulative hyperthermia over the drug release threshold of 39.5°C for between 23-63 minutes without exceeding 47°C, whilst remaining well below the defined CEM_{43} threshold (60 minutes) deeming optimal hyperthermia. It is not practicable to correlate overall hyperthermia time with the level of drug release due to tumour heterogeneity and sampling variability. This said the majority of tumours receiving optimal hyperthermia demonstrated localised radiological response (Section 3.4).

Whilst early cases used 'Dot Mode' (or single shot), later treatments utilised 'Linear Mode' (or moving beam) due to pre-clinical demonstration of improved heating efficiency, especially for clinically-relevant tumour volumes (Section 2.2). Optimal hyperthermia below the CEM_{43} limit was achieved in the target tumour of all Part I patients

except that of TXA103. As expected there was an absence of hyper-echoic grayscale changes on the post-exposure B-mode images of the target in all cases. Each patient is briefly discussed in turn. In each case, experience from the previous treatments was used to optimise treatment.

TXA101 was the only case to use both centrally and peripherally placed thermistors. The first inserted thermistor was deemed to be peripherally placed in the tumour, and, rather than removing it, a decision was made to insert a second, central, thermistor in order to measure the peak tumour bulk temperatures. The vast majority of the tumour was visible on B-mode through a single intercostal space and dot mode with 1 second exposures was used to heat a prescribed volume of 10.5 cm^3 for an estimated tumour volume of 13.7 cm^3. At 50 W in continuous wave, at an estimated 13.7 MPa derated peak-to-peak pressure, over 23 minutes of optimal hyperthermia was achieved centrally (Figure 3.3). In addition, by having a peripheral thermistor, the thermometry for this case demonstrates that hyperthermia can be highly targeted, given the low temperature rise recorded in the periphery.

TXA102 was a larger tumour volume estimated to be 88.4 cm^3. Through a single intercostal window, only a portion of this tumour was accessible for FUS treatment and an estimated volume of 25 cm^3 was prescribed, the exact figure unfortunately was not recorded at the time of treatment. Dot mode, at a power of 70 W and an estimated 11.8 MPa derated peak-to-peak pressure, was initially used to heat this volume. Using longer 2 second exposures, 55 minutes were required to cycle through the prescribed tumour volume (Figure 3.4). The resulting thermometry trace demonstrates the majority of this time was spent under the release threshold, with only short periods above it for a total of nearly 10 minutes. At this point, whilst remaining drug was still circulating, a decision was made to switch to free-hand linear mode and perform localised heating around the vicinity of the thermistor tip. This is represented by the second treatment duration of 20 minutes, from 55 minutes onwards, for which 19 minutes was above the release threshold. Although release temperatures were much more easily sustained using this approach, it

was over a smaller volume than originally intended.

TXA103 was the most technically challenging case encountered. Several attempts at co-axial needle repositioning were required in order to place the needle in a central area of tumour and there was initial difficulty localising the coaxial needle with the JC200, leading to delays. The case was complicated further as air was inadvertently injected into the tumour on instrumenting with the thermistor, making visual and thermal alignment more difficult. Ultimately, whilst temperature elevations were seen with FUS exposure, convincing thermal alignment was not achieved nor was optimal hyperthermia in the planning stages. At this stage, in what was believed to be in the best interests of the patient, a team decision was made to give the drug and expose the tumour with FUS, given the alternative of waking the patient without attempting the intervention. During planning stages, it was identified that the Bair Hugger™ forced-air warming blanket had led to a mild increase in core body temperature, and settings were subsequently changed to ambient cycle. Core body temperature registered at 38°C on commencement of post-drug FUS. As no significant 'spike' artefacts were seen at any point of FUS exposure, it was deemed that in this case, the thermistor sweet spot was close the the treatment volume but either not within it, or rib-shielded. Consequently power settings remained conservative, and based on planning parameters, rather than ramping in an attempt to obtain the necessary registered temperature rises to be deemed optimal. Linear mode at 100 W power (11.8 MPa derated peak-to-peak pressure) was used to treat a prescribed volume of 73.2 cm^3 of an estimated 148.8 cm^3 tumour through a single intercostal space. A complete treatment cycle took 26 minutes with a 12 mm line separation. Subsequently, depth interval was reduced to 8 mm in an attempt to trap more heat, and a second treatment cycle took 40 minutes. For the remaining anaesthetic time, a third treatment cycle was commenced using the same settings, but time did not allow for completion. Ultimately, only 2 seconds above the release threshold were registered by the thermistor, which clearly appears sub-optimal. However, due to gas shielding around the thermistor, this may have under-estimated the real central tumour temperature.

TXA104 used a single thermistor which was deliberately sited slightly more peripheral to the centre of the target tumour in an attempt to avoid the necrotic core, based on the baseline PET scan (Figure 3.59). Through a single intercostal window good thermal alignment was achieved and FUS treatment was performed over a prescribed volume of 73.4 cm^3, covering the majority of the target tumour, which was of similar estimated volume, with the exception of the lateral margins which were shielded by ribs. The treatment proceeded in linear mode using a fixed power of 140 W (18.2 MPa derated peak-to-peak pressure) and a varied DC, making this the first case where pulsed FUS was used. The first full cycle proceeded at a 50% DC and took 26 minutes, achieving temperatures above the release threshold within 5 minutes (Figure 3.6). The second cycle was initially started at a 30% DC in an attempt to maintain temperature, an overall 40% reduction in energy, but an initial temperature decline lead the team to increase the DC to 40% after the first 18 units (rows) of treatment. The difference in the morphology of the thermometry trace between these two treatments can be explained by the fact that for the first cycle an unusual top-to-bottom slice ordering was used, whilst the usual slice-by-slice ordering was used subsequently. The third partial treatment continued at 50% DC to fill the remaining available anaesthetic time. Overall excellent temperature control was achieved over a large tumour volume, for well over an hour, demonstrating the great advantage of linear mode in the clinical cases. This case also demonstrates the advantage of finer DC control at a fixed exposure power. In addition this method has the added advantage of keeping the in-situ pressures fixed, and thus keeping the amount of non-linearity at a constant, theoretically giving a more predictable therapeutic response.

TXA105 was the first case to use a Medtronic T-type thermocouple due to expiry and discontinuation of the AngioDynamics thermistors. As dynamic cold-junction compensation was not used in this first thermocouple case (Section 2.1.2), post-calibration was performed against the oesophageal temperature probe at the end of treatment. The volume for this target tumour is hard to assess as it is the result of several tumours which have merged together with disease progression (Figure 3.7). The more posterior compo-

nent of the target tumour was planned for treatment with an estimated volume of 66.4 cm^3, however ultimately the prescribed volume was 90.9 cm^3, presumably due to difficultly distinguishing tumour boundaries. Of note this was the largest treatment volume attempted and it was achieved by splitting the tumour volume in two sections across two intercostal spaces. Linear mode proceeded at 110 W (17.1 MPa derated peak-to-peak pressure) and 70% DC. However during this treatment it became apparent that time spent translating the transducer from one rib space to the next was highly inefficient, effectively reducing the duty cycle by approximately a third. Consequently slices were skipped in an attempt to maintain heat around the thermistor. At around 35 minutes into the thermometry trace, the treatment was re-planned over a smaller volume of 63.8 cm^3 in a volume containing the thermocouple, and the treatment was recommenced using a higher power of 130 W (18.3 MPa derated peak-to-peak pressure) and 85% DC. Overall, over 56 minutes of hyperthermia over the release threshold were obtained. The lesson learned from this case was not to split a treatment volume in an exposure plan, as it is likely that higher levels of drug could have been delivered if the second treatment plan was performed immediately after infusion. The ethical considerations of treating large tumour volumes in patients with advanced liver disease are discussed in Section 4.5.

3.2.5 Power Predictions

Patients were treated in the order presented in Table 3.7 and then Table 3.8, and anatomical and thermometry data from Part I treatments were used to inform subsequent treatments both in Part I and Part II. For each case cross-sectional imaging, available prior to treatment (baseline MRI or CT scan), was used to obtain basic metrics of the FUS-target tumour, with respect to the propagation path of FUS, including:

1. Distance of transducer from ribs
2. Thickness of layers (skin, fat, connective tissue, normal liver parenchyma)
3. Tumour depth (centre point, closest and furthest borders)

4. Estimated tumour volume

Pennes' bio-heat transfer equation was originally designed to to model heat transfer theory in perfused tissue, and calorimetric experiments were performed in the human forearm to evaluate the model [488]. It has since been applied to the field of FUS [489], and of particular interest here, perfused liver models to predict temperature generation when under exposure [490]. The model includes a tissue and a blood domain, the later responsible for convecting of heat away from a hyperthermia volume of tissue through the circulation. The equations follow for the tissue (subscript t) and blood (subscript b) domains respectively, where the change in temperature, δT, depends on the tissue density ρ, the specific heat capacity C, and the tissue's thermal conductivity k:

$$\rho_t C_t \frac{\delta T}{\delta t} = k_t.\nabla^2 T - \omega_b C_b.(T - T_\infty) + Q \tag{3.5}$$

$$\rho_b C_b \frac{\delta T}{\delta t} = k_b.\nabla^2 T - \rho_b C_b.(\overrightarrow{v}.\nabla T) + Q \tag{3.6}$$

T_∞ refers to the temperature in tissue well away from the point undergoing FUS exposure, and initially will typically be 37°C. The first terms of both equations represent heat diffusion and are dependent on k. The second term in the tissue domain represents convective heat losses through the blood, with a perfusion rate of ω_b, whilst the second term in the blood domain represents advection of heat created by the flow of blood with velocity $\overrightarrow{v}$. The Q term in both equations represents the rate of heat absorbed (produced) in the tissue per unit volume due to the FUS stimulus, and is defined as being proportional to in situ intensity, I, averaged over a sinusoidal signal with amplitude p, where the proportionality constant, α, is the frequency-dependent ultrasound absorption coefficient, and p refers to the acoustic pressure and c is the sound velocity in tissue (assuming a plane wave at the focus):

$$Q = 2\alpha.I, \text{ where } I = \frac{p^2}{2\rho c}, \text{ thus } Q = \alpha.\frac{p^2}{\rho c} \tag{3.7}$$

For our clinical study, Part I treatments have provided real-time thermometry data (δT), for which power and DC are known. Using this simple thermal model and previous Part I thermometry data, it is possible to make predictions about required powers for target tumours at different depths in future patients, based on path length differences. For patients TXA104-105 and TXB101-TXB102, in order to achieve bulk heating above the drug release threshold, the individual JC200 output power requirements were predicted using combination of data acquired from prior patient Part I treatments, namely output power and DC of the first two patients treated, and baseline radiological depth measurements to the centre point of the tumour (Table 3.2). In order to make these power scaling calculations, derated pressures (Table 3.6) were used with the attenuation coefficient approximation of 0.6 dB/cm averaged from the literature (Section 3.2.3). This is a very simplistic approach, which ignores any non-linear contributions to heating, but it never-the-less has proven to be perhaps surprisingly accurate in the clinical cases (Figure 3.9).

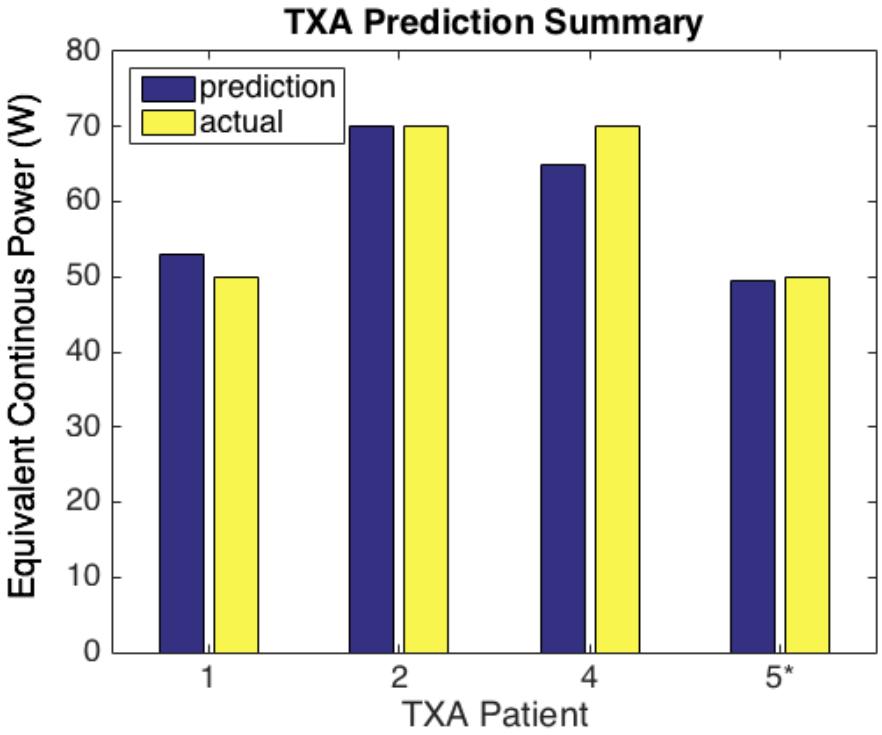


Figure 3.9: Comparison of power predictions for the early Part I patients compared to the actual values used to obtain optimal hyperthermia in the target tumour, in the tumour volume insonated prior to drug delivery. Where duty cycle (DC) was used instead of continuous wave (CW), powers have been reduced to CW-equivalent powers, for ease of comparison. To illustrate by example, as predicted, the equivalent power for TXA105(*) was sufficient to raise the temperature sufficiently in a relatively small 10-20cm^3 volume around the thermometry device. The power ultimately used for drug delivery was higher (Table 3.9), after adjusting for DC, because the tumour volume insonated post-infusion was larger. Patient TXA103 omitted due to technical issues with this treatment. Acknowledgement: Dr. Michael Gray for performing these calculations.

However, the model has inherent limitations, as it makes the following assumptions:

1. Patient-to-patient variation in required output power are only due to tissue path length differences, and does not include, for example, the presence of rib blocking effects.

2. Patient-to-patient variation in non-linear heating is negligible.

3. Patient-to-patient variation in perfusion of liver is negligible.

4. Absorption and attenuation values in human liver are equal between patients [491].

Thus a significantly more sophisticated approach is also being explored to facilitate future treatments in the absence of real-time thermometry. The method is under development and includes an ultrasonic model of the JC200, coupled with a thermal model of perfused tissue and anatomical CT data. The model has the option to include FUS attenuation by rib blocking. The model mimics the JC200 FUS treatment exposures, in terms of FUS paths and slice geometries, in both dot and linear mode. The method is discussed further in Section 4.6.3 on future work. Acknowledgement: Dr. Michael Gray.

TXB101 received a derated FUS pressure of 16.5 MPa peak-to-peak (55% DC) over a prescribed volume of 34.2 cm^3, which incorporated over 90% of the tumour. Three 18 minute cycles were used to cover the volume in linear mode. During drug administration it was noted that the patient had become hypothermic to 34°C, a consequence of conductive cooling through the cold water bath and loss of temperature auto-regulation due to the anaesthesia. Best efforts were made to correct this with the BairHugger™ but temperature was still low, around 35°C, at the time of commencing FUS heating. In addition, for this patient the BMI was high and it was noted that the FUS had to pass through a 5 cm layer of subcutaneous tissues before entering the body. Both of these factors may have been detrimental to obtaining hyperthermia in the target range.

TXB102 Received a derated pressure of 19.4 MPa peak-to-peak (42% DC) over a volume of 50 cm^3, correlating to the more superficial region which was targeted within the extensive tumour volume. Again three complete cycles were used to cover the region in linear mode, and no issues were encountered during the procedure.

TXB103 Received a derated pressure of 17.3 MPa peak-to-peak (44% DC) over a volume of 31 cm^3, again at a superficial region targeted within the extensive tumour volume. Five complete cycles were used to cover the region in linear mode without difficulty.

TXB104 Received a derated pressure of 19.9 MPa peak-to-peak (40% DC) over a volume of 53.9 cm^3, this time covering the vast majority of the tumour volume with only

some of the anterior border missed. Three complete cycles were used to cover the region in linear mode, which again preceded without issue.

3.2.6 Cell Viability by Microscopy

Immunohistochemistry for Microscopy

HIFU-ablated tissue may show characteristics of thermal and mechanical insult on routine H&E staining (nuclear pyknosis, erythrocyte disruption, loss of cell membrane detail, granular protein deposits on vessel walls, endothelial damage and homogenisation of vascular smooth muscle [213, 214]). It follows that a lack of these features would indicate the absence of thermal ablation, which is of interest for the unreleased (B2) and released (B3) biopsies, both of which are obtained from FUS-exposed tumour. However, as discussed in Section 1.3.3, it must be borne in mind that the H&E stain has it inherent limitations when used specifically for this indication.

Formalin-fixed paraffin-embedded sections of clinical tumour samples were stained for H&E (Appendix 5.1.4) and assessed by a consultant histopathologist for general morphology and in addition for characteristics of ablative change (Figures 3.10-3.18). Characteristics of HIFU-ablation (discussed in Section 1.3.3) were absent in all samples. The large variation in background tumour necrosis is apparent across the series, both between tumours (e.g. TXA101 well-differentiated, TXA104 highly necrotic) and from serial samples taken from the same tumour (e.g. TXA105). In addition some of the later Part I biopsies were noted to be contaminated with blood clot (TXA102.B3, TX104.B2). One sample demonstrated the presence of microspheres (TXA102.B2(b)), which corresponds with a previous Systemic Internal Radiotherapy (SIRT) treatment (Section 1.2.2).

Different sections of the same samples were also assessed for apoptosis using Caspase-3 ('Casp3') IHC (Appendix 5.1.4) (Figures 3.19-3.25).

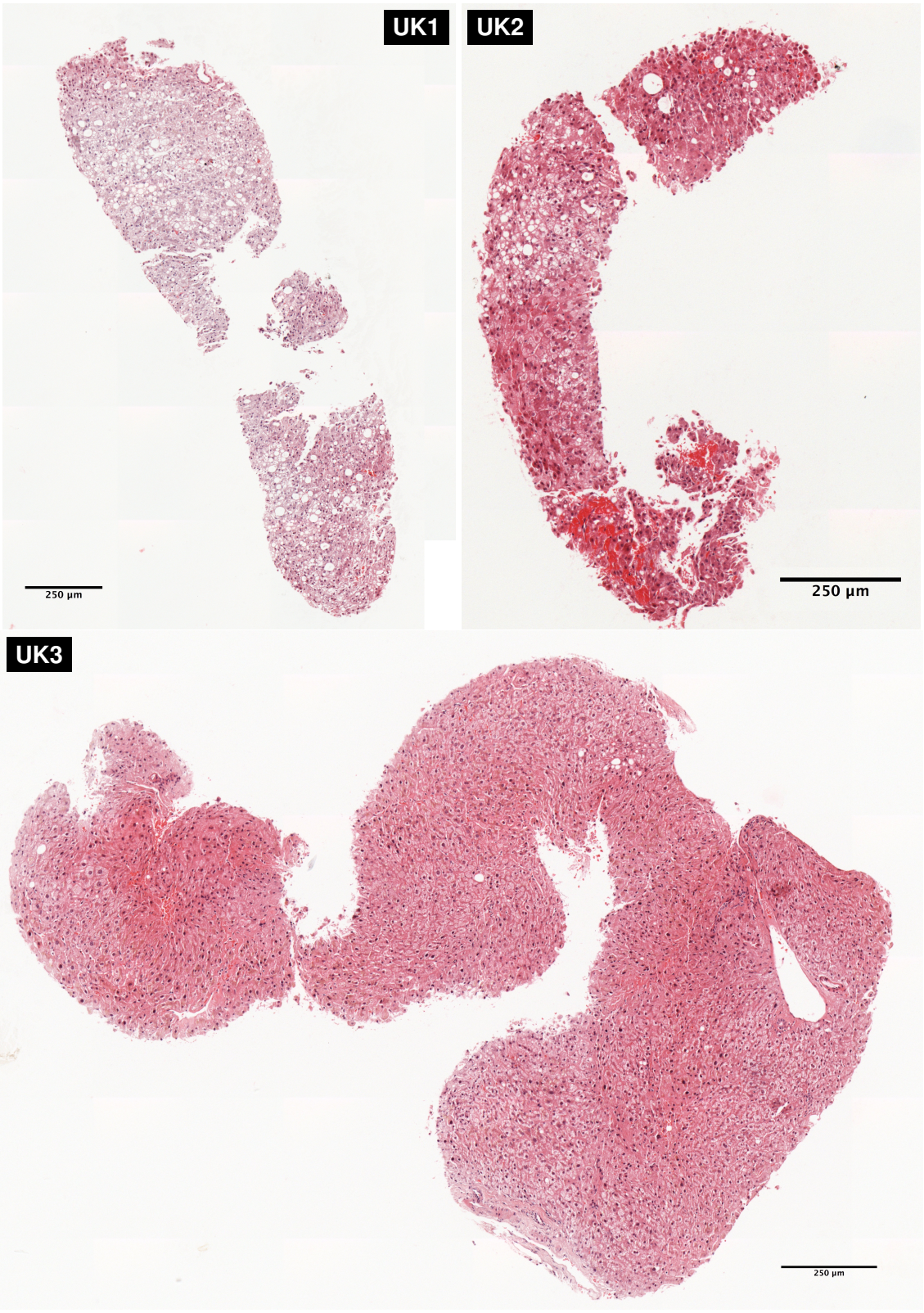


Figure 3.10: H&E microscopy for TXA101 biopsies at x20 magnification, with 250 µm scalebar. Samples are labelled as unknown (UK) as during the fixation process the tissue samples left the embedding cassette used in this first case, and samples had to be retrieved from the formalin solution. Later cases have used cassettes with finer holes to avoid this issue.

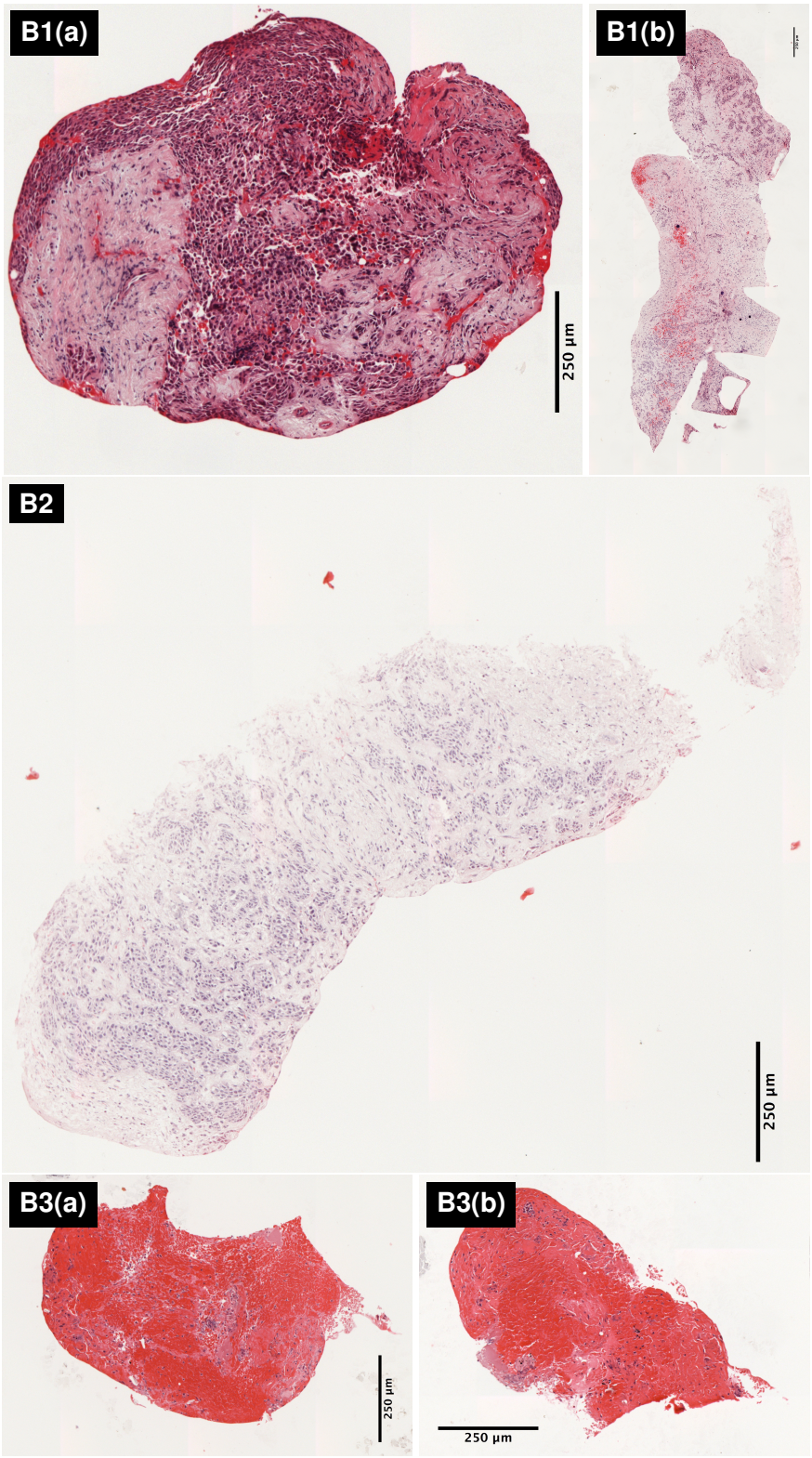


Figure 3.11: H&E microscopy for TXA102 biopsies at x20 magnification, with 250 µm scalebar. For biopsy nomenclature see Section 3.1.2. Short reports by histopathologist follow. B1(a): No liver. Tumour with fibrosis. B1(b): No liver. Tumour set in abundant fibrous stroma (especially centrally). Microspheres are present. B2: No liver. Tumour set in stroma. B3(a): No liver. Almost entirely blood clot and fibrin. Small collections of cells at the centre, not unequivocally tumour. B3(b): No liver. Blood clot and fibrin. For all H&E slides acknowledgements go to Leticia Campo for slide preparation and Prof. Robert Goldin for reporting.

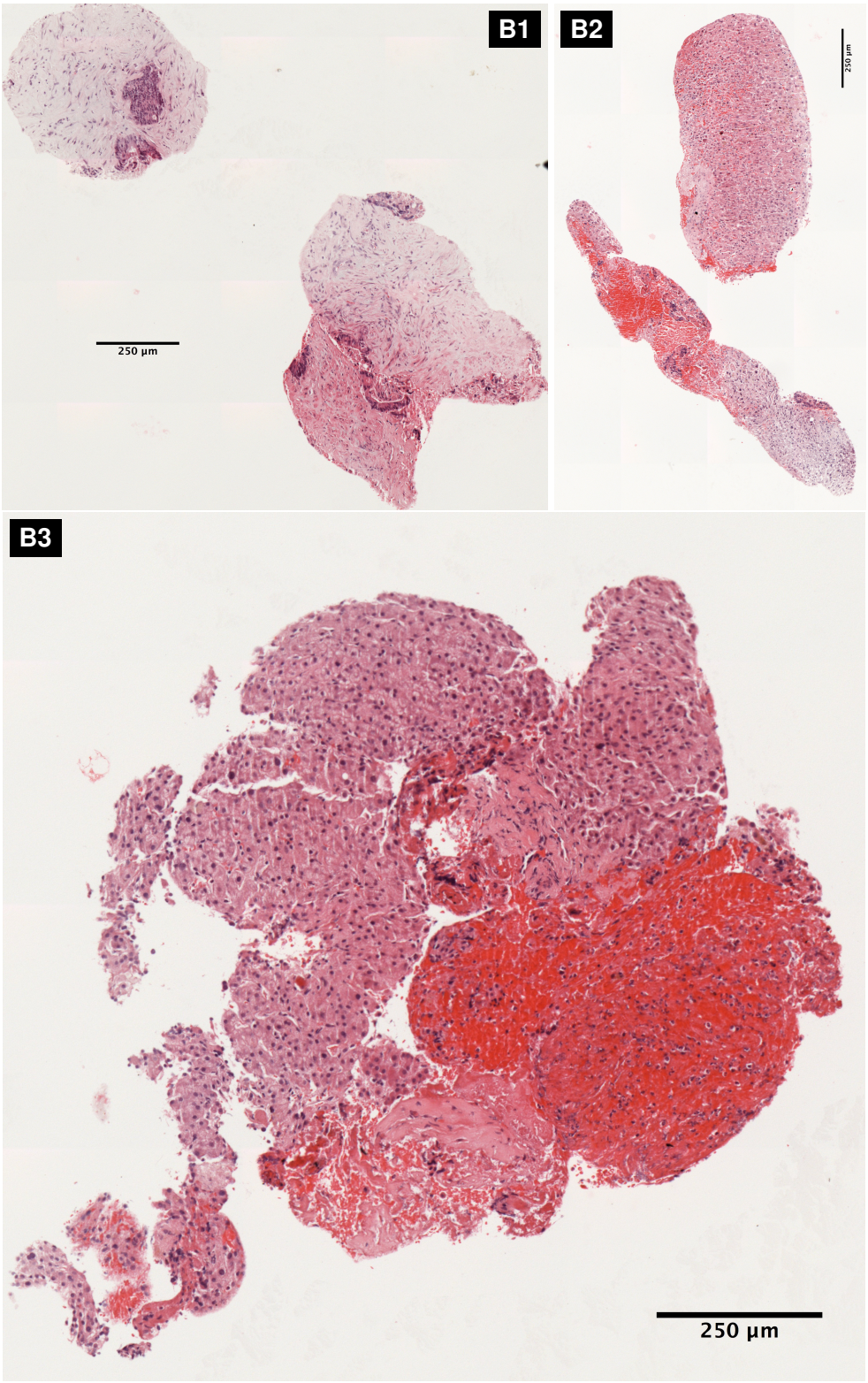


Figure 3.12: H&E microscopy for TXA103 biopsies at x20 magnification, with 250 µm scalebar. Short reports by histopathologist follow. B1: No liver. Tumour set in fibrous stroma. B2: Liver showing damage with prominent apoptotic cells. Also fresh haemorrhage with small collections of cells at the centre, not unequivocally tumour. B3: Normal liver and fresh blood.

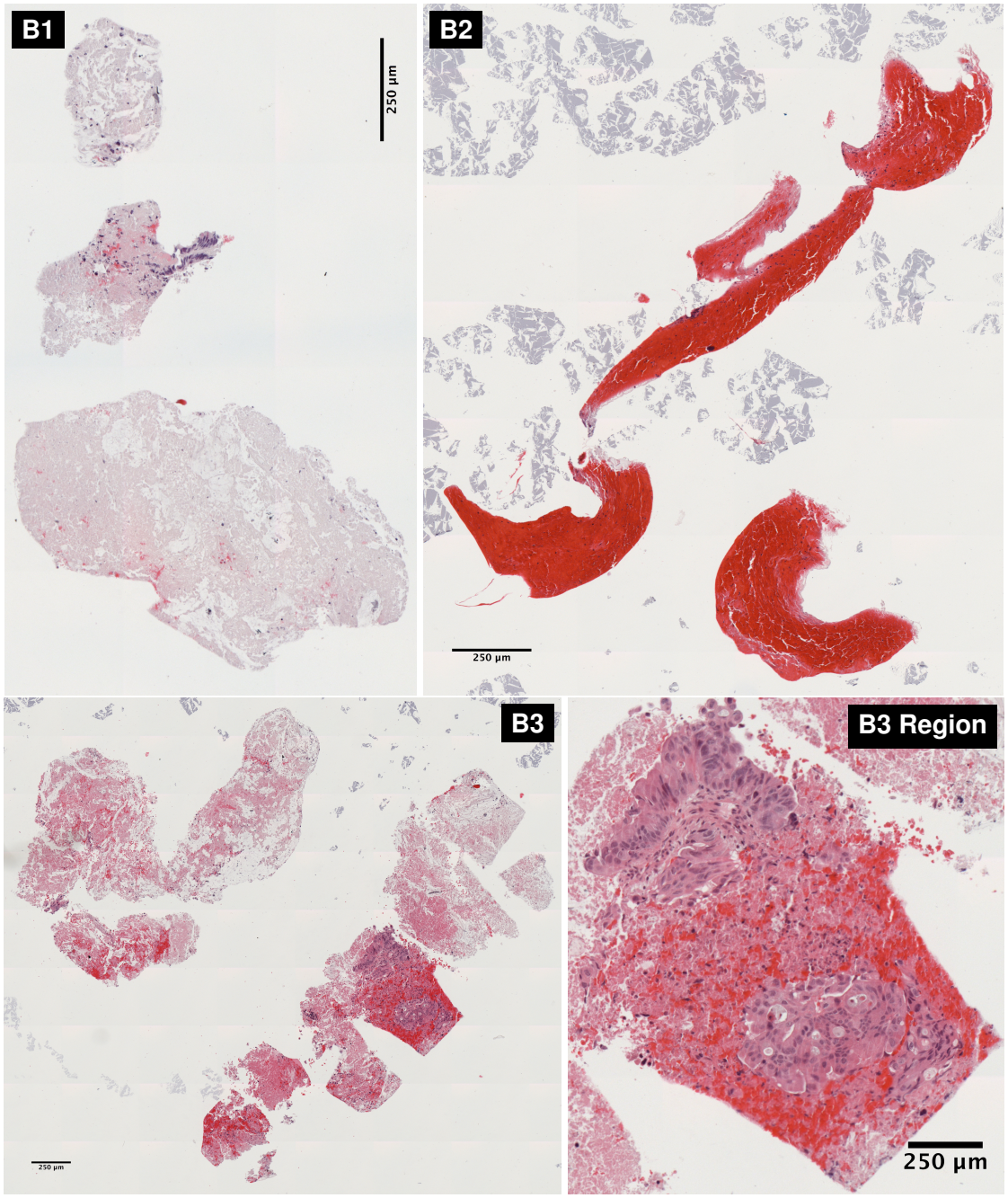


Figure 3.13: H&E microscopy for TXA104 biopsies at x20 magnification, with 250 µm scalebar. Short reports by histopathologist follow. B1: No liver. Necrotic tumour, small amount of viable tumour in the middle fragment. B2: No liver. Blood clot and exogenous material. B3: No liver. Necrotic tumour with a small foci of viable tumour (shown as B3 Region).

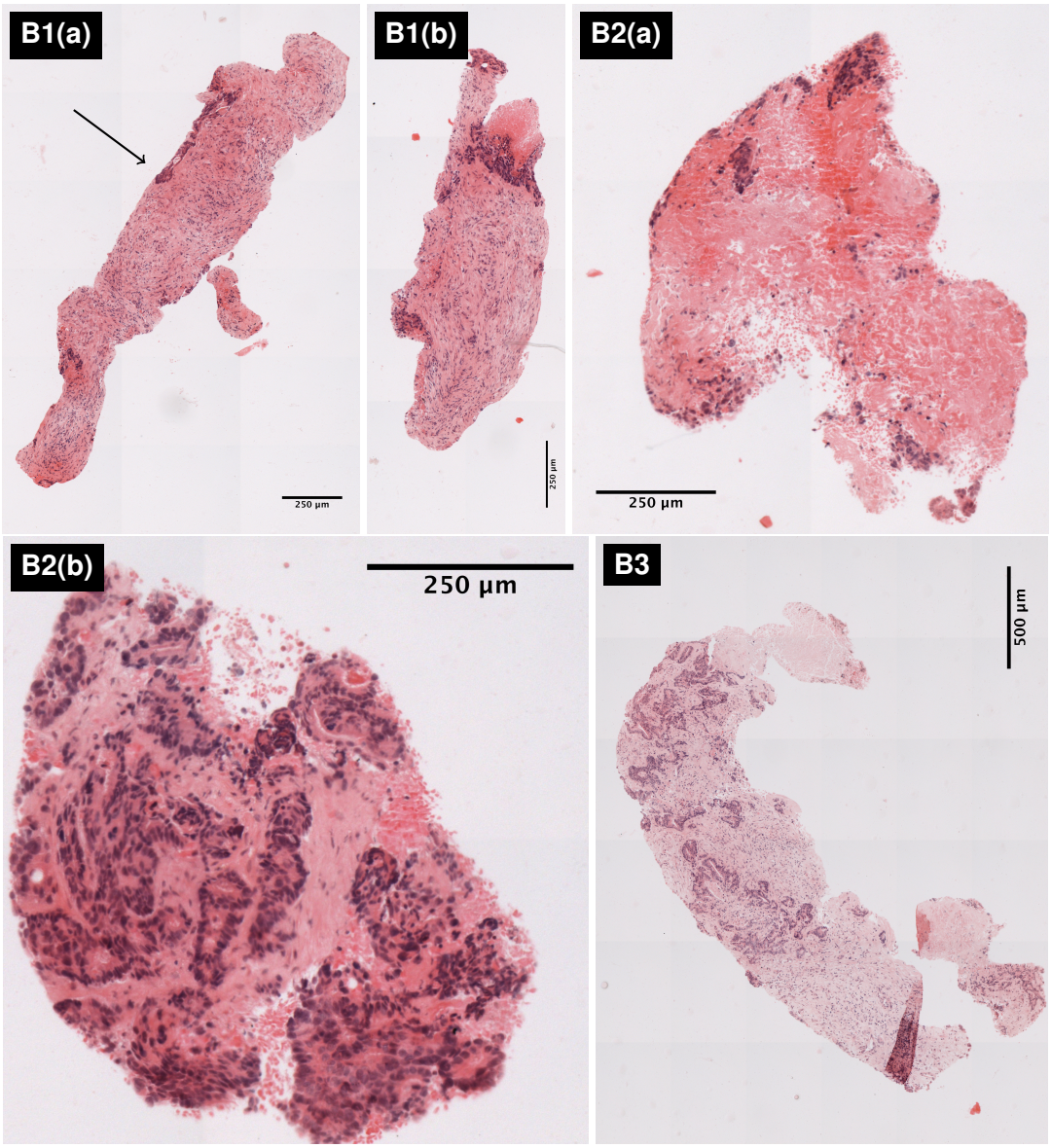


Figure 3.14: H&E microscopy for TXA105 biopsies at x20 magnification, with various scalebars. Short reports by histopathologist follow. B1(a): Fibrous tissue with a small amount of tumour down one edge (see arrow). B1(b): Fibrous tissue with tumour at one end. B2(a): Almost entirely necrotic tumour. There is no evidence of ablative HIFU. B2(b): Viable tumour (adenocarcinoma) set in fibrous tissue. There is no evidence of ablative HIFU. B3: Viable tumour (adenocarcinoma) set in fibrous tissue (more than on B2(b)). There is no evidence of ablative HIFU.

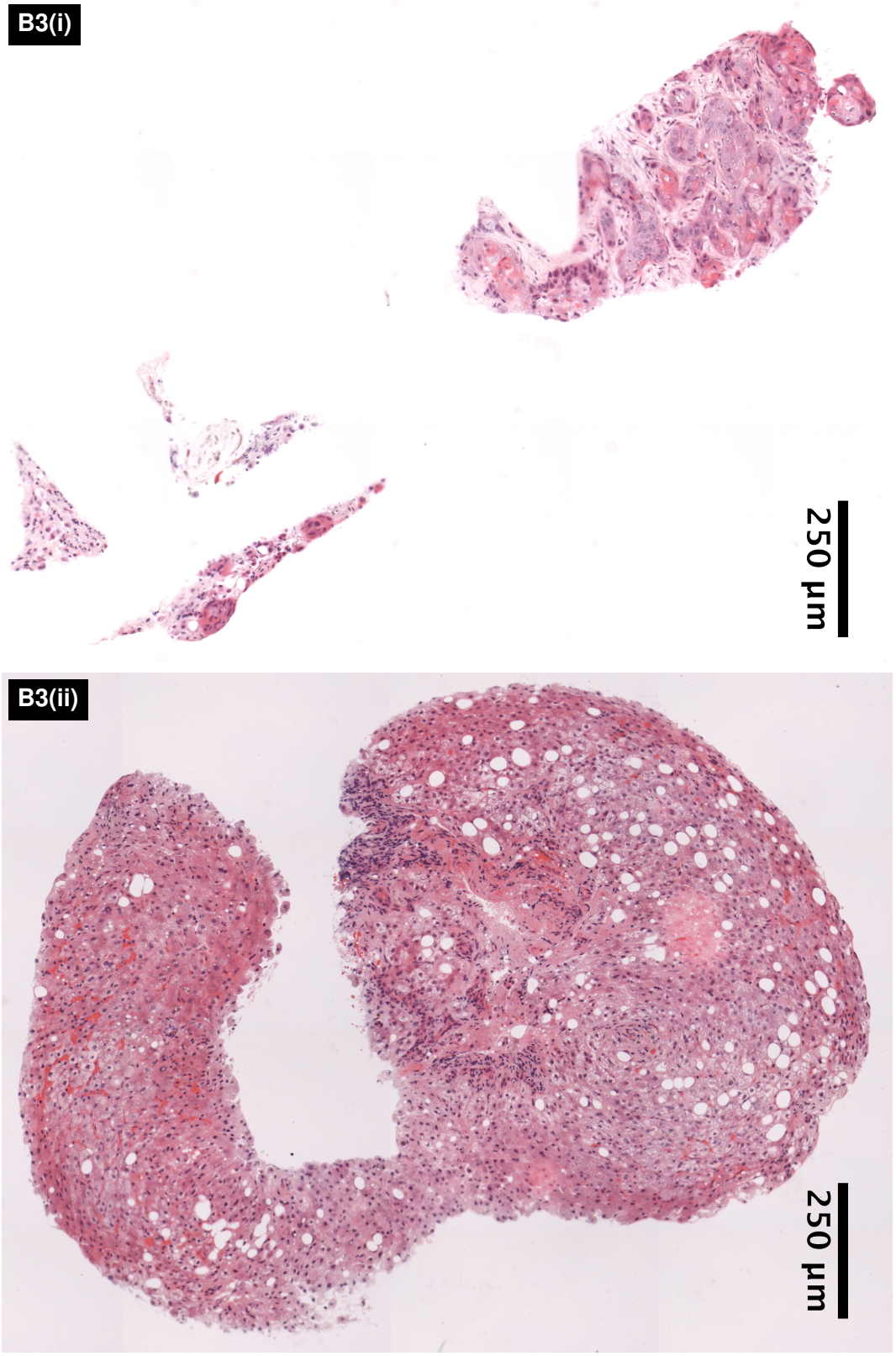


Figure 3.15: H&E microscopy for TXB101 biopsies at x20 magnification, with 250 µm scalebar. Short reports by histopathologist follow. B3(i) Tumour. B3(ii) Normal liver with fatty change.

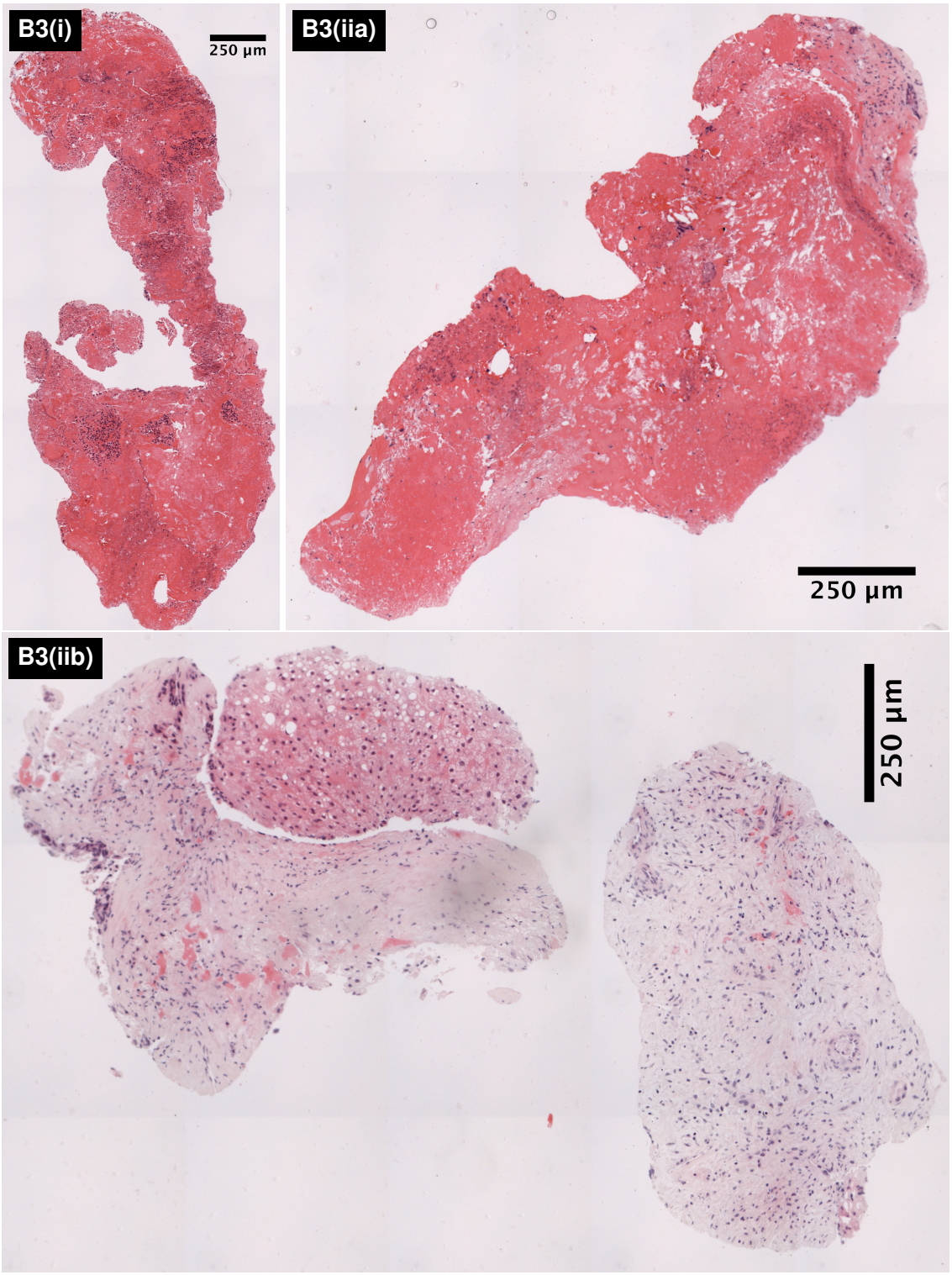


Figure 3.16: H&E microscopy for TXB102 biopsy at x20 magnification, with 250 µm scalebar. Short reports by histopathologist follow. B3(i) Almost entirely necrotic with a small cluster of possible tumour cells. B3(iia) Mostly blood clot; a little fibrous tissue with tumour. B3(iib) Fibrous tissue with tumour and normal liver.

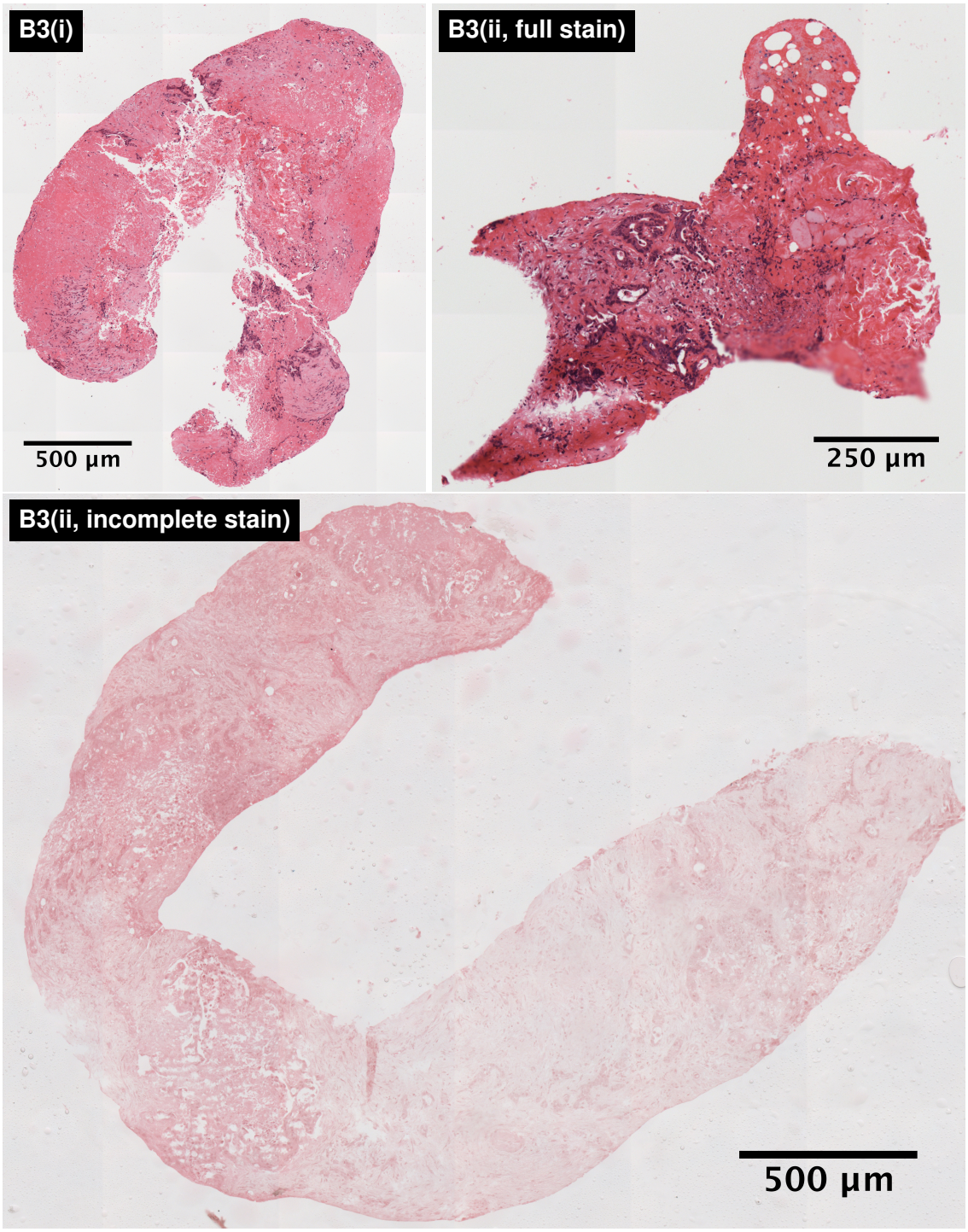


Figure 3.17: H&E microscopy for TXB103 biopsy at x20 magnification, with various scalebars. B3(ii, poor stain) demonstrates the full extent of the tissue sample, but has stained incompletely with H&E. B3(ii, full stain) is a repeat, and full H&E stain, but for a smaller tissue sample due to being almost out of tissue on the paraffin block. Short reports by histopathologist follow. B3(i) Fibrous tissue with tumour, mostly necrosis (80%). B3(iia) Mostly blood clot; a little fibrous tissue with tumour. B3(ii, partial stain) Islands of tumour in fibrous tissue, 20% necrosis. B3(ii, full stain) Fibrous tissue with tumour, small amount of serum. 15% necrosis.

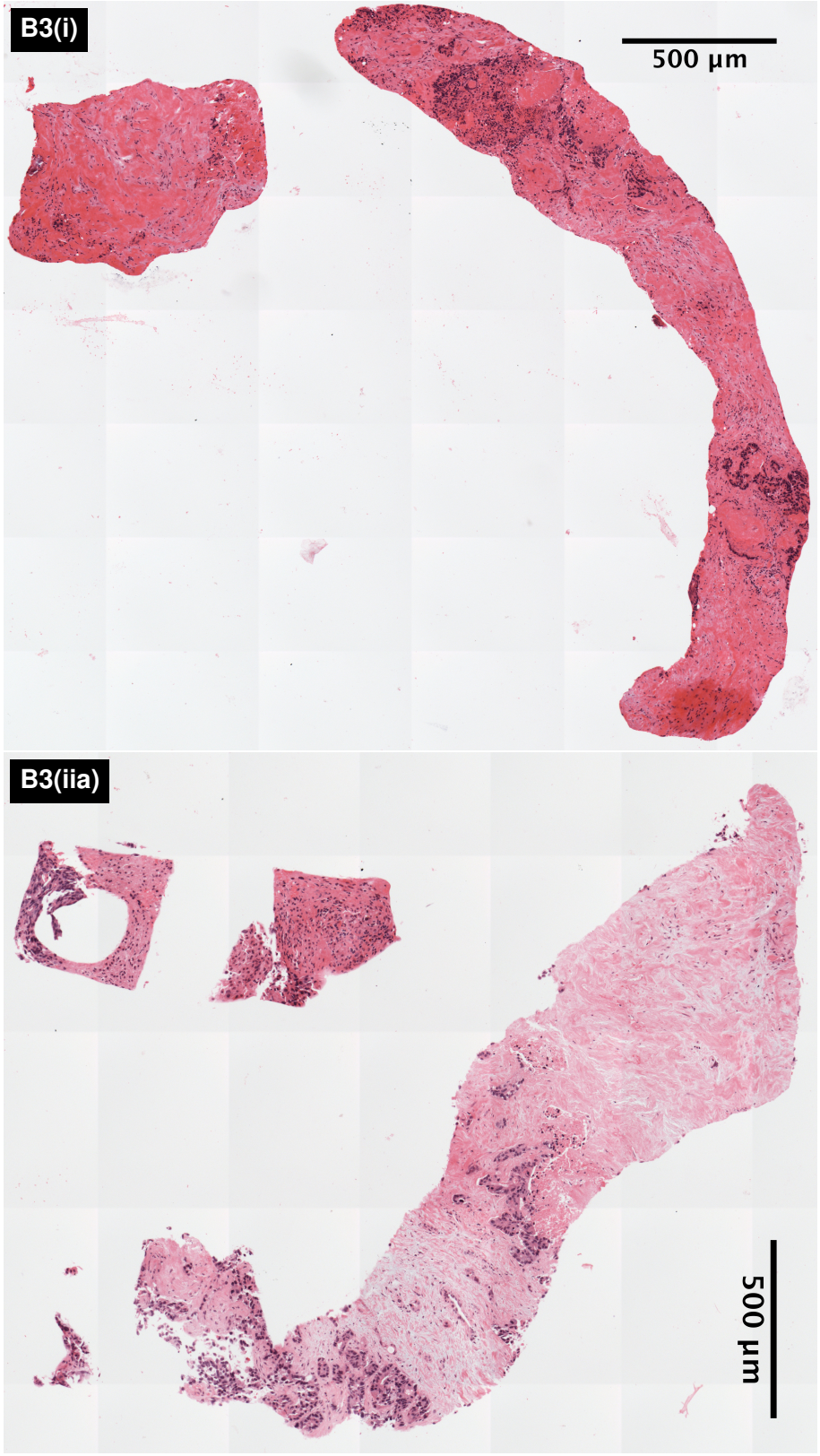


Figure 3.18: H&E microscopy for TXB104 biopsy at x20 magnification, with 500 µm scalebar. Short reports by histopathologist follow. B3(i) Mostly stroma with both viable and early necrotic tumour islands. 10% Necrosis. No coagulative necrosis. B3(ii) Mostly tumour and stroma, with separate early necrotic area. 10% necrosis.

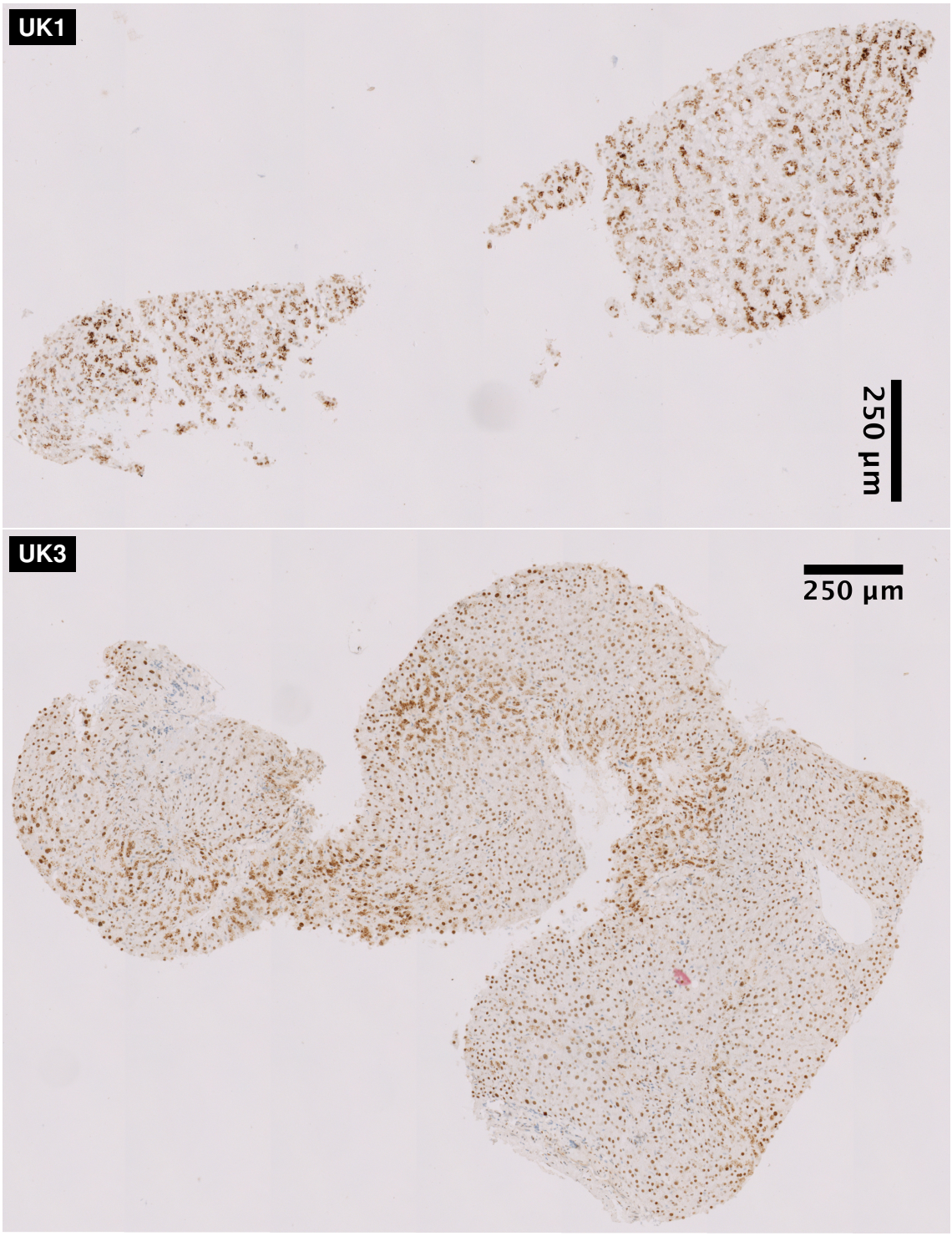


Figure 3.19: Caspase-3 immunohistochemistry microscopy for TXA101 biopsies at x20 magnification, with 250 µm scalebar. Short reports by histopathologist follow. UK1: Widespread Casp3 cytoplasmic staining (90%) with minimal nuclear staining. UK3: Less Casp3 cytoplasmic staining, more Casp3 nuclear staining, demonstrating 90% apoptosis. For all immunohistochemistry slides acknowledgements go to Leticia Campo for slide preparation and Prof. Robert Goldin for reporting.

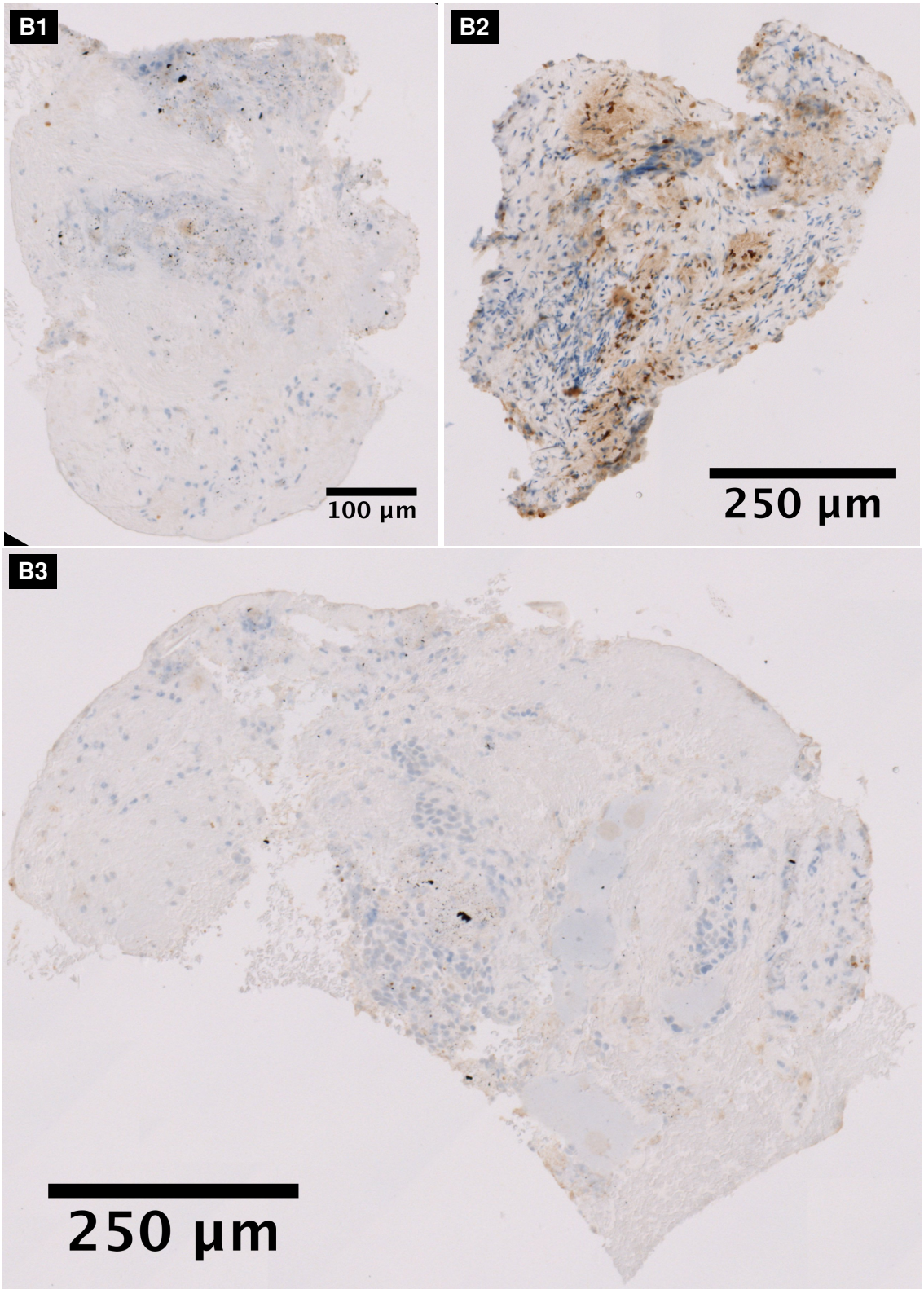


Figure 3.20: Caspase-3 immunohistochemistry microscopy for TXA102 biopsies at x20 magnification, with various scalebars. Short reports by histopathologist follow. B1: No nuclear or cytoplasmic Casp3 staining (0%). B2: Patchy Casp3 staining of cytoplasm (60%) and nuclei (20%) probably of tumour. B3: No Casp3 staining almost all blood clot.

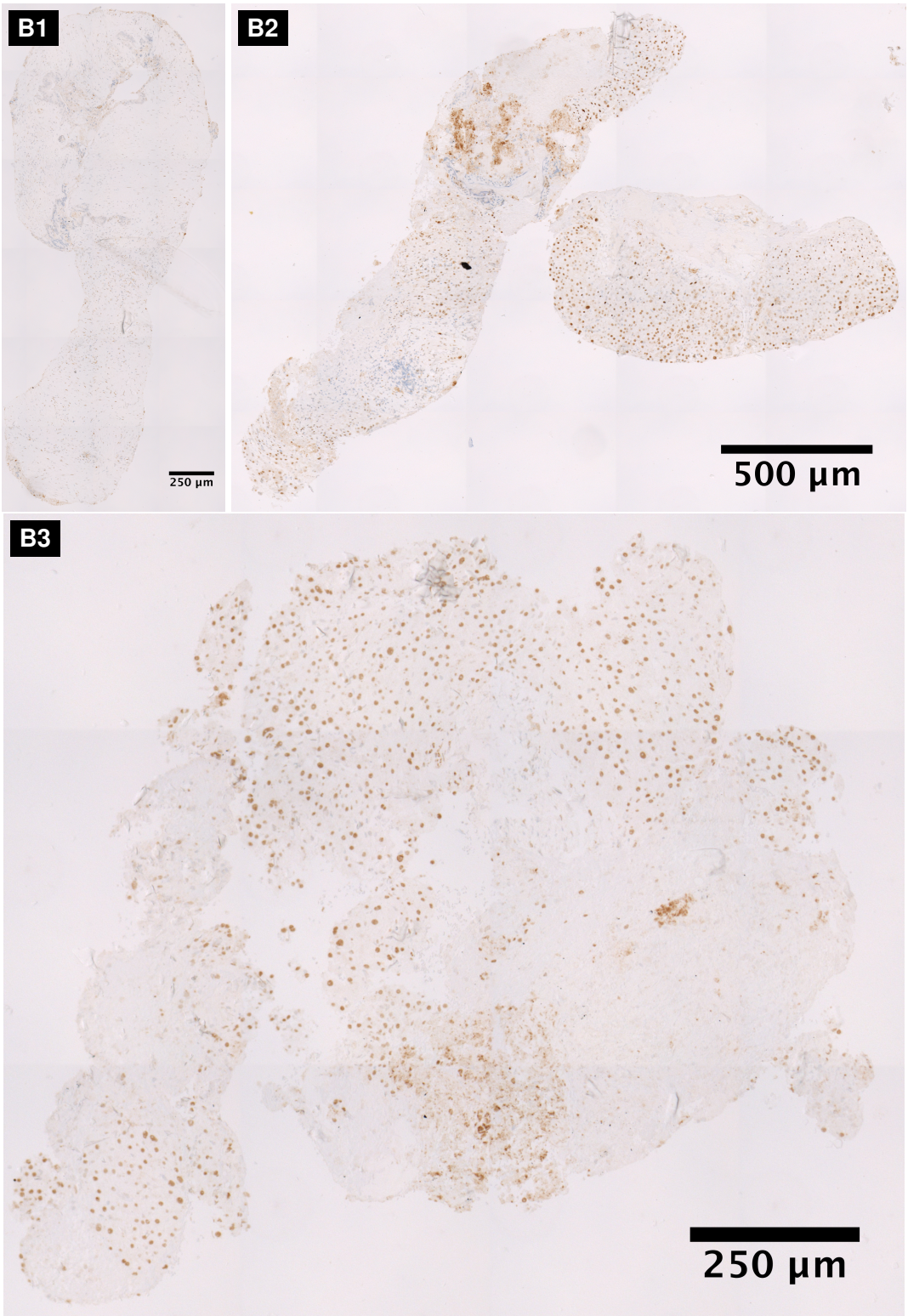


Figure 3.21: Caspase-3 immunohistochemistry microscopy for TXA103 biopsies at x20 magnification, with various scalebars. Short reports by histopathologist follow. B1: Fibrous tissue, 5% of nuclei staining for Casp3. B2: 80% of nuclei and 5% of cytoplasm stains for Casp3. Correlates with increased apoptosis seen on the H&E. B3: 80% of nuclei stain for Casp3, no cytoplasmic staining.

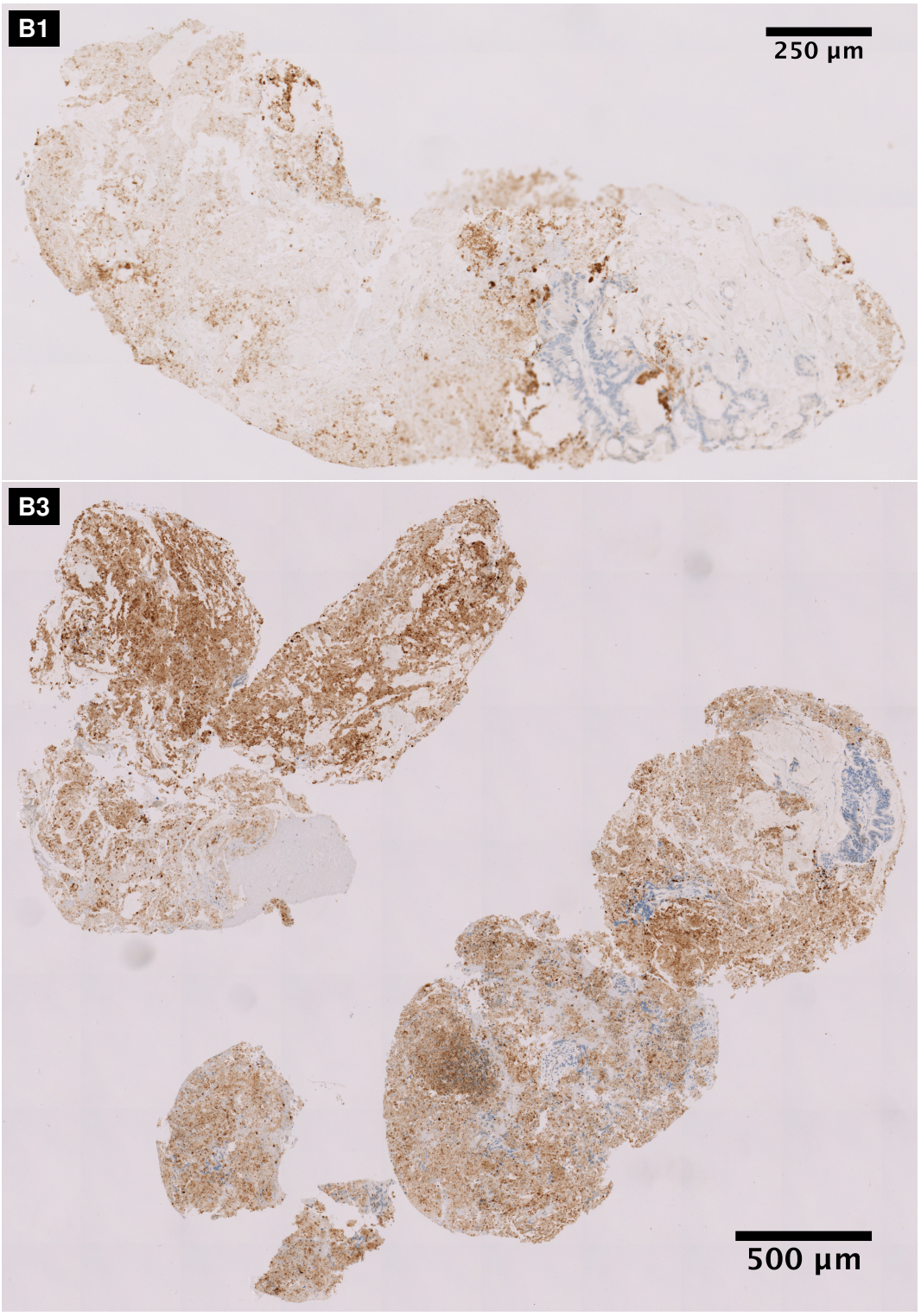


Figure 3.22: Caspase-3 ('Casp3') immunohistochemistry microscopy for TXA104 biopsies at x20 magnification, with various scalebars. Short reports by histopathologist follow. B1: In this necrotic sample, 50% of cytoplasm stains for Casp3. There is minimal staining of the viable tumour, with 1% nuclear staining. B3: In this necrotic sample, 90% of cytoplasm stains for Casp3. There is minimal staining of the viable tumour, with 1% nuclear staining.

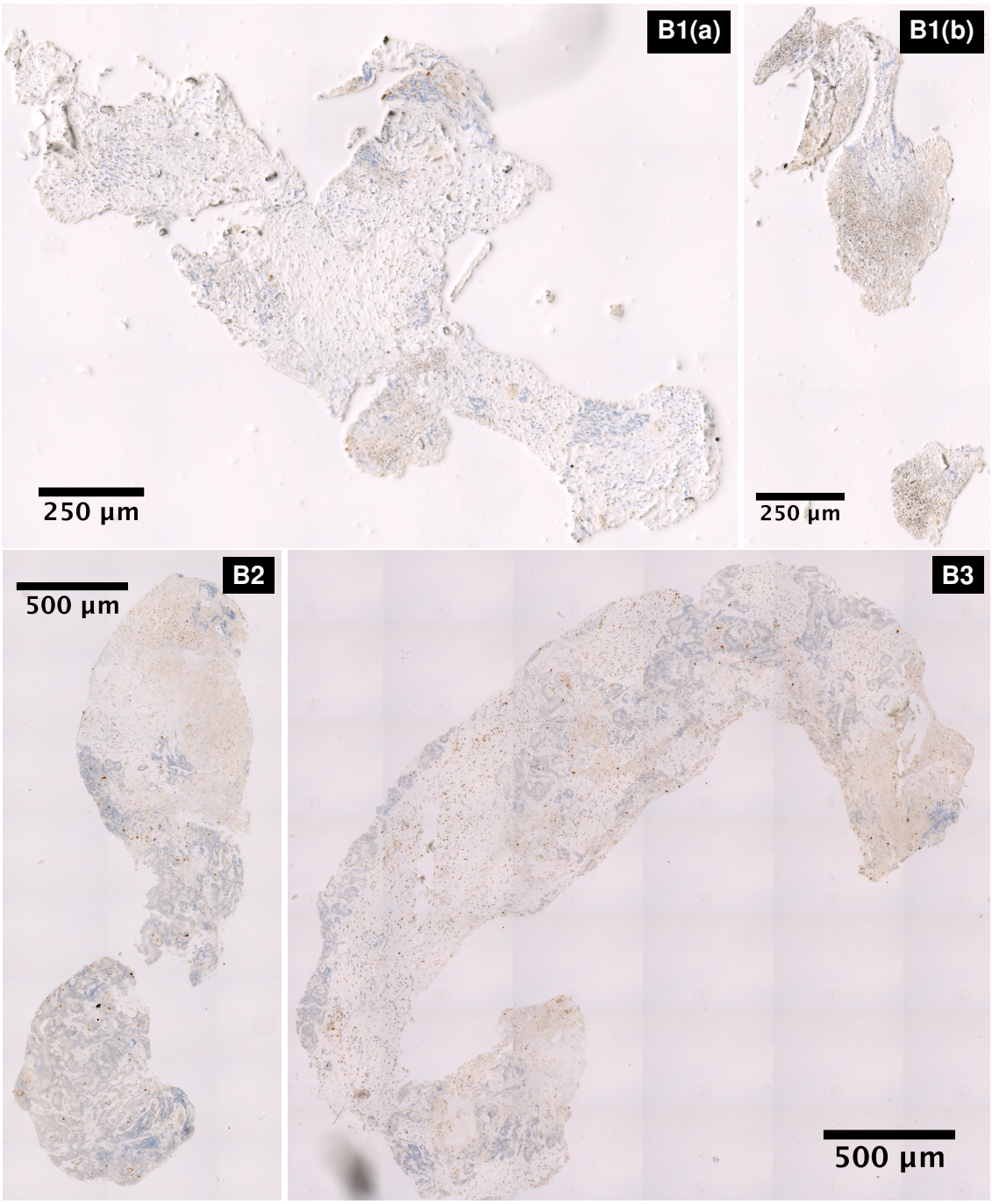


Figure 3.23: Caspase-3 immunohistochemistry microscopy for TXA105 biopsies at x20 magnification, with various scalebars. Short reports by histopathologist follow. B1(a): No definitive Casp3 staining. B1(b): Minimal staining for Casp3 (1% of the cytoplasm only) in this predominately fibrous tissue sample. B2: In the necrotic region, 50% of the cytoplasm stains for Casp3. In the viable tumour, 3% of the cytoplasm and 1% of the nuclei stain for Casp3. B3: In the viable tumour, 30% of the nuclei stain for Casp3. There is only minimal cytoplasmic Casp3 staining.

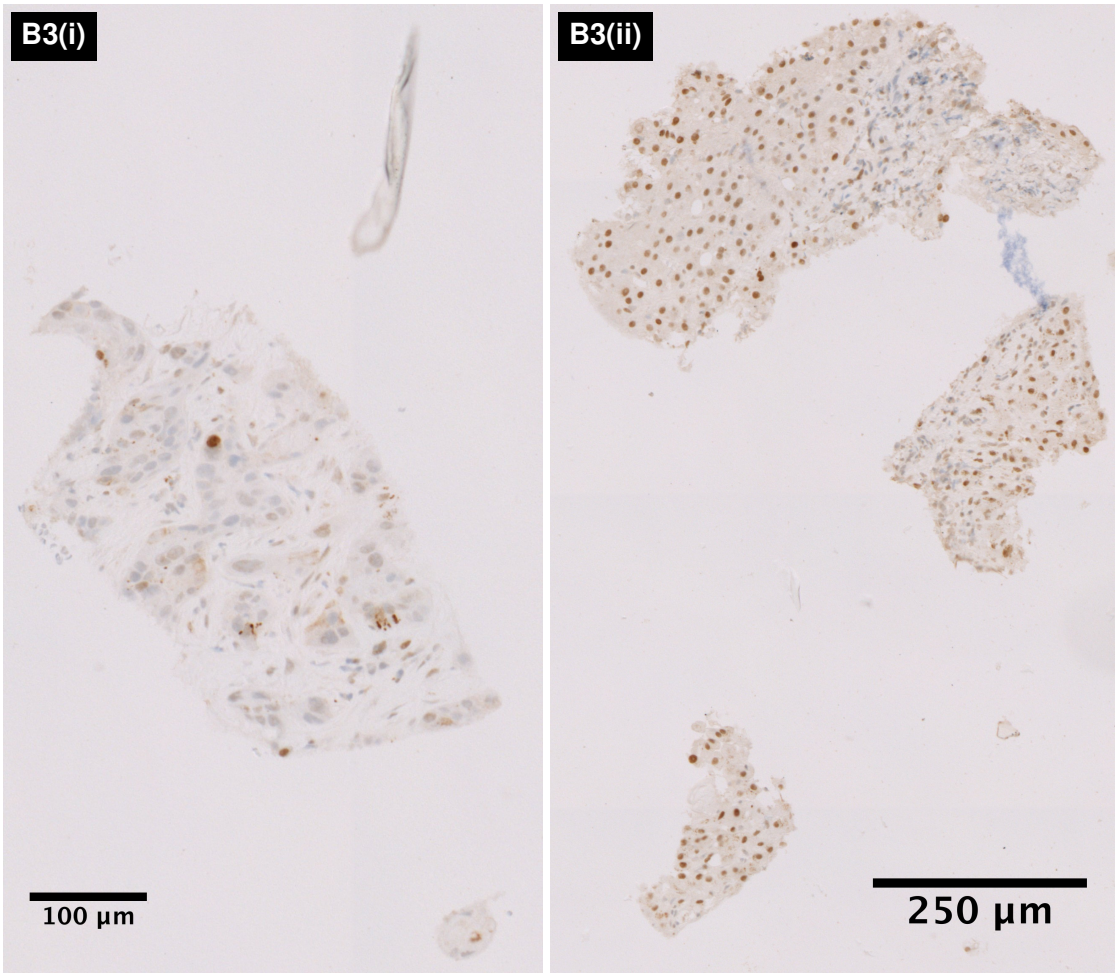


Figure 3.24: Caspase-3 immunohistochemistry microscopy for TXB101 biopsies at x20 magnification, with various scalebars. Short reports by histopathologist follow. B3(i): This small tissue fragment shows 2% nuclear and 5% cytoplasmic Casp3 staining. B3(ii): 90% nuclear Casp3 staining, minimal cytoplasmic staining.

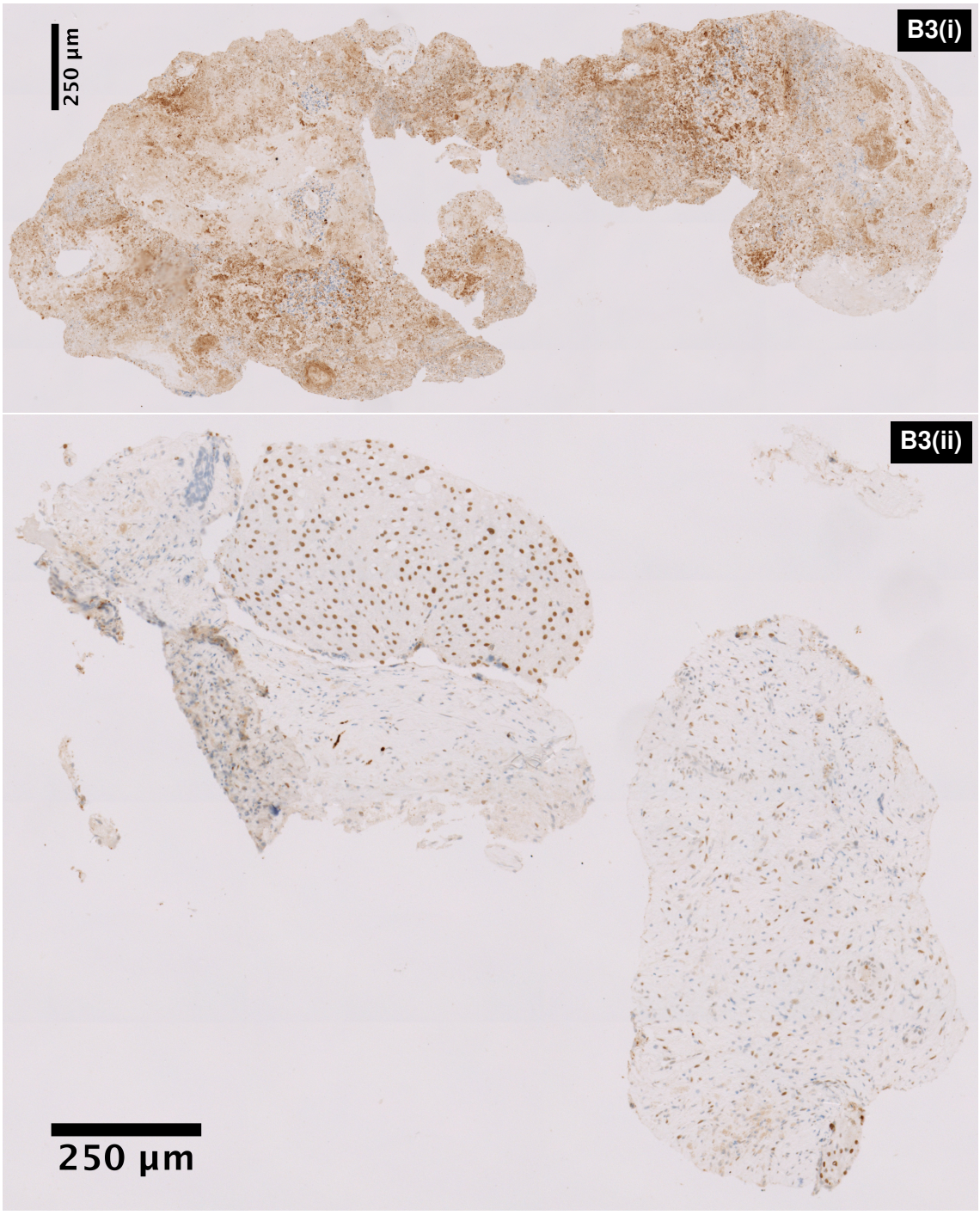


Figure 3.25: Caspase-3 immunohistochemistry microscopy for TXB102 biopsies at x20 magnification, with various scalebars. Short reports by histopathologist follow. B3(i): In this necrotic sample, 80% of the cytoplasm stains for Casp3. In the tumour regions, 5% of the cytoplasm stains for Casp3. There is negligible Casp3 nuclear staining. B3(ii): In the region of normal liver with fatty change, 90% of the nuclei stain for Casp3. In the fibrous tissue, 50% of the nuclei stain for Casp3. In the viable tumour there is negligible Casp3 staining.

Interpretation of Caspase-3 Results

The reports for slides stained for Caspase-3 are included in the figure legends for ease of reference (Figure 3.19-3.25). Strong Caspase-3 nuclear-specific staining suggests that those cells are currently undergoing the process of apoptosis, a process that is complete within a few hours at most [492]. It is difficult to comment on weaker Caspase-3 staining seen outside of the nucleus, which may represent previous cell destruction through apoptosis or may be non-specific. In the context of this study, Caspase-3 staining is limited in its ability to distinguish doxorubicin- and thermally-induced apoptosis, and neither can these be distinguished from pre-existing apoptotic cells within the tumour matrix. Clinical samples demonstrate a wide variation of Caspase-3 expression between patients and between samples from the same patient. Of note, TXA105.B2 demonstrates only 1% of nuclei staining for apoptosis whilst the B3 sample, taken post-delivery, demonstrates ~30% (Figure 3.23). The most likely explanation for this apparent increase in apoptosis is heterogeneity within the tumour sample. Although TXB105.B3 demonstrates high amounts of nuclear doxorubicin (Figure 3.30), it is perhaps less likely that we are seeing mechanisms of doxorubicin-induced apoptosis at play (Section 1.4.2), given the final tissue biopsy is obtained within an hour or two of drug administration. Due to ethical considerations, the study design intentionally has not incorporated a delayed tissue biopsy.

Cytokeratin Immunofluorescence Microscopy

The utility of CK8 vitality staining in assessing tissue ablation has previously been discussed in Section 2.4.2. Immunofluorescence microscopy images for DAPI (nuclear stain), CD31 (vascular marker) and CK8 are shown for the obtained biopsy samples in Figures 3.26-3.33. In one case, additional staining was performed using pan-CK in addition to CK8 (Figure 3.31). Samples were formalin-fixed and paraffin embedded and images acquired using Zeiss 710 Confocal Microscope. The immunofluorescence stain-

ing protocol used to generate these images is summarised in Appendix 5.1.3, Section 5.1.5 along with the fluorophores in Table 5.2). Parameters affecting CK8 fluorescence intensity were matched, thus levels are comparable both for the same patient and between different patients.

Interpretation of Immunofluorescence Results

The interpretation for the IF are included in the figure legends for ease of reference (Figure 3.26-3.33). In summary, CK8 was present heterogeneously across all samples and persisted following FUS-exposures in both Part I and Part II cases, further supporting the absence of ablative levels of FUS energy. Although the duration before which CK8 becomes absent in tumour tissues after HIFU exposure is not currently reported in the literature, pre-clinical results using the pan-CK stain demonstrated the loss of all CK subtypes in samples of *ex vivo* ox liver immediately following HIFU ablation (Section 2.4.2). CD31 IF staining is useful to gain understanding of the vascular distrubution in the tissue sections, and can be correlated to doxorubicin distribution (Section 3.3.4).

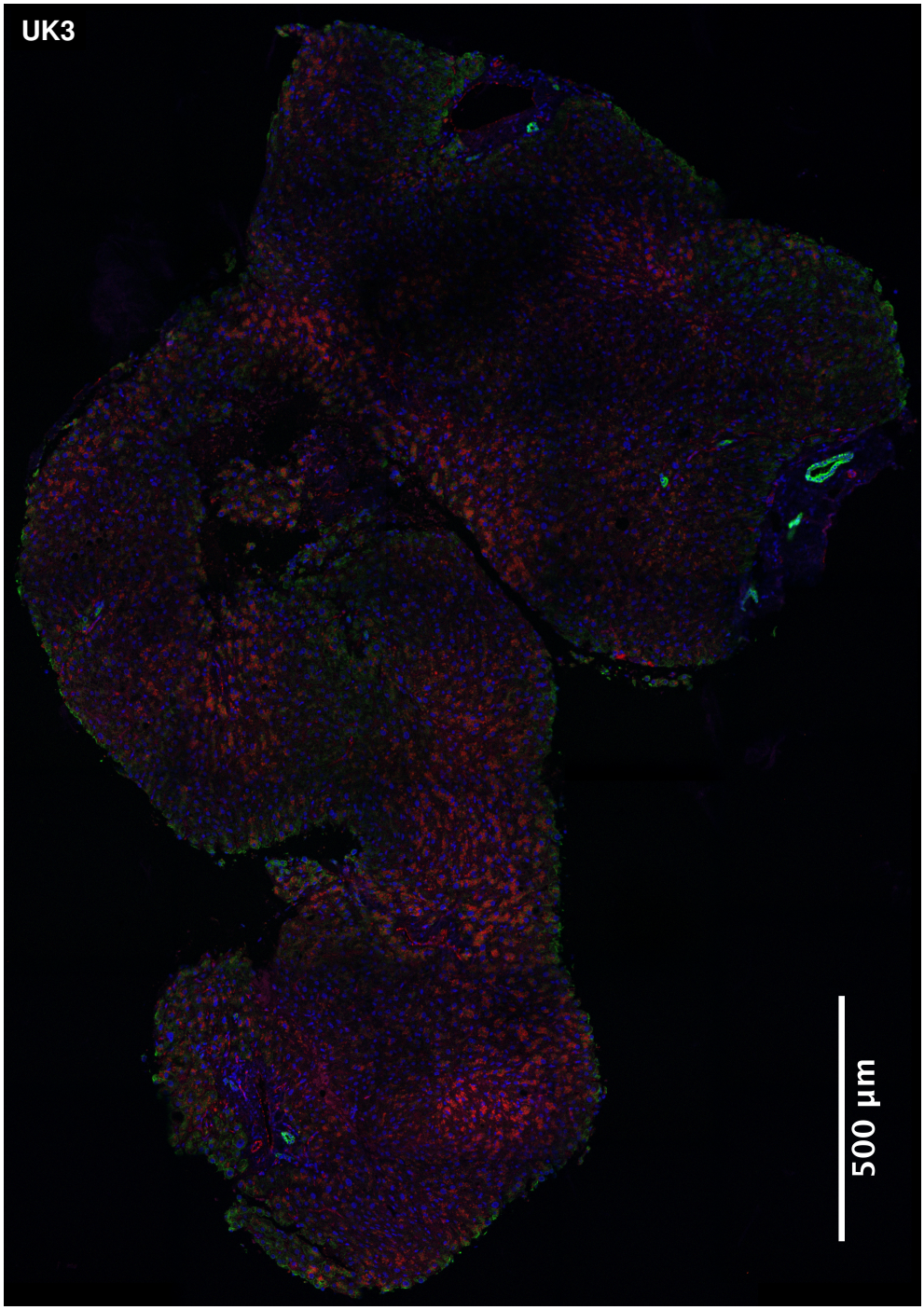


Figure 3.26: Immunofluorescence microscopy for one of the (unknown) TXA101 biopsies, UK3, at x20 magnification, with 500 µm scalebar. DAPI=blue (nucleus), CD31=red (endothelia), CK8=green (viable, epithelia-specific). UK3 was the only sample with adequate tissue remaining at the time of IF. Short report by histologist: Poorly staining for CK8 (bile ducts are a good internal control). Diffuse CD31 staining is supportive of this being HCC. Good correlation with H&E. Cross-reference with H&E, Figure 3.10. **Interpretation:** the UK3 sample stains weakly or negatively for CK8, other than the biliary structures which stain strongly positive and specifically. It is not possible to know the time point at which this particular biopsy was obtained from TXA101, due to the sample handling issues discussed previously. It is not possible to evaluate cell viability in this sample for this reason. For all immunofluorescence images acknowledgements go to Leticia Campo for staining protocol optimisation and slide preparation, Mark Shipman for assistance with image acquisition and Prof. Robert Goldin for reporting.

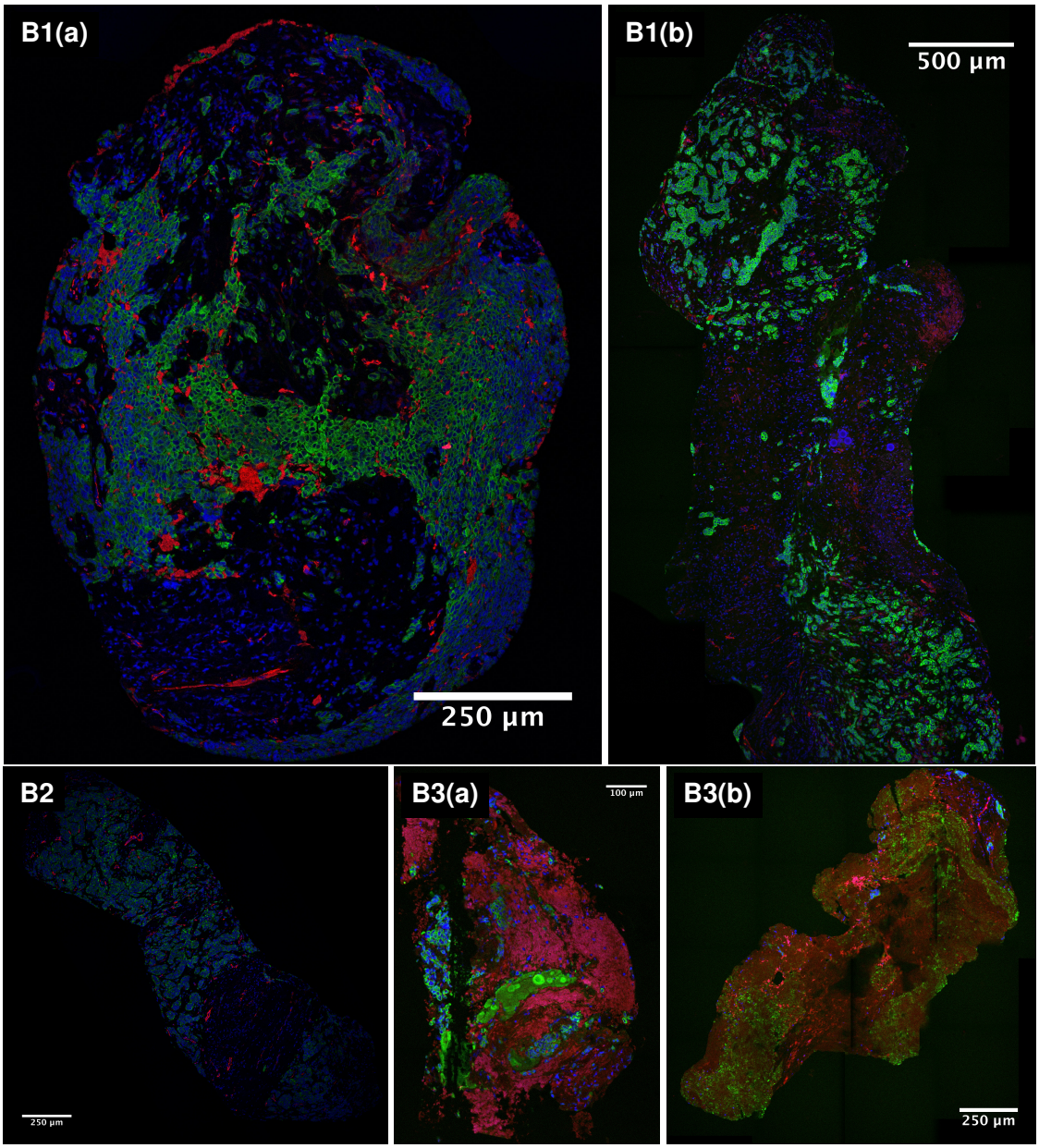


Figure 3.27: Immunofluorescence microscopy for TXA102 biopsies at x20 magnification, with various scalebars. DAPI=blue, CD31=red, CK8=green. Histopathology reports follow. B1(a): CK8 shows very good correlation with tumour. CD31 shows several large vessels. B1(b): CK8 shows good correlation with tumour. CD31 shows several smaller vessels. B2: CK8 shows good correlation with tumour. CD31 shows a few large vessels. B3(a): CK8 shows good correlation with tumour (of which there is very little). Regions of diffuse CD31 staining (presumed blood products as seen on H&E), but no blood vessels (as expected). B3(b): CK8 shows widespread granular staining consistent with necrosis and minimal cell-specific staining (no tumour on H&E). Regions of diffuse CD31 staining (presumed blood products as seen on H&E), but no blood vessels (as expected). Cross-reference with H&E, Figure 3.11. **Interpretation:** Biopsy samples B1-B3 demonstrate strong and specific CK8-positive regions. Despite sample B3 being predominately blood clot, some cellular areas remain which are CK8-positive, suggesting persistence of cell viability immediately post-FUS exposure, i.e. consistent with levels of hyperthermia not HIFU ablation. Note that CD31 also stains white blood cells and platelets, explaining why B3 samples stain highly for it.

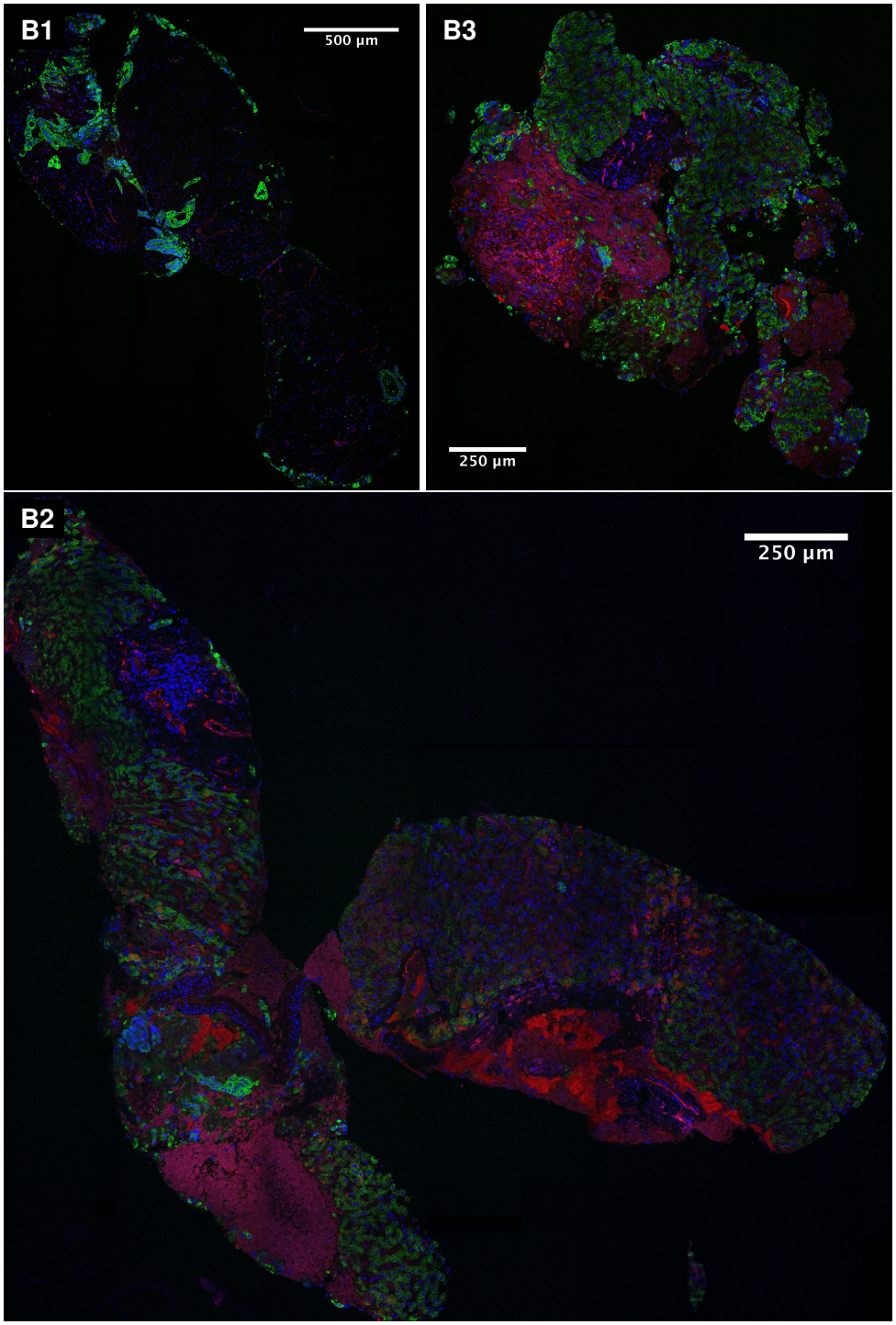


Figure 3.28: Immunofluorescence microscopy for TXA103 biopsies at x20 magnification, with 250 µm scalebar. DAPI=blue, CD31=red, CK8=green. Histopathology reports follow. B1: CK8 shows good correlation with tumour. CD31 shows several small vessels. B2: CK8 shows good correlation with tumour. Regions of diffuse CD31 staining (presumed blood products as seen on H&E), and several small vessels. B3: CK8 shows good correlation with tumour. Regions of diffuse CD31 staining (presumed blood products as seen on H&E), and several small vessels. Cross-reference with H&E morphology, Figure 3.11. **Interpretation:** Biopsy samples B1-B3 demonstrate strong and specific CK8-positive regions, suggesting persistence of cell viability post-FUS exposure.

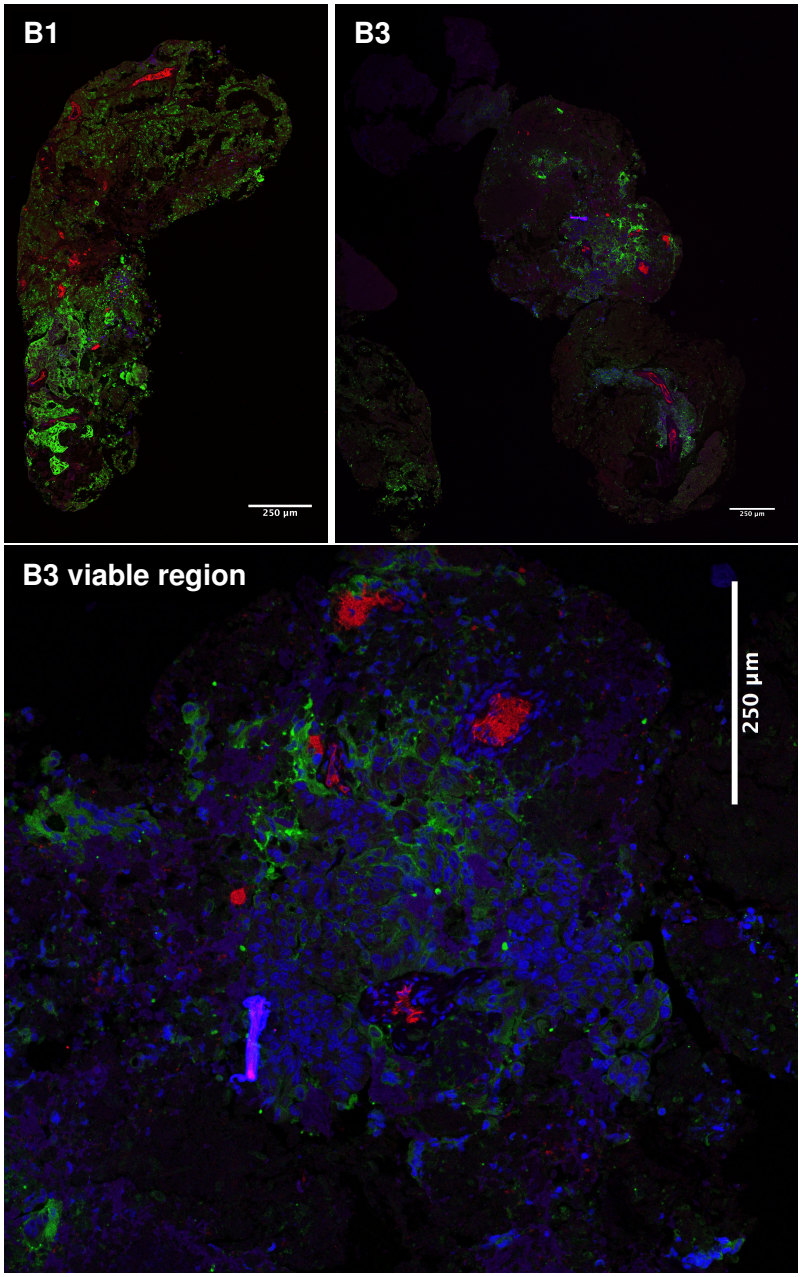


Figure 3.29: Immunofluorescence microscopy for TXA104 B3 biopsies at x20 magnification, with 250 µm scalebar. DAPI=blue, CD31=red, CK8=green. Immunofluorescence for sample B2 was omitted due to being entirely blood clot. The most viable region of the B3 tumour sample is shown at higher magnification rightmost. Histopathology reports follow. B1: CK8 shows widespread granular staining in necrotic regions and cell-specific staining at tumour foci. CD31 shows a few large vessels. Section appears to be a different level to the H&E, which is almost entirely necrotic. B3(a): Mostly necrotic sample, CK8 and CD31 staining in regions of tumour foci only. In these regions a few cells stain positively for CK8 and CD31 shows a few small vessels. B3(b): CK8 shows widespread granular staining consistent with necrosis and minimal cell-specific staining (very little tumour seen on H&E). CD31 shows no blood vessels (as expected). Cross-reference with H&E morphology, Figure 3.13. **Interpretation:** Whilst B3 is certainly more necrotic, both available biopsy samples B1 & B3 demonstrate strong and specific CK8-positive regions, suggesting persistence of cell viability post-FUS exposure. Of note CK8 was found to be strongly positive in viable tumour regions and typically near to micro-vasculature, and absent in adjacent regions of tumour necrosis. This demonstrates the utility of cross-referencing with the H&E counterpart, for which tumour necrosis is easily identified by lack of discernible nuclei.

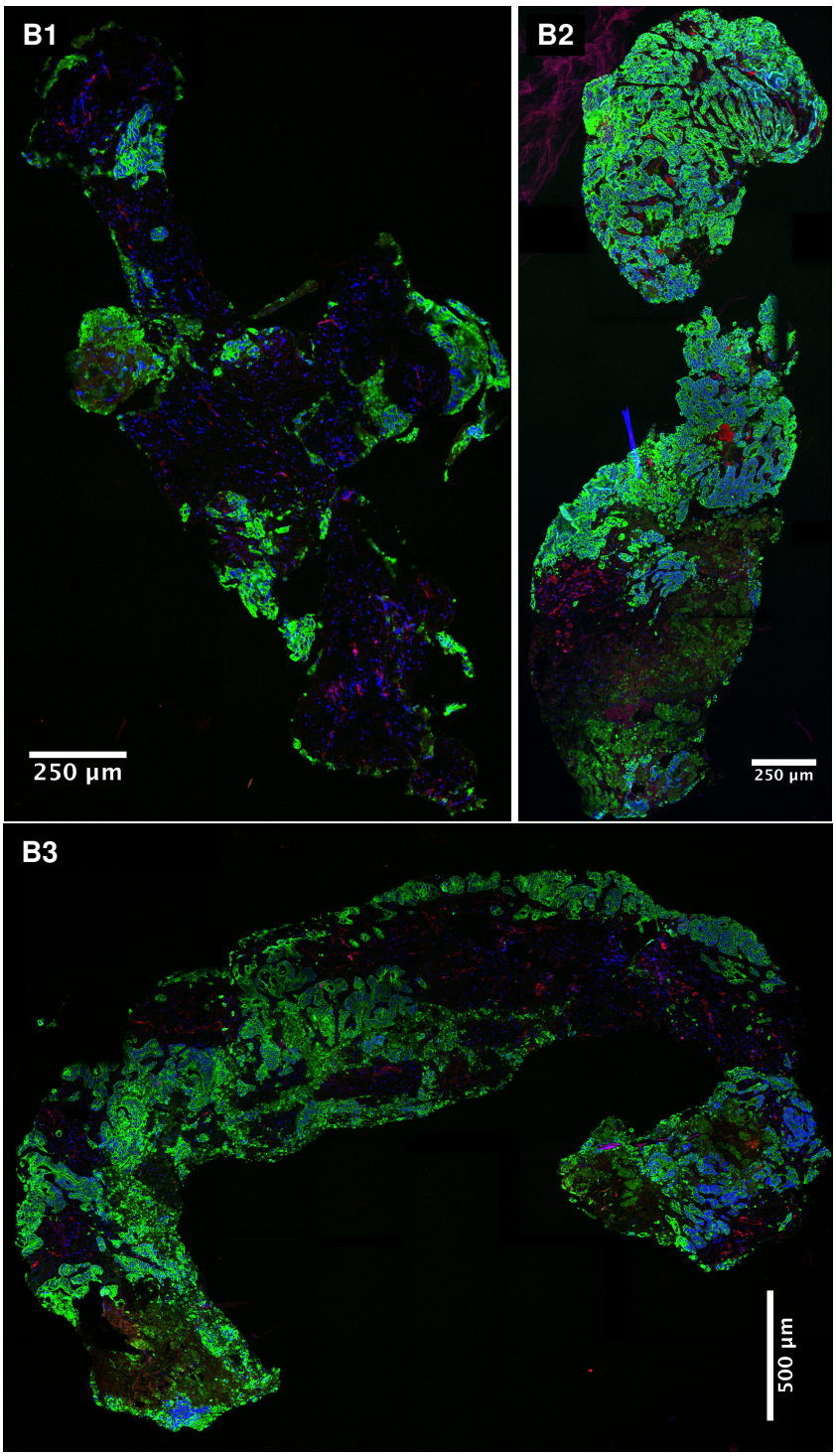


Figure 3.30: Immunofluorescence microscopy for TXA105 biopsies at x20 magnification, with various scalebars. DAPI=blue, CD31=red, CK8=green. Histology reports follow. B1: CK8 shows good correlation with tumour. CD31 shows several small vessels. B2: CK8 shows good correlation with tumour. CD31 shows several small vessels. B3: CK8 shows good correlation with tumour. CD31 shows several medium and small vessels. Cross-reference with panCK (Figure 3.31) and H&E morphology, Figure 3.14. **Interpretation:** Biopsy samples B1-B3 demonstrate strong and specific CK8-positive regions. In this tumour strongly expressive of CK8, the the regions of glandular (epithelial) morphology on the H&E correspond to CK8 regions. Furthermore, the distribution of maximal nuclear doxorubicin (Section 3.3.4, Figure 3.44) also appears to roughly correspond to that of areas staining highly for CD31, an expected finding given doxorubicin delivery is through the tumour micro-vasculature.

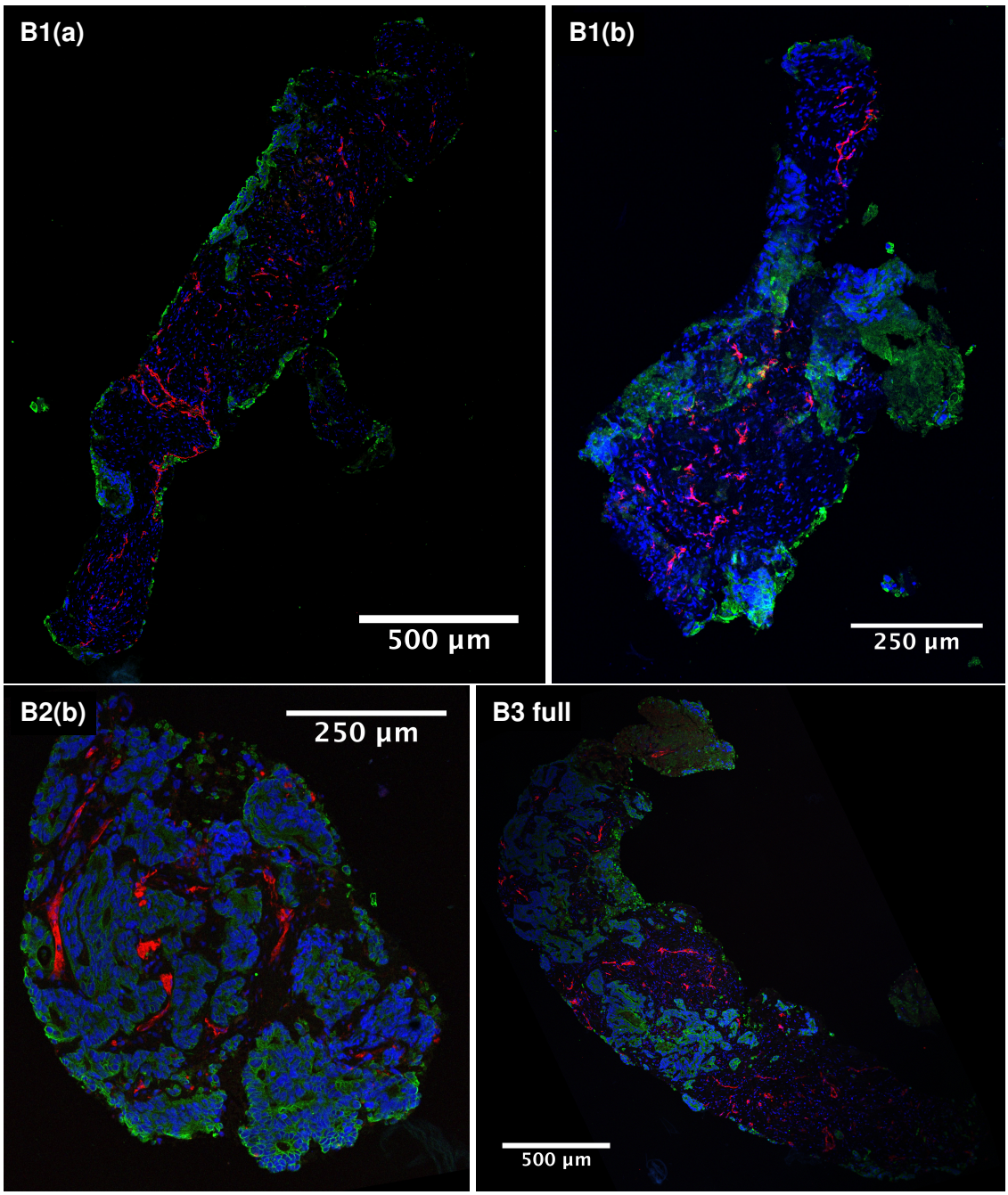


Figure 3.31: Immunofluorescence microscopy for TXA105 biopsies at x20 magnification, with various scalebars. DAPI=blue, CD31=red, pan-CK=green. Cross-reference with H&E morphology, Figure 3.14. TXA105 biopsy samples were additionally stained for pan-CK during method development. **Interpretation:** positive staining across all samples is demonstrated, in a similar distribution to CK8. In sample B1(a) pan-CK appears to be demonstrating an artifactual edge effect possibly due to incomplete penetrance. In sample B3, peripheral parts demonstrate reduced fluorescence in all channels, which is due to a focusing issue for this large sample.

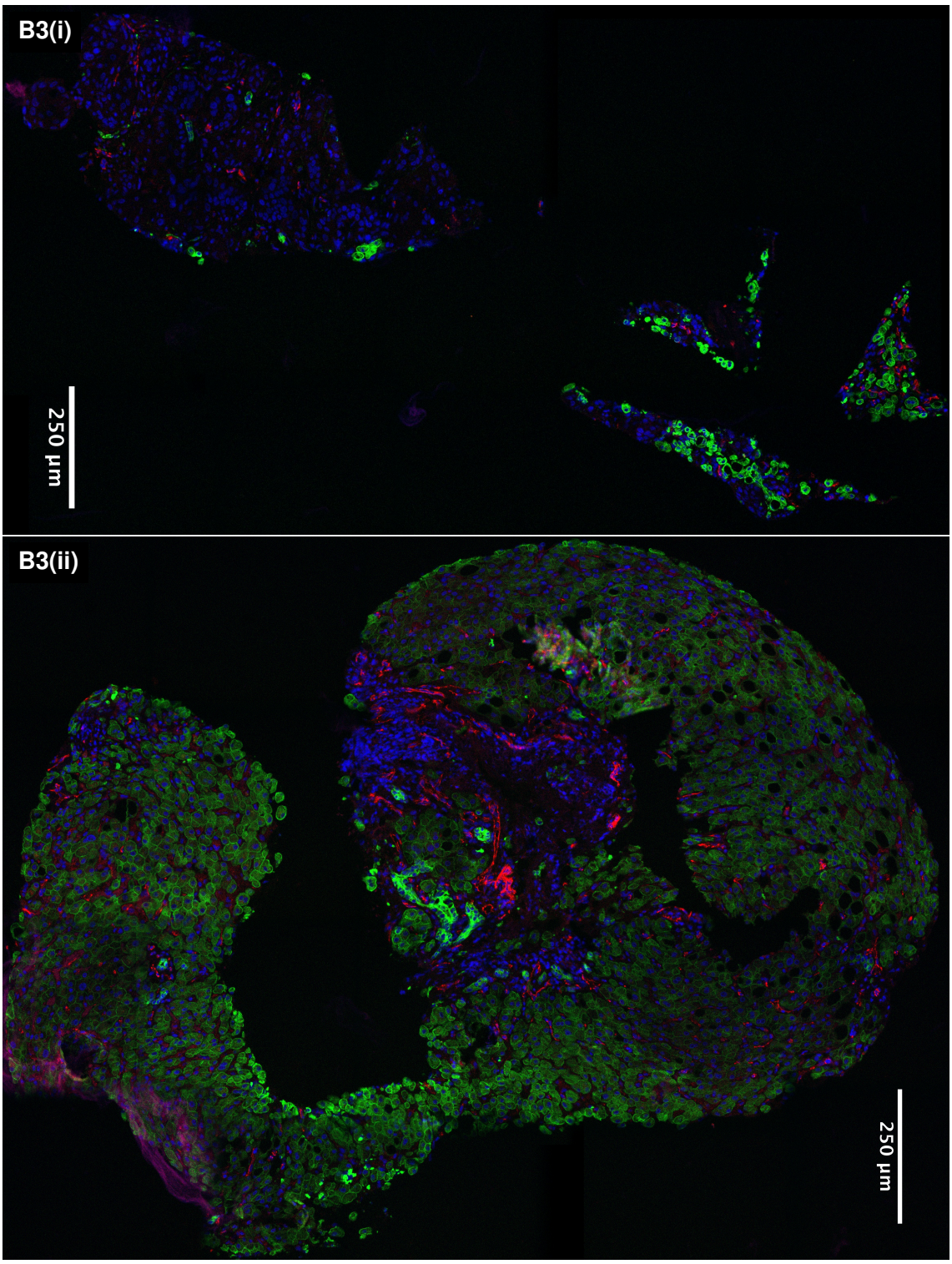


Figure 3.32: Immunofluorescence microscopy for TXB101 B3 biopsies at x20 magnification, with 250 µm scalebars. DAPI=blue, CD31=red, CK8=green. For Part II samples ('TXB'), biopsy is only performed after drug delivery and so B1 and B2 samples are not available. Histopathology reports follow. B3(i): CK8 shows good correlation with normal liver but there is no specific staining of the tumour cells. CD31 shows several small vessels. B3(ii): CK8 shows good correlation with normal (fatty) liver but there is no specific staining of the tumour cells. CD31 shows a few large vessels. Cross-reference with H&E morphology, Figure 3.15. **Interpretation:** sample B3 demonstrates strong and specific CK8-positive regions, suggesting persistence of cell viability post-FUS exposure in Part II.

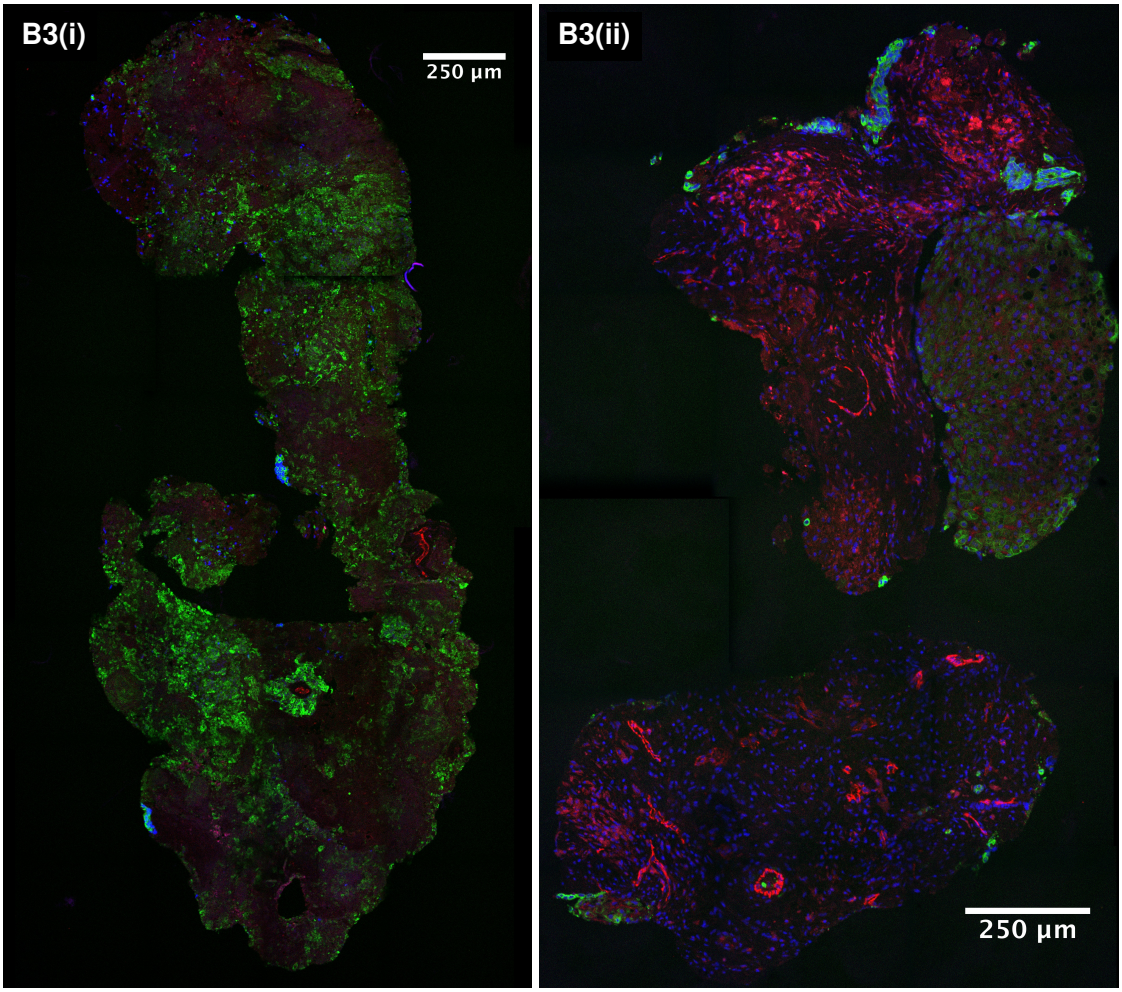


Figure 3.33: Immunofluorescence microscopy for TXB102 B3 biopsies at x20 magnification, with 250 µm scalebars. DAPI=blue, CD31=red, CK8=green. Histopathology reports follow. B3(i): CK8 shows widespread granular staining consistent with necrosis and minimal cell-specific staining at tumour foci (very little tumour seen on H&E). CD31 shows very few blood vessels (as expected). B3(ii): CK8 shows good correlation with normal liver and the small amount of tumour, but does not stain fibrous tissue (correlating with H&E). CD31 shows lots of large vessels. Cross-reference with H&E morphology, Figure 3.16. **Interpretation:** sample B3 demonstrates strong and specific CK8-positive regions, suggesting persistence of cell viability post-FUS exposure in Part II. The (i) and (ii) counterparts represent different cores in Part I and it appears that the first core was taken from a strongly CK8-positive region whilst the second core was taken from a more vascular region which is predominately CK8-negative, but contains some strongly CK8-positive regions.

3.3 Pharmocokinetics & Bio-Distrubution of Doxorubicin

For each patient, the details of the ThermoDox® infusions are shown in Table 3.11.

Patient ID	Infusion Start Time	Infusion End Time	Infusion Duration (mins)	ThermoDox® dose (mg)
TXA101	15:12	15:44	32	91
TXA102	13:39	14:09	30	81
TXA103	13:19	13:50	31	101
TXA104	11:58	12:33	35	70
TXA105	13:05	13:35	30	104
TXB101	10:43	11:11	28	124
TXB102	11:05	11:41	36	82
TXB103	11:06	11:36	30	90
TXB104	11:00	11:30	30	96

Table 3.11: Infusion timings for ThermoDox® for each study intervention. Each infusion is given over 30 minutes in 250 mL of 5% dextrose solution at a dose of 50mg/m^2 body surface area (equivalent to a single standard doxorubicin cycle), with peak circulating levels immediately following end of drug infusion (Figure 2.33). Immediately following infusion a 5 minute saline flush is given.

3.3.1 Doxorubicin Quantification in Plasma by HPLC

The HPLC method previously described in 2.3.1 was used to obtain the total plasma doxorubicin levels for the three time points, as shown in Table 3.12. These data items have been plotted against a published pharmacokinetic curve for patients receiving the same dose (50 mg/m^2) of ThermoDox® but with RFA rather than FUS treatment of the target tumour [316]. There is currently no published clinical PK data for patients receiving ThermoDox® alone, and this data may be difficult to obtain due to ethical considerations of giving the drug without a heating modality to trigger release in a target tumour.

Patient ID	Plasma Sample	Time taken	Mins. after Infusion End	Dox. Conc. µg/mL	Evaluable for 3° Endpoint? Y/N
TXA101	P1	10:40	-	0.0	Y
TXA101	P2	15:47	3	N/E*	N
TXA101	P3	16:41	57	N/E* [a]	N
TXA102	P1	10:56	-	0.0	Y
TXA102	P2	14:10	1	26.2	Y
TXA102	P3	15:30	81	23.5	Y
TXA103	P1	10:49	-	0.0	Y
TXA103	P2	13:55	5	19.9	Y
TXA103	P3	15:18	88	6.0	Y
TXA104	P1	10:56	-	0.0	Y
TXA104	P2	12:44	11	26.2	Y
TXA104	P3	14:05	92	5.4	Y
TXA105	P1	11:45	-	0.0	Y
TXA105	P2	13:36	1	23.7	Y
TXA105	P3	15:05	90	8.0	Y
TXB101	P1	09:49	-	0.0	Y
TXB101	P2	11:13	2	31.9	Y
TXB101	P3	12:47	96	19.3	Y
TXB102	P1	09:56	-	0.0	Y
TXB102	P2	11:41	0	29.8	Y
TXB102	P3	13:35	114	16.0	Y

Table 3.12: Fluorescence HPLC results for total doxorubicin in plasma for patients treated on the study. HPLC analysis of plasma samples for TXB103 and TXB104 had not been performed at time of writing. Acknowledgements: Dr. Lisa Folkes, Dr. Michael Stratford.

[a] *In the first HPLC analysis for plasma, the plasma concentrations for P2 and P3 were off the standard curve and thus they were non-evaluable. For subsequent runs, the SOP was modified to dilute plasma samples to a range back on the curve.

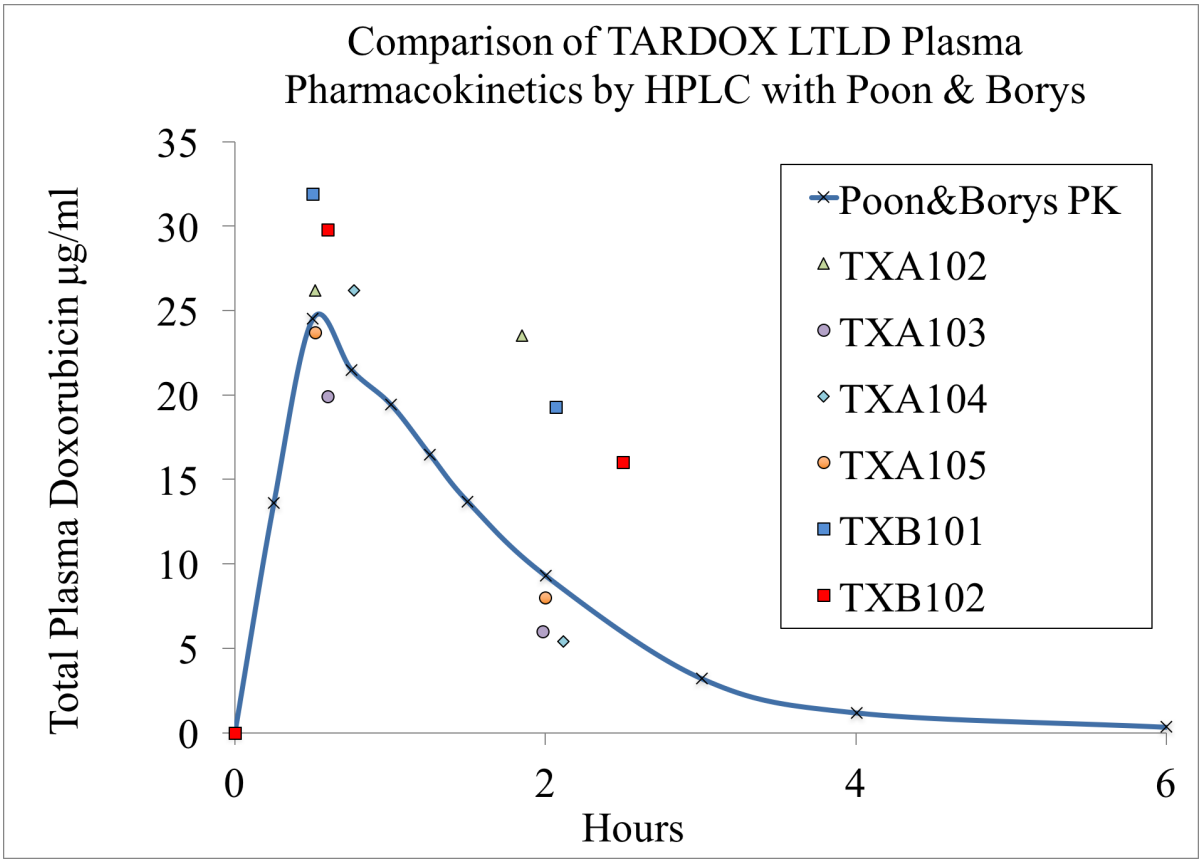


Figure 3.34: HPLC plasma pharmacokinetics for total doxorubicin in patients treated on the study, overlaid with published ThermoDox® pharmacokinetics for total doxorubicin in patients treated with ThermoDox® and RFA [316].

Interpretation of Plasma HPLC Results

The majority of the HPLC plasma data points for total doxorubicin lie close to the published pharmacokinetic curve, which in itself provides further validation of the HPLC assay. The final (Released) plasma sample for patients TXA101, TXA102, TXB101 and TXB102 lie notably above the published curve. The most likely explanation is that blood sampling in these patients was performed from the same arm used to administer the drug, potentially resulting in a venous sampling bias. Whilst best efforts are made to avoid sampling from the same arm as administration, in the cohort of patients referred for the study, having received many previous cycles of chemotherapy, venous access is often very difficult. In these particular cases there were only limited options for cannulation

sites from which the team were able to bleed back in order to sample the circulating venous blood. However this does not explain TXB102, which was the only case to receive ThermoDox® via a peripherally inserted central cannula (PICC line) which eliminates any such bias. Variability between the quantification assays used (fluorescence HPLC vs. liquid chromatography-mass spectrometry) and expected standard errors are also factors to consider.

The *in vivo* ThermoDox® animal study previously performed at the University of Oxford (Section 2.3.2) showed a dramatic shift of drug out of the circulation in the group receiving HIFU over the group receiving ThermoDox® alone (Figure 2.34). For this clinical study, it follows that, for blood samples taken following delivery, circulating levels well below the PK clearance line for the Poon & Borys study may suggest enhanced delivery over that seen with RFA. However, in the clinical case, as the tumour-to-body mass ratio is two orders of magnitude smaller than in murine tumour models, this shift becomes much less significant, even with dramatically enhanced levels of drug delivery (10-20 μg/g). To put this into perspective, for a tumour treatment region of 3x3x3 cm, if this clinical study intervention was effective enough to deliver 20 μg/g of doxorubicin to this ~27 g tumour mass, 540 μg of doxorubicin would be removed from the blood stream, resulting in a drop of 0.18 μg/mL in plasma [4]. This would be from a circulating plasma level of around 10 μg/mL at the 2 hour mark (Figure 3.34), which would be less than a 2% drop. Given the inherent standard error of any PK assay and patient-to-patient variation, identification of such a small change holds little statistical rigour. Thus, whilst the plasma PK data continues to be informative for the TARDOX study in supporting the tumour PK data, for the reasons discussed, the exploratory endpoint relating to plasma PK will not be discussed further.

[4]This calculation makes the assumption that 100% of the circulating doxorubicin is encapsulated, and thus all doxorubicin is confined to the plasma compartment of ~3000 mL, rather than bioavailable doxorubicin which is split relatively evenly between plasma and cellular compartments, depending on the patient's haematocrit [493].

3.3.2 Doxorubicin Quantification in Plasma by Dequenching Assay

HPLC requires destruction of the sample and thus the relative split between encapsulated and non-encapsulated drug cannot be assessed by this method. The dequenching assay for plasma, previously described in Section 2.3.2, goes some way towards establishing the level of drug encapsulation in the circulating plasma. The clinical results of the dequenching assay are shown in Table 3.12. Note that the Unreleased plasma sample for TXA104 is an outlier, which deviates from both the expected curve and the HPLC result and thus is likely to be a spurious result. As the corresponding HPLC value is in range (Figure 3.34), it is unlikely to be due to venous sampling error, and an operator error is a more likely explanation. It is important to appreciate that the purpose of this assay was not to re-validate the corresponding HPLC values for plasma samples, rather to better understand the release profile of circulating ThermoDox® when used in combination with FUS.

Patient ID	Plasma Sample	Mins. after Infusion End	Pre-heated Avg. Fluor. (Equivalent Conc. µg/mL)	Post-heated Avg. Fluor. (Total Conc. µg/mL)	Heated: Pre-heated Fluor. Ratio	Heated: Pre-heated Conc. Ratio
TXA101	P1	-	191 (0.00)	296 (0.00)	-	-
TXA101	P2	3	5813 (5.93*[a])	27945 (32.49*)	4.81	5.48
TXA101	P3	57	4350 (4.41*)	27054 (32.26*)	6.22	7.32
TXA102	P1	-	-81 (0.00)	144 (0.00)	-	-
TXA102	P2	1	5448 (4.62*)	26120 (24.68*)	4.79	5.34
TXA102	P3	81	3354 (2.53*)	20746 (19.38*)	6.19	4.90
TXA103	P1	-	619 (0.00)	364 (0.00)	-	-
TXA103	P2	5	5702 (4.79*)	26559 (24.07*)	4.66	5.03
TXA103	P3	88	2389 (1.74*)	10005 (8.53*)	4.19	4.90
TXA104	P1	-	-142 (0.00)	-275 (0.00)	-	-
TXA104	P2	11	7960 (6.35*)	35909 (42.58*)	4.51	6.71
TXA104	P3	92	2662 (2.00*)	10493 (9.68*)	3.94	4.84
TXA105	P1	-	952 (0.00)	1183 (0.00)	-	-
TXA105	P2	1	6768 (6.15)	23607 (23.60)	3.49	3.84
TXA105	P3	90	3304 (2.63)	10755 (10.07)	3.26	3.82
TXB101	P1	-	-66 (0.00)	-197 (0.00)	-	-
TXB101	P2	1	6229 (6.05)	26189 (27.81)	4.20	4.60
TXB101	P3	96	2707 (2.49)	17618 (17.75)	6.51	7.13
TXB102	P1	-	854 (0.00)	-973 (0.00)	-	-
TXB102	P2	0	5503 (4.56)	28327 (24.85)	5.15	5.45
TXB102	P3	113	1664 (1.27)	17219 (13.11)	10.35	10.29
TXB103	P1	-	-651 (0.00)	-1018 (0.00)	-	-
TXB103	P2	0	5852 (4.30)	27506 (27.26)	4.70	6.34
TXB103	P3	83	1878 (1.17)	11280 (10.86)	6.01	9.25
TXB104	P1	-	-124 (0.00)	388 (0.00)	-	-
TXB104	P2	0	5051 (4.16)	21535 (20.86)	4.23	5.01
TXB104	P3	90	2285 (1.82)	12856 (11.53)	5.63	6.34

Table 3.13: Dequenching fluorescence results for total doxorubicin in plasma for patients treated on the study. All samples were read the same day as the intervention. Fluorescence readings were obtained using POLARstar OPTIMA plate reader using an excitation of 485 nm, an emission of 590 nm and gain of 1700. All fluorescence values are blank-corrected and averaged from two wells, with a 1 in 2 dilution in MPHP. Assay details can be found in Section 2.3.2. Acknowledgements: Dr. Kevin Myers, Nita Fisher, Daniela Tramonti.

[a]Concentrations marked with an asterix (*) have been estimated from the standard curve generated for TXA105. This is because at some unknown point prior to TXA105, the reference standards and QCs became degraded. Standards and QCs were re-made for TXA105 onwards. For these items, the original raw fluorescence values are shown, which are not influenced by the standard curve.

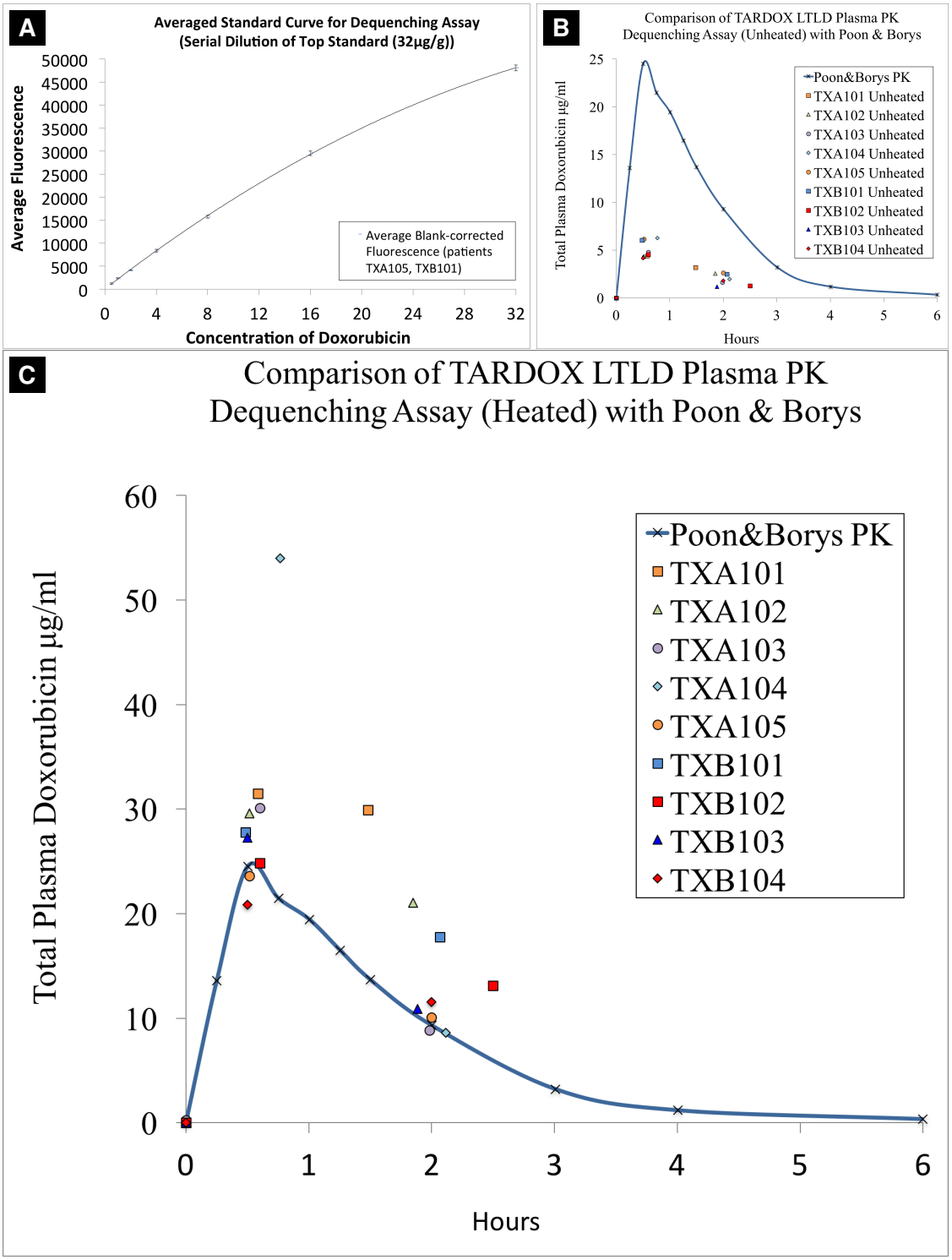


Figure 3.35: A: Standard curve for dequenching plasma assay obtained from validated non-degraded standards (Section 2.3.2) for patients TXA105 & TXB101, with standard error bars. This curve was used to back-calculate plasma levels for patients TXA101-TXA104, where the initial standards for the dequenching assay were identified to have degraded (Figure 2.36). **B:** Plasma pharmacokinetics for total doxorubicin by dequenching assay pre-heating in patients treated on the study, overlaid with published ThermoDox® pharmacokinetics for total doxorubicin in patients treated with ThermoDox® and RFA [316]. **C:** The post-heating (dequenched) results for the same samples. In plots (B) and (C), values for TXA101-104 are estimates only.

Interpretation of Plasma Dequenching Results

Concentrations obtained for plasma samples from patients TXA101-TX104 are estimates, referenced from a more recent standard curve, obtained for patient TXA105. Only estimates can be made for these early cases as there was a deterioration of the original standards and QCs, thought to be due to their storage of -20°C rather than -80°C (Figure 2.36). As there has been little deviation in the fluorescence values obtained from the standard curves generated from patient TXA105 onwards (Figure 3.35), for which standards and QCs were remade, these estimates can be made with a reasonably high degree of confidence. Although similar trends are demonstrated, inevitably comparison of results between the HPLC and dequenching assays demonstrate some level of discrepancy. This is likely to be a consequence of differences in the underlying methods and associated errors. These discrepancies will not be discussed further.

It is the current understanding that following a ThermoDox® infusion, bioavailable doxorubicin accounts for less than a tenth (an estimated 3.7-9.4%) of the total circulating plasma doxorubicin in humans (Christine Swenson, Celsion Corporation, unpublished). The results of the dequenching assay used here are not able to determine the absolute plasma concentrations of free and encapsulated doxorubicin, as in a mixed sample, both components contribute to fluorescence. However the results provide an indication as to the degree of encapsulation. For all samples, the heated vs. pre-heated doxorubicin concentration ratio shows a 3.48-10.29 fold increase in plasma samples (P2 and P3), demonstrating the high-degree of encapsulation persists even 1.5 hours following infusion end. Lower fold increases would suggest the majority of doxorubicin circulating in the plasma has already been released from ThermoDox®. The variation in the degree of encapsulated drug circulating demonstrated between patients and for consecutive samples from the same patient may perhaps be explained by the following:

1. Physiological differences between patients and metabolic pathways
2. Differences in pharmacy timing for drug preparation/collection

3. Differences in ambient temperatures during preparation, storage and delivery of drug

Both assays demonstrate that the final (Released) plasma sample for patients TXA101, TXA102 and TXB101 are above expected clearance levels, where the same arm was used for administration and sampling, reinforcing the possibility of sampling bias previously discussed (Section 3.3.1). Plasma sample P2 of patient TXA104 was reported to be especially high (42.58 μg/mL) by the dequenching assay, whilst in the expected range (26.2 μg/mL) by the HPLC assay. The reason for this spurious result is unknown, and this outlier has been excluded from the plot (Figure 3.35). In any case, in order to determine the concentration of total circulating doxorubicin, the HPLC results should be taken over the dequenching results, due to more extensive validation performed for the HPLC assay.

3.3.3 Doxorubicin Quantification by HPLC in Tumour Biopsy

Table 3.14 summarises the HPLC results for the clinical biopsy samples for Part I and Table 3.15 for Part II. The HPLC fluorescence chromatograms for Part I are shown in Figures 3.36-3.40. Part II chromatograms omitted for brevity.

Patient ID	Biopsy	Time Taken	Biopsy Mass mg	Est. % Necrosis	Dox. Conc. µg/g	HPLC Evaluable? Y/N	Inc. in Interim 1° Endpoint Analysis? (Y/N)	Patient Included in Interim 1° Endpoint Analysis? Y/N	(B2-B3 fold inc.)
TXA101	B1	10:35	2.78	N/E	0.00	Y	-		
TXA101	B2	15:46	2.57	N/E	2.56	Y	Y	Y	x2.1
TXA101	B3	16:40	6.64	N/E	5.32	Y	Y		
TXA102	B1	10:56	2.19	0	0.00	Y	-		
TXA102	B2	14:09	2.81	0	1.02	Y [a]	Y	N [b]	-
TXA102	B3	15:30	4.85	Clot	13.2	N [c]	N		
TXA103	B1	10:48	3.11	0/90	0.00	Y	-		
TXA103	B2	13:55	2.10	0	4.09	Y	Y	N [d]	-
TXA103	B3	15:23	3.94	0	7.89	Y	Y		
TXA104	B1	10:48	1.59	95	0.00	Y	-		
TXA104	B2	12:36	2.31	Clot	1.59	Y	N	N [e]	-
TXA104	B3	13:47	2.77	90	2.09	Y	N		
TXA105	B1	11:45	0.84	0	0.00	Y	-		
TXA105	B2	13:36	2.73	0/95	2.23	Y	Y	Y	x5.2
TXA105	B3	15:05	1.30	10	11.50	Y	Y		

Table 3.14: Part I biopsy HPLC results generated by the Bioanlaysis Core. Acknowledgements: Dr. Lisa Folkes and Dr. Michael Stratford. Estimated percentage necrosis obtained from H&E microscopy by consultant histopathologist (Figures 3.10-3.14).

[a] Repsonse was below the LLOQ as defined in the validation report, however post-analysis has shown linearity in the standards down to this concentration and hence this value can be included in analysis, and in particular averaging for the Part II comparison.

[b] In addition to the assay error, H&E microscopy of the other half of the B3 sample reported mainly blood clot and thus has been excluded in the interim analysis of the primary endpoint.

[c] Estimate only as the internal standard was inadvertantly omitted from this item prior to HPLC processing.

[d] Hyperthermia has been deemed suboptimal in this patient, due to technical difficulties previously discussed (Section 3.2.4). In Part I, only tumours receiving optimal hyperthermia have been included in the interim analysis of the primary endpoint.

[e] Whilst the HPLC result is validated, H&E microscopy of the other half of the B2 sample reported mainly blood clot and thus has been excluded in the interim analysis of the primary endpoint. In addition the B3 sample was from a highly necrotic tumour core.

Patient ID	Biopsy Sample	Time Taken	Biopsy Mass mg	Est. % Necrosis	Dox. Conc. µg/g	HPLC Evaluable? Y/N	Patient Included in Interim 1° Endpoint Analysis? Y/N	Avg. B2(=2.48)-B3 fold inc.)
TXB101	B3(i)	12:47	2.45	0	6.65	Y	Y	x2.7
TXB102	B3(i)	13:35	2.42	95	6.84	Y	Y	x2.8

Table 3.15: Part II biopsy HPLC results generated by the Bioanlaysis Core. HPLC analysis of tissue samples for TXB103 and TXB104 had not been performed at time of writing. Acknowledgements: Dr. Lisa Folkes and Dr. Michael Stratford. Estimated percentage necrosis obtained from H&E microscopy by consultant histopathologist (Figures 3.15-3.16).

HPLC Chromatograms

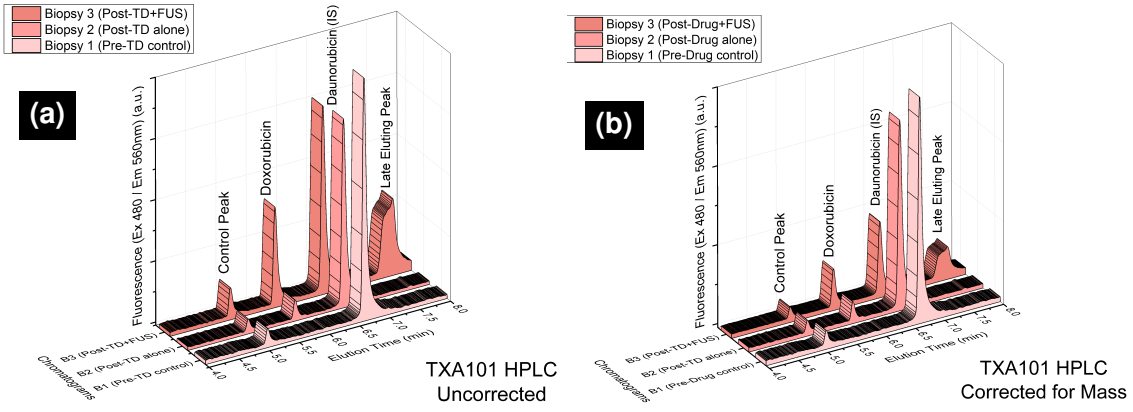


Figure 3.36: HPLC chromatograms for TXA101, both unnormalised (a) and normalised for biopsy mass (b). Note that the broad peak shown at 8 minutes did not interfere with the peaks of the anthracycines. This was later deemed to be a late-eluting peak from a previous run, and subsequently the elution gradient of the assay was modified to avoid this problem in future, and the assay was revalidated. Full details of the HPLC methodology are avaiable in Section 2.3.1.

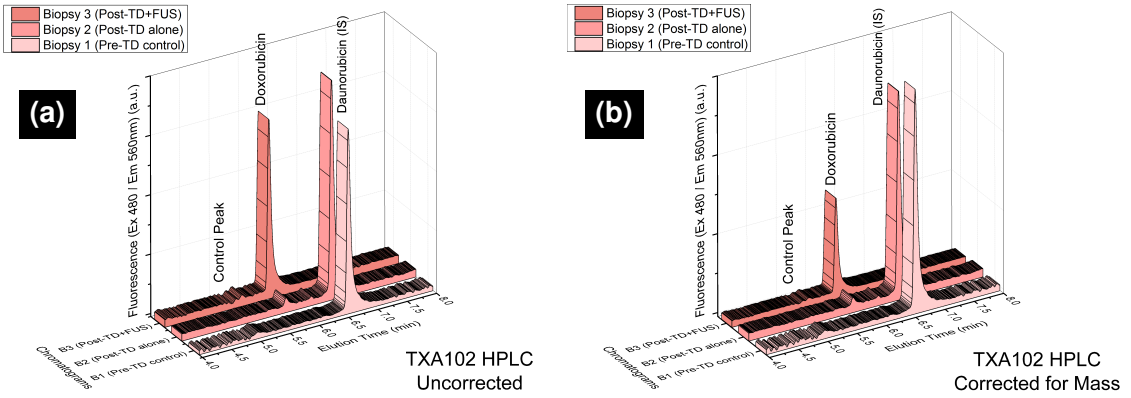


Figure 3.37: HPLC chromatograms for TXA102, both unnormalised (a) and normalised for biopsy mass (b). Note in this particular HPLC run the internal standard was inadvertantly omitted for the third biopsy sample, and the corresponding peak is missing.

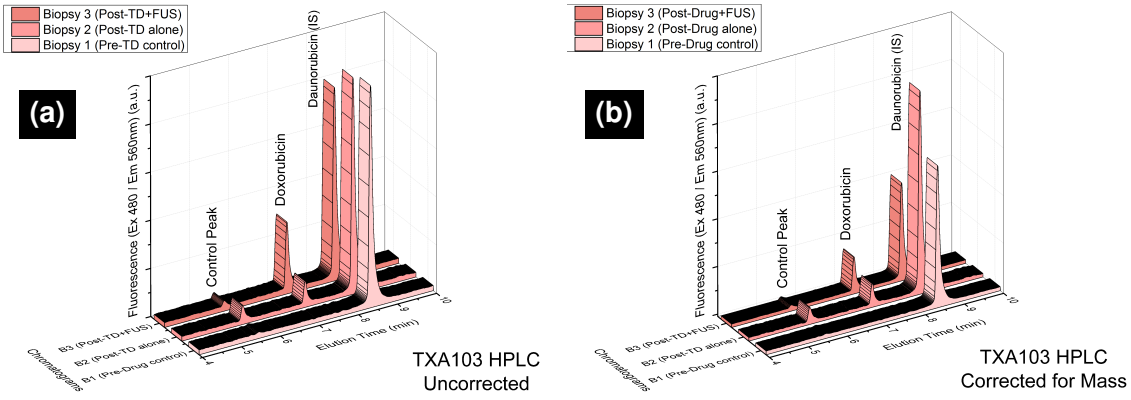


Figure 3.38: HPLC chromatograms for TXA103, both unnormalised (a) and normalised for biopsy mass (b).

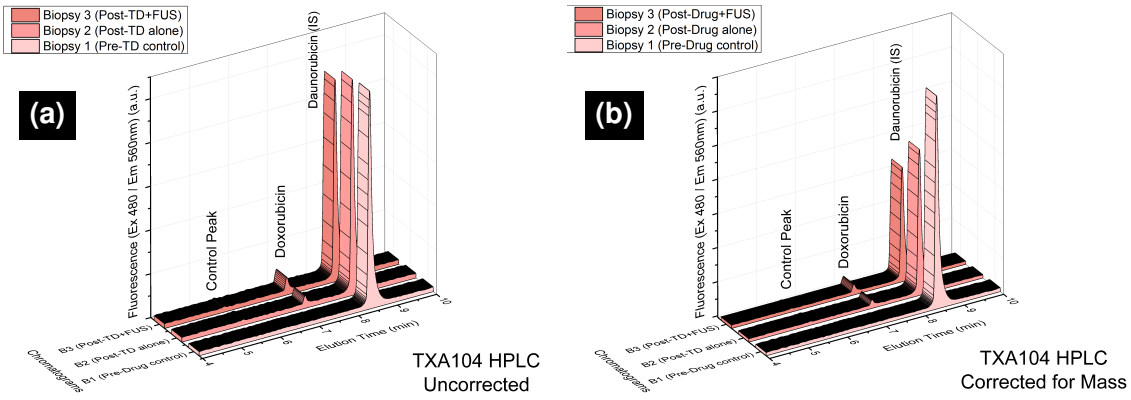


Figure 3.39: HPLC chromatograms for TXA104, both unnormalised (a) and normalised for biopsy mass (b).

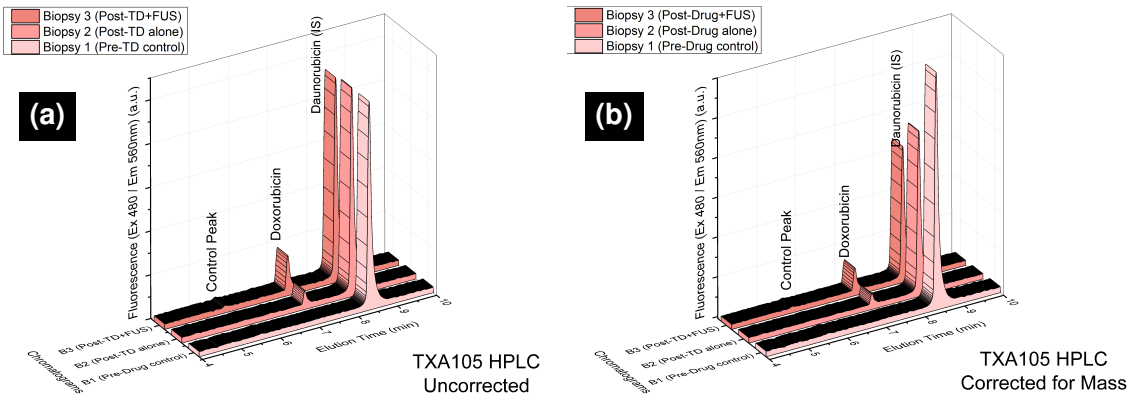


Figure 3.40: HPLC chromatograms for TXA105, both unnormalised (a) and normalised for biopsy mass (b).

Interpretation of Biopsy HPLC Results

HPLC chromatograms are clean with easily distinguishable peaks. Modification of the elution gradient was required to remove late-eluting peaks seen in TXA101 (Figure 3.36). A great advantage of dividing a single biopsy core in two is that it means that HPLC biopsy results can be taken in the context of the H&E microscopy results (Section 3.2.6), which not only allows identification of intratumoral blood clot sampled inadvertently, it also gives an opportunity to estimate the degree of background tumour necrosis (Tables 3.14 and 3.15).

In the first patient treated, **TXA101**, doxorubicin was absent in the Pre-Treatment (B1) sample as would be expected. There was a over 2.1-fold increase in the amount of doxorubicin delivered following targeted FUS in this well-differentiated HCC tumour. The second patient treated, **TXA102**, unfortunately bled into her tumour following earlier biopsies, such that the final biopsy was comprised mainly of clot (Figure 3.11). Consequently, this result has been excluded from the interim analysis of the primary endpoint.

For the third patient, **TXA103**, it was not possible to record optimal hyperthermia due to an number of technical difficulties (Section 3.2.4) and it was deemed that optimal hyperthermia was not achieved. Consequently, although this result is excluded from the interim analysis here, the Unreleased (B2) concentration can be included in the averaging

required to evaluate the primary endpoint in Part II patients and both Unreleased and Released concentrations can be included in final primary endpoint analysis on an intention-to-treat basis. H&E revealed that whilst the B1 sample appears to be well placed in the tumour, the B3 sample, which followed subtle co-axial needle repositioning for biopsy following an initial bloody core, is likely to have been sampled from an area outside of the confines of the tumour as the H&E report reveals normal liver tissue (Figure 3.12), again demonstrating the value of quantitative and qualitative data collection.

The B3 sample for **TXA104** shows an unexpectedly low intratumoral drug concentration of 2.09 μg/g, despite the target receiving optimal hyperthermia. This value is well below the threshold which would be considered therapeutic. This may be explained by the central and highly necrotic region of tumour sampled; the microscopy section of the same biopsy core shows predominately necrosis (>90%) with a small minority of viable tumour cells (Figure 3.13). This is supported by the fact that doxorubicin appears to be localised to the small focus of tumour cells, and absent in the surrounding necrotic tissue (Figure 3.41). If the region demonstrating a localised PET response the tumour periphery (Figure 3.4), was sampled it may have provided a higher yield of information and potentially would have demonstrated a much higher concentration of delivered drug.

TXA105 demonstrated a very encouraging 5.2-fold increase with an intratumoral drug concentration of 11.5 μg/g and this may reflect the quality of the biopsy (Figures 3.13 and 3.41).

TXB101 and **TXB102** demonstrated intratumoral concentrations of 6.65 and 6.84 μg/g respectively, the former being from a tumour sample with low necrosis (Figure 3.15) and the latter being from a highly necrotic tumour sample (Figure 3.16). These results are further discussed as case summaries in Section 4.2.1 in the context of the primary endpoint in Section 4.2.3.

3.3.4 Doxorubicin Bio-availability by Fluorescence Microscopy

Using the same spectral un-mixing technique discussed in Section 2.3.3, the fluorescence signature of doxorubicin was used to determine its distribution in the clinical samples. Clinical slides were prepared using the same method, other than using a soft-setting DAPI mounting media in case the slide was reused for immunofluorescence. However, typically an adjacent slice of the same tissue block was used for this purpose. Analysis for doxorubicin was performed before immunofluorescent (IF) staining for cell nuclei, endothelia and cytokeratins. This was because the heating step required for slide preparation for IF has the effect of dramatically reducing the doxorubicin fluorescence intensity.

Figures for samples TXA101-TXA102 excluded due to the issues previously demonstrated on H&E microscopy (Figures 3.10-3.11) and that for TXA103 excluded due to lack of evidence of optimal hyperthermia (Figure 3.5). Figures 3.41-3.47 show the results from patient TXA104-TXB103 (microscopy for TXB104 not included), in which optimal hyperthermia was either demonstrated for Part I or predicted for Part II. Acquisition parameters affecting doxorubicin fluorescence intensity were matched, thus doxorubicin levels are comparable both for the same patient and between different patients, with the exception of TXB103 and TXB104 where the 468 nm laser power required reduction by 30% due to saturation of the doxorubicin signal.

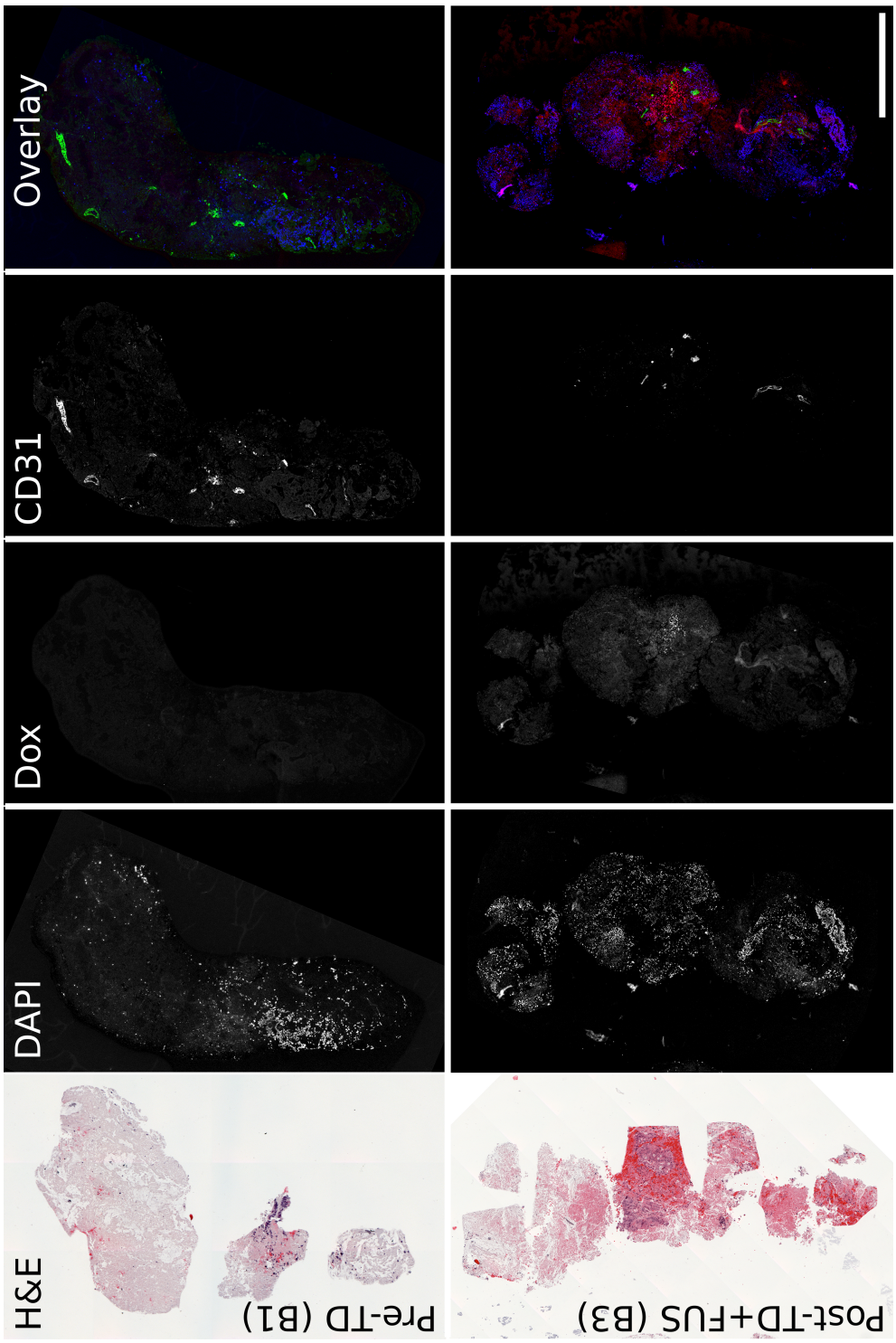


Figure 3.41: H&E, DAPI & Doxorubicin fluorescence microscopy overlayed with immunofluorescence microscopy of Pre-Treatment (B1) & Post-TD+FUS (B3) samples obtained from the targeted colorectal primary liver metastasis for patient TXA104, demonstrating the distrubution of doxorubicin. Post-TD alone (B2) sample omitted due to being a blood clot. Staining is, from left to right, H&E, DAPI (blue, nuclear stain), Doxorubicin (red, unmixed), CD31-IF (green, vascular stain) and composite. Samples formalin-fixed and paraffin embedded, doxorubicin profile spectrally unmixed using Zeiss 710 Confocal Microscope. Acquired at x20 magnification and shown with 500 μm scalebar. Acknowledgment: Mark Shipman of the Ludwig Institute for Cancer Research, University of Oxford, for preparing this figure.

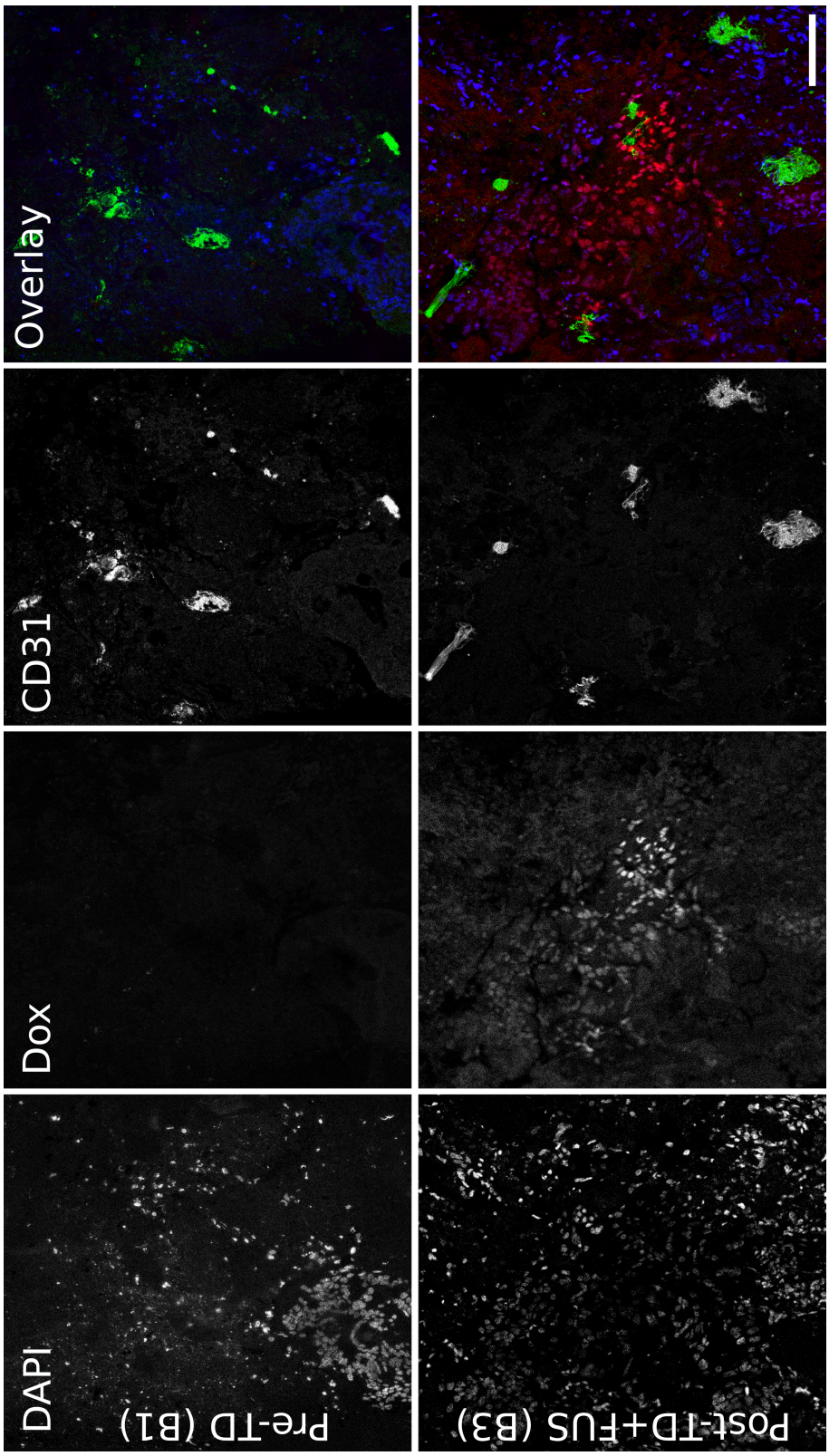


Figure 3.42: DAPI & Doxorubicin fluorescence microscopy overlayed with immunofluorescence microscopy of selected viable tumour region of Pre-Treatment (B1) & Post-TD+FUS (B3) samples for the same patient. Staining is, from left to right, DAPI, Doxorubicin, CD31 and composite (DAPI=blue, Doxorubicin=red, CD31=green). Acquired at x20 magnification and shown with 100 μm scalebar.

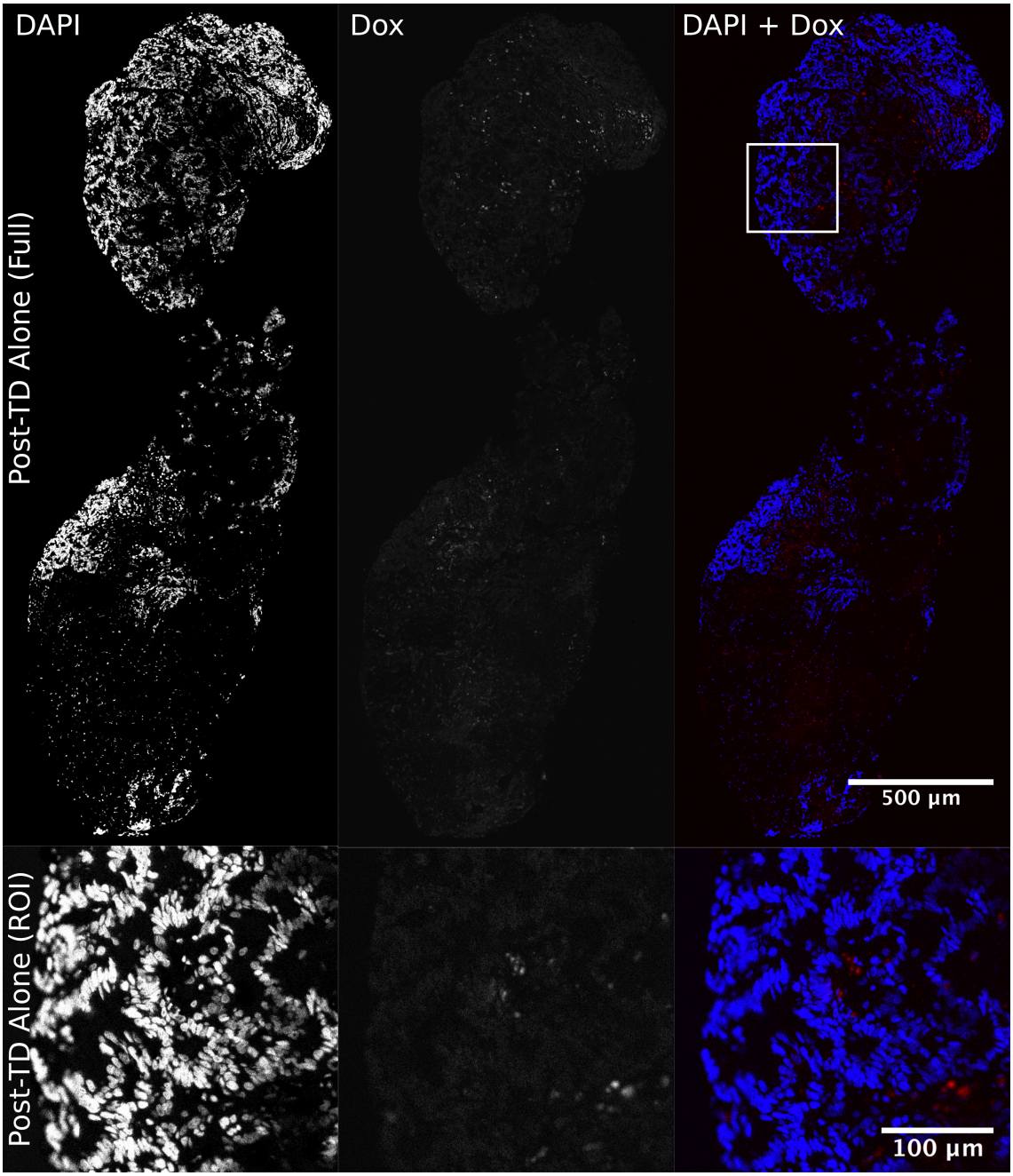


Figure 3.43: DAPI & Doxorubicin fluorescence microscopy of Post-TD alone (B2) sample obtained from the targeted colorectal primary liver metastasis for patient TXA105. Staining is, from left to right, DAPI, Doxorubicin and composite (DAPI=blue, Doxorubicin=red). White box indicates bounds of smaller region of interest (ROI) shown in higher resolution on the final row. Samples formalin-fixed and paraffin embedded, doxorubicin profile spectrally unmixed using Zeiss 710 Confocal Microscope. Acquired at x20 magnification.

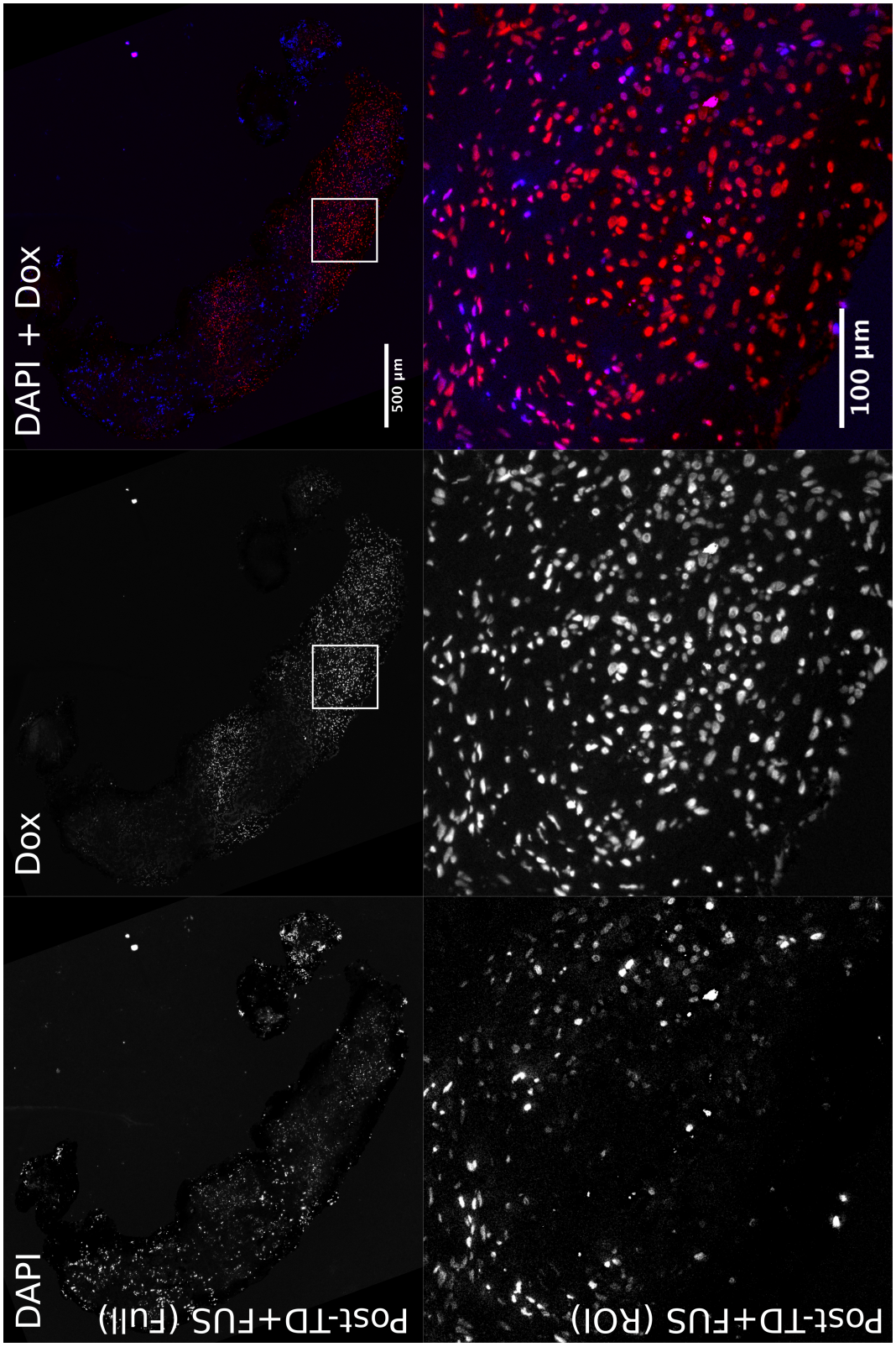


Figure 3.44: DAPI & Doxorubicin fluorescence microscopy of Post-TD+FUS (B3) sample obtained from the targeted colorectal primary liver metastasis for patient TXA105. Staining is, from left to right, DAPI, Doxorubicin and composite (DAPI=blue, Doxorubicin=red). White box indicates bounds of smaller region of interest (ROI) shown in higher resolution on the final row. Samples formalin-fixed and paraffin embedded, doxorubicin profile spectrally unmixed using Zeiss 710 Confocal Microscope. Acquired at x20 magnification.

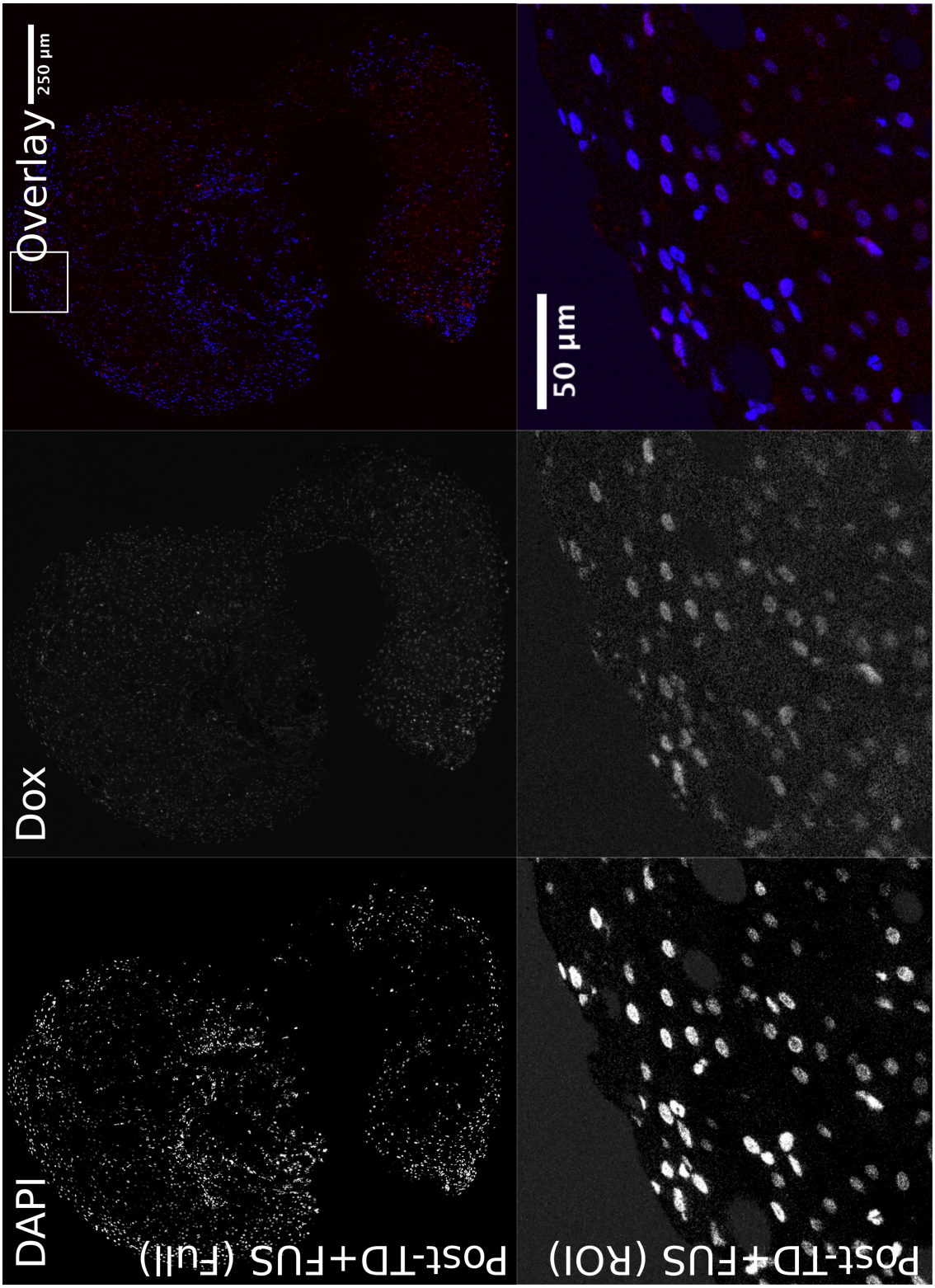


Figure 3.45: DAPI & Doxorubicin fluorescence microscopy of a Post-TD+FUS sample (B3(ii)) obtained from the targeted lung primary liver metastasis for patient TXB101. Staining is, from left to right, DAPI, Doxorubicin and composite (DAPI=blue, Doxorubicin=red). White box indicates bounds of smaller region of interest (ROI) shown in higher resolution on the final row. Samples formalin-fixed and paraffin embedded, doxorubicin profile spectrally unmixed using Zeiss 710 Confocal Microscope. Acquired at x20 magnification.

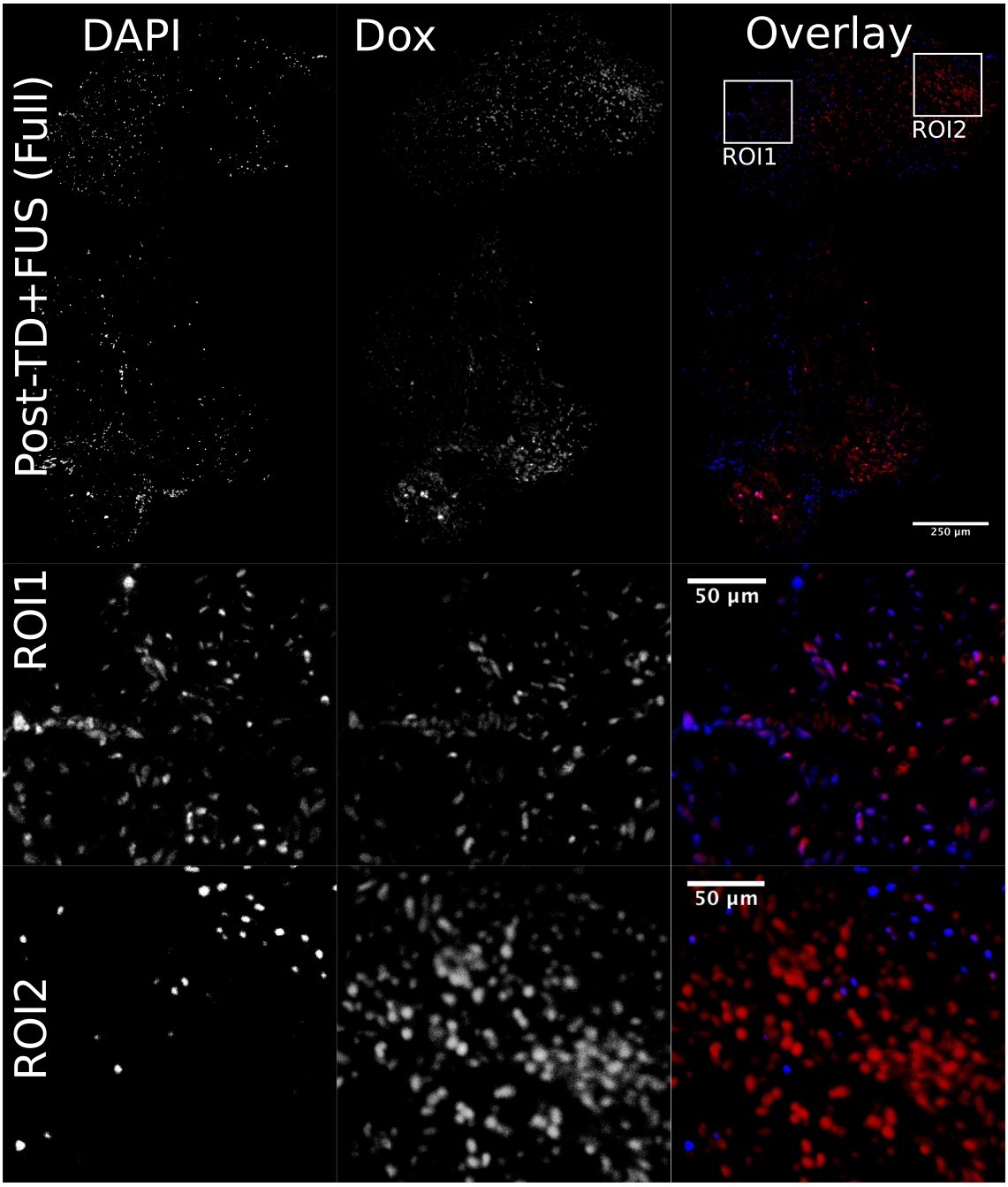


Figure 3.46: DAPI & Doxorubicin fluorescence microscopy of a Post-TD+FUS sample (B3(ii)) obtained from the targeted colorectal liver metastasis for patient TXB102. Staining is, from left to right, DAPI, Doxorubicin and composite (DAPI=blue, Doxorubicin=red). White boxes indicates bounds of smaller regions of interest (ROI) shown in higher resolution on the last two rows. ROI1 shows a moderate level of doxorubicin and nuclear co-localisation with DAPI counter-stain, whereas ROI2 shows a high level of nuclear doxorubicin which appears to out-compete DAPI. Samples formalin-fixed and paraffin embedded, doxorubicin profile spectrally unmixed using Zeiss 710 Confocal Microscope. Acquired at x20 magnification.

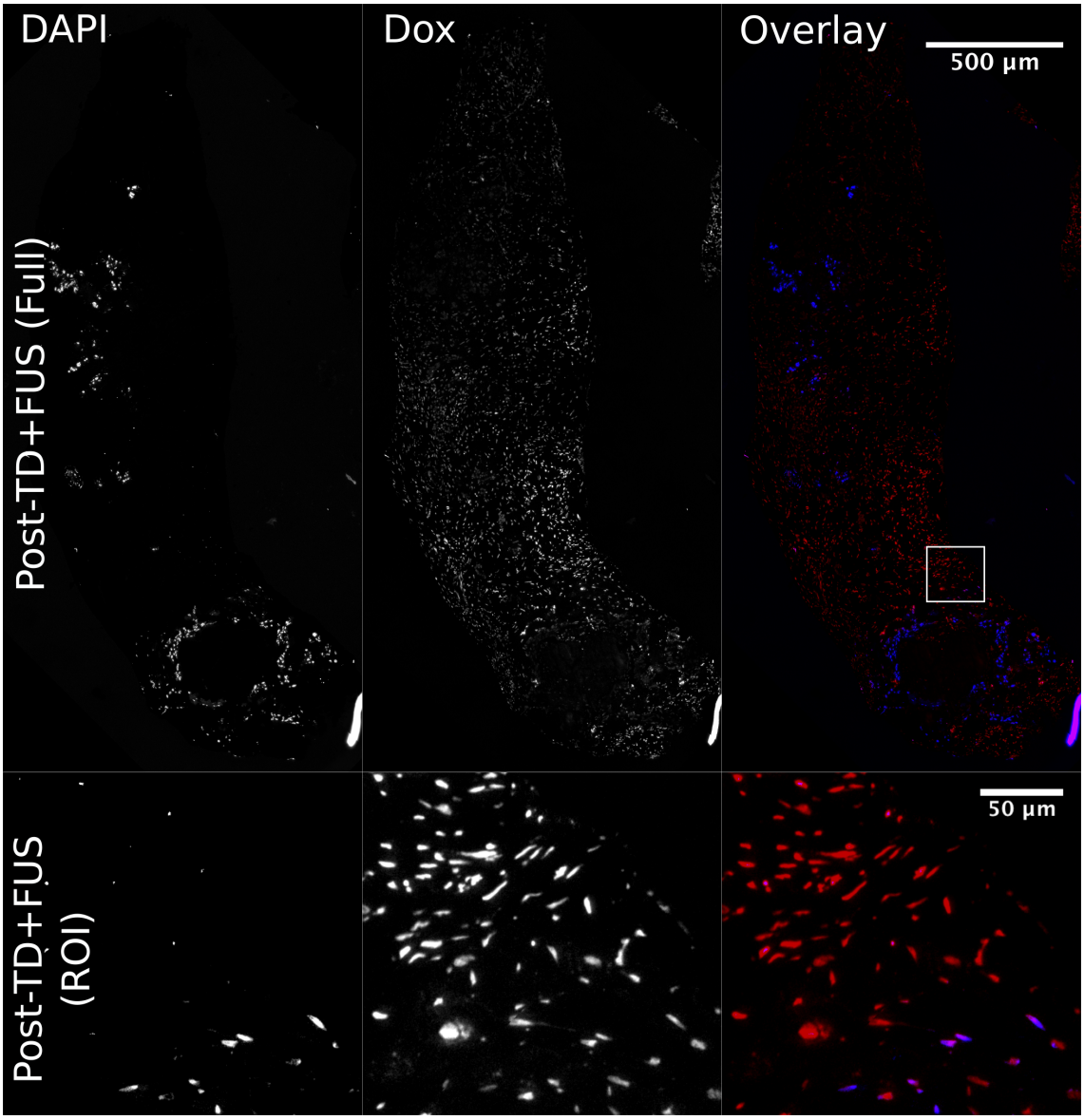


Figure 3.47: DAPI & Doxorubicin fluorescence microscopy of a Post-TD+FUS sample (B3(ii)) obtained from the targeted colorectal liver metastasis for patient TXB103. Staining is, from left to right, DAPI, Doxorubicin and composite (DAPI=blue, Doxorubicin=red). Nuclei staining positive for DAPI are sparse, again presumably due to being out-competed by high levels of doxorubicin. White box indicates bounds of smaller region of interest (ROI) shown in higher resolution on the last row, demonstrating a high level of doxorubicin and nuclear co-localisation with DAPI counter-stain in several nuclei. Samples formalin-fixed and paraffin embedded, doxorubicin profile spectrally unmixed using Zeiss 710 Confocal Microscope. Acquired at x20 magnification.

Interpretation of Fluorescence Microscopy Results

TXA104: The B1 sample demonstrates absence of doxorubicin as would be expected prior to drug infusion (Figure 3.41). The B3 sample demonstrates a background level of

doxorubicin, which is concentrated in regions of viable tumour (Figure 3.42) within this highly necrotic core (Figure 3.11). Pearson's Correlation Rank analysis reveals a strong correlation of DAPI and doxorubicin in this region (rank=0.75), evidencing the presence of nuclear-bound doxorubicin for the first time. This addresses one of the key study hypotheses (Section 1.5.3) and provides strong evidence for FUS-triggered release of LTSLs, perhaps for the first time in man. Noteably, as seen pre-clinically (Section 2.3.3), there is again competition for nuclear binding sites (DAPI weakly staining nuclei where doxorubicin concentration highest). Despite seeing only minimal levels of drug delivery by HPLC (Section 3.3.3), there was a strong radiological response in this tumour (Section 3.4). It is most likely that high levels of doxorubicin were delivered to the metabolically active tumour foci and that biopsy sampling of the necrotic core has under-estimated the concentration of intratumoral drug delivered.

TXA105: Post-delivery the nuclei of the B3 sample are strongly positive for doxorubicin (Figure 3.44) confirming ThermoDox® release and intercalation. This correlates well with both a high level of doxorubicin on HPLC (Section 3.3.3) radiological outcomes (Section 3.4).

TXB101: Nuclei are weakly positive for doxorubicin post-delivery and intercalation is clearly demonstrated in one core (Figure 3.45).

TXB102: Nuclei are strongly positive for doxorubicin in a section of one of the available cores (B3.ii) (Figure 3.46). In this tissue section, DAPI signal is weak or non-existent in many regions, making it difficult to co-localise the two, and this is thought to be due to direct competition for nuclear binding sites. In regions were doxorubicin is weaker, co-localisation in the nuclei is seen using the DAPI counter-stain. Other tissue sections of the same core (B3.ii) and the other available core (B3.i) were highly necrotic (Figure 3.11), demonstrating a high degree of micro-regional tumour heterogeneity. This is likely to explain why these samples demonstrated less impressive doxorubicin delivery (data not shown).

TXB103: Nuclei are strongly positive for doxorubicin in a section of one of the available cores (B3.ii) and reduced laser power was required to avoid saturation (Figure 3.47). Again DAPI signal is weak, presumably due to competition with doxorubicin. The other tissue core taken in this case, B3(i), demonstrates less nuclear intercalation of doxorubicin, most likely as a consequence of being more necrotic and having less viable cells and less nuclei per unit area (data not shown).

TXB104: Nuclei are strongly positive for doxorubicin in both B3 cores, again with reduced laser power (data not shown). In areas where doxorubicin is weaker, DAPI signal is stronger, supporting the idea of nuclear binding site saturation with doxorubicin.

3.4 Radiological Outcomes

Any degree of radiological response (subjective or formally assessed) was not anticipated in this proof of concept study as only a single cycle of standard dose chemotherapy is given. In addition, colorectal cancer metastases, comprising 4/7 of the treated cases, are not classically thought of as being responsive to doxorubicin in the clinical arena [494], although chemotoxic effects may be cell-line dependent [495, 496].

This expectation has been incorporated in the study design, where follow-up imaging for response is exploratory only, reflected by the tertiary endpoints (Section 3.1.3). Response was examined using three independent imaging modalities; perfusion CT and dynamic contrast enhanced MRI of the liver, and full-body ^{18}F-FDG PET-CT. Baseline scans are performed the day prior to intervention.

On the day following the intervention, a contrast MRI scan was performed, which is compared with baseline (Figures 3.48-3.55). The primary purpose of this scan is to demonstrate the absence of ablative changes due to FUS alone (Figure 1.3), as at this time point it is too early to observe effects of chemo-ablation which would manifest several days or weeks later.

Follow-up imaging for response was scheduled at 2 and 4 weeks post-intervention, at the same time as clinical review, however the protocol has the flexibility to perform the final set of imaging up to 60 days post-intervention. Radiological follow-up data is shown in Figures 3.56-3.63. Whilst CT and MRI offer data on tumour size and perfusion, PET scans provide functional information on the tumour status.

Response of the FUS-target tumour was analysed by CHOI [465], RECIST 1.1 [466] and PERCIST [497] criteria. CT and MRI scans were analysed for tumour size on axial sections, using the RECIST criteria. CT scans were analysed for contrast perfusion, using the CHOI criteria. PET-CT scans were analysed for metabolic tumour activity using Standardised Uptake Values (SUV_{max}, SUV_{peak}) and the PERCIST criteria. Although these metrics are typically used to quantify response across several tumours from systemically administered therapies, for this device-targeted drug delivery study, the FUS-target tumours were analysed independently. In addition, in the majority of cases, selected control liver tumours which were exposed to drug alone, were also available for analysis. Response in the FUS-target tumours, but not the control tumours, provides a high level of evidence of successful targeted therapy. Furthermore, the absence of ablative changes on the MRI performed on the day following intervention provides strong evidence that any response is due to chemo-ablation. A summary of these results is provided in Tables 3.16-3.18.

Patient ID	Target/Control	Baseline CT	2wk CT	4wk CT	Baseline MRI	Day 1 MRI	2wk MRI	4wk MRI	RECIST Response
TXA101	T	35	30	25	34	34	26	26	SD
TXA101	C	57,34	57,34	57,35	52,-	57,-	50,-	50,-	SD,SD
TXA102	T	74	68	-	83	86	78	76	SD
TXA102	C	22,26,12	15,-,14	-,-,-	22,36,12	21,38,15	19,36,15	20,35,16	SD,SD,SD
TXA103	T	65	59	62	70	70	74	79	SD
TXA103	C	13,27	16,23	18,29	10,22	13,22	14,25	14,25	PD,SD
TXA104	T	61	61	65	62	62	62	65	SD
TXA104	C	8	8	9	86	88	90	94	SD
TXA105	T	67	71	69	66	71	74	78	SD
TXA105	C	21,39	24,39	26,45	26,44	25,43	28,47	31,48	SD,SD
TXB101	T	34	45	44	33	34	39	41	PD
TXB102	T	88	90	86	98	98	98	95	SD
TXB102	C	33,79	40,79	38,98	42,78	43,78	44,81	52,89	SD,PD
TXB103	T	75	88	-	76	76	93	-	PD
TXB103	C	23,62	23,70	-,-	19,57	19,60	26,65	-,-	PD,SD

Table 3.16: Summary of simplified RECIST analysis and outcomes, used to assess either entire or insonated volume of target tumour for response. Measurements are longest axial dimensions of FUS-target volume (T) and selected control (C) liver tumours in mm. RECIST applied to each as if it were a RECIST target tumour. RECIST non-target lesions not analysed. Key: PR = Partial Response, SD = Stable Disease, PD = Progressive Disease. Analysis performed using Horos V2.1.0.

Patient ID	Target/Control	Baseline CT	2wk CT	4wk CT	4wk CHOI Response
TXA101	T	75	36	28	PR
TXA101	C	75,75	76,75	76,82	SD,SD
TXA102	T	70	67	-	SD
TXA102	C	87,91,40	88,84,51	-	SD,SD,PD
TXA103	T	41	37	39	SD
TXA103	C	39,63	51,60	39,65	PD,SD
TXA104	T	45	40	36	PR
TXA104	C	29	26	-	SD
TXA105	T	63	52	51	PR[a]
TXA105	C	50,40	40,29	40,-	PR,PR
TXB101	T	32	24	32	PD
TXB102	T	64	50	49	PR
TXB102	C	68,33	50,28	51,35	PR,SD
TXB103	T	47	42	-	PD
TXB103	C	66,64.7	73.2,66.6	-,-	PD,SD

Table 3.17: Summary of simplified CHOI analysis and outcomes, used to assess either entire or insonated volume of target tumour for response. In large tumours were FUS exposure was limited to sub-regions, only the FUS-exposed regions were assessed for perfusion, thus this is not a formal CHOI assessment. Measurements are Houndfield Units (HU) of FUS-target (T) and selected control (C) liver tumours. Key: PR = Partial Response, SD = Stable Disease, PD = Progressive Disease. Analysis performed using Horos V2.1.0.

[a]The ~21% decrease in the H.U. intensity in the target tumour is matched by similar decreases in the control lesions and is not isolated to the target region alone. This may be a systemic effect of the drug or may be related to variability in the technique of contrast administration (for example flow rate) or CT scanning parameters (these are standardised wherever possible as per research scan protocols).

Patient ID	Target/Control	Baseline PET SUV_{max}	2wk PET SUV_{max}	4wk PET SUV_{max}	Baseline PET SUV_{peak}	2wk PET SUV_{peak}	4wk PET SUV_{peak}	PERCIST Response
TXA101	T	4.5	3.4	3.8	3.8	3.0	3.2	SMD
TXA101	C	5.3,4.0	4.6,3.5	4.7,4.6	4.5,3.4	3.8,2.8	4.0,2.7	SMD,SMD
TXA102	T	17.8	17.8	-	14.1	14.2	-	SMD
TXA102	C	19.5,14.7,18.6	18.1,14.6,14.3	-	14.8,10.9,16.2	14.0,10.9,12.1	-	SMD,SMD
TXA103	T	20.8	30.8	29.2	17.8	22.8	24.2	PMD
TXA103	C	12.6,11.4	13.7,11.8	19.4,14.2	7.6,9.4	8.7,10.0	12.1,11.3	PMD,SMD
TXA104	T	19.9	18.9	20.6	15.0	13.6	16.4	SMD
TXA104	C	18.2,23.0	22.6,17.0	26.0,14.7	12.8,8.2	16.3,7.2	16.7,7.8	SMD,PMD
TXA105	T	14.6	15.3	17.1	11.9	12.4	13.6	SMD
TXA105	C	8.7,11.8	9.1,13.2	11.0,13.4	7.0,8.9	6.8,9.8	8.0,9.8	-
TXB101	T	9.5	19.0	15.2	7.2	13.8	11.0	PMD
TXB102	T	13.9	16.1	15.7	12.1	11.7	11.6	SMD
TXB102	C	14.5,22.5	16.2,22.4	17.1,23.7	10.8,19.0	11.9,18.8	13.2,21.8	SMD,SMD
TXB103	T	16.8	20.2	-	12.8	16.9	-	PMD
TXB103	C	26.4,20.9	25.3,23.2	-,-	20.8,14.2	21.2,16.9	-,-	SMD,SMD

Table 3.18: Summary of simplified PERCIST analysis and outcomes. Measurements are Standardised Uptake Values (SUV) of ^{18}F-FDG radioactive tracer in FUS-target (T) and selected control (C) liver tumours. Entirety of FUS-target tumour assessed for SUV in each case. Key: PMR = Partial Metabolic Response, SMD = Stable Metabolic Disease, PMD = Progressive Metabolic Disease. PET-CT analysis performed using Hermes Hybrid Viewer V2.5, Hermes Medical Solutions AB, Stockholm, Sweden.

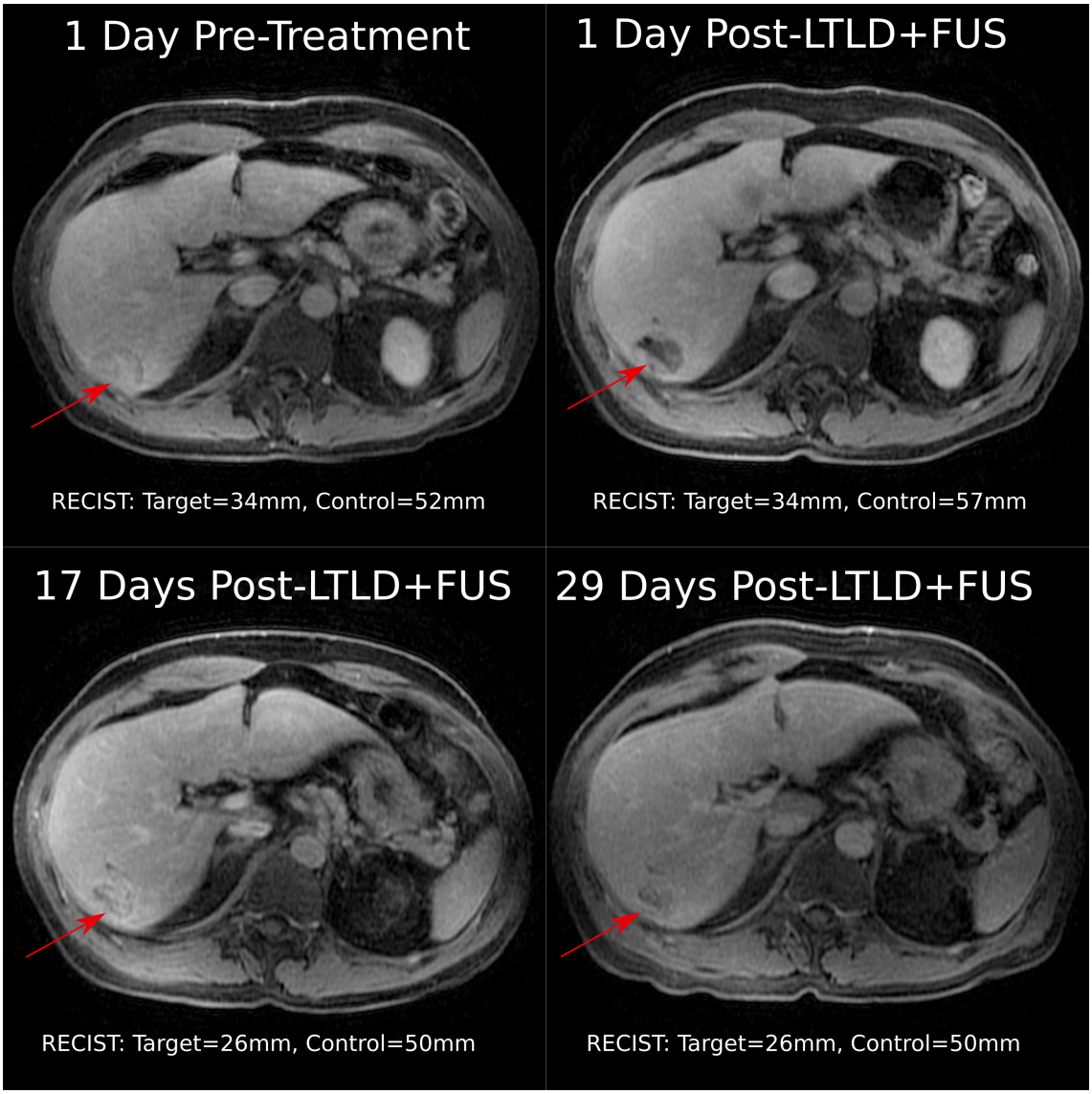


Figure 3.48: Baseline and subsequent follow-up dynamic contrast-enhanced (DCE) MRI images for TXA101, with slices aligned to the target tumour. Images obtained from the Liver Acquisition with Volume Acquisition (LAVA) sequence at matched time points following contrast administration, to allow comparison of perfusion.

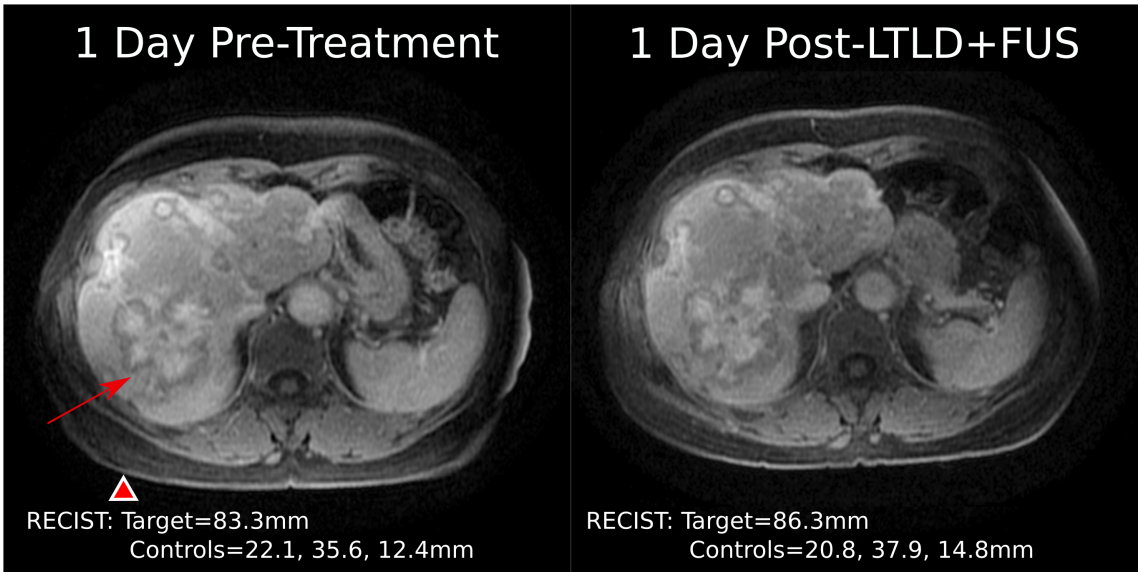


Figure 3.49: Baseline and Day 1 dynamic contrast-enhanced (DCE) MRI images for TXA102, with slices aligned to the target tumour. Images obtained from the Liver Acquisition with Volume Acquisition (LAVA) sequence at matched time points following contrast administration, to allow comparison of perfusion.

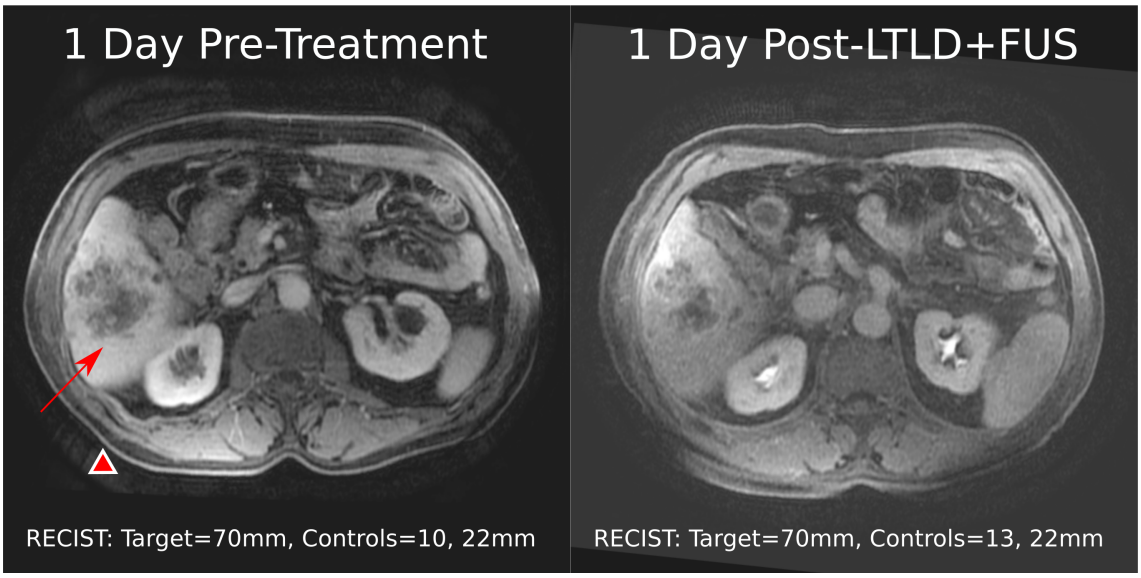


Figure 3.50: Baseline and Day 1 dynamic contrast-enhanced (DCE) MRI images for TXA103, with slices aligned to the target tumour. Images obtained from the Liver Acquisition with Volume Acquisition (LAVA) sequence at matched time points following contrast administration, to allow comparison of perfusion.

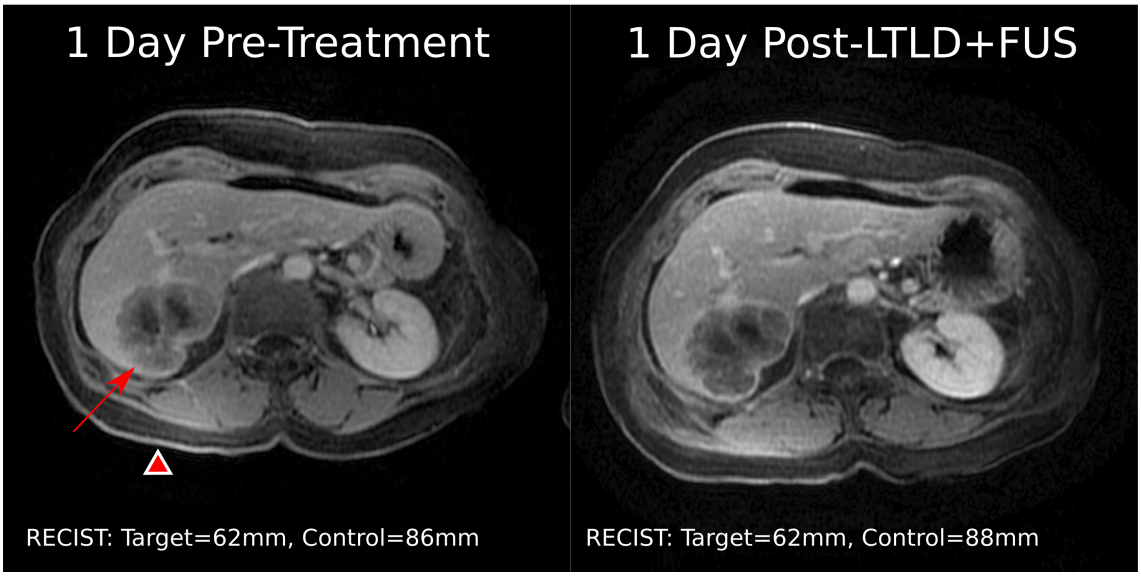


Figure 3.51: Baseline and Day 1 dynamic contrast-enhanced (DCE) MRI images for TXA104, with slices aligned to the target tumour. Images obtained from the Liver Acquisition with Volume Acquisition (LAVA) sequence at matched time points following contrast administration, to allow comparison of perfusion.

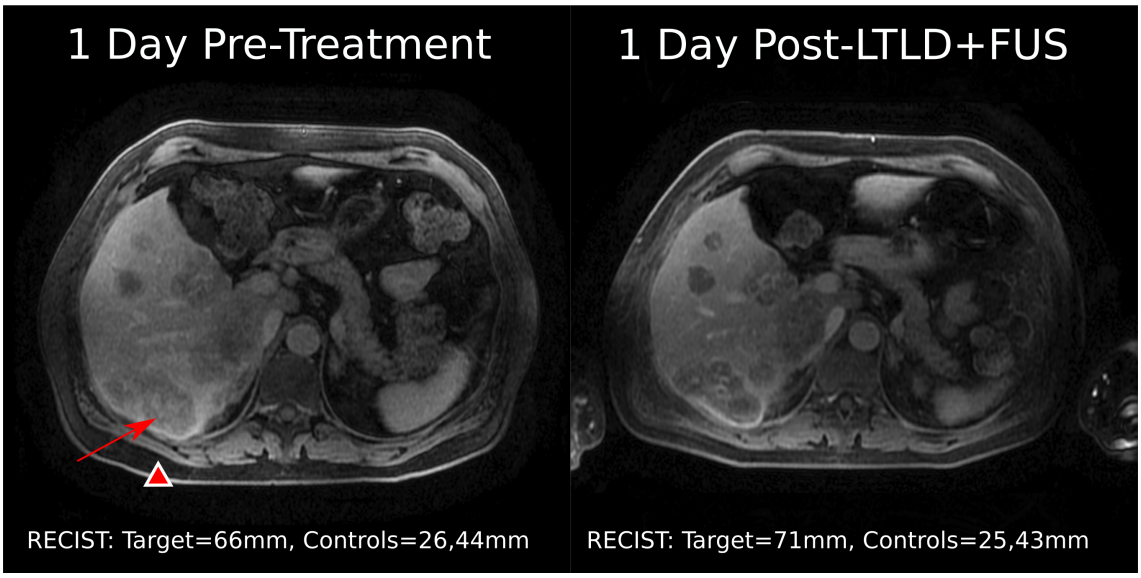


Figure 3.52: Baseline and Day 1 dynamic contrast-enhanced (DCE) MRI images for TXA105, with slices aligned to the target tumour. Images obtained from the Liver Acquisition with Volume Acquisition (LAVA) sequence at matched time points following contrast administration, to allow comparison of perfusion.

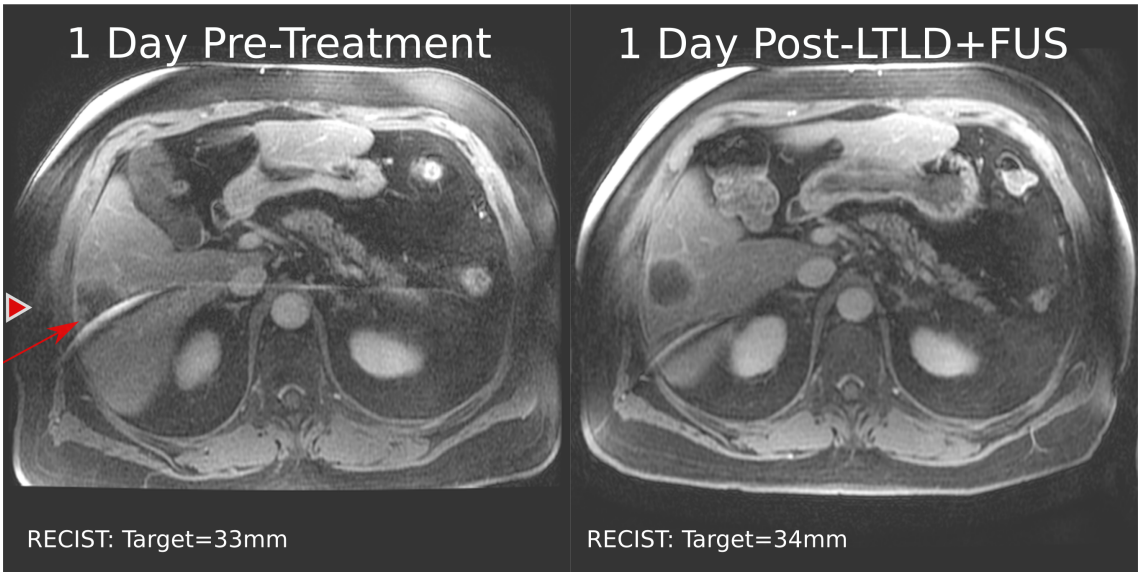


Figure 3.53: Baseline and Day 1 dynamic contrast-enhanced (DCE) MRI images for TXB101, with slices aligned to the target tumour. Images obtained from the Liver Acquisition with Volume Acquisition (LAVA) sequence at matched time points following contrast administration, to allow comparison of perfusion.

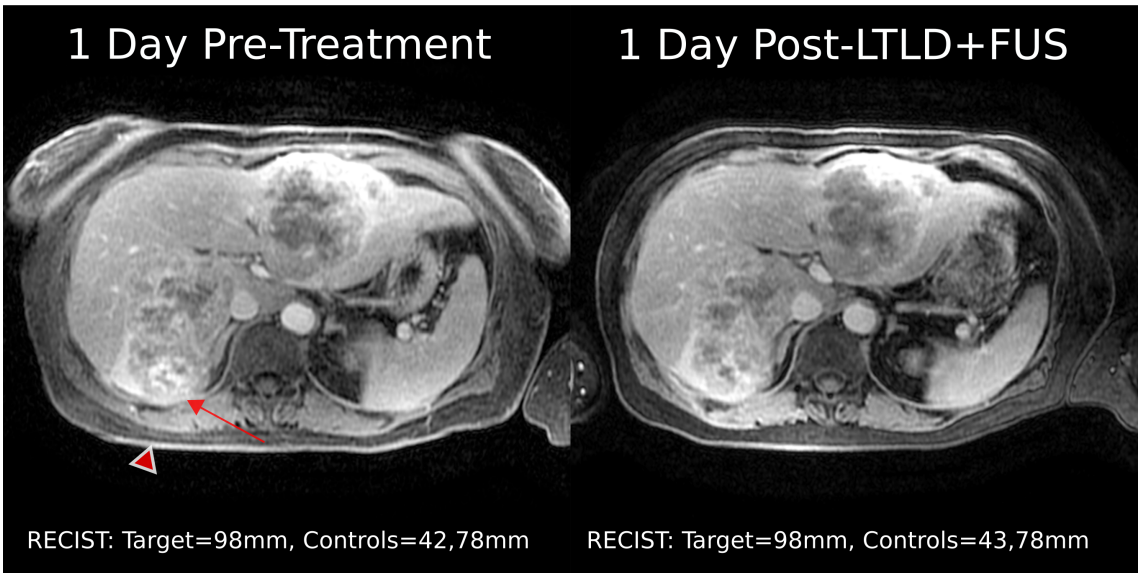


Figure 3.54: Baseline and Day 1 dynamic contrast-enhanced (DCE) MRI images for TXB102, with slices aligned to the target tumour. Images obtained from the Liver Acquisition with Volume Acquisition (LAVA) sequence at matched time points following contrast administration, to allow comparison of perfusion.

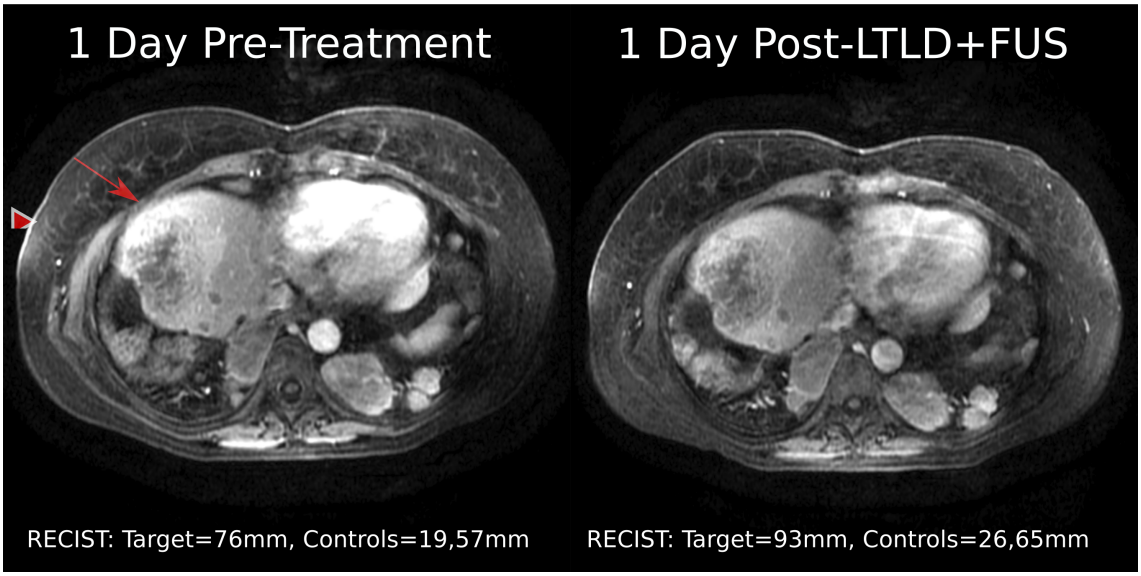


Figure 3.55: Baseline and Day 1 dynamic contrast-enhanced (DCE) MRI images for TXB103, with slices aligned to the target tumour. Images obtained from the Liver Acquisition with Volume Acquisition (LAVA) sequence at matched time points following contrast administration, to allow comparison of perfusion.

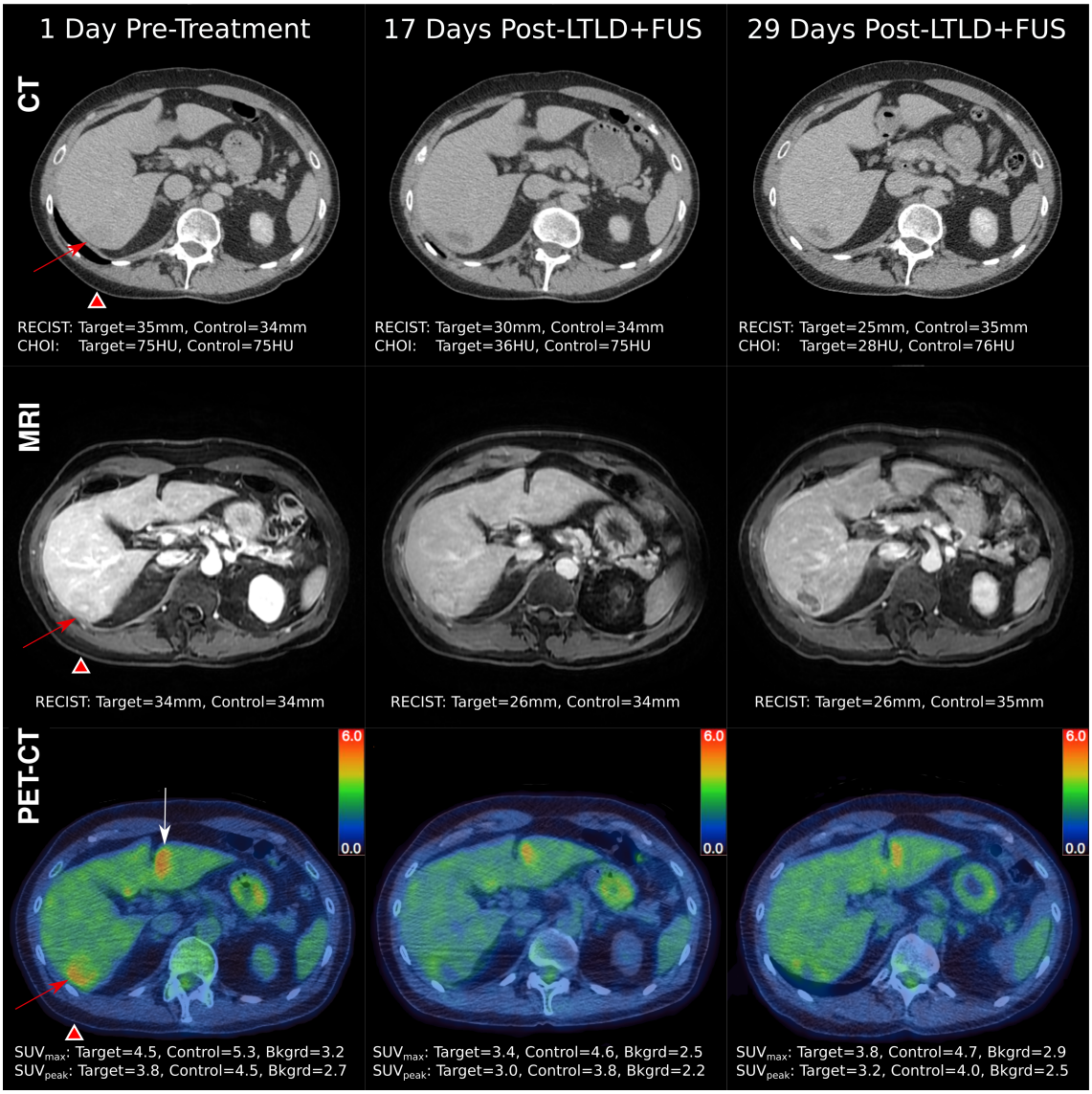


Figure 3.56: Multimodal radiological images for TXA101 in chronological order, all slices aligned to the target tumour. The red triangle indicates approximate orientation and path of FUS, the red arrow indicates the target tumour and the white arrow a control tumour present on the same slice. TOP: Perfusion CT. MIDDLE: Dynamic Contrast Enhanced MRI (LAVA sequence). BOTTOM: ^{18}F-FDG PET-CT.

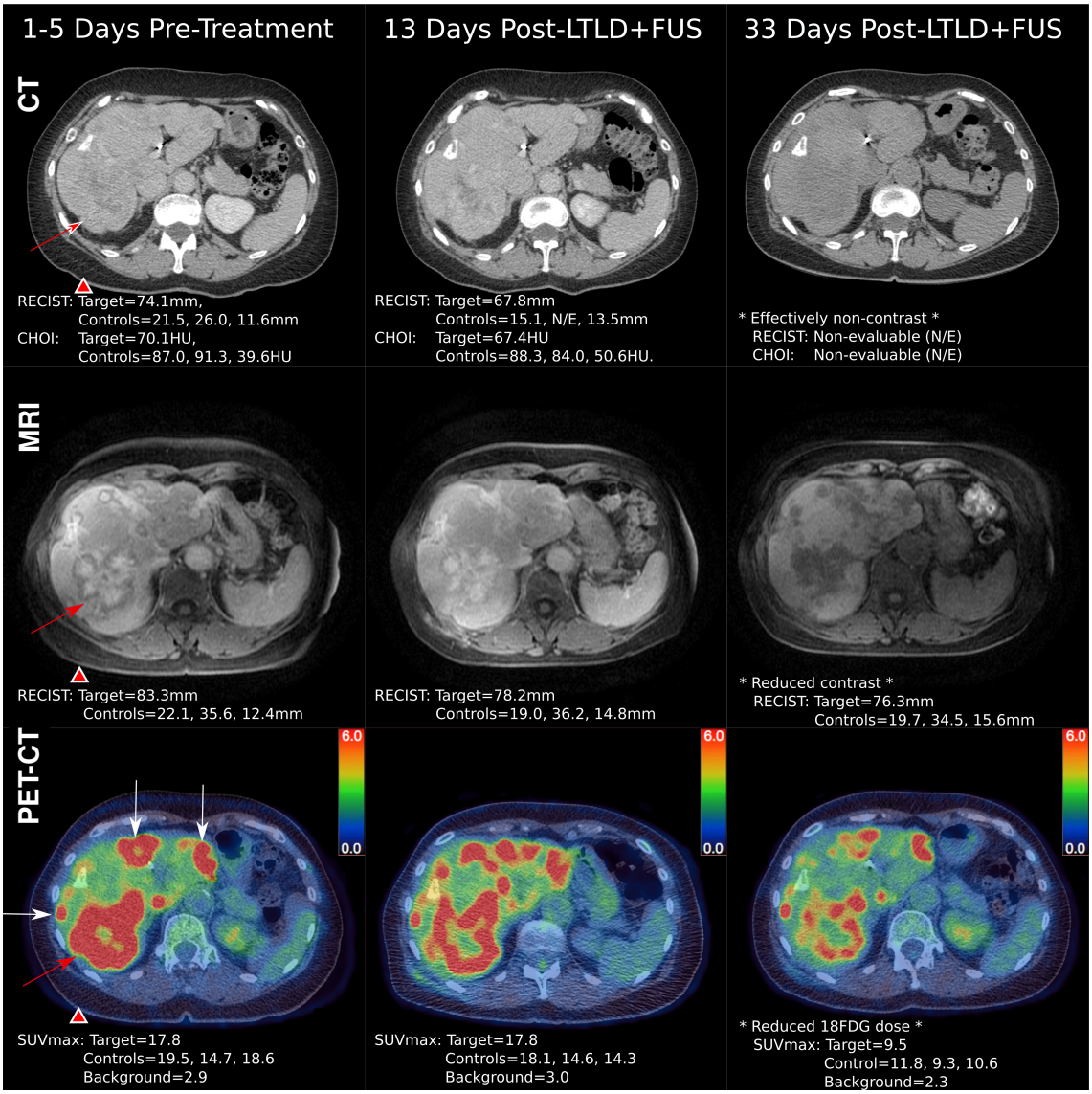


Figure 3.57: Multimodal radiological images for TXA102 in chronological order, all slices aligned to the target tumour. The red triangle indicates approximate orientation and path of FUS, the red arrow indicates the target tumour and the white arrows are control tumours present on the same slice. TOP: Perfusion CT. MIDDLE: Dynamic Contrast Enhanced MRI (LAVA sequence). BOTTOM: ^{18}F-FDG PET-CT. At the final 33 day time point, vascular access was a problem, and it is likely that some degree of extravasation of contrast and radioactive tracer meant these scans were not directly comparable to the previous study scans, and thus these scans have not been interpreted for response.

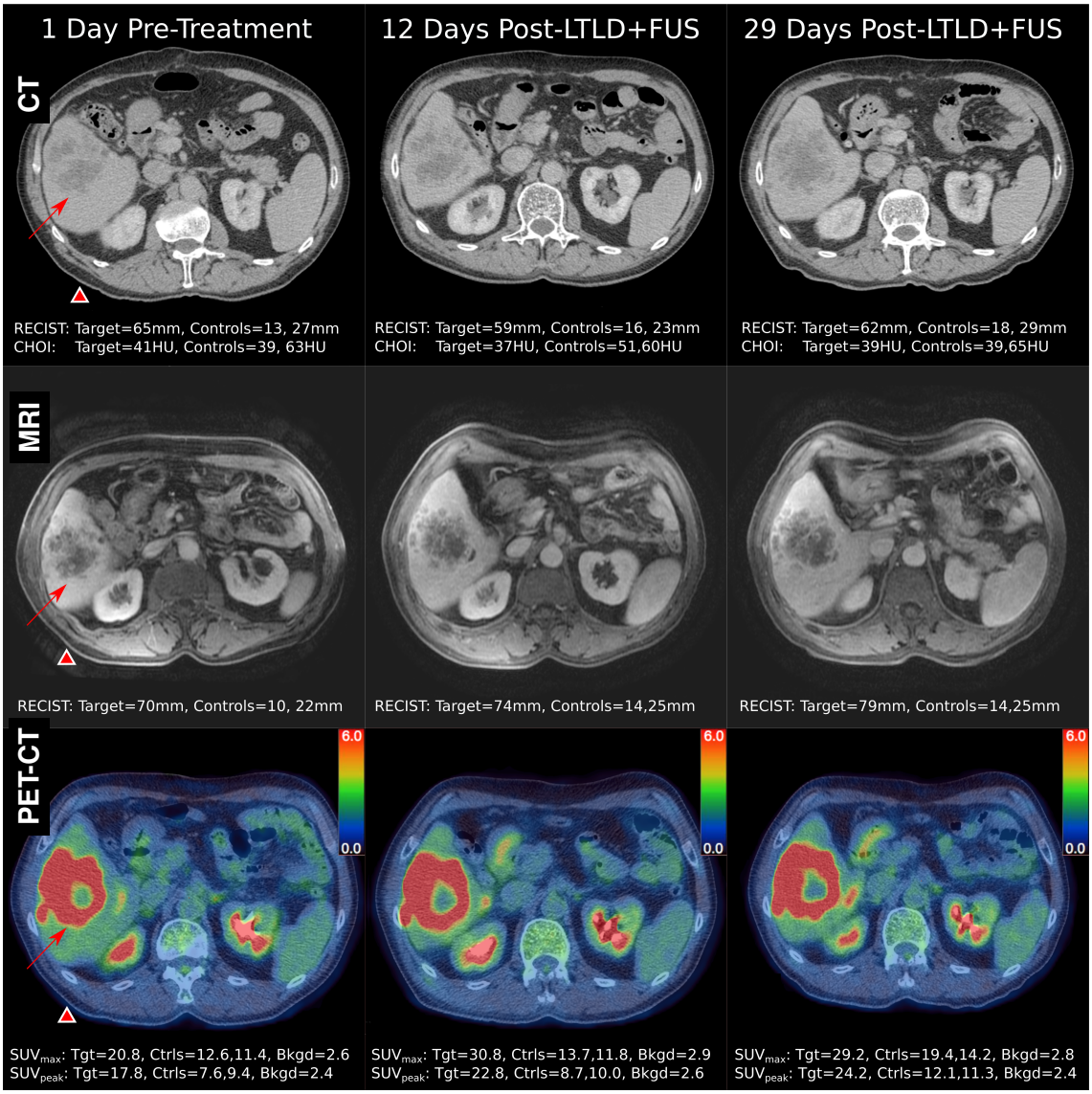


Figure 3.58: Multimodal radiological images for TXA103 in chronological order, all slices aligned to the target tumour. The red triangle indicates approximate orientation and path of FUS and the red arrow indicates the target tumour. Note that as this was a Part I patient, the co-axial needle needed to be placed at the same time as FUS treatment, thus the patient was positioned prone to enable this to happen (Figure 1.9). No control tumours were present on the same slice. TOP: Perfusion CT. MIDDLE: Dynamic Contrast Enhanced MRI (LAVA sequence). BOTTOM: ^{18}F-FDG PET-CT.

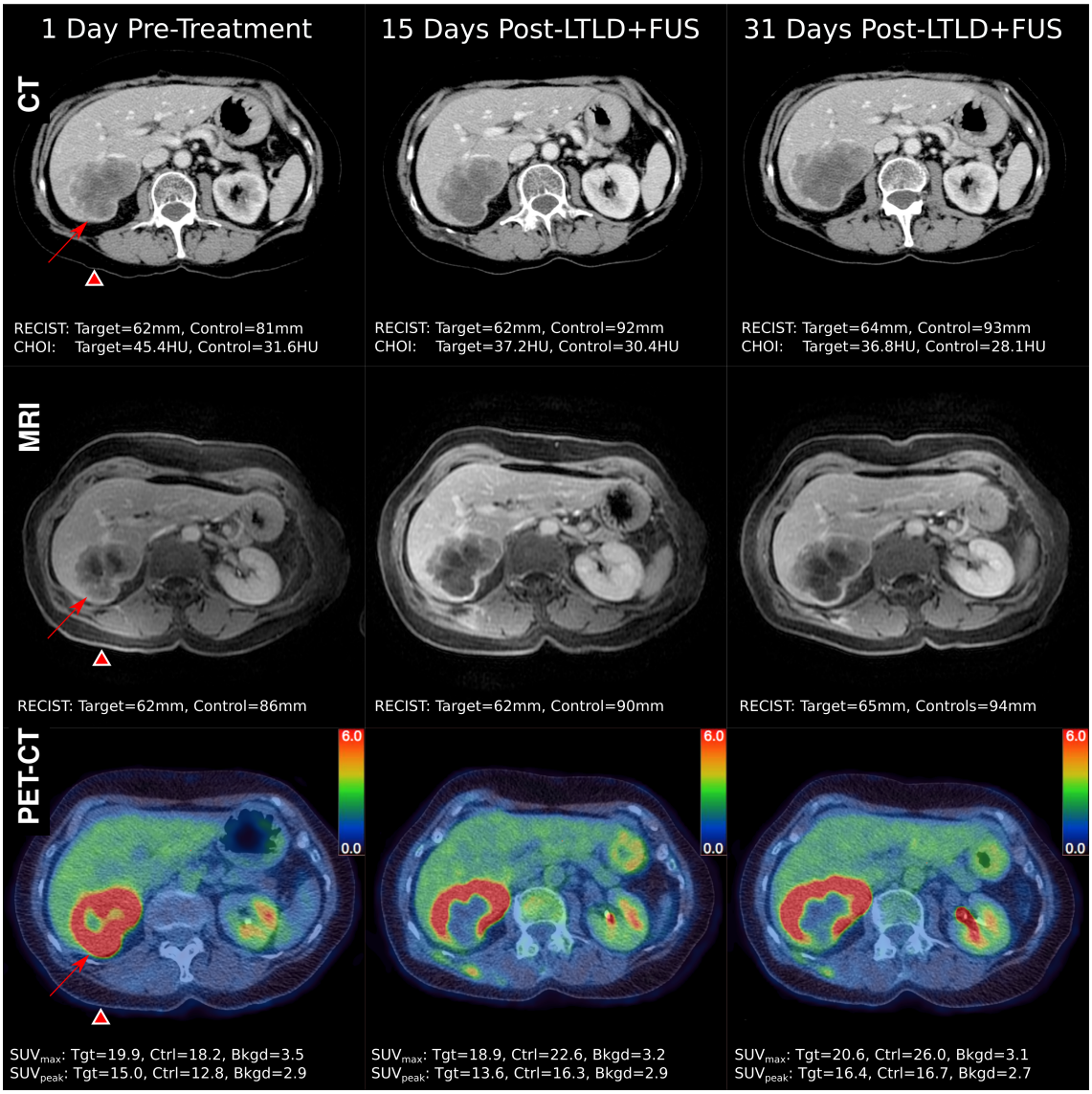


Figure 3.59: Multimodal radiological images for TXA104 in chronological order, all slices aligned to the target tumour. The red triangle indicates approximate orientation and path of FUS and the red arrow indicates the target tumour. No control tumours were present on the same slice. TOP: Perfusion CT. MIDDLE: Dynamic Contrast Enhanced MRI (fat saturation series). BOTTOM: ^{18}F-FDG PET-CT.

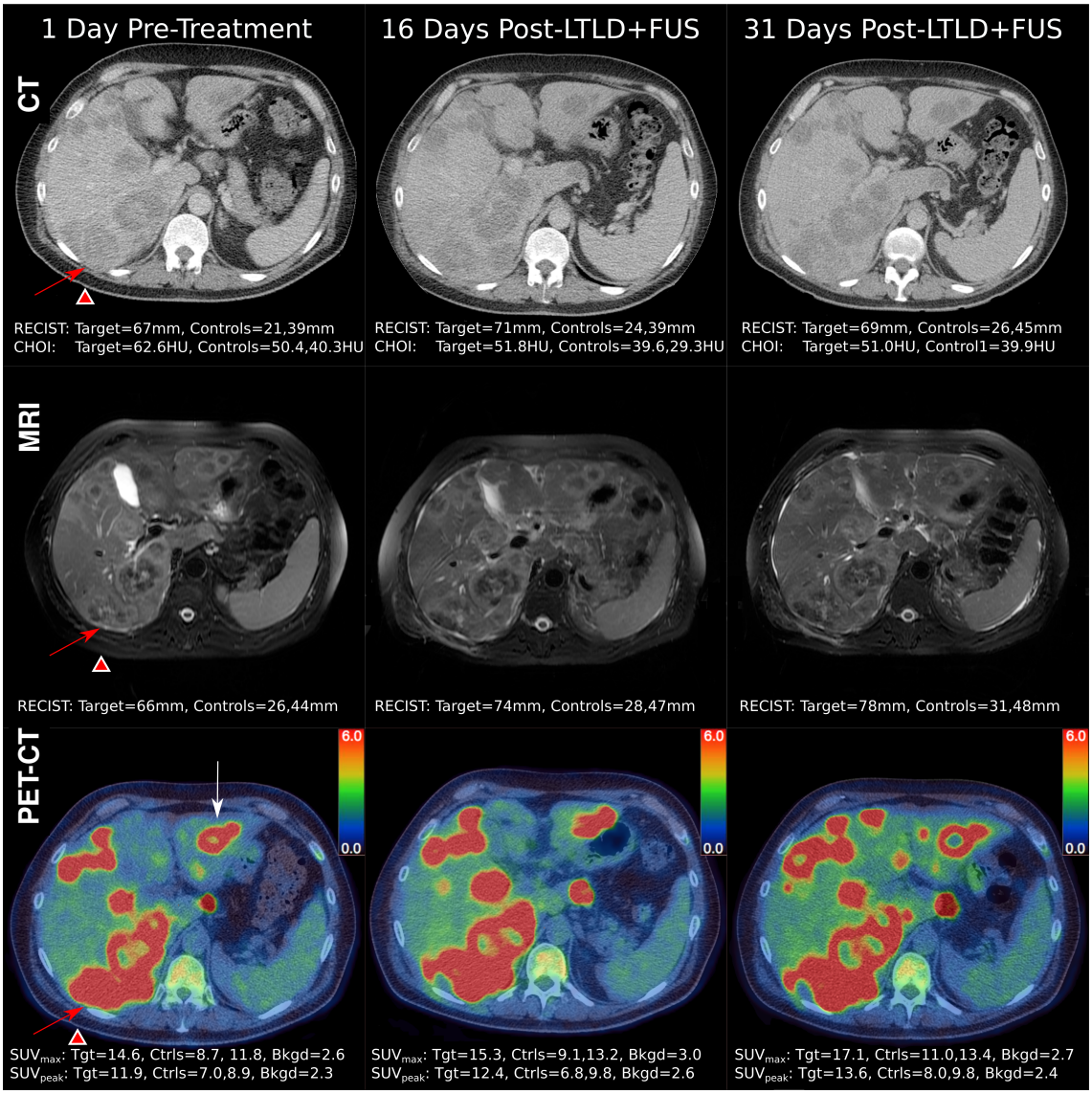


Figure 3.60: Multimodal radiological images for TXA105 in chronological order, all slices aligned to the target tumour. The red triangle indicates approximate orientation and path of FUS, the red arrow indicates the target tumour and the white arrow a control tumour present on the same slice. TOP: Perfusion CT. MIDDLE: Dynamic Contrast Enhanced MRI (fat saturation series). BOTTOM: ^{18}F-FDG PET-CT.

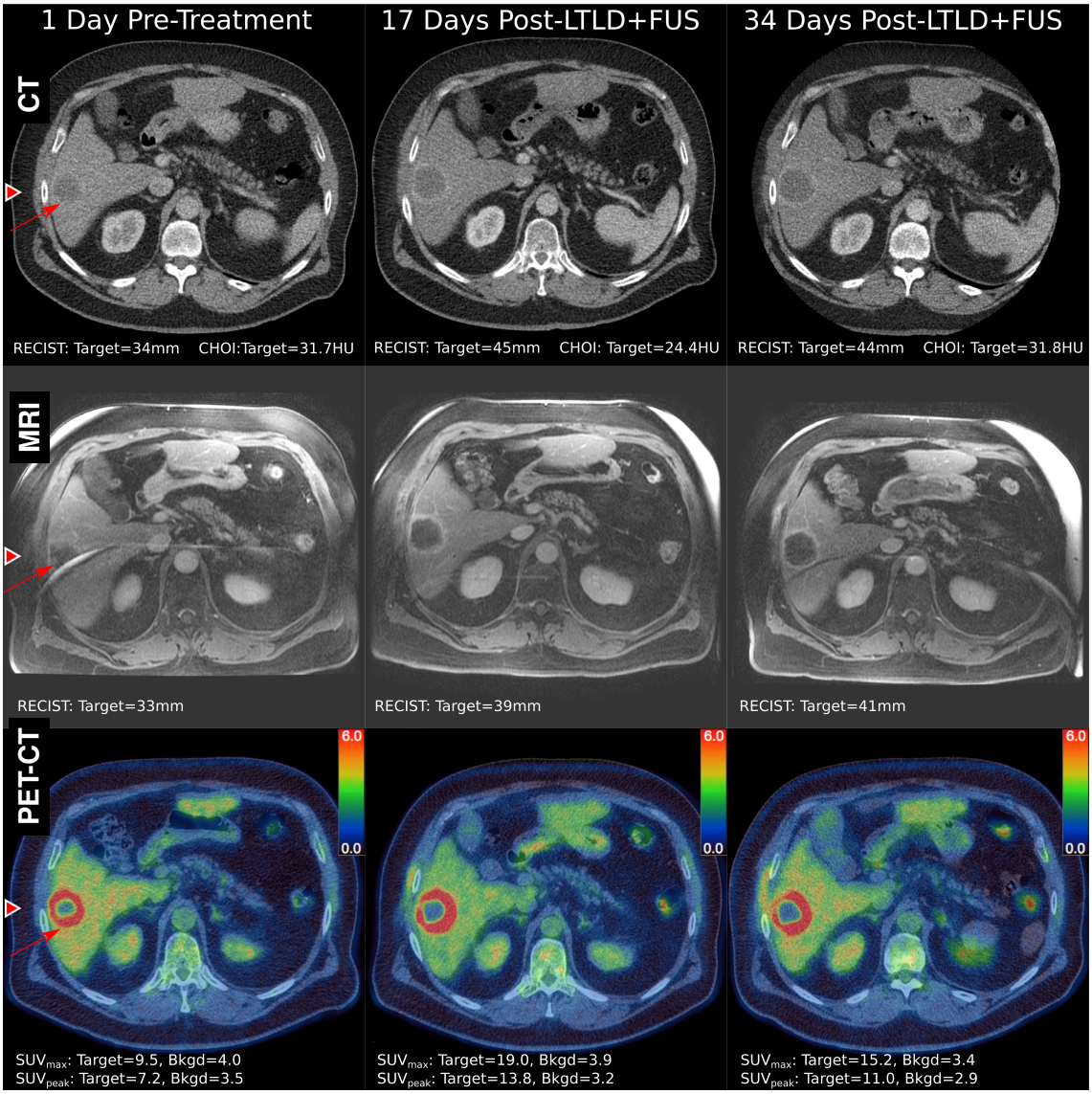


Figure 3.61: Multimodal radiological images for TXB101 in chronological order, all slices aligned to the target tumour. The red triangle indicates approximate orientation and path of FUS, the red arrow indicates the target tumour. No liver control tumours were available for comparison. TOP: Perfusion CT. MIDDLE: Dynamic Contrast Enhanced MRI (LAVA sequence). BOTTOM: ^{18}F-FDG PET-CT.

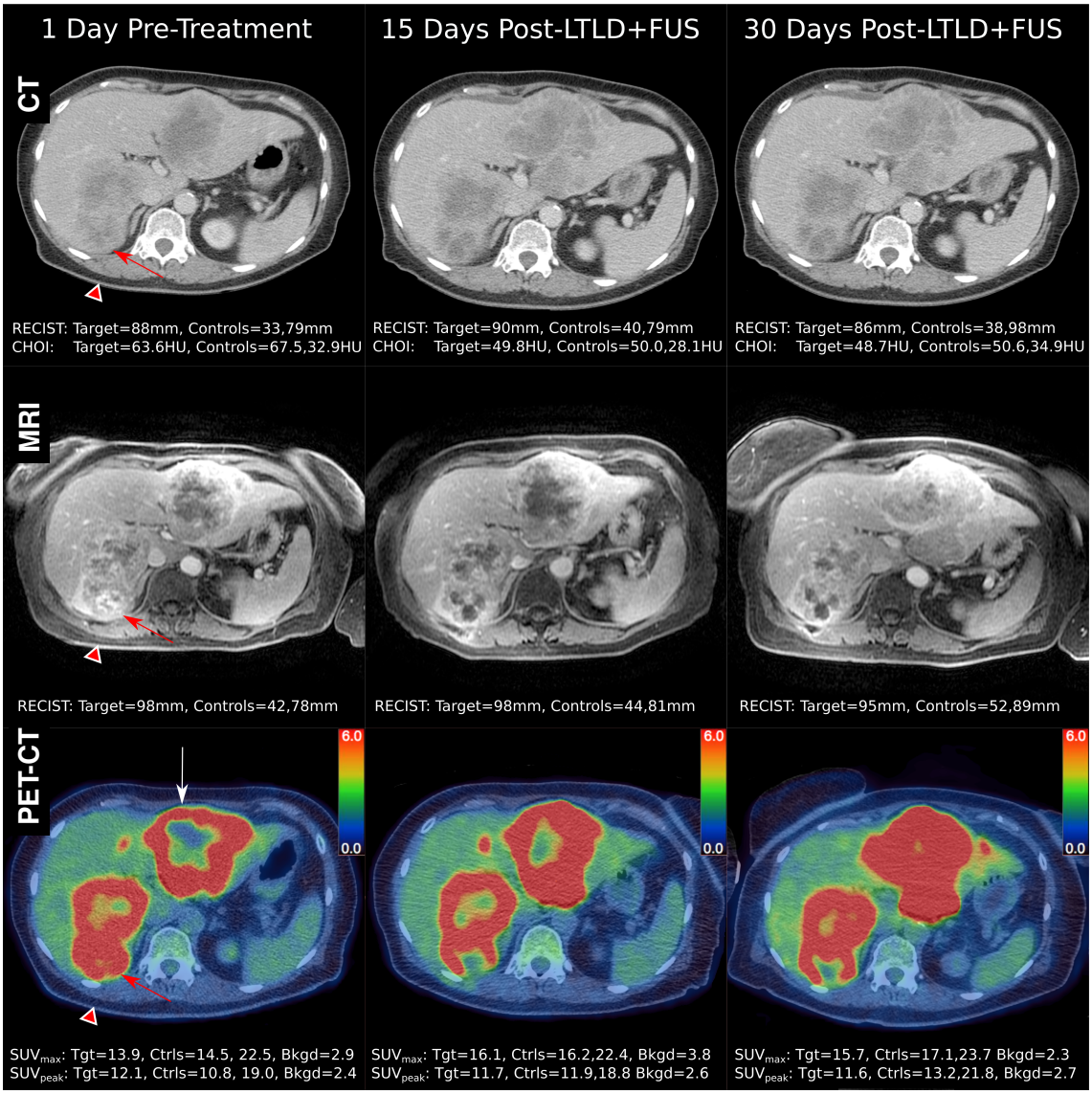


Figure 3.62: Multimodal radiological images for TXB102 in chronological order, all slices aligned to the target tumour. The red triangle indicates approximate orientation and path of FUS, the red arrow indicates the target tumour and the white arrow a control tumour present on the same slice. TOP: Perfusion CT. MIDDLE: Dynamic Contrast Enhanced MRI (LAVA sequence). BOTTOM: ^{18}F-FDG PET-CT.

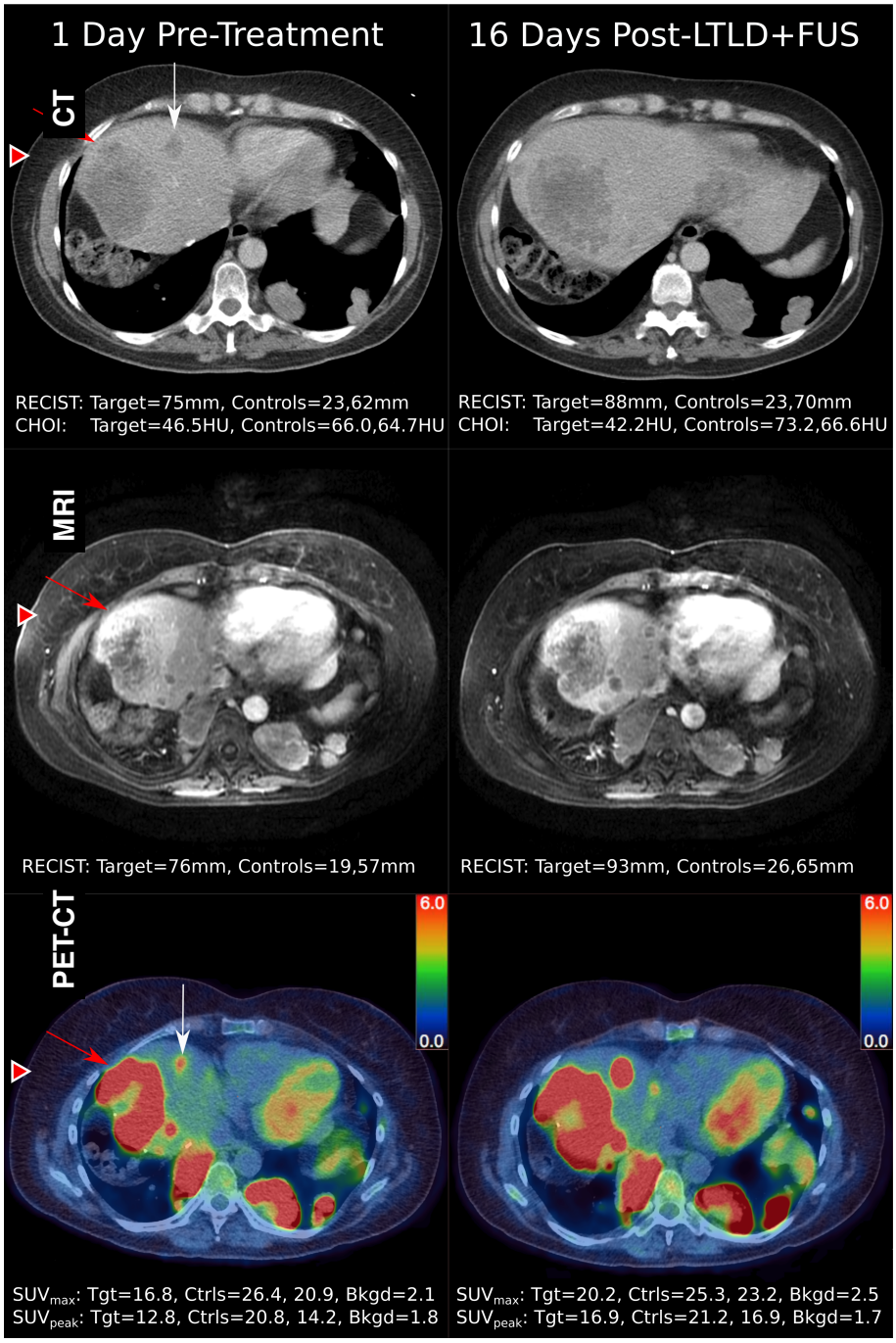


Figure 3.63: Multimodal radiological images for TXB103 in chronological order, all slices aligned to the target tumour. Patient withdrew from the study after 2 week scans due to lethargy thus 4 week scans unavailable. The red triangle indicates approximate orientation and path of FUS, the red arrow indicates the target tumour and the white arrow a control tumour present on the same slice. Note that when the patient was in right lateral decubitus position for treatment, rather than supine for imaging, the liver moved such that the lung no longer sheilded the target tumour. Note also that this patient has previously had a right hepatectomy and that lung metastases are also visible on the patient's left side (right of image). TOP: Perfusion CT. MIDDLE: Dynamic Contrast Enhanced MRI (LAVA sequence). BOTTOM: ^{18}F-FDG PET-CT.

Interpretation of Radiological Response Results

In vivo and subsequent clinical studies have shown that CE-MRI is highly predictive for the coagulated tissue volume at the time of HIFU ablation [498, 499]. The clinical use of CE-MRI in HIFU ablation of tumours is discussed in more detail in Section 1.3.2. The JC200 USgFUS device is not MRI-compatible, and so in this study it was not possible to perform CE-MRI at the same time as intervention. Thus day 1 CE-MRI scans, which are too early for chemotherapeutic response, have been incorporated in the study design. In summary, these CE-MRIs show the absence of changes which would be consistent with HIFU ablation in all cases but one (TXA101). This provides strong evidence to suggest any radiological response at the later follow up time points (typically 2- and 4-weeks) is likely to be due to therapeutic effect of targeted chemotherapy in combination with hyperthermia, rather than ablation. TXA101 is a special case as it appears that there is a decreased perfusion on day 1 following intervention (Figure 3.48). Expert radiological opinion is that what we are seeing here is a transient effect of one or more blood clot(s) which are temporarily reducing perfusion of the tumour, and not ablative change. This deduction has been made as the two week CE-MRI scan shows re-perfusion of the tumour, which is inconsistent with HIFU ablation, where perfusion effects are much longer-lived. This is further supported by interpretation of the H&E samples which do not demonstrate any evidence of ablative change, and one of which being reported has having fresh artifactual haemorrhage (Figure 3.10).

In interpretation of the radiological data for response, it must be stressed that response was not the primary objective of this clinical study design, and radiological endpoints were only exploratory in nature. There are, of course, important ethical considerations in this clinical study of targeted chemotherapy, and attempting to get the best possible radiological outcomes may not necessarily be in the best interests of the patient. These considerations are discussed in more detail in Section 4.5.

Despite the study intervention only consisting of a single cycle of ThermoDox®

several patients previously refractory or progressive on second or third line systemic chemotherapy, have demonstrated localised radiological response in the target tumours across one or more of the imaging modalities. In particular, follow-up PET scans for patients TXA101, TXA104, TXA105, TXB102 and TXB104 demonstrate unequivocal localised photopenia within the volumes of tumour exposed to FUS; an unexpected but very encouraging result for the study. In addition, one of the remaining Part II cases, TXB101, demonstrates *subjective* response in the region of FUS exposure. These regions of localised photopenia are outside of the central necrotic tumour cores, thus increased tumour necrosis due to growth of aggressive tumours during the short follow-up period can be excluded as a cause. In addition, MRI scans performed the day following treatment showed absence of changes present following thermal and mechanical ablation with HIFU (Figures 3.48-3.55), supporting delayed chemo-ablation as the primary mechanism of cell death. This is evidenced further by deepening photopenia in the four week PET scan of TXB104 relative to the two week scan (data not shown). In addition TXA101 follow-up imaging also demonstrated a subjective, and less impressive, response in the control tumours, which may be explained by systemic effects of ThermoDox® or possibly immune-mediated abscopal effects (Section 1.3) following chemo-ablation.

These regional tumour changes have not translated into an objective response as measured by PERCIST, as analysis across the entire FUS-target tumour has been performed in each case. Typically tumours targeted in this clinical study are too big to be heated by FUS in their entirety, due to limited access through the intercostal space, limitations in the heating efficiency of a single element transducer, which must be translated in space to move the focal point, and time constraints whilst under anaesthesia. Using the JC200, the practical upper limit of volume that can be effectively treated with heat in this study is around 64 cm^3, which can take 15 minutes of real-time for a single cycle when a row distance of 12 mm is used (Figure 2.25). Despite the limitation of tumour coverage volume in this study, by CHOI criteria, TXA101 and TXA104 demonstrated a partial response (PR) in the target tumour alone due to decreases in contrast enhancement of 62.7 and

18.6% in the respective FUS-target tumours. RECIST analysis failed to demonstrate any response, although there was clear 23-28% reduction in tumour size in the FUS-target tumour in patient TXA101, with no such reduction seen in the control tumours.

In patients with large target tumours, as frequently seen in this clinical study, it has been a challenge to reliably correlate areas of FUS treatment with subsequent follow-up scans. In Part I, the FUS heating was targeted around the thermistor, but having only ultrasound guidance and without co-registration technology to fuse with cross-sectional imaging, it is not possible to record precisely where the thermistor was located. This has highlighted the importance of planning and communication between the radiology team, and in particular the benefit of planning meetings to discuss the baseline cross-sectional imaging prior to the procedure. In smaller tumours (<50 cm^3) this becomes less of a problem as the entire tumour volume can typically be covered with FUS heating within the practical intervention timescales.

CHAPTER 4

Discussion, Conclusion & Future Work

4.1 Safety & Feasibility

Overall the clinical cases have demonstrated excellent safety profiles, with neutropenia (Grade IV in 4/9 patients) and delayed discharge due to confusion (Grade I in 1/9 patients) being the only SAEs, which self-resolved in all cases. There were no adverse effects related to FUS itself, which is perhaps to be expected given the much lower powers used for hyperthermia (<120 W) when compared to powers required (typically in excess of 250 W), when using the JC200 therapeutic device for ablative regimes. Procedurally, as expected, AEs were associated with the biopsy and long-lie under anaesthetic, and were all relatively benign, mild in severity and self-limiting (Section 3.2, Table 3.4).

Feasibility of inducing optimal hyperthermia in liver tumour volumes ranging from 10-72 cm^3 transcostally has been demonstrated in 4/5 of the patients in Part I of the study. Once correctly aligned, using linear mode, bulk hyperthermia in excess of 39.5°C was generally achieved within around 5 minutes, and could be sustained for periods of time well in excess of 60 minutes (Figures 3.6 & 3.7). The duration of FUS exposure given was driven by the pharmacokinetics of the drug, with an aim for around an hour of hyperthermia in all cases, where achievable within the constraints of available anaesthetic time. Hyperthermia was well controlled in all patients and did not exceed 46°C in any

patient at any time, and results which evidence the lack of FUS-mediated ablation are discussed in Section 4.2.2.

Although feasible in selected tumour anatomies, it is clear that Part I of the study is not practical nor intended for translation into routine clinical use due to fairly lengthy treatment times, often extended by difficulties in aligning two ultrasound sources to the same tumour region in the presence of ribs. Part II of the study proved to be practically much more straight-forward, and this was predominately due to the fact that there was no requirement for insertion of a co-axial needle until after the post-drug FUS exposure. This enabled the patient to be manoeuvred into optimal positions for both FUS and biopsy, and no compromise was required. This is reflected in the mean anaesthetic time of 213.8 minutes for Part II, relative to 368.6 minutes for Part I (Table 3.3). Of most importance, these shorter treatment times reduce overall anaesthetic-related risks (such as chest infection and deep vein thrombosis). In addition a shorter time under anaesthetic is more acceptable to the patient, the referring clinicians and the study team, whilst considerably cheaper with respect to booking required resources including staff.

In more routine practice outside of a Phase I study, using a therapeutic device such as the JC200, treatment times of 2-3 hours would be anticipated to induce 1 hour of hyperthermia over a tumour volumes of up to 64 cm^3 or possibly larger volumes by treatment segmentation. In reality, if and when FUS-targeted delivery becomes a routine treatment option, FUS devices of the future are likely to offer defocused heating to more rapidly induce hyperthermia in treatment volumes, reducing treatment times further. Potentially the use of therapeutic devices with incorporated respiratory gating may remove the need for a general anaesthetic in liver targeting, whilst other organs, such as the brain and breast, which are not affected by respiratory motion could be performed without a GA.

4.2 Summary of Clinical Results

4.2.1 Case Summary

Due to technical limitations consequent on the requirement for thermometry device insertion, the first five Part I cases discussed (TXA101-105) were all performed with the patient in supine or near-supine position, over the water bath. Whilst technically challenging in their own right, these early cases were essential to obtain the thermometry data which allowed progression to Part II of the study.

TXA101 was a successful first case which utilised dot mode heating for a relatively small prescribed volume of 10.5 cm^3 (Figure 3.3). In addition to demonstrating feasibility of Part I, the case demonstrated both increased drug delivery and radiological response. The criteria for the primary endpoint were met with a 2.1-fold increase in doxorubicin dose delivered (Figure 3.36). It was extremely encouraging to see a radiological response, namely CHOI PR and new PET photopenia, in the target tumour alone (Figure 3.56), given the single cycle of chemotherapy administered for this patient with primary HCC. Fluorescence microscopy data is lacking for reasons previously discussed.

For case **TXA102**, an initial period of dot mode was used to attempt to heat a larger estimated volume of 25 cm^3. It became apparent that it was much more challenging to maintain adequate hyperthermia over this larger volume using dot mode clinically than pre-clinically, presumably in large part due to the presence of perfusion. Consequently, whilst ThermoDox® was still in circulation, free-hand linear mode was explored for the first time clinically in a small volume around the thermistor tip (Figure 3.4). Although hyperthermia ultimately proved to be optimal in the localised region around the tip, the final biopsy (B3) was found to be mainly blood clot on H&E (Figure 3.10), resulting in the exclusion of the case from the interim analysis of the primary endpoint. Furthermore, interpretation of radiological outcomes is not possible due to variation in the flow rates and/or volumes of administered contrast (CT, MRI) and radio-active tracer (PET) given

in follow-up scans due to IV access issues.

TXA103 was the first case to use solely linear mode for post-drug coverage of a much larger 73.2 cm^3 target volume, and this heating mode was used going forward for subsequent cases. Row distances of both 12 and 8 mm were attempted, taking ~25 and 40 minutes respectively, the latter resulting in more tightly spaced rows in an attempt to trap more heat (Figure 3.5). However the case was unfortunately subject to several technical difficulties on the day, including gas in the FUS field. The difficulties resulted in sub-optimal heating, and as such the case has been excluded from interim analysis of the primary endpoint. As might be expected in this case, there was no clear radiological response (Figure 3.58).

TXA104 thermometry demonstrates well-controlled hyperthermia over a similarly large volume of 73.4 cm^3, sustained for over an hour. A complete cycle took around 25 minutes to complete with 12 mm row distance - the same time it took to complete a cycle of 10.5 cm^3 in dot mode with an 8 mm row distance (Figure 3.6). Following optimal hyperthermia over this large tumour volume, there was some misfortune in that Unreleased biopsy (B2) obtained from the centrally-placed co-axial needle was deemed to be predominately blood clot, as seen on H&E (Figure 3.13). Furthermore microscopy revealed that the Released biopsy core (B3) was sampled from a highly necrotic tumour region. It is likely that the counterpart half of the same B3 biopsy used for HPLC was also highly necrotic. As necrotic tumour is predominately cellular debris and has a sparsity of viable cells and microvasculature, estimating average intratumoral doxorubicin concentration from a small 1-2 mg sample of a larger heated region is likely to represent a significant under-estimate, especially in the knowledge that the heated region was largely metabolically active (Figure 3.59). Despite this limitation, for the first time clinically, spectral unmixing fluorescence microscopy was able to demonstrate nuclear doxorubicin in a small region of viable cells, evidencing FUS-mediated release of LTSLs (Figure 3.42). Regardless, this case has been excluded from interim analysis of the primary endpoint, given B2 is blood clot. This case highlights the difficulties related to point sampling of a

heterogenous tumour with micro-regional variation which are discussed below (Section 4.3.2).

TXA104 demonstrates a clear localised radiological response on PET (Figure 3.59), a promising outcome given that colorectal metastases are not generally responsive to liposomal doxorubicin in the clinic [494]. With regards to the PET response, the maximal response can be observed posteriorly, i.e. closest to the skin and the FUS source. As one might expect, and as validated in pre-clinical work (Section 2.2) and in the case of TXA101 thermometry (Figure 3.2.4), the core of a FUS-exposed treatment volume remains hottest and the temperature falls off by several degrees in the periphery. This may explain the lack of PET response in the anterior border, furthest from the transducer, of the FUS-exposed tumour. It is certainly possible that slightly higher output powers or DC may have pushed peripheral temperatures sufficiently high as to result in an even larger region of PET response. In addition, for deep parts of the tumour, attenuation may play a part in further derating pressures, reducing in situ pressures and thus thermal conversion (Section 3.2.3). Furthermore, aside from the purely thermal mechanism it has been considered that inertial cavitation may play a role in FUS-mediated drug delivery (Section 3.2.2). It is conceivable that derated peak pressures at depth come below the inertial cavitation threshold, resulting in decreased drug delivery, whilst the closer tumour borders benefit from cavitation mediated delivery at higher pressures. Finally, the lack of response in the lateral aspects of the tumour is most likely explained by a combination of two factors: the cooler peripheries of the tumour and a rib-blocking effect either side of the acoustic window for FUS. Although further optimisation of FUS coverage strategies may lead to improved radiological responses, one must be mindful that the primary rationale for this initial study is to demonstrate enhanced doxorubicin delivery in a target volume, not curative outcomes. The ethical considerations here are discussed further in Section 4.5.

TXA105 demonstrated that when splitting a larger treatment volume of 90.9 cm^3 across two rib spaces, heating was inefficient due to redundant transducer travel time back

and forth over the rib. However, excellent control of hyperthermia was again demonstrated over a smaller volume of 63.8 cm^3 through a single rib space containing the thermocouple (Figure 3.7). Optimal heating resulted in both a 5.2-fold increase in total doxorubicin delivery by HPLC (Figure 3.40) and a localised PET response for this colorectal tumour (Figure 3.60). Again, notably the PET response is demonstrated on the posterior tumour border, closest to the transducer. In addition, the B3 biopsy core was of viable tumour and demonstrated wide-spread doxorubicin DNA intercalation across the biopsy sample at levels high enough to suppress the degree of DAPI counter-staining (Figure 3.44).

Due to having ethics to take a single biopsy at each time point, Part I has suffered somewhat from inadequate biopsy samples (highly-necrotic or haemorrhagic tissue) in a small number of instances. Part II of the study design serves to mitigate this risk by having ethics to take two biopsy cores for the single post-drug delivery (B3) time point, each divided in two for both HPLC and microscopy analysis. By design, this introduces a level of redundancy in case of an inadequate samples or failed HPLC run.

TXB101 was the first Part II case and, with the patient in right lateral decubitus, a 40.7 cm^3 volume was exposed to FUS over three consecutive cycles, taking 18 minutes each (Table 3.8). Microscopic analysis revealed a low level of doxorubicin intercalation in biopsy B3(ii) (Figure 3.45), relative to that previously seen in Part I. Biopsies were intentionally sampled in the metabolically active tumour periphery, away from the necrotic core, by correlation with PET (Figure 4.2). HPLC analysis of B3(i) revealed a moderate intratumoral drug concentration of 6.65 μg/g. Radiological analysis revealed a subjectively larger and more photopenic zone of central tumour necrosis (Figure 3.61), but it is difficult to discern if this is due to natural tumour progression or response. Considering the results for this case as a whole, the lack of substantial radiological response is perhaps more likely to be as a consequence of delivering a drug concentration below that of the therapeutic threshold, rather than resistance of the tumour to doxorubicin. This may have been due in part to the thickness of the subcutaneous fat layer in this particular

patient, which was approximately 5 cm. In the kidney, surrounding perinephric fat has been shown to have an defocusing effect [153]. It is possible that a similar effect occurs through subcutaneous tissues in patients with high BMI, reducing the heating efficiency at the focus. The difficulties faced in maintaining core body temperature in this patient may also have contributed to reducing the delivered dose. Unfortunately in the absence of real-time thermometry for this case, it is not possible to make further deductions. Of note this patient would not have been suitable for Part I given the technical difficulty in triangulating the tumour from two different ultrasound sources. The power settings used for all Part II cases are discussed in Section 3.2.5.

TXB102 proceeded with the patient at 30° tilt from supine, and a larger volume of 49.9 cm^3 was exposed to FUS, again over three consecutive cycles of 20 minutes each (Table 3.8). HPLC analysis revealed a moderate intratumoral drug concentration of 6.84 μg/g in a section of the first core (B3(i)), whilst nuclear doxorubicin was clearly distinguishable in a section from the second core (B3(ii)) (Figure 3.46), which is thus likely to contain higher concentrations. PET demonstrates a localised response in the centre of the region which was exposed to FUS (Figure 3.61). This is the first Part II case to evidence both high levels of doxorubicin intercalation and unequivocal radiological response, in this target colorectal liver metastasis. In particular it confirms that these outcomes are possible without the pre-delivery FUS exposure or the thermometry device required for Part I, and indeed completely non-invasively.

TXB103 proceeded with the patient in right lateral decubitus, and a tumour volume of 30.7 cm^3 was treated with FUS over five consecutive cycles of 12 minutes each (Table 3.8). Microscopic analysis revealed the first core (B3(i)) was moderately necrotic (Figure 3.17) but contained some nuclear doxorubicin (data not shown). The second core (B3(ii)) revealed more viable cells, which demonstrated a strong nuclear doxorubicin signal throughout (Figure 3.47). Accurately co-localising the region for biopsy and the heated region within this very large target tumour was crucially important and careful communication between the radiologist performing the biopsy and study team, with joint

reference to cross sectional imaging, was key to success. Despite clear evidence of release of bioavailable doxorubicin in the tumour, no clear PET response was seen in the target region of the colorectal liver metastasis at two weeks (Figure 3.63), which could possibly be explained by either delivery of sub-therapeutic levels or drug resistance.

TXB104 again proceeded with the patient in right lateral decubitus, and a tumour volume of 53.9 cm^3 was treated with FUS over three consecutive cycles of 22 minutes each (Table 3.8). Microscopy demonstrates strong nuclear doxorubicin and the PET scan shows an unequivocal localised response in the target FUS-tumour alone (data not shown).

At the time of writing, HPLC analysis had not been performed for samples obtained for patients TXB103 or TXB104.

4.2.2 Evidencing Non-Ablative Regimes

Part I patients have demonstrated CEM_{43} thresholds ranging from 35 seconds to 14 minutes 12 seconds (Section 3.2.1), well below the thresholds where ablative changes would be expected, and below the cut off of 60 minutes incorporated into the definition of optimal hyperthermia (Section 3.2.4). In addition, it is important to note that echogenic (grayscale) changes which would be considered to represent ablative changes (Section 1.4.7) were not seen at any stage during the FUS exposures for any of the interventions.

Furthermore, microscopy studies of the Released biopsy samples have shown persistence of similar levels of CK8 cell viability stain (Section 3.2.6) whilst demonstrating nuclear doxorubicin (Section 3.3.4). This is true for patients TXA104, TXA105, TXB101, TXB102, TXB103 and TXB104 where heating was deemed optimal by either thermometry or prediction. Whilst persistence of CK8 stain as a marker of cell viability post-FUS has not be rigorously validated by this study (Section 2.4.2), its utility has been published in several clinical studies across a variety of tissue types and ablative modalities including HIFU (Section 1.3.3).

The final level of evidence for the absence of FUS-mediated ablative changes comes from the contrast MRI scan performed the day following intervention. The original intention of this early scan was two-fold, firstly to perform MR-spectroscopy in an attempt to identify doxorubicin in the liver tumour, and secondly, to demonstrate the absence of changes, such as loss of enhancement, which would be expected in HIFU-ablation (Section 1.3.3). As MR-spectroscopy sequences have not yet become available clinically, the scan can be used solely for the latter purpose. MRI scans performed the day following treatment showed no evidence of ablation, as discussed in Section 3.4.

4.2.3 Interim Analysis of Primary Endpoint

For the five Part I patients treated to date, the four with evaluable Unreleased samples (excluding TXA104) have an average concentration of intratumoral doxorubicin of 2.48 μg/g tissue ± 1.26 SD (Table 3.14). This value may be subject to change if further patients are recruited to Part I. Of the Part I patients, three were excluded from evaluation of the primary endpoint for reasons previously discussed (3.3.3). The remaining two Part I cases, both receiving optimal hyperthermia, met the primary endpoint, demonstrating an enhanced intratumoral delivery of between 2.1-5.2 fold relative to the concentration prior to FUS delivery, with an average post-delivery intratumoral doxorubicin of 8.41 μg/g ± 4.37 SD.

Part II cases analysed to date (TXB101 and TXB102) were both evaluable for HPLC and the average intratumoral doxorubicin across all evaluable Released samples from both Parts I and II was 7.58 μg/g ± 2.70 SD (n=4). For Part II cases, it is not possible to attempt analysis of the primary endpoint until the end of the study, when all Part I cases have been completed, as the average Unreleased concentration from Part I is used as the comparator, in the absence of these biopsy samples in Part II. The primary endpoint of the study requires at least a two fold increase in intratumoral drug concentration following FUS (or Released concentration >10μg/g) in at least 50% of all treated patients in which hyperthermia has been attempted (monitored in Part I, predicted in Part II). The Released

samples in Part II both demonstrate a greater than two-fold increase from the current comparator value, with an average concentration of 6.75 μg/g ± 0.13 SD. Thus, overall, 100% (4/4) of the patients included in this interim analysis currently satisfy criteria for the primary endpoint, based on current averages.

Overall, due to potential issues with obtaining tissue cores inadequate for analysis or failed HPLC run, in retrospect, a more considered primary endpoint for this study might have been satisfied by *either* increased intratumoral doxorubicin concentration, *or*, unequivocal PET radiological response localised to the FUS exposed region alone.

4.3 Key Study Challenges

It has been a privilege to lead this early phase clinical trial from concept through treatment and to clinical data collection. This has only been possible due to numerous excellent existing or on-going pre-clinical research programmes involving the use of LTSLs and FUS in general, and the long-continued research efforts leading to the availability of clinically-approved FUS devices, such as the JC200. The world-class research facilities at Oxford and the continued support of my supervising Professors have facilitated this translational work greatly. A number of logistical, technical and scientific challenges have been encountered and addressed along the way, which are discussed below in turn.

4.3.1 Clinical & Logistical Challenges

In order to progress this Phase I clinical trial to its currently maturing stage, I have personally had to address several key clinical and logistical challenges. This would not have been possible without the great support of the Oncology Clinical Trials Office (OCTO) and the Early Phase Clinical Trials Unit (EPCTU), based at Oxford. Some of the key clinical challenges encountered include:

1. Design, refinement, authorship & implementation of a detailed study protocol in-

corporating a significant degree of complexity and objectives & endpoints encompassing feasibility, safety and efficacy

2. Obtaining the necessary regulatory approvals to allow site initiation

3. Patient recruitment, management, intervention and follow-up

We were pleased to obtain MRHA approval on 12th May 2014 (Appendix 5.2.2) and ethical approval on 29th May 2014 (Appendix 5.2.1), leading to site initiation on 4th July 2014. Despite efforts, recruitment was initially slow for the first year of opening, with just one patient treated during this period. This was due to several factors including competition with several other systemic therapy Phase I studies at Oxford's cancer centre. In addition many patients suitable for the study intervention were also suitable for more established minimally-invasive therapies such as MWA and SIRT. Raising awareness of the TARDOX study in the referring oncology clinicians also took time, as might be expected with any new Phase I study. Furthermore, a high proportion of early referrals made, around half, were not suitable for Part I due to the technical feasibility with respect to tumour location. Until Part II of the study, which allows treatment of a wider range of tumour locations, opened in June 2016, a higher proportion of patients were ineligible for the trial. In addition, even following successful ultrasound screening, several of the advanced cancer patients failed at later screening due to having biochemical abnormalities consistent with liver failure, thus not meeting the inclusion criteria specified in the study protocol. Fortunately the later months of the study saw more referrals and a more fruitful period of recruitment. Study recruitment will remain open until the end of March 2017, by which time it is anticipated that ~10 patients will have been treated in total based on current treatment rates.

In arranging the study intervention for those who were successfully screened, this multidisciplinary study required a great deal of planning in coordination in order to ensure availability of the key members of the team, including the patient themselves, the clinical fellow, the HIFU device operator, the study radiologist, the anaesthetist, the post-

doctoral researcher, the pharmacy technician, the oncology research nurse and the various members of staff involved in sample handling and processing.

4.3.2 Technical Challenges

The technical challenges presented by the study are predominately concerned with difficulties targeting a moving organ and also around use of the co-axial needle for thermometry and tissue sampling. In delivery of the intervention, minimising respiratory motions of the liver is essential to ensure accurate targeting. High-frequency jet ventilation (HFJV), discussed in Section 1.3.2, has previously been used with success for RFA of the liver [192] and MWA of the lung [196]. This technique was used in all Part I and II cases and proved to be invaluable for minimising respiratory-related motion of the liver.

In terms of technical challenges, Part I of the study has proven especially demanding. The technical challenges encountered in Part I are summarised below:

1. The co-axial needle must be placed through a transcostal approach into the target tumour, above the water level, whilst in a position which is compatible with simultaneous FUS exposure, via an independent transcostal approach. Once the co-axial needle is inserted, it would be unsafe to move the patient into a more optimal position for FUS as it would disturb the needle position. This means, in practice, the patient position may not be optimal for FUS exposure of the tumour or the biopsy, and is often based on a compromise. For example, in the supine position which is useful for biopsy of target tumours in Segment VI, the rib space is often less generous than in a position of lateral tilt.

2. In addition, using the diagnostic probe of the JC200 to find the needle and thermometry device can then be a challenge in itself, especially in larger tumours, or where the needle becomes obscured behind a rib. Ensuring the JC200 transducer is positioned in the correct rib space is essential. This has inevitably led to delays and prolonged treatment times in some of the Part I treatments.

3. On one occasion, instrumenting the co-axial needle with a thermometry device has led to the introduction of gas into the ultrasound field. This has the effect of creating a echogenic cloud which obscures the view of the needle and also interacts with FUS to induce cavitation. In practice, when this has happened, waiting a period of time for the gas cloud to disperse has been the best way forward to maintain the integrity of thermometry data.

4. The co-axial needle and/or thermistor, which may remain in the liver for some hours, may become gradually migrate from its initial position during a prolonged treatment, due to continued respiratory movements. This risk was minimised by taping the position of the needle against the skin and securing the thermistor to it, and the use of high-frequency jet ventilation.

5. The insertion of the co-axial needle, when combined with multiple tissue biopsies over prolonged periods, can result in localised bleeding around the needle tip. This has meant that when taking the Unreleased (B2) or Released (B3) biopsy, on occasion, mainly blood clot has been sampled. Where this has been visually apparent, repeat biopsies have been taken from a slightly modified needle position to avoid the blood, which of course risks being outside of the targeted region of the tumour and thus may underestimate the amount of delivered drug.

6. Having only a single biopsy for each time point is a risk to the primary endpoint. If a user error or equipment failure occurs during the HPLC assay, there is no possibility of repeating the assay. Performing repeated biopsies is an ethical consideration as it poses a safety risk to the patient and will likely increase the risk of bleeding into the tumour. In Part II of the study this is rectified by taking two serial biopsies at the B3 time point.

These issues have resulted in lengthy treatment times, which themselves have potential to put the patient at risk of further AEs due to prolonged treatment under a GA. Part

II has also proven to be technically much more straight-forward and the risk of FUS-mediated tumour ablation remains low. The biggest risks in Part II, in the absence of real-time thermometry, relate to the study endpoints and not patient safety:

1. Under-heating the tumour: thermometry data from Part I cases is essential in that it can be used to predict the required treatment parameters for the JC200 (Section 3.2.5). The anatomical attributes for each target tumour will naturally vary, such as thickness of subcutaneous tissues, depth, rib spacing, and perfusion. Thus the more Part I patients who are successfully treated with optimal hyperthermia on the study, the better the primary outcome for Part II patients is likely to be.

2. Over-heating the tumour: as dramatically reduced powers are required for hyperthermia (circa 50-150 W) in comparison to HIFU ablation (typically in excess of 250 W), it is unlikely that inadvertent HIFU-ablation will result. If this did happen, grayscale changes would be apparent on the real-time B-mode console (Figure 4.1). HIFU-ablation is not desirable in this drug delivery study, but if it were to happen, it would be controlled and highly-targeted ablation of tumour tissue and thus not a safety risk to the patient.

3. Mis-sampling in large tumours: sampling part of a large tumour which has not received optimal hyperthermia and thus compromising the primary endpoint. This has effected tumour selection for Part II, such that smaller tumours are favoured for Part II whilst larger tumours are favoured for Part I.

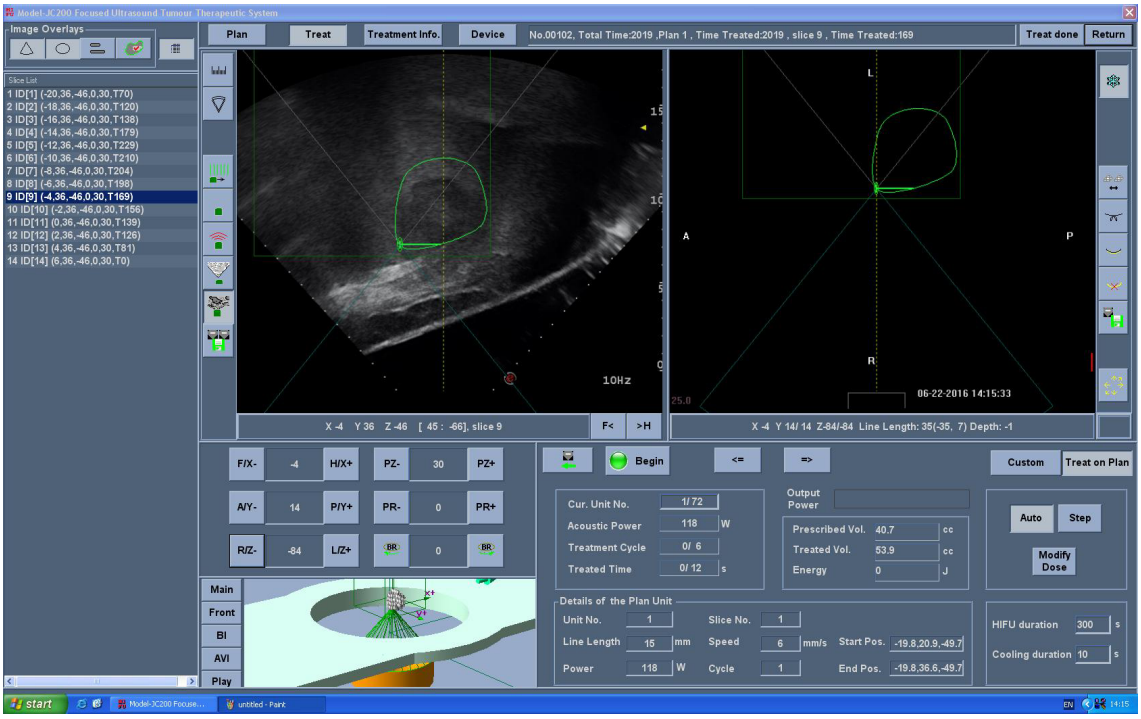


Figure 4.1: Screenshot taken from JC200 operator console during treatment for patient TXB101. The treatment volume was divided into 14 slices, and slice 9 is currently selected and the B-mode shown in the left pane, demonstrating clear tumour margins through the intercostal space. Note the treatment volume prescribed intentionally extends past the visible tumour margin on the B-mode in an attempt to treat the tumour margins. This is only possible in cases with smaller tumour volumes (<~50 cm^2) where complete tumour coverage is attempted. The right B-mode pane would normally contain live treatment images but in this case the screen shot was taken after the patient had been recovered.

A further technical consideration to make during the planning session is optimal selection of the tumour volume for biopsy. Many of the target tumours encountered will have a necrotic core due to tumour growth occurring quicker than neo-vascularisation. This phenomen is perhaps demonstrated most clearly in patient TXB101, where the solitary liver tumour has a clearly demarcated necrotic core on PET (Figure 4.2). If the final Released biopsy is taken from the necrotic core, it is likely that the analysis of the tissue sample will under-represent concentration of drug over the entire tumour. The tissue obtained for patient TXA104 illustrates this issue (Figure 3.13). Despite optimal hyperthermia, the majority of tissue was noted to be devoid of tissue which stained for nuclei positive cells, and of micro-vasculature, and this was consequent with a poor delivery

of doxorubicin (Figure 3.41), which is concentrated only in the micro-regional area of viable tumour cells (Figure 3.42).

The risks of sampling necrotic tumour were considered at the time of study design. At this time it was unknown if there was enough tissue mass for both HPLC and microscopic analysis, and a primary endpoint which was dependent on both sets of data would have been a risk. Consequently it was deemed that the primary endpoint is required to be met in 50 % or more of patients, for the study outcome to be considered successful. In practical terms, in the planning stages for all cases, it is prudent to carefully examine the baseline PET scan to determine the optimal approach to avoid sampling necrotic tissue wherever possible.

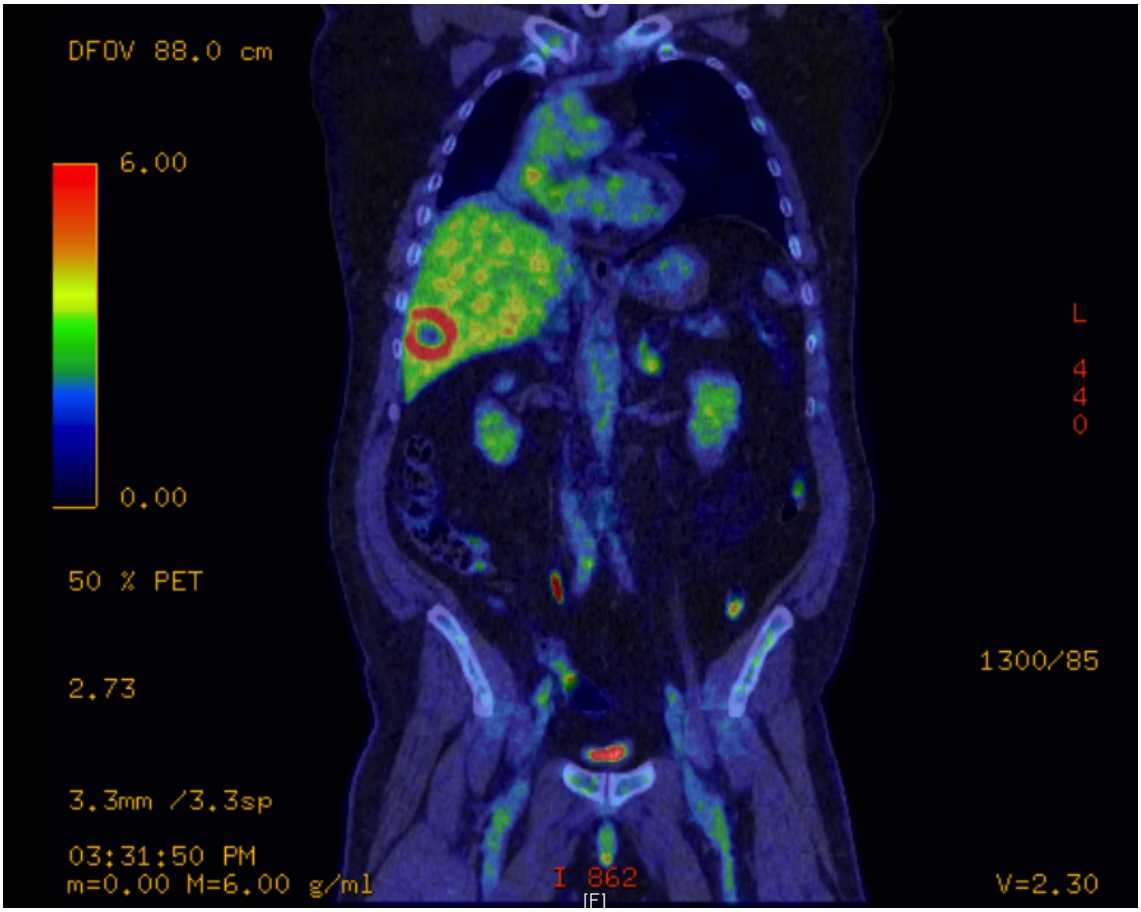


Figure 4.2: Coronal image of baseline ^{18}F-FDG PET-CT scan demonstrating the solitary target lesion in the liver. The core of the tumour appears to be necrotic as its metabolic activity is below that of normal liver parenchyma.

4.3.3 Scientific Challenges

The scientific challenges which I have addressed to conclusion, with the assistance of the Institute of Biomedical Engineering, University of Oxford (IBME), the Good Clinical Practice Laboratories, Bio-analysis Core and Department of Radiology, Oxford, include:

1. Optimised strategies for induction and maintenance of controlled volumetric hyperthermia in *ex-vivo* liver tissue, using a clinical FUS device

2. Translation of optimised heating strategies for clinical application to perfused tumour volumes

3. From biopsy tissue alone, development of laboratory methods to assess efficacy of LTSL and FUS as a combination therapy, above LTSL alone, which include:

   Quantification of intratumoral doxorubicin concentration

   Quantification of doxorubicin pharmacokinetics in the plasma, including bioavailability studies

4. From biopsy tissue alone, development of microscopy methods to assess bioavailability of doxorubicin cronsequent with liposomal release

5. Application of the principles of published methods to assess isolated radiological response in the target tumour across three imaging modalities

With regard to the first and second items, the FUS regime used to target tumours for drug delivery is key to maximising levels of vascular permeability, doxorubicin delivery and chemosensitisation of the tumour cells. Clearly inadequate heating of the target tumour is likely to fail to release intravascular ThermoDox® within the tumour microvasculature to therapeutic concentrations. Conversely, overheating the tumour to temperatures above 43 °C may result in decreased perfusion, as discussed in Section 1.4.6, and thus decreased opportunity for drug delivery. Higher temperatures still may approach CEM_{43}

limits and thermal ablation may destroy the very microvasculature crucial for intratumoral drug delivery. In addition to maintaining tight temperature control of 41-43 °C, consideration should also be given to the derated in situ peak pressures, and the potential role for cavitation-enhanced delivery has previously been discussed (Section 3.2.2).

In the absence of a non-invasive methods of measuring temperature, pressure or cavitation threshold, large anatomical variation in tumour location and the FUS approach, and with a wide variation in quoted literature values for liver attenuation (Section 3.2.3) and perfusion between patients, obtaining this delicate balance perhaps becomes the greatest challenge of all.

4.4 Study Limitations

This Phase I clinical study has several limitations which have all previously been discussed individually, and are summarised as follows:

1. Ethical considerations of treating a single tumour in patients with disseminated cancer (Section 4.5)

2. Inability to quantify liver perfusion and attenuation for individual patients, information, which could better predict and optimise FUS parameters. For example, it is well reported that there is a wide variation in ultrasound attenuation in cirrhotic liver relative to normal liver parenchyma [482, 484].

3. Obstruction of FUS propagation path by ribs, often limiting full tumour exposure

4. Limitation of the volume that can be practically heated in time available using the single element transducer of the JC200 (64 cm^3), despite use of moving beam mode

5. Enhanced drug delivery in Part I patients may be argued to be, in part, due to 'priming' of the vasculature with FUS in the planning exposure, prior to drug administration

6. Lack of real-time thermometry feedback in Part II

7. Inability to perfectly correlate FUS treatment volume with the biopsy position in Part II, especially in larger tumours, due to lack of co-registration method

8. Inherent error in biopsy tissue sampling within a large and heterogenous tumour environment (e.g. sampling of necrotic core)

9. Lack of the tissue biopsy from non-FUS exposed control tumours (ethical considerations)

10. Inability to perfectly correlate follow-up radiological imaging with FUS treatment volume, due to lack of co-registration method

Many of these limitations result from the difficulties in translation to a clinical study, introducing further ethical considerations, and tumour volumes an order of magnitude greater than those seen pre-clinically. Despite these limitations this early study continues to generate a wealth of valuable data which is likely to inform future clinical studies in this field.

4.5 Ethical Considerations

In this proof of concept study, patients receive a single chemotherapy cycle, and the primary and secondary endpoints intentionally make no reference to radiological response of the tumour or survival. Whilst the study may potentially offer improved outcomes in patients with small tumour targets in oligo-metastatic disease, on the whole the study is unlikely to provide any prognostic benefit, even if there is a good response in the target tumour. This is unfortunately an expectation of Phase I trials, which typically focus on feasibility and safety, and altruism becomes the overriding driver for most patients. Given early TARDOX cases demonstrated some localised response on radiological follow-up (Section 3.4) there is a temptation to cover larger tumour volumes with FUS for longer

periods in subsequent patients. However whilst it is the duty of a doctor to do good, first and foremost doctors are bound by the Hippocratic oath to do no harm (*Primum non nocere*), and patient safety will always be the first priority. Prolonging anaesthesia to heat larger volumes for longer periods in order to obtain greater degrees of radiological response is associated with increased patient risk, and may not necessarily be the best interests of the study patients, who by definition have disseminated disease. In addition to prolonging treatment time, obtaining optimal hyperthermia in larger tumour volumes (prescribed volumes over 64cm^3) rapidly becomes challenging within the confines of the current USgFUS therapeutic device (Section 2.2.3). Thus, in the interests of the patients being treated and the integrity of the trial, which may potentially benefit cancer patients of the future, insonated volumes have been kept to this order of magnitude (Tables 3.7 & 3.8). When the study team consult with study patients, in order to avoid false hope, the projected outcomes are discussed at length with the patient during the consent process, such that any participant is fully informed that direct prognostic benefit is likely to be small, if anything, in this particular clinical study. In a special case, best efforts were made to cover the full extent of the target tumour and margin with FUS in a patient with primary lung cancer and a single liver tumour (TXB101), in the hope of maximising the potential prognostic benefit.

4.6 Future Work

4.6.1 Other Clinical Studies

In the translation of this targeted drug delivery paradigm to a clinically approved standard, there are several challenges yet to be overcome. Safety of both the drug and the device becomes of paramount importance and early phase studies will typically concentrate on these safety aspects, whilst the focus will shift to efficacy in later phase studies. Although it is trivial to harvest the targeted tumour in pre-clinical studies, this is clearly

not the case in clinical studies. In cases of neoadjuvant chemotherapy the study design provides tissue obtained following surgical resection, for example mastectomy after targeted delivery to a breast tumour. However for targeted delivery studies without the option of resection, such as the TARDOX study [132], endpoints involving intratumoral drug quantification and penetrance necessitate biopsy, and tissue mass limits the extent of analysis. Whilst non-invasive methods of quantifying surrogate markers of release are under investigation [311, 381, 382], they are not yet available for clinical use. Some study designs have thus concentrated on anti-tumour efficacy quantified through survival outcomes and/or radiological response; for example the primary endpoint of the HEAT and OPTIMA studies involves progression-free survival [392, 396]. Yarmolenko *et al.* have discussed the difficulties associated with making comparisons of response across different tumour types and different patient groups [378].

Despite these challenges, it is anticipated that the next decade will see a continued worldwide research effort leading to completion of further clinical studies using the FUS/LTSL model, demonstrating feasibility, safety and enhanced oncological outcomes. Further regulatory approvals for the use of FUS in drug delivery would then follow, and such treatments may become routine clinical practice in the healthcare systems across the globe, both for oncological treatments and beyond.

4.6.2 Technological Advances

Advances in Focused Ultrasound Devices

In the non-invasive treatment of solid organ cancers, the great potential for combining clinical FUS devices with drug delivery systems such as LTSLs has been discussed. Future developments may see further improvements in phased array technology to provide of more efficient FUS exposures and to allow transcranial focusing [500]. Furthermore, development of defocused transducers will improve the efficiency of regional heat deposition, thereby reducing treatment times [501, 502]. Further ultrasound advancements are

likely to include improved guidance and real-time monitoring techniques including 3D ultrasound, dual-mode ultrasound, passive acoustic mapping of cavitation and ultrasound thermography with higher spatial and temporal resolution than MRI thermometry can offer. There is even potential for the development of devices combining unique features of both MRgFUS and USgFUS [93]. Most recently, in 2016, an MRgFUS phased array system (Insightec Exablate Neuro System) has received FDA approval for trans-cranial focusing for treatment of essential tremor, the first FDA approval of a FUS device for use on the brain. Review articles on the use of FUS for drug delivery are available [503, 504].

Potential modifications to defocus an existing clinically-approved USgFUS-device, such as the JC200, have been suggested by Dr. Michael Gray. Direct application of a ring of absorbing material to the periphery of the transducer could potentially achieve expansion of the JC200 ultrasound beam by reducing the aperture (Figure 4.3). The main advantage would be more efficient heating of tumour volumes due to the reduction in the number of rows and slices required to cover a large tumour volume. Modelling shows that a ring reducing the transducer outer radius by 1 cm would reduce the intensity at the axial focus by approximately half, whilst increasing the full-width half maximum (FWHM) beam width by 2.6 mm. Reduced pressures at the focus would likely require some degree of compensation in order to maintain the necessary levels of heat deposition for drug delivery. Levels of cavitation could potentially be reduced, depending on the level of compensation required, which may have an unfavourable effect on drug delivery (Section 3.2.2). Clearly before clinical application, such a modification would require thorough pre-clinical investigation to characterise beam pattern changes at the focus and focal pressures, and this is outside the scope of this thesis.

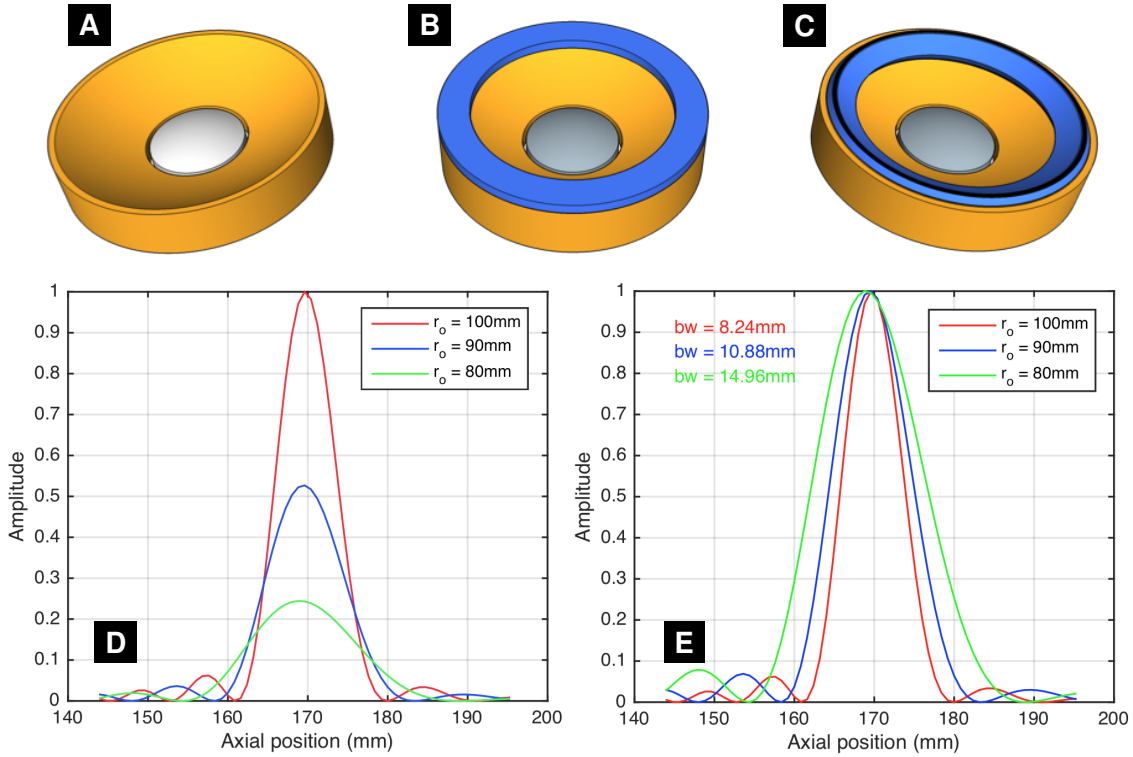


Figure 4.3: Baseline JC200 (A) with flat ring absorber (B) or reduced profile conformal absorber (C). D: Predicted axial beam intensity patterns for transducer outer radii of 100 (the radius of the unmodified JC200 transducer), 90 and 80 mm. E: Normalised axial beam pattern for the same, where the coloured text (bw) represents full-width at half maximum (FWHM) values. Acknowledgement: Dr. Michael Gray, IBME.

Pharmacological Advances

The last 50 years have seen continued research and development in liposomal formulation since the conceptualisation of the liposome by Bangham *et al.* in 1965 [265]. Whilst ThermoDox® remains the only LTSLs approved for investigational use in the clinic, many liposomal formulations of the future are in the development pipeline. In addition to ThermoDox®, the potential scope for other classes of therapeutic agent to be delivered using LTSLs by FUS is large. Advances in liposome formulations include antibody conjugation, leading to a new generation of "immunoliposomes", which offer the potential for specific cellular targeting. Thermo-sensitive formulations are now beginning to emerge, such as the monoclonal antibody-targeted TSLs (TTSL-Ab) [505], which can provide targeting on both anatomical and molecular levels. Furthermore a wide range

of hydrophilic chemotherapy agents could potentially be delivered by LTSLs and several thermo-sensitive formulations, including carriers for cisplastin [506] and melphalan [507], have already been produced. Although not yet available in thermo-sensitive forms, the broad range of other liposomal therapeutic agents under investigation includes viral therapies (virosomes) [508–510], siRNA [511, 512], rhematologics [513] and analgesics [514].

As previously discussed in Section 1.4.8, the FUS research community eagerly anticipate the emergence of approved theranostic LTSLs, which co-encapsulate paramagnetic MRI contrast agents [311, 381, 382] for non-invasive monitoring of drug delivery. Although not yet available in thermo-sensitive forms, a broad range of other liposomal therapeutic agents under investigation includes viral therapies (virosomes)[515–517], siRNA [518, 519], rhematologics [520] and analgesics [521]. This expanding research field is covered by several excellent reviews covering thermosensitive liposomes [522–524] and paramagnetic liposomes for MR-guided drug delivery [525].

Future developments in the FUS/LTSL delivery mechanism may include co-administration of liposomes with micron-sized cavitation-promoting agents in order to further increase penetration depth of the released drug [526]. Indeed the strategy of using ultrasound-mediated cavitation for enhanced drug penetrance may potentially also be employed to deliver other chemotherapeutics, including biologics such as Anti-PD1 and Anti-ICOS, avoiding the need for liposomal reformulation of a huge range of existing approved drugs.

4.6.3 Simulating Parameters for Volumetric Hyperthermia

Here in Oxford, using 3D conformational data from CT scans in each clinical case, custom *in silico* FUS modelling is being explored with a view to predict required FUS parameters for optimal hyperthermia of a target liver tumour volume. Development of this model, which employs JC200 incident field measurements, CT data, and both measured

and literature-based tissue properties all as inputs into finite element calculations, is ongoing.

4.7 Conclusions

When the clinical evidence is taken collectively, it supports that the use of ThermoDox® in combination with FUS for hyperthermia can achieve non-invasive and targeted release of doxorubicin in liver tumours. Furthermore, clinical evidence supports that using this method, a single treatment cycle of standard dose doxorubicin can achieve highly targeted chemo-ablation in a variety of tumour types, including colorectal metastases.

Whilst this early study is one of the very first to achieve clinical translation, preliminary results have demonstrated feasibility of targeted liposomal release and have shown promise in terms of efficacy and even localised chemo-ablative response from a single ThermoDox® cycle.

It is anticipated that the thermometry and radiological data acquired in this early proof of concept study may lead to further similar USgFUS or MRgFUS drug delivery studies performed non-invasively with FUS parameters based on patient-specific simulations. This early clinical experience highlights the real clinical need for robust non-invasive methods of monitoring temperature and cavitation simultaneously, potentially integrating both ultrasound-based methods for cavitation detection [102] and MR for thermometry. Several other MRgFUS studies incorporating the use of ThermoDox® are already in the pipeline and results are highly anticipated across the clinical and FUS research communities alike.

4.8 Summary

Whilst the field of minimally-invasive targeted cancer therapies continues to grow, FUS is the only modality to offer non-invasive and non-ionising solid-organ tumour targeting.

Whilst molecularly targeted chemotherapeutics offer great promise in systemic cancer therapy, the challenge of achieving penetration of therapeutic concentrations of drug into the difficult tumour micro-environment is not addressed [238, 239, 527]. The use of FUS in combination with systemically-circulating agent(s), such as LTSLs, offers the unique potential to deliver greatly enhanced concentrations of therapeutic agents, beyond the perivascular space, to unsurpassed tumour penetration depths. Technology is already available to test this hypothesis clinically, and the TARDOX study is one of the very earliest studies to demonstrate the promising capabilities of such targeted therapy. Not only has this study demonstrated the potential of FUS to *release* LTSLs at *enhanced concentrations* in liver tumours, local *tumour response* in refractory colorectal tumours has been observed from a single standard chemotherapy cycle of doxorubicin, which is not a typical indication for the drug. The study would not have been possible without a great number of pre-clinical and clinical research contributions dating back to the conception of therapeutic HIFU (1940s) and development of the first liposome (1960s).

With exclusion of chemotherapeutics that target on a molecular level, the use of targeted FUS offers the only truly non-invasive solution for the drug delivery problem to date. FUS-mediated delivery through thermal and/or cavitational mechanisms has the potential to deliver greater concentrations of therapeutic agents beyond the perivascular space to unsurpassed tumour penetration depths, without increasing systemic dose and in the absence of direct ablative effects. Coupled with advances in radiological methods for non-invasive monitoring of delivery, release and subsequent clinical response, such device and drug combinations have the potential to transform the future of the management of solid organ cancers.

CHAPTER 5

Appendices

5.1 Laboratory Methods

5.1.1 Live/Dead Staining of a Cell Suspension for Flow Cytometry

The live/dead staining method described uses a commercial fluorescence based cell viability kit, which has far-red fluorescence emission spectra, distinct from that of doxorubicin (LifeSciences Far Red LIVE/DEAD®, Fixable Far Red Dead Cell Stain Kit for 633 or 635 nm excitation, Ref: L10120 (L/D stain). For cell suspensions, viability staining was performed immediately without fixation, but the L/D stain also offers the opportunity for fixation and analysis at a later time. For each stained sample a matched unstained control of equivalent volume and cell concentration was used.

1. L/D stain was reconstituted in DMSO as per product instructions, and stored in aliquots of 5 μL at 80 °C

2. 1 μL of a thawed L/D stain aliquot was added to samples for staining only and gently vortexed.

   The remaining steps were then performed to both the unstained and stained FACS tubes in parallel:

3. Samples were incubated for 15 mins at room temperature and protected from light.

4. Centrifugation was performed at 400g RCF for 5 minutes and the pellet retained.

5. Where fixation was required for delayed analysis, samples were re-suspended in 1 mL of 4% NBF diluted in PBS (Scigen 10% Buffered Neutral Formalin, Ref: FX2040), incubated for a minimum of 15 minutes and a maximum of 24 hours at room temperature, whilst protecting from light, and centrifugation was repeated.

6. Fixed and unfixed samples were re-suspended in 650 μL of PBS and aliquot into two 300 μL sterile lidded FACS tubes (one spare) and refrigerated for up to 7 days until analysis.

7. Analysis was performed using a BD FACSCalibur™ flow cytometer and the FL4 channel for the red laser (633 nm), in logarithmic 4-colour mode.

Acknowledgement: Mick Woodcock of the Bio-analysis Core for demonstrating the capabilities and teaching the techniques of flow cytometry.

5.1.2 Tissue Cell Recovery Protocol

A cell recovery protocol involving tissue disaggregation and enzymatic digestion was optimised using small (from 4-100 mg) samples of *ex-vivo* fresh mouse liver. The following protocol may be adapted for other tissue types including clinical samples:

1. Post-treatment tissue samples were placed in individual petri dishes, covered by a few drops of sterile DMEM and then kept on ice.

2. Tissue was macerated between two crossed scalpels into a pulp, avoiding crushing and scraping.

3. Samples were washed in up to 10 mL of DMEM media and transferred to 15 ml centrifuge tubes

4. 200 μL of 1 mg/mL Collagenase/Dyspase® diluted in PBS (100 mL, Roche, Ref: 10269638001) was added for digestion of the connective tissues, vortexed and incubated in a water bath at 37°C for 30 minutes.

5. Samples were filtered through cell strainer (BD Falcon Cell Strainer 70 μm nylon mesh, Ref: 352350) into a fresh 50 mL centrifuge tube.

6. 2mL of RBC lysis buffer diluted in deionised water (Red Blood Cell Lysis Buffer, 100 mL, Sigma, Ref: R5575) was added and each sample kept on ice for 5 minutes.

7. Samples were centrifuged at 400 g (RCF) at 10°C for 5 minutes and the supernatant was discarded to leave pellet (not visible by eye for smaller mass samples).

8. Cells were re-suspended in 5 mL FACS buffer (2% foetal calf serum in PBS), re-filtered through a fresh cell strainer into a centrifuge tube and topped up to 15 ml with FACS buffer.

9. Centrifugation was repeated and cells were re-suspended in 2.1 mL of PBS and vortexed.

10. 1 mL aliquots were transferred into two 15 mL centrifuge tubes (one for staining, one unstained control).

11. For each sample, cell counts were performed using haemocytometer and, in the case of larger tissue masses, diluted in PBS to approximately 1 million cells/mL if exceeding this concentration.

Acknowledgements: Mr. Alex Gordon-Weeks of the Nuffield Department of Surgical Sciences and Dr. Philip Jakeman of the Department of Oncology, University of Oxford for sharing and demonstrating their cell recovery protocols, which have both contributed to the development of this protocol.

5.1.3 Markers & Fluorophores Used in Fluorescence Microscopy

Fluorescent Marker	**Purpose**	**Primary Ab.**	**Secondary Ab.**	**Optimal Ex./Em. (nm)**
Doxorubicin (Apollo Scientific, Ref: BID0120)	Determine drug penetrance & bioavailability	N/A	N/A	485/590
Hard-setting DAPI Mounting Media (Vecta-Shield)	Determine co-localisation with doxorubicin in cell nuclei	N/A	N/A	358/461
CK8 (BD Scientific, Cytokeratin-8 antibody (CAM 5.2))	Cell viability stain to determine the absence of thermal ablation in epithelial cells	Anti-Cytokeratin (CK8) (CAM 5.2, BD, Ref: 345779)	Goat anti-Mouse IgG2a, Alexa Fluor® 488 conjugate (Green) (ThermoFisher Scientific, Ref: A-21131)	490/525
panCK (Abcam®, Anti-wide spectrum Cytokeratin antibody ab9377)	Determine if epithelial cells are thermally ablated	Anti-wide spectrum Cytokeratin antibody (AbCam, Ref: ab9377)	Goat anti-Rabbit IgG (H&L), Alexa Fluor® 568 conjugate (Red) (ThermoFisher Scientific, Ref: A-11011)	490/525

Table 5.1: Fluorescent markers, anti-bodies (Ab.) and excitation/emission values for immunofluorescent fluorophores used for pre-clinical microscopy studies (Sections 2.3.3 and 2.4.2). Acknowledgement: Leticia Campo for fluorophore selection.

Fluorescent Marker	**Purpose**	**Primary Ab.**	**Secondary Ab.**	**Optimal Ex./Em. (nm)**
Doxorubicin (encapsulated within or released from clinical-grade ThermoDox®)	Determine drug penetrance & bioavailability	N/A	N/A	485/590
Soft-setting DAPI Mounting Media (Vecta-Shield)	Determine co-localisation with doxorubicin in cell nuclei	N/A	N/A	358/461
CK8 (BD Scientific, Cytokeratin-8 antibody (CAM 5.2))	Cell viability stain to determine the absence of thermal ablation in epithelial cells	Anti-Cytokeratin (CK8) (CAM 5.2, BD, Ref: 345779)	Goat anti-Mouse IgG2a, Alexa Fluor® 488 conjugate (Green) (ThermoFisher Scientific, Ref: A-21131)	490/525
CD31	Vascular stain	Monoclonal mouse anti-human CD31 (endothelial) clone JC70A IgG1-Ab (i.e. isotype 1) (DAKO, Ref: M0823)	Donkey anti-Mouse IgG, Alexa Fluor® 488 (Green, Thermo Fisher A-21202)	490/525

Table 5.2: Fluorescent markers, anti-bodies (Ab.) and excitation/emission values for immunofluorescent fluorophores used in microscopy of clinical biopsy samples obtained on the TARDOX study (Sections 3.3.4 and 3.2.6). Acknowledgement: Leticia Campo for fluorophore selection.

5.1.4 Stains Used in Immunohistochemistry for Microscopy

Marker	Purpose	Primary Ab.	Secondary Ab.
H&E	Gold standard for tissue morphology	N/A	N/A
Caspase-3	Marker of apoptosis	Cleaved Caspase-3 (Asp175 D3E9 Cell Signal 9579 Rb)	Leica Bond Polymer Refine Detection Kit (Ref: DS9800)

Table 5.3: Immunohistochemical (IHC) stains used in microscopy of clinical biopsy samples obtained on the TARDOX study (Section 3.2.6). Acknowledgement: Leticia Campo for marker selection.

5.1.5 Summary of Microscopy Protocols

Summary of Doxorubicin Protocol for Fluorescence Microscopy

1. Slides were cut at 4 μm using the Leica RM2235 Microtome
2. Slide were mounted with Vectashield non-permanent with DAPI, using coverslip No. 1.5 (0.17 mm thick)

Acknowledgement: Leticia Campo for optimisation of this microscopy protocol.

Summary of CD31 & CK8 Immunofluorescence Protocol for Microscopy

1. Slides either reused from previous doxorubicin studies, or new tissue slice taken from corresponding block
2. Staining was performed on the Leica Biosystems BOND-MAX Auto-Stainer
3. Antigen retrieval was performed using 40' with ER2
4. A custom protocol was used whereby the mixture of primary antibodies was incubated for 1 hour and after addition of secondary antibodies, a further incubation period of 1 hour was used

5. Dilutions: CD31 was used at a dilution of 1 in 20, CK8 was used neat and Alexafluor was used at 1 in 200

6. Slides were mounted with VectaShield hard set + DAPI, using coverslip No. 1.5 (0.17 mm thick)

Acknowledgement: Leticia Campo for optimisation of this microscopy protocol.

Summary of Caspase-3 Immunohistochemistry Protocol for Microscopy

1. IHC staining was performed on the Lecia Biosystems BOND-MAX Auto-Stainer

2. Dilution: Caspase-3 antibody was diluted 1 in 200

3. Standard protocol F60 was used, which involves a 60 minute primary antibody incubation period

4. Antigen retrieval was performed using 40' ER2

Acknowledgement: Leticia Campo for optimisation of this microscopy protocol.

5.2 Regulatory Approvals

5.2.1 Research Ethics Committee Approval

NHS
Health Research Authority
NRES Committee North East - York
Room 002
Jarrow Business Centre
Viking Business Park
Rolling Mill Road
Jarrow, Tyne & Wear
NE32 3DT

Telephone: 0191 4283545

13 May 2014

Mark Middleton
University of Oxford
Cancer Centre, Churchill Hospital
Oxford
OX3 7LE

Dear Mr Middleton

Study title:	**A Proof of Concept Study to Investigate the Feasibility of Targeted Release of Doxorubicin from Lyso-thermosensitive Liposomal (LTSL) Doxorubicin (ThermoDox®) Using Focused Ultrasound in Patients with Liver Metastases from Lung, Breast or Colorectal Primary Tumours**
REC reference:	**14/NE/0124**
Protocol number:	**OCTO_040**
EudraCT number:	**2014-000514-61**
IRAS project ID:	**150000**

The Research Ethics Committee reviewed the above application at the meeting held on 09 May 2014.

We plan to publish your research summary wording for the above study on the HRA website, together with your contact details, unless you expressly withhold permission to do so. Publication will be no earlier than three months from the date of this favourable opinion letter. Should you wish to provide a substitute contact point, require further information, or wish to withhold permission to publish, please contact the REC Manager at nrescommittee.northeast-york@nhs.net

Ethical opinion

The Committee reviewed the above study

In discussion, the Committee noted the following ethical issues.

Professor Constantin Coussios, Chief Scientist and Mr Paul Lyon, Clinical research fellow attended to discuss the application on your behalf.

The Committee informed the researchers that they were very impressed by the way in which the research had been presented.

1. The Committee queried the Sponsorship of the study.

   The researchers informed the Committee the study was in collaboration with Celsion in the USA. Celsion's role in the study is to provide the study drug free of charge and quality assurance of releasing the drug in the UK. There only obligation to Celsion is to update them on the trial and to provide anonymised data. The researchers went on to inform the Committee that the University of Oxford is their sponsor and that the trial was not commercially sponsored.

2. Page 4 of the PIS documents that a relative or friend can sign the consent form on behalf of the participant and the Committee required further information under what circumstances this would be.

   The researchers explained that this is standard wording for this type of trial and that this is for those participants who may have a physical disability.

3. The Committee noted the recruitment methods and queried whether this would allow an adequate enrolment of participants, given the long list of exclusion criteria.

   The researchers acknowledged that the list does appear to be quite long however, this does have an overlap in normal doxorubicin therapy. They reiterated that there are plenty of people in the UK who receive doxorubicin and estimate that between 14-28 participants would be recruited within two years.

4. It was unclear whether the participants would be able to sustain a general anaesthetic, as this is not included in the inclusion criteria.

   The researchers informed the Committee that when the participant is undergoing their ultra sound, the anaesthetic allows for easier control of the diaphragm allowing the liver therefore to remain as still as possible. If the participant was not felt to be fit enough, they would be excluded from the study. The researchers informed the Committee that they have previous experience in 14 participants.

5. The Committee discussed the significant intellectual property.

   The researchers confirmed there to be a great clinical intellectual property where the same amount of chemotherapy is injected. Their animal studies have shown 10-25% can be injected into the tumour and that their long-term goal was to see if it was possible to lower the dose of chemotherapy to achieve the same effect.

6. The Committee queried whether there was an indication for treating another organ.

The Researchers explained that this study was a platform phase 1 study and that they are starting to administer the drug into the liver primarily. They hope to encapsulate the drug for other diseases such as kidney, pancreas and breast but would also like to look at other drugs.

7. The Committee informed the researchers that the IRAS form (A17-1) makes no reference to mental capacity, which must be a potential factor with the patients concerned. The Committee explained that should the participants be found to lack capacity and this would raise issues, this must be included in the inclusion/exclusion criteria.

The researchers agreed to amend their inclusion/exclusion criteria.

The researchers went on to inform the Committee of an error in their amendment form. The researchers explained that they should have selected the option 'Clinical trial of an unlicensed investigational medicinal product'. Doxorubicin is licensed but not its formulation.

The Committee informed the Researchers that this section of the IRAS form should be amended to read 'Clinical trial of an unlicensed investigational medicinal product'.

The researchers agreed.

The researchers left the meeting.

Decision – Favourable with Conditions

The members of the Committee present gave a favourable ethical opinion of the above research on the basis described in the application form, protocol and supporting documentation, subject to the conditions specified below.

1. To amend your Exclusion criteria to state that, any participants found to be lacking capacity, will be excluded from the study.

2. Section A8 of the IRAS form to be amended to read 'Clinical trial of an unlicensed investigational medicinal product'.

3. Within the PIS under the heading 'What is the purpose of the study' to state that no patients will progress from part 1 to 2 of the study.

Ethical review of research sites

NHS Sites

A Research Ethics Committee established by the Health Research Authority

The favourable opinion applies to all NHS sites listed in the application, subject to management permission being obtained from the NHS/HSC R&D office prior to the start of the study (see "Conditions of the favourable opinion" below).

Non NHS sites

The Committee has not completed any site-specific assessment (SSA) for the non-NHS research site(s) taking part in this study. The favourable opinion does not therefore apply to any non-NHS site at present. I will write to you again as soon as an SSA application(s) has been reviewed. In the meantime, no study procedures should be initiated at non-NHS sites.

Conditions of the favourable opinion

The favourable opinion is subject to the following conditions being met prior to the start of the study.

You should notify the REC in writing once all conditions have been met (except for site approvals from host organisations) and provide copies of any revised documentation with updated version numbers. The REC will acknowledge receipt and provide a final list of the approved documentation for the study, which can be made available to host organisations to facilitate their permission for the study. Failure to provide the final versions to the REC may cause delay in obtaining permissions.

Management permission or approval must be obtained from each host organisation prior to the start of the study at the site concerned.

Management permission ("R&D approval") should be sought from all NHS organisations involved in the study in accordance with NHS research governance arrangements.

Guidance on applying for NHS permission for research is available in the Integrated Research Application System or at http://www.rdforum.nhs.uk.

Where a NHS organisation's role in the study is limited to identifying and referring potential participants to research sites ("participant identification centre"), guidance should be sought from the R&D office on the information it requires to give permission for this activity.

For non-NHS sites, site management permission should be obtained in accordance with the procedures of the relevant host organisation.

Sponsors are not required to notify the Committee of approvals from host organisations

Registration of Clinical Trials

All clinical trials (defined as the first four categories on the IRAS filter page) must be registered on a publically accessible database within 6 weeks of recruitment of the first participant (for medical device studies, within the timeline determined by the current registration and publication trees).

There is no requirement to separately notify the REC but you should do so at the earliest opportunity e.g when submitting an amendment. We will audit the registration details as part of the annual progress reporting process.

To ensure transparency in research, we strongly recommend that all research is registered but for non clinical trials this is not currently mandatory.

If a sponsor wishes to contest the need for registration they should contact Catherine Blewett (catherineblewett@nhs.net), the HRA does not, however, expect exceptions to be made. Guidance on where to register is provided within IRAS.

Clinical trial authorisation must be obtained from the Medicines and Healthcare products Regulatory Agency (MHRA).

The sponsor is asked to provide the Committee with a copy of the notice from the MHRA, either confirming clinical trial authorisation or giving grounds for non-acceptance, as soon as this is available.

It is responsibility of the sponsor to ensure that all the conditions are complied with before the start of the study or its initiation at a particular site (as applicable).

Approved documents

The documents reviewed and approved at the meeting were:

Document	*Version*	*Date*
Covering Letter	Lucy Boyle	09 April 2014
GP/Consultant Information Sheets	1.0	08 April 2014
Investigator CV	Professor Middleton	15 May 2012
Investigator's Brochure		11 October 2013
Letter from Sponsor		09 April 2014
Participant Consent Form	1.0	08 April 2014
Participant Information Sheet	1.0	08 April 2014
Protocol	1.0	08 April 2014
REC application	3.5	08 April 2014

Membership of the Committee
The members of the Ethics Committee who were present at the meeting are listed on the attached sheet.

Statement of compliance
This Committee is recognised by the United Kingdom Ethics Committee Authority under the Medicines for Human Use (Clinical Trials) Regulations 2004, and is authorised to carry out the ethical review of clinical trials of investigational medicinal products.

The Committee is fully compliant with the Regulations as they relate to ethics committees and

the conditions and principles of good clinical practice.

The Committee is constituted in accordance with the Governance Arrangements for Research Ethics Committees and complies fully with the Standard Operating Procedures for Research Ethics Committees in the UK.

After ethical review

Reporting requirements

The attached document "After ethical review – guidance for researchers" gives detailed guidance on reporting requirements for studies with a favourable opinion, including:

- Notifying substantial amendments
- Adding new sites and investigators
- Notification of serious breaches of the protocol
- Progress and safety reports
- Notifying the end of the study

The NRES website also provides guidance on these topics, which is updated in the light of changes in reporting requirements or procedures.

Feedback

You are invited to give your view of the service that you have received from the National Research Ethics Service and the application procedure. If you wish to make your views known please use the feedback form available on the website.

Further information is available at National Research Ethics Service website > After Review

14/NE/0124 **Please quote this number on all correspondence**

We are pleased to welcome researchers and R & D staff at our NRES committee members' training days – see details at http://www.hra.nhs.uk/hra-training/

With the Committee's best wishes for the success of this project.

Yours sincerely

pp H Hendry

Professor Peter Heasman
Chair

Email: nrescommittee.northeast-york@nhs.net

A Research Ethics Committee established by the Health Research Authority

Enclosures:	*List of names and professions of members who were present at the meeting and those who submitted written comments* *"After ethical review – guidance for researchers" [SL-AR1]*
Copy to:	Ms Heather House, University of Oxford

A Research Ethics Committee established by the Health Research Authority

NRES Committee North East - York

Attendance at Committee meeting on 09 May 2014

Committee Members:

Name	*Profession*	*Present*	*Notes*
Dr Sarah Bartlett	Consultant Child & Adolescent Psychiatrist	Yes	
Dr David Cairns	Principal Statistician	Yes	
Ms Linda Chadd	Lay Member	Yes	
Mr Steve Chandler	Retired Consultant Medical Physicist	Yes	
Dr Mary Connor	Coaching & Mentoring Consultant	No	
Mr Malcolm G Harrison	Lawyer - Retired	Yes	
Mrs Janet Hattle	Head of Pharmacy	Yes	
Professor Peter Heasman (Chair)	Professor of Periodontology	Yes	
Mrs Fan Hutchison	Principal Teacher	Yes	
Mr Malcolm Khan	Lawyer - Retired	No	
Dr Giles McCracken	Senior Clinical Lecturer	Yes	
Dr Rikesh Patel	Clinical Research Fellow	Yes	
Dr Ian Woollands	Retired Clinical Director, Occupational Health	Yes	
Ms Lorraine Wright	Senior Research Nurse	Yes	

Also in attendance:

Name	*Position (or reason for attending)*
Mia Porteous	Observer
Natasha Dyer	Observer
Mrs Hayley Henderson	REC Manager

NHS
Health Research Authority
NRES Committee North East - York
Jarrow Business Centre
Viking Business Park
Rolling Mill Road
Jarrow, Tyne & Wear
NE32 3DT

Telephone: 0191 4283545

29 May 2014

Lucy Boyle
TARDOX Clinical trial Coordinator
Oncology Clinical Trials Office
Department of Oncology
University of Oxford
Headlington
Oxford
OX3 7DQ

Dear Ms Boyle

Study title:	**A Proof of Concept Study to Investigate the Feasibility of Targeted Release of Doxorubicin from Lyso-thermosensitive Liposomal (LTSL) Doxorubicin (ThermoDox) Using Focused Ultrasound in Patients with Liver Metastases from Lung, Breast or Colorectal Primary Tumours**
REC reference:	**14/NE/0124**
Protocol number:	**OCTO_040**
EudraCT number:	**2014-000514-61**
IRAS project ID:	**150000**

Thank you for your letter of 28th May 2014. I can confirm the REC has received the documents listed below and that these comply with the approval conditions detailed in our letter dated 13 May 2014

Documents received

The documents received were as follows:

Document	*Version*	*Date*
Other [Response to conditions of favourable opinion]		28 May 2014
Participant information sheet (PIS) [Clean/Tracked]	2.0	15 May 2014

Approved documents
The final list of approved documentation for the study is therefore as follows:

Document	*Version*	*Date*
Covering letter on headed paper	Lucy Boyle	09 April 2014
GP/consultant information sheets or letters	1.0	08 April 2014

Investigator's brochure / IMP Dossier		11 October 2013
Letter from sponsor		09 April 2014
Other [Response to conditions of favourable opinion]		28 May 2014
Participant consent form	1.0	08 April 2014
Participant information sheet (PIS) [Clean/Tracked]	2.0	15 May 2014
REC Application Form	3.5	08 April 2014
Research protocol or project proposal	1.0	08 April 2014
Summary CV for Chief Investigator (CI)	Professor Middleton	15 May 2012

You should ensure that the sponsor has a copy of the final documentation for the study. It is the sponsor's responsibility to ensure that the documentation is made available to R&D offices at all participating sites.

14/NE/0124 **Please quote this number on all correspondence**

Yours sincerely

H Hendn

Mrs Hayley Henderson
REC Manager

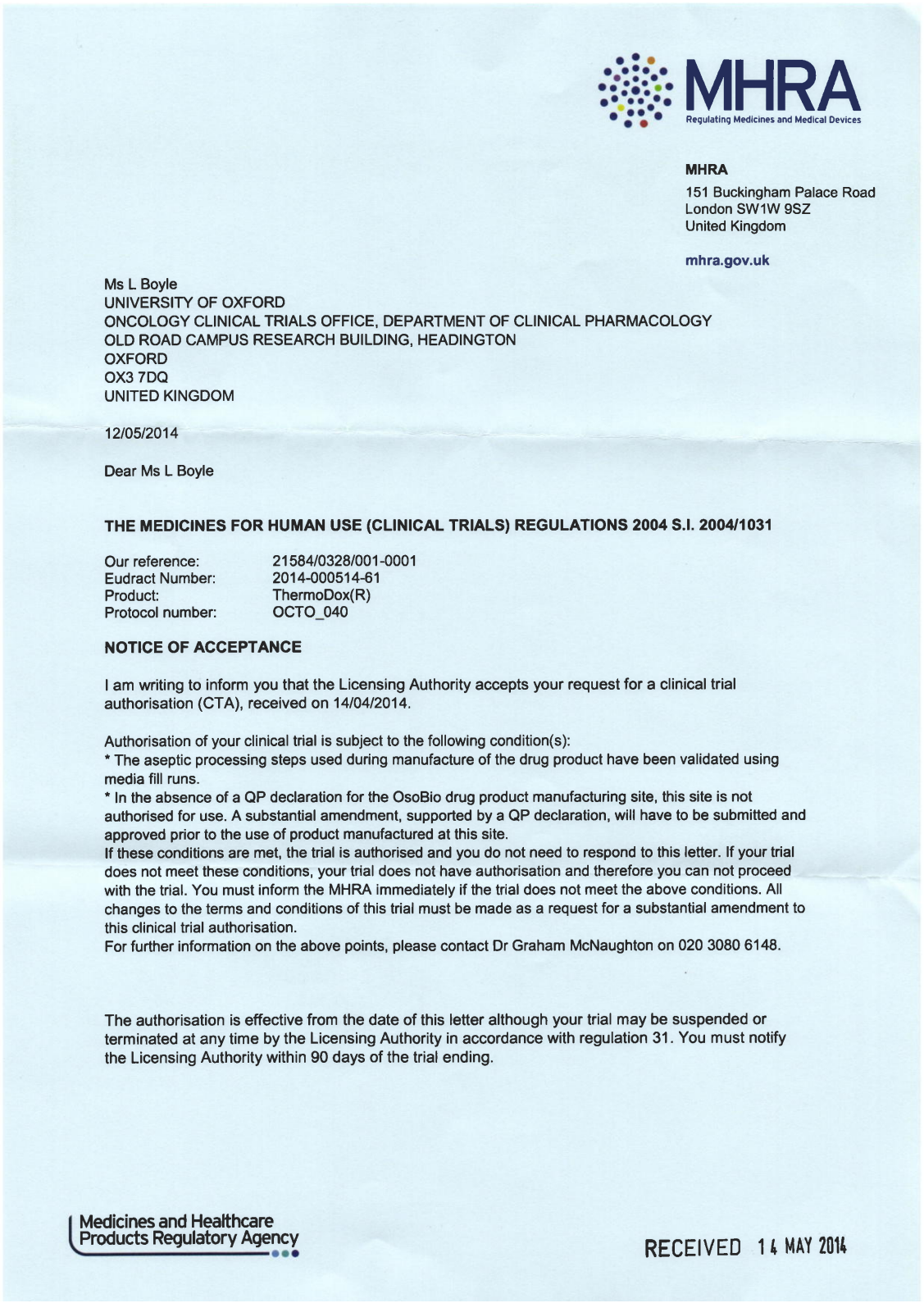
E-mail: nrescommittee.northeast-york@nhs.net

Copy to: Mark Middleton, University of Oxford

Ms Heather House, University of Oxford

A Research Ethics Committee established by the Health Research Authority

5.2.2 Medicines and Healthcare products Regulatory Agency Approvals



MHRA
Regulating Medicines and Medical Devices

MHRA
151 Buckingham Palace Road
London SW1W 9SZ
United Kingdom

mhra.gov.uk

Ms L Boyle
UNIVERSITY OF OXFORD
ONCOLOGY CLINICAL TRIALS OFFICE, DEPARTMENT OF CLINICAL PHARMACOLOGY
OLD ROAD CAMPUS RESEARCH BUILDING, HEADINGTON
OXFORD
OX3 7DQ
UNITED KINGDOM

12/05/2014

Dear Ms L Boyle

THE MEDICINES FOR HUMAN USE (CLINICAL TRIALS) REGULATIONS 2004 S.I. 2004/1031

Our reference:	21584/0328/001-0001
Eudract Number:	2014-000514-61
Product:	ThermoDox(R)
Protocol number:	OCTO_040

NOTICE OF ACCEPTANCE

I am writing to inform you that the Licensing Authority accepts your request for a clinical trial authorisation (CTA), received on 14/04/2014.

Authorisation of your clinical trial is subject to the following condition(s):
* The aseptic processing steps used during manufacture of the drug product have been validated using media fill runs.
* In the absence of a QP declaration for the OsoBio drug product manufacturing site, this site is not authorised for use. A substantial amendment, supported by a QP declaration, will have to be submitted and approved prior to the use of product manufactured at this site.
If these conditions are met, the trial is authorised and you do not need to respond to this letter. If your trial does not meet these conditions, your trial does not have authorisation and therefore you can not proceed with the trial. You must inform the MHRA immediately if the trial does not meet the above conditions. All changes to the terms and conditions of this trial must be made as a request for a substantial amendment to this clinical trial authorisation.
For further information on the above points, please contact Dr Graham McNaughton on 020 3080 6148.

The authorisation is effective from the date of this letter although your trial may be suspended or terminated at any time by the Licensing Authority in accordance with regulation 31. You must notify the Licensing Authority within 90 days of the trial ending.

Medicines and Healthcare Products Regulatory Agency

RECEIVED 14 MAY 2014

MHRA
Regulating Medicines and Medical Devices

Finally, you are reminded that a favourable opinion from the Ethics Committee is also required before this trial can proceed.

Yours sincerely,

Clinical Trials Unit
MHRA

Medicines and Healthcare Products Regulatory Agency

RECEIVED 14 MAY 2014

MHRA
151 Buckingham Palace Road
London SW1W 9SZ
United Kingdom

mhra.gov.uk

Ms L Boyle
UNIVERSITY OF OXFORD
ONCOLOGY CLINICAL TRIALS OFFICE, DEPARTMENT OF CLINICAL PHARMACOLOGY
OLD ROAD CAMPUS RESEARCH BUILDING, HEADINGTON
OXFORD
OX3 7DQ
UNITED KINGDOM

13/05/2016

Dear Ms L Boyle

THE MEDICINES FOR HUMAN USE (CLINICAL TRIALS) REGULATIONS 2004 S.I. 2004/1031

Our Reference:	21584/0328/001-0004
Eudract Number:	2014-000514-61
Product:	ThermoDox(R)
Protocol number:	OCTO_040
Substantial Amendment Code Number:	Code Number: TARDOX_SubsAmend005_14Mar2016
Version: 1.0	
Date: 2016/03/14	

NOTICE OF ACCEPTANCE OF AMENDMENT

I am writing to inform you that the Licensing Authority accepts the proposed amendment to your clinical trial authorisation (CTA), received on 08/04/2016.

Medical point:
Authorisation of your substantial amendment is subject to the following condition(s) and to be submitted at the next IB submission:

- The IB must be clearly stated if there have been any changes to the Reference Safety Information (RSI). In addition, the IB should have a clear RSI. If the RSI is within IB it should be a clearly identified separate section. This section should include a list of 'expected' adverse reactions, e.g. in the form of a table, where all related adverse events (i.e. adverse reactions) are listed by nature and severity including frequency in numbers (see CT1 section 2.3. (32.), CT3 section 7.2.3.2. (51 to 53))
- Information on severity must be provided to the expected table to determine the expectedness and thus SUSAR reporting (see CT-3, paragraph 50). NOTE: Fatal reactions are always unexpected due to the concept of increased severity
- The sponsor should always submit a track changes version of the IB

For further information on the above points, please contact Mrs Hedwig Ganguly on 020 3080 7059 or hedwig.ganguly@mhra.gsi.gov.uk

Medicines and Healthcare Products Regulatory Agency



This amendment may therefore be made.

You are reminded that where it is appropriate, the Ethics Committee should also be notified of amendments.

Yours sincerely,

Clinical Trials Unit
MHRA



5.3 Previous Medical Histories

Patient ID	Diagnosis	Clinical background & Prior treatments
TXA101	2008: Primary HCC / Hepatoma 2008, diffuse multi-lobar, biopsy proven	April 2009, Nemorubicin & Cisplatin. November 2019, Pemetrexed, Cisplatin & PARP inhibitor (A4991014 early phase trial), stopped after having reaction to Cisplatin, surveillance since. Other co-morbidities: Cardiac septal defect repair as child, well-controlled asthma.
TXA102	1996: right-sided grade 2, node positive, ER positive breast cancer	Neoadjuvant FEC x6 and adjuvant Tamoxifen four years. 2001, new left-sided primary tumour, grade 2, ER, PR positive, lymph node negative. Treated with surgery, radiotherapy and adjuvant Arimidex, stopped in 2006. July 2010, relapsed with bone met., started on Exemestane + single fraction of 8 Gy palliative radiotherapy to the right hip. Nov 2011, developed two liver mets. Exemestane changed to Tamoxifen and Alendronic acid commenced. November 2012, radiotherapy to right hip, patient commenced on Faslodex. April 2012, progressive disease in the liver, Faslodex stopped and Capecitabine commenced. Progressive disease to the liver June 2013, Capecitabine stopped. SIRT for liver met. (800 MBq to right hepatic artery and 300 MBq to left hepatic artery) Sept 2013 with good response on MRI scan November 2013. Progression of bone met. on MRI Nov 2013. Denosumab commenced. Megace commenced Dec 2013, discontinued April 2014 due to disease progression. Oral Vinorelbine commenced May 2014, well tolerated at the higher dose of 80 mg/m^2. Elevated CA 15-3.

Table 5.4 – *Continued from previous page*

Patient ID	**Diagnosis**	**Prior Treatment**
TXA103	2011: pT3,pN0,M1 adenocarcinoma of the rectosigmoid junction (KRAS mutation in codon 12)	Anterior resection Dec 2011. Treated with 10 cycles of neoadjuvant Irinotecan and modified de Gramont and Bevacizumab chemotherapy Resection ablation for segment 2 of the liver with RFA to the right-sided lesion. Progressive pulmonary mets. treated with 12 cycles of Irinotecan and modified de Gramont plus Bevacizumab April to September 2013. Further disease progression in May 2014 treated with CAPOX until November 2014 with further progressive progression. March 2015, AZD0424 early phase clinical trial, with progressive disease May 2015. Removed from BAY17437 dose escalation trial (targeted drug targeting intracellular proteins) due to adverse event of extreme headache. Co-morbidities: pulmonary embolus, atrial fibrillation.
TXA104	2013: mCRC (RAS mutant)	1st line 5-FU + Bevacizumab - 18 months. 2nd line Irinotecan + 5-FU x 6 cycles - no response, discontinued May 2015. Residual GU neuropathy. Removed from BAY1238097 - BETI- CID-7 study Sept 2015 due to adverse events of extreme vomiting and headache. Co-morbidities: osteoporosis.
TXA105	2014: mCRC to lung and liver (KRAS mutant)	FOLFOX and FOLFIRI. CT Nov 2015 showed increased hepatic mets with decreased pulmonary mets.
TXB101	Metastatic lung cancer (T2a,N2,M0 SCC), mediastinal lymphadenopathy	1st line - radical chemo-radiotherapy with Cisplatin + Etoposide + 66 Gy 33 fractions. PET showed progression with solitary liver met. in April 2015. 2nd line - Paclitaxel + AZD2014 (TAX-TORC study) gave partial response, stopped after 3 cycles due to residual peripheral neuropathy and diabetes. Co-morbidities: gout, hypertension, hypercholesterolaemia. smoker of 39 pack-years.

Table 5.4 – *Continued from previous page*

Patient ID	**Diagnosis**	**Prior Treatment**
TXB102	mCRC - Dukes C1 carcinoma of sigmoid colon, G2 T4 N2 (10/18 nodes) (KRAS, NRAS, BRAF wild type)	Sigmoid colectomy June 2013. Adjuvant Oxaliplatin + Capecitabine completed Jan 2014, Oxaliplatin omitted from cycle 6 onwards due to severe neuropathy. CT showed disease recurrence with peritoneal mets. and ovarian secondary in August 2014. 1st line palliative chemotherapy FOLFIRI + Cetuximab Oct 2014-Jan 2015. CT showed marked progression in Jan 2015. Extensive proximal deep vein thrombosis excluded use of Bevacizumab. Instead received two cycles of Mytomycin C + Capecitabine, stopped due to progressive disease. Palliative laparotomy and hysterectomy for Krukenburg tumour May 2016. Co-morbidities: ablated Wolf-Parkinson-White, NIDDM, endometrial polyps.
TXB103	mCRC - rectal tumour (KRAS mutation, codon 12) with liver mets.	1st line - Oxaliplatin + 5-FU. Right hemihepatectomy and cholecystectomy Aug 2015, complicated by a pneumothorax, found to have lung secondaries and a new 2cm liver deposit in recovery period. 2nd line - Irinotecan + Capectiabine Nov 2015, with progressive disease at 3 months. 3rd line - Oxaliplatin Feb 2016, 4 cycles before progressive disease. Co-morbidities: pulmonary embolus, deep vein thrombosis following first line of chemotherapy, SVT mesh filter in situ, appendicectomy, c-sections, gestational diabetes, solitary rectal polyp.
TXB104	mCRC (pT4b, N1(1/15), KRAS mutation).	Laparoscopic right hemicolectomy Sept 2013. 1st line - SCOT trial (Oxaliplatin + Capecitabine), 8 cycles completed March 2014. 2nd line - Irinotecan + 5-FU Sept-Dec 2015, 6 cycles. 3rd line - Oxaliplatin + 5-FU March-Dec 2016. Co-morbidities: depression, hypertension, transient ischaemic attack.

Table 5.4: Prior treatment history of the patients who received the study intervention (met.=metastasis, HCC=hepatocellular carcinoma, mCRC=metastatic colorectal cancer, SCC=squamous cell carcinoma, NIDDM=non insulin dependent diabetes).

Bibliography

[1] Forman D. Bray F Ferlay J. SI, Ervik M. Cancer incidence and mortality worldwide. *IARC CancerBase No. 11. Lyon, France: International Agency for Research on Cancer*, 2013.

[2] World Heath Organisation. International agency for research on cancer: Fact sheet, 2012. Jan 2014.

[3] Sunita Padman, Robert Padbury, Carol Beeke, Christos S Karapetis, Sarwan Bishnoi, Amanda R Townsend, Guy Maddern, and Timothy J Price. Liver only metastatic disease in patients with metastatic colorectal cancer: impact of surgery and chemotherapy. *Acta Oncol*, 52(8):1699–706, Nov 2013.

[4] J Ruiterkamp, M F Ernst, L de Munck, M van der Heiden-van der Loo, E Bastiaannet, L V van de Poll-Franse, K Bosscha, V C G Tjan-Heijnen, and A C Voogd. Improved survival of patients with primary distant metastatic breast cancer in the period of 1995-2008. a nationwide population-based study in the netherlands. *Breast Cancer Res Treat*, 128(2):495–503, Jul 2011.

[5] H. J. Wanebo, C. Semoglou, F. Attiyeh, and Jr. Stearns, M. J. Surgical management of patients with primary operable colorectal cancer and synchronous liver metastases. *Am J Surg*, 135(1):81–5, 1978.

[6] J. P. Welch and G. A. Donaldson. The clinical correlation of an autopsy study of recurrent colorectal cancer. *Ann Surg*, 189(4):496–502, 1979.

[7] S Bengmark and L Hafström. The natural history of primary and secondary malignant tumors of the liver. i. the prognosis for patients with hepatic metastases from colonic and rectal carcinoma by laparotomy. *Cancer*, 23(1):198–202, Jan 1969.

[8] B M Jaffe, W L Donegan, F Watson, and J S Spratt, Jr. Factors influencing survival in patients with untreated hepatic metastases. *Surg Gynecol Obstet*, 127(1):1–11, Jul 1968.

[9] R Stangl, A Altendorf-Hofmann, R M Charnley, and J Scheele. Factors influencing the natural history of colorectal liver metastases. *Lancet*, 343(8910):1405–10, Jun 1994.

[10] Evangelos P Misiakos, Nikolaos P Karidis, and Gregory Kouraklis. Current treatment for colorectal liver metastases. *World J Gastroenterol*, 17(36):4067–75, Sep 2011.

[11] O. F. Bathe, I. G. Kaklamanos, F. L. Moffat, J. Boggs, D. Franceschi, and A. S. Livingstone. Metastasectomy as a cytoreductive strategy for treatment of isolated pulmonary and hepatic metastases from breast cancer. *Surg Oncol*, 8(1):35–42, 1999.

[12] G M Clark, G W Sledge, Jr, C K Osborne, and W L McGuire. Survival from first recurrence: relative importance of prognostic factors in 1,015 breast cancer patients. *J Clin Oncol*, 5(1):55–61, Jan 1987.

[13] A Goldhirsch, R D Gelber, and M Castiglione. Relapse of breast cancer after adjuvant treatment in premenopausal and perimenopausal women: patterns and prognoses. *J Clin Oncol*, 6(1):89–97, Jan 1988.

[14] A Insa, A Lluch, F Prosper, I Marugan, A Martinez-Agullo, and J Garcia-Conde. Prognostic factors predicting survival from first recurrence in patients with metastatic breast cancer: analysis of 439 patients. *Breast Cancer Res Treat*, 56(1):67–78, Jul 1999.

[15] S M O'Reilly, M A Richards, and R D Rubens. Liver metastases from breast cancer: the relationship between clinical, biochemical and pathological features and survival. *Eur J Cancer*, 26(5):574–7, 1990.

[16] L Wyld, E Gutteridge, S E Pinder, J J James, S Y Chan, K L Cheung, J F R Robertson, and A J Evans. Prognostic factors for patients with hepatic metastases from breast cancer. *Br J Cancer*, 89(2):284–90, Jul 2003.

[17] Atlanta: American Cancer Society. Cancer facts and figures 2014. *American Cancer Society*, 2014.

[18] L E Quint, S Tummala, L J Brisson, I R Francis, A S Krupnick, E A Kazerooni, M D Iannettoni, R I Whyte, and M B Orringer. Distribution of distant metastases from newly diagnosed non-small cell lung cancer. *Ann Thorac Surg*, 62(1):246–50, Jul 1996.

[19] S G Hilsenbeck, W A Raub, Jr, and K S Sridhar. Prognostic factors in lung cancer based on multivariate analysis. *Am J Clin Oncol*, 16(4):301–9, Aug 1993.

[20] L A Ries. Influence of extent of disease, histology, and demographic factors on lung cancer survival in the seer population-based data. *Semin Surg Oncol*, 10(1):21–30, 1994.

[21] D Max Parkin, Freddie Bray, J Ferlay, and Paola Pisani. Global cancer statistics, 2002. *CA Cancer J Clin*, 55(2):74–108, 2005.

[22] Cancer Research UK. Liver cancer: Cancer statistics, November 2014.

[23] National Cancer Intelligence Network. Trends in incidence of primary liver cancer subtypes, May 2012.

[24] Shahid A Khan, Shireen Emadossadaty, Nimzing G Ladep, Howard C Thomas, Paul Elliott, Simon D Taylor-Robinson, and Mireille B Toledano. Rising trends in cholangiocarcinoma: is the icd classification system misleading us? *J Hepatol*, 56(4):848–54, Apr 2012.

[25] J Rothbarth and C J H van de Velde. Treatment of liver metastases of colorectal cancer. *Ann Oncol*, 16 Suppl 2:ii144–9, 2005.

[26] H Bismuth, R Adam, F Lévi, C Farabos, F Waechter, D Castaing, P Majno, and L Engerran. Resection of nonresectable liver metastases from colorectal cancer after neoadjuvant chemotherapy. *Ann Surg*, 224(4):509–20; discussion 520–2, Oct 1996.

[27] Eren Berber, Robert Pelley, and Allan E Siperstein. Predictors of survival after radiofrequency thermal ablation of colorectal cancer metastases to the liver: a prospective study. *J Clin Oncol*, 23(7):1358–64, Mar 2005.

[28] K S Hughes, R Simon, S Songhorabodi, M A Adson, D M Ilstrup, J G Fortner, B J Maclean, J H Foster, J M Daly, and D Fitzherbert. Resection of the liver for colorectal carcinoma metastases: a multi-institutional study of patterns of recurrence. *Surgery*, 100(2):278–84, Aug 1986.

[29] Y Fong, J Fortner, R L Sun, M F Brennan, and L H Blumgart. Clinical score for predicting recurrence after hepatic resection for metastatic colorectal cancer: analysis of 1001 consecutive cases. *Ann Surg*, 230(3):309–18; discussion 318–21, Sep 1999.

[30] Dominique Elias and Daniela Di Pietroantonio. Surgery for liver metastases from breast cancer. *HPB (Oxford)*, 8(2):97–9, 2006.

[31] Giorgio Ercolani, Matteo Ravaioli, Gian Luca Grazi, Matteo Cescon, Giovanni Varotti, Massimo Del Gaudio, Gaetano Vetrone, Matteo Zanello, Alfonso Principe, and Antonio Daniele Pinna. The role of liver resections for metastases from lung carcinoma. *HPB (Oxford)*, 8(2):114–5, 2006.

[32] N Kemeny and A Schneider. Regional treatment of hepatic metastases and hepatocellular carcinoma. *Curr Probl Cancer*, 13(4):197–283, 1989.

[33] N.P. Doroshow. Modulation of fluorouracil by leucovorin in patients with advanced colorectal cancer: evidence in terms of response rate. advanced colorectal cancer meta-analysis project. *J Clin Oncol*, 10(6):896–903, Jun 1992.

[34] P Piedbois, P Rougier, M Buyse, J Pignon, L Ryan, R Hansen, B Zee, B Weinerman, J Pater, and C Leichman. Efficacy of intravenous continuous infusion of fluorouracil compared with bolus administration in advanced colorectal cancer. meta-analysis group in cancer. *J Clin Oncol*, 16(1):301–8, Jan 1998.

[35] S Barni and M Mandalà. Chemotherapy for metastatic breast cancer. *Ann Oncol*, 16 Suppl 4:iv23–27, May 2005.

[36] R Fossati, C Confalonieri, V Torri, E Ghislandi, A Penna, V Pistotti, A Tinazzi, and A Liberati. Cytotoxic and hormonal treatment for metastatic breast cancer: a systematic review of published randomized trials involving 31,510 women. *J Clin Oncol*, 16(10):3439–60, Oct 1998.

[37] S Peters, A A Adjei, C Gridelli, M Reck, K Kerr, E Felip, and ESMO Guidelines Working Group. Metastatic non-small-cell lung cancer (nsclc): Esmo clinical practice guidelines for diagnosis, treatment and follow-up. *Ann Oncol*, 23 Suppl 7:vii56–64, Oct 2012.

[38] Josep M Llovet, Andrew Burroughs, and Jordi Bruix. Hepatocellular carcinoma. *Lancet*, 362(9399):1907–17, Dec 2003.

[39] Jordi Bruix, Morris Sherman, and Practice Guidelines Committee, American Association for the Study of Liver Diseases. Management of hepatocellular carcinoma. *Hepatology*, 42(5):1208–36, Nov 2005.

[40] J Bruix, M Sherman, J M Llovet, M Beaugrand, R Lencioni, A K Burroughs, E Christensen, L Pagliaro, M Colombo, J Rodés, and EASL Panel of Experts on HCC. Clinical management of hepatocellular carcinoma. conclusions of the barcelona-2000 easl conference. european association for the study of the liver. *J Hepatol*, 35(3):421–30, Sep 2001.

[41] Josep M Llovet, Sergio Ricci, Vincenzo Mazzaferro, Philip Hilgard, Edward Gane, Jean-Frédéric Blanc, Andre Cosme de Oliveira, Armando Santoro, Jean-Luc Raoul, Alejandro Forner, Myron Schwartz, Camillo Porta, Stefan Zeuzem, Luigi Bolondi, Tim F Greten, Peter R Galle, Jean-François Seitz, Ivan Borbath, Dieter Häussinger, Tom Giannaris, Minghua Shan, Marius Moscovici, Dimitris Voliotis, Jordi Bruix, and SHARP Investigators Study Group. Sorafenib in advanced hepatocellular carcinoma. *N Engl J Med*, 359(4):378–90, Jul 2008.

[42] National Institute for Health and Care Excellence. Sorafenib for the treatment of advanced hepatocellular carcinoma, May 2010.

[43] D H Palmer, S A Hussain, A J Smith, S Hargreaves, Y T Ma, D Hull, P J Johnson, and P J Ross. Sorafenib for advanced hepatocellular carcinoma (hcc): impact of rationing in the united kingdom. *Br J Cancer*, 109(4):888–90, Aug 2013.

[44] M P Coleman, G Gatta, A Verdecchia, J Estève, M Sant, H Storm, C Allemani, L Ciccolallo, M Santaquilani, F Berrino, and EUROCARE Working Group. Eurocare-3 summary: cancer survival in europe at the end of the 20th century. *Ann Oncol*, 14 Suppl 5:v128–49, 2003.

[45] J W Valle, H Wasan, P Johnson, E Jones, L Dixon, R Swindell, S Baka, A Maraveyas, P Corrie, S Falk, S Gollins, F Lofts, L Evans, T Meyer, A Anthoney, T Iveson, M Highley, R Osborne, and J Bridgewater. Gemcitabine alone or in combination with cisplatin in patients with advanced or metastatic cholangiocarcinomas or other biliary tract tumours: a multicentre randomised phase ii study - the uk abc-01 study. *Br J Cancer*, 101(4):621–7, Aug 2009.

[46] David Li, Josephine Kang, Benjamin J Golas, Vincent W Yeung, and David C Madoff. Minimally invasive local therapies for liver cancer. *Cancer Biol Med*, 11(4):217–36, Dec 2014.

[47] Vincent L Flanders and Debra A Gervais. Ablation of liver metastases: current status. *J Vasc Interv Radiol*, 21(8 Suppl):S214–22, Aug 2010.

[48] L Solbiati, T Livraghi, S N Goldberg, T Ierace, F Meloni, M Dellanoce, L Cova, E F Halpern, and G S Gazelle. Percutaneous radio-frequency ablation of hepatic metastases from colorectal cancer: long-term results in 117 patients. *Radiology*, 221(1):159–66, Oct 2001.

[49] Richard M Goldberg, Daniel J Sargent, Roscoe F Morton, Charles S Fuchs, Ramesh K Ramanathan, Stephen K Williamson, Brian P Findlay, Henry C Pitot, and Steven R Alberts. A randomized controlled trial of fluorouracil plus leucovorin, irinotecan, and oxaliplatin combinations in patients with previously untreated metastatic colorectal cancer. *J Clin Oncol*, 22(1):23–30, Jan 2004.

[50] S Giacchetti, M Itzhaki, G Gruia, R Adam, R Zidani, F Kunstlinger, S Brienza, E Alafaci, F Bertheault-Cvitkovic, C Jasmin, M Reynes, H Bismuth, J L Misset, and F Lévi. Long-term survival of patients with unresectable colorectal cancer liver metastases following infusional chemotherapy with 5-fluorouracil, leucovorin, oxaliplatin and surgery. *Ann Oncol*, 10(6):663–9, Jun 1999.

[51] Tito Livraghi, Luigi Solbiati, Franca Meloni, Tiziana Ierace, S Nahum Goldberg, and G Scott Gazelle. Percutaneous radiofrequency ablation of liver metastases in potential candidates for resection: the "test-of-time approach". *Cancer*, 97(12):3027–35, Jun 2003.

[52] Heather Higgins and David L Berger. Rfa for liver tumors: does it really work? *Oncologist*, 11(7):801–8, 2006.

[53] E Berber and A E Siperstein. Perioperative outcome after laparoscopic radiofrequency ablation of liver tumors: an analysis of 521 cases. *Surg Endosc*, 21(4):613–8, Apr 2007.

[54] A. R. Gillams and W. R. Lees. Five-year survival in 309 patients with colorectal liver metastases treated with radiofrequency ablation. *Eur Radiol*, 19(5):1206–13, 2009.

[55] J K Seifert and D L Morris. Prognostic factors after cryotherapy for hepatic metastases from colorectal cancer. *Ann Surg*, 228(2):201–8, Aug 1998.

[56] Albert A Nemcek. Complications of radiofrequency ablation of neoplasms. *Semin Intervent Radiol*, 23(2):177–87, Jun 2006.

[57] Shirley Yuk-Wah Liu, Kit-Fai Lee, and Paul Bo-San Lai. Needle track seeding: a real hazard after percutaneous radiofrequency ablation for colorectal liver metastasis. *World J Gastroenterol*, 15(13):1653–5, Apr 2009.

[58] Giuseppe Cabibbo and Antonio Craxì. Needle track seeding following percutaneous procedures for hepatocellular carcinoma. *World J Hepatol*, 1(1):62–6, Oct 2009.

[59] Nishant Kumar, Ron C Gaba, M Grace Knuttinen, Benedictta O Omene, Brandon K Martinez, Charles A Owens, and James T Bui. Tract seeding following radiofrequency ablation for hepatocellular carcinoma: prevention, detection, and management. *Semin Intervent Radiol*, 28(2):187–92, Jun 2011.

[60] Tito Livraghi, Luigi Solbiati, M Franca Meloni, G Scott Gazelle, Elkan F Halpern, and S Nahum Goldberg. Treatment of focal liver tumors with percutaneous radio-frequency ablation: complications encountered in a multicenter study. *Radiology*, 226(2):441–51, Feb 2003.

[61] T Ruers, C Punt, F Van Coevorden, J P E N Pierie, I Borel-Rinkes, J A Ledermann, G Poston, W Bechstein, M A Lentz, M Mauer, E Van Cutsem, M P Lutz, B Nordlinger, and EORTC Gastro-Intestinal Tract Cancer Group, Arbeitsgruppe Lebermetastasen und—tumoren in der Chirurgischen Arbeitsgemeinschaft Onkologie (ALM-CAO) and the National Cancer Research Institute Colorectal Clinical Study Group (NCRI CCSG). Radiofrequency ablation combined with systemic treatment versus systemic treatment alone in patients with non-resectable colorectal liver metastases: a randomized eortc intergroup phase ii study (eortc 40004). *Ann Oncol*, 23(10):2619–26, Oct 2012.

[62] T Lorentzen, B O Skjoldbye, and C P Nolsoe. Microwave ablation of liver metastases guided by contrast-enhanced ultrasound: experience with 125 metastases in 39 patients. *Ultraschall Med*, 32(5):492–6, Oct 2011.

[63] Ryan T Groeschl, Charles H C Pilgrim, Erin M Hanna, Kerri A Simo, Ryan Z Swan, David Sindram, John B Martinie, David A Iannitti, Mark Bloomston, Carl Schmidt, Hooman Khabiri, Lawrence A Shirley, Robert C G Martin, Susan Tsai, Kiran K Turaga, Kathleen K Christians, William S Rilling, and T Clark Gamblin. Microwave ablation for hepatic malignancies: a multiinstitutional analysis. *Ann Surg*, 259(6):1195–200, Jun 2014.

[64] Tito Livraghi, Franca Meloni, Luigi Solbiati, Giorgio Zanus, and Collaborative Italian Group using AMICA system. Complications of microwave ablation for liver tumors: results of a multicenter study. *Cardiovasc Intervent Radiol*, 35(4):868–74, Aug 2012.

[65] Robert C G Martin, Charles R Scoggins, and Kelly M McMasters. Safety and efficacy of microwave ablation of hepatic tumors: a prospective review of a 5-year experience. *Ann Surg Oncol*, 17(1):171–8, Jan 2010.

[66] ClinicalTrials.gov. Resection versus microwave ablation for resectable colorectal cancer liver metastases, 2016.

[67] J L McCall, M W Booth, and D L Morris. Hepatic cryotherapy for metastatic liver tumours. *Br J Hosp Med*, 54(8):378–81, 1995.

[68] C K Leow, W Y Lau, and A K Li. Cryoablation of unresectable malignant liver tumors. *Am J Surg*, 172(5):607, Nov 1996.

[69] A J Sheen, G J Poston, and D J Sherlock. Cryotherapeutic ablation of liver tumours. *Br J Surg*, 89(11):1396–401, Nov 2002.

[70] Tom Mala. Cryoablation of liver tumours – a review of mechanisms, techniques and clinical outcome. *Minim Invasive Ther Allied Technol*, 15(1):9–17, 2006.

[71] C Tellez, A B Benson, 3rd, M T Lyster, M Talamonti, J Shaw, M A Braun, A A Nemcek, Jr, and R L Vogelzang. Phase ii trial of chemoembolization for the treatment of metastatic colorectal carcinoma to the liver and review of the literature. *Cancer*, 82(7):1250–9, Apr 1998.

[72] C Breedis and G Young. The blood supply of neoplasms in the liver. *Am J Pathol*, 30(5):969–77, 1954.

[73] V P Chuang and S Wallace. Hepatic artery embolization in the treatment of hepatic neoplasms. *Radiology*, 140(1):51–8, Jul 1981.

[74] M E Clouse, R G Lee, E J Duszlak, J J Lokich, C Trey, M R Alday, D C Yoburn, J Diamond, A W Crosson, and P Costello. Peripheral hepatic artery embolization for primary and secondary hepatic neoplasms. *Radiology*, 147(2):407–11, May 1983.

[75] R S Stubbs and S K Wickremesekera. Selective internal radiation therapy (sirt): a new modality for treating patients with colorectal liver metastases. *HPB (Oxford)*, 6(3):133–9, 2004.

[76] Belen Gil-Alzugaray, Ana Chopitea, Mercedes Iñarrairaegui, Jose I Bilbao, Macarena Rodriguez-Fraile, Javier Rodriguez, Alberto Benito, Inés Dominguez, Delia D'Avola, Jose I Herrero, Jorge Quiroga, Jesus Prieto, and Bruno Sangro. Prognostic factors and prevention of radioembolization-induced liver disease. *Hepatology*, 57(3):1078–87, Mar 2013.

[77] Bruno Sangro, Belen Gil-Alzugaray, Javier Rodriguez, Iosu Sola, Antonio Martinez-Cuesta, Antonio Viudez, Ana Chopitea, Mercedes Iñarrairaegui, Javier Arbizu, and Jose I Bilbao. Liver disease induced by radioembolization of liver tumors: description and possible risk factors. *Cancer*, 112(7):1538–46, Apr 2008.

[78] Michael B Pitton, Roman Kloeckner, Christian Ruckes, Gesine M Wirth, Waltraud Eichhorn, Marcus A Wörns, Arndt Weinmann, Mathias Schreckenberger, Peter R Galle, Gerd Otto, and Christoph Dueber. Randomized comparison of selective internal radiotherapy (sirt) versus drug-eluting bead transarterial chemoembolization (deb-tace) for the treatment of hepatocellular carcinoma. *Cardiovasc Intervent Radiol*, 38(2):352–60, Apr 2015.

[79] ClinicalTrials.gov. Folfox6m plus sir-spheres microspheres vs folfox6m alone in patients with liver mets from primary colorectal cancer (foxfireglobal), Oct 2012.

[80] Stephen J Beebe, Paula M Fox, Laura J Rec, E Lauren K Willis, and Karl H Schoenbach. Nanosecond, high-intensity pulsed electric fields induce apoptosis in human cells. *FASEB J*, 17(11):1493–5, Aug 2003.

[81] Robert C G Martin, 2nd, Kelli McFarland, Susan Ellis, and Vic Velanovich. Irreversible electroporation in locally advanced pancreatic cancer: potential improved overall survival. *Ann Surg Oncol*, 20 Suppl 3:S443–9, Dec 2013.

[82] Govindarajan Narayanan and Mehul H Doshi. Irreversible electroporation (ire) in renal tumors. *Curr Urol Rep*, 17(2):15, Feb 2016.

[83] Vincenza Granata, Elisabetta de Lutio di Castelguidone, Roberta Fusco, Orlando Catalano, Mauro Piccirillo, Raffaele Palaia, Francesco Izzo, Adolfo D'Errico Gallipoli, and Antonella Petrillo. Irreversible electroporation of hepatocellular carcinoma: preliminary report on the diagnostic accuracy of magnetic resonance, computer tomography, and contrast-enhanced ultrasound in evaluation of the ablated area. *Radiol Med*, 121(2):122–31, Feb 2016.

[84] Christine Ball, Kenneth R Thomson, and Helen Kavnoudias. Irreversible electroporation: a new challenge in "out of operating theater" anesthesia. *Anesth Analg*, 110(5):1305–9, May 2010.

[85] Joern Wulf, Matthias Guckenberger, Ulrich Haedinger, Ulrich Oppitz, Gerd Mueller, Kurt Baier, and Michael Flentje. Stereotactic radiotherapy of primary liver cancer and hepatic metastases. *Acta Oncol*, 45(7):838–47, 2006.

[86] Karyn A Goodman, Ellen A Wiegner, Katherine E Maturen, Zhigang Zhang, Qianxing Mo, George Yang, Iris C Gibbs, George A Fisher, and Albert C Koong. Dose-escalation study of single-fraction stereotactic body radiotherapy for liver malignancies. *Int J Radiat Oncol Biol Phys*, 78(2):486–93, Oct 2010.

[87] Alexander Kirichenko, Olivier Gayou, David Parda, Vijay Kudithipudi, Kusum Tom, Akhtar Khan, Peter Abrams, Molly Szramowski, Jose Oliva, Dulabh Monga, Moses Raj, and Ngoc Thai. Stereotactic body radiotherapy (sbrt) with or without surgery for primary and metastatic liver tumors. *HPB (Oxford)*, 18(1):88–97, Jan 2016.

[88] Jason Chia-Hsien Cheng, Jian-Kuen Wu, Chao-Ming Huang, Hua-Shan Liu, David Y Huang, Skye Honguin Cheng, Stella Y Tsai, James Jer-Min Jian, Yu-Mong Lin, Tsun-I Cheng, Cheng-Fang Horng, and Andrew T Huang. Radiation-induced liver disease after three-dimensional conformal radiotherapy for patients with hepatocellular carcinoma: dosimetric analysis and implication. *Int J Radiat Oncol Biol Phys*, 54(1):156–62, Sep 2002.

[89] Charlie C Pan, Brian D Kavanagh, Laura A Dawson, X Allen Li, Shiva K Das, Moyed Miften, and Randall K Ten Haken. Radiation-associated liver injury. *Int J Radiat Oncol Biol Phys*, 76(3 Suppl):S94–100, Mar 2010.

[90] C K Holland and R E Apfel. Thresholds for transient cavitation produced by pulsed ultrasound in a controlled nuclei environment. *J Acoust Soc Am*, 88(5):2059–69, Nov 1990.

[91] C. C. Coussios, C. H. Farny, G. T. Haar, and R. A. Roy. Role of acoustic cavitation in the delivery and monitoring of cancer treatment by high-intensity focused ultrasound (hifu). *Int J Hyperthermia*, 23(2):105–20, 2007.

[92] T Leighton. *The acoustic bubble*. Academic press, 2012.

[93] E. S. Ebbini and G. Ter Haar. Ultrasound-guided therapeutic focused ultrasound: Current status and future directions. *Int J Hyperthermia*, 31(2):77–89, 2015.

[94] C D Kowal and J R Bertino. Possible benefits of hyperthermia to chemotherapy. *Cancer Res*, 39(6 Pt 2):2285–9, Jun 1979.

[95] T Feyerabend, R Steeves, G J Wiedemann, E Richter, and H I Robins. Rationale and clinical status of local hyperthermia, radiation, and chemotherapy in locally advanced malignancies. *Anticancer Res*, 17(4B):2895–7, 1997.

[96] T S Herman and B A Teicher. Summary of studies adding systemic chemotherapy to local hyperthermia and radiation. *Int J Hyperthermia*, 10(3):443–9, 1994.

[97] M H Falk and R D Issels. Hyperthermia in oncology. *Int J Hyperthermia*, 17(1):1–18, 2001.

[98] P Wust, B Hildebrandt, G Sreenivasa, B Rau, J Gellermann, H Riess, R Felix, and P M Schlag. Hyperthermia in combined treatment of cancer. *Lancet Oncol*, 3(8):487–97, Aug 2002.

[99] Wei Rao, Zhong-Shan Deng, and Jing Liu. A review of hyperthermia combined with radiotherapy/chemotherapy on malignant tumors. *Crit Rev Biomed Eng*, 38(1):101–16, 2010.

[100] S. Dromi, V. Frenkel, A. Luk, B. Traughber, M. Angstadt, M. Bur, J. Poff, J. Xie, S. K. Libutti, K. C. Li, and B. J. Wood. Pulsed-high intensity focused ultrasound and low temperature-sensitive liposomes for enhanced targeted drug delivery and antitumor effect. *Clin Cancer Res*, 13(9):2722–7, 2007.

[101] Tove J Evjen, Eirik Hagtvet, Alexei Moussatov, Sibylla Røgnvaldsson, Jean-Louis Mestas, R Andrew Fowler, Cyril Lafon, and Esben A Nilssen. In vivo monitoring of liposomal release in tumours following ultrasound stimulation. *Eur J Pharm Biopharm*, 84(3):526–31, Aug 2013.

[102] J. J. Choi, R. C. Carlisle, C. Coviello, L. Seymour, and C. C. Coussios. Non-invasive and real-time passive acoustic mapping of ultrasound-mediated drug delivery. *Phys Med Biol*, 59(17):4861–77, 2014.

[103] Susan M Graham, Robert Carlisle, James J Choi, Mark Stevenson, Apurva R Shah, Rachel S Myers, Kerry Fisher, Miriam-Bazan Peregrino, Len Seymour, and Constantin C Coussios. Inertial cavitation to non-invasively trigger and monitor intratumoral release of drug from intravenously delivered liposomes. *J Control Release*, 178:101–7, Mar 2014.

[104] Tong Li, Hong Chen, Tatiana Khokhlova, Yak-Nam Wang, Wayne Kreider, Xuemei He, and Joo Ha Hwang. Passive cavitation detection during pulsed hifu exposures of ex vivo tissues and in vivo mouse pancreatic tumors. *Ultrasound Med Biol*, 40(7):1523–34, Jul 2014.

[105] Alison Burgess, Kairavi Shah, Olivia Hough, and Kullervo Hynynen. Focused ultrasound-mediated drug delivery through the blood-brain barrier. *Expert Rev Neurother*, 15(5):477–91, May 2015.

[106] Christopher J Harvey, James M Pilcher, Robert J Eckersley, Martin J K Blomley, and David O Cosgrove. Advances in ultrasound. *Clin Radiol*, 57(3):157–77, Mar 2002.

[107] Burov AK. High-intensity ultrasonic vibrations for action on animal and human malignant tumours. *Dokl Akad Nauk SSSR*, (106):239–41, 1956.

[108] S. Madersbacher and M. Marberger. *Therapeutic applications of ultrasound in urology.*, pages 115–136. Oxford: ISIS, marberger m. edition, 1995.

[109] F. J. Fry and L. K. Johnson. Tumor irradiation with intense ultrasound. *Ultrasound Med Biol*, 4(4):337–41, 1978.

[110] R. Yang, C. R. Reilly, F. J. Rescorla, P. R. Faught, N. T. Sanghvi, F. J. Fry, Jr. Franklin, T. D., L. Lumeng, and J. L. Grosfeld. High-intensity focused ultrasound in the treatment of experimental liver cancer. *Arch Surg*, 126(8):1002–9; discussion 1009–10, 1991.

[111] J. Y. Chapelon, J. Margonari, F. Vernier, F. Gorry, R. Ecochard, and A. Gelet. In vivo effects of high-intensity ultrasound on prostatic adenocarcinoma dunning r3327. *Cancer Res*, 52(22):6353–7, 1992.

[112] Stephen Goss and Francis J. Fry. The effect of high intensity ultrasonic irradiation on tumor growth. *Sonics and Ultrasonics, IEEE Transactions on*, 31(5):491–496 0018–9537, 1984.

[113] G. O. Oosterhof, E. B. Cornel, G. A. Smits, F. M. Debruyne, and J. A. Schalken. Influence of high-intensity focused ultrasound on the development of metastases. *Eur Urol*, 32(1):91–5, 1997.

[114] A. Gelet and JY. Chapelon. *Effects of high-intensity focused ultrasound on malignant cells and tissues*, pages 107–114. Oxford: ISIS, marberger m. edition, 1995.

[115] Martijn Hmgm den Brok, Roger P. M. Sutmuller, Robbert van der Voort, Erik J. Bennink, Carl G. Figdor, Theo J. M. Ruers, and Gosse J. Adema. In situ tumor ablation creates an antigen source for the generation of antitumor immunity. *Cancer research*, 64(11):4024–4029

[116] Z. Hu, X. Y. Yang, Y. Liu, M. A. Morse, H. K. Lyerly, T. M. Clay, and P. Zhong. Release of endogenous danger signals from hifu-treated tumor cells and their stimulatory effects on apcs. *Biochem Biophys Res Commun*, 335(1):124–31, 2005.

[117] Z. Hu, X. Y. Yang, Y. Liu, G. N. Sankin, E. C. Pua, M. A. Morse, H. K. Lyerly, T. M. Clay, and P. Zhong. Investigation of hifu-induced anti-tumor immunity in a murine tumor model. *J Transl Med*, 5:34, 2007.

[118] F. Wu, Z. B. Wang, P. Lu, Z. L. Xu, W. Z. Chen, H. Zhu, and C. B. Jin. Activated anti-tumor immunity in cancer patients after high intensity focused ultrasound ablation. *Ultrasound Med Biol*, 30(9):1217–22, 2004.

[119] Z. L. Xu, X. Q. Zhu, P. Lu, Q. Zhou, J. Zhang, and F. Wu. Activation of tumor-infiltrating antigen presenting cells by high intensity focused ultrasound ablation of human breast cancer. *Ultrasound Med Biol*, 35(1):50–7, 2009.

[120] Rebecca Waitz and Stephen B Solomon. Can local radiofrequency ablation of tumors generate systemic immunity against metastatic disease? *Radiology*, 251(1):1–2, Apr 2009.

[121] Christopher Bastianpillai, Neophytos Petrides, Taimur Shah, Stephanie Guillaumier, Hashim U Ahmed, and Manit Arya. Harnessing the immunomodulatory effect of thermal and non-thermal ablative therapies for cancer treatment. *Tumour Biol*, 36(12):9137–46, Dec 2015.

[122] Carmel Mothersill and Colin B Seymour. Radiation-induced bystander effects–implications for cancer. *Nat Rev Cancer*, 4(2):158–64, Feb 2004.

[123] Joseph M Kaminski, Eric Shinohara, James Bradley Summers, Kenneth J Niermann, Allan Morimoto, and Jeffrey Brousal. The controversial abscopal effect. *Cancer Treat Rev*, 31(3):159–72, May 2005.

[124] Peter J Wersäll, Henric Blomgren, Pavel Pisa, Ingmar Lax, Karl-Mikael Kälkner, and Christer Svedman. Regression of non-irradiated metastases after extracranial stereotactic radiotherapy in metastatic renal cell carcinoma. *Acta Oncol*, 45(4):493–7, 2006.

[125] Shankar Siva, Michael P MacManus, Roger F Martin, and Olga A Martin. Abscopal effects of radiation therapy: a clinical review for the radiobiologist. *Cancer Lett*, 356(1):82–90, Jan 2015.

[126] Jan T Poleszczuk, Kimberly A Luddy, Sotiris Prokopiou, Mark Robertson-Tessi, Eduardo G Moros, Mayer Fishman, Julie Y Djeu, Steven E Finkelstein, and Heiko Enderling. Abscopal benefits of localized radiotherapy depend on activated t-cell trafficking and distribution between metastatic lesions. *Cancer Res*, 76(5):1009–18, Mar 2016.

[127] D. Cranston. A review of high intensity focused ultrasound in relation to the treatment of renal tumours and other malignancies. *Ultrason Sonochem*, 27:654–8, 2015.

[128] F. Wu, Z. B. Wang, W. Z. Chen, W. Wang, Y. Gui, M. Zhang, G. Zheng, Y. Zhou, G. Xu, M. Li, C. Zhang, H. Ye, and R. Feng. Extracorporeal high intensity focused ultrasound ablation in the treatment of 1038 patients with solid carcinomas in china: an overview. *Ultrason Sonochem*, 11(3-4):149–54, 2004.

[129] R. O. Illing, J. E. Kennedy, F. Wu, G. R. ter Haar, A. S. Protheroe, P. J. Friend, F. V. Gleeson, D. W. Cranston, R. R. Phillips, and M. R. Middleton. The safety and feasibility of extracorporeal high-intensity focused ultrasound (hifu) for the treatment of liver and kidney tumours in a western population. *Br J Cancer*, 93(8):890–5, 2005.

[130] Islam Ahmed Shehata. Treatment with high intensity focused ultrasound: secrets revealed. *Eur J Radiol*, 81(3):534–41, Mar 2012.

[131] T A Leslie, J E Kennedy, R O Illing, G R Ter Haar, F Wu, R R Phillips, P J Friend, I S D Roberts, D W Cranston, and M R Middleton. High-intensity focused ultrasound ablation of liver tumours: can radiological assessment predict the histological response? *Br J Radiol*, 81(967):564–71, Jul 2008.

[132] ClinicalTrials.gov. A proof of concept study to investigate the feasibility of targeted release of doxorubicin from lyso-thermosensitive liposomal (ltsl) doxorubicin (thermodox®) using focused ultrasound in patients with primary or secondary liver tumours, 2014.

[133] L. A. Frizzell, C. A. Linke, E. L. Carstensen, and C. W. Fridd. Thresholds for focal ultrasonic lesions in rabbit kidney, liver, and testicle. *Biomedical Engineering, IEEE Transactions on*, (4):393–396 0018–9294, 1977.

[134] E. L. Carstensen, M. W. Miller, and C. A. Linke. Biological effects of ultrasound. *Journal of Biological Physics*, 2(4):173–192, 1974.

[135] K J Taylor and C C Connolly. Differing hepatic lesions caused by the same dose of ultrasound. *J Pathol*, 98(4):291–3, Aug 1969.

[136] S Q Cheng, X D Zhou, Z Y Tang, Y Yu, H Z Wang, S S Bao, and D C Qian. High-intensity focused ultrasound in the treatment of experimental liver tumour. *J Cancer Res Clin Oncol*, 123(4):219–23, 1997.

[137] G. Vallancien, D. Chopin, C. Davila, B. Guiillonneau, E. Perreira, B. Veillon, J. M. Brisset, and J. Andre-Bougaran. [focused extracorporeal pyrotherapy. initial experimental results]. *Prog Urol*, 1(1):149–53, 1991.

[138] G. Vallancien, M. Harouni, B. Veillon, A. Mombet, D. Prapotnich, J. M. Brisset, and J. Bougaran. Focused extracorporeal pyrotherapy: feasibility study in man. *Journal of Endourology*, 6(2):173–181

[139] R Yang, N T Sanghvi, F J Rescorla, C A Galliani, F J Fry, S L Griffith, and J L Grosfeld. Extracorporeal liver ablation using sonography-guided high-intensity focused ultrasound. *Invest Radiol*, 27(10):796–803, Oct 1992.

[140] F Prat, M Centarti, A Sibille, F A Abou el Fadil, L Henry, J Y Chapelon, and D Cathignol. Extracorporeal high-intensity focused ultrasound for vx2 liver tumors in the rabbit. *Hepatology*, 21(3):832–6, Mar 1995.

[141] A Sibille, F Prat, J Y Chapelon, F abou el Fadil, L Henry, Y Theilliere, T Ponchon, and D Cathignol. Characterization of extracorporeal ablation of normal and tumor-bearing liver tissue by high intensity focused ultrasound. *Ultrasound Med Biol*, 19(9):803–13, 1993.

[142] A. G. Visioli, I. H. Rivens, G. R. Ter Haar, A. Horwich, R. A. Huddart, E. Moskovic, A. Padhani, and J. Glees. Preliminary results of a phase i dose escalation clinical trial using focused ultrasound in the treatment of localised tumours. *European journal of ultrasound*, 9(1):11–18 1999.

[143] G. ter Haar, D. Sinnett, and I. Rivens. High intensity focused ultrasound-a surgical technique for the treatment of discrete liver tumours. *Physics in medicine and biology*, 34(11):1743 1989.

[144] S. Vaezy, X. Shi, R. W. Martin, E. Chi, P. I. Nelson, M. R. Bailey, and L. A. Crum. Real-time visualization of high-intensity focused ultrasound treatment using ultrasound imaging. *Ultrasound Med Biol*, 27(1):33–42, 2001.

[145] S. N. Goldberg, C. J. Grassi, J. F. Cardella, J. W. Charboneau, 3rd Dodd, G. D., D. E. Dupuy, D. A. Gervais, A. R. Gillams, R. A. Kane, Jr. Lee, F. T., T. Livraghi, J. McGahan, D. A. Phillips, H. Rhim, S. G. Silverman, L. Solbiati, T. J. Vogl, B. J. Wood, S. Vedantham, D. Sacks, Committee Society of Interventional Radiology Technology Assessment, and Ablation the International Working Group on Image-guided Tumor. Image-guided tumor ablation: standardization of terminology and reporting criteria. *J Vasc Interv Radiol*, 20(7 Suppl):S377–90, 2009.

[146] Doron Kopelman, Yael Inbar, Arik Hanannel, Gillian Dank, David Freundlich, Azriel Perel, David Castel, Adrian Greenfeld, Tal Salomon, Merab Sareli, Adrian Valeanu, and Moshe Papa. Magnetic resonance-guided focused ultrasound surgery (mrgfus). four ablation treatments of a single canine hepatocellular adenoma. *HPB (Oxford)*, 8(4):292–8, 2006.

[147] Doron Kopelman, Yael Inbar, Arik Hanannel, David Freundlich, David Castel, Azriel Perel, Adrian Greenfeld, Tal Salamon, Merab Sareli, Adrian Valeanu, and Moshe Papa. Magnetic resonance-guided focused ultrasound surgery (mrgfus): ablation of liver tissue in a porcine model. *Eur J Radiol*, 59(2):157–62, Aug 2006.

[148] D. R. Daum, N. B. Smith, R. King, and K. Hynynen. In vivo demonstration of noninvasive thermal surgery of the liver and kidney using an ultrasonic phased array. *Ultrasound Med Biol*, 25(7):1087–98, 1999.

[149] D. R. Daum, M. T. Buchanan, T. Fjield, and K. Hynynen. Design and evaluation of a feedback based phased array system for ultrasound surgery. *IEEE Trans Ultrason Ferroelectr Freq Control*, 45(2):431–8, 1998.

[150] R. J. McGough, M. L. Kessler, E. S. Ebbini, and C. A. Cain. Treatment planning for hyperthermia with ultrasound phased arrays. *IEEE Transactions on Ultrasonics, Ferroelectrics, and Frequency Control*, 43(6):1074–1084, Nov 1996.

[151] Y Y Botros, E S Ebbini, and J L Volakis. Two-step hybrid virtual array ray (var) technique for focusing through the rib cage. *IEEE Trans Ultrason Ferroelectr Freq Control*, 45(4):989–1000, 1998.

[152] Y Y Botros, J L Volakis, P VanBaren, and E S Ebbini. A hybrid computational model for ultrasound phased-array heating in presence of strongly scattering obstacles. *IEEE Trans Biomed Eng*, 44(11):1039–50, Nov 1997.

[153] R. Ritchie, J. Collin, C. Coussios, and T. Leslie. Attenuation and de-focusing during high-intensity focused ultrasound therapy through peri-nephric fat. *Ultrasound Med Biol*, 39(10):1785–93, 2013.

[154] L. Chen, G. ter Haar, C. R. Hill, M. Dworkin, P. Carnochan, H. Young, and J. P. Bensted. Effect of blood perfusion on the ablation of liver parenchyma with high-intensity focused ultrasound. *Phys Med Biol*, 38(11):1661–73, 1993.

[155] R. W. Ritchie, T. Leslie, R. Phillips, F. Wu, R. Illing, G. ter Haar, A. Protheroe, and D. Cranston. Extracorporeal high intensity focused ultrasound for renal tumours: a 3-year follow-up. *BJU Int*, 106(7):1004–9, 2010.

[156] Kennedy J.E. *An Assessment of the Capacity of High-Intensity Focused Ultrasound to Treat Tumours of the Liver and Kidney*. PhD thesis, University of Oxford, 2004.

[157] S. Ellis, V. Rieke, M. Kohi, and A. C. Westphalen. Clinical applications for magnetic resonance guided high intensity focused ultrasound (mrghifu): present and future. *J Med Imaging Radiat Oncol*, 57(4):391–9, 2013.

[158] Mougenot C-Andreae T. Köhler M, Enholm J. Philips mr-guided high intensity focused ultrasound (white paper). *Philips Healthcare*, 2012.

[159] W. J. Elias, D. Huss, T. Voss, J. Loomba, M. Khaled, E. Zadicario, R. C. Frysinger, S. A. Sperling, S. Wylie, S. J. Monteith, J. Druzgal, B. B. Shah, M. Harrison, and M. Wintermark. A pilot study of focused ultrasound thalamotomy for essential tremor. *N Engl J Med*, 369(7):640–8, 2013.

[160] C. Lafon, D. Melodelima, R. Salomir, and J. Y. Chapelon. Interstitial devices for minimally invasive thermal ablation by high-intensity ultrasound. *Int J Hyperthermia*, 23(2):153–63, 2007.

[161] M. Abel, H. Ahmed, E. Leen, E. Park, M. Chen, H. Wasan, P. Price, L. Monzon, W. Gedroyc, and P. Abel. Ultrasound-guided trans-rectal high-intensity focused ultrasound (hifu) for advanced cervical cancer ablation is feasible: a case report. *J Ther Ultrasound*, 3:21, 2015.

[162] G. R. Meininger, H. Calkins, L. Lickfett, P. Lopath, T. Fjield, R. Pacheco, P. Harhen, E. R. Rodriguez, R. Berger, H. Halperin, and S. B. Solomon. Initial experience with a novel focused ultrasound ablation system for ring ablation outside the pulmonary vein. *J Interv Card Electrophysiol*, 8(2):141–8, 2003.

[163] L. Mearini and M. Porena. Transrectal high-intensity focused ultrasound for the treatment of prostate cancer: past, present, and future. *Indian J Urol*, 26(1):4–11, 2010.

[164] G. T. Haar and C. Coussios. High intensity focused ultrasound: physical principles and devices. *Int J Hyperthermia*, 23(2):89–104, 2007.

[165] J. B. Adams, R. G. Moore, J. H. Anderson, J. D. Strandberg, F. F. Marshall, and L. R. Davoussi. High-intensity focused ultrasound ablation of rabbit kidney tumors. *J Endourol*, 10(1):71–5, 1996.

[166] R. F. Paterson, E. Barret, Jr. Siqueira, T. M., T. A. Gardner, J. Tavakkoli, V. V. Rao, N. T. Sanghvi, L. Cheng, and A. L. Shalhav. Laparoscopic partial kidney ablation with high intensity focused ultrasound. *J Urol*, 169(1):347–51, 2003.

[167] K. U. Köhrmann, M. S. Michel, J. Gaa, E. Marlinghaus, and P. Alken. High intensity focused ultrasound as noninvasive therapy for multilocal renal cell carcinoma: case study and review of the literature. *The Journal of urology*, 167(6):2397–2403

[168] Christopher Rowland Hill, Jeff C. Bamber, and Gail ter Haar. *Physical principles of medical ultrasonics*, volume 2. Wiley Online Library, 2004.

[169] Faqi Li, Xiaobo Gong, Kai Hu, Chongyan Li, and Zhibiao Wang. Effect of ribs in hifu beam path on formation of coagulative necrosis in goat liver. *AIP Conference Proceedings*, 829(1):477–480, 2006.

[170] John Civale, Robert Clarke, Ian Rivens, and Gail Ter Haar. The use of a segmented transducer for rib sparing in hifu treatments. *Ultrasound in medicine and biology*, 32(11):1753–1761, 2006.

[171] Youssry Y. Botros, John L. Volakis, Philip VanBaren, and Emad S. Ebbini. A hybrid computational model for ultrasound phased-array heating in presence of strongly scattering obstacles. *Biomedical Engineering, IEEE Transactions on*, 44(11):1039–1050

[172] Youssry Y. Botros, Emad S. Ebbini, and John L. Volakis. Two-step hybrid virtual array ray (var) technique for focusing through the rib cage. *Ultrasonics, Ferroelectrics, and Frequency Control, IEEE Transactions on*, 45(4):989–1000, 1998.

[173] D. R. Daum and K. Hynynen. A 256-element ultrasonic phased array system for the treatment of large volumes of deep seated tissue. *IEEE Trans Ultrason Ferroelectr Freq Control*, 46(5):1254–68, 1999.

[174] J. Y. Chapelon, D. Cathignol, C. Cain, E. Ebbini, J. U. Kluiwstra, O. A. Sapozhnikov, G. Fleury, R. Berriet, L. Chupin, and J. L. Guey. New piezoelectric transducers for therapeutic ultrasound. *Ultrasound Med Biol*, 26(1):153–9, 2000.

[175] M. Pernot, J. F. Aubry, M. Tanter, J. L. Thomas, and M. Fink. High power transcranial beam steering for ultrasonic brain therapy. *Phys Med Biol*, 48(16):2577–89, 2003.

[176] E. S. Ebbini, H. Yao, and A. Shrestha. Dual-mode ultrasound phased arrays for image-guided surgery. *Ultrason Imaging*, 28(2):65–82, 2006.

[177] Mickaël Tanter, Mathieu Pernot, J. F. Aubry, Gabriel Montaldo, Fabrice Marquet, and Mathias Fink. Compensating for bone interfaces and respiratory motion in high-intensity focused ultrasound. *International Journal of Hyperthermia*, 23(2):141–151 0265–6736, 2007.

[178] J. W. Hand, A. Shaw, N. Sadhoo, S. Rajagopal, R. J. Dickinson, and L. R. Gavrilov. A random phased array device for delivery of high intensity focused ultrasound. *Phys Med Biol*, 54(19):5675–93, 2009.

[179] X. Ji, J. F. Bai, G. F. Shen, and Y. Z. Chen. High-intensity focused ultrasound with large scale spherical phased array for the ablation of deep tumors. *J Zhejiang Univ Sci B*, 10(9):639–47, 2009.

[180] E. Cochard, C. Prada, J. F. Aubry, and M. Fink. Ultrasonic focusing through the ribs using the dort method. *Med Phys*, 36(8):3495–503, 2009.

[181] E. Cochard, J. F. Aubry, M. Tanter, and C. Prada. Adaptive projection method applied to three-dimensional ultrasonic focusing and steering through the ribs. *J Acoust Soc Am*, 130(2):716–23, 2011.

[182] S. Qiao, G. Shen, J. Bai, and Y. Chen. Transcostal high-intensity focused ultrasound treatment using phased array with geometric correction. *J Acoust Soc Am*, 134(2):1503–14, 2013.

[183] J. W. Choi, J. Y. Lee, E. J. Hwang, I. Hwang, S. Woo, C. J. Lee, E. J. Park, and B. I. Choi. Portable high-intensity focused ultrasound system with 3d electronic steering, real-time cavitation monitoring, and 3d image reconstruction algorithms: a preclinical study in pigs. *Ultrasonography*, 33(3):191–9, 2014.

[184] Feng Wu. High intensity focused ultrasound: a noninvasive therapy for locally advanced pancreatic cancer. *World J Gastroenterol*, 20(44):16480–8, Nov 2014.

[185] Eduardo Moros. *Physics of thermal therapy: fundamentals and clinical applications*. CRC Press, 2012.

[186] J. E. Kennedy, F. Wu, G. R. ter Haar, F. V. Gleeson, R. R. Phillips, M. R. Middleton, and D. Cranston. High-intensity focused ultrasound for the treatment of liver tumours. *Ultrasonics*, 42(1-9):931–5, 2004.

[187] C. L. Yao, T. Trinh, G. T. Wong, and M. G. Irwin. Anaesthesia for high intensity focused ultrasound (hifu) therapy. *Anaesthesia*, 63(8):865–72, 2008.

[188] L. H. Schwartz, J. Richaud, L. Buffat, E. Touboul, and M. Schlienger. Kidney mobility during respiration. *Radiother Oncol*, 32(1):84–6, 1994.

[189] B. Bussels, L. Goethals, M. Feron, D. Bielen, S. Dymarkowski, P. Suetens, and K. Haustermans. Respiration-induced movement of the upper abdominal organs: a pitfall for the three-dimensional conformal radiation treatment of pancreatic cancer. *Radiother Oncol*, 68(1):69–74, 2003.

[190] J. H. Campos. An update on bronchial blockers during lung separation techniques in adults. *Anesth Analg*, 97(5):1266–74, 2003.

[191] J. B. Brodsky. Lung separation and the difficult airway. *Br J Anaesth*, 103 Suppl 1:i66–75, 2009.

[192] P. Biro, D. R. Spahn, and T. Pfammatter. High-frequency jet ventilation for minimizing breathing-related liver motion during percutaneous radiofrequency ablation of multiple hepatic tumours. *Br J Anaesth*, 102(5):650–3, 2009.

[193] P. E. Perkins. High-frequency jet ventilation during radiofrequency ablation: a case report. *AANA J*, 76(3):209–12, 2008.

[194] Jr. Goode, J. S., R. L. Taylor, C. W. Buffington, M. M. Klain, and D. Schwartzman. High-frequency jet ventilation: utility in posterior left atrial catheter ablation. *Heart Rhythm*, 3(1):13–9, 2006.

[195] Jr. Goode, J. S., R. L. Ranier, C. W. Buffington, M. M. Klain, and D. Schwartzman. To the editor–on the safety and efficacy of high-frequency jet ventilation during posterior left atrial ablation. *Heart Rhythm*, 8(8):e1; author reply e1–2, 2011.

[196] D. Y. Chung, D. M. Tse, P. Boardman, F. V. Gleeson, M. W. Little, S. H. Scott, and E. M. Anderson. High-frequency jet ventilation under general anesthesia facilitates ct-guided lung tumor thermal ablation compared with normal respiration under conscious analgesic sedation. *J Vasc Interv Radiol*, 25(9):1463–9, 2014.

[197] Senay Mihcin, Jan Strehlow, Daniel Demedts, Michael Schwenke, Yoav Levy, and Andreas Melzer. Evidence-based cross validation for acoustic power transmission for a novel treatment system. *Minim Invasive Ther Allied Technol*, pages 1–14, Jan 2017.

[198] F. J. Fry. Intense focused ultrasound in medicine. some practical guiding physical principles from sound source to focal site in tissue. *Eur Urol*, 23 Suppl 1:2–7, 1993.

[199] C R Hill and G R ter Haar. Review article: high intensity focused ultrasound–potential for cancer treatment. *Br J Radiol*, 68(816):1296–1303, Dec 1995.

[200] G. R. ter Haar and D. Robertson. Tissue destruction with focused ultrasound in vivo. *Eur Urol*, 23 Suppl 1:8–11, 1993.

[201] M. Susani, S. Madersbacher, C. Kratzik, L. Vingers, and M. Marberger. Morphology of tissue destruction induced by focused ultrasound. *Eur Urol*, 23 Suppl 1:34–8, 1993.

[202] L. Chen, I. Rivens, G. ter Haar, S. Riddler, C. R. Hill, and J. P. Bensted. Histological changes in rat liver tumours treated with high-intensity focused ultrasound. *Ultrasound Med Biol*, 19(1):67–74, 1993.

[203] J. B. Fowlkes, J. A. Ivey, E. A. Gardner, J. M. Rubin, and P. L. Carson. New acoustical approaches to perfusion and other vascular dynamics. *The Journal of the Acoustical Society of America*, 95(5):2855–2855

[204] Shahram Vaezy, Roy Martin, Peter Kaczkowski, George Keilman, Bryan Goldman, Hadi Yaziji, Steve Carter, Michael Caps, and Lawrence Crum. Use of high-intensity focused ultrasound to control bleeding. *Journal of vascular surgery*, 29(3):533–542 1999.

[205] F. Wu, W. Z. Chen, J. Bai, J. Z. Zou, Z. L. Wang, H. Zhu, and Z. B. Wang. Tumor vessel destruction resulting from high-intensity focused ultrasound in patients with solid malignancies. *Ultrasound Med Biol*, 28(4):535–42, 2002.

[206] J. Denekamp. Inadequate vasculature in solid tumours: consequences for cancer research strategies. *BJR Suppl*, 24:111–7, 1992.

[207] H. M. Sweetland, A. Wyman, and K. Rogers. Evaluation of the effect of interstitial laser hyperthermia on experimental subcutaneous tumours. *Lasers in medical science*, 8(2):107–112

[208] David L. Liu, Stefan Andersson-Engels, Christian Sturesson, Katarina Svanberg, Carl H. Håkansson, and Sune Svanberg. Tumour vessel damage resulting from laser-induced hyperthermia alone and in combination with photodynamic therapy. *Cancer letters*, 111(1):157–165, 1997.

[209] G. ter Haar. Ultrasound focal beam surgery. *Ultrasound Med Biol*, 21(9):1089–100, 1995.

[210] R. Warwick and J. Pond. Trackless lesions in nervous tissues produced by high intensity focused ultrasound (high-frequency mechanical waves). *J Anat*, 102(Pt 3):387–405, 1968.

[211] C. A. Linke, E. L. Carstensen, L. A. Frizzell, A. Elbadawi, and C. W. Fridd. Localized tissue destruction by high-intensity focused ultrasound. *Arch Surg*, 107(6):887–91, 1973.

[212] B. Walter, T. Weiss, F. Hofstadter, A. Gaumann, A. Hartmann, S. Rogenhofer, R. Ganzer, S. Wach, D. Engehausen, W. F. Wieland, and A. Blana. Utility of immunohistochemistry markers in the interpretation of post-high-intensive focussed ultrasound prostate biopsy cores. *World J Urol*, 31(5):1129–33, 2013.

[213] F. Wu, W. Z. Chen, J. Bai, J. Z. Zou, Z. L. Wang, H. Zhu, and Z. B. Wang. Pathological changes in human malignant carcinoma treated with high-intensity focused ultrasound. *Ultrasound Med Biol*, 27(8):1099–106, 2001.

[214] R. W. Ritchie, T. A. Leslie, G. D. Turner, I. S. Roberts, L. D'Urso, D. Collura, A. Demarchi, G. Muto, and M. E. Sullivan. Laparoscopic high-intensity focused ultrasound for renal tumours: a proof of concept study. *BJU Int*, 107(8):1290–6, 2011.

[215] F. Wu, Z. B. Wang, Y. D. Cao, Z. L. Xu, Q. Zhou, H. Zhu, and W. Z. Chen. Heat fixation of cancer cells ablated with high-intensity-focused ultrasound in patients with breast cancer. *Am J Surg*, 192(2):179–84, 2006.

[216] P. R. Mueller and A. U. Adam. *Interventional Oncology: A Practical Guide for the Interventional Radiologist*. Springer New York, 2011.

[217] L. Jiang, B. Hu, Q. Guo, and L. Chen. Sonographic and histological development of high-intensity focused ultrasound in rabbit muscle. *Exp Ther Med*, 5(1):33–38, 2013.

[218] M. Ichihara, K. Sasaki, S. Umemura, M. Kushima, and T. Okai. Blood flow occlusion via ultrasound image-guided high-intensity focused ultrasound and its effect on tissue perfusion. *Ultrasound Med Biol*, 33(3):452–9, 2007.

[219] I. J. Rowland, I. Rivens, L. Chen, C. H. Lebozer, D. J. Collins, G. R. ter Haar, and M. O. Leach. Mri study of hepatic tumours following high intensity focused ultrasound surgery. *Br J Radiol*, 70:144–53, 1997.

[220] R. A. Neumann, R. M. Knobler, F. Pieczkowski, and W. Gebhart. Enzyme histochemical analysis of cell viability after argon laser-induced coagulation necrosis of the skin. *J Am Acad Dermatol*, 25(6 Pt 1):991–8, 1991.

[221] J. K. Anderson, M. Baker, O. Jaffers, M. S. Pearle, G. L. Lindberg, and J. A. Cadeddu. Time course of nicotinamide adenine dinucleotide diaphorase staining after renal radiofrequency ablation influences viability assessment. *J Endourol*, 21(2):223–7, 2007.

[222] Y. N. Wang, T. Khokhlova, M. Bailey, J. H. Hwang, and V. Khokhlova. Histological and biochemical analysis of mechanical and thermal bioeffects in boiling histotripsy lesions induced by high intensity focused ultrasound. *Ultrasound Med Biol*, 39(3):424–38, 2013.

[223] D. L. Kreb, K. Bosscha, M. F. Ernst, M. J. Rutten, G. J. Jager, P. J. van Diest, and J. C. van der Linden. Use of cytokeratin 8 immunohistochemistry for assessing cell death after radiofrequency ablation of breast cancers. *Biotech Histochem*, 86(6):404–12, 2011.

[224] U. Lindner, N. Lawrentschuk, R. A. Weersink, S. R. Davidson, O. Raz, E. Hlasny, D. L. Langer, M. R. Gertner, T. Van der Kwast, M. A. Haider, and J. Trachtenberg. Focal laser ablation for prostate cancer followed by radical prostatectomy: validation of focal therapy and imaging accuracy. *Eur Urol*, 57(6):1111–4, 2010.

[225] G. J. Van Leenders, H. P. Beerlage, E. T. Ruijter, J. J. de la Rosette, and C. A. van de Kaa. Histopathological changes associated with high intensity focused ultrasound (hifu) treatment for localised adenocarcinoma of the prostate. *J Clin Pathol*, 53(5):391–4, 2000.

[226] Kai-Uwe Schassburger, Lars Lofgren, Ulla Lagerstedt, Karin Leifland, Karin Thorneman, Bengt Sandstedt, Gert Auer, and Hans Wiksell. Minimally-invasive treatment of early stage breast cancer: a feasibility study using radiofrequency ablation under local anesthesia. *Breast*, 23(2):152–158, Apr 2014.

[227] Kennedy J. E. Dphil thesis: An assessment of the capacity of high-intensity focused ultrasound to treat tumours of the liver and kidney. 2004.

[228] J Belghiti, K Hiramatsu, S Benoist, P Massault, A Sauvanet, and O Farges. Seven hundred forty-seven hepatectomies in the 1990s: an update to evaluate the actual risk of liver resection. *J Am Coll Surg*, 191(1):38–46, Jul 2000.

[229] Ralph V. Clayman. From knife to needle to nothing: the waning of the wound. *Braz J Urol*, 27:209–214, 2001.

[230] K. R. Yabroff, J. Lund, D. Kepka, and A. Mariotto. Economic burden of cancer in the united states: estimates, projections, and future research. *Cancer Epidemiol Biomarkers Prev*, 20(10):2006–14, 2011.

[231] D. Schrag. The price tag on progress–chemotherapy for colorectal cancer. *N Engl J Med*, 351(4):317–9, 2004.

[232] Andrew I Minchinton and Ian F Tannock. Drug penetration in solid tumours. *Nat Rev Cancer*, 6(8):583–92, Aug 2006.

[233] R. H. Thomlinson and L. H. Gray. The histological structure of some human lung cancers and the possible implications for radiotherapy. *Br J Cancer*, 9(4):539–49, 1955.

[234] K. L. Bennewith and S. Dedhar. Targeting hypoxic tumour cells to overcome metastasis. *BMC Cancer*, 11:504, 2011.

[235] R. K. Jain. The next frontier of molecular medicine: delivery of therapeutics. *Nat Med*, 4(6):655–7, 1998.

[236] S. Goel, D. G. Duda, L. Xu, L. L. Munn, Y. Boucher, D. Fukumura, and R. K. Jain. Normalization of the vasculature for treatment of cancer and other diseases. *Physiol Rev*, 91(3):1071–121, 2011.

[237] A. S. Narang and S. Varia. Role of tumor vascular architecture in drug delivery. *Adv Drug Deliv Rev*, 63(8):640–58, 2011.

[238] R. K. Jain. Transport of molecules across tumor vasculature. *Cancer Metastasis Rev*, 6(4):559–93, 1987.

[239] R. K. Jain. Delivery of molecular and cellular medicine to solid tumors. *Adv Drug Deliv Rev*, 26(2-3):71–90, 1997.

[240] R. K. Jain. Delivery of molecular and cellular medicine to solid tumors. *Adv Drug Deliv Rev*, 64(Suppl):353–365, 2012.

[241] H. F. Dvorak, J. A. Nagy, J. T. Dvorak, and A. M. Dvorak. Identification and characterization of the blood vessels of solid tumors that are leaky to circulating macromolecules. *Am J Pathol*, 133(1):95–109, 1988.

[242] L. E. Gerlowski and R. K. Jain. Microvascular permeability of normal and neoplastic tissues. *Microvasc Res*, 31(3):288–305, 1986.

[243] R. K. Jain. Normalization of tumor vasculature: an emerging concept in antiangiogenic therapy. *Science*, 307(5706):58–62, 2005.

[244] A. Krol, J. Maresca, M. W. Dewhirst, and F. Yuan. Available volume fraction of macromolecules in the extravascular space of a fibrosarcoma: implications for drug delivery. *Cancer Res*, 59(16):4136–41, 1999.

[245] I. K. Choi, R. Strauss, M. Richter, C. O. Yun, and A. Lieber. Strategies to increase drug penetration in solid tumors. *Front Oncol*, 3:193, 2013.

[246] A. J. Primeau, A. Rendon, D. Hedley, L. Lilge, and I. F. Tannock. The distribution of the anticancer drug doxorubicin in relation to blood vessels in solid tumors. *Clin Cancer Res*, 11(24 Pt 1):8782–8, 2005.

[247] A. Pluen, Y. Boucher, S. Ramanujan, T. D. McKee, T. Gohongi, E. di Tomaso, E. B. Brown, Y. Izumi, R. B. Campbell, D. A. Berk, and R. K. Jain. Role of tumor-host interactions in interstitial diffusion of macromolecules: cranial vs. subcutaneous tumors. *Proc Natl Acad Sci U S A*, 98(8):4628–33, 2001.

[248] R H Blum and S K Carter. Adriamycin. a new anticancer drug with significant clinical activity. *Ann Intern Med*, 80(2):249–59, Feb 1974.

[249] G. N. Hortobagyi. Anthracyclines in the treatment of cancer. an overview. *Drugs*, 54 Suppl 4:1–7, 1997.

[250] Hernán Cortés-Funes and Cyntia Coronado. Role of anthracyclines in the era of targeted therapy. *Cardiovasc Toxicol*, 7(2):56–60, 2007.

[251] T Skovsgaard and N I Nissen. Membrane transport of anthracyclines. *Pharmacol Ther*, 18(3):293–311, 1982.

[252] K Kiyomiya, S Matsuo, and M Kurebe. Mechanism of specific nuclear transport of adriamycin: the mode of nuclear translocation of adriamycin-proteasome complex. *Cancer Res*, 61(6):2467–71, Mar 2001.

[253] Ken-ichi Kiyomiya, Jun Satoh, Hiroshi Horie, Masaru Kurebe, Hiroshi Nakagawa, and Saburou Matsuo. Correlation between nuclear action of anthracycline anticancer agents and their binding affinity to the proteasome. *Int J Oncol*, 21(5):1081–5, Nov 2002.

[254] A Marco and F Arcamone. Dna complexing antibiotics: daunomycin, adriamycin and their derivatives. *Arzneimittelforschung*, 25(3):368–74, Mar 1975.

[255] Yves Pommier, Elisabetta Leo, HongLiang Zhang, and Christophe Marchand. Dna topoisomerases and their poisoning by anticancer and antibacterial drugs. *Chem Biol*, 17(5):421–33, May 2010.

[256] Zhong-Xiang Li, Ting-Ting Wang, Yan-Ting Wu, Chen-Ming Xu, Min-Yue Dong, Jian-Zhong Sheng, and He-Feng Huang. Adriamycin induces h2ax phosphorylation in human spermatozoa. *Asian J Androl*, 10(5):749–57, Sep 2008.

[257] Marek Gniazdowski, William A Denny, Stephanie M Nelson, and Malgorzata Czyz. Effects of anticancer drugs on transcription factor-dna interactions. *Expert Opin Ther Targets*, 9(3):471–89, Jun 2005.

[258] Sylvia Mansilla and José Portugal. Sp1 transcription factor as a target for anthracyclines: effects on gene transcription. *Biochimie*, 90(7):976–87, Jul 2008.

[259] L Gille and H Nohl. Analyses of the molecular mechanism of adriamycin-induced cardiotoxicity. *Free Radic Biol Med*, 23(5):775–82, 1997.

[260] R. M. Schiffelers and G. Storm. Liposomal nanomedicines as anticancer therapeutics: beyond targeting tumor cells. *Int J Pharm*, 364(2):258–64, 2008.

[261] T. Lammers, W. E. Hennink, and G. Storm. Tumour-targeted nanomedicines: principles and practice. *Br J Cancer*, 99(3):392–7, 2008.

[262] H. K. Sajja, M. P. East, H. Mao, Y. A. Wang, S. Nie, and L. Yang. Development of multifunctional nanoparticles for targeted drug delivery and noninvasive imaging of therapeutic effect. *Curr Drug Discov Technol*, 6(1):43–51, 2009.

[263] T. M. Allen and P. R. Cullis. Drug delivery systems: entering the mainstream. *Science*, 303(5665):1818–22, 2004.

[264] David Needham. Materials engineering of lipid bilayers for drug carrier performance. *Mrs Bulletin*, 24(10):32–41, 1999.

[265] A. D. Bangham, M. M. Standish, and J. C. Watkins. Diffusion of univalent ions across the lamellae of swollen phospholipids. *J Mol Biol*, 13(1):238–52, 1965.

[266] G. Gregoriadis, P. D. Leathwood, and B. E. Ryman. Enzyme entrapment in liposomes. *FEBS Lett*, 14(2):95–99, 1971.

[267] G. Gregoriadis and B. E. Ryman. Liposomes as carriers of enzymes or drugs: a new approach to the treatment of storage diseases. *Biochem J*, 124(5):58P, 1971.

[268] G. Gregoriadis. Drug entrapment in liposomes. *FEBS Lett*, 36(3):292–6, 1973.

[269] G. Gregoriadis. The carrier potential of liposomes in biology and medicine (first of two parts). *N Engl J Med*, 295(13):704–10, 1976.

[270] G Gregoriadis. The carrier potential of liposomes in biology and medicine (second of two parts). *N Engl J Med*, 295(14):765–70, Sep 1976.

[271] N v Rooijen and R v Nieuwmegen. Liposomes in immunology: Multilamellar phosphatidylcholine liposome as a simple biodegradable and harmless adjuvant without any immunogenic activity of its own. *Immunol commun*, 9:243–56, 1980.

[272] Danilo D Lasic. *Liposomes: from physics to applications*. Elsevier Science Ltd, 1993.

[273] A L Klibanov, K Maruyama, V P Torchilin, and L Huang. Amphipathic polyethyleneglycols effectively prolong the circulation time of liposomes. *FEBS Lett*, 268(1):235–7, Jul 1990.

[274] D Papahadjopoulos, T M Allen, A Gabizon, E Mayhew, K Matthay, S K Huang, K D Lee, M C Woodle, D D Lasic, and C Redemann. Sterically stabilized liposomes: improvements in pharmacokinetics and antitumor therapeutic efficacy. *Proc Natl Acad Sci U S A*, 88(24):11460–4, Dec 1991.

[275] J Senior, C Delgado, D Fisher, C Tilcock, and G Gregoriadis. Influence of surface hydrophilicity of liposomes on their interaction with plasma protein and clearance from the circulation: studies with poly(ethylene glycol)-coated vesicles. *Biochim Biophys Acta*, 1062(1):77–82, Feb 1991.

[276] P R Cullis. Lateral diffusion rates of phosphatidylcholine in vesicle membranes: effects of cholesterol and hydrocarbon phase transitions. *FEBS Lett*, 70(1):223–8, Nov 1976.

[277] T J McIntosh. The effect of cholesterol on the structure of phosphatidylcholine bilayers. *Biochim Biophys Acta*, 513(1):43–58, Oct 1978.

[278] Pranali P Deshpande, Swati Biswas, and Vladimir P Torchilin. Current trends in the use of liposomes for tumor targeting. *Nanomedicine (Lond)*, 8(9):1509–28, Sep 2013.

[279] Vladimir P Torchilin. Recent advances with liposomes as pharmaceutical carriers. *Nat Rev Drug Discov*, 4(2):145–60, Feb 2005.

[280] D. Needham and M. W. Dewhirst. The development and testing of a new temperature-sensitive drug delivery system for the treatment of solid tumors. *Adv Drug Deliv Rev*, 53(3):285–305, 2001.

[281] A Gabizon, R Catane, B Uziely, B Kaufman, T Safra, R Cohen, F Martin, A Huang, and Y Barenholz. Prolonged circulation time and enhanced accumulation in malignant exudates of doxorubicin encapsulated in polyethylene-glycol coated liposomes. *Cancer Res*, 54(4):987–92, Feb 1994.

[282] N D James, R J Coker, D Tomlinson, J R Harris, M Gompels, A J Pinching, and J S Stewart. Liposomal doxorubicin (doxil): an effective new treatment for kaposi's sarcoma in aids. *Clin Oncol (R Coll Radiol)*, 6(5):294–6, 1994.

[283] T. M. Allen and P. R. Cullis. Liposomal drug delivery systems: from concept to clinical applications. *Adv Drug Deliv Rev*, 65(1):36–48, 2013.

[284] Maurie Markman. Pegylated liposomal doxorubicin in the treatment of cancers of the breast and ovary. *Expert Opin Pharmacother*, 7(11):1469–74, Aug 2006.

[285] M E R O'Brien, N Wigler, M Inbar, R Rosso, E Grischke, A Santoro, R Catane, D G Kieback, P Tomczak, S P Ackland, F Orlandi, L Mellars, L Alland, C Tendler, and CAELYX Breast Cancer Study Group. Reduced cardiotoxicity and comparable efficacy in a phase iii trial of pegylated liposomal doxorubicin hcl (caelyx/doxil) versus conventional doxorubicin for first-line treatment of metastatic breast cancer. *Ann Oncol*, 15(3):440–9, Mar 2004.

[286] Carmela Pisano, Sabrina Chiara Cecere, Marilena Di Napoli, Carla Cavaliere, Rosa Tambaro, Gaetano Facchini, Cono Scaffa, Simona Losito, Antonio Pizzolorusso, and Sandro Pignata. Clinical trials with pegylated liposomal doxorubicin in the treatment of ovarian cancer. *J Drug Deliv*, 2013:898146, 2013.

[287] G. Batist, J. Barton, P. Chaikin, C. Swenson, and L. Welles. Myocet (liposome-encapsulated doxorubicin citrate): a new approach in breast cancer therapy. *Expert Opin Pharmacother*, 3(12):1739–51, 2002.

[288] C. E. Petre and D. P. Dittmer. Liposomal daunorubicin as treatment for kaposi's sarcoma. *Int J Nanomedicine*, 2(3):277–88, 2007.

[289] Michael L Etheridge, Stephen A Campbell, Arthur G Erdman, Christy L Haynes, Susan M Wolf, and Jeffrey McCullough. The big picture on nanomedicine: the state of investigational and approved nanomedicine products. *Nanomedicine*, 9(1):1–14, Jan 2013.

[290] H. Maeda. The enhanced permeability and retention (epr) effect in tumor vasculature: the key role of tumor-selective macromolecular drug targeting. *Adv Enzyme Regul*, 41:189–207, 2001.

[291] H. Maeda. Tumor-selective delivery of macromolecular drugs via the epr effect: background and future prospects. *Bioconjug Chem*, 21(5):797–802, 2010.

[292] G. Kong, R. D. Braun, and M. W. Dewhirst. Hyperthermia enables tumor-specific nanoparticle delivery: effect of particle size. *Cancer Res*, 60(16):4440–5, 2000.

[293] F. Yuan, M. Leunig, S. K. Huang, D. A. Berk, D. Papahadjopoulos, and R. K. Jain. Microvascular permeability and interstitial penetration of sterically stabilized (stealth) liposomes in a human tumor xenograft. *Cancer Res*, 54(13):3352–6, 1994.

[294] Stefan Wilhelm, Anthony J Tavares, Qin Dai, Seiichi Ohta, Julie Audet, Harold F Dvorak, and Warren CW Chan. Analysis of nanoparticle delivery to tumours. *Nature Reviews Materials*, 1:16014, 2016.

[295] T. D. Tailor, G. Hanna, P. S. Yarmolenko, M. R. Dreher, A. S. Betof, A. B. Nixon, I. Spasojevic, and M. W. Dewhirst. Effect of pazopanib on tumor microenvironment and liposome delivery. *Mol Cancer Ther*, 9(6):1798–808, 2010.

[296] D. C. Drummond, C. O. Noble, M. E. Hayes, J. W. Park, and D. B. Kirpotin. Pharmacokinetics and in vivo drug release rates in liposomal nanocarrier development. *J Pharm Sci*, 97(11):4696–740, 2008.

[297] A. Gabizon, H. Shmeeda, and Y. Barenholz. Pharmacokinetics of pegylated liposomal doxorubicin: review of animal and human studies. *Clin Pharmacokinet*, 42(5):419–36, 2003.

[298] Y. Barenholz. Doxil(r)–the first fda-approved nano-drug: lessons learned. *J Control Release*, 160(2):117–34, 2012.

[299] L. Harris, G. Batist, R. Belt, D. Rovira, R. Navari, N. Azarnia, L. Welles, E. Winer, and Tlc D. Study Group. Liposome-encapsulated doxorubicin compared with conventional doxorubicin in a randomized multicenter trial as first-line therapy of metastatic breast carcinoma. *Cancer*, 94(1):25–36, 2002.

[300] M. R. Ranson, S. Cheeseman, S. White, and J. Margison. Caelyx (stealth liposomal doxorubicin) in the treatment of advanced breast cancer. *Crit Rev Oncol Hematol*, 37(2):115–20, 2001.

[301] G. Kong, G. Anyarambhatla, W. P. Petros, R. D. Braun, O. M. Colvin, D. Needham, and M. W. Dewhirst. Efficacy of liposomes and hyperthermia in a human tumor xenograft model: importance of triggered drug release. *Cancer Res*, 60(24):6950–7, 2000.

[302] A. Sharma, U. S. Sharma, and R. M. Straubinger. Paclitaxel-liposomes for intracavitary therapy of intraperitoneal p388 leukemia. *Cancer Lett*, 107(2):265–72, 1996.

[303] K. M. Laginha, S. Verwoert, G. J. Charrois, and T. M. Allen. Determination of doxorubicin levels in whole tumor and tumor nuclei in murine breast cancer tumors. *Clin Cancer Res*, 11(19 Pt 1):6944–9, 2005.

[304] K. R. Hande. The importance of drug scheduling in cancer chemotherapy: Etoposide as an example. *Oncologist*, 1(4):234–239, 1996.

[305] A. S. Janoff. Lipids, liposomes, and rational drug design. *Lab Invest*, 66(6):655–8, 1992.

[306] A. Gabizon, D. Tzemach, L. Mak, M. Bronstein, and A. T. Horowitz. Dose dependency of pharmacokinetics and therapeutic efficacy of pegylated liposomal doxorubicin (doxil) in murine models. *J Drug Target*, 10(7):539–48, 2002.

[307] M. B. Yatvin, J. N. Weinstein, W. H. Dennis, and R. Blumenthal. Design of liposomes for enhanced local release of drugs by hyperthermia. *Science*, 202(4374):1290–3, 1978.

[308] J. N. Weinstein, R. L. Magin, M. B. Yatvin, and D. S. Zaharko. Liposomes and local hyperthermia: selective delivery of methotrexate to heated tumors. *Science*, 204(4389):188–91, 1979.

[309] D. Needham, G. Anyarambhatla, G. Kong, and M. W. Dewhirst. A new temperature-sensitive liposome for use with mild hyperthermia: characterization and testing in a human tumor xenograft model. *Cancer Res*, 60(5):1197–201, 2000.

[310] Gopal R Anyarambhatla and David Needham. Enhancement of the phase transition permeability of dppc liposomes by incorporation of mppc: a new temperature-sensitive liposome for use with mild hyperthermia. *Journal of Liposome Research*, 9(4):491–506, 1999.

[311] M. de Smet, E. Heijman, S. Langereis, N. M. Hijnen, and H. Grull. Magnetic resonance imaging of high intensity focused ultrasound mediated drug delivery from temperature-sensitive liposomes: an in vivo proof-of-concept study. *J Control Release*, 150(1):102–10, 2011.

[312] G Kong and M W Dewhirst. Hyperthermia and liposomes. *Int J Hyperthermia*, 15(5):345–70, 1999.

[313] Jeffrey K Mills and David Needham. Lysolipid incorporation in dipalmitoylphosphatidylcholine bilayer membranes enhances the ion permeability and drug release rates at the membrane phase transition. *Biochim Biophys Acta*, 1716(2):77–96, Oct 2005.

[314] L. H. Lindner, M. E. Eichhorn, H. Eibl, N. Teichert, M. Schmitt-Sody, R. D. Issels, and M. Dellian. Novel temperature-sensitive liposomes with prolonged circulation time. *Clin Cancer Res*, 10(6):2168–78, 2004.

[315] M. Hossann, M. Wiggenhorn, A. Schwerdt, K. Wachholz, N. Teichert, H. Eibl, R. D. Issels, and L. H. Lindner. In vitro stability and content release properties of phosphatidylglyceroglycerol containing thermosensitive liposomes. *Biochim Biophys Acta*, 1768(10):2491–9, 2007.

[316] R. T. Poon and N. Borys. Lyso-thermosensitive liposomal doxorubicin: a novel approach to enhance efficacy of thermal ablation of liver cancer. *Expert Opin Pharmacother*, 10(2):333–43, 2009.

[317] C. E. Swenson, L. E. Bolcsak, G. Batist, Jr. Guthrie, T. H., K. H. Tkaczuk, H. Boxenbaum, L. Welles, S. C. Chow, R. Bhamra, and P. Chaikin. Pharmacokinetics of doxorubicin administered i.v. as myocet (tlc d-99; liposome-encapsulated doxorubicin citrate) compared with conventional doxorubicin when given in combination with cyclophosphamide in patients with metastatic breast cancer. *Anticancer Drugs*, 14(3):239–46, 2003.

[318] Eleonora Mylonopoulou. *Enhancement and Mapping of Ultrasonic Drug Release for Thermosensitive Liposomes by Acoustic Cavitation*. Thesis, 2011.

[319] T Karino, S Koga, and M Maeta. Experimental studies of the effects of local hyperthermia on blood flow, oxygen pressure and ph in tumors. *Jpn J Surg*, 18(3):276–83, May 1988.

[320] C. W. Song, H. J. Park, C. K. Lee, and R. Griffin. Implications of increased tumor blood flow and oxygenation caused by mild temperature hyperthermia in tumor treatment. *Int J Hyperthermia*, 21(8):761–7, 2005.

[321] S L Brown, J W Hunt, and R P Hill. Differential thermal sensitivity of tumour and normal tissue microvascular response during hyperthermia. *Int J Hyperthermia*, 8(4):501–14, 1992.

[322] A. Gasselhuber, M. R. Dreher, A. Partanen, P. S. Yarmolenko, D. Woods, B. J. Wood, and D. Haemmerich. Targeted drug delivery by high intensity focused ultrasound mediated hyperthermia combined with temperature-sensitive liposomes: computational modelling and preliminary in vivovalidation. *Int J Hyperthermia*, 28(4):337–48, 2012.

[323] G. Kong, R. D. Braun, and M. W. Dewhirst. Characterization of the effect of hyperthermia on nanoparticle extravasation from tumor vasculature. *Cancer Res*, 61(7):3027–32, 2001.

[324] B. Hildebrandt, P. Wust, O. Ahlers, A. Dieing, G. Sreenivasa, T. Kerner, R. Felix, and H. Riess. The cellular and molecular basis of hyperthermia. *Crit Rev Oncol Hematol*, 43(1):33–56, 2002.

[325] F. K. Storm. Clinical hyperthermia and chemotherapy. *Radiol Clin North Am*, 27(3):621–7, 1989.

[326] J. D. Cohen and H. I. Robins. Whole body hyperthermia and intraperitoneal carboplatin in residual ovarian cancer. *Adv Exp Med Biol*, 267:197–202, 1990.

[327] G. J. Wiedemann, H. I. Robins, D. M. Katschinski, M. Mentzel, F. D'Oleire, M. Kutz, and T. Wagner. Systemic hyperthermia and ice chemotherapy for sarcoma patients: rationale and clinical status. *Anticancer Res*, 17(4B):2899–902, 1997.

[328] C. D. Kowal and J. R. Bertino. Possible benefits of hyperthermia to chemotherapy. *Cancer Res*, 39(6 Pt 2):2285–9, 1979.

[329] R. Engelhardt. Rational for clinical application of hyperthermia and drugs. *Rev Med Chir Soc Med Nat Iasi*, 91(2):347–52, 1987.

[330] T. S. Herman. Temperature dependence of adriamycin, cis-diamminedichloroplatinum, bleomycin, and 1,3-bis(2-chloroethyl)-1-nitrosourea cytotoxicity in vitro. *Cancer Res*, 43(2):517–20, 1983.

[331] J. Overgaard. Combined adriamycin and hyperthermia treatment of a murine mammary carcinoma in vivo. *Cancer Res*, 36(9 pt.1):3077–81, 1976.

[332] G. M. Hahn, J. Braun, and I. Har-Kedar. Thermochemotherapy: synergism between hyperthermia (42-43 degrees) and adriamycin (of bleomycin) in mammalian cell inactivation. *Proc Natl Acad Sci U S A*, 72(3):937–40, 1975.

[333] Q. Chen, S. Tong, M. W. Dewhirst, and F. Yuan. Targeting tumor microvessels using doxorubicin encapsulated in a novel thermosensitive liposome. *Mol Cancer Ther*, 3(10):1311–7, 2004.

[334] Q. Chen, A. Krol, A. Wright, D. Needham, M. W. Dewhirst, and F. Yuan. Tumor microvascular permeability is a key determinant for antivascular effects of doxorubicin encapsulated in a temperature sensitive liposome. *Int J Hyperthermia*, 24(6):475–82, 2008.

[335] ClinicalTrials.gov. Phase 1/2 study of thermodox with approved hyperthermia in treatment of breast cancer recurrence at the chest wall (dignity), 2009.

[336] K. Hynynen. The threshold for thermally significant cavitation in dog's thigh muscle in vivo. *Ultrasound Med Biol*, 17(2):157–69, 1991.

[337] Anthony Novell, Chantal Al Sabbagh, Jean-Michel Escoffre, Cédric Gaillard, Nicolas Tsapis, Elias Fattal, and Ayache Bouakaz. Focused ultrasound influence on calcein-loaded thermosensitive stealth liposomes. *Int J Hyperthermia*, 31(4):349–58, Jun 2015.

[338] ConstantinâĂŘC Coussios, Caleb H. Farny, Charles R. Thomas, Robin O. Cleveland, R. Glynn Holt, and Ronald A. Roy. Cavitation detection during and following hifu exposure in vitro. *The Journal of the Acoustical Society of America*, 115(5):2448–2448

[339] B. A. Rabkin, V. Zderic, and S. Vaezy. Hyperecho in ultrasound images of hifu therapy: involvement of cavitation. *Ultrasound Med Biol*, 31(7):947–56, 2005.

[340] R. Seip and E. S. Ebbini. Noninvasive estimation of tissue temperature response to heating fields using diagnostic ultrasound. *IEEE Trans Biomed Eng*, 42(8):828–39, 1995.

[341] C. Simon, P. Vanbaren, and E. S. Ebbini. Two-dimensional temperature estimation using diagnostic ultrasound. *IEEE Trans Ultrason Ferroelectr Freq Control*, 45(4):1088–99, 1998.

[342] R. M. Arthur, W. L. Straube, J. D. Starman, and E. G. Moros. Noninvasive temperature estimation based on the energy of backscattered ultrasound. *Med Phys*, 30(6):1021–9, 2003.

[343] R. M. Arthur, J. W. Trobaugh, W. L. Straube, and E. G. Moros. Temperature dependence of ultrasonic backscattered energy in motion-compensated images. *IEEE Trans Ultrason Ferroelectr Freq Control*, 52(10):1644–52, 2005.

[344] R. M. Arthur, W. L. Straube, J. W. Trobaugh, and E. G. Moros. In vivo change in ultrasonic backscattered energy with temperature in motion-compensated images. *Int J Hyperthermia*, 24(5):389–98, 2008.

[345] R. Maass-Moreno and C. A. Damianou. Noninvasive temperature estimation in tissue via ultrasound echo-shifts. part i. analytical model. *J Acoust Soc Am*, 100(4 Pt 1):2514–21, 1996.

[346] R. Maass-Moreno, C. A. Damianou, and N. T. Sanghvi. Noninvasive temperature estimation in tissue via ultrasound echo-shifts. part ii. in vitro study. *J Acoust Soc Am*, 100(4 Pt 1):2522–30, 1996.

[347] C. Mougenot, R. Salomir, J. Palussiere, N. Grenier, and C. T. Moonen. Automatic spatial and temporal temperature control for mr-guided focused ultrasound using fast 3d mr thermometry and multispiral trajectory of the focal point. *Magn Reson Med*, 52(5):1005–15, 2004.

[348] B. Quesson, F. Vimeux, R. Salomir, J. A. de Zwart, and C. T. Moonen. Automatic control of hyperthermic therapy based on real-time fourier analysis of mr temperature maps. *Magn Reson Med*, 47(6):1065–72, 2002.

[349] R. Salomir, J. Palussiere, F. C. Vimeux, J. A. de Zwart, B. Quesson, M. Gauchet, P. Lelong, J. Pergrale, N. Grenier, and C. T. Moonen. Local hyperthermia with mr-guided focused ultrasound: spiral trajectory of the focal point optimized for temperature uniformity in the target region. *J Magn Reson Imaging*, 12(4):571–83, 2000.

[350] C. Mougenot, B. Quesson, B. D. de Senneville, P. L. de Oliveira, S. Sprinkhuizen, J. Palussiere, N. Grenier, and C. T. Moonen. Three-dimensional spatial and temporal temperature control with mr thermometry-guided focused ultrasound (mrghifu). *Magn Reson Med*, 61(3):603–14, 2009.

[351] Max O Köhler, Charles Mougenot, Bruno Quesson, Julia Enholm, Brigitte Le Bail, Christophe Laurent, Chrit T W Moonen, and Gösta J Ehnholm. Volumetric hifu ablation under 3d guidance of rapid mri thermometry. *Med Phys*, 36(8):3521–35, Aug 2009.

[352] A. Partanen, P. S. Yarmolenko, A. Viitala, S. Appanaboyina, D. Haemmerich, A. Ranjan, G. Jacobs, D. Woods, J. Enholm, B. J. Wood, and M. R. Dreher. Mild hyperthermia with magnetic resonance-guided high-intensity focused ultrasound for applications in drug delivery. *Int J Hyperthermia*, 28(4):320–36, 2012.

[353] S. A. Sapareto and W. C. Dewey. Thermal dose determination in cancer therapy. *Int J Radiat Oncol Biol Phys*, 10(6):787–800, 1984.

[354] A. Meshorer, S. D. Prionas, L. F. Fajardo, J. L. Meyer, G. M. Hahn, and A. A. Martinez. The effects of hyperthermia on normal mesenchymal tissues. application of a histologic grading system. *Arch Pathol Lab Med*, 107(6):328–34, 1983.

[355] W. Schramm, D. Yang, B. J. Wood, F. Rattay, and D. Haemmerich. Contribution of direct heating, thermal conduction and perfusion during radiofrequency and microwave ablation. *Open Biomed Eng J*, 1:47–52, 2007.

[356] B. D. de Senneville, C. Mougenot, B. Quesson, I. Dragonu, N. Grenier, and C. T. Moonen. Mr thermometry for monitoring tumor ablation. *Eur Radiol*, 17(9):2401–10, 2007.

[357] D. J. Kerr, A. M. Kerr, R. I. Freshney, and S. B. Kaye. Comparative intracellular uptake of adriamycin and 4'-deoxydoxorubicin by non-small cell lung tumor cells in culture and its relationship to cell survival. *Biochem Pharmacol*, 35(16):2817–23, 1986.

[358] H. E. Skipper. Perspectives in cancer chemotherapy: Therapeutic design. *Cancer Res*, 24:1295–302, 1964.

[359] A. Gasselhuber, M. R. Dreher, F. Rattay, B. J. Wood, and D. Haemmerich. Comparison of conventional chemotherapy, stealth liposomes and temperature-sensitive liposomes in a mathematical model. *PLoS One*, 7(10):e47453, 2012.

[360] E. Mylonopoulou, M. Bazan-Peregrino, C. D. Arvanitis, and C. C. Coussios. A non-exothermic cell-embedding tissue-mimicking material for studies of ultrasound-induced hyperthermia and drug release. *Int J Hyperthermia*, 29(2):133–44, 2013.

[361] T. Kobayashi, S. Tsukagoshi, and Y. Sakurai. Enhancement of the cancer chemotherapeutic effect of cytosine arabinoside entrapped in liposomes on mouse leukemia l-1210. *Gan*, 66(6):719–20, 1975.

[362] E. Mayhew, D. Papahadjopoulos, Y. M. Rustum, and C. Dave. Inhibition of tumor cell growth in vitro and in vivo by 1-beta-d-arabinofuranosylcytosine entrapped within phospholipid vesicles. *Cancer Res*, 36(12):4406–11, 1976.

[363] R L Magin and M R Niesman. Temperature-dependent drug release from large unilamellar liposomes. *Cancer Drug Deliv*, 1(2):109–17, 1984.

[364] J L Merlin. In vitro evaluation of the association of thermosensitive liposome-encapsulated doxorubicin with hyperthermia. *Eur J Cancer*, 27(8):1031–4, 1991.

[365] S. K. Huang, P. R. Stauffer, K. Hong, J. W. Guo, T. L. Phillips, A. Huang, and D. Papahadjopoulos. Liposomes and hyperthermia in mice: increased tumor uptake and therapeutic efficacy of doxorubicin in sterically stabilized liposomes. *Cancer Res*, 54(8):2186–91, 1994.

[366] K. Maruyama, S. Unezaki, N. Takahashi, and M. Iwatsuru. Enhanced delivery of doxorubicin to tumor by long-circulating thermosensitive liposomes and local hyperthermia. *Biochim Biophys Acta*, 1149(2):209–16, 1993.

[367] S. Unezaki, K. Maruyama, N. Takahashi, M. Koyama, T. Yuda, A. Suginaka, and M. Iwatsuru. Enhanced delivery and antitumor activity of doxorubicin using long-circulating thermosensitive liposomes containing amphipathic polyethylene glycol in combination with local hyperthermia. *Pharm Res*, 11(8):1180–5, 1994.

[368] S. Ning, K. Macleod, R. M. Abra, A. H. Huang, and G. M. Hahn. Hyperthermia induces doxorubicin release from long-circulating liposomes and enhances their anti-tumor efficacy. *Int J Radiat Oncol Biol Phys*, 29(4):827–34, 1994.

[369] Y. Nishimura, K. Ono, M. Hiraoka, S. Masunaga, S. Jo, Y. Shibamoto, K. Sasai, M. Abe, K. Iga, and Y. Ogawa. Treatment of murine scc vii tumors with localized hyperthermia and temperature-sensitive liposomes containing cisplatin. *Radiat Res*, 122(2):161–7, 1990.

[370] C. van Bree, J. J. Krooshoop, R. C. Rietbroek, J. B. Kipp, and P. J. Bakker. Hyperthermia enhances tumor uptake and antitumor efficacy of thermostable liposomal daunorubicin in a rat solid tumor. *Cancer Res*, 56(3):563–8, 1996.

[371] M. H. Gaber, N. Z. Wu, K. Hong, S. K. Huang, M. W. Dewhirst, and D. Papahadjopoulos. Thermosensitive liposomes: extravasation and release of contents in tumor microvascular networks. *Int J Radiat Oncol Biol Phys*, 36(5):1177–87, 1996.

[372] S. A. Sapareto, L. E. Hopwood, W. C. Dewey, M. R. Raju, and J. W. Gray. Effects of hyperthermia on survival and progression of chinese hamster ovary cells. *Cancer Res*, 38(2):393–400, 1978.

[373] S. A. Sapareto. Thermal isoeffect dose: addressing the problem of thermotolerance. *Int J Hyperthermia*, 3(4):297–305, 1987.

[374] W C Dewey. Arrhenius relationships from the molecule and cell to the clinic. *Int J Hyperthermia*, 25(1):3–20, Feb 2009.

[375] M. L. Hauck, S. M. LaRue, W. P. Petros, J. M. Poulson, D. Yu, I. Spasojevic, A. F. Pruitt, A. Klein, B. Case, D. E. Thrall, D. Needham, and M. W. Dewhirst. Phase i trial of doxorubicin-containing low temperature sensitive liposomes in spontaneous canine tumors. *Clin Cancer Res*, 12(13):4004–10, 2006.

[376] V. Frenkel, A. Etherington, M. Greene, J. Quijano, J. Xie, F. Hunter, S. Dromi, and K. C. Li. Delivery of liposomal doxorubicin (doxil) in a breast cancer tumor model: investigation of potential enhancement by pulsed-high intensity focused ultrasound exposure. *Acad Radiol*, 13(4):469–79, 2006.

[377] R. Staruch, R. Chopra, and K. Hynynen. Localised drug release using mri-controlled focused ultrasound hyperthermia. *Int J Hyperthermia*, 27(2):156–71, 2011.

[378] P. S. Yarmolenko, Y. Zhao, C. Landon, I. Spasojevic, F. Yuan, D. Needham, B. L. Viglianti, and M. W. Dewhirst. Comparative effects of thermosensitive doxorubicin-containing liposomes and hyperthermia in human and murine tumours. *Int J Hyperthermia*, 26(5):485–98, 2010.

[379] B. L. Viglianti, A. M. Ponce, C. R. Michelich, D. Yu, S. A. Abraham, L. Sanders, P. S. Yarmolenko, T. Schroeder, J. R. MacFall, D. P. Barboriak, O. M. Colvin, M. B. Bally, and M. W. Dewhirst. Chemodosimetry of in vivo tumor liposomal drug concentration using mri. *Magn Reson Med*, 56(5):1011–8, 2006.

[380] A. M. Ponce, B. L. Viglianti, D. Yu, P. S. Yarmolenko, C. R. Michelich, J. Woo, M. B. Bally, and M. W. Dewhirst. Magnetic resonance imaging of temperature-sensitive liposome release: drug dose painting and antitumor effects. *J Natl Cancer Inst*, 99(1):53–63, 2007.

[381] A. H. Negussie, P. S. Yarmolenko, A. Partanen, A. Ranjan, G. Jacobs, D. Woods, H. Bryant, D. Thomasson, M. W. Dewhirst, B. J. Wood, and M. R. Dreher. Formulation and characterisation of magnetic resonance imageable thermally sensitive liposomes for use with magnetic resonance-guided high intensity focused ultrasound. *Int J Hyperthermia*, 27(2):140–55, 2011.

[382] T. Tagami, W. D. Foltz, M. J. Ernsting, C. M. Lee, I. F. Tannock, J. P. May, and S. D. Li. Mri monitoring of intratumoral drug delivery and prediction of the therapeutic effect with a multifunctional thermosensitive liposome. *Biomaterials*, 32(27):6570–8, 2011.

[383] A. Ranjan, G. C. Jacobs, D. L. Woods, A. H. Negussie, A. Partanen, P. S. Yarmolenko, C. E. Gacchina, K. V. Sharma, V. Frenkel, B. J. Wood, and M. R. Dreher. Image-guided drug delivery with magnetic resonance guided high intensity focused ultrasound and temperature sensitive liposomes in a rabbit vx2 tumor model. *J Control Release*, 158(3):487–94, 2012.

[384] R. M. Staruch, M. Ganguly, I. F. Tannock, K. Hynynen, and R. Chopra. Enhanced drug delivery in rabbit vx2 tumours using thermosensitive liposomes and mri-controlled focused ultrasound hyperthermia. *Int J Hyperthermia*, 28(8):776–87, 2012.

[385] R. M. Staruch, K. Hynynen, and R. Chopra. Hyperthermia-mediated doxorubicin release from thermosensitive liposomes using mr-hifu: Therapeutic effect in rabbit vx2 tumours. *Int J Hyperthermia*, 31(2):118–33, 2015.

[386] T. Tagami, M. J. Ernsting, and S. D. Li. Efficient tumor regression by a single and low dose treatment with a novel and enhanced formulation of thermosensitive liposomal doxorubicin. *J Control Release*, 152(2):303–9, 2011.

[387] S. M. Park, M. S. Kim, S. J. Park, E. S. Park, K. S. Choi, Y. S. Kim, and H. R. Kim. Novel temperature-triggered liposome with high stability: formulation, in vitro evaluation, and in vivo study combined with high-intensity focused ultrasound (hifu). *J Control Release*, 170(3):373–9, 2013.

[388] S Rizzitelli, P Giustetto, D Faletto, D Delli Castelli, S Aime, and E Terreno. The release of doxorubicin from liposomes monitored by mri and triggered by a combination of us stimuli led to a complete tumor regression in a breast cancer mouse model. *J Control Release*, 230:57–63, Apr 2016.

[389] Pierangela Giustetto, Daniela Delli Castelli, Cinzia Boffa, Silvia Rizzitelli, Davide Durando, Juan Carlos Cutrin, Silvio Aime, and Enzo Terreno. Release of a paramagnetic magnetic resonance imaging agent from liposomes triggered by low intensity non-focused ultrasound. *Journal of Medical Imaging and Health Informatics*, 3(3):356–366, 2013.

[390] Silvia Rizzitelli, Pierangela Giustetto, Cinzia Boffa, Daniela Delli Castelli, Juan Carlos Cutrin, Silvio Aime, and Enzo Terreno. In vivo mri visualization of release from liposomes triggered by local application of pulsed low-intensity non-focused ultrasound. *Nanomedicine*, 10(5):901–4, Jul 2014.

[391] ClinicalTrials.gov. Heat activated liposomal doxorubicin and radiofrequency ablation in treating patients with primary or metastatic liver tumors, Oct 2004.

[392] ClinicalTrials.gov. A phase iii, randomized, double blind, dummy-controlled study of thermodox® (lyso-thermosensitive liposomal doxorubicin-ltld) in hepatocellular carcinoma (hcc) using standardized radiofrequency ablation (rfa) treatment time âL'ě 45 minutes for solitary lesions âL'ě 3 cm to âL'd' 7 cm, 2014.

[393] G. Lopez-Berestein, V. Fainstein, R. Hopfer, K. Mehta, M. P. Sullivan, M. Keating, M. G. Rosenblum, R. Mehta, M. Luna, E. M. Hersh, and et al. Liposomal amphotericin b for the treatment of systemic fungal infections in patients with cancer: a preliminary study. *J Infect Dis*, 151(4):704–10, 1985.

[394] A. Gabizon, T. Peretz, A. Sulkes, S. Amselem, R. Ben-Yosef, N. Ben-Baruch, R. Catane, S. Biran, and Y. Barenholz. Systemic administration of doxorubicin-containing liposomes in cancer patients: a phase i study. *Eur J Cancer Clin Oncol*, 25(12):1795–803, 1989.

[395] ClinicalTrials.gov. A study of thermodox™ in combination with radiofrequency ablation (rfa) in primary and metastatic tumors of the liver, Feb 2007.

[396] ClinicalTrials.gov. A phase iii, randomized, double-blinded, dummy-controlled study of the efficacy and safety of thermodox® (thermally sensitive liposomal doxorubicin) in combination with radiofrequency ablation (rfa) compared to rfa-alone in the treatment of non-resectable hepatocellular carcinoma, 2008.

[397] R. T. Poon. Phase 3 randomized, double-blind, dummy controlled trial of radiofrequency ablation (rfa) + lyso-thermosensitive liposomal doxorubicin for hepatocellular carcinoma (hcc) lesions 3-7 cm. In *International Liver Cancer Association 7th Annual Conference*, 2013.

[398] Celsion. Thermodox® lyso-thermosensitive liposomal doxorubicin (ltld) investigator's brochure. Report, Celsion, 21 September 2015 2015.

[399] E. A. Lefrak, J. Pitha, S. Rosenheim, and J. A. Gottlieb. A clinicopathologic analysis of adriamycin cardiotoxicity. *Cancer*, 32(2):302–14, 1973.

[400] A. M. Rahman, S. W. Yusuf, and M. S. Ewer. Anthracycline-induced cardiotoxicity and the cardiac-sparing effect of liposomal formulation. *Int J Nanomedicine*, 2(4):567–83, 2007.

[401] T. M. Zagar, Z. Vujaskovic, S. Formenti, H. Rugo, F. Muggia, B. O'Connor, R. Myerson, P. Stauffer, I. C. Hsu, C. Diederich, W. Straube, M. K. Boss, A. Boico, O. Craciunescu, P. Maccarini, D. Needham, N. Borys, K. L. Blackwell, and M. W. Dewhirst. Two phase i dose-escalation/pharmacokinetics studies of low temperature liposomal doxorubicin (ltld) and mild local hyperthermia in heavily pretreated patients with local regionally recurrent breast cancer. *Int J Hyperthermia*, 30(5):285–94, 2014.

[402] P. Therasse, S. G. Arbuck, E. A. Eisenhauer, J. Wanders, R. S. Kaplan, L. Rubinstein, J. Verweij, M. Van Glabbeke, A. T. van Oosterom, M. C. Christian, and S. G. Gwyther. New guidelines to evaluate the response to treatment in solid tumors. european organization for research and treatment of cancer, national cancer institute of the united states, national cancer institute of canada. *J Natl Cancer Inst*, 92(3):205–16, 2000.

[403] S. R. Urva, B. S. Shin, V. C. Yang, and J. P. Balthasar. Sensitive high performance liquid chromatographic assay for assessment of doxorubicin pharmacokinetics in mouse plasma and tissues. *J Chromatogr B Analyt Technol Biomed Life Sci*, 877(8-9):837–41, 2009.

[404] D A Gewirtz. A critical evaluation of the mechanisms of action proposed for the antitumor effects of the anthracycline antibiotics adriamycin and daunorubicin. *Biochem Pharmacol*, 57(7):727–41, Apr 1999.

[405] ClinicalTrials.gov. Blood-brain barrier disruption using transcranial mri-guided focused ultrasound, Jan 2015.

[406] V. Rieke and K. Butts Pauly. Mr thermometry. *J Magn Reson Imaging*, 27(2):376–90, 2008.

[407] B Quesson, J A de Zwart, and C T Moonen. Magnetic resonance temperature imaging for guidance of thermotherapy. *J Magn Reson Imaging*, 12(4):525–33, Oct 2000.

[408] P T S Borman, C Bos, T de Boorder, B W Raaymakers, C T W Moonen, and S P M Crijns. Towards real-time thermometry using simultaneous multislice mri. *Phys Med Biol*, 61(17):N461–77, Sep 2016.

[409] M. Gyongy and C. C. Coussios. Passive cavitation mapping for localization and tracking of bubble dynamics. *J Acoust Soc Am*, 128(4):EL175–80, 2010.

[410] M. Gyongy and C. C. Coussios. Passive spatial mapping of inertial cavitation during hifu exposure. *IEEE Trans Biomed Eng*, 57(1):48–56, 2010.

[411] V. A. Salgaonkar, S. Datta, C. K. Holland, and T. D. Mast. Passive cavitation imaging with ultrasound arrays. *J Acoust Soc Am*, 126(6):3071–83, 2009.

[412] C. Coviello, R. Kozick, J. Choi, M. Gyongy, C. Jensen, P. P. Smith, and C. C. Coussios. Passive acoustic mapping utilizing optimal beamforming in ultrasound therapy monitoring. *J Acoust Soc Am*, 137(5):2573–85, 2015.

[413] C. R. Jensen, R. W. Ritchie, M. Gyongy, J. R. Collin, T. Leslie, and C. C. Coussios. Spatiotemporal monitoring of high-intensity focused ultrasound therapy with passive acoustic mapping. *Radiology*, 262(1):252–61, 2012.

[414] P. C. van Zijl and N. N. Yadav. Chemical exchange saturation transfer (cest): what is in a name and what isn't? *Magn Reson Med*, 65(4):927–48, 2011.

[415] G. T. Haar and C. Coussios. High intensity focused ultrasound: past, present and future. *Int J Hyperthermia*, 23(2):85–7, 2007.

[416] Robert C Ward, Terrance T Healey, and Damian E Dupuy. Microwave ablation devices for interventional oncology. *Expert Rev Med Devices*, 10(2):225–38, Mar 2013.

[417] K Hynynen, C J Martin, D J Watmough, and J R Mallard. Errors in temperature measurement by thermocouple probes during ultrasound induced hyperthermia. *Br J Radiol*, 56(672):969–70, Dec 1983.

[418] Hugh Morris, Ian Rivens, Adam Shaw, and Gail Ter Haar. Investigation of the viscous heating artefact arising from the use of thermocouples in a focused ultrasound field. *Phys Med Biol*, 53(17):4759–76, Sep 2008.

[419] Eleonora Mylonopoulou, Miriam Bazán-Peregrino, Costas D Arvanitis, and Constantin C Coussios. A non-exothermic cell-embedding tissue-mimicking material for studies of ultrasound-induced hyperthermia and drug release. *Int J Hyperthermia*, 29(2):133–44, 2013.

[420] Jason R Cook, Richard R Bouchard, and Stanislav Y Emelianov. Tissue-mimicking phantoms for photoacoustic and ultrasonic imaging. *Biomed Opt Express*, 2(11):3193–206, Nov 2011.

[421] S. M. Howard and C. I. Zanelli. HIFU Transducer Characterization Using a Robust Needle Hydrophone. In C.-C. Coussios and G. Ter Haar, editors, *6th International Symposium on Therapeutic Ultrasound*, volume 911 of *American Institute of Physics Conference Series*, pages 8–14, May 2007.

[422]

[423] Qifeng Wang, Rui Guo, Shunkang Rong, Gang Yang, Que Zhu, Yonghong Jiang, Changming Deng, Dichuan Liu, Qi Zhou, Qi Wu, Shunhe Wang, Jun Qian, Qi Wang, Han Lei, Tong-Chuan He, Zhibiao Wang, and Jing Huang. Noninvasive renal sympathetic denervation by extracorporeal high-intensity focused ultrasound in a pre-clinical canine model. *J Am Coll Cardiol*, 61(21):2185–92, May 2013.

[424] Bramaramba Gnapareddy, Sreekantha Reddy Dugasani, Taewoo Ha, Bjorn Paulson, Taehyun Hwang, Taesung Kim, Jae Hoon Kim, Kyunghwan Oh, and Sung Ha Park. Chemical and physical characteristics of doxorubicin hydrochloride drug-doped salmon dna thin films. *Sci Rep*, 5:12722, 2015.

[425] Nai-Tzu Chen, Chia-Yan Wu, Chao-Yu Chung, Yeukuang Hwu, Shih-Hsun Cheng, Chung-Yuan Mou, and Leu-Wei Lo. Probing the dynamics of doxorubicin-dna intercalation during the initial activation of apoptosis by fluorescence lifetime imaging microscopy (flim). *PLoS One*, 7(9):e44947, 2012.

[426] Jan Rothuizen and David C Twedt. Liver biopsy techniques. *Vet Clin North Am Small Anim Pract*, 39(3):469–80, May 2009.

[427] Ahmed M Al-Abd, Nam Ho Kim, Soo-Chang Song, Seung Jin Lee, and Hyo-Jeong Kuh. A simple hplc method for doxorubicin in plasma and tissues of nude mice. *Arch Pharm Res*, 32(4):605–11, Apr 2009.

[428] G L Scherphof, J Dijkstra, H H Spanjer, J T Derksen, and F H Roerdink. Uptake and intracellular processing of targeted and nontargeted liposomes by rat kupffer cells in vivo and in vitro. *Ann N Y Acad Sci*, 446:368–84, 1985.

[429] S M Moghimi and J Szebeni. Stealth liposomes and long circulating nanoparticles: critical issues in pharmacokinetics, opsonization and protein-binding properties. *Prog Lipid Res*, 42(6):463–78, Nov 2003.

[430] N Z Wu, R D Braun, M H Gaber, G M Lin, E T Ong, S Shan, D Papahadjopoulos, and M W Dewhirst. Simultaneous measurement of liposome extravasation and content release in tumors. *Microcirculation*, 4(1):83–101, Mar 1997.

[431] Darren C Wu and Clyde M Ofner, 3rd. Adsorption and degradation of doxorubicin from aqueous solution in polypropylene containers. *AAPS PharmSciTech*, 14(1):74–7, Mar 2013.

[432] P Loverock, G ter Haar, M G Ormerod, and P R Imrie. The effect of ultrasound on the cytotoxicity of adriamycin. *Br J Radiol*, 63(751):542–6, Jul 1990.

[433] Ondřej Hovorka, Vladimír Subr, David Větvička, Lubomír Kovář, Jiří Strohalm, Martin Strohalm, Aleš Benda, Martin Hof, Karel Ulbrich, and Blanka Ríhová. Spectral analysis of doxorubicin accumulation and the indirect quantification of its dna intercalation. *Eur J Pharm Biopharm*, 76(3):514–24, Nov 2010.

[434] Regine Lüpertz, Wim Wätjen, Regine Kahl, and Yvonni Chovolou. Dose- and time-dependent effects of doxorubicin on cytotoxicity, cell cycle and apoptotic cell death in human colon cancer cells. *Toxicology*, 271(3):115–21, May 2010.

[435] Gregory J R Charrois and Theresa M Allen. Drug release rate influences the pharmacokinetics, biodistribution, therapeutic activity, and toxicity of pegylated liposomal doxorubicin formulations in murine breast cancer. *Biochim Biophys Acta*, 1663(1-2):167–77, May 2004.

[436] D J Kerr, A M Kerr, R I Freshney, and S B Kaye. Comparative intracellular uptake of adriamycin and 4'-deoxydoxorubicin by non-small cell lung tumor cells in culture and its relationship to cell survival. *Biochem Pharmacol*, 35(16):2817–23, Aug 1986.

[437] Timo Zimmermann, Jens Rietdorf, and Rainer Pepperkok. Spectral imaging and its applications in live cell microscopy. *FEBS Lett*, 546(1):87–92, Jul 2003.

[438] J Kapuscinski. Dapi: a dna-specific fluorescent probe. *Biotech Histochem*, 70(5):220–33, Sep 1995.

[439] Nicolas Brosseau, Emil Andreev, and Dindial Ramotar. Complementation of the yeast model system reveals that caenorhabditis elegans oct-1 is a functional transporter of anthracyclines. *PLoS One*, 10(7):e0133182, 2015.

[440] G C Rice, G Fisher, M Devlin, G M Humphries, S Qasim Mehdi, and G M Hahn. Use of n-sigma-dansyl-l-lysine and flow cytometry to identify heat-killed mammalian cells. *Int J Hyperthermia*, 1(2):185–91, 1985.

[441] M A Mackey, S L Anolik, and J L Roti Roti. Changes in heat and radiation sensitivity during long duration, moderate hyperthermia in hela s3 cells. *Int J Radiat Oncol Biol Phys*, 24(3):543–50, 1992.

[442] G P Raaphorst, D P Heller, A Bussey, and C E Ng. Thermal radiosensitization by 41 degrees c hyperthermia during low dose-rate irradiation in human normal and tumour cell lines. *Int J Hyperthermia*, 10(2):263–70, 1994.

[443] G C Li, N F Mivechi, and G Weitzel. Heat shock proteins, thermotolerance, and their relevance to clinical hyperthermia. *Int J Hyperthermia*, 11(4):459–88, 1995.

[444] M Yonezawa, T Otsuka, N Matsui, H Tsuji, K H Kato, A Moriyama, and T Kato. Hyperthermia induces apoptosis in malignant fibrous histiocytoma cells in vitro. *Int J Cancer*, 66(3):347–51, May 1996.

[445] I B Shchepotin, V Soldatenkov, J T Wroblewski, A Surin, M Shabahang, R R Buras, R J Nauta, H Pulyaeva, and S R Evans. Apoptosis induced by hyperthermia and verapamil in vitro in a human colon cancer cell line. *Int J Hyperthermia*, 13(5):547–57, 1997.

[446] T Nishida, K Akagi, and Y Tanaka. Correlation between cell killing effect and cell membrane potential after heat treatment: analysis using fluorescent dye and flow cytometry. *Int J Hyperthermia*, 13(2):227–34, 1997.

[447] B Z Leal, M L Meltz, N Mohan, J Kuhn, T J Prihoda, and T S Herman. Interaction of hyperthermia with taxol in human mcf-7 breast adenocarcinoma cells. *Int J Hyperthermia*, 15(3):225–36, 1999.

[448] Y Rong and P Mack. Apoptosis induced by hyperthermia in dunn osteosarcoma cell line in vitro. *Int J Hyperthermia*, 16(1):19–27, 2000.

[449] F Zölzer and C Streffer. Quiescence in s-phase and g1 arrest induced by irradiation and/or hyperthermia in six human tumour cell lines of different p53 status. *Int J Radiat Biol*, 76(5):717–25, May 2000.

[450] T Ohtsubo, H J Park, J C Lyons, T Ohnishi, and C W Song. Effect of acidic environment and p53 on apoptosis induction by hyperthermia. *Int J Hyperthermia*, 16(6):481–91, 2000.

[451] K Kameda, T Kondo, K Tanabe, Q L Zhao, and H Seto. The role of intracellular ca(2+) in apoptosis induced by hyperthermia and its enhancement by verapamil in u937 cells. *Int J Radiat Oncol Biol Phys*, 49(5):1369–79, Apr 2001.

[452] Chang-Uk Lim, Ying Zhang, and Michael H Fox. Cell cycle dependent apoptosis and cell cycle blocks induced by hyperthermia in hl-60 cells. *Int J Hyperthermia*, 22(1):77–91, Feb 2006.

[453] Joseph L Roti Roti. Cellular responses to hyperthermia (40-46 degrees c): cell killing and molecular events. *Int J Hyperthermia*, 24(1):3–15, Feb 2008.

[454] Satoko Adachi, Satoshi Kokura, Tetsuya Okayama, Takeshi Ishikawa, Tomohisa Takagi, Osamu Handa, Yuji Naito, and Toshikazu Yoshikawa. Effect of hyperthermia combined with gemcitabine on apoptotic cell death in cultured human pancreatic cancer cell lines. *Int J Hyperthermia*, 25(3):210–9, May 2009.

[455] Alfred S Song, Amer M Najjar, and Kenneth R Diller. Thermally induced apoptosis, necrosis, and heat shock protein expression in 3d culture. *J Biomech Eng*, 136(7), Jul 2014.

[456] K K Karukstis, E H Thompson, J A Whiles, and R J Rosenfeld. Deciphering the fluorescence signature of daunomycin and doxorubicin. *Biophys Chem*, 73(3):249–63, Jul 1998.

[457] I Vermes, C Haanen, and C Reutelingsperger. Flow cytometry of apoptotic cell death. *J Immunol Methods*, 243(1-2):167–90, Sep 2000.

[458] W Swat, L Ignatowicz, and P Kisielow. Detection of apoptosis of immature cd4+8+ thymocytes by flow cytometry. *J Immunol Methods*, 137(1):79–87, Mar 1991.

[459] Z Darzynkiewicz, S Bruno, G Del Bino, W Gorczyca, M A Hotz, P Lassota, and F Traganos. Features of apoptotic cells measured by flow cytometry. *Cytometry*, 13(8):795–808, 1992.

[460] Howard M Shapiro. *Practical flow cytometry*. John Wiley & Sons, 2005.

[461] K J Bloom, K Dowlat, and L Assad. Pathologic changes after interstitial laser therapy of infiltrating breast carcinoma. *Am J Surg*, 182(4):384–8, Oct 2001.

[462] N F LaRusso. Morphology, physiology, and biochemistry of biliary epithelia. *Toxicol Pathol*, 24(1):84–9, 1996.

[463] P Van Eyken, R Sciot, F Callea, K Van der Steen, P Moerman, and V J Desmet. The development of the intrahepatic bile ducts in man: a keratin-immunohistochemical study. *Hepatology*, 8(6):1586–95, 1988.

[464] Charles Gawad, Winston Koh, and Stephen R Quake. Single-cell genome sequencing: current state of the science. *Nat Rev Genet*, 17(3):175–88, Mar 2016.

[465] Haesun Choi, Chuslip Charnsangavej, Silvana C Faria, Homer A Macapinlac, Michael A Burgess, Shreyaskumar R Patel, Lei L Chen, Donald A Podoloff, and Robert S Benjamin. Correlation of computed tomography and positron emission tomography in patients with metastatic gastrointestinal stromal tumor treated at a single institution with imatinib mesylate: proposal of new computed tomography response criteria. *J Clin Oncol*, 25(13):1753–9, May 2007.

[466] E A Eisenhauer, P Therasse, J Bogaerts, L H Schwartz, D Sargent, R Ford, J Dancey, S Arbuck, S Gwyther, M Mooney, L Rubinstein, L Shankar, L Dodd, R Kaplan, D Lacombe, and J Verweij. New response evaluation criteria in solid tumours: revised recist guideline (version 1.1). *Eur J Cancer*, 45(2):228–47, Jan 2009.

[467] Paul E Kinahan and James W Fletcher. Positron emission tomography-computed tomography standardized uptake values in clinical practice and assessing response to therapy. *Semin Ultrasound CT MR*, 31(6):496–505, Dec 2010.

[468] B Fisher, A M Brown, N V Dimitrov, R Poisson, C Redmond, R G Margolese, D Bowman, N Wolmark, D L Wickerham, and C G Kardinal. Two months of doxorubicin-cyclophosphamide with and without interval reinduction therapy compared with 6 months of cyclophosphamide, methotrexate, and fluorouracil in positive-node breast cancer patients with tamoxifen-nonresponsive tumors: results from the national surgical adjuvant breast and bowel project b-15. *J Clin Oncol*, 8(9):1483–96, Sep 1990.

[469] William C Dewey, Chris J Diederich, and Mark W Dewhirst. Hyperthermia classic commentary: 'arrhenius relationships from the molecule and cell to the clinic' by william dewey, int. j. hyperthermia, 10:457-483, 1994. *Int J Hyperthermia*, 25(1):21–4, Feb 2009.

[470] C Damianou and K Hynynen. The effect of various physical parameters on the size and shape of necrosed tissue volume during ultrasound surgery. *J Acoust Soc Am*, 95(3):1641–9, Mar 1994.

[471] Ellen L Jones, James R Oleson, Leonard R Prosnitz, Thaddeus V Samulski, Zeljko Vujaskovic, Daohai Yu, Linda L Sanders, and Mark W Dewhirst. Randomized trial of hyperthermia and radiation for superficial tumors. *J Clin Oncol*, 23(13):3079–85, May 2005.

[472] David Schlesinger, Stanley Benedict, Chris Diederich, Wladyslaw Gedroyc, Alexander Klibanov, and James Larner. Mr-guided focused ultrasound surgery, present and future. *Med Phys*, 40(8):080901, Aug 2013.

[473] Aradhana M Venkatesan, Ari Partanen, Tajana Klepac Pulanic, Matthew R Dreher, John Fischer, Robert K Zurawin, Raja Muthupillai, Sham Sokka, Heikki J Nieminen, Ninet Sinaii, Maria Merino, Bradford J Wood, and Pamela Stratton. Magnetic resonance imaging-guided volumetric ablation of symptomatic leiomyomata: correlation of imaging with histology. *J Vasc Interv Radiol*, 23(6):786–794.e4, Jun 2012.

[474] Isaac A Chang. Considerations for thermal injury analysis for rf ablation devices. *Open Biomed Eng J*, 4:3–12, 2010.

[475] S. J. Graham, L. Chen, M. Leitch, R. D. Peters, M. J. Bronskill, F. S. Foster, R. M. Henkelman, and D. B. Plewes. Quantifying tissue damage due to focused ultrasound heating observed by mri. *Magn Reson Med*, 41(2):321–8, 1999.

[476] Olivier Seror, Matthieu Lepetit-Coiffé, Brigitte Le Bail, Baudouin Denis de Senneville, Hervé Trillaud, Chrit Moonen, and Bruno Quesson. Real time monitoring of radiofrequency ablation based on mr thermometry and thermal dose in the pig liver in vivo. *Eur Radiol*, 18(2):408–16, Feb 2008.

[477] Pavel S Yarmolenko, Eui Jung Moon, Chelsea Landon, Ashley Manzoor, Daryl W Hochman, Benjamin L Viglianti, and Mark W Dewhirst. Thresholds for thermal damage to normal tissues: an update. *Int J Hyperthermia*, 27(4):320–43, 2011.

[478] M W Dewhirst, B L Viglianti, M Lora-Michiels, M Hanson, and P J Hoopes. Basic principles of thermal dosimetry and thermal thresholds for tissue damage from hyperthermia. *Int J Hyperthermia*, 19(3):267–94, 2003.

[479] Anna Yudina and Chrit Moonen. Ultrasound-induced cell permeabilisation and hyperthermia: strategies for local delivery of compounds with intracellular mode of action. *Int J Hyperthermia*, 28(4):311–9, 2012.

[480] Feng Wu, Zhi-Biao Wang, Wen-Zhi Chen, Hui Zhu, Jin Bai, Jian-Zhong Zou, Ke-Quan Li, Cheng-Bing Jin, Fang-Lin Xie, and Hai-Bing Su. Extracorporeal high intensity focused ultrasound ablation in the treatment of patients with large hepatocellular carcinoma. *Ann Surg Oncol*, 11(12):1061–9, Dec 2004.

[481] Sacha D Nandlall, Edward Jackson, and Constantin-C Coussios. Real-time passive acoustic monitoring of hifu-induced tissue damage. *Ultrasound Med Biol*, 37(6):922–34, Jun 2011.

[482] N F Maklad, J Ophir, and V Balsara. Attenuation of ultrasound in normal liver and diffuse liver disease in vivo. *Ultrason Imaging*, 6(2):117–25, Apr 1984.

[483] B S Garra, T H Shawker, M Nassi, and M A Russell. Ultrasound attenuation measurements of the liver in vivo using a commercial sector scanner. *Ultrason Imaging*, 6(4):396–407, Oct 1984.

[484] K J Parker, M S Asztely, R M Lerner, E A Schenk, and R C Waag. In-vivo measurements of ultrasound attenuation in normal or diseased liver. *Ultrasound Med Biol*, 14(2):127–36, 1988.

[485] A Duerinckx, K Rosenberg, J Hoefs, D Aufrichtig, C Cole-Beuglet, G Kanel, S Lottenberg, and L A Ferrari. In vivo acoustic attenuation in liver: correlations with blood tests and histology. *Ultrasound Med Biol*, 14(5):405–13, 1988.

[486] B W Dong, M Wang, K Xie, and M H Chen. In vivo measurements of frequency-dependent attenuation in tumors of the liver. *J Clin Ultrasound*, 22(3):167–74, 1994.

[487] Yasutomo Fujii, Nobuyuki Taniguchi, Kouichi Itoh, Kouichiro Shigeta, Yi Wang, Jing-Wen Tsao, Kenji Kumasaki, and Takashi Itoh. A new method for attenuation coefficient measurement in the liver: comparison with the spectral shift central frequency method. *J Ultrasound Med*, 21(7):783–8, Jul 2002.

[488] H H Pennes. Analysis of tissue and arterial blood temperatures in the resting human forearm. *J Appl Physiol*, 1(2):93–122, Aug 1948.

[489] M C Kolios, M D Sherar, and J W Hunt. Blood flow cooling and ultrasonic lesion formation. *Med Phys*, 23(7):1287–98, Jul 1996.

[490] F P Curra, P D Mourad, V A Khokhlova, R O Cleveland, and L A Crum. Numerical simulations of heating patterns and tissue temperature response due to high-intensity focused ultrasound. *IEEE Trans Ultrason Ferroelectr Freq Control*, 47(4):1077–89, 2000.

[491] M E Lyons and K J Parker. Absorption and attenuation in soft tissues. ii. experimental results. *IEEE Trans Ultrason Ferroelectr Freq Control*, 35(4):511–21, 1988.

[492] A H Wyllie. Apoptosis: an overview. *Br Med Bull*, 53(3):451–65, 1997.

[493] E Piazza, M Broggini, A Trabattoni, N Natale, A Libretti, and M G Donelli. Adriamycin distribution in plasma and blood cells of cancer patients with altered hematocrit. *Eur J Cancer Clin Oncol*, 17(10):1089–96, Oct 1981.

[494] A F Shields, L M Lange, and M M Zalupski. Phase ii study of liposomal doxorubicin in patients with advanced colorectal cancer. *Am J Clin Oncol*, 24(1):96–8, Feb 2001.

[495] E G Mayhew, M H Goldrosen, J Vaage, and Y M Rustum. Effects of liposome-entrapped doxorubicin on liver metastases of mouse colon carcinomas 26 and 38. *J Natl Cancer Inst*, 78(4):707–13, Apr 1987.

[496] S Oudard, A Thierry, T J Jorgensen, and A Rahman. Sensitization of multidrug-resistant colon cancer cells to doxorubicin encapsulated in liposomes. *Cancer Chemother Pharmacol*, 28(4):259–65, 1991.

[497] Richard L Wahl, Heather Jacene, Yvette Kasamon, and Martin A Lodge. From recist to percist: Evolving considerations for pet response criteria in solid tumors. *J Nucl Med*, 50 Suppl 1:122S–50S, May 2009.

[498] A H Chung, F A Jolesz, and K Hynynen. Thermal dosimetry of a focused ultrasound beam in vivo by magnetic resonance imaging. *Med Phys*, 26(9):2017–26, Sep 1999.

[499] Nathan McDannold, Clare M Tempany, Fiona M Fennessy, Minna J So, Frank J Rybicki, Elizabeth A Stewart, Ferenc A Jolesz, and Kullervo Hynynen. Uterine leiomyomas: Mr imaging-based thermometry and thermal dosimetry during focused ultrasound thermal ablation. *Radiology*, 240(1):263–72, Jul 2006.

[500] N. McDannold, N. Vykhodtseva, F. A. Jolesz, and K. Hynynen. Mri investigation of the threshold for thermally induced blood-brain barrier disruption and brain tissue damage in the rabbit brain. *Magn Reson Med*, 51(5):913–23, 2004.

[501] K. Sasaki, T. Azuma, K. I. Kawabata, M. Shimoda, E. I. Kokue, and S. I. Umemura. Effect of split-focus approach on producing larger coagulation in swine liver. *Ultrasound Med Biol*, 29(4):591–9, 2003.

[502] P. R. Patel, A. Luk, A. Durrani, S. Dromi, J. Cuesta, M. Angstadt, M. R. Dreher, B. J. Wood, and V. Frenkel. In vitro and in vivo evaluations of increased effective beam width for heat deposition using a split focus high intensity ultrasound (hifu) transducer. *Int J Hyperthermia*, 24(7):537–49, 2008.

[503] A. Schroeder, J. Kost, and Y. Barenholz. Ultrasound, liposomes, and drug delivery: principles for using ultrasound to control the release of drugs from liposomes. *Chem Phys Lipids*, 162(1-2):1–16, 2009.

[504] C. P. Phenix, M. Togtema, S. Pichardo, I. Zehbe, and L. Curiel. High intensity focused ultrasound technology, its scope and applications in therapy and drug delivery. *J Pharm Pharm Sci*, 17(1):136–53, 2014.

[505] Z. S. Al-Ahmady, O. Chaloin, and K. Kostarelos. Monoclonal antibody-targeted, temperature-sensitive liposomes: in vivo tumor chemotherapeutics in combination with mild hyperthermia. *J Control Release*, 196:332–43, 2014.

[506] K. Iga, N. Hamaguchi, Y. Igari, Y. Ogawa, K. Gotoh, K. Ootsu, H. Toguchi, and T. Shimamoto. Enhanced antitumor activity in mice after administration of thermosensitive liposome encapsulating cisplatin with hyperthermia. *J Pharmacol Exp Ther*, 257(3):1203–7, 1991.

[507] T. P. Chelvi, S. K. Jain, and R. Ralhan. Hyperthermia-mediated targeted delivery of thermosensitive liposome-encapsulated melphalan in murine tumors. *Oncol Res*, 7(7-8):393–8, 1995.

[508] H. S. Kim and Y. S. Park. Gene transfection by quantitatively reconstituted sendai envelope proteins into liposomes. *Cancer Gene Ther*, 9(2):173–7, 2002.

[509] J. Schneider, H. Falk, and G. Hunsmann. Virosomes constructed from lipid and purified friend leukaemia virus glycoprotein. *J Gen Virol*, 64 Pt 3:559–65, 1983.

[510] Y. Kaneda. Virosomes: evolution of the liposome as a targeted drug delivery system. *Adv Drug Deliv Rev*, 43(2-3):197–205, 2000.

[511] O. B. Garbuzenko, M. Saad, S. Betigeri, M. Zhang, A. A. Vetcher, V. A. Soldatenkov, D. C. Reimer, V. P. Pozharov, and T. Minko. Intratracheal versus intravenous liposomal delivery of sirna, antisense oligonucleotides and anticancer drug. *Pharm Res*, 26(2):382–94, 2009.

[512] K. A. Whitehead, R. Langer, and D. G. Anderson. Knocking down barriers: advances in sirna delivery. *Nat Rev Drug Discov*, 8(2):129–38, 2009.

[513] B. Kapoor, S. K. Singh, M. Gulati, R. Gupta, and Y. Vaidya. Application of liposomes in treatment of rheumatoid arthritis: quo vadis. *ScientificWorldJournal*, 2014:978351, 2014.

[514] E. R. Viscusi, R. Sinatra, E. Onel, and S. L. Ramamoorthy. The safety of liposome bupivacaine, a novel local analgesic formulation. *Clin J Pain*, 30(2):102–10, 2014.

[515] Hong Sung Kim and Yong Serk Park. Gene transfection by quantitatively reconstituted sendai envelope proteins into liposomes. *Cancer Gene Ther*, 9(2):173–7, Feb 2002.

[516] J Schneider, H Falk, and G Hunsmann. Virosomes constructed from lipid and purified friend leukaemia virus glycoprotein. *J Gen Virol*, 64 Pt 3:559–65, Mar 1983.

[517] Y Kaneda. Virosomes: evolution of the liposome as a targeted drug delivery system. *Adv Drug Deliv Rev*, 43(2-3):197–205, Sep 2000.

[518] Olga B Garbuzenko, Maha Saad, Seema Betigeri, Min Zhang, Alexandre A Vetcher, Viatcheslav A Soldatenkov, David C Reimer, Vitaly P Pozharov, and Tamara Minko. Intratracheal versus intravenous liposomal delivery of sirna, antisense oligonucleotides and anticancer drug. *Pharm Res*, 26(2):382–94, Feb 2009.

[519] Kathryn A Whitehead, Robert Langer, and Daniel G Anderson. Knocking down barriers: advances in sirna delivery. *Nat Rev Drug Discov*, 8(2):129–38, Feb 2009.

[520] Bhupinder Kapoor, Sachin Kumar Singh, Monica Gulati, Reena Gupta, and Yogyata Vaidya. Application of liposomes in treatment of rheumatoid arthritis: quo vadis. *ScientificWorldJournal*, 2014:978351, 2014.

[521] Eugene R Viscusi, Raymond Sinatra, Erol Onel, and Sonia L Ramamoorthy. The safety of liposome bupivacaine, a novel local analgesic formulation. *Clin J Pain*, 30(2):102–10, Feb 2014.

[522] K. Cho, X. Wang, S. Nie, Z. G. Chen, and D. M. Shin. Therapeutic nanoparticles for drug delivery in cancer. *Clin Cancer Res*, 14(5):1310–6, 2008.

[523] B. Kneidl, M. Peller, G. Winter, L. H. Lindner, and M. Hossann. Thermosensitive liposomal drug delivery systems: state of the art review. *Int J Nanomedicine*, 9:4387–98, 2014.

[524] H. Grull and S. Langereis. Hyperthermia-triggered drug delivery from temperature-sensitive liposomes using mri-guided high intensity focused ultrasound. *J Control Release*, 161(2):317–27, 2012.

[525] S. Langereis, T. Geelen, H. Grull, G. J. Strijkers, and K. Nicolay. Paramagnetic liposomes for molecular mri and mri-guided drug delivery. *NMR Biomed*, 26(7):728–44, 2013.

[526] James J Kwan, Rachel Myers, Christian M Coviello, Susan M Graham, Apurva R Shah, Eleanor Stride, Robert C Carlisle, and Constantin C Coussios. Ultrasound-propelled nanocups for drug delivery. *Small*, 11(39):5305–14, Oct 2015.

[527] R. K. Jain. Delivery of molecular and cellular medicine to solid tumors. *J Control Release*, 53(1-3):49–67, 1998.